

QC  
880  
.A46  
1976

ATDL-77/23

QC  
880  
A4  
10/106  
77/23

# Environmental Research Laboratories

Air Resources

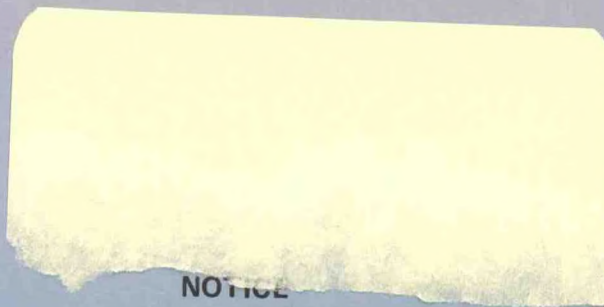
Atmospheric Turbulence and Diffusion Laboratory,

Oak Ridge, Tennessee.

September 1977

## 1976 ANNUAL REPORT





#### NOTICE

This report was prepared as an account of work sponsored by the United States Government. Neither the United States nor the United States Department of Energy, nor any of their employees, nor any of their contractors, subcontractors, or their employees, makes any warranty, express or implied, or assumes any legal liability or responsibility for the accuracy, completeness or usefulness of any information, apparatus, product or process disclosed, or represents that its use would not infringe privately owned rights.

This report has been reproduced directly from the best available copy.

Available from the National Technical Information Service, U. S. Department of Commerce, Springfield, Virginia 22161.

Price: Paper Copy \$19.00  
Microfiche \$3.00

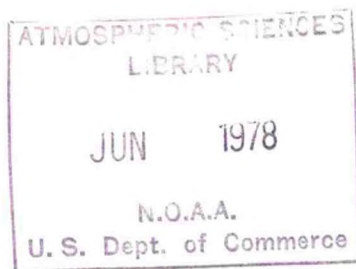


QC  
880  
.A46  
1976

## Foreword

The following is a compilation of research contributions from the National Oceanic and Atmospheric Administration Air Resources Atmospheric Turbulence and Diffusion Laboratory for the calendar year 1976. It was prepared by the Technical Information Center, U. S. Energy Research and Development Administration, Oak Ridge, Tennessee. Subsequent volumes will be issued on an annual basis. The research reported in this document was performed under an agreement between the U. S. Energy Research and Development Administration and the National Oceanic and Atmospheric Administration.

F. A. Gifford  
Director  
Atmospheric Turbulence  
and Diffusion Laboratory



78 2045







# CONTENTS

SUMMARY OF ACTIVITIES AND PLANS - FISCAL YEARS 1977 AND 1978 - Rayford P. Hosker, Jr. and Ruth A. Green .....	1
SCALE HEIGHT APPROXIMATIONS FOR DEPOSITION ESTIMATES AT EXTENDED DISTANCES - W. M. Culkowski .....	19✓
A COMPREHENSIVE ATMOSPHERIC TRANSPORT AND DIFFUSION MODEL - Walter M. Culkowski and Malcolm R. Patterson .....	37✓
LOCAL AND GLOBAL TRANSPORT AND DISPERSION OF AIRBORNE EFFLUENTS - S. R. Hanna .....	159✓
FOREST METEOROLOGY RESEARCH WITHIN THE OAK RIDGE SITE, EASTERN DECIDUOUS FOREST BIOME, USIBP - B. A. Hutchison and D. R. Matt .....	177 <sup>Dpl</sup> ✓
EFFECTS OF SKY BRIGHTNESS DISTRIBUTION UPON DIFFUSE RADIATION WITHIN A DECIDUOUS FOREST - B. A. Hutchison and D. R. Matt .....	237
OBSERVED AND PREDICTED COOLING TOWER PLUME RISE AT THE JOHN E. AMOS POWER PLANT, WEST VIRGINIA - Steven R. Hanna ...	239 <sup>done</sup>
SULCAL - A MODEL OF SULFUR CHEMISTRY IN A PLUME - C. F. Baes, Jr., J. T. Holdeman, and W. M. Culkowski .....	245
THE ANNUAL CYCLE OF SOLAR RADIATION IN A DECIDUOUS FOREST - B. A. Hutchison and D. R. Matt .....	327 <sup>done</sup>
THE SIMULATION OF ATMOSPHERIC TRANSPORT USING OBSERVED AND ESTIMATED WINDS - Carmen J. Nappo, Jr. ....	339
TROPOSPHERIC RELATIVE DIFFUSION OBSERVATIONS - F. A. Gifford .....	347 <sup>done</sup>
FIRST ANNUAL REPORT ON WEATHER MODIFICATION EFFECTS OF COOLING TOWERS - S. R. Hanna and R. P. Hosker, Jr. ....	351
COMMENTS ON "OBSERVATIONS OF AN INDUSTRIAL CUMULUS" - Steven R. Hanna .....	459
REGIONAL TRANSPORT MODEL OF ATMOSPHERIC SULFATES - K. S. Rao, I. Thomson, and B. A. Egan .....	461✓



REVIEW - PHYSICS OF THE BIOSPHERE - B. A. Hutchison .....	475
THE DISTRIBUTION OF SOLAR RADIATION WITHIN A DECIDUOUS FOREST - Boyd A. Hutchison and Detlef R. Matt .....	<i>done</i> 477
EFFECTS OF ATMOSPHERIC PARAMETERS ON THE CONCENTRATION OF PHOTOCHEMICAL AIR POLLUTANTS - F. A. Gifford and Steven R. Hanna .....	501
DAILY OBSERVATIONS OF VISIBLE PLUME LENGTH AT TVA'S PARADISE COOLING TOWERS - Steven R. Hanna and Martin Pike .....	511✓
SECONDARY MOTIONS IN A COOLING TOWER PLUME - Steven R. Hanna and Martin Pike .....	523✓
PREDICTED CLIMATOLOGY OF COOLING TOWER PLUMES FROM ENERGY CENTERS - Steven R. Hanna .....	<i>done</i> 531
MEETING REVIEW - THIRD SYMPOSIUM ON ATMOSPHERIC TURBULENCE, DIFFUSION, AND AIR QUALITY, AMS, 19-22 OCTOBER 1976, RALEIGH, N.C. - Steven R. Hanna .....	557
PREDICTIONS OF NOCTURNAL MIXING LAYER PARAMETERS - Gary A. Briggs .....	<i>out</i> 561✓
HYDROMETEOROLOGICAL ASPECTS OF ELECTRIC POWER PRODUCTION Steven R. Hanna .....	<i>done</i> 563
DRIFT - MODELING AND MONITORING COMPARISONS - Norbert C. J. Chen and Steven R. Hanna .....	<i>done</i> 597

Summary of  
Activities and Plans  
FY 1977 - 1978

Air Resources  
Atmospheric Turbulence and Diffusion Laboratory  
National Oceanic and Atmospheric Administration  
Oak Ridge, Tennessee  
July 1977

Rayford P. Hosker, Jr.  
and  
Ruth A. Green



## I. Preface and Summary

### A. Scope.

The Atmospheric Turbulence and Diffusion Laboratory (ATDL) in Oak Ridge, Tennessee, is operated for the Energy Research and Development Administration (ERDA) by the National Oceanic and Atmospheric Administration's (NOAA) Air Resources Laboratories, a group of research units generally concerned with problems of environmental pollution and its control. Major funding is from ERDA's Division of Biomedical and Environmental Research. ATDL works closely with various divisions of Oak Ridge National Laboratory (ORNL) on environmental projects of joint interest, and also functions as a meteorological consultant and advisor to that laboratory.

The ATDL is organized to perform research studies on atmospheric diffusion, transport, removal, and effects of pollutants, including heat and moisture, with most emphasis on scales up to regional size (up to  $\sim 200$  km). Current research programs include air transport studies, especially for the eastern Tennessee region; air pollution studies; the meteorological effects of cooling towers and energy production; research on plume and wake behavior, including effects of buoyancy, active thermal convection, building wake interaction, and removal processes; extension of atmospheric transport, diffusion, and effluent removal models to special situations such as over-water and over-forest flows; and study of the role of forest structure on the energy balance and on diffusion.

### B. FY 1977 Highlights.

The first phase of the Tennessee Valley Prediction Model (TVPM) was completed and is now being tested. The model attempts real time prediction of the transport and diffusion of atmospheric pollutants released from continuous or instantaneous point sources. The Tennessee Valley Assessment Model (TVAM) was also completed and testing is now under way. The purpose of this model is the generation of climatological estimates of air pollution patterns in the Tennessee Valley region from existing and proposed nuclear coal-burning power plants. The ATDL one-dimensional planetary boundary layer (PBL) model was expanded so that several parameterizations of the same processes can be simultaneously tested. A new one-dimensional time-dependent PBL model, based on a second-order turbulence closure theory, was developed to simulate the diurnal variation of the structure of the Ekman layer. A simple analytic model was developed for the nocturnal boundary layer. Data gathered during the Eastern Tennessee Trajectory Experiment (ETTEX) were published. A workshop on mesoscale transport and diffusion modeling using puffs and plumes was held at the ATDL.



In connection with studies of Meteorological Effects of Thermal Energy Releases (METER), cooling tower drift deposition modeling and monitoring techniques were critically reviewed and a report published. The one-dimensional plume and cloud growth model was run using input data from cooling towers at the John E. Amos power plant, the Chalk Point power plant, and refineries in St. Louis and Los Angeles. Time-sequence photographs were made of cooling tower plumes at TVA's Paradise, Kentucky, steam plant. A comprehensive state-of-the-art literature survey was completed of mathematical formulations of deep or shallow moist convection, and of numerical prediction models for cumulus cloud formation and growth. A review of Deardorff's 3-D numerical simulation of the planetary boundary layer with subgrid-scale turbulence modeling was completed, and a detailed report prepared. The diurnal variability of the dimensionless parameter,  $C$ , in the ATDL simple urban diffusion model,  $X = CQ/u$ , was evaluated for carbon monoxide using observed values of  $X$ ,  $Q$ , and  $u$  from many stations in the states of Maryland, New Jersey, and Colorado. Project "Prairie Grass" diffusion coefficients were reanalyzed using convective similarity theory. The Monte Carlo mesoscale diffusion model was applied to several test days on which ETTEX wind observations were available. A comparison of plume deposition models was completed. An experiment was conducted at the National Engineering Test Site in Idaho Falls to compare estimates of plume dispersion made from high-altitude and/or satellite photographs to those obtained from simultaneous releases of an inert gaseous tracer ( $SF_6$ ).

The low-speed wind tunnel purchased under an ERDA-EPA agreement for cooling tower research was installed in a new building behind the present ATDL offices, and tested. Building systems "shakedown" has been completed. Specialized wind tunnel instruments have been procured and installed, and a fast digital data system has been ordered. Modifications of the tunnel test sections for boundary layer modeling are underway. The water flow channel is being modified to accommodate deeper water to facilitate modeling of mesoscale transport phenomena.

Tower erection at the new deciduous forest meteorology site on Walker Branch Watershed was completed, and installation of instrumentation was begun. Preliminary determinations of forest structure at this site have been made. A cooperative study with the ORNL Environmental Sciences Division was conducted of elemental and sulfate inputs to the watershed via wetfall and dryfall. Aerosol concentrations were measured above and within the canopy. Analysis of micrometeorological data collected in the tulip poplar forest continued. The annual cycle of radiation in and above this forest was reconstructed using available data collected onsite and



continuous data collected at the Oak Ridge weather station. The wiring and instrumentation on the in-forest tower at the pine plantation site were completely overhauled, with particular attention to lightning protection measures. A digital data logging system is now recording data onto magnetic tape for easy analysis.

A research grade solar radiation station has been established at the Walker Branch site. The facility will serve as a cooperative station in the National Weather Service's new nationwide network of solar stations.

C. FY 1978 Highlights.

Initial coding and testing of the two-dimensional mesoscale model will be completed. Work will continue on development of the Tennessee Valley Prediction Model (TVPM), and the Tennessee Valley Assessment Model (TVAM) will be expanded to include washout, rainout, and ground deposition. The ATDL one-dimensional model will be used to test higher order turbulence closure schemes, and the new one-dimensional time-dependent PBL model will be used to study the detailed structure and behavior of the convective and nocturnal boundary layers. Work will resume on the potential flow model for complex terrain. Preliminary design of ETTEX II will begin.

Development and testing of a 2-D shallow cloud model for the METER study will continue. Chalk Point project observations will be used to test the drift deposition and plume cloud growth models. A new set of observations from the Paradise, Kentucky, steam plant will be studied in order to determine empirical formulas for predicting visible plume length based on measurements of meteorological variables near the surface. Studies of cooling tower plume-wake interactions will begin in the ATDL wind tunnel, with the object of parameterizing major effects for inclusion in the numerical models of plume rise and cloud growth.

The ATDL Applied Fluid Dynamics Laboratory will begin full-scale operation. Wind tunnel simulation of the atmospheric boundary layer for a variety of turbulence generator configurations will be completed and documented. Studies of cooling towers and isolated building wakes will begin. Initial water table visualizations of mesoscale advection over complex terrain will be completed. A model of the Walker Branch forest meteorology site and its surroundings will be tested to

elucidate flow patterns about the ridges, and to assist in proper instrument placement in the field. The new parameterizations for plume dispersion coefficients will be tested. The Monte Carlo diffusion model will be generalized. The Idaho smoke data will be analyzed and a new experiment planned. A second edition of Plume Rise will be completed, incorporating an analysis of data from the first ETTEX field experiment.

Analysis of micrometeorological data from the tulip poplar forest will continue. Studies of energy partitioning in an oak-hickory forest (Walker Branch site) will be conducted and related to synoptic climatic conditions and to forest structure. The turbulent flux measuring systems will be tested and placed in use during selected time periods. Data from the pine plantation site will be collected and stratified by prevailing weather conditions for a period of one year. A higher-order-closure numerical model of flow in a forest will be initiated, making use of data obtained at both field sites to simplify the equations of motion.

## II. FY 77 Accomplishments - ATDL

### A. Air Transport Studies.

The first phase of the Tennessee Valley Prediction Model (TVPM) is complete and testing is underway. The purpose of this model is the real time prediction of the transport and diffusion of atmospheric pollutants released from continuous or instantaneous point sources. The model is composed of three parts, a predictor, transporter and diffuser. The predictor consists of an array of up to 25 one-dimensional planetary boundary layer models. These models predict local winds throughout the Tennessee Valley Region. The transporter uses these winds to calculate the trajectories of air parcels which are used to simulate a continuous plume. In the diffuser section, plume dispersion due to atmospheric turbulence is simulated by calculating the spread of individual air parcels. Testing consists of comparing the calculated concentration patterns from several sources using the ETTEX wind observations with the patterns, using numerically calculated winds.

The Tennessee Valley Assessment Model (TVAM) has been completed and is being tested. The purpose of this model is the generation of climatological estimates of air pollution patterns in the Tennessee Valley region from existing and proposed nuclear and coal burning power plants. This model is similar to TVPM except that winds are not predicted but are estimated using the Tennessee Valley Authority (TVA) meteorological observations throughout the region.



Work continued on updating the ATDL-ORNL Atmospheric Transport Model (ATM). Principal emphasis was placed on developing objective techniques to determine stability classifications from local meteorology data. A paper to that effect was presented at the Air Pollution Control Association's annual meeting.

The ATDL one-dimensional planetary boundary layer (PBL) model has been expanded so that several parameterizations of the same processes can be simultaneously tested. The following parameterizations have been analyzed: constant flux layer calculations prescribed or calculated surface temperatures; turbulence eddy coefficients; stationary and time-dependent boundary conditions; atmospheric long-wave radiative cooling; and explicit and implicit finite differencing schemes. In addition, an extensive computer graphics package has been added so that 24-hour time-height cross-sections and vertical profiles of the meteorological variables can be plotted when desired.

A new one-dimensional time-dependent PBL model, based on a second-order turbulence closure theory, was developed to simulate the diurnal variation of the structure of the Ekman layer. The boundary conditions can be specified on the mean quantities or turbulent fluxes at the surface using the local equilibrium flux-profile relations.

A simple analytic model was developed for the nocturnal boundary layer. It was described and compared with more complex models and with data from field experiments in a paper submitted to Boundary Layer Meteorology.

Coding has begun on a two-dimensional mesoscale model using simple K-theory closure. Eventually this model will be expanded to three dimensions with higher order closure and used to assess the potential for adverse weather modifications of large nuclear power parks.

Computer codes have been written to test finite differencing schemes used in two and three-dimensional models, and relaxation techniques used in the solution of Poisson's equation. These tests are a necessary first step in the development of two and three dimensional mesoscale models.

The ETTEX data were published. These data include pilot balloon soundings, radiosondes, TVA meteorological tower observations, tetron position observations and surface meteorological observations. The report also includes a synopsis of ETTEX and discussions of significant results concerning wind fields over complex terrain, trajectory calculations and studies of relative diffusion.

A workshop on transport and diffusion modeling using puffs and plumes was held at ATDL on January 26 and 27. The workshop concentrated on the technical and theoretical considerations involved in modeling using puffs and plumes.

Work on the potential flow model for the eastern Tennessee river valley using both finite element and finite difference techniques has been delayed, pending the addition of a scientist-programmer-research assistant to the present staff.

## B. Atmospheric Pollution.

In cooperation with Oak Ridge National Laboratory, cooling tower drift deposition modeling and monitoring techniques were critically reviewed and a report published. Using several years of observations of the TVA Paradise cooling towers, correlations between plume geometry and meteorological variables were developed. Time-lapse movies of plumes from mechanical draft cooling towers at the Oak Ridge Gaseous Diffusion Plant were used to estimate tangential speeds in secondary vortices in the plume. Time-lapse photographs were taken of the plumes from the natural draft cooling towers at the Paradise plant, and are being similarly analyzed.

The one-dimensional plume and cloud growth model was run using input data from cooling towers at the John E. Amos power plant, the Chalk Point power plant, and refineries in St. Louis and Los Angeles. Predicted visible plume lengths, cloud bases, and liquid water contents agree fairly well with observations.

For the METER (Meteorological Effects of Thermal Energy Releases) project, a comprehensive state-of-the-art literature survey was completed of mathematical formulations of deep or shallow moist convection, and numerical prediction models for cumulus cloud formation and growth. Particular attention was given to cloud microphysics and turbulence parameterizations.

A steady-state 2-D shallow cloud model was also developed for the METER study. The model carries a full set of exact equations for mean wind velocities, potential temperature, water vapor and liquid water, as well as equations for the corresponding turbulent fluxes which are closed approximately. Bulk microphysics is included in terms of saturation adjustments and precipitation of liquid water. The power park is treated as a continuous area source at the grid lower boundary and its heat and vapor emission fluxes are directly input as boundary conditions with sinusoidal distributions over a specified downwind distance. The latter depends on the mean wind direction with respect to the line of cooling towers. The program is being tested and preliminary results are encouraging.



In relation to the study of possible concentration of vorticity by power parks, a review of Deardorff's 3-D numerical simulation of the planetary boundary layer with subgrid-scale turbulence modeling was completed, and a detailed report prepared. This report outlines the rationale for the subgrid-scale approach, its advantages and drawbacks, and problems likely to be encountered in its adaptation to the METER study.

A nonprecipitating 3-D shallow-convection cloud model was formulated for use in the study of meteorological effects of heat and moisture rejection by power parks. The model uses conservative variables, and the dynamical turbulence modeling is based on a higher-order turbulence closure theory. A report outlining the model assumptions, governing equations, boundary conditions, and possible simplifications has been prepared.

A chapter on the "Atmospheric Effects of Energy Generation" was completed for Atmospheric Science and Power Production (the successor to Meteorology and Atomic Energy - 1968).

The diurnal variability of the dimensionless parameter,  $C$ , in the ATDL simple urban diffusion model,  $X = CQ/u$ , was evaluated for carbon monoxide (CO) using observed values of  $X$ ,  $Q$ , and  $u$  from many stations in the states of Maryland, New Jersey, and Colorado. Due to the effects of atmospheric stability,  $C$  is five times as great at 2 a.m. as it is during the day. The new values of  $C$  were validated using independent CO data from Los Angeles.

#### C. Plume and Wake Behavior.

Diffusion coefficients measured in the "Prairie Grass" field experiment were re-analyzed in terms of recently advanced convective scaling parameters. This was a joint effort with members of the Atmospheric Sciences Department at North Carolina University.

The Monte Carlo mesoscale diffusion model was applied to several test days on which ETTEX wind observations were available. Reasonable results were obtained for relative diffusion, but the predicted diffusion was not fast enough for the single particle case.

Comparisons of the source-depletion, partial-reflection, surface-depletion, and ADPIC deposition models with each other and with field data were completed in collaboration with ORNL staff. The results will be submitted to Atmospheric Environment.



The low-speed wind tunnel purchased under an ERDA-EPA agreement for cooling tower research has been installed in a new building behind the ATDL offices. Specialized instruments such as hot-film anemometers, an electronic manometer, and temperature and trace gas concentration sensors have been procured. Time-lapse 16mm and 35mm camera systems are on hand for flow visualization studies. An on-site darkroom has been established to permit rapid processing of test results. A digital data logging system is being ordered. Flow conditions in the as-delivered tunnel have been carefully documented in an initial report. Experiments are underway to simulate atmospheric boundary layer flow in the modified 1mx1mx9m test section. When these are complete, studies of the flow and plume behavior close to model cooling towers will begin. A chapter on "Flow and Diffusion Near Obstacles" was completed for Atmospheric Science and Power Production.

The recirculating 1.2mx6m water flow table is being modified to carry a 30 cm deep flow. The facility is to be used for visualization of flow patterns near obstacles, over hills and ridges (e.g., the Walker Branch forestry site), and over mesoscale rough terrain (e.g., eastern Tennessee river valley). Dye injectors for this work are being designed.

A series of experiments on plume rise in calm, stable environments was designed and analyzed by ATDL personnel. (The work was carried out at the EPA fluid modeling facility by the staff of that facility). Also, data on maximum ground concentrations for neutral and unstable conditions. The results of these analyses and other recent advances in plume rise prediction were incorporated in a draft of a chapter for Atmospheric Science and Power Production.

An experiment was attempted at the National Engineering Test Site in Idaho Falls to compare estimates of plume dispersion made from high-altitude or satellite photographs to those obtained from simultaneous releases of an inert trace gas (SF<sub>6</sub>). Weather difficulties resulted in little usable data--however, most of the expendable materials such as the SF<sub>6</sub> are still on hand. The experiment will be attempted again late next year, hopefully with more favorable wind and sky cover conditions.

#### D. Forest Meteorology.

Tower erection at the deciduous forest meteorology site on Walker Branch Watershed was completed, and installation of instrumentation was started. Preliminary determinations of forest structure at this site have been made. A cooperative study (with Environmental Sciences Division, ORNL) was conducted of elemental and sulphate inputs to the watershed via wetfall and dryfall. In addition, aerosol concentrations were measured



above and within the canopy. Results of this study will be published in the proceedings of a Smithsonian Institute workshop on watershed research in Eastern North America. Instrumentation for measurement and recording (in both analog and digital form) of turbulent fluxes of heat, mass, and momentum were assembled and means of deployment designed. Preliminary measurements of the vertical fluxes of sensible heat, water vapor, and momentum in the oak-hickory forest at the Walker Branch site are underway.

Analysis of micrometeorologic data collected in the tulip poplar forest continued. The annual cycle of radiation in and above this forest was reconstructed using periodic data collected onsite and continuous data collected at the Oak Ridge weather stations. The resulting paper is in press in Agricultural Meteorology. In addition, radiant flux density distributions observed within this forest have been shown to closely approximate incomplete gamma functions throughout the year and under all kinds of weather conditions. This implies that the use of mean radiation for the prediction of rates of processes such as photosynthesis or evapotranspiration which vary nonlinearly with radiation leads to error. Relationships between the parameters defining the gamma functions and forest structure and weather conditions are under study.

The instrumentation on the in-forest tower at the pine plantation site has been completely overhauled. New transient-protected signal and power cables have been installed. Low-threshold heated sensor anemometers have been added at five levels within the canopy to supplement the cup-type units above. Temperature and humidity instruments have been recalibrated and reinstalled in aspirated shelters at ten levels. A digital data logging system is now recording data on to magnetic tape for easy analysis. Use of the turbulent flux instrumentation mentioned above is also planned for this forest.

#### E. Climatology.

A research grade solar radiation station for the Walker Branch site has been designed and necessary instrumentation acquired. This facility will serve as a cooperative station in the National Weather Service's new nationwide network of solar stations. Data collected at this site will be archived as part of the National Weather Service's solar radiation data set as well as being made available to other research programs at ORNL and elsewhere in this region.



The 22-year record of meteorological data collected at the Oak Ridge weather station was edited, calibrated, and stored on line on disk at the ORNL computer center. As such, this data set is now directly accessible via computer by ATDL and ORNL staff. Such data are particularly useful to ecosystem and regional modeling efforts underway at ORNL.

### III. FY 1978 Goals - ATDL.

#### A. Air Transport Studies.

Initial coding and testing of the two-dimensional mesoscale model should be completed. At this time, more efficient differencing schemes and computing techniques will be tested so that the most efficient running can be obtained. Initial coding of a three-dimensional mesoscale model will begin.

Development of the Tennessee Valley Prediction Model (TVPM) will continue. The results of boundary layer modeling studies will be incorporated into the TVPM as well as new and more accurate diffusion schemes. Washout, rainout, and ground deposition parameterizations will also be included in the code. Contact will be made with the ORNL Health Physics Division to start a real-time implementation of TVPM. This will give ORNL the ability to make rational decisions in case of a nuclear emergency.

The Tennessee Valley Assessment Model (TVAM) will be expanded to include washout, rainout, and ground deposition. The model will be modified to read the TVA meteorological data tapes. Using these input data as well as sulfur source emissions and measured concentrations, the TVAM will be tested and verified.

Work will continue on techniques (such as subroutines to the Air Transport Model) to establish valid, objective stability criteria based on local meteorological data and experience. Particular emphasis will be placed on verifying models in the unstable cases, since the economic penalties of miscalculation are most severe for the short distance cases.

The ATDL one-dimensional model will be used to test higher order turbulence closure schemes. An implicit finite differencing scheme will also be tested. Knowledge gained in these studies will be applied to the predictor section of the Tennessee Valley Prediction Model.

The new one-dimensional time-dependent PBL model will be used to study the detailed structure and behavior of the convective and nocturnal boundary layers, and related diffusion studies. The simple down-gradient diffusion model will be

improved to simulate the counter-gradient fluxes observed in the convective mixed layers.

Work on potential flow over complex terrain will be restarted.

Proposals for doing another ETTEX-type experiment will be drawn up, with a target date of winter of 1979.

#### B. Atmospheric Pollution.

The development and testing of a 2-D shallow cloud model for the METER study will continue. Attempts will be made to validate the model utilizing available observations of visible plumes and cumulus clouds over power centers, refineries, etc. The second-order turbulence closure model will be considerably simplified by using approximate diagnostic equations for turbulent fluxes. The results of both models will be compared. Conservative variables will be used to further simplify the model and reduce the computing time. Several alternate schemes of estimating the fraction of saturation in the grid volume will be tested. A Poisson equation for pressure will be included in a time-dependent version of the 2-D model.

Recent observations for the Chalk Point project will be used to test the drift deposition and plume cloud growth models. The latter model will be modified so that it is time dependent, in order to simulate the "pumping" and diurnal variability of cooling tower plumes, as observed in the time-lapse films from Keystone and Paradise.

A new set of observations from the TVA's Paradise, Kentucky, steam plant will be studied in order to determine empirical formulas for predicting visible plume length based on measurements of meteorological variables near the surface. Time lapse films will be analyzed to determine tangential speeds in secondary vortices at natural draft towers.

Studies of flow and plume behavior near single cooling towers will be well underway. A range of wind speeds, plume characteristics, upwind flow conditions, and tower sizes and types will be examined. The digital data logging system will be in operation, permitting rapid processing of test data using ORNL's computer system and ATDL's remote terminals. The object of this work is to parameterize important near-tower effects such as plume downwash for inclusion in the numerical models.

A critical review of urban diffusion models will be conducted.



### C. Plume and Wake Behavior.

The new ATDL Applied Fluid Dynamics Laboratory (AFDL) will be in full operation. Wind tunnel simulations of the atmospheric boundary layer will be completed and documented for a variety of turbulence generator modifications in the tunnel test section. Studies of cooling towers, mentioned above, and of wake structure near isolated building-like objects will begin. Detailed measurements for a variety of structure geometries and approach flow conditions will be carried out.

Tests of downwash of effluents released near buildings will be carried out at the EPA fluid modeling facility. Building shape, stack height, and efflux momentum will be varied, and rules-of-thumb for avoidance of downwash will be followed. Lift-off of buoyant plumes released in a turbulent wake will also be modeled.

Initial water table visualizations of mesoscale advection over complex terrain will be completed. The work will primarily be directed toward instrumenting the channel, building scale models, and testing flow visualization and photographic techniques. A model of the Walker Branch forest meteorology site and its surroundings will be tested to elucidate flow patterns about the ridges, and to assist in proper instrument placement in the field.

Further tests of the new parameterizations for plume diffusion coefficients will be made using published field data. A new field experiment may be contemplated and designed.

The Monte Carlo diffusion model will be put in a general form so that it can be used to estimate mesoscale diffusion. The only input needed is a turbulent energy spectrum and a two or three-dimensional field of wind speeds.

The limited data from the first Idaho Falls experiment on photographic estimates of plume dispersion will be analyzed and reported. Extrapolation of the results to satellite photos of long plumes will be attempted. Planning of the second experiment will begin.

A second edition of Plume Rise will be completed, incorporating an analysis of the data from the first ETTEX field experiment for possible convective turbulent effects on plume rise.

#### D. Forest Meteorology.

Analysis of micrometeorologic data from the tulip poplar forest will continue. Solar radiation distribution data will be used to test several models of radiation penetration into vegetation reported in the literature. In addition, comparisons of radiation data from the multi-storied tulip poplar forest and single-storied oak-hickory forest will be made.

Studies of energy partitioning in an oak-hickory forest (Walker Branch site) will be conducted and related to synoptic climatic conditions and to forest structure. Preliminary turbulence data will be analyzed and power spectra examined for conformance with similarity theory.

Data from the pine plantation site will be collected and stratified by prevailing weather conditions for a period of one year. Plots of the wind and temperature fields will be generated. Turbulent flux measurements will be performed, and the data compared to those from the Walker Branch site.

A higher-order-closure numerical model of flow in a forest will be initiated. Data from both active forest sites and from the literature will be examined to determine where the various terms in the governing equations may be conveniently parameterized or even neglected.

#### E. Climatology.

The solar radiation station will routinely accumulate data. The information will be supplied to the National Weather Service's archives, and also to solar energy research programs underway at ORNL and elsewhere.

#### IV. Laboratory Staff.

During FY 1977 the ATDL staff totaled approximately 21. Of this number, 11 were professional scientists and five were technical and administrative personnel. Several part-time workers, mostly students, account for the remainder. No overall increase in staff is planned for FY 1978, but it is expected that one professional position will be filled that was delayed during FY 1977. The staff is frequently augmented by visiting scientists from abroad. Several have come via International Atomic Energy Agency-National Research Council Fellowships, to work on problems



of nuclear meteorology. Others have been assigned here to work on basic problems of atmospheric diffusion through various programs, such as Oak Ridge Associated Universities (ORAU) faculty research fellowships. Also much use of university students at various levels is made, including part-time undergraduate workers, summer fellowship students, "co-op" students, and part-time graduate students. University students in these various capacities supplied approximately three person-years in FY 1977, a substantial fraction (~15%) of the ATDL total.

Publications and Reports FY-1977

- Chen, N. C. J., and S. R. Hanna, 1976: Drift - Modeling and Monitoring Comparisons. Presented at the Cooling Tower Institute Meeting, Houston, Texas, January 21, 1977 - February 2, 1977. National Oceanic and Atmospheric Admin., Envir. Res. Labs., Atmospheric Turbulence and Diffusion Lab., Rept. ATDL 76/24, 30 pp.
- Crawford, T. V., R. P. Hosker, Jr., et al., 1977: Environmental Transport, Panel Report II, Effects of Trace Contaminants from Coal Combustion, R. I. Van Hook and W. D. Shults, Editors, ERDA 77-64, 21-37.
- Culkowski, Walter M., 1977: Average daily solar radiation for Oak Ridge, Tennessee, 1956 through 1975. National Oceanic and Atmospheric Admin., Envir. Res. Labs., Atmospheric Turbulence and Diffusion Lab., Rept. ATDL 77/2, 5 pp., 21 tables.
- Culkowski, Walter M., 1977: An investigation of various atmospheric stability criteria at the one-hundred meter level in East Tennessee. Session 58, Meteorology III with Emphasis on Atmospheric Modeling, The 70th Annual Meeting of the Air Pollution Control Association, Toronto, Ontario, Canada, June 20-24, 1977, Paper No. 77-58,4.
- Gifford, F. A., and S. R. Hanna, 1976: Effects of atmospheric parameters on the concentration of photochemical air pollutants. National Oceanic and Atmospheric Admin., Envir. Res. Labs., Atmospheric Turbulence and Diffusion Lab., Rept. ATDL 76/17, 6 pp., 3 tables.
- Gifford, F. A., 1977: Comments on "Multiple-source plume models of urban air pollution - their general structure." To be published in Atmospheric Environ.
- Gifford, F. A., 1977: Bulletin Advertising: An Index to Expertise in Environmental Pollution. Bull. Am. Meteorol. Soc., 58, 598.
- Gifford, F. A., 1977: Similarity theory of the dispersion of buoyant power plant plumes with sulfur reactions. National Oceanic and Atmospheric Admin., Envir. Res. Labs., Atmospheric Turbulence and Diffusion Lab., Rept. ATDL 77/12, 7 pp.
- Gifford, F. A., R. P. Hosker, Jr., and K. S. Rao, 1977: Diffusion - deposition patterns in Martian streaks. National Oceanic and Atmospheric Admin., Envir. Res. Labs., Atmospheric Turbulence and Diffusion Lab., Rept. ATDL 77/18, 29 pp.
- Hanna, S. R., 1976: Climatology of cooling tower plume types from energy centers. J. Appl. Meteorol., 16, No. 9.
- Hanna, S. R., 1976: Symposium review: Third Symposium on Atmospheric Turbulence, Diffusion, and Air Quality. Bull. Am. Meteorol. Soc. 57, 242-244



- Hanna, S. R., 1976: Hydrometeorological aspects of electric power production. Presented at the Conference on "Water for Energy Development" held in Pacific Grove, California, December 6-10, 1976. National Oceanic and Atmospheric Admin., Envir. Res. Labs., Atmospheric Turbulence and Diffusion Lab., Rept. ATDL 76/23, 33 pp.
- Hanna, S. R., 1977: Urban modeling of inert substances. To be published by ASTM in Proceedings of Conference on Air Quality Meteorology, held 1-3 August in Boulder, Colorado.
- Hanna, S. R., 1977: Atmospheric effects of energy generation. To be published in Atmospheric Science and Power Production.
- Hanna, S. R., 1977: Model predictions and observations of clouds formed by oil refineries in Los Angeles. To be published in the Proceedings of the Sixth Conference on Inadvertent and Planned Weather Modification, October 10-13, 1977, Champaign-Urbana, Illinois.
- Hanna, S. R., 1977: A stability correction term for a simple urban dispersion model. To be published in the Proceedings of the Joint Conference on Applications on Air Pollution Meteorology, November 28 - December 2, 1977, Salt Lake City, Utah.
- Hanna, S. R. and F. A. Gifford, 1977: Applications of the ATDL simple urban dispersion model to Frankfurt, West Germany. To be published in the Proceedings of the 8th International Technical Meeting on Air Pollution Modeling and Its Application, September 20-23, 1977, in Louvain-la-Neuve, Belgium.
- Hanna, S. R., 1977: Diurnal variation of the stability factor in the simple ATDL urban dispersion model. National Oceanic and Atmospheric Admin., Envir. Res. Labs., Atmospheric Turbulence and Diffusion Lab., Rept. ATDL 77/19, 13 pp.
- Hosker, R. P., Jr., 1977: Flow and diffusion near obstacles. To be published in Atmospheric Science and Power Production.
- Hutchison, Boyd A., 1977: Atmospheric Turbulence and Diffusion Laboratory deciduous forest meteorology research program: An overview. National Oceanic and Atmospheric Adm., Envir. Res. Labs., Atmospheric Turbulence and Diffusion Lab., Rept. No. 77/1, 11 pp.
- Hutchison, Boyd A., Detlef R. Matt, and Robert T. McMillen, 1977: The characterization of deciduous forest radiation regimes. Weather-Climate Modeling for Real-Time Applications in Agriculture and Forest Meteorology, 61-62. (Proceedings of the 13th Conference on Agricultural and Forest Meteorology, Purdue University, April 4-6, 1977)

- Lindberg, S. E., R. R. Turner, N. M. Ferguson, and D. Matt, 1977: Walker Branch Watershed trace element studies: Collection and analysis of wetfall for trace constituents. National Oceanic and Atmospheric Adm., Envir., Res. Labs., Atmospheric Turbulence and Diffusion Lab., Rept. No. 77/6, 20 pp, 2 figures, 9 tables.
- Matt, Detlef R., Boyd A. Hutchison, and Robert T. McMillen, 1977: Analytical representation of solar radiation flux density distribution in a deciduous forest. Weather-Climate Modeling for Real-Time Applications in Agriculture and Forest Meteorology, 93-94. (Proceedings of the 13th Conference on Agricultural and Forest Meteorology, Purdue University, April 4-6, 1977.)
- Nappo, Carmen J., Jr., 1977: Mesoscale flow over complex terrain during the Eastern Tennessee Trajectory Experiment (ETTEX). To be published in the J. of Appl. Meteorol.
- Nappo, Carmen J., Jr., 1977: Horizontal variability of mesoscale winds over complex terrain. To be published in the Proceedings of the Joint Conference on Applications on Air Pollution Meteorology, November 28 - December 2, 1977, Salt Lake City, Utah.
- Rao, K. S., J. C. Wyngaard, and O. R. Cote, 1977: A numerical study of warm-air advection fog. To be published in the Proceedings of the Third Conference on Numerical Weather Predictions, April 26-28, 1977, Omaha, Nebraska.
- Rao, K. S., V. W. Nee, and K. T. Yang, 1977: Mass diffusion from a point source in a neutral turbulent shear layer. Trans. ASME, J. Heat Transfer, 99, 433-438.
- Weber, A. H., K. R. McDonald, and G. A. Briggs, 1977: Turbulence classification schemes for stable and unstable conditions. To be published in the Proceedings of the Joint Conference on Applications on Air Pollution Meteorology, November 28 - December 2, 1977, Salt Lake City, Utah.



# Environmental Research Laboratories

Air Resources

Atmospheric Turbulence and Diffusion Laboratory

Oak Ridge, Tennessee

FEBRUARY, 1976

SCALE HEIGHT APPROXIMATIONS FOR DEPOSITION ESTIMATES  
AT EXTENDED DISTANCES

W. M. CULKOWSKI

U. S. DEPARTMENT OF COMMERCE  
NATIONAL OCEANIC AND ATMOSPHERIC ADMINISTRATION

Scale Height Approximations for Deposition  
Estimates at Extended Distances

Walter M. Culkowski

Air Resources Atmospheric Turbulence and  
Diffusion Laboratory

National Oceanic and Atmospheric Administration  
Oak Ridge, Tennessee

February 18, 1976

ABSTRACT

As airborne materials travel beyond  $10^5$  meters, the vertical profile of material concentration becomes a function of three parameters; the height of the boundary layer, the deposition velocity, and the vertical diffusivity. The effects of these parameters are examined and some simple approximate relationships are presented for the vertical distribution and surface concentration of material with particular reference to surface deposition estimates.

ATDL Contribution File No. 76/1



## INTRODUCTION

The usual assumption that a plume may be corrected for the surface deposition effect by adjusting the source term has been questioned. Horst's (1) differentiation between "source removal" and the more physically realistic "surface removal" showed that the difference between the two processes ranged from negligible during unstable conditions to orders of magnitude for stable conditions out to  $10^5$  meters.

In attempting to extend a computer model of atmospheric transport and diffusion by Culkowski and Patterson (2) to mesoscale and greater distances, it became obvious that simply extending the usual plume estimates was inappropriate. Computers can, of course, be programmed to simulate any physical process, but often at enormous cost in computer time and programming. Accordingly, the following treatment is intended to enable a modeler to more realistically approximate deposition and concentration with minimal cost in computer time as a result of simplified programming techniques.

# THE SCALE HEIGHT

It will be convenient for the following considerations to define a scale height,  $H_1$ , as:

$$H_1 = Q / \int_{b-1/2}^{b+1/2} \int_{a-1/2}^{a+1/2} \chi(1) dx dy \quad (1)$$

$Q$  = total amount of material present over a unit area (grams)

$a, x$  = downwind distance (meters)

$b, y$  = crosswind distance (meters)

$\chi(1)$  = the concentration of material at the height of one meter (grams/meter<sup>3</sup>).

$H_1$  is a (usually) fictitious height enabling the investigator to employ distribution free methods if the scale height and surface concentrations are available. For convenience,  $Q$  is generally considered to be the crosswind integrated value, i.e.

$$H_1 = Q / \int_{-\infty}^{\infty} \int_{a-1/2}^{a+1/2} \chi(1) dx dy \quad (1a)$$

and will be considered as such in all subsequent references.



## ASSUMPTIONS AND SIMPLIFICATIONS

Utilizing a given scale height is valid only after the vertical distribution achieves an equilibrium state. The time  $T$ , required to reach the equilibrium state may be written as:

$$T = f(H \cdot V_g / K_z) \quad (2)$$

where  $T$  = time required to reach an equilibrium distribution in the vertical co-ordinate

$H$  = "mixing depth" of the atmosphere

$V_g$  = deposition velocity

$K_z$  = representative vertical diffusivity for a given stability condition

$T$  ranges from  $10^3$  seconds for  $(HV_g/K_z) = .25$  to  $10^6$  seconds when  $HV_g/K_z = 8$ . For the most part, however, all cases approach equilibrium sufficiently by  $10^5$  seconds of downwind travel to assure the viability of the methods outlined below. As a practical matter, as shown in tables II and III, below, deposition and concentration estimates may be made assuming the equilibrium configuration had constantly been operating over the entire  $10^5$  seconds.

No single stability condition would be expected to apply over the range of times and mixing depths involved here, and generalized vertical diffusivities are arbitrarily assigned for purposes of comparison to determine the steady state condition.

Moreover, the real atmosphere includes wind shear, multiple stable layers etc., which are ignored here, as is usually done in other long range computer diffusion models. The purpose of this paper is to show how an additional step toward realism, i.e. a treatment of deposition, can be applied to the more general models without undue cost in computer time.

#### VALIDITY OF DEPOSITION ASSUMPTIONS

At greater times and distances, removal processes other than deposition must be considered. Washout, defined by Chamberlain (3) as the removal of material by rainfall, does not alter the vertical distribution of material. Coagulation of aerosols becomes a real possibility and has been considered an important removal mechanism by many, (Lushnikov and Smirnov (4) Zuyev et al. (5) and Junge (6)) but disputed by others such as Brock (7). Calculations of the removal problem on a computer show that the half lives of surface emitted materials vary primarily as a function of stability and mixing depth. Table I shows the estimated half lives of an aerosol, calculated by means of the commonly assigned deposition velocity of  $V_g = 0.01$  meters/second.

Table I

Half Lives of Aerosols,  $V_g = 0.01$  meters/second (Source at Surface)

Stability	A	B	C	D	E	F
Mixing Depth (m)	3200	1600	800	400	200	100
$K_z$ ( $m^2/sec$ )	110	35	11	4	1	.25
1/2 Life (Hours)	53	22	8.3	3.3	1.7	0.2



Half lives of between 8 and 1000 hours have been estimated in the literature by McDonald (8), Fischer (9), and Esmen and Corn (10), by examining vertical profiles of material and assuming losses by coagulation. Table I shows that deposition is a competing, if not dominating, factor in effluent removal.

#### CALCULATIONS AND SCALING

The arbitrary values of  $H$ ,  $K_z$  and  $V_g$  were combined into a vertical dispersion model computed for a time scale of up to  $10^7$  seconds on an IBM 360/91. The results are given in Tables II and III. In addition to the runs shown in the tables, various other combinations of parameters were tried to determine if a simple approximation scheme could be found. To a very close (generally better than 10%) approximation one may write

$$H_1 = H(2.56 + HV_g/K_z)/2.56 \quad (3)$$

By analogy to the classic heat flow problems, one might expect to find the vertical distribution to be a sine function, and, indeed, after examining the computed profiles,

$$\text{for} \quad \theta \equiv \arcsin (H/H_1) \quad (3a)$$

$$\int_{-\infty}^{\infty} \chi(z) dy = Q_0 \exp(-V_g t/H_1) \sin \left[ \theta + z(90^\circ - \theta)/H \right] \quad (3b)$$

where  $t$  = elapsed time

$z$  = height above the surface

The following tables were constructed using deposition velocities of .01 (Table II) and 0.10 (Table III) meters/second. The former figure is commonly assumed to be the deposition velocity of very small particles and many gases over low-roughness terrain. The latter figure was included to explore the possible effects of extended wooded areas which have been reported by Sehmel et al (11), Slinn (12), Hosker (13), and Waldron (14) to increase the net deposition velocity by an order of magnitude or more.

The original distribution of material in the vertical was uniform, (i.e. a "box model"), although subsequent calculations employing point sources located at various elevations lead to exactly the same scale height. Starting with the "box" model has two effects; (1) equilibrium is achieved within  $10^5$  seconds and, (2) the depletion factor  $Q/Q_0$  will be smaller or larger if the source is a surface or elevated release, respectively.

The value of  $Q/Q_0$  for  $K_z = \infty$  was calculated by

$$Q/Q_0 = \exp (-V_g t/H) \quad , \quad (4)$$

The values of  $Q/Q_0$  for  $K_z < \infty$  were generated by a combinatorial generating function on an IBM 360/91 computer, but one finds  $t$  to a very close approximation

$$Q/Q_0 = \exp(-V_g t/H_1), \quad (4a)$$

indicating that equation (4a) may be used over the entire period, without having to calculate intermediate scale heights.



TABLE II

Comparison of Uniform ( $K_z = \infty$ ) With Parameter Dependent  
Concentrations After  $10^5$  Seconds

$$V_g = 0.01 \text{ meters/second}$$

STABILITY	H	$K_z$	Q/Qo	$H_1$	$K_z$	Q/Qo	$\exp(-V_g t/H_1)$
A	3200	$\infty$	.73	3518	110	.73	.75
B	1600	$\infty$	.54	1846	35	.57	.58
C	800	$\infty$	.29	999	11	.36	.37
D	400	$\infty$	.08	539	4	.15	.16
E	200	$\infty$	$7 \times 10^{-3}$	343	1	.05	.05
F	100	$\infty$	$5 \times 10^{-5}$	249	.25	.02	.02

TABLE III

Comparison of Uniform ( $K_z = \infty$ ) With Parameter  
Dependent Concentrations After  $10^5$  Seconds

$V_g = 0.10$  meters/second

STABILITY	H	$K_z$	Q/Qo	$H_1$	$K_z$	Q/Qo	$\exp(-V_g t/H_1)$
A	3200	$\infty$	.04	6615	110	.21	.22
B	1600	$\infty$	$2 \times 10^{-3}$	4334	35	.09	.10
C	800	$\infty$	$4 \times 10^{-6}$	3020	11	.03	.04
D	400	$\infty$	$1 \times 10^{-11}$	1946	4	.005	.006
E	200	$\infty$	$2 \times 10^{-22}$	1773	1	.003	.004
F	100	$\infty$	$4 \times 10^{-44}$	1690	.25	.002	.003



Perhaps the most significant finding that emerges from comparing Tables II and III is that increasing the deposition velocity by an order of magnitude decreases the remaining inventory, after  $10^5$  seconds, by approximately a factor of ten, an extreme divergence from the "box model" for most stability conditions.

#### INTERMEDIATE SCALE HEIGHT

Although comparing the results of Tables II and III with equation (4a), shows computations of intermediate scale height to be generally unnecessary, the rate of rise of the scale height from the mixing depth (generally achieved by the time an effluent travels  $10^5$  meters), and the time the equilibrium scale height is achieved (about  $10^5$  seconds) may be of occasional interest. Unfortunately, this author has so far failed to find a satisfactory interpolation formula. However, a fair representation may be achieved by

$$H_2 = [(H_1 - H)t] \exp[-(5.0 + 1.1 \log 10t)] + H \quad 10 \leq t \leq 10^5 \text{ seconds} \quad (5)$$

where  $H_2$  = intermediate scale height

$H_2$  calculated with the preceding approximation is accurate within 5% when the assumptions listed in Table II are used.

Table IV lists the intermediate scale heights from which equation (5) was obtained.

TABLE IV

Intermediate Scale Heights Resulting From Changing  
 A Uniform To A Parameter Dependent Distribution.  
 (Parameters as Given in Table II)

TIME	Scale Heights (Meters)					
	Stability					
	A	B	C	D	E	F
10 seconds	3207	1604	806	405	205	105
$10^2$ seconds	3229	1624	823	420	220	121
$10^3$ seconds	3294	1682	874	461	263	167
$10^4$ seconds	3442	1805	977	532	338	244
$10^5$ seconds	3518	1846	999	539	343	249



## EFFECTS OF MIXING HEIGHT VARIATIONS

Tables I - III illustrate the effects of stability on the net amount of material remaining after an extended time, and reference has been made to the effect that the  $(Q/Q_0)$  values are in reasonable agreement with estimated residence times found in the literature. Because of the variation of the mixing depth with time as shown by Holzworth (15). However, much of the aerosol or reactive gas inventory is unavailable; e.g., an aerosol cloud released during an "A" condition will have most of its material dispersed above the assumed 100 meter mixing depth which may follow that night, permitting less than 10% of the material to circulate below the height of the mixing layer. This would help in explaining the long (4 days or greater) residence times of surface emitted aerosols found by various isotope ratio methods such as Blifford et al. (16) Haxel and Schumann (17) and Lehmann and Sittkus (18) The work of Poet, et al, (19) seems appropriate to the atmospheric modeler. They find, for all dry removal processes:

$$Q/Q_0 = \exp(-t/T_1) \quad (6)$$

where  $T_1$  = residence time of 4 days ( $3.5 \times 10^5$  seconds).

Suprisingly, there is little or no seasonal variation in residence time. The residence time,  $T_1$ , may be considered dimensionally

in distribution-free methods :

$$T_1 = H_1/Vg \quad (7)$$

Equating  $H_1$  with  $T_1$  and a  $Vg$  of 0.01 meters/second, we find the "A" condition to be most representative, in terms of Scale Heights, for estimating deposition over extended times.

#### CONCLUSIONS AND RECOMMENDATIONS

Extending present computer models of surface concentrations and deposition can be accomplished rather easily by applying the Scale Height concept beyond the  $10^4$ - $10^5$  meters normally covered by the Sutton or Pasquill-Gifford dispersion parameters. Whatever vertical dispersion parameters are assumed to be operating at  $10^5$  meters form the basis of the assumed "box model" which will be transformed to the equilibrium model by equation (3)

For deposition velocities of the order of  $Vg = 0.01$  or less, the modeler is particularly fortunate in that he may retain the "box model" if he so chooses since, by Table II, there is very little difference between the box and most representative equilibrium model. Larger deposition velocities require surprisingly little correction as illustrated in Table III.



The simplest method of employing present models to greater distances is simply to extend the present vertical dispersion graphs or tables, (after corrections for each wind speed group), linearly to an  $H_1$  of 3500 meters. Table V below shows that assuming a constant  $H_1$  of 3500 meters is not unrealistic, physically. G. I. Taylor in 1917, (20) determined the average monthly  $K_z$  from heat flux measurements at the Eiffel Tower. Fitting equation (3) to the lowest and highest readings we find that the assumed mixing depths are in good agreement with typical mean afternoon mixing depths for the U.S. (15).

TABLE V

Lowest and Highest Average Daily  $K_z$  as Found by  
G. I. Taylor and Resulting Mixing Depths if  $H_1 = 3500$  meters

MONTH	$K_z(m^2/sec)$	$H_1$ (meters)	H(meters)
February	1.6	3500	1010
August	30.1	3500	2613

In conclusion, the employment of "source removal," or "box model" methods often found implicitly or explicitly over a period of  $10^5$  seconds or longer would need little

correction provided the deposition velocity were on the order of 0.01 meters per second or smaller, and the mixing depth or the equivalent vertical dispersion parameter was approximately 3500 meters. Existing models may easily be extended to account for increased deposition velocities using the methods outlined above.



## REFERENCES

1. Horst, T. W., "A Surface Depletion Model for Deposition from a Gaussian Plume," Atmosphere-Surface Exchange of Particulate and Gaseous Pollutants - 1974 Symposium, September 4-6, 1974, Battelle.
2. Culkowski, Walter M. and Malcolm R. Patterson, "A Comprehensive Atmospheric Transport and Diffusion Model," ORNL-NSF-EATC-17.
3. Chamberlain, A. C., 1953, "Aspects of Travel and Deposition of Aerosol and Vapor Clouds," British Report AERE-HP/R-1261.
4. Lushnikov, A. A. and V. I. Smirnov, "Stationary Coalescence and Particle Size Distribution of Atmospheric Aerosols," Izv., Atmospheric and Oceanic Physics, Vol. 11, No. 2, 1975, pp. 139-152.
5. Zuyev, V. Ye.; L. S. Ivlev; and K. Ya. Kondrat'Yev, "Recent Results from Studies of Atmospheric Aerosols," Izv., Atmospheric and Oceanic Physics, Vol. 9, No. 4, 1973, pp. 371-385.
6. Junge, Christian E., Air Chemistry and Radioactivity, 1963, Academic Press New York and London.
7. Brock, J. R., "Condensational Growth of Atmospheric Aerosols," Journal of Colloid and Interface Science, Vol 39, No. 1, April 1972.
8. McDonald, James E., "Mean Atmospheric Residence Times for Particulate Air Pollutants," Bulletin of the American Meteorological Society, Vol. 42, No. 9, September, 1961, pp. 664-665.
9. Fischer, William H., "Residence Time of Particles in Urban Air," Atmospheric Environment, 1971, Vol 5, pp. 1059-1060.
10. Esmen, Nurtan A. and Morton Corn, "Residence Time of Particles in Urban Air," Atmospheric Environment, 1971, Vol 5, pp. 571-578.
11. Sehmel, G. A., Sutter, S. L., and Dana, M.T., "Dry deposition processes", in Pacific Northwest Laboratory Annual Report for 1972 to the U.S.A.E.C. Division of Biomedical and Environmental Research, vol. II, part 1, BNWL-1751 PT1, UC-53 (April, 1973), 43.
12. Slinn, W.G.N., "On the dry deposition of sea salt nuclei", in Pacific Northwest Laboratory Annual Report for 1971 to the U.S.A.E.C. Division of Biomedical and Environmental Research, vol. II, part 1, BNWL-1651 PT1, UC-53 (Dec., 1972) 51.

13. Hosker, R. P., "Estimates of Dry Deposition and Plume Depletion over Forests and Grassland," IAEA Symposium on the Physical Behavior of Radioactive Contaminants in the Atmosphere, Vienna, Austria, Nov. 12-16, 1973.
14. Waldron, A. W., jr., "Expected Instantaneous Surface Line Source and Point Source Behavior in a Forest Environment," U.S. Army Test and Evaluation Command Technical Note DTC-TN-72-601, AD-887 032, August, 1971.
15. Holzworth, George C., "Mixing Heights, Wind Speeds, and Potential for Urban Air Pollution Throughout the Contiguous United States," Environmental Protection Agency, January 1972.
16. Blifford, I. H., L. B. Lockhart, Jr. and H. B. Rosknstock (1952). "On the Natural Radioactivity in the Air," J. Geophys. Research 57, 499-509.
17. Haxel, O. and G. Schumann (1955). "Selbstreinigung der Atmosphere," Z. Physik 142, 127-132.
18. Lehmann, L. and A. Stitkus (1959). Bestimmung von Aerosolverweilzeiten aus dem RaD und RaF-Gehalt der atmospharischen Luft und des Niederschlages. Naturwissenschaften 46, 9-10.
19. Poet, S. E.; H. E. Moore; and E. A. Martell. "Lead 210, Bismuth 210, and Polonium 210 in the Atmosphere: Accurate Ratio Measurement and Application to Aerosol Residence Time Determination," Journal of Geophysical Research, Vol. 77, No. 33, November 20, 1972.
20. "Phenomena Connected with Turbulence in the Lower Atmosphere," Proceedings of the Royal Society, A, vol. XCIV (1917), pp. 137-55.



# **A COMPREHENSIVE ATMOSPHERIC TRANSPORT and DIFFUSION MODEL**

Walter M. Culkowski

Malcolm R. Patterson

## ERRATA

ORNL/NSF/EATC-17

A COMPREHENSIVE ATMOSPHERIC  
TRANSPORT AND DIFFUSION MODEL

by

W. M. Culkowski and M. R. Patterson

Page 12: Omit eq (15). Eq (16) should read:

$$Q = Q_0 \exp \left[ -\sqrt{\frac{2}{\pi}} \left( \frac{v_g}{u} \right) \int_0^x \frac{\exp \left( -h^2 / 2\sigma_z^2 z \right)}{\sigma_z} dx' \right]$$

Page 19: Following eq (26), the statements should read:

 $\Delta h = 1.6 (F_B)^{1/3} u^{-1} (3.5x^*)^{2/3}$  for A,B,C,D stabilities (See below)

 $X^* = 14m (F_B/m^4/sec^3)^{1/3}$ , if  $F_B \leq 55m^4/sec^3$ ,

 $X^* = 34m (F_B/m^4/sec^3)^{1/3}$ , if  $F_B > 55m^4/sec^3$ , or
change all  $\mu$ 's to  $u$ 's.

Page 30: Data Block 6 should read:

READ(INFREQ,481)KDUMMY

READ(INFREQ,620)(FREQ(ISEA,I,J,K),J=1,NWINDS)

620 FFORMAT (6X,6F8.2)

Page 32: The second sentence should read:

This number is typically six or seven and must be seven or less in the current version.

Page 40: The first two columns labeled SO<sub>2</sub> Output are in fact sulfur output. The values in the last two columns should be multiplied by 2 to give SO<sub>2</sub>. This will not affect the correlations listed in Table 2.



Page 58: Statement number 1602 should read:

1602 T1P=(GPHI(I)-PPHI(J))\*CØS(GTHA(I))

Statement number 164 et. seq. should read:

164 DIRP(I,J)=180.\*(ATAN2(T1P,T2P))/PI  
IF(DIRP(I,J).LT.0.0) DIRP(I,J)=360.+DIRP(I,J)  
IF(KTAG.EQ.2)GO TO 190

Statement number 1903 should read:

1903 T1A=(GPHI(I)-APHI(K))\*CØS(GTHA(I))

Page 59: Statement number 194 et. seq. should read:

194 DIRA(I,K)=180.\*(ATAN2(T1A,T2A))/PI  
IF(DIRA(I,K).LT.0.0) DIRA(I,K)=360.+DIRA(I,K)  
IF(KTAG.EQ.2) GO TO 220

Page 60: An instruction preceding instruction number 281 should be inserted, the instruction from numbers 280 to 281 should read:

280 TH1(I,K)=TH1(I,K)+11.25  
IF(TH1(I,K).LT.0.0) TH1(I,K)=TH1(I,K)+360.  
TH2(I,K)=TH1(I,K)+DTH(I,K)

281 CONTINUE

Page 66: Changes to DD, FAC1, D1RL and a factor "A" added. Beginning at the top of page 66 and continuing to about the middle of the page (the 3rd statement below statement number 3040) should read:

H=HGL(L)  
DD=R\*SQRT((LSTHA(L)-LFTHA(L))\*\*2+CØS(LSTHA(L))\*CØS  
(LFTHA(L))

&\*2)  
DD=DD/9.

DTHL=(LFTHA(L)-LSTHA(L))/9.

DPHL=(LFPHI(L)-LSPHI(L))/9.

DØ 3050 NN=1,9

THAL=LSTHA(L)+(NN-1)\*DTHL+DTHL/2.

PHIL=LSPHI(L)+(NN-1)\*DPHL+DPHL/2.

DL=R\*SQRT((GTHA(I)-THAL)\*\*2+CØS(GTHA(I))\*COS(THAL)\*  
(GPHI(I)-PHIL)\*

&\*2)

A=DD/DL\*2.546479

C\*\*\* A REPRESENTS THE RATIO ØF ANGLE SUBTENDED BY DD

```

C*** AT A DISTANCE DL TØ SECTØR ØF 22.5 DEGREES.
C*** 2.546479=180./PI/22.5
      FAC1=A*LQIO(L,M,MØN)
      FACWET=FAC1*2.543*CLAMDA(M)*WW
      T1L=(GPHI(I)-PHIL)*CØS(GTHA(I))
      T2L=THAL-GTHA(I)
      IF(T1L.NE.0.0) GØ TØ 3040
      IF(T2L.NE.0.0) GØ TØ 3040
      WRITE(KØUT,3039)
3039  FORMAT(////,10X,'*****SAMPLING PØINT MAY NØT CØINCIDE
      WITH LINE SØU
      &RCE*****',//)
      CALL ERRØR
3040  CØNTINUE
      D1RL=180.*(ATAN2(T1L,T2L))/PI
      IF(D1RL.LE.0.0) D1RL=D1RL+360.
      DTSTL=D1RL+11.25

```

Page 82: The wind speeds used (0.894, etc.) came from the following breakdown of wind speeds:

<u>WIND SPEEDS</u> (mph)	<u>AVERAGE</u> (mph)	<u>AVERAGE</u> m/sec
0.6-3.4	2.0	0.894
3.4-7.4	5.4	2.41
7.4-12.4	9.9	4.43
12.4-18.4	15.4	6.88
18.4-24.4	21.4	9.57
>24.4		

If you use a different classification, such as knots, these values should be changed accordingly.

Page 107: Change SO<sub>2</sub> to S in line 29 or multiply all source terms by 2.

Page 114: All values in the table should be multiplied by 2 to give SO<sub>2</sub> data.

Page 62: Change line 38 as follows:  
CALL WASH(IPTYPE,DF1,DF2,GRATE)

Page 78: Line 4, change 2,8 to 2.8

Page 66: Just before 78 CONTINUE, Insert IF(HH.LT.0.0) HH = 0.0

Page 38: First Line: note that density must be specified in gm/m<sup>3</sup>,  
not gm/cm<sup>3</sup>.



Page 72: In the current version of ATM, the computations of FX(I) and FX(IKP) may result in exponent underflows, causing abnormal termination of the program. This can be corrected by limiting the maximum value that the exponents can have. The following statements can be substituted in Function QQP to limit the exponents to -40:

In place of FX(I) = . . .

```
YY=0.5*(HH/SIGTAB(NS,I))**2
IF(YY.GT.40.0) YY=40.0
FX(I)=SQRTPI*EXP(-YY)/SIGTAB(NS,I)
```

In place of FX(IKP) = . . .

```
ZZ=0.5*(HH/SMA)**2
IF(ZZ.GT.40.0) ZZ=40.0
FX(IKP)=SQRTPI*EXP(-ZZ)/SMA
```

Page 59: The current version of ATM does not handle small area sources properly. The following changes should be made in the 8th and 9th lines after 221 CONTINUE.

```
R1(I,K)=DA(I,K)-4.0*AREA(K)/(PI*DA(I,K))
R2(I,K)=DA(I,K)+4.0*AREA(K)/(PI*DA(I,K))
```

The factor of 4 comes from NDIR/4.

Page 9: The expressions with Figure 4(a) should be changed as follows:

$$R1 = R - \frac{4A}{\pi R} \quad R2 = R + \frac{4A}{\pi R}$$

Contract No. W-7405-eng-26

COMPUTER SCIENCES DIVISION

## A COMPREHENSIVE ATMOSPHERIC TRANSPORT AND DIFFUSION MODEL

Walter M. Culkowski\* and Malcolm R. Patterson\*\*

APRIL 1976

Work Supported by the National Science Foundation-RANN Environmental  
Aspects of Trace Contaminants Program Under NSF Interagency  
Agreement No. AEN72-01243A03

\*Atmospheric Turbulence and Diffusion Laboratory, NOAA, Oak Ridge, Tennessee.

\*\*Computer Sciences Division.

OAK RIDGE NATIONAL LABORATORY  
Oak Ridge, Tennessee 37830  
operated by  
UNION CARBIDE CORPORATION  
for the  
ENERGY RESEARCH AND DEVELOPMENT ADMINISTRATION



## CONTENTS

LIST OF FIGURES .....	v
ACKNOWLEDGEMENTS .....	vii
ABSTRACT .....	1
I. INTRODUCTION .....	2
II. BASIC CALCULATIONS .....	3
Plume Depletion .....	10
Dryfall Deposition .....	11
Wetfall Deposition .....	13
Summary of Model Calculations .....	13
III. THE ATMOSPHERIC TRANSPORT MODEL PROGRAM .....	15
Subroutine Descriptions .....	17
MAIN .....	17
Subroutine DCAL .....	18
Subroutine FALL .....	21
Subroutine FRXTRN .....	22
Subroutine GEOMET .....	22
Subroutine MAXCON .....	23
Function QQP .....	23
Subroutine SIGA .....	25
Subroutine SIGMA .....	25
Subroutine WASH .....	27
Subroutine WNDSCF .....	28
Subroutines SIMPUN and YLAG .....	29
IV. INPUT TO THE ATMOSPHERIC TRANSPORT MODEL .....	29
V. RESULTS .....	39
Conclusions .....	39
REFERENCES .....	41
APPENDICES .....	43
A. List of Symbols .....	45
B. Program Listing .....	47
C. Input Data .....	81
D. Output .....	109

## LIST OF FIGURES

Fig. 1. Pasquill-Gifford Horizontal Dispersion Coefficients versus Distance .....	5
Fig. 2. Pasquill-Gifford Vertical Dispersion Coefficients versus Distance .....	6
Fig. 3. Smith's $\sigma_z(x)$ Compared to Pasquill-Gifford $\sigma_z(x)$ for all Stability Categories and Two Roughness Lengths.....	7
Fig. 4. Initial and Transformed Area Sources. Part a, $\sqrt{A}/R < 2$ ; Part b, $2 < \sqrt{A}/R < \sqrt{4\pi}$ ; Part c, $\sqrt{A}/R > \sqrt{4\pi}$ .....	9
Fig. 5. Structure of the Atmospheric Transport Model .....	16
Fig. 6. Input to the Main Program of the Atmospheric Transport Model .....	30

## ACKNOWLEDGEMENTS

The authors express their sincere gratitude to Ms. C. L. Begovich for her skillful help in assembling the code, unifying the report, and providing valuable technical assistance in clarifying parts of the manuscript. We also appreciate comments made during review of the report by Drs. J. K. Munro, B. D. Murphy, N. M. Larson, and R. J. Raridon.



# A COMPREHENSIVE ATMOSPHERIC TRANSPORT AND DIFFUSION MODEL

by

Walter M. Culkowski and Malcolm R. Patterson

## ABSTRACT

A comprehensive version of the Atmospheric Transport Model is described that includes the effect of aerodynamic roughness on dispersion constants, clarifies the roles of the terminal velocity and deposition velocity, incorporates a tilting plume for heavy particulates, and includes an episodic calculation of exposure maxima. This model also limits the maximum value of the dispersion constants in order to retain the emitted material in the planetary boundary layer. The structure of the program has been modularized in order to clarify the flow of calculation and allow more flexibility. Values for atmospheric concentration as well as both wetfall and dryfall deposition are calculated. The model is applied to the vicinity of three power plants, and correlations between model predictions and observed values are presented.

## I. INTRODUCTION

Under the sponsorship of the National Science Foundation-Research Applied to National Needs Program (NSF-RANN), Mills and Reeves<sup>1</sup> developed and published a model describing the movement of trace materials through the atmosphere. This model provides a means of calculating input deposition of trace contaminants to a watershed; the subsequent movement of the contaminants through the watershed by hydrologic processes can then be traced using hydrologic transport models. The Atmospheric Transport Model has enjoyed considerable success. It has been applied to studies of transport of trace metals and of SO<sub>2</sub> from both point and area sources and includes the capability for the consideration of line sources. It has been coupled to the Wisconsin Hydrologic Transport Model to provide estimates of input wetfall and dryfall depositions. A version of it has been applied to the movement of uranium or tailings from concentrate piles in New Mexico. The model is currently being applied to the transport of toxic metals in the vicinity of a lead smelter in the New Lead Belt of southeastern Missouri.

Since publication of the Mills and Reeves report, several new capabilities have been added to the Atmospheric Transport Model (ATM). Its scope has been expanded and its limitations are more clearly understood. The purpose of the present report is to provide a specific, standardized version of the Atmospheric Transport Model that includes those capabilities that have been added since the last publication. This new document will provide a reference for subsequent standardization and incorporation in the final form of the Unified Transport Model. These additional capabilities include Hosker's<sup>2</sup> formulation of the sigma dispersion constants to include the effect of aerodynamic roughness length. It also allows for coupling the Atmospheric Transport Model to the Unified Transport Model in order to compute parameters necessary for calculation of wetfall deposition. It includes a clarification of the roles of terminal velocity and deposition velocity. The model also incorporates a tilting of the plume for heavy particulates and an episodic (hourly) version which will calculate exposure maxima for conditions of adverse meteorology. The model also includes constraints on the maximum value of the dispersion parameters allowed, and it incorporates the concept of a mixing depth to limit the dispersion of the emitted material to the planetary boundary layer. The range to which the model is applicable has been more clearly delineated.

In addition, this report describes more fully the structure of the model and gives more background in the derivation and theory of application of the model. A discussion of those calculations necessary to include the input parameters for plume rise is incorporated. The program itself has been considerably streamlined and modularized so that it is easier to follow the flow of the calculation. Certain sections of the printout have been condensed and new flexibility has been introduced in application. The input data have been reorganized and structured in a way that allows the user to construct scenarios using available climatology and variable source strengths for periods of projected study. The table of Pasquill-Gifford<sup>3</sup> dispersion parameters which were read in as data in the previous version of the model have been incorporated into a block data subprogram, obviating the need for reading these data from the input data stream and wasting computer time. The addition of the Hosker formulation of the Briggs<sup>4</sup> and Smith<sup>5</sup> dispersion parameters has effectively extended the applicable range of this Atmospheric Transport Model to 50 km, without sacrificing accuracy for ranges of the order of 1 km that were already inherent in the Pasquill-Gifford dispersion parameters.



We stress that these contributions to this Atmospheric Transport Model have extended the scope of that model and have made the model easier to use. The model is not drastically different in content from the previous version and is again a standard, straight line, Gaussian plume type of model. This generic type of model has enjoyed successful application over a period of at least fifteen years and has been validated under the Ecology and Analysis of Trace Contaminants Project in applications for SO<sub>2</sub> and for trace metal transport in the vicinity of large fossil burning power plants. In particular, this model has been used for calculation of input depositions to the Walker Branch Watershed, a well instrumented watershed on the Oak Ridge reservation. The results obtained from this model have also been validated by comparison with data furnished by the Tennessee Valley Authority that were measured in the vicinity of these same large steam plants. Within the stated range of less than 50 km, we feel that this model has successfully undergone as extensive a set of validation calculations as any model of which we know.

The model may best be described as a mathematical distillation of the relevant parts of *Meteorology and Atomic Energy* (1968),<sup>6</sup> which is a standard reference in the field of air pollution. Though reflecting what we feel to be the latest accepted thinking in atmospheric modeling, we stress that this is a mesoscale (100 m to 50 km) model based on restrictive assumptions, such as that of a straight line wind field. The detailed description of the model given below enumerates most of these restrictions and assumptions and mentions alternate approaches to extend or restrict the model as the individual investigator may require.

## II. BASIC CALCULATIONS

The development of the Gaussian plume model has been well described in preceding publications, for example see Gifford (1968).<sup>7</sup> We review here the parts of that development which seem most applicable to the considerations of the present model in order to provide the setting for use of this model. First, let us consider the simplest case, that of one point source. For each point source, an image source at an equal distance below the surface has been employed to make the flux of matter at the surface of the earth be zero. The employment of this image source has been described in the earlier publication by Mills and Reeves<sup>1</sup> and is a well accepted practice in atmospheric pollution studies. Material in the plume is removed by wet and dry deposition processes, as is described later. The dryfall mechanism employs a deposition velocity concept such that the net flux of material is from the plume to the landscape surface at a rate proportional to the atmospheric concentration in the layer adjacent to the ground surface. We stress that the following is not given as a derivation but is a formulation of the very successful techniques that have been evolved over a period of years.

By analogy with the classical equation for the conduction of heat in a solid, the concentration of matter suspended in a turbulent fluid may be written as

$$\frac{dq}{dt} = \frac{\partial}{\partial x} \left( K_x \frac{\partial q}{\partial x} \right) + \frac{\partial}{\partial y} \left( K_y \frac{\partial q}{\partial y} \right) + \frac{\partial}{\partial z} \left( K_z \frac{\partial q}{\partial z} \right) ,$$



where,  $K_x$ ,  $K_y$ , and  $K_z$  are eddy diffusivities in the  $x$ ,  $y$ , and  $z$  directions, respectively,  $q$  is the concentration of material per unit volume, and  $t$  is time. In the case of a smoke plume from a point source,  $x$  is considered to be the distance the plume travels downwind,  $y$  the horizontal distance to the plume's centerline, and  $z$  a vertical distance normal to the plume's centerline.

For smoke plumes,  $K_x = 0$ , eliminating the first term on the right in Eq. (1).  $K_y$ ,  $K_z$ , and wind speed (implicit in the left term in Eq. (1)) vary with height and time. Although a myriad of solutions have appeared in the literature, the most often used is the "Gaussian plume model"

$$q(x, y, z) = \frac{Q}{2\pi\sigma_y\sigma_z u} \exp \left[ - \left( \frac{y^2}{2\sigma_y^2} + \frac{z^2}{2\sigma_z^2} \right) \right] \quad (2)$$

where  $Q$  = the release rate of a pollutant from a point source (gm/sec),  
 $u$  = the wind speed (m/sec),  
 $\sigma_y, \sigma_z$  = diffusion coefficients in the  $Y$  and  $z$  directions, respectively.

It is of fundamental importance in extending, using or understanding any Gaussian plume model, to realize that Eq. (2) is not an exact solution and its application is very restricted. The  $\sigma_y, \sigma_z$  and  $u$ 's chosen are empirically determined, largely from observations at the ground level. Inferences of plume concentrations at any place but the surface (from Eq. (2) and the published  $\sigma$ 's) is certain to introduce additional errors into the calculations.

Finally, let us generalize this model by considering the concept of a wind rose. The wind rose is built into the model as a frequency table, which is a table of the fractional occurrence during a given time period of a particular combination of stability class type, wind direction, and wind speed class. The wind direction has been broken into sixteen subcardinal directions proceeding clockwise in 22.5 degree increments from wind from the north as direction *one* through wind from the north-northwest as direction *sixteen*. Correspondingly, the wind speed classes have been broken into six categories that proceed from roughly 1 m/sec through 14 m/sec. The six stability classes correspond to the conventional Pasquill-Gifford classification scheme proceeding from stability class A, called 1 in the program, through stability class F, called 6 in the program. The Pasquill-Gifford dispersion parameters are displayed in Figs. 1 and 2, and were intended to be applied on scales less than 10 km. The Hosker formulation of the Briggs-Smith dispersion parameters is correspondingly displayed on the larger scale out to 50 km in Fig. 3 and is included here for reference. It is necessary to limit each of these dispersion parameters to values that are of the order of or less than the mixing height of the planetary boundary layer. For each wind speed class a mixing depth value has been incorporated in the program for that purpose.

In addition to the point source equation described above, the model includes the concept of line and area sources. The consideration of line sources has been described to a limited extent in the previous work;<sup>1</sup> however, we note that the line is broken into its intercepts with the subcardinal directions and each of these into ten segments. Each segment is modeled as a point source concentrated at the center of that line segment of the line source. In order to maintain the generality

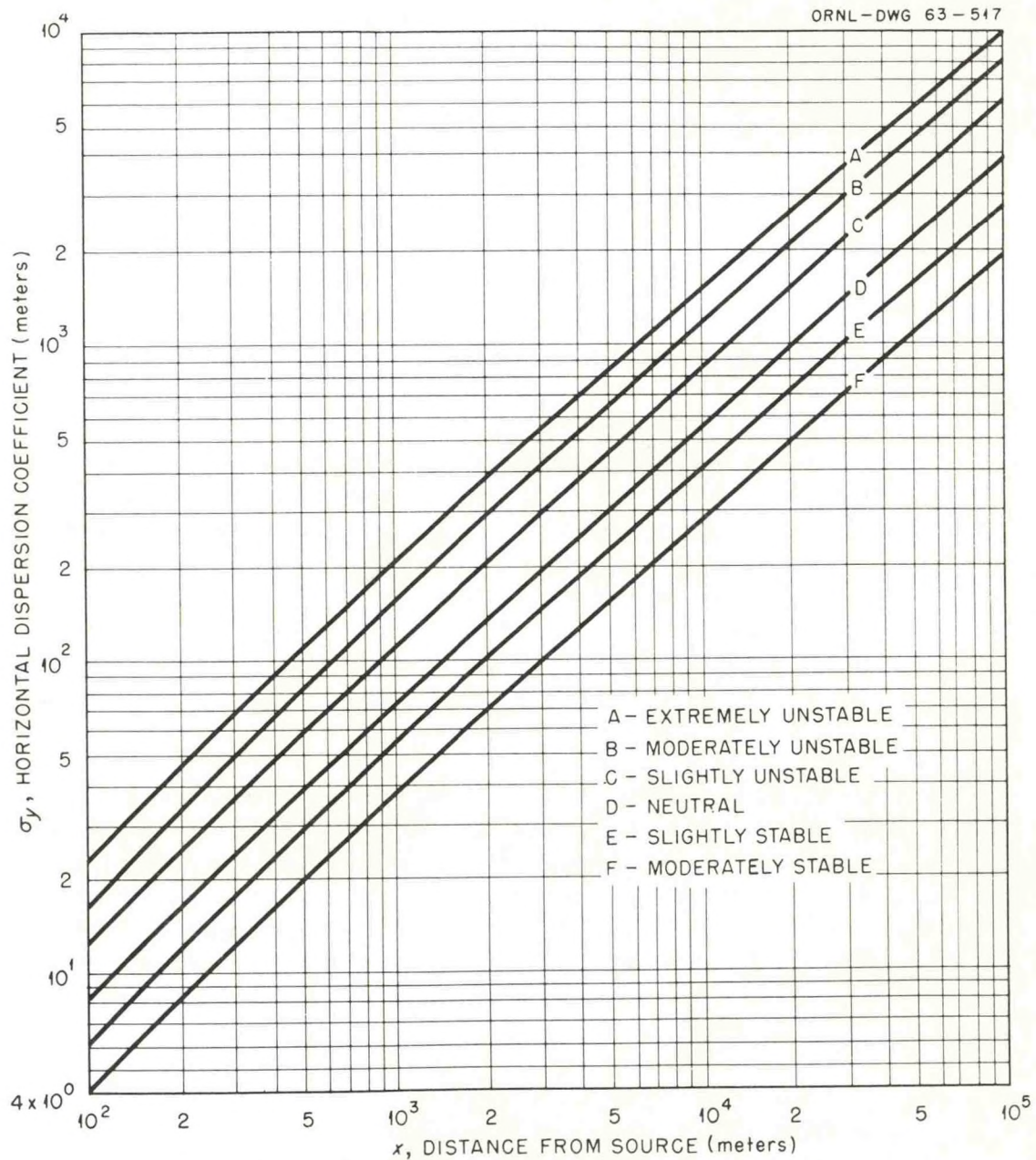


Fig. 1. Pasquill-Gifford Horizontal Dispersion Coefficients versus Distance.



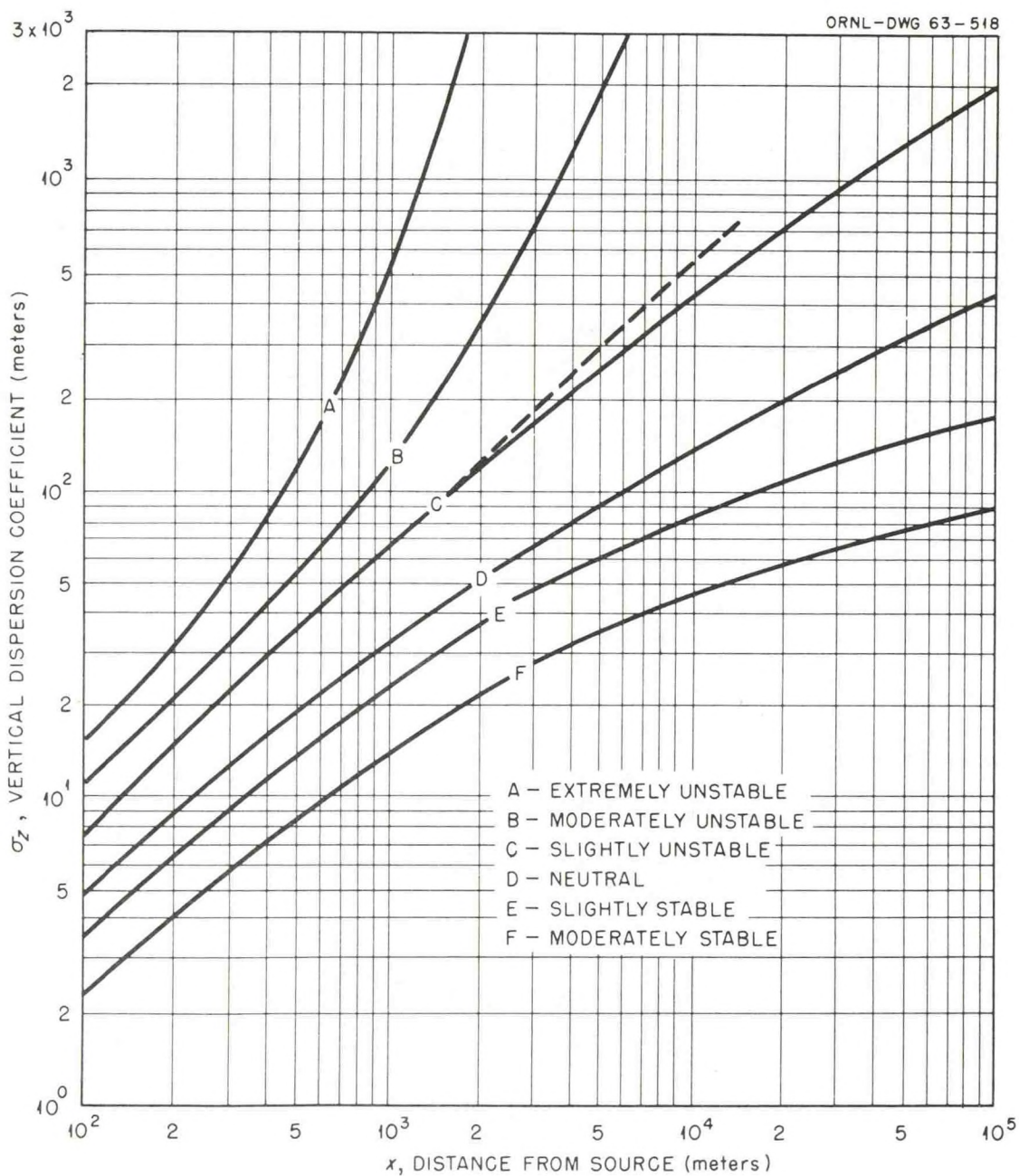


Fig. 2. Pasquill-Gifford Vertical Dispersion Coefficients versus Distance.



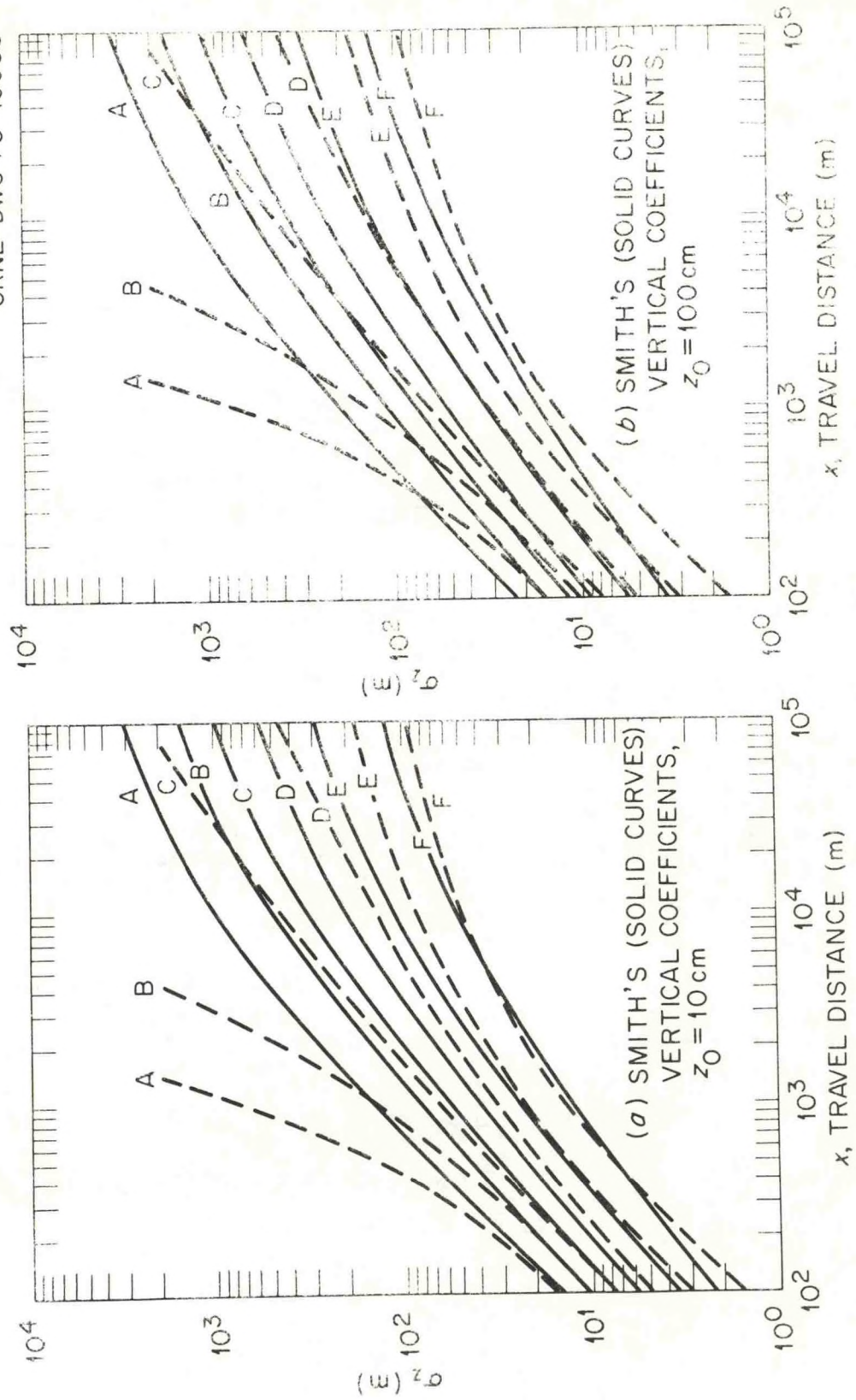


Fig. 3. Smith's  $\alpha_2(x)$  Compared to Pasquill-Gifford  $\alpha_2(x)$  for all Stability Categories and Two Roughness Lengths.

of the program, the coordinate system for reference of point, area, and line sources, as well as the receptor gauge at which the deposition calculations are performed, has been carried in terms of latitude and longitude. The corresponding calculations of distances and angles are also done in the reference of a spherical geometry approach. A portion of the previous report is included below for clarification of the treatment of area sources.

"The situation for the area sources presented somewhat of a problem, since an exact specification of the boundaries of the area source would require large amounts of computer time and storage. Our solution was to take advantage of the radial dependence of the stability wind rose and map each area into the appropriate polar area. We then treat each differential segment of that polar area as an equivalent point source. The only restriction is that the area should initially be roughly square or circular in shape. Elongated areas may be broken up into several nearly circular area sources with the same source strength per unit area as the original area source. In order to preserve the roughly circular character of the area sources and leave the distance to the centroid approximately the same, we make the following requirements for the transformed polar area sources..." (Fig. 4a).

We require that the radial value  $R$  of the centroid of an area source be at the average distance of that area source from the receptor. Thus

$$R = \frac{R_1 + R_2}{2} \quad (3)$$

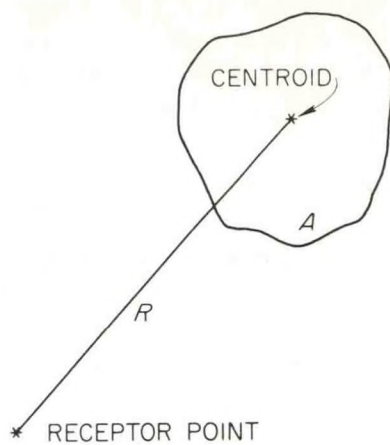
where  $R_1$  and  $R_2$  are parameters of the transformed polar area. Further we require that this transformed area be approximately "rectangular" in its shape. Thus we require that its arc length in the  $\theta$  direction be approximately the same as its depth in the radial direction:

$$R_2 - R_1 = \frac{(R_1 + R_2) \Delta\theta}{2} \quad (4)$$

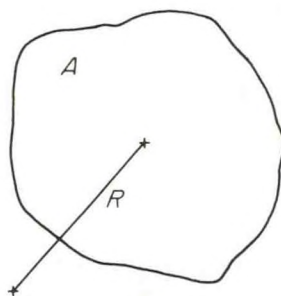
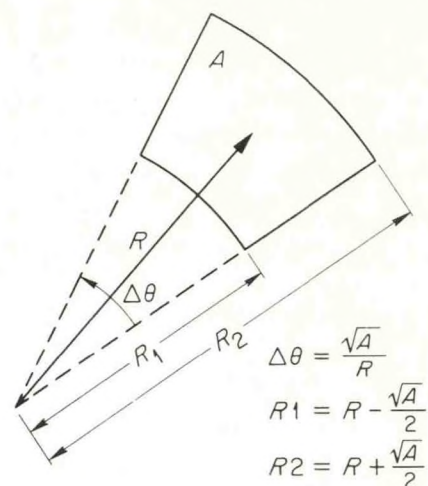
Finally, we require that the area of the actual source and that of the transformed source be the same, thus

$$A = \frac{\Delta\theta}{2} (R_2^2 - R_1^2) \quad , \quad (5)$$

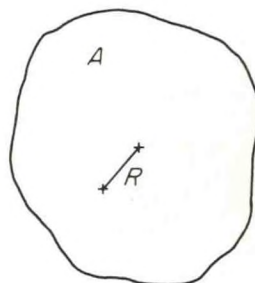
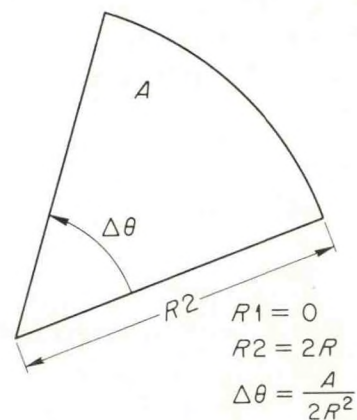
from which



(a)



(b)



(c)

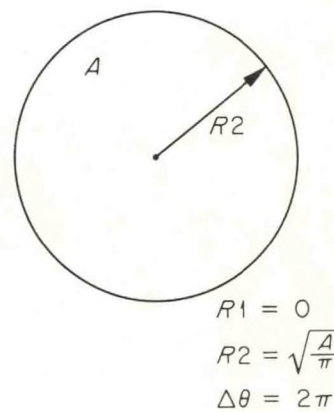


Fig. 4. Initial and Transformed Area Sources. Part a,  $\sqrt{A}/R < 2$ ; Part b,  $2 < \sqrt{A}/R < \sqrt{4\pi}$ ; Part c,  $\sqrt{A}/R > \sqrt{4\pi}$ .



$$\Delta\theta = \frac{\sqrt{A}}{R}$$

$$R_1 = R - \frac{\sqrt{A}}{2} \quad (6)$$

$$R_2 = R + \frac{\sqrt{A}}{2}$$

The conditions given above can no longer be satisfied if the angle  $\delta\theta$  is larger than two radians because its radial dimension would have to be larger than the radius out to the point of the centroid. In that case (Fig. 4b) we require that the transformed area be a sector of a circle with the following dimensions

$$R_1 = 0$$

$$R_2 = 2R \quad (7)$$

$$A = \frac{R_2^2 \Delta\theta}{2}$$

which yields

$$\Delta\theta = \frac{A}{2R^2} \quad (8)$$

Finally, if the value of  $\delta\theta$  calculated from the above equations is larger than  $2\pi$  we then consider the transformed area to be a circle of radius

$$R_2 = \sqrt{\frac{A}{\pi}} \quad (9)$$

centered about the area source centroid as shown in Fig. 4c.

### Plume Depletion

Plume depletion is the generic term which describes the removal of material from airborne concentrations by deposition of this material on landscape surfaces rather than by simple dilution. Plume depletion can occur by precipitation scavenging to input wetfall deposition to the watershed (washout), by dryfall deposition during periods of no rain which again deposits material on the landscape surface (dryfall), and also by rainout deposition by formation of raindrops in clouds which are impacted by the plume, leading to a subsequent transport of the material from the

cloud to the landscape surface inside the raindrop (rainout). This model considers only the washout, wetfall and dryfall deposition processes and does not concern itself with rainout, because rainout generally occurs at heights above that of the planetary boundary layer. The general effect of plume depletion processes is that of reducing the effective source strength of the plume at increasing distances away from the injection point. This effective reduction of the plume source strength has been handled in a perturbative fashion by first considering the calculation of what the concentration and subsequent deposition values would be if there were no diminution of the source strength. This zeroth order estimate of the concentration is then modified by incorporating a first-order value for the effective source strength, reduced by the amount of material which has been deposited. Two deposition mechanisms are described below.

### Dryfall Deposition

The value of the atmospheric concentration of the particular species under consideration has been given above in Eq. (2). This concentration is repeated below at the ground level surface for an effective stack height  $h$  and including the dispersion in both  $z$ -direction and the transverse  $y$ -direction

$$q = \frac{Q}{2\pi\sigma_y\sigma_z u} \exp\left(\frac{-y^2}{2\sigma_y^2} - \frac{h^2}{2\sigma_z^2}\right) \quad (10)$$

This atmospheric concentration leads to an aerial deposition given by the following formula

$$\omega = v_g \cdot \frac{Q}{\pi\sigma_y\sigma_z u} \exp\left[-\frac{y^2}{2\sigma_y^2} - \frac{h^2}{2\sigma_z^2}\right] \quad (11)$$

where the deposition velocity  $v_g$  has been multiplied by the atmospheric concentration to yield the deposition per unit area of the material emitted at the source. We note that the variation of this concentration and the consequent deposition in the transverse  $y$ -direction is Gaussian, as the name Gaussian plume implies, and that its effective measure of the width of the plume is the value of the dispersion parameter  $\sigma_y$ . The value of  $\sigma_y$  is ordinarily of an order less than or equal to the average variations during the time period of approximately one month with which this report is concerned. Consequently, the transverse variation is integrated out and the values of the atmospheric concentration and the deposition are averaged over the one-sixteenth of a circle included in each of the sixteen subcardinal directions. The dryfall deposition that occurs from a plume to the landscape surface can be included, as mentioned above, in a perturbative sense by calculation of the rate of change of the effective source strength as a function of distance away from the source by consideration of the following equation

$$\frac{dQ}{dx} = - \int \omega dy \quad (12)$$

Substituting the value for the aerial deposition determined above we obtain

$$\frac{dQ}{dx} = - \int_0^{y'} \frac{v_g Q e^{-\frac{h^2}{2\sigma_z^2}}}{\pi \sigma_y \sigma_z u} e^{-\frac{y^2}{2\sigma_y^2}} dy \quad (13)$$

Those terms which are not a function of the lateral direction  $y$  can then be brought outside the integral. Because of the small contribution of the concentration in the region outside of  $2\sigma$  in lateral distance the integral may be extended from minus infinity to plus infinity without introducing large errors. This integration yields the following result

$$\frac{dQ}{dx} = - v_g \sqrt{\frac{2}{\pi}} \cdot \frac{Q e^{-\frac{h^2}{2\sigma_z^2}}}{\sigma_z u} \quad (14)$$

This differential equation can be cast in an easily integrable form as given below

$$Q(x) = Q_0 - \int_{x'=0}^x \frac{dQ}{dx'} dx' \quad (15)$$

The solution for an effective source strength is

$$Q = Q_0 e^{-\sqrt{\frac{2}{\pi}} \frac{v_g}{u} \int_0^x \frac{e^{-\frac{h^2}{2\sigma_z^2}}}{\sigma_z} dx'} \quad (16)$$

Note that the above equation includes the still basically Gaussian shape in the form of an indefinite integral from the point of emission  $x'=0$  to the point of calculation at  $x'=x$ . The evaluation of this integral cannot be done analytically because of the dependence of the dispersion coefficient  $\sigma_z$  on the distance  $x'$ ; consequently it must be evaluated numerically. For reference, we mention that this evaluation of the numerical integral is carried out in the subroutine QQP described below. This formulation of the effective dryfall source strength is incorporated in an equation given at the end of the next chapter.



### Wetfall Deposition

Wetfall deposition is defined here as that plume depletion that occurs as washout of either particulates or gaseous substances by the passage of already-formed raindrops through the plume. This type of plume depletion is described by Englemann (1968)<sup>8</sup> and is summarized below. The depletion of material by washout can be taken to be proportional to the amount of material in the plume. This relationship is displayed in the differential equation given below, which states that the time rate of depletion of the material is proportional through the constant  $\lambda$  to the material remaining in suspension

$$\frac{dQ}{dt} = -\lambda Q \quad (17)$$

Again, this equation can be cast in a readily integrable form as

$$\int \frac{dQ}{Q} = \int -\lambda dt \quad , \quad (18)$$

which can be solved to yield the exponential form,

$$Q = Q_0 e^{-\lambda t} \quad . \quad (19)$$

In turn the transit or residence time of the material in the suspended state can be approximated as the ratio of the distance traveled to the wind speed for this specific speed class as

$$t = \frac{x}{u} \quad . \quad (20)$$

Finally the effective source strength, as modified by washout, is given here in the form that depends on distance and wind speed in an exponential decay:

$$Q = Q_0 e^{-\frac{\lambda x}{u}} \quad . \quad (21)$$

### Summary of Model Calculations

The diminution of source strength by the dryfall and washout processes described above can be incorporated into the Gaussian plume formulation along with the frequency table for occurrence of

stability type, wind direction, and wind speed by multiplying the equation for a single point source with unidirectional wind flow by the appropriate factors given in the following equation

$$X_i(x, \theta) = \sum_{p=1}^{N_s} \sum_{r=1}^{N_w} \frac{2.032 F_{pr}(\theta) \bar{Q}_{ipr}(x)}{\sigma_p(x) u_r x} \exp \left[ \frac{-h_{pr}^2}{2\sigma_p^2(x)} \right] \quad (22)$$

Here  $X_i(x, \theta)$  = ground level air concentration of pollutant  $i$ , in direction  $\theta$ , at a distance  $x$  from the source,  
 $\theta$  = one of sixteen cardinal wind direction sectors (N, NNE, NE, etc.),  
 $r$  = one of eight wind speed classes,  
 $F_{pr}(\theta)$  = fraction of time during which the wind blows from direction sector  $\theta$ , with wind speed class  $r$ , and stability class  $s$  (Stability Wind Rose),  
 $\bar{Q}_{ipr}(x)$  = point source strength for pollutant  $i$ , modified by depletion due to fallout and washout occurring at distances less than  $x$ ,  
 $N_s$  = number of stability classes,  
 $N_w$  = number of wind speed classes,  
 $\sigma_p(x)$  = vertical dispersion parameter appropriate for stability class  $p$  and distance  $x$ ,  
 $h_{pr}$  = effective stack height,  
 $p$  = one of six wind stability classes (A,B,C,D,E,F) changing from extremely unstable to moderately stable.

Finally, the form given above can be generalized to include many point sources at many receptor sites by summing over the contributions to a given receptor by the nearby, i.e., closer than 50 km, point sources to give

$$X_i = \sum_{p=1}^{N_s} \sum_{r=1}^{N_w} \sum_{j=1}^{N_j} \frac{2.032 F_{pr}(\theta_j) \bar{Q}_{ipr}(x_j)}{\sigma_p(x_j) u_r x_j} \exp \left[ \frac{-h_{pr}^2}{2\sigma_p^2(x_j)} \right] \quad (23)$$

where  $N_j$  is the number of point sources. Note that implicit in this equation is the dependence on distance that is contained in the dispersion coefficients  $\sigma$ . The somewhat complicated-looking formalism simply implies that contributions from many different point sources have been included, that the wind flows from a given direction with a given fractional occurrence during the climatological period of reference (which is generally taken to be one month), and that



the transverse dependence of the atmospheric concentration has been integrated out and assigned to the sixteen subcardinal directions. Thus the material is assumed to be uniformly distributed within each of these subcardinal directions during that part of the time that the wind direction is from the point source to the receptor.

### III. THE ATMOSPHERIC TRANSPORT MODEL PROGRAM

The code for calculation of the results described above has been written in FORTRAN IV, which is the most generally available type of FORTRAN compiler. In particular, the FORTRAN IV version described here can be readily implemented on most IBM, CDC, and UNIVAC machines with, in some cases, no changes to the source program. We have attempted to maintain this generality of the source programming in order to make the Atmospheric Transport Model readily transferable from this site to other potential users. Indeed, the purpose of this documentation is to describe the full scope of this particular model in order that other potential users of the code can address varied demanding problems in atmospheric transport without being forced to program all of those processes which have been incorporated in the current model. The current model is relatively simple in its computing facility requirements, storage requirements, and machine running time. These properties will be discussed at length below.

The structure of the Atmospheric Transport Model is displayed in Fig. 5. The function of the main program is to read in and report back out the input data that are fed to the model to describe the wind frequency table, the source strengths, the locations of point sources, line sources, area sources, and resuspension sources along with the sites of the particular receptor points at which the calculated values of deposition and concentration are desired. The main program in turn calls a more detailed subprogram GEOMET, which calculates the solid geometry relating receptors and point and area sources. In addition, fraction of time during which washout occurs is transmitted to the main program from the subroutine FRXTRN. In this subroutine the default values can be set from available climatological data for average rainfall intensity and the fraction of the time during which rainfall occurs, if the program is operated in a stand-alone version, uncoupled from the Unified Transport Model. In the mode of operation in which the ATM is coupled to the UTM, these quantities are calculated from the available precipitation that are contained in the PRECIP link of the Wisconsin Hydrologic Transport Model. The program also includes a subroutine WNDSCF for calculation of resuspension contributions from area sources such as tailings piles; however, this capability has not yet been evaluated in detail, and this part of the model is now considered unvalidated but potentially useful.

In turn the detailed input data and the calculated geometric relationships are passed to a subroutine called DCAL, which stands for "Detailed Calculations," in which the evaluation of the specific forms given above for atmospheric concentration and deposition is calculated. The subroutine DCAL evaluates the dispersion coefficients by calls to the subroutine SIGMA and evaluates the indefinite integral in the subroutine QQP by means of a Simpson's integration (SIMPUN) taken from Westley (1969).<sup>9</sup> Values for washout coefficients are calculated in the subroutine WASH.

For consideration of episodic contributions to atmospheric concentrations, the subroutine MAXCON can be employed on an hourly scale. This subroutine retains the dependence of the plume concentration on the lateral dispersion coefficient  $\sigma_y$  and evaluates the lateral dispersion



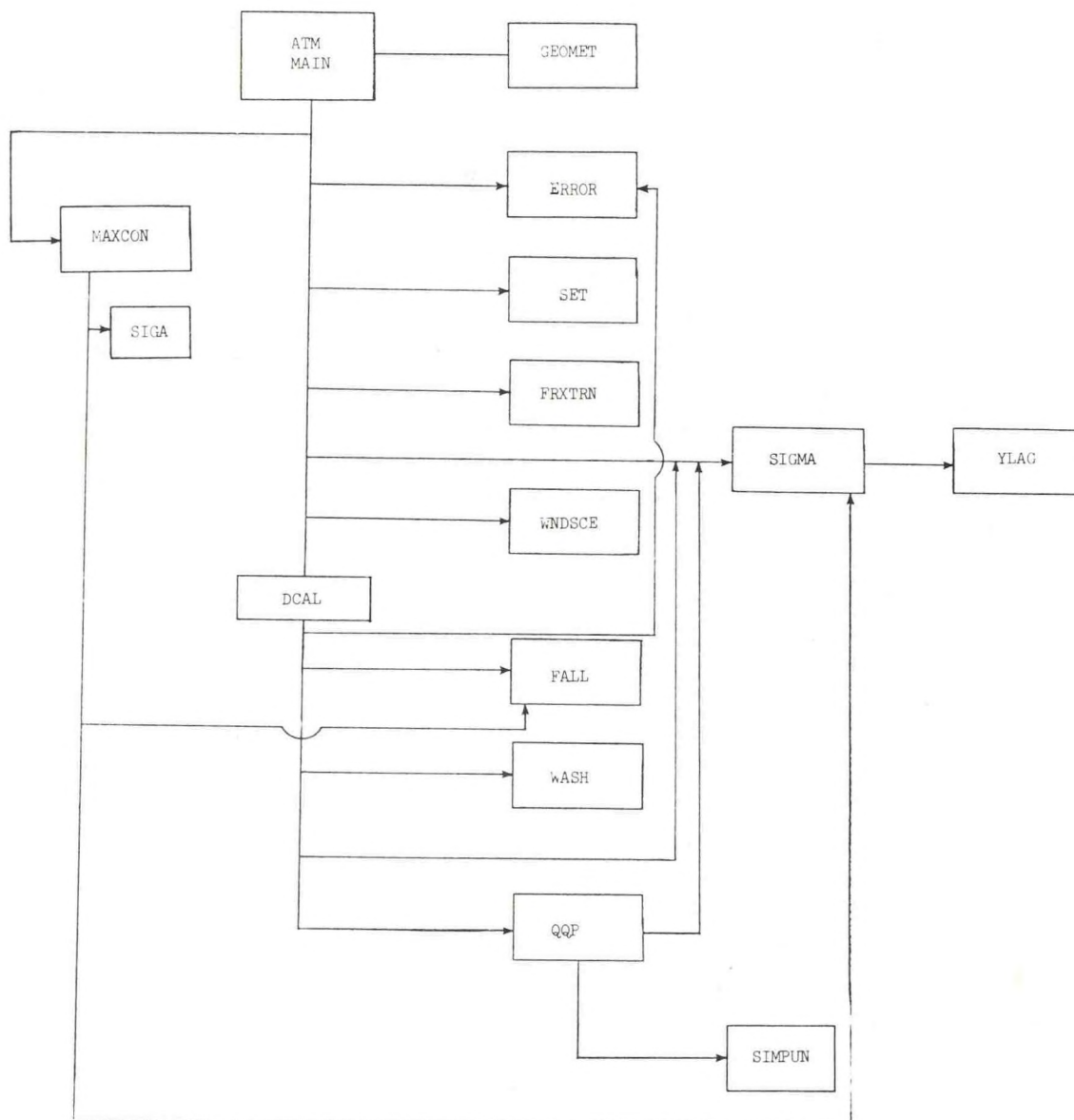


Fig. 5. Structure of the Atmospheric Transport Model.

coefficient by calls to function SIGA. The employment of this particular mode of operation of the ATM, the episodic version MAXCON, requires a considerable amount of computer time; the user would be well advised to consider carefully beforehand which calculations are most germane to his considerations. Discussions of each of the major subprograms are given below. These subprograms are described here in alphabetic order; constant reference should be made to Fig. 5 showing the structure and relative ordering of the employment of these subroutines. An attempt has been made to keep all of the input in the main program, with subsequent transfer of these input data to the needed subprograms, which perform their detailed functions in specifically structured ways that can be modified by the user if necessary.

To summarize, the program consists of twelve sections, the main program and subprograms DCAL, SIGMA, QQP, FRXTRN, FALL, WASH, SIMPUN, WINDSCE, YLAG, MAXCON, and SIGA. Briefly, their functions are

- MAIN - the section of the program that reads in the bulk of the data-set, calculates directions and distances from sources to receptors, and "idealizes" area source geometrics,
- DCAL - (**Detailed Calculations**) calls most of remaining subroutines to calculate required output,
- FALL - calculates terminal and deposition velocities for particulates, and deposition velocity for gases,
- FRXTRN - (**Fraction of Time it Rains**) a subroutine to insert monthly rainfall information into the program,
- GEOMET - Calculates **geometric** relationships of source-to-receptor gauge distances and directions, given the latitude and longitude of each source or gauge,
- MAXCON - (**Maximum Concentration**) finds the single highest concentration possible at a specific location from a number of point sources. Specifies "worst" condition of wind speed, wind direction, month and stability condition, within five degrees,
- QQP - calculates attenuation of source strength due to deposition, washout, or fallout,
- SIGA - (**Sigma Azimuth**) calculates distances of receptor to plume centerlines, and appropriate horizontal dispersion parameters,
- SIGMA - calculates *vertical* diffusivities,
- SIMPUN - (Simpson's rule) employed by QQP to calculate the integral describing attenuation of the material source strength,
- WASH - (**Washout**) calculates washout coefficients for particles and gases,
- WINDSCE - (**Windblown sources**) calculates resuspension of materials by the wind,
- YLAG - a double precision subroutine employed by function SIGMA.

### Subroutine Descriptions

The following description of subroutines primarily describes the function of each subprogram.

#### MAIN

The MAIN program has two basic functions: 1) to read in the bulk of the data set, and 2) to process the data set for more efficient handling in the subroutine DCAL. Refer to Chapter 4 or the MAIN program itself for details on input format, etc.

### Subroutine DCAL

This subroutine is the "workhorse" of the entire program. Its function is to call the various subprograms (except MAXCON and SIGA) into several calculation modes, depending on the source types, and print the results.

In the MAIN program a data set was called in which established a monthly or annual matrix of wind speeds, wind velocities, and stability categories. MAIN then calculated and stored these data as the fraction of time each element of that matrix occurred.

To estimate the concentration for point sources, Eq. (23) is employed and the total point source concentration is obtained.

Deposition, both wet and dry are obtained from the subroutines WASH and FALL.

Dry deposition is calculated as

$$\omega_i(x, \theta) = \sum_{p=1}^{N_s} \sum_{r=1}^{N_{i,r}} \frac{F_{pr}(\theta)}{\sigma_p(x) u_r x} 2.032 v_i W_f \exp \left[ \frac{-h^2}{2\sigma_p^2(x)} \right] Q_{i,pr} \quad (24)$$

where  $\omega_i(x, \theta)$  = deposition rate of pollutant  $i$ , in direction  $\theta$ , at a distance  $x$  from the source,

$W_f$  = fraction of time in which only dry deposition occurs,

$v_i$  = deposition velocity of pollutant  $i$ .

Similarly, wet deposition, (washout) is calculated by

$$\omega_i(x, \theta) = \sum_{p=1}^{N_s} \sum_{r=1}^{N_{i,r}} \frac{F_{pr}(\theta)}{\sigma_p(x) u_r x} 2.453 \lambda_i W_w Q_{i,pr}(x) \sigma_p(x) \quad (25)$$

where  $W_w$  = fraction of time both washout and dry deposition are occurring,

$\lambda_i$  = washout coefficient of pollutant  $i$ .

The program sums over wet and dry deposition for each source and receptor in a similar manner for concentration.

Point, area, and line sources are treated virtually identically except for the windblown sources as a subgroup of the area sources. For point area and line sources, the plume is assumed to "tilt" at the terminal velocity of the particle in question. For gases the plume does not tilt. As explained in subroutine QQP, the deposition velocity is assumed equal to the terminal velocity if the terminal velocity exceeds .01 m/sec; otherwise all material is assumed to have a deposition velocity of .01 m/sec.



The type of vegetative cover, which governs the amount of dry deposition, may differ at the gauge from the assumed general type of cover governing removal by deposition in subroutine QQP. Although the program initializes the gauges to the general type of ground cover (SURF (I) = KCOVER; I = gauge number), each surface type may be overridden after "DO" loop 983.

Point sources are permitted to rise through buoyancy via the PKAPPA (Unstable) and QKAPPA (Stable) parameters established in the data input. Total height of rise is restricted, however, to 1500 meters, a typical height of the tropospheric "mixing depth."

The values assigned PKAPPA and QKAPPA are considered typical of coal fired steam plants. They are based on the Tennessee Valley Authority's Allen Steam Plant near Memphis, Tennessee. The following condensation is based on Briggs<sup>10</sup> formulation, and should be incorporated whenever the appropriate parameters are known or can be reasonably estimated.

The effective stack height  $h$  will be greater than the actual stack height  $h_o$  due to the buoyancy of the plume. This increase in effective stack height  $\Delta h$  is called the plume rise

$$h = h_o + \Delta h \quad , \quad (26)$$

where  $\Delta h = 1.6 F_B u^{-1} (3.5 x^*)^{2/3}$  for A,B,C,D stabilities (see below)  
 $x^* = 14 \text{ m } (F_B / \text{m}^4 / \text{sec}^3)^{5/8}$ , if  $f < 55 \text{ m}^4 / \text{sec}^3$ ,  
 $x^* = 34 \text{ m } (F_B / \text{m}^4 / \text{sec}^3)^{2/5}$ , if  $f > 55 \text{ m}^4 / \text{sec}^3$ , or

$$\Delta h = 2.9 \left( \frac{F_B}{\mu s} \right)^{1/3} \text{ for E and F stabilities, where}$$

$$F_B = g W r^2 \frac{T_S - T_E}{T_E} \text{ , in which}$$

$g$  = gravitational acceleration ( $9.8 \text{ m/sec}^2$ ),

$W$  = stack gas ejection velocity ( $\text{m/sec}$ ),

$r$  = radius of the stack ( $\text{m}$ ),

$T_S$  = stack gas temperature ( $^{\circ}\text{K}$ ),

$T_E$  = air temperature ( $^{\circ}\text{K}$ ),

$$s = \frac{d\theta}{dz} \left( \frac{g}{T_E} \right) \text{ , and}$$

$$\frac{d\theta}{dz} = \text{potential temperature gradient.}$$

The plume rise parameters used in the sample run are given below:

$$T_S = 394^{\circ}\text{K},$$

$$T_E = 289^{\circ}\text{K},$$

$$\pi r^2 W = 387 \text{ m}^3 / \text{sec},$$

$$\frac{d\theta}{dz} = 1^\circ\text{K}/100\text{m (approximately true for slightly stable or moderately stable conditions), which results in}$$

$$\Delta h = \frac{1490}{u}(\text{m}) \text{ for A,B,C,D stabilities (i.e., PKAPPA} = 1490), \text{ or}$$

$$\Delta h = \frac{317}{u^{1/3}}(\text{m}) \text{ for E and F stabilities (i.e., QKAPPA} = 317).$$

Area sources are difficult to define, and hence difficult to deal with. True "area sources" are fields and forests emitting water vapor, ammonia, etc. Generally, however, areas which have numerous points of emission, low in height, and more or less uniform in strength (such as household emissions of coal smoke) are classified as area sources. The programmer must exercise judgment concerning the location, boundary, and source strength of such areas. Note, however, that the program does not preclude having numerous (separate) point sources within the boundaries of an area source. In the MAIN program, the boundaries are idealized for computational purposes. Anticipating that each may be quite large, the program breaks each area into three regions of equal source strength. By so doing, the objections to using a single centroid (point source) approximation are substantially mitigated. Nevertheless, the subject of area sources is complex, and the reservations enumerated in the discussion of the MAIN program should be carefully considered.

The windblown source estimate in the area source section utilizes an eclectic approximation to concentration and deposition estimates. Sutton<sup>11</sup> derived a model which served as a mainstay for concentration estimates for many years. It was well verified for short distances and low source heights and had the advantage of being integrable. Although Sutton used a different set of dispersion parameters, it is possible to use Csanady's<sup>12</sup> form of the Sutton approximation to fit the present model.

$$\omega_i(x, \theta) = \sum_{p=1}^{N_s} \sum_{r=1}^{N_w} \frac{1.016 Q_s F_{pr}(\theta) F_d \delta A f}{\sigma_p(x) u_r x} \exp\left(\frac{-fx/u_r - h}{2\sigma_p^2}\right)^2 \times \left[ 2 - \frac{2}{\left(1 - \frac{n_p}{2}\right) \left(\frac{u_r - h}{xf} - 1\right) + 2} \right] \quad (27)$$

$Q_s$  = area source strength (velocity dependent),

$f$  = settling velocity of dust particle (m/sec),

$$n_p = - \frac{2x}{\sigma_{p,z}} \frac{d\sigma_p}{dx} + 2 ,$$

$h$  = source height (m),

$F_d$  = fraction of time the windblown source remains dry,

$\delta A$  = element of area.

The line source treatment is, again, based on the Gaussian point source calculation, but each line source is broken into ten centroids to approximate a continuous line source.



### Subroutine FALL

It is a common practice to ignore effluent removal as the plume moves downwind; this is termed the "conservative" approach and, of course, for gases and small particles maximizes the effluent concentration at every point. This approach is generally quite good; by avoiding the variable of effluent removal one may often show that a maximum allowable concentration is never exceeded, even without taking credit for the diminished strength of the plume.

Often, however, it is desirable to model all the plume processes, and the present model does so by including effluent removal by three processes: 1) fallout; 2) deposition; and 3) washout. The first two processes are generally termed "dry removal" and the third is termed "wet removal." The first two processes are covered by the subroutine "FALL," the third by subroutine "WASH."

It is of fundamental importance to distinguish between the often confused terms *fallout* and *deposition*, since both have the units of velocity. *Fallout* is the process whereby a particle falls of its own weight. The forcing constant is gravity and applies throughout the depth of the atmosphere. *Deposition* is normally given in units of velocity (though it need not be) but is a surface phenomenon, independent of gravity. Gases such as SO<sub>2</sub> will deposit on a surface; hence, they have a deposition velocity, even though they have no terminal velocity (fallout).

For particles, the program assumes that the material will have a vertical settling velocity given by Stokes' law:

$$V_s = D^2 \cdot S \cdot 3 \times 10^{-5} \quad , \quad (28)$$

where  $V_s$  = terminal velocity of particle (m/sec),

$D$  = diameter of the particle (microns),

$S$  = density of particle (gm/cm<sup>3</sup>).

The actual net terminal velocity in a turbulent medium has, so far, not yielded to a satisfactory theoretical treatment. One would expect, for example, that  $V_s$  would appreciably diminish as the size of the turbulent elements (analogous to a "mean free path") increased. Nevertheless, the assumption that an aggregate of particles will behave with a mean terminal velocity has been used in plume work since Schmidt<sup>13</sup> in 1925. The theoretical objections are not very restrictive in practice, however, since a 10 micron particle of unit density is calculated to fall only twelve meters in one hour. For very large, or very dense particles, where the terminal velocity becomes important, the effect of turbulence on slowing terminal velocities is apparently not very great for *average* dustfall (Csanady, 1972).<sup>14</sup>

When particles are of the magnitude of 100 microns and about 2.5 gm/cm<sup>2</sup> in density, the plume will sink at the rate of approximately one meter per second. Accordingly, the centerline of the plume reaches the surface in less than one hour. Since the centerline of the plume contains the maximum concentration it is not "conservative" to ignore fallout (i.e., terminal velocity).

In the absence of turbulence, terminal velocities and deposition velocities would remain very similar, but turbulent air rapidly increases the deposition velocities of small particles (i.e., those below 10 microns), which are the most abundant (the order of 10<sup>12</sup> particles per cubic meter of air). The program approximates the increased deposition velocity by assigning a deposition velocity of 0.01 m/sec for terminal velocities below this amount.

*Deposition* is generally given in the units of velocity introduced by Chamberlain;<sup>15</sup> that is, the amount of material deposited per second per m<sup>2</sup>/concentration is

$$v_g = \omega/\chi$$



where  $v_g$  = deposition velocity (m/sec),  
 $\omega$  = rate of deposition (parts/m<sup>2</sup>),  
 $\chi$  = concentration at the surface (parts/m<sup>3</sup>).

The physical processes incorporated into the deposition velocity are complex and not thoroughly understood, depending on the material being deposited, the receptor surface, and turbulence. The present program provides a data set for calculating the deposition velocity of a gas from the turbulence type and molecular diffusivity, as suggested by Chamberlain:<sup>15</sup>

$$v_g = \alpha \cdot K_z / \ln (K_z / D) \quad (29)$$

where  $K_z$  = diffusion constant (m<sup>2</sup>/sec),  
 $D$  = molecular diffusivity (m<sup>2</sup>/sec),  
 $\alpha$  = 1.0 (meter)<sup>-1</sup>.

Unfortunately, sufficient experimental verification is lacking for uncritical acceptance of Eq. (29); the program defaults to  $v_g = .01$  m/sec, a value found to be acceptable for SO<sub>2</sub>. The programmer may choose either one, or, of course, insert another value in this subroutine.

The net result of subroutine FALL is that particles are assigned a terminal and deposition velocity according to Stokes' law. The terminal velocities are later used for plume tilt. Gases are assigned a deposition velocity of .01 m/sec and a terminal velocity of zero, unless otherwise specified. Later in subroutine DCAL, the particles will assume a minimum deposition velocity, and both gases and particles will be removed by varying rates in subroutine DCAL and function QQP. Sehmal and Hodgson<sup>16</sup> give excellent theoretical and experimental values of particulate deposition, should the reader care to pursue the matter further.

#### Subroutine FRXTRN

The role of this subroutine is discussed in subroutine WASH. The number of hours of measurable precipitation (.01 inch or more) divided by the total hours each month yields the fraction (FRACT) of time it rains each month. The total rainfall divided by the number of hours of rainfall is the average rate (AVRAT) used in the program. As explained in subroutine WASH, more detailed programming may prove necessary where wind direction and rainfall are highly correlated.

#### Subroutine GEOMET

The distances and angular relationships of source points and receptor gauges are calculated in subroutine GEOMET. A source point, receptor gauge, and the North Pole form the end points of a spherical triangle. Knowing the latitude and longitude of source and receptor and using the relationship between the sides and angles of a spherical triangle, both source-receptor gauge distance and the angular direction from north from the gauge are computed.

### Subroutine MAXCON

This subroutine uses Eq. (2) and subroutine SIGA to find the set of circumstances that produces the greatest one hour concentration of material at one or more locations from a number of point sources, employing monthly point source, stack height, and plume rise parameters from the program. It consumes a large amount of computer time if 360° is scanned at one degree intervals (e.g., two gauges, four point sources requires about twenty minutes of computer time on an IBM 360/91).

No removal mechanisms (washout or deposition) are used in this subroutine, primarily for reasons of economy of computer time. One would anticipate that this subroutine would be employed relatively near large stacks where deposition could not contribute to a loss of emission inventory of more than a few percent. If deposition is thought to be a major consideration, however, the function QQP may be employed in exactly the same relative location as in subroutine DCAL. Note that the plume will tilt, but one degree resolution is required if the "F" conditions are the greatest contributors to concentration. To save computer time, a run of five degree intervals (about the resolution of a "C" or "3" condition) can be used to determine the most troublesome directions, and one degree sweeps used on successive runs. The subroutine prints the month, wind direction, speed and stability conditions that produces the maximum hourly concentration.

### Function QQP

As wet and dry deposition attenuate the strength of the plume downwind, the model calculates the fraction of material remaining by using the function QQP. As defined in subroutine FALL, the deposition rate over any given area can be written as

$$\omega = x \cdot v_g \quad . \quad (30)$$

Since the deposition  $\omega$  removes material from the plume, the amount removed while the plume traverses the distance  $dx$  must be integrated over the crosswind direction  $y$

$$\frac{dQ}{dx} = - \int_{-\infty}^{\infty} x \cdot v_g \, dy \quad (31)$$

From Eq. (31) we may write

$$\frac{dQ}{dx} = - (Qv_g/\mu) \int_{-\infty}^{\infty} f(x) \, dy \quad (32)$$

which may be integrated to give

$$Q/Q_0 = (f(x) \cdot \exp(-v_g/\mu)) \quad (33)$$

where

$$f(x) = \sqrt{2/\pi} \int_0^x \exp(-h^2/2\sigma_z^2) dx \quad . \quad (34)$$

Here  $f(x)$  is approximated by employing Simpson's rule (subroutine SIMPSON). By Eq. (34) for dry deposition, and for dry periods,

$$QQP = Q/Q_0 \quad . \quad (35)$$

Similarly, as described in subroutine WASH

$$dQ = -\lambda Q dt \quad (36)$$

$$Q/Q_0 = \exp(-\lambda t) \quad . \quad (37)$$

The time of travel "t" is estimated by

$$x = \mu t \quad (38)$$

$$t = x/\mu \quad (39)$$

$$Q/Q_0 = \exp(-\lambda x/\mu) \quad . \quad (40)$$

During periods of washout, the dry deposition process is assumed to be operating, so for washout plus dry deposition

$$QQP = Q/Q_0 = \exp(-x\lambda/\mu) + f(x) \exp(-v_g/\mu) \quad . \quad (41)$$

Attenuation of material by dry deposition is rapidly increased over a forest. Sehmal et al.,<sup>16</sup> Slinn,<sup>17</sup> Hori<sup>18</sup> and Baumgartner<sup>19</sup> have reported effective deposition velocities of over 10 cm/sec over forested regions. The causes of this increased deposition are complex and not fully understood. Certainly, the increased surface area itself leads to higher total deposition, though not an increase in  $v_g$ . The boundary layer physics and the wind fields of a forest obviously differ grossly from respective grassland parameters. In this code, however, we choose not to alter  $v_g$  itself, but to



introduce an "effective area" argument, i.e., to approximate the effective increase in deposition by ascribing a net increase of surface area over that of grassland. Thus, if one assumed that the deposition was eight times as much as that over a grassy plain, one would assign  $KCOVER = 8$ , and function QQP would multiply each surface increment in Simpson's rule by a factor of eight. Should the plume travel over heavily forested land and then an equal amount of grassland, the programmer might assign a value of  $KCOVER = 4$  or  $KCOVER = 5$ .

It is possible to assign a specific  $KCOVER$  to each appropriate distance increment, or even let the model specify the cover type (by a subprogram similar to the area source modifications in the MAIN Program), but the penalty in computer time is large if many area sources are used.

As explained in subroutine FALL, heavy particles settle out in the aggregate, at a rate approximating Stokes' law. The net effect of this settling is to tilt the plume's centerline downward at the settling rate. For particles with a terminal velocity greater than .01 m/sec the centerline of the plume is tilted in this subroutine. These particles are assumed to have a deposition velocity equal to this terminal velocity. Particles which settle at a rate of less than .01 m/sec are assigned a deposition velocity of .01 m/sec in subroutine DCAL, for reasons which are covered in the description of that subroutine. These particles are assigned a new terminal velocity of zero in subprogram QQP.

There have been many objections, on theoretical grounds, to using the Gaussian plume model for deposition estimates. It has been pointed out that removal from the bottom of a Gaussian plume automatically changes the basic assumption that it remains Gaussian in shape. Defenders of the method argue that vertical mixing is sufficient to support a Gaussian approximation, and, as pointed out in the basic calculations, the assumed Gaussian shape cannot be rigorously defended in any case. Horst<sup>20</sup> compared the effects of a mathematical model that removed only surface material with that which removed the inventory from the entire plume, as does this model. The comparison indicates that for  $v_g/\text{wind speed} \leq .01$  the two models agree well down to stability D. For F stability and/or  $v_g/\text{wind speed} \geq .01$ , the errors increase as  $v_g$  increases. This indicates that one should exercise caution in interpreting the results when forest cover is assumed. On the other hand, the complexities of flow over (and through) a forested region are not fully understood, and Horst's corrections are unsubstantiated in this case. The investigator may do well to compare the results of the present model for  $KCOVER = 1$  and  $KCOVER = 10$ , and assume these bracket the true value.

### Subroutine SIGA

This subroutine, **Sigma Azimuthal**, not only computes the horizontal dispersion parameters (SIGY) required in Eq. (2), but also calculates the distance (DIS) of a normal from the gauge to the plume's centerline, and a new distance (DIS2) from source to the intersection of the normal to the plume.

### Subroutine SIGMA

Equation (2) lists the six basic parameters of the Gaussian plume equation, source strength, wind speed, horizontal and vertical distance from the plume's centerline and the horizontal and vertical dispersion parameters. As will be seen in subroutine DCAL, the horizontal dispersion plays no part in calculating average concentrations over extended periods. The remaining parameters are either known or amenable to estimation.

The remaining parameter,  $\sigma_z$ , reflects a broad range of conditions, from the initial height of the stack to the stability of the atmosphere. Atmospheric stability is determined by the gradient of



temperature (more accurately *potential* temperature). If the temperature were to decrease at the rate of  $1^{\circ}\text{C}$  per 100 meters elevation, the stability would be neutral, or a "D," (in the model a "4") category; a particle of air would be free to move by inertia only, with no buoyant forces acting upon it. Since the atmosphere is warmed from the earth's surface upward, primarily buoyant (unstable) conditions occur for most daylight hours. On cloudy, somewhat windy days, this instability will be slight (a "C" or "3" condition) with slow warming of the surface layers. For days with intense sunlight and little wind, very unstable ("A" or "1") conditions exist. Similarly, a night cooling of the air from the earth's surface reverses the processes, and vertical motions are intensively damped. Superimposed upon this process are other factors such as terrain, moisture and synoptic weather. Note, however, that since the stability conditions grow from the surface upward, it is common to have unstable air at low altitudes and stable air aloft, and, conversely, very stable air at the surface with less stable air aloft.

As noted earlier, the  $\sigma_z$ 's found in the literature are empirically based on functions of distance. The investigator has a choice of two basic methods of estimating  $\sigma_z$ 's, the Pasquill-Gifford<sup>3</sup> method (P-G), and Hosker's method of obtaining more recent values suggested by F. B. Smith<sup>5</sup> and G. A. Briggs.<sup>4</sup> The discussion below on which diffusion scheme to use is based on arguments in a paper by Gifford.<sup>21</sup> It should be emphasized that these are not really competing approaches. The difference in values between the models is largely a function of the source of emission, rather than any fundamental theoretical difference. In the atmosphere, the wind vector and diffusivities change rapidly with height, often with marked discontinuities. The  $\sigma_z$ 's encompass the average vertical characteristics of the atmosphere for each stability, but only as they effect surface distributions.

Pasquill has indicated that his curves work well for point sources up to 100 meters in height. Based on the "Prairie Grass"<sup>22</sup> experiments and other data, the Pasquill approach is capable of providing criteria for estimating stability and has found wide and well deserved acceptance. Its use in this program is recommended when the primary sources of pollutants are non-buoyant and are emitted from a height of no more than 100 meters. Thus if one is concerned primarily with line or area sources, normally the P-G curves should be chosen. Also if the point sources are from industries with non-buoyant (or negatively buoyant) plumes, such as cement plants and industries using roof vents, the P-G curves would again be applicable. Note, however, a strong caveat:  $\sigma_z$  must be limited to below 3200 meters for the "A" condition, 1600 meters for the "B," 800 meters for the "C," 500 meters for the "D," 200 meters for the "E," and 100 meters for the "F." These limitations reflect the physical reality of the plume becoming uniformly mixed within the planetary boundary layer in the vertical direction as it proceeds downwind.

For the majority of cases, however, the primary interest will probably be in the emission from tall stacks with buoyant plumes. Plume behavior from these stacks is obviously different from plumes emitted near the ground. Initial turbulent dispersion is low, since such plumes are well above the height of maximum turbulence due to surface roughness, and buoyant currents from the earth's surface are in the process of being damped. The present model calculates these vertical dispersion parameters using a slightly altered version of the method introduced by Hosker,<sup>2</sup> based on the works of Briggs and F. B. Smith. Briggs, using TVA plume studies and the St. Louis Dispersion Study,<sup>23</sup> generated a theoretical framework to obtain  $\sigma_z$ 's from elevated, buoyant plumes. F. B. Smith incorporated roughness and thermal influences in a formal treatment to obtain  $\sigma_z$ 's over a wide range of conditions. Hosker evolved a computation scheme suitable for smaller calculators which is incorporated in the data set of function SIGMA. Generally, this second set of curves is to be

preferred. They have the benefit of an additional parameter (roughness) for more physical realism and more than a decade of theoretical work behind them.

Normally the difference in results between using either set of curves (correctly) should not exceed 10-20%. The greatest difference (a factor of ten) occurs at the limit of validity of the P-G curves for stability condition "A" and a roughness length of 0.1 meters. Otherwise, the overall differences are slight.

### Subroutine WASH

Rainfall is a very important factor in removing effluent from the atmosphere. One-third or more of the suspended material below cloud level may be removed from the atmosphere by rainfall in one hour. Washout is considered to attenuate the entire plume at a uniform rate as it travels downwind. Consequently, washout has the units of time, and the material inventory downwind is given by

$$Q = Q_0 \exp (-\lambda t)$$

where  $Q_0$  = original source strength,  
 $\lambda$  = washout coefficient (sec)<sup>-1</sup>,  
 $t$  = time of travel (sec).

Broadly speaking, rainfall is about ten times more efficient in removing material than dry deposition. Within the first few hundred meters of a tall stack, washout is the only method of transferring material from the plume to the surface.

The program calculates washout of particles and gases through the information on the average amount of rainfall, supplied by subroutine FRXTRN.

The particulate washout estimate is based on Fig. 5.9 of *Meteorology and Atomic Energy*.<sup>5</sup> A data set was constructed to match the appropriate curves; the washout coefficient is calculated using the particle's diameter and density, then interpolating between the curves.

Washout for gases is more direct, following the Kelkar-Hanford curve of Fig. 5.11 in *Meteorology and Atomic Energy*.<sup>5</sup>

$$\lambda = 5.55 R^{0.6} \quad (42)$$

where  $\lambda$  = washout coefficient,  
 $R$  = rainfall rate in millimeters per hour.

The investigator should note two important items. First, the units used in FRXTRN are for rainfall in hundredths of an inch per hour (the standard U.S. Weather Service reporting unit). The conversion to millimeters is performed in subroutine WASH. Second, the *average* rainfall rate is used, implying that rainfall is independent of atmospheric stability, wind direction and wind speed. In many areas a definite correlation exists between wind vectors and rainfall, however; subroutines FRXTRN and WASH as well as the MAIN program and the calling subprogram DCAL should reflect this dependence. The National Weather Records Center, Asheville, North Carolina, can supply joint rainfall and wind vector tables upon request.



### Subroutine WNDSCF

In some places, principally in mining and smelting areas, material previously deposited may be re-entrained into the atmosphere during periods of dry windy weather. Thus a rather specialized area source is created, with sources strength dependent on wind speed and the physical properties of the source itself.

These properties are, unfortunately, not easily determined without additional studies. Once deposited, the physical structure of the material will change due to weathering, agglomeration, solubility, etc. It is incorrect to assume that the material re-entrained is physically identical to that which was deposited. Relying principally on Bagnold's work,<sup>24</sup> Mills<sup>25</sup> used the following model of re-entrainment.

Dust (diameter  $< 0.1$  mm) cannot be directly transported into the atmosphere by turbulent diffusion, since the drag force for such small grains is spread over a large area rather than an individual particle. The process of dust suspension is assumed to take place in three steps:

(1) The larger grains are set into motion across the surface (a process known as saltation) as the wind speed increases. The threshold velocity for the onset of saltation is given by

$$v_t = 0.575 \sqrt{\frac{\sigma - \rho}{\rho} g d} \log_{10} \left( \frac{z}{k} \right) \quad (43)$$

where  $z$  = height of wind measurement ( $\sim 1$  m),

$k$  = surface roughness during saltation ( $\sim 0.01$  m),

$g$  = gravitational acceleration,

$d$  = grain diameter (m),

$\sigma$  = density of sand grains ( $\text{gm/m}^3$ ),

$\rho$  = density of air ( $\text{gm/m}^3$ ).

The saltation rate  $q$  (gm/meter/sec) may then be calculated as

$$q = \alpha C \sqrt{\frac{d}{D}} \frac{\rho}{g} (u - v_t)^3 \quad (44)$$

where  $\alpha = 1 / \left( 5.75 \log_{10} \left( \frac{z}{k} \right) \right)^3$

$D$  = standard grain diameter (0.00025 m),

$u$  = wind speed (m/sec),

$C$  = constant depending upon particle size distribution (nearly uniform sand,  $C = 1.5$ ; naturally graded sand,  $C = 1.8$ ; wide range of grain size,  $C = 2.8$ ).

(2) The suspension of the dust size grains by *impaction* of the larger sand particles will be a function of the saltation rate. As a first approximation we take the suspension rate  $Q_s$  to be proportional to the saltation rate  $q$

$$Q_s = R_f q \quad (45)$$

$R_f^{-1}$  has the dimension of length and could be considered roughly proportional to the average distance traveled by the sand grains between ground impacts. From the agricultural erosion data of Gillette, et al.,<sup>26</sup> one may infer a value of  $R_f$  of about  $10^{-5}\text{m}^{-1}$ . This value is only a rough approximation and should be measured for the area in question.

This source strength is used as an area source input in subroutine DCAL.

### Subroutines SIMPUN and YLAG

Subroutines SIMPUN and YLAG are "in-house" subroutines at ORNL. SIMPUN, a program constructed by J. Barish to implement Simpson's rule for integration, is used in subroutine QQP. Subroutine YLAG is a double precision interpolation routine used in subroutine SIGMA.

## IV. INPUT TO THE ATMOSPHERIC TRANSPORT MODEL

The Atmospheric Transport Model has been structured such that the first input data are concerned with definition of atmospheric stability class. Wind speeds for each wind speed class and the wind rose for each wind speed class, stability class, direction, and period of the year comprise these data. Data pertaining to the geographic location of the receptor gauges, point sources, area sources, line sources, and wind-blown sources follow next; logical variables (switches) are also included which describe whether or not the particular gauge or source is to be included in the subsequent calculations. The locations are specified in the input stream in terms of latitude and longitude of each of these types of points. Heights and plume rise parameters for point sources are next, along with the heights for area and line sources. The number of pollutants that are to be included in the calculation is next in the input string, along with the pollutant type, whether it is a particulate or a gas, and the characteristics of that particular pollutant. Finally the source strengths are included in order for point, area, and line sources.

This structure has been used in order to allow the user of the program to specify the detailed climatology, for example, on an annual basis, then run several different cases with different numbers of sources, pollutants, effective source heights, and emission rates, all of which depend on the same climatology and geographic location that have been established in preceding data. This type of input structure should add to the flexibility of the program and to its use in the calculation of extended scenarios for long term effects. It also minimizes the internal core storage required by the program, because the data can be read in the input data stream, used immediately to perform the needed calculations, and then flushed out as data are read in describing the new source strengths. We have attempted to keep the input data fields either five characters or ten characters wide. In addition, we have attempted to reuse each format in succeeding input data acquisition statements as much as possible to reduce the number of required formats. A simplified version of input to the main program of the Atmospheric Transport Model is given in Fig. 6. This figure represents all of the READ statements for acquisition of data in the Atmospheric Transport Model, and has simply been listed from the main program. The schematic shown in Fig. 5 indicates the logic which determines whether the next input data block is to be read or not.

In the following part of this chapter we describe twenty-three input data blocks, where each data block consists of the data acquired by a single READ statement in the main program. Under each of these data blocks we describe the input variable names, their units, and their formats.



Data Block 1	22	READ(IN,22) A FORMAT(10A8)
Data Block 2	481	READ(IN,481) KDISP,KTAG,KSEA,ROUGH FORMAT( 15,E10.0)
Data Block 3		READ(IN,10) NWINDS,NDIR,NFSTAB,JSTAB(I),I=1,NFSTAB)
Data Block 4	541	READ(IN,230) (WINDSD(I),I=1,NWINDS)
Data Block 5	23	READ(IN,23) (SEANAM(ISEA),ISEA=1,KSEA) FORMAT(7(2X,A8))
Data Block 6	620	READ(IN,620) (FREQ(ISEA,I,J,K),J=1,NWINDS) FORMAT(6X,6F8.2)
Data Block 7	770	READ(IN,10) NG,NP,NA,NL,NWS 10 FORMAT(16I5)
Data Block 8	14	IF(NG.GT.0) READ(IN,112) (SKIPG(I),I=1,NG) 112 FORMAT(16I5)
Data Block 9		IF(NP.NE.0) READ(IN,112) (SKIPP(I),I=1,NP)
Data Block 10		IF(NA.NE.0) READ(IN,112) (SKIPA(I),I=1,NA)
Data Block 11		IF(NL.NE.0) READ(IN,112) (SKIPL(I),I=1,NL)
Data Block 12	40	READ(IN,40) GLATD,GLATM,GLATS,GLOND,GLONM,GLONS,GNAME(I) FORMAT(6F10.5,12X,A8)
Data Block 13		READ(IN,40) PLATD,PLATM,PLATS,PLOND,PLONM,PLONS,PNAME(J)
Data Block 14		READ(IN,40) ALATD,ALATM,ALATS,ALOND,ALONM,ALONS,ANAME(K)
Data Block 15		READ(IN,40) LLATDS,LLATMS,LLATSS,LLONDS,LLONMS,LLONSS,LLNAM(L)
Data Block 16		READ(IN,40) LLATDF,LLATMF,LLATSF,LLONDF,LLONMF,LLONSF
Data Block 17	230	READ(IN,230) (AREA(K),K=1,NA) FORMAT(7E10.3)
Data Block 18		READ(IN,230) (HGT(I),I=1,NP)
Data Block 19		READ(IN,230) (PKAPPA(J),J=1,NP)
Data Block 20		READ(IN,230) (QKAPPA(J),J=1,NP)
Data Block 21		READ(IN,230) (HGA(K),K=1,NA)
Data Block 22		READ(IN,230) (HGL(L),L=1,NL)
Data Block 23		READ(IN,10) NPOL,KCOVER
Data Block 24	956	READ(IN,112) (SKIPOL(I),I=1,NPOL)
Data Block 25	957	READ(IN,957) (IPTYPE(M),DF1(M),DF2(M),POLNAM(M),M=1,NPOL) FORMAT(15,2E10.0,2X,A8)
Data Block 26		READ(IN,230) (PQIO(I,M,MON),MON=1,KSEA)
Data Block 27		READ(IN,230) (AQIO(K,M,MON),MON=1,KSEA)
Data Block 28		READ(IN,230) (LQIO(L,M,MON),MON=1,KSEA)
Data Block 29		IF(NWS.NE.0) READ(IN,960) (ITYPE(I),DEN(I),DSALT(I),DSUSP(I),I=1,NWS)
Data Block 30		IF(NWS.NE.0) READ(IN,230) (CONCF(K,M),M=1,NPOL)
Data Block 31		IF(NWS.NE.0) READ(IN,230) (FDRY(MON),MON=1,KSEA)
Data Block 32		IF(NWS.NE.0) READ(IN,230) (SSCON(I),I=1,NWS)
Data Block 33	10	READ(IN,10) ICHO FORMAT(15)

Fig. 6. Input to the Main Program of the Atmospheric Transport Model.

Data Block 1        READ(IN,22) A  
                     22    FORMAT(10A8)

A        = 80 character name of this particular computer run. This choice of name is completely left to the user and is simply printed out as a heading at the beginning of the calculation.

Data Block 2        READ(IN,481) KDISP,KTAG,KSEA,ROUGH  
                     481    FORMAT(3I5,E10.0)

KDISP    = control variable for calculation of sigma dispersion coefficients:  
          = 1 implies Pasquill-Gifford stability parameters are used,  
          = 2 implies Hosker's formulation of Briggs-Smith dispersion parameters are to be calculated in subroutine SIGMA, rather than Pasquill-Gifford dispersion coefficients.

KTAG     = control variable for whether detailed printout of dispersion parameters and wind rose frequency table is desired:  
          = 1 implies detailed printout requested,  
          = 2 implies no detailed printout requested.

KSEA     = number of time periods (seasons) to be considered in this run. KSEA must be less than or equal to fourteen in the current version. The names of these time periods will be read in a following READ statement. The number of time intervals (months, emissions, etc.) used in the wind frequency tables should also be the number used in the source inventories, or the results may be misleading. For example, were one to use an annual wind frequency data set run against a *monthly* source inventory, the output might show that *each* month had a large concentration pattern southeast and northeast of a source (from northwest and southwest winds, respectively). In reality, the winter months may have exhibited the predominantly northwest winds, while the summer months had the southwest winds, hence the true output would be very different from that of a mismatched data set.

ROUGH    = roughness parameter for use in the Hosker formulation of the dispersion coefficients. This effective roughness parameter is approximately 1/100th of the height of protuberances into the free air stream (meters).

Data Block 3        READ(IN,10) NWINDS,NDIR,NFSTAB,(JSTAB(I),I=1,NFSTAB)  
                     10    FORMAT(16I5)

NWINDS   = number of wind speed classes included in the following wind rose frequency table, must be less than or equal to eight in the current version.

NDIR     = number of subcardinal directions included in the frequency wind rose. This number should always be sixteen in the current version. However, provision is made for reading other than sixteen wind directions, if corresponding modifications are made in subroutine GEOMET.



NFSTAB = number of stability types included in the wind rose frequency table. This number typically is six or seven and must be less than seven in the current version. The accompanying stability type must be assigned in the following array JSTAB to one of the six Pasquill-Gifford stability types A-F, corresponding to 1-6.

JSTAB = Pasquill-Gifford stability type as used by the frequency wind rose and determined by the criterion described by Gifford.

**Data Block 4** 541 READ(IN,230) (WINDSD(I),I=1,NWINDS)  
230 FORMAT(7E10.3)

WINDSD = wind speed for each of the wind speed classes NWINDS described above. This value is the mean wind speed in meters per second (m/sec) for the frequency table determined above.

**Data Block 5** READ(IN,23) (SEANAM(ISEA=1,KSEA)  
23 FORMAT(7(2X,A8))

SEANAM = eight-character name of each time period corresponding to the total number of periods KSEA described in Data Block 2 above. There should be one name right-adjusted in each field of ten columns. Seven season names can be accommodated per input data card. If there are more than seven, another card identical in format should follow in the input data stream until the total number of periods equal KSEA.

**Data Block 6** READ(IN,620) (FREQ(ISEA,I,J,K),J=1,NWINDS)  
620 FORMAT(6X,6F8.2)

FREQ = raw data from which the frequency wind rose is calculated. The input units for this array are arbitrary. However, the same set of units must be used within each time period ISEA. Thus, within a given period the same units of measurement for the frequency occurrence of a given stability class type, wind speed, and wind direction should be used, for example, hours. The array FREQ will be renormalized within the main program such that the sum of the elements of FREQ for the period ISEA is unity. Each input data card should contain six values for the relative occurrence of the wind speed class for the given wind stability type and wind direction.

**Data Block 7** 770 READ(IN,10) NG,NP,NA,NL,NWS  
10 FORMAT(16I5)

NG = number of receptor gauges ( $\leq 10$ ) at which the values of deposition and concentration are desired,  
NP = number of point sources ( $\leq 10$ ) from which the pollutants emanate,  
NA = number of area sources ( $\leq 10$ ) from which emissions occur,  
NL = number of line sources ( $\leq 10$ ) from which emissions occur, and

NWS = number of wind blown sources from which resuspension occurs. The number of wind blown sources should be included in the count of total area sources, NA, and the number of area sources which are not wind blown resuspension sources is equal to the difference NA-NWS.

**Data Block 8** 14 IF(NG.GT.O) READ(IN,112) (SKIPG(I),I=1,NG)  
112 FORMAT(16L5)

If the number of gauge points is greater than zero, values for the logical variable SKIPG must be read describing whether or not the calculations are to be *skipped* for that receptor gauge or not. This logical variable is read in the format such that it is a field five characters wide, and sixteen gauges can be specified on one input data card. The value *T* must occur within each five-column field if the gauge is to be skipped in the ensuing calculation, or the value *F* must be punched anywhere within that five column field or the field left blank if the calculations are to be performed for that particular receptor gauge.

**Data Block 9** IF(NP.NE.O) READ(IN,112) (SKIPP(I),I=1,NP)

Similarly, if the point sources number more than zero, one must specify for each of the point sources the value

SKIPP = T if the particular point source is to be skipped during the ensuing calculation, or  
= F or five spaces if the calculations are to be performed.

**Data Block 10** IF(NA.NE.O) READ(IN,112) (SKIPA(I),I=1,NA)

If there are more than zero area sources NA, a logical variable SKIPA must be read for each area source which describes whether or not this area source is to be skipped during the calculations.

SKIPA = T implies the calculations for this area source are to be skipped, or  
= F or blank implies do not skip these area sources.

**Data Block 11** IF(NL.NE.O) READ(IN,112) (SKIPL(I),I=1,NL)

If there are no line sources, no logical variables SKIPL for the line sources need be read. However, if NL is greater than zero, logical variables describing whether to skip the particular line source must be read.

SKIPL = T implies skip this line source in the calculation, or  
= F or blank implies perform the calculations for this line source.



**Data Block 12**      READ(IN,40) GLATD,GLATM,GLATS,GLOND,  
                          GLONM,GLONS,GNAME(I)  
                          40   FORMAT(6F10.5,12X,A8)

GLATD    = receptor gauge latitude in degrees,  
 GLATM    = gauge latitude in minutes,  
 GLATS    = gauge latitude in seconds,  
 GLOND    = gauge longitude in degrees,  
 GLONM    = gauge longitude in minutes,  
 GLONS    = gauge longitude in seconds, and  
 GNAME    = eight-character name adjusted to fall in the field of columns 73-80, giving a name to this particular receptor gauge. This name is simply printed out as an identification in the following calculations.

**Data Block 13**      READ(IN,40) PLATD,PLATM,PLATS,PLOND,  
                          PLONM,PLONS,PNAME(J)

PLATD    = point source latitude in degrees,  
 PLATM    = point source latitude in minutes,  
 PLATS    = point source latitude in seconds,  
 PLOND    = point source longitude in degrees,  
 PLONM    = point source longitude in minutes,  
 PLONS    = point source longitude in seconds, and  
 PNAME    = eight-character name of point source adjusted to fall in columns 73-80. This name also serves to identify the point source and is printed out in the following calculations.

**Data Block 14**      READ(IN,40) ALATD,ALATM,ALATS,ALOND,  
                          ALONM,ALONS,ANAME(K)

ALATD    = area source latitude in degrees,  
 ALATM    = area source latitude in minutes,  
 ALATS    = area source latitude in seconds,  
 ALOND    = area source longitude in degrees,  
 ALONM    = area source longitude in minutes,  
 ALONS    = area source longitude in seconds, and  
 ANAME    = area source name adjusted to fall in columns 73-80. This area source name will be printed out in the following calculations for identification purposes.

**Data Block 15**      READ(IN,40) LLATDS,LLATMS,LLATSS,LLONDS,  
                          LLONMS,LLONSS,LLNAME(L)

LLATDS    = line start latitude in degrees,  
 LLATMS    = line start latitude in minutes,  
 LLATSS    = line start latitude in seconds,

LLONDS = line start longitude in degrees,  
 LLONMS = line start longitude in minutes,  
 LLONSS = line start longitude in seconds, and  
 LLNAME = line source name adjusted to fall in columns 73-80 of the input data card. This name will also be used for identification in the following printout.

**Data Block 16**      READ(IN,40) LLATDF,LLATMF,LLATSF,LLONDF,  
                          LLONMF,LLONSF

LLATDF = line finish latitude in degrees,  
 LLATMF = line finish latitude in minutes,  
 LLATSF = line finish latitude in seconds,  
 LLONDF = line finish longitude in degrees,  
 LLONMF = line finish longitude in minutes, and  
 LLONSF = line finish longitude in seconds.

Note that there are no alphanumeric names attached to the finish of the given line source latitude and longitude card. The same name that is attached to these occurs on the previous card defining the start of this particular line source. A name can be inserted in this field; however, that name will not be printed out in the following calculations.

**Data Block 17**      READ(IN,230) (AREA(K),K=1,NA)  
                          230    FORMAT(7E10.3)

AREA      = area of corresponding area source in square meters. Seven such areas are read per card, and the data should continue on the next card if there are more than seven area sources. The maximum number of area sources allowed in the current program is ten.

**Data Block 18**      READ(IN,230) (HGT(I),I=1,NP)

HGT      = height of point source in meters. Seven such heights are read per card, if the number of point sources is greater than zero.

**Data Block 19**      READ(IN,230) (PKAPPA(J),J=1,NP)

If the number of point sources is greater than zero, a value of PKAPPA must be read in this data block for each point source. Seven values occur per card. The value PKAPPA specifies the plume rise parameter for stability classes 1-4, corresponding to stability classes A-D of Pasquill-Gifford.



**Data Block 20**      `READ(IN,230) (QKAPPA(J),J=1,NP)`

**QKAPPA** = corresponding plume rise parameter for stability classes E and F (stability classes 5 and 6). If the number of point sources is greater than zero, seven such plume rise parameters will be read from each card. These stability classes occur only for daytime conditions.

**Data Block 21**      `READ(IN,230) (HGA(K),K=1,NA)`

**HGA** = height of area source in meters (m). If the number of area sources is greater than zero, a maximum of seven values for HGA are read per card.

**Data Block 22**      `READ(IN,230) (HGL(L),L=1,NL)`

**HGL** = height of line source in meters. If the number of line sources is greater than zero, as many as seven such values are read per card.

**Data Block 23**      `READ(IN,10) NPOL,KCOVER`

**NPOL** = number of pollutants for which the following calculations are to be performed,

**KCOVER** = cover type specification, which is an integer between 1 and 10. This cover specification enhances the deposition velocity that is assumed by default to 0.01 m/sec all pollutants. This parameter is basically related to the type of vegetation cover which occurs in the area being modeled. A value of one is appropriate for grassland, and a value of ten is appropriate for dense forest. Intermediate cover is defined to change from grassland cover to forest cover for  $KCOVER \geq 5$ .

**Data Block 24**    956    `READ(IN,112) (SKIPOL(I),I=1,NPOL)`

**SKIPOL** = logical variable defining whether each particular pollutant is to be skipped in the following calculations or whether these calculations are to be performed:

= T implies skip this particular pollutant in the following calculation, or

= F or blank implies perform the calculations for this pollutant.

**Data Block 25**      `READ(IN,957) (IPTYPE(M),DF1(M),DF2(M),  
POLNAM(M),M=1,NPOL)  
957    FORMAT(I5,2E10.0,2X,A8)`

**IPTYPE** = pollutant type, particulate or gas:

= 1 implies pollutant is a particulate, or

= 2 implies pollutant is a gas;

DF1 = diameter of particle if IPTYPE=1 ( $10^{-6}$  m), or  
 = boundary layer thickness if IPTYPE=2 (m);  
 DF2 = density of particle if IPTYPE=1 ( $\text{g}/\text{cm}^3$ ), or  
 = diffusivity of gas in air if IPTYPE=2 ( $\text{m}^2/\text{sec}$ ); and  
 POLNAM = eight character name of pollutant of interest. This name is simply printed out as an identification during the remainder of the calculation.

**Data Block 26**      READ(IN,230) (PQI0(I,M,MON),MON=1,KSEA)

PQI0 = pollutant source strength for a point source in grams per second ( $\text{g}/\text{sec}$ ). Note that on each card the number of periods of time MON covered by this calculation must be read on this and any continuation card, at the rate of seven such source strengths per card, until the total number of entries equals KSEA. These cards must be repeated for each pollutant M, as the next ordering of the input data. After a complete cycle has been run through for the pollutants emitted from this source, then a cycle for each of the point sources I must be included.

**Data Block 27**      READ(IN,230) (AQI0(K,M,MON),MON=1,KSEA)

AQI0 = area source strength in grams per square meter per second ( $\text{g}/\text{m}^2/\text{sec}$ ). Seven such values should appear on each card. The most rapidly varying variable is the time period MON, and seven time periods are accommodated per card. When values for the next pollutant M are to be read, the next card should start at the beginning in columns 1-10 and cycle through the KSEA values for that pollutant. After a complete cycle through the number pollutants has been made, a similar set of cards must be inserted for each additional area source K.

**Data Block 28**      READ(IN,230) (LQI0(L,M,MON),MON=1,KSEA)

LQI0 = line source strength in grams per meter ( $\text{g}/\text{m}$ ). Seven such line source strengths can be read per card, where the time period MON is the most rapidly varying index. The next card continues in columns 1-10, if KSEA is greater than seven. The next most rapidly varying index is the number of pollutants M, and the data for the next pollutant M should start in columns 1-10 and cycle through the number of time periods on the remainder of this or any additional cards. Finally, these cards should be repeated until the input is defined for each of the NL line sources.

**Data Block 29**      READ(IN,960) (ITYPE(I),DEN(I),DSALT(I),DUSP(I),I=1,NWS)

ITYPE = 1 for nearly uniform sand  
 = 2 for naturally graded sand  
 = 3 for wide range of grain sizes



DEN = density of the grain ( $\text{gm}/\text{m}^3$ )  
DSALT = saltation diameter (m)  
DSUSP = suspension diameter (m)

**Data Block 30**      READ(IN,230) (CONCF(K,M),M=1,NPOL)

CONCF = the fraction of the total concentration of the windblown source which is pollutant

**Data Block 31**      READ(IN,230) (FDRY(MON),MON=1,KSEA)

FDRY = the fraction of time the source remains dry during each season

**Data Block 32**      READ(IN,230) (SSCON(I),I=1,NWS)

SSCON = suspension to saltation ratio for the source ( $\text{m}^{-1}$ )

**Data Block 33**      READ(IN,10) ICHO  
10    FORMAT(I5)

ICHO = control parameter for calculation of either climatological (monthly average) results or episodic results:  
= 1 implies that climatological (monthly average) calculations will be performed by calling the subroutine DCAL, or  
= 2 implies that episodic calculations will be performed for all the stability classes and time periods of interest.

This summary of the input data read in the main program of the Atmospheric Transport Model is detailed but should provide sufficient information for the user to generate a corresponding data set applicable to a new problem. To illustrate the structure of a particular data set, data are presented in Appendix C of this report as a sample case for calculation with this model. The column numbers are not shown in the appendix; however, the position of the leader at the beginning of the left most input column is specified at the top of each page. Note that much of the input data is required to define the frequency table *FREQ* for the stability wind rose. These data can be stored on an alternative direct input device, such as a disk, if calculations are to be often repeated using these climatological variables. The wind rose can then be read in from such a direct access device at each run, without having to read data cards each time. We have chosen to store these data on such a device, a data cell. The input unit for the *FREQ* data is logical unit *IFREQ* and is set in the main program.

## V. RESULTS

Appendix D lists the results of operation of the program for the several months of the given data set, the entire data set and program being too large to reproduce concisely. The results of one run, assuming forest cover, are listed below. The meteorological, effluent, and monitoring data were supplied by the Tennessee Valley Authority (TVA) and Oak Ridge National Laboratory. As listed in the data set, two very large TVA steam plants are in the Oak Ridge area, as well as one moderate size steam plant located at the Y-12 plant. For validation, data from a TVA monitoring station located 4100 meters northeast of the Bull Run steam plant and 39,000 meters northeast of the Kingston plant, are compared to results calculated by the model. Table 1 below lists the monthly output of  $\text{SO}_2$  at each steam plant, the average observed monthly  $\text{SO}_2$  concentration at the monitoring station, and the concentration and deposition estimates produced by the model.

As can readily be seen from Table 1 the output from Kingston was fairly constant, whereas the output from Bull Run varied considerably from month to month. The observed  $\text{SO}_2$  concentrations at the monitoring station correlate with the output of Bull Run quite well ( $r = .68$ ). The fact that the model exceeds this correlation is an indication of its validity. Several points should be noted first, however, before the results are examined in detail. First, the quality of the observations, their interpretation as to stability class, etc., are fundamental to the model. Second, the meteorological data are essentially hourly summed over a month's period, whereas the source strength data are averaged monthly, since an hour-to-hour match of meteorology to power output would be very costly. A slight mismatch of data will obviously occur, since the hourly output of a steam plant is not constant. Third, the reported values of TVA  $\text{SO}_2$  data are truncated; e.g., hourly values below .01 ppm are considered zero, consequently the values in Table 1 do not reflect any background  $\text{SO}_2$  data.

Table 2 lists the correlations between observed  $\text{SO}_2$  and the output of Bull Run, the predicted concentration and the predicted overhead inventory.

The output correlates very well ( $r = 0.80$ ) with observed values of  $\text{SO}_2$  concentration. The overhead plume inventory was obtained from the wet deposition rate at an assumed removal of  $\lambda = 5 \times 10^{-4} \text{ sec}^{-1}$  (see the WASHOUT subroutine). Since washout occurs over the entire plume, it is independent of stability class and plume height. The overhead plume inventory also correlates extremely well ( $r = 0.91$ ) with observations.

## Conclusions

From the predicted  $\text{SO}_2$  concentration and the plume inventory calculations one may conclude the following: (1) The model serves very well as a predictor for  $\text{SO}_2$  concentration. (2) The input wind data are adequate (i.e., wind direction, frequency, and speed). (3) The stability classification of the data must also be very good, since it resulted in excellent (within thirty percent) agreement of predicted and observed concentrations. For the period in question, at least, it appears that the stability classes were more constant than the data showed. This is encouraging to those with limited observational equipment. This model could have been run assuming a "B" (number 2) conditions throughout, and the concentration would have correlated well ( $r = 0.91$ ) with observations.



Table 1

Monthly SO<sub>2</sub> Output of TVA Steam Plants Compared  
with Observed and Calculated Values of Concentration

Month	SO <sub>2</sub> Output Kingston	GMS/sec Bull Run	Observed SO <sub>2</sub> ppm	Predicted SO <sub>2</sub> ppm	Predicted Overhead SO <sub>2</sub> Mass GM/M <sup>2</sup>
July 72	2750	826	.0041	.0037	.00047
Aug. 72	2800	784	.0019	.0026	.00019
Sept. 72	2450	761	.0033	.0031	.00028
Oct. 72	2410	803	.0018	.0027	.00018
Nov. 72	2510	767	.0016	.0026	.00014
Dec. 72	2280	783	.0033	.0032	.00020
Jan. 73	2470	708	.0013	.0024	.00015
Feb. 73	2540	784	.0021	.0027	.00019
Mar. 73	2220	608	.0006	.0019	.00012
Apr. 73	2460	711	.0015	.0029	.00016
May 73	2310	517	.0014	.0026	.00017
June 73	2560	0	.0005	.0018	.00001
July 73	2760	63	.0007	.0029	.00005
Aug. 73	2860	0	.0006	.0009	.00001

Table 2

Correlations Between Observed SO<sub>2</sub>  
and Observed and Predicted Values

Monitor vs Bull Run Output	r = 0.68
Monitor vs Predicted SO <sub>2</sub>	r = 0.80
Monitor vs Overhead Inventory	r = 0.91

## REFERENCES

1. M. T. Mills and M. Reeves, *A Multi-Source Atmospheric Transport Model for Deposition of Trace Contaminant*, ORNL/NSF/EATC/2, October, 1973.
2. R. P. Hosker, Jr., *Estimates of Dry Deposition and Plume Depletion over Forests and Grassland*, IAEA-SM-181/19, Air Resources Atmospheric Turbulence and Diffusion Laboratory, November, 1973.
3. W. F. Hilsmeier and F. A. Gifford, Jr., *Graphs for Estimating Atmospheric Dispersion*, USAEC Report ORO-545, Weather Bureau, Oak Ridge, Tennessee, 1962.
4. G. A. Briggs, *Diffusion Estimation for Small Emissions*, U.S. Dept. of Commerce, NOAA-ERL-ARATDL contribution no. 79 (Draft), Oak Ridge, Tennessee, May, 1973.
5. F. B. Smith, "A Scheme for Estimating the Vertical Dispersion of a Plume from a Source Near Ground Level," Chapter XVII, *Proceedings of the Third Meeting of the Panel on Air Pollution Modeling*, N.A.T.O. Committee on the Challenges of Modern Society, Paris, France, October 2-3, 1972. Proceedings No. 14, Air Pollution Tech. Information Center, U.S.E.P.A., Research Triangle Park, North Carolina, 1973.
6. D. H. Slade (Ed.), *Meteorology and Atomic Energy 1968*, U.S. Energy Research and Development Administration, TID-24190, July, 1968.
7. F. A. Gifford, Jr., "An Outline of Theories of Diffusion in the Lower Layers of the Atmosphere," Chapter III, *Meteorology and Atomic Energy* (D. Slade, Ed.), U.S. Energy Research and Development Administration, TID-24190, 1968.
8. R. J. Engelmann, *Rain Scavenging of Particulates*, U.S. Energy Research and Development Administration Report 10, 79382, Hanford Atomic Products Operation, 1963.
9. G. W. Westley and J. A. Watts (Eds.), *The Computing Technology Center Numerical Analyses Library*, CTC-39, Oak Ridge National Laboratory, October, 1970.
10. G. A. Briggs, *Plume Rise*, TID-25075, 1969.
11. O. G. Sutton, "A Theory of Eddy Diffusion in the Atmosphere," *Proc. Ray. Soc.*, (London), Ser. A, 135:143-165, 1932.
12. G. T. Csanady, "Deposition of Dust Particles from Industrial Stacks," *Aust. Journal of Applied Science*, 9, 1958.
13. W. Schmidt, "Der Massenaustausch in freier Luft und verwandte Erscheinungen," *Probleme der Kosmischen Physik*, Hamburg, Verlag von Henri Grand, 1925.
14. G. T. Csanady, *Atmospheric Diffusion of Buoyant and Heavy Clouds*, NYO-3635-24, Final Report on U.S.E.R.D.A. Project NYO-3685, 1972.
15. A. C. Chamberlain, *Aspects of Travel and Deposition of Aerosol and Vapour Clouds*, A.E.R.E., HP/R 1261, H.M.S.O., 1953.
16. G. A. Sehmel and W. H. Hodgson, "Particle and Gaseous Removal in the Atmosphere by Dry Deposition," *Proceedings of the Symposium on Atmospheric Diffusion and Air Pollution, Santa Barbara, California, September 9-13, 1974*.
17. W.G.N. Slinn, "On the Dry Deposition of Sea Salt Nuclei," in Pacific Northwest Laboratory Annual Report for 1971 to the U.S.E.R.D.A. Division of Biomedical and Environmental Research, vol. II, part 1, BNWL-1651 PT1, UC-53, December, 1972.



18. T. Hori (Editor), *Studies of Fogs in Relation to Fog-preventing Forest* (Hokkaido University, Sapporo, Japan), 1953.
19. A. Baumgartner, "Untersuchungen über den warme-und wasserhaushalt eines jungen waldes," *Berichte des Deutschen Wetterdienstes* 5, 1956.
20. Thomas W. Horst, "A Surface Depletion Model for Deposition from a Gaussian Plume," *Proceedings of 1974 Symposium on Surface Exchange of Particulate and Gaseous Pollutants, Richland, Washington, September 4-6, 1974*.
21. F. A. Gifford, "Atmospheric Dispersion Models for Environmental Pollution Applications," presented at American Meteorological Society (AMS) Workshop on Meteorology and Environmental Assessment, Boston, Massachusetts, October, 1975.
22. H. E. Cramer, F. A. Record, and H. C. Vaughan, *The Study of the Diffusion of Gases or Aerosols in the Lower Atmosphere*, Massachusetts Institute of Technology, AFCRC-TR-58-239, May 15, 1958.
23. J. L. McElroy and F. Pooler, *St. Louis Dispersion Study, Volume II - Analysis*, U.S.E.P.A., NAPCA Publication No. AP-53, 1968.
24. R. A. Bagnold, *The Physics of Blown Land and Desert Dunes*, Methuen and Co. Ltd, London, 1959.
25. M. T. Mills, R. G. Dahlman, and J. S. Olson, *Ground Level Air Concentrations from a Tailings Area During a Windstorm*, ORNL/TM/4375, Oak Ridge National Laboratory, September, 1975.
26. D. A. Gillette, I. H. Blifford, Jr., and C. R. Fenster, "Measurements of Aerosol Size Distributions and Vertical Fluxes of Aerosols on Land Subject to Wind Erosion," *Journal of Applied Meteorology*, 11, p. 977, 1972.

## APPENDICES



## APPENDIX A. LIST OF SYMBOLS

C	sand uniformity constant
d	grain diameter (cm)
D	standard grain diameter (cm)
f	settling velocity of dust particle (m/sec)
$F_B$	buoyancy flux ( $\text{m}^4/\text{sec}^3$ )
$F_d$	fraction of time windblown source remains dry
$F_{pr}(\theta)$	fraction of the time the wind blows from direction $\theta$ , with wind speed class $r$ , and stability class $p$
g	gravitational acceleration ( $\text{m}/\text{sec}^2$ )
h	effective stack height (m)
$h_o$	actual stack height (m)
k	surface roughness during saltation (cm)
$K_x, K_z$	eddy diffusivities ( $\text{m}^2/\text{sec}$ )
$n_p$	stability power law parameter
p	stability index
q	volume concentration of particulates ( $\text{gm}/\text{m}^3$ )
Q	effective source strength ( $\text{gm}/\text{sec}$ )
r	stack radius (m)
R	distance from receptor gauge to area source centroid (m)
$R_f$	suspension to saltation ratio ( $\text{m}^1$ )
$R_1$	distance from receptor gauge to nearest boundary of polar area source (m)
$R_2$	distance from receptor gauge to farthest boundary of polar area source (m)
s	temperature profile parameter ( $\text{sec}^2$ )
t	time (sec)
$T_E$	air temperature ( $^{\circ}\text{K}$ )
$T_s$	stack gas temperature ( $^{\circ}\text{K}$ )
u	wind speed in the x-direction ( $\text{m}/\text{sec}$ )
v	deposition velocity ( $\text{m}/\text{sec}$ )
$v_t$	threshold wind speed for saltation ( $\text{cm}/\text{sec}$ )
W	stack ejection velocity ( $\text{m}/\text{sec}$ )
$W_f$	fraction of time only dry deposition occurs
$W_w$	fraction of time both wet and dry deposition occur
x	distance downwind from source (m)
X	ground level air concentration ( $\text{gm}/\text{m}^3$ )
$x^*$	cutoff distance downwind for plume rise (m)
y	distance crosswind from the plume axis (m)
z	vertical distance from ground (m)
$\Delta h$	plume rise (m)
$\Delta\theta$	angular spread of polar area source (radians) as seen from a receptor gauge
$\theta$	one of sixteen principal compass directions clockwise from north
$\lambda$	washout coefficient ( $\text{sec}^1$ )
$\sigma_y, \sigma_z$	horizontal and vertical dispersion (m)
$\omega$	deposition rate ( $\text{gm}/\text{m}^2/\text{sec}$ )

# APPENDIX B. PROGRAM LISTING

```

MAIN PROGRAM ATM (AIR TRANSPORT MODEL)
IMPLICIT REAL*4 (A-H,O-Z)
LOGICAL SKIP, SKIPA, SKIPL, SKIPG, SKIPOL
INTEGER YEAR
INTEGER*4 STNFRD(10)/' 1',9*0/
REAL*4 LSTHA,LFTHA,LSEPHI,LFPHI
REAL*4 LLATDS,LLATMS,LLATSS
REAL*4 LLATDF,LLATMF,LLATSF
REAL*4 LLONDS,LLONMS,LLONSS
REAL*4 LLONDF,LLONMF,LLONSF
REAL*4 LQIO
REAL*8 ATITLE,SEANAM,GNAME,PNAME,ANAME,LNAME,POLNAM
COMMON/C1/XM(50),SIGTAB(6,50),SIGMAX(7),V(5),DV(5),
1 CLAMDA(5),DLAMDA(10,14,5),NDIST,NSTAB
COMMON/C2/H
COMMON/C3/PI,F,KOUT
COMMON/C4/DP(10,10),DA(10,10),DIRP(10,10),DIRA(10,10),AREA(10)
COMMON/C5/DTH(10,10),R1(10,10),R2(10,10),TH1(10,10),TH2(10,10)
COMMON/C6/FREQ(14,7,8,16),HGT(10),PQIO(10,5,14),
1 AQIO(10,5,14),LQIO(10,5,14)
COMMON/C7/DEPP(10,5,14),DEPA(10,5,14),DEPI(10,5,14)
COMMON/C8/NG,NP,NA,NL,NWS,NPOL,NFSTAB,NWINDS,WW,WF,FDRY(14)
COMMON/C9/DEPT(10,5,14),DRYDEF(10,5,14),WETDEF(10,5,14)
COMMON/C10/LSTHA(5),LFTHA(5),LSEPHI(5),LFPHI(5)
COMMON/C11/GTHA(10),GPHI(10),PTH(10),PPHI(10),ATHA(10),APHI(10)
COMMON/C12/WQIO(3,5,8),VFALL(3)
COMMON/C13/HGA(10),HGL(5)
COMMON/C14/KDISP,KCOVER,ROUGH
COMMON/C15/SKIPP(10),SKIPA(10),SKIPL(10),SKIPG(10),SKIPOL(10)
COMMON/C16/MOB,MOE,KSEA
COMMON/C17/SURF(10)
COMMON/C18/COMP(32),F(32,10,20),ATITLE(10),SEANAM(14),GNAME(10),
1 PNAME(10),ANAME(10),LNAME(10),POLNAM(5)
COMMON/C19/CONCP(3,5),SSCON(3),DEN(3),DSALT(3),DSUSP(3),
1 ITYPE(3)
DIMENSION PKAPPA(10),WINDSD(8)
DIMENSION QKAPPA(10)
DIMENSION JSTAB(7)
DIMENSION FRACT(14),AVRATE(14),GRATE(10,14),GFRACT(10,14)
DIMENSION IPTYPE(5),DF1(5),DF2(5)
C*** NPOL=NUMBER OF POLLUTANTS
C*** R=EARTH'S RADIUS IN METERS, NG=NUMBER OF RAIN GAUGES, NP=NUMBER OF
C*** POINT SOURCES, NA=NUMBER OF AREA SOURCES, (GLATD,GLATM,GLATS)=LATI
C*** TUDE OF RAIN GAUGE IN DEGREES,MINUTES,AND SECONDS, (GLOND,GLONM,GL
C*** ONS)=LONGITUDE OF RAIN GAUGE IN DEGREES,MINUTES,AND SECONDS,
C*** (PLATD,PLATM,PLATS)=LATITUDE OF POINT SOURCE IN DEGREES,MINUTES,
C*** AND,SECONDS, (PLOND,PLONM,PLONS)=LONGITUDE OF POINT SOURCE IN
C*** DEGREES,MINUTES,AND SECONDS, (ALATD,ALATM,ALATS)=LATITUDE OF
C*** CENTROID OF AREA SOURCE IN DEGREES,MINUTES,AND SECONDS, (ALOND,
C*** ALONM,ALONS)=LONGITUDE OF CENTROID OF AREA SOURCE IN DEGREES,MIN-
C*** UTES,AND SECONDS
C*** DP(I,J)=DISTANCE IN METERS FROM GAUGE I TO POINT SOURCE J
C*** DA(I,K)=DISTANCE IN METERS FROM GAUGE I TO CENTROID OF AREA SOURCE
C*** K
C*** DIRP(I,J)=DIRECTION IN DEGREES FROM GAUGE I TO POINT SOURCE J(MEAS
C*** URED CLOCKWISE FROM DUE NORTH)

```



```

C*** DIRA(I,K)=DIRECTION IN DEGREES FROM GAUGE I TO CENTROID OF AREA
C*** SOURCE K(MEASURED CLOCKWISE FROM NORTH)
C*** AREA(K)=AREA OF AREA SOURCE K IN METERS**2
C*** (LLATDS,LLATMS,LLATSS)=LATITUDE OF THE STARTING POINT OF THE LINE
C*** SOURCE IN DEGREES,MINUTES,AND SECONDS
C*** (LLONDS,LLONMS,LLONSS)=LONGITUDE OF THE STARTING POINT OF THE LINE
C*** SOURCE IN DEGREES,MINUTES,AND SECONDS
C*** (LLATDF,LLATMF,LLATSF)=LATITUDE OF THE TERMINATION POINT OF THE
C*** LINE SOURCE IN DEGREES,MINUTES,AND SECONDS
C*** (LLONDF,LLONMF,LLONSF)=LONGITUDE OF THE TERMINATION POINT OF THE
C*** LINE SOURCE IN DEGREES,MINUTES,AND SECONDS
C*** IPTYPE(M)=1, POLLUTANT M IS A PARTICULATE
C*** IPTYPE(M)=2, POLLUTANT M IS A GAS
C*** AND PARTICLE SIZE DATA
IN=50
C***** INFREQ IS THE UNIT NUMBER THAT THE FREQUENCY TABLE WILL
C***** WILL BE READ FROM. IF INFREQ=50, IT WILL BE ASSUMED TO BE READ
C***** FROM THE CARD INPUT STREAM. IF INFREQ=XX IT WILL READ FROM
C***** A DISK.
INFREQ=50
KOUT=51
YEAR=74
R=6.367E+6
PI=3.1415927
PI180=PI/180.0
C*** NA=NUMBER OF AREA SOURCES(INCLUDING WINDBLOWN AREA SOURCES)
C*** NWS=NUMBER OF WINDBLOWN AREA SOURCES
C*** DATA FOR WINDBLOWN SOURCES LISTED AFTER THAT FOR THE
C*** ORDINARY AREA SOURCES
C*** IN OTHER WORDS, IF YOU HAVE 4 AREA SOURCES, 2 OF WHICH
C*** ARE WINDBLOWN, AREA SOURCES 1 AND 2 WILL BE ORDINARY
C*** AND 3 AND 4 WILL BE WINDBLOWN
READ(IN,22) ATITLE
22 FORMAT(10A8)
WRITE(KOUT,21) ATITLE
21 FORMAT('1',10X,10A8)
C*** NDIST=NUMBER OF DISTANCES IN THE STABILITY TABLE
C*** NSTAB=NUMBER OF STABILITIES IN THE TABLE
C*** SIGTAB=VARIOUS PASQUILL STABILITIES
C*** KDISP=1, USE PASQUILL STABILITY TABLE
C*** KDISP=2, USE SMITH'S STABILITY FORMULATION WITH MODIFICATION
C*** DUE TO SURFACE ROUGHNESS(SEE R.F. HOSKER'S PAPER)
C*** KCOVER=1-5, GRASS COVER
C*** KCOVER=6-10 FOREST COVER
C*** ROUGH= ROUGHNESS OF THE LAND SURFACE(METERS)
READ(IN,481) KDISP,KTAG,KSEA,ROUGH
481 FORMAT(3I5,E10.0)
C*** KTAG=1 WILL PRINT DATA ON WIND DIRECTION FREQUENCY
C*** TABLES,AREA AND LINE SOURCE PARAMETERS.ONCE RUN ,THESE
C*** MAY BE BYPASSED BY KTAG=2
IF(KDISP.EQ.2) GO TO 483
WRITE(KOUT,482)
482 FORMAT('0 PASQUILL STABILITIES USED'/)
GO TO 4835
483 WRITE(KOUT,484)
484 FORMAT('0 PASQUILL STABILITIES NOT USED--STABILITIES FOUND IN
&SUBROUTINE SIGMA'/)
DO 4834 IP=1,NSTAB

```

```

      DO 4834 I=1,NDIST
      SIGTAB(IP,I)=SIGMA(IP,XM(I),IDUM,ADUM)
4834 CONTINUE
4835 IF(KTAG.EQ.2) GO TO 501
      WRITE(KOUT,470)
470 FORMAT('0 DISPERSION COEFFICIENTS FOR STABILITY CLASS'/
      & '0',18X,'X',17X,'A',14X,'B',14X,'C',14X,'D',14X,'E',14X,'F'/)
      WRITE(KOUT,480) (XM(I),(SIGTAB(IP,I),IP=1,NSTAB),I=1,NDIST)
480 FORMAT(10X,F9.1,5X,6E15.5)
501 WRITE(KOUT,489) ROUGH
489 FORMAT('0 ROUGHNESS=',2X,E10.3,2X,'METERS')
C*** NWINDS=NUMBER OF WIND SPEEDS IN THE FREQUENCY TABLE
C*** NDIR=NUMBER OF DIRECTIONS IN THE FREQUENCY TABLE
C*** NFSTAB=NUMBER OF WIND STABILITIES IN THE FREQUENCY TABLE
C*** JSTAB(I)=INDEX OF STABILITIES TO BE USED
      READ(IN,10) NWINDS,NDIR,NFSTAB,(JSTAB(I),I=1,NFSTAB)
      WRITE(KOUT,490) NWINDS,NDIR,NFSTAB,(JSTAB(I),I=1,NFSTAB)
490 FORMAT('0 NUMBER OF WIND SPEEDS=',I5,'/',10X,'NUMBER OF WIND DI
      & RECTIONS=',I5,'/',10X,'NUMBER OF WIND STABILITIES=',I5,'/',10X,'STABIL
      & ILITIES USED---',I7)
C*** SIGMAX(IP)=MAXIMUM VALUE OF VERTICAL DISPERSION FOR EACH STABILITY
      WRITE(KOUT,510) (SIGMAX(IP),IP=1,NSTAB)
510 FORMAT('0 SIGMAX FOR EACH STABILITY IN THE TABLE=',7E10.3)
C*** WINDSD(I)=WIND SPEED IN METERS/SEC FOR WIND SPEED CLASS I
541 READ(IN,230) (WINDSD(I),I=1,NWINDS)
      DO 560 I=1,NWINDS
      WRITE(KOUT,570) I,WINDSD(I)
560 CONTINUE
570 FORMAT('0 WIND SPEED FOR WIND CLASSES'/(7(I5,F10.3)))
C*** KSEA=NUMBER OF MONTHS OF DATA FOR WIND ROSE
      READ(IN,23) (SEANAM(ISEA),ISEA=1,KSEA)
23 FORMAT(7(2X,A8))
      READ(INFREQ,481) KDUMMY
      DO 645 ISEA=1,KSEA
      SUM=0.0
      DO 600 I=1,NFSTAB
      DO 600 K=1,NDIR
      READ(INFREQ,620) (FREQ(ISEA,I,J,K),J=1,NWINDS)
620 FORMAT(6X,6F8.2)
      DO 642 J=1,NWINDS
      SUM=SUM+FREQ(ISEA,I,J,K)
642 CONTINUE
600 CONTINUE
      DO 644 I=1,NFSTAB
      DO 644 K=1,NDIR
      DO 644 J=1,NWINDS
      FREQ(ISEA,I,J,K)=FREQ(ISEA,I,J,K)/SUM
644 CONTINUE
645 CONTINUE
      IF(KTAG.EQ.2) GO TO 770
      DO 760 ISEA=1,KSEA
860 WRITE(KOUT,665) ISEA,SEANAM(ISEA)
665 FORMAT('0 STABILITY WIND ROSE DATA FOR PERIOD',I4,2X,A8)
      DO 750 I=1,NFSTAB
      WRITE(KOUT,710) JSTAB(I)
710 FORMAT(50X,'STABILITY CLASS',I5)
      WRITE(KOUT,720) (WINDSD(LL),LL=1,NWINDS)
720 FORMAT(' WINDSPEEDS',/,18X,6F12.4)

```



```

DO 740 K=1,NDIR
  WRITE(KOUT,730) K,(FREQ(ISEA,I,J,K),J=1,NWINDS)
730 FORMAT(1X,'DIRECTION',I3,5X,6F12.6)
740 CONTINUE
750 CONTINUE
760 CONTINUE
770 READ(IN,10) NG,NP,NA,NL,NWS
  10 FORMAT(16I5)
  IF(NG.EQ.0) GO TO 13
  IF(NP.NE.0) GO TO 14
  IF(NA.NE.0) GO TO 14
  IF(NL.NE.0) GO TO 14
  WRITE(KOUT,12)
  12 FORMAT(//,10X,'NO SOURCES',//)
  CALL ERROR
  13 WRITE(KOUT,1300)
1300 FORMAT(//,10X,'NO GAUGES',//)
  CALL ERROR
C*** SKIPG(I)=T GAUGE I NOT USED, =F USED
C*** SKIPF(I)=T POINT SOURCE I NOT USED, =F USED
C*** SKIPF(I)=T AREA SOURCE I NOT USED, =F USED
C*** SKIPL(I)=T LINE SOURCE I NOT USED, =F USED
  14 IF(NG.GT.0) READ(IN,112) (SKIPG(I),I=1,NG)
112 FORMAT(16I5)
  IF(NP.NE.0) READ(IN,112) (SKIPF(I),I=1,NP)
  IF(NA.NE.0) READ(IN,112) (SKIPF(I),I=1,NA)
  IF(NL.NE.0) READ(IN,112) (SKIPL(I),I=1,NL)
  WRITE(KOUT,20)
  20 FORMAT('0 LATITUDE AND LONGITUDE OF GAUGE SAMPLING POINTS'/'0')
  WRITE(KOUT,41)
  41 FORMAT(' ID NUMBER',6X,'NAME',5X,'LATITUDE',22X,'LONGITUDE'/'
  1 23X,'DEGREES',3X,'MINUTES',3X,'SECONDS',
  2 3X,'DEGREES',3X,'MINUTES',3X,'SECONDS')
  DO 60 I=1,NG
  READ(IN,40) GLATD,GLATM,GLATS,GLOND,GLONM,GLONS,GNAME(I)
  40 FORMAT(6F10.5,12X,A8)
  IF(SKIPG(I)) GO TO 60
  WRITE(KOUT,50) I,GNAME(I),GLATD,GLATM,GLATS,GLOND,GLONM,GLONS
  50 FORMAT(I10,2X,A8,6F10.2)
  GIHA(I)=PI180*(GLATD+(GLATM+GLATS/60.0)/60.0)
  GPHI(I)=PI180*(GLOND+(GLONM+GLONS/60.0)/60.0)
  60 CONTINUE
  IF(NP.EQ.0) GO TO 91
  WRITE(KOUT,70)
  70 FORMAT('0 LATITUDE AND LONGITUDE OF POINT SOURCES'/'0')
  WRITE(KOUT,41)
  DO 90 J=1,NP
  READ(IN,40) PLATD,PLATM,PLATS,PLOND,PLONM,PLONS,PNAME(J)
  IF(SKIPF(J)) GO TO 90
  WRITE(KOUT,50) J,PNAME(J),PLATD,PLATM,PLATS,PLOND,PLONM,PLONS
  PTHA(J)=PI180*(PLATD+(PLATM+PLATS/60.0)/60.0)
  PPHI(J)=PI180*(PLOND+(PLONM+PLONS/60.0)/60.0)
  90 CONTINUE
  91 IF(NA.EQ.0) GO TO 121
  WRITE(KOUT,100)
  100 FORMAT('0 LATITUDE AND LONGITUDE OF AREA SOURCE CENTROIDS'/'0')
  WRITE(KOUT,41)
  DO 120 K=1,NA

```

04 24 75

```

      READ(IN,40) ALATD,ALATM,ALATS,ALOND,ALONM,ALONS,ANAME(K)
      IF(SKIPA(K))GO TO 120
      WRITE(KOUT,50) K,ANAME(K), ALATD,ALATM,ALATS,ALOND,ALONM,ALONS
      ATHA(K)=PI180*(ALATD+(ALATM+ALATS/60.0)/60.0)
      APHI(K)=PI180*(ALOND+(ALONM+ALONS/60.0)/60.0)
120 CONTINUE
121 IF(NL.EQ.0) GO TO 126
      WRITE(KOUT,1211)
1211 FORMAT('0 LATITUDE AND LONGITUDE OF LINE SOURCE ENDPOINTS'/)
      WRITE(KOUT,41)
      DO 125 L=1,NL
      READ(IN,40) LLATDS,LLATMS,LLATSS,LLONDS,LLONMS,LLONSS,LNAME(L)
      READ(IN,40) LLATDF,LLATMF,LLATSF,LLONDF,LLONMF,LLONSF
      IF(SKIPL(L))GO TO 125
      WRITE(KOUT,50) L,LNAME(L),LLATDS,LLATMS,LLATSS,LLONDS,LLONMS,LLONSS
      WRITE(KOUT,50) L,LNAME(L),LLATDF,LLATMF,LLATSF,LLONDF,LLONMF,LLONSF
      LSTHA(L)=PI180*(LLATDS+(LLATMS+LLATSS/60.0)/60.0)
      LFTHA(L)=PI180*(LLATDF+(LLATMF+LLATSF/60.0)/60.0)
      LSPHI(L)=PI180*(LLONDS+(LLONMS+LLONSS/60.0)/60.0)
      LFPHI(L)=PI180*(LLONDF+(LLONMF+LLONSF/60.0)/60.0)
125 CONTINUE
126 WRITE(KOUT,160)
160 FORMAT('0')
      IF(NA.LE.0)GO TO 165
      READ(IN,230) (AREA(K),K=1,NA)
230 FORMAT(7E10.3)
      WRITE(KOUT,225)
225 FORMAT('0 AREA SOURCE AREAS IN METEFS**2')
      DO 240 K=1,NA
      IF(SKIPA(K))GO TO 240
      WRITE(KOUT,250) K,ANAME(K),AREA(K)
250 FORMAT(' AREA SOURCE',I3,2X,A8,2X,1PE10.3)
240 CONTINUE
165 CALL GEOMET(KTAG)
C*** HGT(I)=HEIGHT OF POINT SOURCE I
C*** HGA(K)=HEIGHT OF AREA SOURCE K
C*** HGL(L)=HEIGHT OF LINE SOURCE L
      IF(NP.EQ.0) GO TO 841
      READ(IN,230) (HGT(I),I=1,NP)
      PKAPPA(J)=PLUME RISE PARAMETER IN THE EFFECTIVE SOURCE CALCULATION
      FOR EACH POINT SOURCE FOR STABILITIES 1,2,3,4
      QKAPPA(J)=PLUME RISE PARAMETER IN THE EFFECTIVE SOURCE CALCULATION
      FOR EACH POINT SOURCE FOR STABILITIES 5,6
      READ(IN,230) (PKAPPA(J),J=1,NP)
      READ(IN,230) (QKAPPA(J),J=1,NP)
      WRITE(KOUT,825)
825 FORMAT('0'/'0')
      WRITE(KOUT,826)
826 FORMAT('0 SOURCE',6X,'NAME',6X,'HEIGHT',6X,'PKAPPA',6X,'QKAPPA')
      DO 840 I=1,NP
      IF(SKIPL(I))GO TO 840
      WRITE(KOUT,830) I,PNAME(I),HGT(I),PKAPPA(I),QKAPPA(I)
830 FORMAT(' POINT',I5,2X,A8,2X,3(1PE12.3))
840 CONTINUE
841 IF(NA.EQ.0) GO TO 842
      READ(IN,230) (HGA(K),K=1,NA)
      DO 8401 K=1,NA
      IF(SKIPA(K))GO TO 8401

```

04 28 75

05 05 75

04 28 75

04 28 75

04 28 75



```

      WRITE(KCUT,831) K,ANAME(K),HGA(K)
831  FORMAT(' AFEA ',I5,2X,A8,2X,1PE12.3)
8401 CONTINUE
842  IF(NL.EQ.0) GO TO 843
      READ(IN,230) (HGL(L),L=1,NL)
      DO 8402 L=1,NL
        IF(SKIP(L)) GO TO 8402
        WRITE(KOUT,832) L,LNAME(L),HGL(L)
832  FORMAT(' LINE ',I5,2X,A8,2X,1PE12.3)
8402 CONTINUE
843  CONTINUE
      READ(IN,10) NPCI,KCOVER
      IF(KCOVER.GT.5) GO TO 486
      WRITE(KOUT,485) KCOVER
485  FORMAT('O GRASS COVER',I5)
      GO TO 488
486  WRITE(KOUT,487) KCOVER
487  FORMAT('O FOREST COVER',I5)
488  CONTINUE
      IF(NPOL.GT.0) GO TO 956
      WRITE(KOUT,17)
17  FORMAT(//,10X,'NO POLLUTANTS',//)
      CALL ERROR
C*** SKIPOL(I)=T POLLUTANT I NOT USED, =F USED
956  READ(IN,112) (SKIPOL(I),I=1,NPOL)
      READ(IN,957) (IPTYPE(M),DF1(M),DF2(M),POLNAM(M),M=1,NPOL)
957  FORMAT(I5,2E10.0,2X,A8)
      WRITE(KOUT,825)
      DO 958 M=1,NPOL
        IF(IPTYPE(M).EQ.2) GO TO 9802
        WRITE(KOUT,9801) M,POLNAM(M),DF1(M),DF2(M)
9801  FORMAT(10X,'DATA FOR POLLUTANT',I4,2X,A8,1X,' (A PARTICULATE)',/
1      ,10X,'PARTICLE DIAMETER=',E12.3,2X,'MICRONS',/
2      ,10X,'PARTICLE DENSITY=',E12.3,2X,'GM/CM**3')
        GO TO 958
9802  WRITE(KOUT,9803) M,POLNAM(M),DF1(M),DF2(M)
9803  FORMAT(10X,'DATA FOR POLLUTANT',I4,2X,A8,1X,' (A GAS)',/
1      ,10X,'BOUNDARY LAYER THICKNESS=',E12.3,2X,'METERS',/
2      ,10X,'DIFFUSION CONSTANT FOR WASHOUT=',E12.3,2X,'METER**2/SEC')
958  CONTINUE
C*** PQIO(I,M,MON)=EMISSION RATE OF POLLUTANT M DURING MONTH MON FROM
C*** PCINT SOURCE I IN GRAMS/SEC
851  IF(NP.EQ.0) GO TO 901
      DO 860 I=1,NP
        DO 855 M=1,NPOL
          READ(IN,230) (PQIO(I,M,MON),MON=1,KSEA)
855  CONTINUE
860  CONTINUE
          WRITE(KOUT,825)
          WRITE(KOUT,9002) (MON,SEANAM(MON),MON=1,KSEA)
9002  FORMAT('1 PCINT SOURCE EMISSIONS FOR PERIODS'/(8(I5,2X,A8)))
          DO 900 I=1,NP
            IF(SKIPP(I)) GO TO 900
            DO 890 M=1,NPOL
              IF(SKIPOL(M)) GO TO 890
              WRITE(KOUT,880) I,M,(PQIO(I,M,MON),MON=1,KSEA)
880  FORMAT('O EMISSION RATE FROM POINT SOURCE',I4,2X,'OF POLLUTANT',
& I4,2X,'IN GRAMS/SEC'/(8(1PE15.4)))

```

```

890 CONTINUE
900 CONTINUE
9001 CONTINUE
C*** AQIO(K,M,MON)=EMISSION RATE OF POLLUTANT M DURING MONTH MON FROM
C*** AREA SOURCE K IN GRAMS/METER**2/SEC
901 IF(NA.EQ.0) GO TO 951
    NAP=NA-NWS
    DC 920 K=1,NAP
    DO 915 M=1,NPOL
        READ(IN,230) (AQIO(K,M,MON),MON=1,KSEA)
915 CONTINUE
920 CONTINUE
    WRITE(KOUT,9502) (MON,SEANAM(MON),MON=1,KSEA)
9502 FORMAT('0 AREA SOURCE EMISSIONS FOR PERIODS'/(8(I5,2X,A8)))
    DO 950 K=1,NAP
        IF(SKIPA(K))GO TO 950
        DC 940 M=1,NPOL
        IF(SKIPOL(M))GO TO 940
        WRITE(KOUT,930) K,M,(AQIO(K,M,MON),MON=1,KSEA)
930 FORMAT('0 EMISSION RATE FROM AREA SOURCE',I4,2X,'OF POLLUTANT',
        & I4,2X,'IN GRAMS/M**2/SEC'/(8(1PE15.4)))
940 CONTINUE
950 CONTINUE
C*** LQIO(L,M,MON)=EMISSION RATE OF POLLUTANT M DURING MONTH MON FROM
C*** LINE SOURCE L IN GRAMS/METER/SEC
951 IF(NL.EQ.0) GO TO 111
    DC 952 L=1,NL
    DO 2511 M=1,NPOL
        READ(IN,230) (LQIO(L,M,MON),MON=1,KSEA)
2511 CONTINUE
952 CONTINUE
    WRITE(KOUT,825)
    WRITE(KOUT,9552) (MON,SEANAM(MON),MON=1,KSEA)
9552 FORMAT('0 LINE SOURCE EMISSIONS FOR PERIODS'/(8(I5,2X,A8)))
    DC 955 L=1,NL
    IF(SKIPL(L))GO TO 955
    DC 954 M=1,NPOL
    IF(SKIPOL(M))GO TO 954
    WRITE(KOUT,953) L,M,(LQIO(L,M,MON),MON=1,KSEA)
953 FORMAT('0 EMISSION RATE FROM LINE SOURCE',I4,2X,'OF POLLUTANT',I
    & 4,2X,'IN GRAMS/M/SEC'/(8(1PE15.4)))
954 CONTINUE
955 CONTINUE
111 DO 11 I=1,NG
    CALL FRXTRN(STNFRD(I),YEAR,FRACT,AVRATE,KSEA)
    DC 11 MON=1,KSEA
    GRATE(I,MON)=AVRATE(MON)
    GFRACT(I,MON)=FRACT(MON)
11 CONTINUE
C*** V(M)=FALLOUT DEPOSITION VELOCITY OF POLLUTANT M IN METERS/SEC
C*** CLAMDA(M)=WASHCUT COEFFICIENT OF POLLUTANT M IN SEC(-1)
    IF(NWS.EQ.0) GO TO 1010
    WRITE(KOUT,160)
    DO 1000 N=1,NWS
        NN=NA-NWS+N
        WRITE(KOUT,990) NN,N,ANAME(NN)
990 FORMAT('0 AREA SOURCE',I4,2X,'=',2X,'WINDBLOWN SOURCE',I4,2X,A8)
1000 CONTINUE

```

04 28 75



```

C*****THE FOLLOWING LINES WERE ADDED SO THAT ALL READS ARE DON IN MAIN.
      READ (IN,960) (ITYPE(I),DEN(I),DSALT(I),DSUSP(I),I=1,NWS)
960    FORMAT(I10,3E10.0)
      WRITE(KOUT,965) (I,ITYPE(I),DEN(I),DSALT(I),DSUSP(I),I=1,NWS)
965    FORMAT(////'CINFORMATION FOR WINDELOWN SOURCE',I4//
+ (10X,'ITYPE=',I4,/10X,'DENSITY=',E12.4,2X,'GM/M**3'/
+10X,'SALTATION DIAMETER=',E12.4,2X,'METERS'/
+10X,'SUSPENSION DIAMETER=',E12.4,2X,'METERS'/))
      DO 967 K=1,NWS
      READ (IN,230) (CONCF(K,M),M=1,NPCL)
      WRITE(KOUT,970) K,(M,CONCF(K,M),M=1,NPCL)
970    FORMAT(10X,'CONCENTRATION FACTOR FOR WINDBLOWN SOURCE',I5//
+ (10X,'POLLUTANT',I5,1PE15.4/))
967    CCNTINUE
      READ (IN,230) (FDRY(MON),MON=1,KSEA)
      WRITE(KOUT,975) (MON,FDRY(MON),MON=1,KSEA)
975    FORMAT(10X,'FRACTION OF TIME SOURCE REMAINS DRY DURING'/
+ (10X,'SEASON',I5,2X,'=',F10.5))
      READ (IN,230) (SSCON(I),I=1,NWS)
      WRITE(KOUT,980) (I,SSCON(I),I=1,NWS)
980    FORMAT(//10X,'SUSPENSION TO SALTATION RATIOS FOR SOURCE'
+I4,2X,'=',E12.4,2X,'1/METER')
C*****THIS IS THE END OF THE ADDED LINES.
      CALL WINDSCE(WINDSD)
1010 CONTINUE
      READ (IN,1012) ICHO
1012 FORMAT(I5)
      IF (ICHC.EQ.2) GO TO 1013
      CALL DCAL(PKAPPA,QKAPPA,WINDSD,JSTAB,GRATE,GFRACT,
&ITYPE,DF1,DF2)
      GO TO 1011
1013 CALL MAXCON(PKAPPA,QKAPPA,WINDSD,JSTAB,GRATE,
1 GFRACT,ITYPE,DF1,DF2)
1011 RETURN
      END

```

04 28 75

04 28 75

04 28 75

```

BLOCK DATA
COMMON/C1/XM(50),SIGTAB(6,50),SIGMAX(7),V(5),DV(5),
1 CLAMDA(5),DLAMDA(10,14,5),NEIST,NSTAB
DIMENSION SIGTA1(6,19),SIGTA2(6,19),SIGTA3(6,12)
EQUIVALENCF (SIGTAB(1,1),SIGTA1(1,1)),(SIGTAB(1,20),
1 SIGTA2(1,1)),(SIGTAB(1,39),SIGTA3(1,1))
DATA NDIST/50/,NSTAB/6/
DATA SIGMAX/0.320E4,0.160E4,0.800E3,0.500E3,0.200E3,0.100E3/
DATA XM/
& 1.000E+00,2.000E+00,3.000E+00,4.000E+00,5.000E+00,
& 1.000E+01,1.500E+01,2.000E+01,2.500E+01,3.000E+01,
& 3.500E+01,4.000E+01,4.500E+01,5.000E+01,1.500E+02,
& 2.000E+02,3.000E+02,4.000E+02,5.000E+02,6.000E+02,
& 7.000E+02,8.000E+02,9.000E+02,1.000E+03,1.100E+03,
& 1.200E+03,1.300E+03,1.400E+03,1.600E+03,1.800E+03,
& 2.000E+03,2.500E+03,3.000E+03,3.500E+03,4.000E+03,
& 4.500E+03,5.000E+03,6.000E+03,7.000E+03,8.000E+03,
& 1.000E+04,1.500E+04,2.000E+04,3.000E+04,4.000E+04,
& 5.000E+04,6.000E+04,7.000E+04,8.000E+04,1.000E+05/
DATA SIGTA1/
& 7.963E-02,1.000E-01,1.070E-01,9.319E-02,4.744E-02,1.924E-02,
& 1.752E-01,2.000E-01,2.025E-01,1.681E-01,8.856E-02,3.743E-02,
& 2.778E-01,3.000E-01,2.941E-01,2.374E-01,1.276E-01,5.524E-02,
& 3.854E-01,4.000E-01,3.832E-01,3.033E-01,1.653E-01,7.282E-02,
& 4.968E-01,5.000E-01,4.704E-01,3.668E-01,2.021E-01,9.021E-02,
& 1.093E+00,1.000E+00,8.900E-01,6.618E-01,3.773E-01,1.755E-01,
& 1.733E+00,1.500E+00,1.292E+00,9.346E-01,5.435E-01,2.590E-01,
& 2.404E+00,2.000E+00,1.684E+00,1.194E+00,7.042E-01,3.413E-01,
& 3.099E+00,2.500E+00,2.067E+00,1.444E+00,8.610E-01,4.229E-01,
& 3.813E+00,3.000E+00,2.445E+00,1.686E+00,1.015E+00,5.037E-01,
& 4.544E+00,3.500E+00,2.817E+00,1.923E+00,1.166E+00,5.841E-01,
& 5.290E+00,4.000E+00,3.186E+00,2.154E+00,1.313E+00,6.639E-01,
& 6.048E+00,4.500E+00,3.550E+00,2.382E+00,1.462E+00,7.434E-01,
& 6.818E+00,5.000E+00,3.912E+00,2.605E+00,1.607E+00,8.225E-01,
& 2.379E+01,1.500E+01,1.075E+01,6.638E+00,4.322E+00,2.361E+00,
& 3.300E+01,2.000E+01,1.400E+01,8.480E+00,5.600E+00,3.112E+00,
& 6.255E+01,3.129E+01,2.053E+01,1.198E+01,8.129E+00,4.593E+00,
& 9.847E+01,4.299E+01,2.694E+01,1.530E+01,1.059E+01,6.054E+00,
& 1.400E+02,5.500E+01,3.326E+01,1.850E+01,1.300E+01,7.500E+00/
DATA SIGTA2/
& 2.113E+02,6.965E+01,3.951E+01,2.137E+01,1.493E+01,8.720E+00,
& 2.994E+02,8.505E+01,4.570E+01,2.414E+01,1.678E+01,9.904E+00,
& 4.047E+02,1.011E+02,5.184E+01,2.682E+01,1.857E+01,1.106E+01,
& 5.281E+02,1.178E+02,5.794E+01,2.944E+01,2.031E+01,1.219E+01,
& 6.696E+02,1.350E+02,6.400E+01,3.200E+01,2.200E+01,1.330E+01,
& 9.152E+02,1.562E+02,6.962E+01,3.421E+01,2.345E+01,1.430E+01,
& 1.217E+03,1.785E+02,7.517E+01,3.636E+01,2.486E+01,1.527E+01,
& 1.583E+03,2.017E+02,8.068E+01,3.846E+01,2.623E+01,1.623E+01,
& 2.018E+03,2.259E+02,8.613E+01,4.050E+01,2.756E+01,1.717E+01,
& 3.126E+03,2.772E+02,9.690E+01,4.448E+01,3.014E+01,1.900E+01,
& 4.599E+03,3.319E+02,1.075E+02,4.830E+01,3.261E+01,2.077E+01,
& 6.500E+03,3.900E+02,1.180E+02,5.200E+01,3.500E+01,2.250E+01,
& 1.844E+04,6.131E+02,1.421E+02,6.022E+01,3.991E+01,2.506E+01,
& 4.321E+04,8.874E+02,1.653E+02,6.789E+01,4.443E+01,2.736E+01,
& 8.880E+04,1.213E+03,1.879E+02,7.514E+01,4.864E+01,2.947E+01,
& 1.657E+05,1.590E+03,2.100E+02,8.203E+01,5.262E+01,3.143E+01,

```



```

& 2.873E+05,2.019E+03,2.316E+02,8.864E+01,5.639E+01,3.327E+01,
& 4.700E+05,2.500E+03,2.528E+02,9.500E+01,6.000E+01,3.500E+01,
& 1.925E+06,3.818E+03,2.942E+02,1.052E+02,6.576E+01,3.782E+01/
DATA SIGTA3/
& 6.340E+06,5.461E+03,3.345E+02,1.147E+02,7.105E+01,4.038E+01,
& 1.781E+07,7.445E+03,3.738E+02,1.236E+02,7.598E+01,4.274E+01,
& 1.000E+08,1.250E+04,4.500E+02,1.400E+02,8.500E+01,4.700E+01,
& 4.300E+09,3.835E+04,6.161E+02,1.750E+02,9.884E+01,5.422E+01,
& 6.200E+10,8.499E+04,7.700E+02,2.050E+02,1.100E+02,6.000E+01,
& 2.666E+12,2.415E+05,1.003E+03,2.479E+02,1.254E+02,6.645E+01,
& 3.844E+13,5.066E+05,1.210E+03,2.837E+02,1.376E+02,7.145E+01,
& 3.046E+14,9.000E+05,1.400E+03,3.150E+02,1.479E+02,7.558E+01,
& 1.653E+15,2.357E+06,1.558E+03,3.480E+02,1.569E+02,7.913E+01,
& 6.906E+15,5.321E+06,1.705E+03,3.786E+02,1.649E+02,8.227E+01,
& 2.383E+16,1.077E+07,1.843E+03,4.072E+02,1.721E+02,8.508E+01,
& 1.889E+17,3.500E+07,2.100E+03,4.600E+02,1.850E+02,9.000E+01/
END

```

```

SUBROUTINE GROMET(KTAG)
C      PROGRAM CALCULATES GEOMETRIC VARIABLES FOR POINT AND AREA
      IMPLICIT REAL*4 (A-H,O-Z)
      LOGICAL SKIP, SKIPA, SKIPL, SKIPG, SKIPOL
      COMMON/C3/PI, P, KOUT
      COMMON/C4/DE(10,10), DA(10,10), DIRP(10,10), DIRA(10,10), AREA(10)
      COMMON/C5/DTH(10,10), R1(10,10), R2(10,10), TH1(10,10), TH2(10,10)
      COMMON/C8/NG, NP, NA, NL, NWS, NPOL, NFSTAB, NWINDS, WW, WF, FDRY(14)
      COMMON/C11/GTHA(10), GPHI(10), PTHA(10), PPHI(10), ATHA(10), APHI(10)
      COMMON/C15/SKIP(10), SKIPA(10), SKIPL(10), SKIPG(10), SKIPOL(10)
      COMMON/C18/COMP(32), F(32,10,20)
      IF(NP.EQ.0) GO TO 1901
      DO 189 I=1, NG
      IF(SKIPG(I))GO TO 189
      DO 190 J=1, NP
      IF(SKIPG(J))GO TO 190
      IF(ABS(GTHA(I)-PTHA(J)).GT. 0.0524) GO TO 1601
      IF(ABS(GPHI(I)-PPHI(J)).GT. 0.0524) GO TO 1601
      DP(I,J)=R*SQRT((GTHA(I)-PTHA(J))**2+COS(GTHA(I))*COS(PTHA(J))*(GPHI(I)-PPHI(J))**2)
      GO TO 1602
1601 DP(I,J)=R*ARCCOS(COS(GTHA(I))*COS(PTHA(J))*COS(GPHI(I)-PPHI(J))+SIN
      &(GTHA(I))*SIN(PTHA(J)))
1602 T1P=(GPHI(I)-PPHI(J))
      T2P=PTHA(J)-GTHA(I)
      IF(T1P.NE.0.0 .OR. T2P.NE.0.0)GO TO 164
      WRITE(KOUT,163)
163  FORMAT(1X,'*****SAMPLING POINT MAY NOT COINCIDE WITH POINT SOURCE'
      &*****')
      CALL ERROR
164  DIRP(I,J)=180.*ARCCOS((SIN(PTHA(J))-COS(DE(I,J)/P)
      +SIN(GTHA(I)))/(SIN(DE(I,J)/R)*COS(GTHA(I)))/PI
      IF(SIN(GPHI(I)-PPHI(J)).LT.0.) DIRP(I,J)=360.-DIRP(I,J)
      IF(KTAG.EQ.2)GO TO 190
      WRITE(KOUT,170) I,J,DP(I,J)
170  FORMAT(10X,'DISTANCE IN METERS FROM GAUGE',I3,1X,'TO POINT SOURCE'
      &,I3,1X,'=',E10.3,/)
      WRITE(KOUT,180) I,J,DIRP(I,J)
180  FORMAT(10X,'DIRECTION IN DEG. CW FROM NORTH FROM GAUGE',I3,1X,'TO
      &POINT SOURCE',I3,1X,'=',E10.3,/)
190  CONTINUE
189  CONTINUE
1901  CONTINUE
      IF(NA.EQ.0) GO TO 431
      DO 221 I=1, NG
      IF(SKIPG(I))GO TO 221
      DO 220 K=1, NA
      IF(SKIPA(K))GO TO 220
      IF(ABS(GTHA(I)-ATHA(K)).GT. 0.0524) GO TO 1902
      IF(ABS(GPHI(I)-APHI(K)).GT. 0.0524) GO TO 1902
      DA(I,K)=R*SQRT((GTHA(I)-ATHA(K))**2+COS(GTHA(I))*COS(ATHA(K))*(GPHI(I)-APHI(K))**2)
      GO TO 1903
1902 DA(I,K)=R*ARCCOS(COS(GTHA(I))*COS(ATHA(K))*COS(GPHI(I)-APHI(K))+SIN
      &(GTHA(I))*SIN(ATHA(K)))
1903 T1A=(GPHI(I)-APHI(K))

```



```

T2A=ATHA(K)-GTHA(I)
IF(T1A.NE.0.0 .OR. T2A.NE.0.0)GO TO 194
WRITE(KOUT,193)
193 FORMAT(10X,'SAMPLING POINT COINCIDES WITH AREA SOURCE CENTROID')
DA(I,K)=1.0E-5
GO TO 220
194 DIRA(I,K)=180.*ARCOS((SIN(ATHA(K))-COS(DA(I,K)/R)
+*SIN(GTHA(I)))/(SIN(DA(I,K)/R)*COS(GTHA(I)))/PI
IF(SIN(GPHI(I)-APHI(K)).LT.0.) DIRA(I,K)=360.-DIRA(I,K)
IF(KTAG.EQ.2) GO TO 220
WRITE(KOUT,200) I,K,DA(I,K)
200 FORMAT(10X,'DISTANCE IN METERS FROM GAUGE',I3,1X,'TO AREA SOURCE',
&I3,1X,'=',E10.3,/)
WRITE(KOUT,210) I,K,DIRA(I,K)
210 FORMAT(10X,'DIRECTION IN DEG. CW FROM NORTH FROM GAUGE',I3,1X,'TO
&AREA SOURCE',I3,1X,'=',E10.3,/)
220 CONTINUE
221 CONTINUE
DO 282 I=1,NG
IF(SKIPG(I))GO TO 282
DO 281 K=1,NA
IF(SKIPA(K))GO TO 281
DTH(I,K)=SQRT(AREA(K))/DA(I,K)
DTH(I,K)=DTH(I,K)*180./PI
IF(DTH(I,K).GE.114.591) GO TO 260
R1(I,K)=DA(I,K)-SQRT(AREA(K))/2.
R2(I,K)=DA(I,K)+SQRT(AREA(K))/2.
TH1(I,K)=DIRA(I,K)-DTH(I,K)/2.
TH2(I,K)=DIRA(I,K)+DTH(I,K)/2.
GO TO 275
260 DTH(I,K)=AREA(K)/(2.0*DA(I,K)**2)
DTH(I,K)=DTH(I,K)*180./PI
IF(DTH(I,K).GE.360.) GO TO 270
TH1(I,K)=DIRA(I,K)-DTH(I,K)/2.
TH2(I,K)=DIRA(I,K)+DTH(I,K)/2.
DIS=2.0*DA(I,K)
R1(I,K)=0.
R2(I,K)=DIS
IF(KTAG.EQ.2) GO TO 280
WRITE(KOUT,290) I,K,DTH(I,K),DIS
290 FORMAT(//,10X,'ANGULAR SPREAD(GREATER THAN 2 RADIANS) FROM GAUGE',
&I3,1X,'TO AREA',I3,1X,'=',E10.3,/,10X,'R1=0.0 R2=',1X,E10.3)
GO TO 280
270 DISP=SQRT(AREA(K)/PI)
R1(I,K)=0.
R2(I,K)=DISP
TH1(I,K)=0.0
TH2(I,K)=0.0
IF(KTAG.EQ.2) GO TO 280
WRITE(KOUT,300) I,K,DISP
300 FORMAT(10X,'ANGULAR SPREAD =2*PI FROM GAUGE',I3,1X,'TO AREA',I3,
&,10X,'R1=0.0 R2=',1X,E10.3)
GO TO 280
275 IF(KTAG.EQ.2) GO TO 280
WRITE(KOUT,310) I,K,DTH(I,K),R1(I,K),R2(I,K)
310 FORMAT(//,10X,'ANGULAR SPREAD(LESS THAN 2 RADIANS) FROM GAUGE',I3,
&I3,1X,'TO AREA',I3,1X,'=',E10.3,/,10X,'R1=',1X,E10.3,2X,'R2=',1X,E10.
&3)

```

```

280 TH1(I,K)=TH1(I,K)+11.25
    TH2(I,K)=TH2(I,K)+11.25
    IF (TH2(I,K).LT.0.0) TH2(I,K)=TH2(I,K)+360.
    IF (TH1(I,K).LT.0.0) TH1(I,K)=TH1(I,K)+360.
281 CONTINUE
282 CONTINUE
C*** ID=IDENTIFIER FOR THE SIXTEEN CARDINAL COMPASS POINTS
C*** ID=1=NORTH, ID=2=NORTH NORTH EAST, ETC.
C*** FOR PLACEMENT OF THE TRANSFORMED AREA INTO THE PROPER SECTORS, WE
C*** GO AROUND THE CIRCLE TWICE (ID=1,32)
C*** F(ID,I,K)=FRACTION OF SECTOR ID OCCUPIED BY THE TRANSFORMED AREA
C*** SEGMENT FROM GAUGE I TO AREA SOURCE K.
DO 330 ID=1,32
    COMP(ID)=22.5*ID
    DO 330 I=1,NG
        DO 330 K=1,NA
            F(ID,I,K)=0.0
330 CONTINUE
    DO 386 I=1,NG
        IF (SKIPG(I)) GO TO 386
        DO 385 K=1,NA
            IF (SKIPA(K)) GO TO 385
            DO 380 ID=1,32
                IF (DTH(I,K).GE.360.) GO TO 378
                IF (COMP(ID).GT.TH1(I,K)) GO TO 350
                GO TO 380
350 IF (COMP(ID).GT.TH2(I,K)) GO TO 360
                GO TO 370
360 F(ID,I,K)=1.0
                GO TO 385
370 F(ID,I,K)=(COMP(ID)-TH1(I,K))/22.5
                ID1=ID+1
                IF (ID1.GT.31) GO TO 385
                DO 375 IDP=ID1,32
                    IDS=IDP-1
                    IF (COMP(IDP).GT.TH2(I,K)) GO TO 372
                    F(IDP,I,K)=1.0
                    GO TO 375
372 F(IDP,I,K)=(TH2(I,K)-COMP(IDS))/22.5
                    GO TO 385
375 CONTINUE
378 F(ID,I,K)=1.0
380 CONTINUE
385 CONTINUE
386 CONTINUE
    DO 396 I=1,NG
        IF (SKIPG(I)) GO TO 396
        DO 394 K=1,NA
            IF (SKIPA(K)) GO TO 394
            DO 390 ID=17,32
                IDT=ID-16
                FTEST=F(IDT,I,K)**2
                IF (FTEST.LT.1.0E-10) F(IDT,I,K)=F(ID,I,K)
390 CONTINUE
394 CONTINUE
396 CONTINUE
    IF (KTAG.EQ.2) GO TO 431
    WRITE(KOUT,400)

```

04 28 75

04 24 75

04 24 75

04 24 75

04 24 75

04 24 75

04 24 75

04 24 75

04 24 75



```

400 FORMAT('0',10X,'SECTOR FRACTIONS FOR AREA SOURCES',/'0')
DO 430 I=1,NG
IF(SKIPG(I))GO TO 430
DO 426 K=1,NA
IF(SKIPA(K))GO TO 426
WRITE(KOUT,410) I,K
410 FORMAT('0',10X,'SECTOR FRACTIONS FOR GAUGE',I3,1X,'AND AREA SOURCE
&',I3,/)
DO 424 ID=1,16
FTEST2=DIH(I,K)/22.5
TEST3=F(ID,I,K)
IF(FTEST2.GE.1.0) FIEST2=1.0
IF(TEST3.GE.1.0) F(ID,I,K)=FTEST2
C***** 02 08 76
WRITE(KOUT,420) ID,F(ID,I,K)
420 FORMAT(10X,'FRACTION FOR SECTOR',I3,1X,'=',F10.5)
424 CONTINUE
426 CONTINUE
430 CONTINUE
431 RETURN
END

```

04 24 75  
04 24 75  
04 24 75

04 24 75

04 24 75  
04 24 75

```

SUBROUTINE DCAL(PKAPPA,QKAPPA,WINDSE,JSTAB,GRATE,GFRACT,
8 IPTYPE,DF1,DF2)
LOGICAL SKIP,SKIPA,SKIPL,SKIPG,SKIPOL
REAL*4 LSTHA,LFTHA,LSEHI,LFPHI
REAL*4 LQIO
REAL*8 ATITLE,SEANAM,GNAME,PNAME,ANAME,LNAME,PCINAM
DIMENSION PKAPPA(10),WINDSE(8),JSTAB(7)
DIMENSION GRATE(10,14),GFRACT(10,14),IPTYPE(5),DF1(5),DF2(5)
DIMENSION QKAPPA(10)
COMMON/C1/XM(50),SIGTAB(6,50),SIGMAX(7),V(5),DV(5),
1 CLAMDA(5),DLAMDA(10,14,5),NDIST,NSTAB
COMMON/C2/H
COMMON/C3/PI,R,KOUT
COMMON/C4/DP(10,10),DA(10,10),DIRP(10,10),DIRA(10,10),AREA(10)
COMMON/C5/DTH(10,10),R1(10,10),R2(10,10),TH1(10,10),TH2(10,10)
COMMON/C6/FRFQ(14,7,8,16),HGT(10),PCIO(10,5,14),
1 AQIO(10,5,14),LQIO(10,5,14)
COMMON/C7/DEPP(10,5,14),DEPA(10,5,14),DEPL(10,5,14)
COMMON/C8/NG,NP,NA,NL,NWS,NPOL,NPSTAB,NWINDS,WW,WF,EDRY(14)
COMMON/C9/DEPT(10,5,14),DRYDEP(10,5,14),WETDEP(10,5,14)
COMMON/C10/LSTHA(5),LFTHA(5),LSEHI(5),LFPHI(5)
COMMON/C11/GTHA(10),GPHI(10),PTHA(10),PPhi(10),ATHA(10),APHI(10)
COMMON/C12/WQIO(3,5,8),VFALL(3)
COMMON/C13/HGA(10),HGL(5)
COMMON/C14/KDISP,KCOVER,ROUGH
COMMON/C15/SKIP(10),SKIPA(10),SKIPL(10),SKIPG(10),SKIPOL(10)
COMMON/C16/MOB,MOE,KSEA
COMMON/C17/SURF(10)
COMMON/C18/COMP(32),F(32,10,20),ATITLE(10),SEANAM(14),GNAME(10),
1 PNAME(10),ANAME(10),LNAME(10),PCINAM(5)
DIMENSION COPP(10,5,14),CCPA(10,5,14),COPL(10,5,14),COPT(10,5,14)
DEPP(I,M,MON)=DEPOSITION RATE IN GRAMS/METER**2/SEC FOR POLLUTANT
C** M,AT SAMPLING POINT I, DURING MONTH MON
C** IT1=1 FOR WETFALL CALL IN QQP, IT2=2 FOR DRYFALL CALL IN QQP
C** IT1=1
C** IT2=2
CALL FALL(V,DV,IPTYPE,DF1,DF2,JSTAB)
CALL WASH(IPTYPE,DF1,DF2,GRATE,CLAMDA)
C***SURF(N) SPECIFIES SURFACE CONDITIONS AT THE RECEPTOR
C***UNLESS EXPLICITLY OVERRIDDEN VALUES DEFAULT TO KCOVER
DC 983 I=1,NG
983 SURF(I)=KCOVER
IKPM=1
DO 984 I=1,NG
DO 984 M=1,NPOL
DO 984 MON=1,KSEA
DEPP(I,M,MON)=0.
DEPA(I,M,MON)=0.
DEPL(I,M,MON)=0.
WETDEP(I,M,MON)=0.
DRYDEP(I,M,MON)=0.
COPP(I,M,MON)=0.0
COPA(I,M,MON)=0.0
COPL(I,M,MON)=0.0
COPT(I,M,MON)=0.0
984 CONTINUE

```



```

IF(NF.EQ.0) GO TO 1091
DO 1060 I=1,NG
IF(SKIPG(I))GO TO 1060
DO 1050 MON=1,KSEA
TSEA=MON
DO 1040 M=1,NPCI
IF(SKIPOL(M))GO TO 1040
C*** WW=WASHOUT WEIGHT,THE FRACTIONAL AMOUNT OF TIME DURING WHICH BOTH
C*** WASHOUT AND FALLOUT OCCURS
C*** WF=FALLOUT WEIGHT,FRACTIONAL AMOUNT OF TIME DURING WHICH ONLY
C*** FALLOUT OCCURS
WW=GFACT(I,MON)
WF=1.0-WW
CLAMDA(M)=DLAMDA(I,MON,M)
997 DO 1030 J=1,NP
IF(SKIPP(J))GO TO 1030
FAC1=PQIO(J,M,MON)/DP(I,J)
FACWET=2.543*CLAMDA(M)*WW*FAC1
DO 1020 II=1,NFSTAB
SMA=SIGMA(JSTAB(II),DP(I,J),IKPM,F)
FACDRY=2.032*FAC1/SMA
FACEXP=-0.5/SMA**2
DO 1010 JJ=1,NWINDS
IF(JSTAB(II).GT.4) GO TO 998
H=HGT(J)+PKAPPA(J)/WINDSD(JJ)
GO TO 999
998 H=HGT(J)+QKAPPA(J)/((WINDSD(JJ))**.3333333)
999 CONTINUE
IF(H.GT.1500.0) H=1500.0
HH = H
IF(IPTYPE(M).EQ.2)GO TO 75
C THE PLUME WILL TILL FOR HEAVY PARTICLES
HH=H-V(M)*DP(I,J)/WINDSD(JJ)
IF(HH.LT.0.0) HH=0.0
75 CONTINUE
QQP1=QQP(JSTAB(II),M,DP(I,J),WINDSD(JJ),IT1,IPTYPE(M),I,KCOVER)
QQP2=QQP(JSTAB(II),M,DP(I,J),WINDSD(JJ),IT2,IPTYPE(M),I,KCOVER)
DTST=DIRP(I,J)+11.25
IF(DTST.GT.360.) DTST=DTST-360.
DTST=DTST/22.51
KK=DTST
KK=KK+1
FREQW=FREQ(MON,II,JJ,KK)/WINDSD(JJ)
DRY=FREQW*QQP2*FACDRY*EXP(FACEXP*HH**2)
COPP(I,M,MON)=COPP(I,M,MON) + DRY
DRY=DRY*WF*SUFF(I)*DV(M)
WET=FREQW*QQP1*FACWET
DEPP(I,M,MON)=DEPP(I,M,MON)+DRY+WET
DRYDEP(I,M,MON)=DRYDEP(I,M,MON)+DRY
WETDEP(I,M,MON)=WETDEP(I,M,MON)+WET
1010 CONTINUE
1020 CONTINUE
1030 CONTINUE
1040 CONTINUE
1050 CONTINUE
1060 CONTINUE
DO 1080 M=1,NPOL
IF(SKIECL(M))GO TO 1080

```

03 23 73

05 24 73

05 24 73

05 07 75

05 07 75

03 28 73

05 07 75

05 07 75

07 18 74

05 22 74

05 22 74

05 22 74

05 22 74

05 07 75

05 07 75

05 07 75

05 07 75

10 01 73

10 01 73

10 01 73

```

WRITE(KOUT,1094)M,POLNAM(M)
1094 FORMAT('1 POLLUTANT',I3,' ',A8,5X,
1 'POINT SOURCE DEPOSITION RATE (GM/M**2/SEC) ')
WRITE(KOUT,1090) (SEANAM(MCN),MON=1,KSEA)
1090 FORMAT('0 GAGE POL',12(2X,A8)/10X,(12(2X,A8)))
DO 1081 I=1,NG
IF(SKIPG(I))GO TO 1081
WRITE(KOUT,1092) I,M,(DEPP(I,M,MCN),MON=1,KSEA)
1092 FORMAT(2I5,12(1PE10.3)/10X,(12(1PE10.3)))
1081 CONTINUE
WRITE(KOUT,1095)
1095 FORMAT(30X,'PCINT SOURCE INCREMENT TO CONCENTRATION (G/M**3) ')
DO 1082 I=1,NG
IF(SKIPG(I))GO TO 1082
WRITE(KOUT,1092) I,M,(COFF(I,M,MCN),MON=1,KSEA)
1082 CONTINUE
1080 CONTINUE
C** * DEPA(I,M,MON)=DEPOSITION RATE IN GRAMS/MEIER**2/SEC FOR POLLUTANT
C** * M,AT SAMPLING PCINT I,DURING MONTH MON, FOR ALL AREA SOURCES
1091 IF(NA.EQ.0) GO TO 2121
PI8=PI/8.0
NDIFF=NA-NWS
DO 2080 I=1,NG
IF(SKIPG(I))GO TO 2080
DO 207C MON=1,KSEA
ISFA=MCN
WW=GPRACT(I,MON)
WP=1.0-WW
DO 2060 M=1,NPOL
IF(SKIPOL(M))GO TO 2060
CLAMDA(M)=DLAMDA(I,MON,M)
DO 2050 K=1,NA
IF(SKIPA(K))GO TO 2050
KW=K-NWS
H=HGA(K)
DELA=(F2(I,K)-R1(I,K))/3.
DELAPA=DELA*PI8*AQIO(K,M,MON)
FACWET=2.543*DELAPA*WW*CLAMDA(M)
DO 2040 MM=1,3
ADIS=R1(I,K)+MM*DELA-DELA/2.
DO 2030 II=1,NFSTAB
SMA=SIGMA(JSTAB(II),ADIS,IKPM,P)
DPAS=DELAPA/SMA
FACDRY=2.032*DPAS
FACFXP=-0.5/SMA**2
P=P+2.0
DO 2020 JJ=1,NWINDS
IF(K.GT.NDIFF) GO TO 2005
QQA1=QQP(JSTAB(II),M,ADIS,WINDSD(JJ),IT1,IPTYPE(M),I,KCOVER)
QQA2=QQP(JSTAB(II),M,ADIS,WINDSD(JJ),IT2,IPTYPE(M),I,KCOVER)
DO 2005 IF(K.GT.NDIFF) GO TO 2015
HH=H
IP(IPTYPE(M).EQ.2) GO TO 76
HH=H-V(M)*ADIS/WINDSD(JJ)
IF(HH.LT.0.0) HH=0.0
76 CONTINUE
QDRY=FACDRY*QQA2/WINDSD(JJ)*EXP(FACFXP*HH**2)
QWET=FACWET*QQA1/WINDSD(JJ)

```

05 07 75  
03 27 73

05 24 73  
05 24 73

05 24 73

06 14 73  
05 01 73  
09 12 73  
05 07 75  
05 07 75  
09 12 73  
06 15 73  
03 27 73  
05 07 75  
05 07 75  
05 07 75  
05 07 75

05 07 75  
05 07 75  
05 07 75

05 07 75



```

DO 2010 KK=1,16
FFREQ=F(KK,I,K)*FREQ(MON,II,JJ,KK)
DRY=FFREQ*QDRY
COPA(I,M,MON)=COPA(I,M,MON)+DRY
DRY=DRY*WF*SURF(I)*DV(M)
WET=FFREQ*QWET
DEPA(I,M,MON)=DEPA(I,M,MON)+DRY+WET
DRYDEP(I,M,MON)=DRYDEP(I,M,MON)+DRY
WETDEP(I,M,MON)=WETDEP(I,M,MON)+WET
2010 CONTINUE
GO TO 2020
2015 DO 2017 KK=1,16
DRY=(1.016*WQIO(KW,M,JJ)*F(KK,I,K)*FREQ(
&ISEA,II,JJ,KK)*FDRY(ISEA)*DELA*(PI/8.)*VFALL(KW)/(SMA*WINDSD(JJ)))
&*EXP(-(VFALL(KW)/WINDSD(JJ))*ADIS-HH)**2/(2.*SMA**2))*{2.-2./
& ((1.-0.5*D)*(WINDSD(JJ)*HH/(ADIS*VFALL(KW))-1.))+2.))
COPA(I,M,MON)=COPA(I,M,MON)+(DRY/VFALL(KW))
WET=0.
DRYDEP(I,M,MON)=DRYDEP(I,M,MON)+DRY
DEPA(I,M,MON)=DEPA(I,M,MON)+DRY
2017 CONTINUE
2020 CONTINUE
2030 CONTINUE
2040 CONTINUE
2050 CONTINUE
2060 CONTINUE
2070 CONTINUE
2080 CONTINUE
DO 1180 M=1,NPCL
IF(SKIPOL(M))GO TO 1180
WRITE(KOUT,1194)M,POLNAM(M)
1194 FORMAT('0 POLLUTANT',I3,' ', 'A8,5X,
1 'AREA SOURCE DEPOSITION RATE (GM/M**2/SEC)')
DO 1181 I=1,NG
IF(SKIPG(I))GO TO 1181
WRITE(KOUT,1092)I,M,(DEPA(I,M,MON),MON=1,KSEA)
1181 CONTINUE
WRITE(KOUT,1096)
1096 FORMAT(30X,'AREA SOURCE INCREMENT TO CONCENTRATION (G/M**3)')
DO 1182 I=1,NG
IF(SKIPG(I))GO TO 1182
WRITE(KOUT,1092)I,M,(COPA(I,M,MON),MON=1,KSEA)
1182 CONTINUE
1180 CONTINUE
C*** DEPL(I,M,MON)=DEPOSITION RATE IN GRAMS/METER**2/SEC FOR POLLUTANT
C*** M,AT SAMPLING POINT I, DURING MONTH MON, FOR ALL LINE SOURCES
2121 IF(NL.EQ.0) GO TO 3125
DO 3100 I=1,NG
IF(SKIPG(I))GO TO 3100
DO 3080 MON=1,KSEA
ISEA=MON
WW=GFRACT(I,MON)
WF=1.0-WW
DO 3070 M=1,NPCL
IF(SKIPOL(M))GO TO 3070
CLAMDA(M)=DLAMDA(I,MON,M)
DO 3060 L=1,NL
IF(SKIPL(L))GO TO 3060

```

```

H=HGL(I)
DD=R*SQRT((LSTHA(L)-LFTHA(L))**2+COS(LSTHA(L))*COS(LFTHA(L))*(LFPH03 05 01 73
EI(L)-LSEPHI(L))**2) 03 23 73
DD=DD/10. 03 23 73
DTHL=(LFTHA(L)-LSTHA(L))/10. 03 23 73
DPHL=(LFPHI(L)-LSPHI(L))/10. 03 23 73
DO 3050 NN=1,10 03 23 73
THAL=LSTHA(L)+(NN-1)*DTHL+DTHL/2. 03 23 73
PHIL=LSPHI(L)+(NN-1)*DPHL+DPHL/2. 03 23 73
DL=P*SQRT((GTHA(I)-THAL)**2+COS(GTHA(I))*COS(THAL)*(GPHI(I)-PHIL)*03 23 73
S*2) 03 23 73
FAC1=DD/DL*LQIO(L,M,MON) 05 07 75
FACWET=FAC1*2.543*CLAMDA(M)*WW 05 07 75
T1L=(GPHI(I)-PHIL) 09*15*75
T2L=THAL-GTHA(I) 03 23 73
IF(T1L.NE.0.0) GO TO 3040 03 23 73
IF(T2L.NE.0.0) GO TO 3040 03 23 73
WRITE(KCUT,3039) 03 23 73
3039 FORMAT(///,10X,'*****SAMPLING POINT MAY NOT COINCIDE WITH LINE SOU03 23 73
PRCE****',///) 03 23 73
CALL FPROF 03 23 73
3040 CONTINUE 03 23 73
DIRL=180.*ARCOS((SIN(THAL)-COS(DL/P)
+*SIN(GTHA(I)))/(SIN(DL/R)*COS(GTHA(I))))/PI 09*15*75
IF(SIN(GPHI(I)-PHIL).LT.C.) DIRL=360.-DIRL 09*15*75
DTSTL=DIRL+11.25 03 23 73
IF(DTSTL.GT.360.) DTSTL=DTSTL-360. 03 23 73
DTSTL=DTSTL/22.51 03 23 73
KK=DTSTL 03 23 73
KK=KK+1 03 23 73
DO 3030 II=1,NFSTAB 03 23 73
SMA=SIGMA(JSTAB(II),DL,IKFM,P) 03 28 73
FACDRY=FAC1/SMA*2.032 05 07 75
FACEXP=-0.5/SMA**2 05 07 75
DO 3020 JJ=1,NWINDS
HH=H
IF(IPTYPE(M).EQ.2) GO TO 78
HH=H-V(M)*DL/WINDSD(JJ)
78 CONTINUE
QQL1=QCP(JSTAB(II),M,DL,WINDSD(JJ),IT1,IPTYPE(M),I,KCOVER) 05 07 75
QQL2=QCP(JSTAB(II),M,DL,WINDSD(JJ),IT2,IPTYPE(M),I,KCOVER) 05 07 75
FACFW=FREQ(MON,II,JJ,KK)/WINDSD(JJ) 05 07 75
DRY=FACFW*FACDRY*QQL2*EXP(FACEXP*HH**2)
COPL(I,M,MON)=COPL(I,M,MON)+DRY
DRY=DRY*WF*SURF(I)*DV(M)
WET=FACFW*FACWET*QQL1 05 07 75
DEPL(I,M,MON)=DEPL(I,M,MON)+WET+DRY 10 01 73
DRYDEP(I,M,MON)=DRYDEP(I,M,MON)+DRY 10 01 73
WETDEP(I,M,MON)=WETDEP(I,M,MON)+WET 10 01 73
3020 CONTINUE 03 23 73
3030 CONTINUE 03 23 73
3050 CONTINUE 03 23 73
3060 CONTINUE 03 23 73
3070 CONTINUE 03 23 73
3080 CONTINUE 03 23 73
3100 CONTINUE 03 23 73
DO 1280 M=1,NPOL
IF(SKIPOL(M)) GO TO 1280

```



```

      WRITE(KOUT,1294)M,POLNAM(M)
1294 FORMAT('O POLLUTANT',I3,' ', 'A8,5X,
1 'LINE SOURCE DEPOSITION RATE (GM/M**2/SEC)')
      DO 1281 I=1,NG
      IF(SKIPG(I))GO TO 1281
      WRITE(KOUT,1092)I,M,(DEPL(I,M,MON),MON=1,KSEA)
1281 CONTINUE
      WRITE(KOUT,1097)
1097 FORMAT(30X,'LINE SOURCE INCREMENT TO CONCENTRATION (G/M**3)')
      DO 1282 I=1,NG
      IF(SKIPG(I))GO TO 1282
      WRITE(KOUT,1092)I,M,(COPL(I,M,MON),MON=1,KSEA)
1282 CONTINUE
1280 CONTINUE
C**1 DEPT(I,M,MON) =DEPOSITION RATE(TOTAL) IN GRAMS/METER**2/SEC FOR
C**2 POLLUTANT M, AT SAMPLING PCINT I, DURING MONTH MON
3125 WRITE(KOUT,2200)ATITLE
2200 FORMAT('1 ',10A8)
      DO 2175 M=1,NPCL
      IF(SKIPOL(M))GO TO 2175
      WRITE(KOUT,2201)M,POLNAM(M)
2201 FORMAT('O POLLUTANT',I3,' ', 'A8/
1 'ORAGE POL PERIOD',12X,'DRYDEP',9X,'WETDEP',8X,'TOTAL DEP',
2 11X,'CONC',30X,'G/M**2/SEC',5X,'G/M**2/SEC',5X,'G/M**2/SEC',
3 9X,'G/M**3')
      DO 2176 I=1,NG
      IF(SKIPG(I)) GO TO 2176
      WRITE(KOUT,2)
2 FORMAT('O ')
      DO 217 MON=1,KSEA
      DEPT(I,M,MON)=DEPP(I,M,MON)+DEPA(I,M,MON)+DEPL(I,M,MON)
      COPT(I,M,MON)=COPP(I,M,MON)+COPA(I,M,MON)+COPL(I,M,MON)
      WRITE(KOUT,2185) I,M,MON,SEANAM(MCN),DRYDEP(I,M,MON),
1 WETDEP(I,M,MON),DEPT(I,M,MON),COPT(I,M,MON)
2185 FORMAT(3I5,2X,A8,4(1PE15.3))
217 CONTINUE
2176 CONTINUE
2175 CONTINUE
      RETURN
      END

```

10 02 73

05 24 73

03 21 75

10 02 73

```

SUBROUTINE PRXTRN(I, YEAR, FRACT, AVRATE, KSEA)
  DIMENSION FRACT(14), AVRATE(14)
C FRACT IS THE FRACTION OF THE MONTH PRECIP OCCURS
C AVRATE IS THE AVERAGE RATE OF PRECIP IN HUNDRETHS
C   OF AN INCH PER HOUR
    DO 10 MONT=1, KSEA
      FRACT(MONT)=0.07
      AVRATE(MONT)=08.5
10 CONTINUE
  RETURN
  END

```

04 28 75

04 28 75



```

SUBROUTINE FALL(V,DV,IPTYPE,DF1,DF2,JSTAB)
REAL*4 MU/182.7E-6/,G/980.0/
REAL*4 KZ(7)/1.25,0.625,0.375,0.250,0.085,0.050,0.050/
DIMENSION V(5),DV(5),IPTYPE(5),DF1(5),DF2(5)
COMMON/C8/NG,NF,NA,NL,NWS,NPOL,NFSTAB,NWINDS,WW,WF,FDRY(14)
COMMON/C14/KDISP,KCOVER,ROUGH
C SUBROUTINE FALL CALCULATES THE TERMINAL VELOCITY OF PARTICLES
C AND THE DEPOSITION VELOCITY OF GASES.
C     VDEF IS THE DEFAULT DEPOSITION VELOCITY, NOT INCL. COVER
C     V(M) IS TERMINAL VELOCITY, DV(M) IS DEPOSITION VEL. INCL.
C     COVER, DVEFF=EFFECTIVE DEP. VEL. INCL. COVER
      GMU=G/(18.0*MU)
      VDEF=0.01
      DVEFF=KCOVER*VDEF
101 DO 100 M=1,NPOL
      IF(IPTYPE(M).EQ.2) GO TO 50
C CONVERT FROM MICRONS TO CM
      D=DF1(M)*1.0E-4
      V(M)=D**2*GMU*DF2(M)
C CONVERT FROM CM/SEC TO M/SEC
      V(M)=0.01*V(M)
      DV(M)=V(M)
      IF(DVEFF.GE.V(M)) DV(M)=VDEF
C V(M) IS A TERMINAL VELOCITY FOR PARTICLES AT THIS POINT.
      GO TO 100
50 CONTINUE
C TO CALCULATE THE DEPOSITION VELOCITY OF A GAS
C FROM THE SHEPPARD-PASQUILL DERIVATION, REMOVE C'S FROM THE
C THREE INSTRUCTIONS BELOW. ADD C TO THE FOURTH.
C     R=KZ(JSTAB)/DF2(M)
C     R=ALOG(R)
C     V(M)=KZ(JSTAB)/R
      V(M)=0.0
      DV(M)=VDEF
100 CONTINUE
      RETURN
      END

```

	SUBROUTINE MAXCON(PKAPPA,QKAPPA,WINDSD,JSTAB,GRATE,GFRACT,	06 04 75
8	IPTYPE,DF1,DF2)	
	LOGICAL SKIPP,SKIP,SKIPL,SKIPG,SKIPOL	04 21 75
	REAL*4 IQIO	
	DIMENSION PKAPPA(10),WINDSD(8),JSTAB(7),CP1(10,10)	05 05 75
	DIMENSION GRATE(10,14),GFRACT(10,14),IPTYPE(5),DF1(5),DF2(5)	05 24 73
	DIMENSION QKAPPA(10)	
	COMMON/C1/XM(50),SIGTAB(6,50),SIGMAX(7),V(5),DV(5),	
1	CLAMDA(5),DLAMDA(10,14,5),NEIST,NSTAB	
	COMMON/C2/H	
	COMMON/C3/PI,R,KOUT	04 28 75
	COMMON/C4/DP(10,10),DA(10,10),DIEP(10,10),DIRA(10,10),AREA(10)	
	COMMON/C6/FREQ(14,7,8,16),HGT(10),PQIO(10,5,14),	04 28 75
1	AQIO(10,5,14),LQIO(10,5,14)	04 28 75
	COMMON/C8/NG,NP,NA,NL,NWS,NPOL,NFSTAB,NWINDS,WW,WF,FDRY(14)	04 28 75
	COMMON/C9/DEPT(10,5,14),DRYDEP(10,5,14),WETDEP(10,5,14)	04 28 75
	COMMON/C15/SKIEP(10),SKIP(10),SKIPL(10),SKIPG(10),SKIPOL(10)	04 21 5
	COMMON/C16/MOE,MOE,KSEA	04 28 75
	CALL FALL(V,DV,IPTYPE,DF1,DF2,JSTAB)	
	IF(NP.EQ.0) GO TO 1091	03 23 73
	IKPM=1	09 12 73
	DO 984 I=1,10	
	DO 984 J=1,10	
984	CP1(I,J)=0.0	05 05 75
	DO 1070 I=1,NG	
	IF(SKIPG(I)) GO TO 1070	05 05 75
	DO 1060 M=1,NPOL	
	IF(SKIPOL(M)) GO TO 1060	05 05 75
	DO 1050 MON=1,KSEA	05 05 75
	DO 1040 JWD=1,360,5	
	DO 1030 JJ=1,NWINDS	
	DO 1020 II=1,NFSTAB	
	SUM=0.0	
	IQZ=JSTAB(II)	
	IF(JSTAB(II).GT.4) GO TO 998	
	H=HGT(J)+PKAPPA(J)/WINDSD(JJ)	
	GO TO 999	
998	H=HGT(J)+QKAPPA(J)/((WINDSD(JJ))**.3333333)	
999	CONTINUE	
	IF(H.GT.1500.0) H=1500.0	07 18 74
	HH=H	05 22 74
	IF(IPTYPE(M).EQ.2) GO TO 75	05 22 74
C THE	PLUME WILL NOW TILT FOR HEAVY PARTICLES	
	HH=H-V(M)*DIS2/WINDSD(JJ)	
	IF(HH.LT.0.0) HH=0.0	05 22 74
75	CONTINUE	05 22 74
	DO 1010 J=1,NP	
	IF(SKIPP(J)) GO TO 1010	05 05 75
	DIS=DP(I,J)	
	DIR=DIRP(I,J)	
	CALL SIGA(DIR,DIS,IQZ,SIGY,JWD,DIS2)	
	SMA=SIGMA(JSTAB(II),DIS2,IKPM,P)	
	DRY1=0.5*(HH/SMA)**2	
	IF(DRY1.GT.50.0) DRY1=50.0	
	DRY1=PQIO(J,M,MON)*SIGY*EXP(-DRY1)	
	DRY2=3.14*SMA*WINDSD(JJ)	



```

      TAX=DRY1/DRY2
      SUM=SUM+TAX
      IF (SUM.LE.CP1(I,M)) GO TO 1010
      CP1(I,M)=SUM
      LMON =MON
      LJWD=JWD
      LJJ=JJ
      LII=II
1010  CONTINUE
1020  CONTINUE
1030  CONTINUE
1040  CONTINUE
1050  CONTINUE
      WRITE(KOUT,1061) I,M
      WRITE(KOUT,1062) LMON
      WRITE(KOUT,1063) LJWD
      WRITE(KOUT,1064) WINDSD(LJJ)
      WRITE(KOUT,1065) LII
      WRITE(KOUT,1066) CP1(I,M)
1061  FORMAT(10X,'MAXIMUM HOURLY CONCENTRATION FOR GAUGE',
      &I4,1X,'AND POLLUTANT',I4,1X,'OCCURS DURING---',)
1062  FORMAT(10X,'MONTH',I5)
1063  FORMAT(10X,'WIND DIRECTION',I5)
1064  FORMAT(10X,'WIND SPEED',F10.3)
1065  FORMAT(10X,'STABILITY',I5)
1066  FORMAT(10X,'CONCENTRATION=',E10.3,'GMS/M**3')
1060  CONTINUE
1070  CONTINUE
1091  RETURN
      END

```

```

FUNCTION QQP(JSTAB,M,DIS,WIND,ISIG,IPTYPE,IGN,KCOVER)
DIMENSION XX(50),FX(50),AX(50)
COMMON/C1/XM(50),SIGTAB(6,50),SIGMAX(7),V(5),DV(5),
1 CLAMDA(5),DLAMDA(10,14,5),NDIST,NSTAB
COMMON/C2/H
COMMON/C3/PI,P,KOUT
COMMON/C17/SUPF(10)
NS=JSTAB
IF(NS.GT.6) NS=6
IKPM=1
SMA=SIGMA(NS,DIS,IKPM,P)
SQRTPI=SQRT(2.0/PI)*KCOVER
IKP=IKPM+1
DO 20 I=1,IKPM
XX(I)=XM(I)
HH = H -V(M)*XM(I)/WIND
IF(HH.LT.0.0) HH = 0.0
PX(I)=SQRTPI*EXP(-0.5*(HH/SIGTAB(NS,I))**2)/SIGTAB(NS,I)
20 CCNTINUE
XX(IKP)=DIS
PX(IKP)=SQRTPI*EXP(-0.5*(HH/SMA)**2)/SMA
L=1
CALL SIMPUN(XX,PX,IKP,L,AX)
IF(ISIG.EQ.1) GO TO 30
QQP=EXP(-(DV(M)*AX(IKP)/DIS)*(DIS/WIND))
GO TO 40
30 QQP=EXP(-(CLAMDA(M)+DV(M)*AX(IKP)/DIS)*(DIS/WIND))
40 RETURN
END

```

06 04 75

04 28 75

05 01 75

05 01 75

03 27 73

05 17 73



```

FUNCTION SIGMA(JSTAB,DIS,IKPM,P)
REAL*8 CONF,DCONE,CTWO,DTWO,RGH,ABS,YLAG
COMMON/C1/XM(50),SIGTAB(6,50),SIGMAX(7),V(5),DV(5),
      CLAMDA(5),DLAMDA(10,14,5),NDIST,NSTAB
COMMON/C14/KDISP,KCOVER,ROUGH
DIMENSION ACONE(6),BONE(6),ATWO(6),BTWO(6),CONE(6),DONE(6),
      CTWO(6),DTWO(6),RGH(6)
DATA ACONE/0.112,0.130,0.112,0.098,0.0609,0.0638/
DATA BONE/1.06,0.950,0.920,0.889,0.895,0.783/
DATA ATWO/5.38E-4,6.52E-4,9.05E-4,1.35E-3,1.96E-3,1.36E-3/
DATA BTWO/0.815,0.750,0.718,0.688,0.684,0.672/
DATA CCNF/1.56,2.02,2.72,5.16,7.37,11.7/
DATA DONE/0.0480,0.0269,0.,-0.060,-0.0957,-0.128/
DATA CTWO/6.25E-4,7.76E-4,0.,186.,4.29E+3,4.59E+4/
DATA DTWO/0.45,0.37,0.,-0.225,-0.60,-0.78/
DATA RGH/0.01,0.04,0.10,0.40,1.0,4.0/
P=0.0
NTYPE=JSTAB
IF(NTYPE.GT.6) NTYPE=6
DO 8 I=1,50
IKP=I
IF(XM(I).GT.DIS) GO TO 9
8 CONTINUE
9 IF(IKP.LT.2) IKP=2
IKPM=IKP-1
IF(KDISP.EQ.2) GO TO 50
C PASQUILL-GIFFORD DISPERSION VALUES
DO 10 I=1,IKPM
IKP=I+1
IF(SIGTAB(NTYPE,I).GT.SIGMAX(NTYPE)) GO TO 30
10 CONTINUE
P=ALOG(SIGTAB(NTYPE,IKP)/SIGTAB(NTYPE,IKPM))/ALOG(XM(IKP)/XM(IKPM))
8)
A=SIGTAB(NTYPE,IKP)/XM(IKP)**P
SIGMA=A*DIS**P
GO TO 40
C HOSKER'S FORMULATION OF BRIGGS-SMITH DISPERSION VALUES
50 ABS=ROUGH
C1=YLAG(ABS,RGH,CONE,0,3,6,0)
D1=YLAG(ABS,RGH,DONE,0,2,6,0)
C2=YLAG(ABS,RGH,CTWO,0,3,6,0)
D2=YLAG(ABS,RGH,DTWO,0,2,6,0)
G=ACONE(NTYPE)*DIS**BCONE(NTYPE)/(1.0+ATWO(NTYPE)*DIS**BTWO(NTYPE))
F=C1*(DIS**D1)
F=ALOG(F)
IF(ROUGH.LE.0.10) GO TO 60
F=F+ALOG(1.+1./(C2*DIS**D2))
GO TO 70
60 F=F-ALOG(1.+C2*DIS**D2)
70 SIGMA=G*F
IF(SIGMA.LT.1.0) SIGMA=1.0
40 IF(SIGMA.LT.SIGMAX(NTYPE)) GO TO 99
30 SIGMA=SIGMAX(NTYPE)
99 RETURN
END

```

```

SUBROUTINE SIGA(DIR,DIS,NTYPE,SIGY,JWD,DIS2)
REAL*4 C3(7)/0.22,0.16,0.11,0.08,0.06,0.04,0.04/
WD=JWD
A=DIP-WD
A=ABS(A)
ACID=360.0-A
IF(A.GE.270.0) A=ACID
IF(A.GT.90.0) GO TO 10
A=A*0.01745
Y=DIS*SIN(A)
DIS2=DIS*COS(A)
IF(DIS2.LT.1.0) GO TO 10
SIGY=DIS2*C3(NTYPE)/SQRT(1.0+0.0001*DIS2)
B=Y/SIGY
IF(B.GT.25.0) GO TO 10
B=B*2.0
IF(B.GT.50.0) GO TO 10
B=EXP(-B)
SIGY=B/SIGY
GO TO 11
10 SIGY=0.0
11 CONTINUE
RETURN
END

```

05 05 75  
05 05 75

05 05 75



```

      SUBROUTINE SIMPUN (XX,FX,NX,I,AX)
C   PROGRAM AUTHOR      J. BARISH,
C   COMPUTING TECHNOLOGY CENTER, UNION CARBIDE CORP., NUCLEAR DIV.,
C   OAK RIDGE, TENN.
C
      DIMENSION XX(2),FX(2),AX(2)
      IF (I.LT.0) GO TO 30
      AX(1)=0.0
      DO 10 IX=2,NX,2
          D1=XX (IX)-XX (IX-1)
          AX (IX)=AX (IX-1)+D1/2.0*(FX (IX)+FX (IX-1))
          IF (NX.EQ.IX) GO TO 20
          D2=XX (IX+1)-XX (IX-1)
          D3=D2/D1
          A2=D3/6.0*D2**2/(XX (IX+1)-XX (IX))
          A3=D2/2.0-A2/D3
      10  AX (IX+1)=AX (IX-1)+(D2-A2-A3)*FX (IX-1)+A2*FX (IX)+A3*FX (IX+1)
      20  RETURN
      30  AX (NX)=0.0
      DO 40 IX=2,NX,2
          IC=NX+1-IX
          D1=XX (IC+1)-XX (IC)
          AX (IC)=AX (IC+1)+D1/2.0*(FX (IC+1)+FX (IC))
          IF (NX.EQ.IX) GO TO 20
          D2=XX (IC+1)-XX (IC-1)
          D3=D2/(XX (IC)-XX (IC-1))
          A2=D3/6.0*D2**2/D1
          A3=D2/2.0-A2/D3
      40  AX (IC-1)=AX (IC+1)+(D2-A2-A3)*FX (IC-1)+A2*FX (IC)+A3*FX (IC+1)
      RETURN
      END

```

```

SUBROUTINE WASH(IPTYPE,DF1,DF2,GRATE)
LOGICAL SKIPD,SKIPA,SKIPL,SKIPG,SKIPOL
DIMENSION IPTYPE(5),DF1(5),DF2(5)
DIMENSION GRATE(10,14)
REAL*4 A(7)/0.0,0.09549,0.034507,0.0239916,8.11996E-03,
1 9.59721E-03,0.0104141/
REAL*4 B(7)/0.333333,0.8405,0.493444,0.305593,0.321280,
1 0.281789,0.249265/
REAL*4 A2RHO(7)/4.0,7.8,16.0,41.0,81.0,169.0,400.0/
1 ,AA/5.546E-4/,PE/0.604229/
COMMON/C1/XM(50),SIGTAB(6,50),SIGMAX(7),V(5),DV(5),
1 CLAMDA(5),DLAMDA(10,14,5),NEIST,NSTAB
COMMON/C8/NG,NP,NA,NL,NWS,NPOL,NFSTAB,NWINDS,WW,Wf,FDRY(14)
COMMON/C15/SKIPP(10),SKIPA(10),SKIPL(10),SKIPG(10),SKIPOL(10)
COMMON/C16/MOB,MOE,KSEA
DO 500 M=1,NPOL
IF(SKIPOL(M))GO TO 500
IF(IPTYPE(M).EQ.2) GO TO 250
ITAG=0
C THE THREE INITIALIZATIONS TO FOLLOW ARE
C NECESSARY DUE TO FORTRAN OPTIMIZATION TECHNIQUES
IKP=1
IKPP=2
FAC=C.0
ASR=DF1(M)**2*DF2(M)/4.
IF(A2RHO(1).GT.ASR) GO TO 2
GO TO 3
2 ITAG=1
FAC=ASR/A2RHO(1)
GO TO 4
3 IF(ASR.LE.A2RHO(7)) GO TO 4
ITAG=2
4 CONTINUE
IF(ITAG.NE.0) GO TO 30
DO 10 ITEST=2,6
IKP=ITEST
IF(ASF.GT.A2RHO(ITEST)) GO TO 20
10 CONTINUE
20 CONTINUE
IKPP=IKP+1
FAC=(ASR-A2RHO(IKP))/(A2RHO(IKPP)-A2RHO(IKP))
30 CONTINUE
DO 60 I=1,NG
IF(SKIPG(I))GO TO 60
DO 50 MON=1,KSEA
X=GRATE(I,MON)*0.254
IF(ITAG.NE.1) GO TO 35
Y=FAC*(B(1)*X)
DLAMDA(I,MON,M)=1.0E-04*Y
GO TO 50
35 IF(ITAG.NE.2) GO TO 45
Y=(-B(7)+SQRT(B(7)**2+4.*A(7)*X))/(2.*A(7))
DLAMDA(I,MON,M)=1.0E-04*Y
GO TO 50
45 CONTINUE
Y1=(-B(IKP)+SQRT(B(IKP)**2+4.*A(IKP)*X))/(2.*A(IKP))

```

06 04 75  
04 21 75  
05 02 75

04 28 75  
04 21 5  
04 28 75

```

      Y2=(-B(IKPP)+SQRT(B(IKPP)**2+4.*A(IKPP)*Y))/(2.*A(IKPP))
      Y=Y1*(1.-FAC)+Y2*FAC
      DLAMDA(I,MON,M)=1.0E-04*Y
50  CONTINUE
60  CONTINUE
    GO TO 500
250 CONTINUE
      DF2M=DF2(M)*10000.0
                                     05 05 75
      DO 300 I=1,NG
      IF(SKIPG(I))GO TO 300
      DO 290 MON=1,KSEA
      X=GPATE(I,MON)*0.254
      Y=AA*X**PP
      DLAMDA(I,MON,M)=Y*DF2M
                                     05 05 75
290 CONTINUE
300 CONTINUE
500 CONTINUE
      RETURN
      END

```



```

SUBROUTINE WINDSCE(WINDSD)
INTEGER IN/50/,KOUT/51/
REAL*4 MU/182.7E-4/,G/9.8/,A/0.1/,RHO/1.22E+3/,
1 Z/1.0/,RK/1.E-2/,C(3)/1.5,1.8,2.8/
DIMENSION WINDSD(8)
COMMON/C8/NG,NE,NA,NL,NWS,NPOL,NFSTAR,NWINDS,WW,WV,FDRY(14)
COMMON/C12/WQIO(3,5,8),VFALL(3)
COMMON/C16/MOB,MCE,KSEA
COMMON/C19/CCNCF(3,5),SSCON(3),DEN(3),DSALT(3),DSUSP(3),
+ITYPE(3)
C*** DSALT=AVERAGE DIAMETER(IN METERS) FOR SALTATING PARTICLES
C*** DSUSP=AVERAGE DIAMETER(IN METERS) FOR SUSPENDED PARTICLES
C*** WQIO(I,J,K)=EMISSION RATE IN GM/METER**2/SEC OF POLLUTANT J FROM
C*** WINDBLOWN SOURCE I DURING TIME OF WINDSPEED CLASS K
C*** CCNCF(I,J)=CONCENTRATION FACTOR FOR POLLUTANT J FROM WIND-
C*** BLOWN SOURCE I
C*** FDRY=FRACTION OF TIME WINDBLOWN SOURCE IS DRY
C*** A=SAND PARTICLE THRESHOLD VELOCITY PROPORTIONALITY CONSTANT(0.1)
C*** RHO=DENSITY OF AIR= 1.22E+3 GM/ M**3
C*** Z=HEIGHT FOR WIND SPEED MEASUREMENT(USUALLY TAKEN AS 1 M)
C*** RK=SURFACE ROUGHNESS(USUALLY TAKEN AS .01M)
C*** G=GRAVITATIONAL ACCELERATION IN M/SEC**2
C*** ITYPE=1---NEARLY UNIFORM SAND, C=1.5
C*** ITYPE=2---NATURALLY GRADED SAND, C=1.8
C*** ITYPE=3---WIDE RANGE OF GRAIN SIZE, C=2.8
C*** DEN=DENSITY OF WINDBLOWN MATERIAL
C*** MU=DYNAMIC VISCOSITY OF AIR(G/M/SEC)
GMU=G/(18.0*MU)
C*** CALCULATE SETTLING VELOCITIES FOR SUSPENDED PARTICLES
DO 70 I=1,NWS
VFALL(I)=DSUSP(I)**2*GMU*DEN(I)
WRITE(KOUT,65) I,VFALL(I)
65 FORMAT(/,10X,'DEPOSITION VELOCITY FOR WINDBLOWN SOURCE',I4,2X,'=',
&E12.4,2X,'METERS/SEC')
70 CONTINUE
ALPHA=1./(5.75*ALOG10(Z/RK))**3
DSTAND=0.00025
BETA=ALPHA*PHO/G
DO 200 I=1,NWS
WRITE(KOUT,110) I
110 FORMAT(///,10X,'EMISSION DATA FROM WINDBLOWN SOURCE',I4,/)
VT=5.75*A*SQRT(((DEN(I)-RHO)/RHO)*G*DSALT(I))*ALOG10(Z/RK)
ITYPE=ITYPE(I)
CS=C(ITYPE)
BETACS=BETA*CS*SQRT(DSALT(I)/DSTAND)
DO 200 JJ=1,NWINDS
VR=WINDSD(JJ)
IF(VR.IT.VT) GO TO 120
QST=BETACS*(VR-VT)**3
GO TO 130
120 QST=0.
130 CONTINUE
DO 180 J=1,NPOL
WQIO(I,J,JJ)=SSCON(I)*CCNCF(I,J)*QST
WRITE(KOUT,140) J,JJ,WQIO(I,J,JJ)
140 FORMAT(10X,'POLLUTANT',I4,2X,'WIND',I4,2X,'SOURCE',

```

```
+ ' STRENGTH=' , E12.4 , 2X , 'GM/M**2/SEC')  
180 CONTINUE  
200 CONTINUE  
  RETURN  
  END
```

DOUBLE PRECISION FUNCTION YLAG(XI,X,Y,IND1,N1,IMAX, IEX)	YLAG	0
C PROGRAM AUTHORS A. A. BROCKS AND E.C. LONG,	YLAG	5
C COMPUTING TECHNOLOGY CENTER, UNION CARBIDE CCRP., NUCLEAR DIV.,	YLAG	10
C OAK RIDGE, TENN.	YLAG	15
C	YLAG	20
C LAGRANGIAN INTERPOLATION	YLAG	25
C XI IS INTERPOLATED ENTRY INTO X-ARRAY	YLAG	30
C N IS THE ORDER OF LAGRANGIAN INTERPOLATION	YLAG	35
C Y IS ARRAY FROM WHICH YLAG IS OBTAINED BY INTERPOLATION	YLAG	40
C IND IS THE MIN-I FOR X(I).GT.XI	YLAG	45
C IF IND=0,X-ARRAY WILL BE SEARCHED	YLAG	50
C IMAX IS MAX INDEX OF X-AND Y-ARRAYS	YLAG	55
C EXTRAPOLATION CAN OCCUR,IEX=-1 OR +1	YLAG	60
C	YLAG	65
C	YLAG	70
C	YLAG	75
DIMENSION X(1),Y(1)	YLAG	80
DOUBLE PRECISION P,D,S,XD,XI,X,Y,YLAG	YLAG	85
IND=IND1	YLAG	90
N=N1	YLAG	95
IEX=0	YLAG	100
IF (N.LE.IMAX) GO TO 10	YLAG	105
N=IMAX	YLAG	110
IEX=N	YLAG	115
10 IF (IND.GT.0) GO TO 40	YLAG	120
DO 20 J = 1,IMAX	YLAG	125
IF (XI-X(J)) 30,130,20	YLAG	130
20 CONTINUE	YLAG	135
IEX=1	YLAG	140
GO TO 70	YLAG	145
30 IND=J	YLAG	150
40 IF (IND.GT.1) GO TO 50	YLAG	155
IEX=-1	YLAG	160
50 INL=IND-(N+1)/2	YLAG	165
IF (INL.GT.0) GO TO 60	YLAG	170
INL=1	YLAG	175
60 INU=INL+N-1	YLAG	180
IF (INU.LE.IMAX) GO TO 80	YLAG	185
70 INL=IMAX-N+1	YLAG	190
INU=IMAX	YLAG	195
80 S=0.	YLAG	200
P=1.	YLAG	205
DO 110 J=INL,INU	YLAG	210
P=P*(XI-X(J))	YLAG	215
D=1.	YLAG	220
DO 100 I=INL,INU	YLAG	225
IF (I.NE.J) GO TO 90	YLAG	230
XD=XI	YLAG	235
GO TO 100	YLAG	240
90 XD=X(J)	YLAG	245
100 D=D*(XD-X(I))	YLAG	250
110 S=S+Y(J)/D	YLAG	255
YLAG=S*P	YLAG	260
120 RETURN	YLAG	265
130 YLAG=Y(J)	YLAG	270
GO TO 120	YLAG	275
END		



## APPENDIX C. INPUT DATA

## WALKER BRANCH CALCULATIONS, JULY 72 THRU AUG 73

PREF BRANCH CALCULATIONS, DUE TO						72 HRS 180° W						
2	2	14	3.5			4	5	6	7	NWINDS,DDIR,NFSTAB,JSATB(6)		
6	16	7	1	2	3					14.0	WINDSD	
.894		2.42		4.42			6.87	9.53				
JUL 72	AUG 72	SEP 72	OCT 72	NOV 72	DEC 72	JAN 73	FEB 73	MAR 73	APR 73			
FEB 73	MAR 73	APR 73	MAY 73	JUN 73	JUL 73	AUG 73						

	1						KSIG--1=SEASONAL, 0=ANNUAL
N	0.28	0.00	0.00	0.00	0.00	0.00	0.28
NNE	0.71	0.00	0.00	0.00	0.00	0.00	0.71
NE	1.42	0.14	0.00	0.00	0.00	0.00	1.56
ENE	1.85	0.14	0.00	0.00	0.00	0.00	1.99
E	0.28	0.00	0.00	0.00	0.00	0.00	0.28
ESE	0.57	0.00	0.00	0.00	0.00	0.00	0.57
SE	0.57	0.00	0.00	0.00	0.00	0.00	0.57
SSE	0.43	0.00	0.00	0.00	0.00	0.00	0.43
S	0.43	0.00	0.00	0.00	0.00	0.00	0.43
SSW	2.84	0.57	0.14	0.00	0.00	0.00	3.55
SW	3.84	1.14	0.99	0.14	0.00	0.00	6.11
WSW	1.56	0.14	0.28	0.00	0.00	0.00	1.98
W	0.85	0.57	0.00	0.00	0.00	0.00	1.42
WNW	0.00	0.00	0.00	0.00	0.00	0.00	0.00
NW	0.14	0.00	0.00	0.00	0.00	0.00	0.14
NNW	0.14	0.00	0.00	0.00	0.00	0.00	0.14
N	0.00	0.00	0.00	0.00	0.00	0.00	0.00
NNE	0.43	0.00	0.00	0.00	0.00	0.00	0.43
NE	0.71	0.14	0.00	0.00	0.00	0.00	0.85
ENE	0.00	0.00	0.00	0.00	0.00	0.00	0.00
E	0.28	0.00	0.00	0.00	0.00	0.00	0.28
ESE	0.00	0.00	0.00	0.00	0.00	0.00	0.00
SE	0.00	0.00	0.00	0.00	0.00	0.00	0.00
SSE	0.00	0.00	0.00	0.00	0.00	0.00	0.00
S	0.14	0.00	0.00	0.00	0.00	0.00	0.14
SSW	0.14	0.14	0.00	0.00	0.00	0.00	0.28
SW	0.28	0.43	0.57	0.00	0.00	0.00	1.28
WSW	0.14	0.28	0.14	0.14	0.14	0.00	0.84
W	0.00	0.00	0.00	0.00	0.00	0.00	0.00
WNW	0.00	0.00	0.00	0.00	0.00	0.00	0.00
NW	0.00	0.00	0.00	0.00	0.00	0.00	0.00
NNW	0.14	0.00	0.00	0.00	0.00	0.00	0.14
N	0.00	0.00	0.00	0.00	0.00	0.00	0.00
NNE	0.14	0.28	0.00	0.00	0.00	0.00	0.42
NE	0.43	0.00	0.00	0.00	0.00	0.00	0.43
ENE	0.28	0.00	0.00	0.00	0.00	0.00	0.28
E	0.00	0.00	0.00	0.00	0.00	0.00	0.00
ESE	0.00	0.00	0.00	0.00	0.00	0.00	0.00
SE	0.00	0.00	0.00	0.00	0.00	0.00	0.00
SSE	0.00	0.00	0.00	0.00	0.00	0.00	0.00
S	0.00	0.00	0.00	0.00	0.00	0.00	0.00
SSW	0.00	0.14	0.00	0.00	0.00	0.00	0.14
SW	0.00	0.14	0.00	0.00	0.00	0.00	0.14
WSW	0.14	0.00	0.28	0.00	0.00	0.00	0.42
W	0.14	0.00	0.00	0.00	0.00	0.00	0.14
WNW	0.00	0.14	0.00	0.00	0.00	0.00	0.14
NW	0.00	0.00	0.00	0.00	0.00	0.00	0.00
NNW	0.14	0.00	0.00	0.00	0.00	0.00	0.14
N	0.00	0.00	0.00	0.00	0.00	0.00	0.00
NNE	0.43	2.41	0.00	0.00	0.00	0.00	2.84
NE	0.99	0.43	0.00	0.00	0.00	0.00	1.42
ENE	0.99	0.00	0.00	0.00	0.00	0.00	0.99
E	0.28	0.00	0.00	0.00	0.00	0.00	0.28
ESE	0.00	0.00	0.00	0.00	0.00	0.00	0.00
SE	0.00	0.14	0.00	0.00	0.00	0.00	0.14
SSE	0.14	0.00	0.00	0.00	0.00	0.00	0.14
S	0.43	0.00	0.14	0.14	0.00	0.00	0.71
SSW	0.85	0.43	0.14	0.00	0.00	0.00	1.42
SW	0.71	0.85	2.13	0.99	0.43	0.00	5.11
WSW	1.14	1.14	0.99	0.28	0.00	0.00	3.55
W	0.00	0.28	0.00	0.43	0.00	0.00	0.71



WNW	0.00	0.00	0.28	0.00	0.00	0.00	0.28
WW	0.00	0.00	0.00	0.00	0.00	0.00	0.00
WNW	0.00	0.00	0.00	0.00	0.00	0.00	0.00
W	0.57	0.57	0.00	0.00	0.00	0.00	1.14
WNE	0.99	1.85	0.00	0.00	0.00	0.00	2.84
NE	0.99	0.28	0.00	0.00	0.00	0.00	1.27
ENE	0.57	0.00	0.00	0.00	0.00	0.00	0.57
E	0.14	0.00	0.00	0.00	0.00	0.00	0.14
ESE	0.14	0.00	0.00	0.00	0.00	0.00	0.14
SE	0.14	0.28	0.00	0.00	0.00	0.00	0.42
SSE	0.99	0.14	0.00	0.00	0.00	0.00	1.13
S	0.43	0.14	0.00	0.00	0.00	0.00	0.57
SSW	1.56	0.43	0.99	0.28	0.00	0.00	3.26
SW	1.56	1.70	2.84	1.70	0.28	0.00	8.08
WSW	0.99	2.98	1.85	0.71	0.00	0.00	6.53
W	0.71	0.71	0.57	0.28	0.14	0.00	2.41
WNW	0.14	0.43	0.00	0.00	0.00	0.00	0.57
WW	0.14	0.14	0.00	0.00	0.00	0.00	0.28
WNW	0.71	0.28	0.00	0.00	0.00	0.00	0.99
N	0.14	0.00	0.00	0.00	0.00	0.00	0.14
WNE	2.84	0.99	0.00	0.00	0.00	0.00	3.83
NE	1.14	0.85	0.28	0.00	0.00	0.00	2.27
ENE	0.99	0.14	0.00	0.00	0.00	0.00	1.13
E	0.57	0.00	0.00	0.00	0.00	0.00	0.57
ESE	0.71	0.00	0.00	0.00	0.00	0.00	0.71
SE	0.28	0.00	0.00	0.00	0.00	0.00	0.28
SSE	0.00	0.00	0.00	0.00	0.00	0.00	0.00
S	0.43	0.00	0.28	0.00	0.00	0.00	0.71
SSW	0.57	0.00	0.00	0.00	0.00	0.00	0.57
SW	3.27	0.00	0.14	0.00	0.00	0.00	3.41
WSW	1.56	0.28	0.14	0.14	0.00	0.00	2.12
W	1.28	0.28	0.14	0.00	0.00	0.00	1.70
WNW	0.43	0.14	0.00	0.00	0.00	0.00	0.57
WW	0.71	0.14	0.00	0.00	0.00	0.00	0.85
WNW	0.14	0.00	0.00	0.00	0.00	0.00	0.14
N	0.00	0.00	0.00	0.00	0.00	0.00	0.00
WNE	0.43	0.14	0.00	0.00	0.00	0.00	0.57
NE	0.71	0.14	0.00	0.00	0.00	0.00	0.85
ENE	0.00	0.00	0.00	0.00	0.00	0.00	0.00
E	0.00	0.00	0.00	0.00	0.00	0.00	0.00
ESE	0.14	0.00	0.00	0.00	0.00	0.00	0.14
SE	0.14	0.00	0.00	0.00	0.00	0.00	0.14
SSE	0.00	0.00	0.00	0.00	0.00	0.00	0.00
S	0.00	0.00	0.00	0.00	0.00	0.00	0.00
SSW	0.00	0.00	0.00	0.00	0.00	0.00	0.00
SW	0.14	0.00	0.00	0.00	0.00	0.00	0.14
WSW	0.00	0.00	0.00	0.00	0.00	0.00	0.00
W	0.14	0.14	0.00	0.00	0.00	0.00	0.28
WNW	0.00	0.00	0.00	0.00	0.00	0.00	0.00
WW	0.00	0.00	0.00	0.00	0.00	0.00	0.00
WNW	0.00	0.00	0.00	0.00	0.00	0.00	0.00
N	0.13	0.27	0.00	0.00	0.00	0.00	0.40
WNE	0.40	1.08	0.27	0.00	0.00	0.00	1.75
NE	0.67	1.88	0.81	0.00	0.00	0.00	3.36
ENE	0.13	0.81	0.54	0.00	0.00	0.00	1.48
E	0.27	0.13	0.00	0.00	0.00	0.00	0.40
ESE	0.40	0.00	0.00	0.00	0.00	0.00	0.40
SE	0.27	0.27	0.00	0.00	0.00	0.00	0.54
SSE	0.13	0.13	0.00	0.00	0.00	0.00	0.26
S	0.54	0.27	0.00	0.00	0.00	0.00	0.81
SSW	0.27	1.08	3.10	0.00	0.00	0.00	4.45
SW	0.40	2.42	3.50	0.81	0.00	0.00	7.13
WSW	0.27	1.08	0.67	0.13	0.00	0.00	2.15
W	0.00	0.27	1.48	0.13	0.00	0.00	1.88
WNW	0.27	0.13	0.00	0.27	0.00	0.00	0.67
WW	0.54	0.00	0.00	0.00	0.00	0.00	0.54

NNW	0.13	0.13	0.13	0.00	0.00	0.00	0.39
N	0.00	0.00	0.00	0.00	0.00	0.00	0.00
NNE	0.00	0.40	0.40	0.00	0.00	0.00	0.80
NE	0.13	0.40	0.00	0.00	0.00	0.00	0.53
ENE	0.00	0.13	0.13	0.00	0.00	0.00	0.26
E	0.00	0.13	0.00	0.00	0.00	0.00	0.13
ESE	0.00	0.00	0.00	0.00	0.00	0.00	0.00
SE	0.13	0.00	0.00	0.00	0.00	0.00	0.13
SSE	0.00	0.00	0.00	0.00	0.00	0.00	0.00
S	0.00	0.00	0.00	0.00	0.00	0.00	0.00
SSW	0.00	0.13	0.00	0.00	0.00	0.00	0.13
SW	0.00	0.00	0.27	0.00	0.00	0.00	0.27
WSW	0.00	0.00	0.00	0.00	0.00	0.00	0.00
W	0.00	0.00	0.13	0.00	0.00	0.00	0.13
WNW	0.00	0.00	0.00	0.00	0.00	0.00	0.00
NW	0.00	0.00	0.00	0.00	0.00	0.00	0.00
NNW	0.00	0.00	0.00	0.00	0.00	0.00	0.00
N	0.00	0.13	0.00	0.00	0.00	0.00	0.13
NNE	0.00	0.00	0.13	0.27	0.00	0.00	0.40
NE	0.00	0.40	0.40	0.00	0.00	0.00	0.80
ENE	0.00	0.13	0.13	0.00	0.00	0.00	0.26
E	0.00	0.00	0.00	0.00	0.00	0.00	0.00
ESE	0.00	0.00	0.00	0.00	0.00	0.00	0.00
SE	0.00	0.13	0.00	0.00	0.00	0.00	0.13
SSE	0.00	0.00	0.00	0.00	0.00	0.00	0.00
S	0.00	0.00	0.00	0.00	0.00	0.00	0.00
SSW	0.00	0.00	0.13	0.00	0.00	0.00	0.13
SW	0.00	0.00	0.27	0.27	0.00	0.00	0.54
WSW	0.00	0.27	0.27	0.00	0.00	0.00	0.54
W	0.00	0.00	0.13	0.00	0.00	0.00	0.13
WNW	0.00	0.13	0.13	0.00	0.00	0.00	0.26
NW	0.00	0.00	0.00	0.00	0.00	0.00	0.00
NNW	0.00	0.00	0.00	0.00	0.00	0.00	0.00
N	0.00	0.13	0.13	0.13	0.00	0.00	0.39
NNE	0.13	0.27	0.94	0.67	0.00	0.00	2.01
NE	0.13	0.81	1.35	0.54	0.00	0.00	2.83
ENE	0.27	0.00	0.13	0.00	0.00	0.00	0.40
E	0.00	0.00	0.00	0.00	0.00	0.00	0.00
ESE	0.00	0.13	0.00	0.00	0.00	0.00	0.13
SE	0.00	0.00	0.13	0.00	0.00	0.00	0.13
SSE	0.00	0.00	0.00	0.00	0.00	0.00	0.00
S	0.00	0.13	0.00	0.00	0.00	0.00	0.13
SSW	0.00	0.40	0.27	0.00	0.00	0.00	0.67
SW	0.27	0.81	0.27	0.94	0.13	0.00	2.42
WSW	0.13	0.27	0.54	0.27	0.13	0.13	1.47
W	0.13	0.13	0.27	0.00	0.00	0.00	0.53
WNW	0.00	0.13	0.13	0.00	0.00	0.00	0.26
NW	0.00	0.13	0.00	0.00	0.00	0.00	0.13
NNW	0.00	0.00	0.81	0.27	0.00	0.00	1.08
N	0.13	0.13	0.54	0.13	0.00	0.00	0.93
NNE	0.40	0.81	2.56	2.29	0.00	0.00	6.06
NE	0.13	0.54	1.88	1.08	0.13	0.00	3.76
ENE	0.27	0.27	0.13	0.00	0.00	0.00	0.67
E	0.00	0.40	0.13	0.00	0.00	0.00	0.53
ESE	0.54	0.40	0.13	0.00	0.00	0.00	1.07
SE	0.13	0.27	0.00	0.00	0.00	0.00	0.40
SSE	0.13	0.13	0.00	0.00	0.00	0.00	0.26
S	0.00	0.00	0.27	0.00	0.00	0.00	0.27
SSW	0.27	0.67	0.27	0.54	0.13	0.00	1.88
SW	0.40	1.35	2.42	2.96	0.27	0.00	7.40
WSW	0.13	0.13	2.42	1.88	0.27	0.00	4.83
W	0.54	0.13	0.94	0.27	0.13	0.00	2.01
WNW	0.13	0.81	0.54	0.00	0.00	0.00	1.48
NW	0.13	0.27	0.00	0.00	0.00	0.00	0.40
NNW	0.13	0.13	0.27	0.13	0.00	0.00	0.66
N	0.81	0.13	0.13	0.00	0.00	0.00	1.07

NNE	0.27	0.81	0.81	2.15	0.13	0.00	4.17
NE	0.40	0.67	1.35	1.21	0.00	0.00	3.63
ENE	0.13	0.67	0.54	0.00	0.00	0.00	1.34
E	0.13	0.13	0.00	0.00	0.00	0.00	0.26
ESE	0.27	0.00	0.00	0.00	0.00	0.00	0.27
SE	0.54	0.00	0.00	0.00	0.00	0.00	0.54
SSE	0.13	0.00	0.00	0.00	0.00	0.00	0.13
S	0.13	0.13	0.00	0.00	0.00	0.00	0.26
SSW	0.13	0.13	0.13	0.13	0.00	0.00	0.52
SW	0.13	0.54	1.62	0.40	0.13	0.00	2.82
WSW	0.27	0.27	1.62	0.54	0.00	0.00	2.70
W	0.40	0.13	0.54	0.00	0.00	0.00	1.07
WNW	0.27	0.00	0.00	0.00	0.00	0.00	0.27
NW	0.54	0.67	0.00	0.00	0.00	0.00	1.21
NNW	0.13	0.27	0.00	0.00	0.00	0.00	0.40
N	0.00	0.00	0.00	0.00	0.00	0.00	0.00
NNE	0.00	0.13	0.40	0.13	0.00	0.00	0.66
NE	0.00	0.13	0.00	0.13	0.00	0.00	0.26
ENE	0.00	0.00	0.00	0.00	0.00	0.00	0.00
E	0.00	0.00	0.00	0.00	0.00	0.00	0.00
ESE	0.00	0.00	0.00	0.00	0.00	0.00	0.00
SE	0.00	0.00	0.00	0.00	0.00	0.00	0.00
SSE	0.00	0.00	0.00	0.00	0.00	0.00	0.00
S	0.00	0.00	0.00	0.00	0.00	0.00	0.00
SSW	0.00	0.00	0.00	0.00	0.00	0.00	0.00
SW	0.00	0.00	0.00	0.00	0.00	0.00	0.00
WSW	0.00	0.00	0.00	0.00	0.00	0.13	0.13
W	0.13	0.00	0.00	0.00	0.00	0.00	0.13
WNW	0.00	0.00	0.00	0.00	0.00	0.00	0.00
NW	0.00	0.13	0.00	0.00	0.00	0.00	0.13
NNW	0.13	0.00	0.00	0.00	0.00	0.00	0.13
N	0.56	0.42	0.14	0.00	0.00	0.00	1.12
NNE	0.14	0.69	0.69	0.69	0.00	0.00	2.21
NE	0.42	0.97	0.14	0.14	0.00	0.00	1.67
ENE	0.83	0.14	0.00	0.00	0.00	0.00	0.97
E	0.42	0.42	0.00	0.00	0.00	0.00	0.84
ESE	0.00	0.28	0.00	0.00	0.00	0.00	0.28
SE	0.42	0.28	0.00	0.00	0.00	0.00	0.70
SSE	0.14	0.14	0.00	0.00	0.00	0.00	0.28
S	0.14	0.14	0.00	0.00	0.00	0.00	0.28
SSW	0.69	2.78	0.97	0.28	0.00	0.00	4.72
SW	0.42	3.19	3.06	0.83	0.14	0.00	7.64
WSW	0.42	1.11	0.97	0.83	0.00	0.00	3.33
W	0.14	0.56	0.42	0.00	0.00	0.00	1.12
WNW	0.28	0.97	0.14	0.00	0.00	0.00	1.39
NW	0.28	0.00	0.00	0.00	0.00	0.00	0.28
NNW	0.42	0.28	0.00	0.00	0.00	0.00	0.70
N	0.00	0.00	0.14	0.28	0.00	0.00	0.42
NNE	0.14	0.28	0.00	0.83	0.14	0.00	1.39
NE	0.00	0.00	0.14	0.14	0.00	0.00	0.28
ENE	0.28	0.00	0.00	0.00	0.00	0.00	0.28
E	0.00	0.00	0.00	0.00	0.00	0.00	0.00
ESE	0.14	0.00	0.00	0.00	0.00	0.00	0.14
SE	0.28	0.00	0.00	0.00	0.00	0.00	0.28
SSE	0.00	0.14	0.00	0.00	0.00	0.00	0.14
S	0.00	0.00	0.14	0.00	0.00	0.00	0.14
SSW	0.14	0.14	0.00	0.14	0.00	0.00	0.42
SW	0.00	0.00	0.28	0.56	0.00	0.00	0.84
WSW	0.00	0.42	0.00	0.00	0.00	0.00	0.42
W	0.00	0.28	0.00	0.00	0.14	0.00	0.42
WNW	0.00	0.00	0.14	0.00	0.00	0.00	0.14
NW	0.00	0.14	0.00	0.00	0.00	0.00	0.14
NNW	0.00	0.14	0.00	0.00	0.14	0.00	0.28
N	0.00	0.00	0.14	0.00	0.00	0.00	0.14
NNE	0.00	0.28	0.14	0.00	0.00	0.00	0.42
NE	0.00	0.00	0.00	0.14	0.00	0.00	0.14



ENE	0.00	0.14	0.00	0.00	0.00	0.00	0.14
E	0.00	0.00	0.00	0.00	0.00	0.00	0.00
ESE	0.00	0.00	0.00	0.00	0.00	0.00	0.00
SE	0.00	0.00	0.00	0.00	0.00	0.00	0.00
SSE	0.00	0.00	0.00	0.00	0.00	0.00	0.00
S	0.00	0.00	0.00	0.00	0.00	0.00	0.00
SSW	0.00	0.00	0.00	0.00	0.00	0.00	0.00
SW	0.00	0.14	0.28	0.14	0.00	0.00	0.56
WSW	0.28	0.14	0.00	0.14	0.00	0.00	0.56
W	0.00	0.00	0.00	0.00	0.00	0.00	0.00
WNW	0.00	0.00	0.00	0.14	0.00	0.00	0.14
NW	0.00	0.00	0.00	0.00	0.00	0.00	0.00
NNW	0.00	0.00	0.00	0.00	0.14	0.00	0.14
N	0.56	0.14	0.14	0.00	0.00	0.00	0.84
NNE	0.00	0.97	0.42	1.11	0.00	0.00	2.50
NE	0.28	0.83	0.42	0.28	0.14	0.00	1.95
ENE	0.28	0.14	0.00	0.00	0.00	0.00	0.42
E	0.00	0.28	0.00	0.00	0.00	0.00	0.28
ESE	0.00	0.14	0.00	0.00	0.00	0.00	0.14
SE	0.00	0.00	0.14	0.00	0.00	0.00	0.14
SSE	0.00	0.42	0.00	0.00	0.00	0.00	0.42
S	0.56	0.14	0.14	0.00	0.00	0.00	0.84
SSW	0.56	0.56	0.28	0.14	0.00	0.00	1.54
SW	0.14	1.25	0.97	2.08	0.00	0.00	4.44
WSW	0.14	0.56	0.97	0.56	0.00	0.00	2.23
W	0.00	0.28	0.56	0.00	0.00	0.00	0.84
WNW	0.14	0.14	0.28	0.00	0.00	0.00	0.56
NW	0.00	0.00	0.28	0.00	0.00	0.00	0.28
NNW	0.28	0.14	0.28	0.14	0.14	0.00	0.98
N	0.14	0.14	0.14	0.14	0.00	0.00	0.56
NNE	0.00	0.42	1.67	0.56	0.00	0.00	2.65
NE	0.00	0.42	1.53	2.08	1.25	0.00	5.28
ENE	0.14	0.14	0.14	0.14	0.00	0.00	0.56
E	0.42	0.14	0.14	0.00	0.00	0.00	0.70
ESE	0.14	0.14	0.00	0.00	0.00	0.00	0.28
SE	0.00	0.00	0.00	0.00	0.00	0.00	0.00
SSE	0.00	0.42	0.14	0.00	0.00	0.00	0.56
S	0.14	0.56	0.00	0.00	0.00	0.00	0.70
SSW	0.14	0.69	1.11	0.00	0.00	0.00	1.94
SW	0.42	1.11	2.08	1.39	0.14	0.00	5.14
WSW	0.28	1.67	2.36	0.28	0.00	0.00	4.59
W	0.28	1.11	0.56	0.00	0.00	0.00	1.95
WNW	0.00	0.56	0.00	0.00	0.00	0.00	0.56
NW	0.00	0.14	0.00	0.00	0.00	0.00	0.14
NNW	0.00	0.42	0.14	0.14	0.00	0.00	0.70
N	0.42	0.69	0.00	0.00	0.00	0.00	1.11
NNE	0.00	0.42	0.69	0.14	0.00	0.00	1.25
NE	0.14	0.28	0.97	0.14	0.00	0.00	1.53
ENE	0.56	0.00	0.42	0.28	0.00	0.00	1.26
E	0.00	0.00	0.00	0.00	0.00	0.00	0.00
ESE	0.28	0.00	0.00	0.00	0.00	0.00	0.28
SE	0.00	0.00	0.14	0.00	0.00	0.00	0.14
SSE	0.00	0.69	0.14	0.00	0.00	0.00	0.83
S	0.00	0.14	0.14	0.00	0.00	0.00	0.28
SSW	0.00	0.56	0.56	0.14	0.00	0.00	1.26
SW	0.42	1.11	1.39	0.42	0.14	0.00	3.48
WSW	0.28	1.25	1.67	0.14	0.00	0.00	3.34
W	0.14	1.25	0.28	0.00	0.00	0.00	1.67
WNW	0.28	0.14	0.00	0.00	0.00	0.00	0.42
NW	0.28	0.00	0.00	0.00	0.00	0.00	0.28
NNW	0.00	0.28	0.00	0.00	0.00	0.00	0.28
N	0.00	0.00	0.00	0.00	0.00	0.00	0.00
NNE	0.00	0.00	0.00	0.00	0.00	0.00	0.00
NE	0.00	0.00	0.00	0.00	0.00	0.00	0.00
ENE	0.00	0.00	0.00	0.00	0.00	0.00	0.00
E	0.00	0.14	0.00	0.00	0.00	0.00	0.14

130

SSE	0.14	0.00	0.00	0.00	0.00	0.14	0.28
S	0.14	0.00	0.00	0.00	0.00	0.00	0.14
SSW	0.00	0.14	0.28	0.28	0.14	0.14	0.98
SW	0.14	0.28	0.70	1.12	0.28	0.28	2.80
WSW	0.14	0.28	1.26	0.70	0.00	0.00	2.38
W	0.00	0.14	0.28	0.98	0.00	0.00	1.40
WNW	0.00	0.00	0.14	0.00	0.00	0.00	0.14
WW	0.14	0.28	0.00	0.00	0.00	0.00	0.42
NNW	0.00	0.14	0.00	0.00	0.00	0.00	0.14
N	0.00	0.28	0.28	0.00	0.28	0.28	1.12
NNE	0.00	0.70	0.98	1.54	0.00	0.14	3.36
NE	0.14	0.56	1.26	1.68	1.12	0.28	5.04
ENE	0.14	0.42	0.56	0.42	0.00	0.14	1.68
E	0.42	0.56	0.56	0.14	0.00	0.14	1.82
ESE	0.28	0.28	0.28	0.00	0.00	0.28	1.12
SE	0.28	0.28	0.14	0.00	0.00	0.42	1.12
SSE	0.00	0.28	0.00	0.00	0.00	0.56	0.84
S	0.28	0.00	0.14	0.00	0.00	0.00	0.42
SSW	0.14	0.42	0.28	0.28	0.00	0.14	1.26
SW	0.00	0.42	1.12	0.14	0.00	0.00	1.68
WSW	0.00	0.42	0.42	0.56	0.14	0.00	1.54
W	0.14	0.00	0.28	0.28	0.00	0.00	0.70
WNW	0.00	0.00	0.00	0.00	0.00	0.00	0.00
WW	0.14	0.14	0.14	0.14	0.00	0.00	0.56
NNW	0.14	0.00	0.14	0.00	0.14	0.00	0.42
N	0.14	0.14	0.00	0.00	0.00	0.14	0.42
NNE	0.00	0.42	0.70	1.12	0.00	0.00	2.24
NE	0.00	0.14	0.70	0.14	0.00	0.00	0.98
ENE	0.14	0.70	0.70	0.00	0.00	0.14	1.68
E	0.00	0.42	0.14	0.00	0.00	0.00	0.56
ESE	0.14	0.14	0.00	0.00	0.00	0.00	0.28
SE	0.14	0.00	0.14	0.00	0.00	0.14	0.42
SSE	0.00	0.00	0.14	0.00	0.00	0.00	0.14
S	0.00	0.00	0.00	0.00	0.00	0.00	0.00
SSW	0.00	0.00	0.28	0.00	0.00	0.00	0.28
SW	0.28	0.56	0.14	0.14	0.00	0.00	1.12
WSW	0.42	0.28	0.28	0.56	0.00	0.00	1.54
W	0.14	0.14	0.56	0.00	0.00	0.00	0.84
WNW	0.14	0.00	0.14	0.00	0.00	0.00	0.28
WW	0.28	0.14	0.00	0.00	0.00	0.00	0.42
NNW	0.00	0.42	0.00	0.00	0.00	0.00	0.42
N	0.00	0.00	0.00	0.00	0.00	0.00	0.00
NNE	0.14	0.00	0.00	0.00	0.00	0.00	0.14
NE	0.00	0.00	0.56	0.00	0.00	0.00	0.56
ENE	0.14	0.00	0.14	0.00	0.00	0.00	0.28
E	0.14	0.14	0.14	0.00	0.00	0.00	0.42
ESE	0.00	0.00	0.00	0.00	0.00	0.00	0.00
SE	0.00	0.00	0.00	0.00	0.00	0.00	0.00
SSE	0.00	0.00	0.00	0.00	0.00	0.00	0.00
S	0.14	0.00	0.00	0.00	0.00	0.00	0.14
SSW	0.00	0.00	0.00	0.00	0.00	0.00	0.00
SW	0.14	0.14	0.00	0.00	0.00	0.00	0.28
WSW	0.00	0.00	0.14	0.00	0.00	0.00	0.14
W	0.00	0.00	0.00	0.00	0.00	0.00	0.00
WNW	0.14	0.00	0.00	0.00	0.00	0.00	0.14
WW	0.00	0.00	0.00	0.00	0.00	0.00	0.00
NNW	0.00	0.00	0.00	0.00	0.00	0.00	0.00
N	0.00	0.83	0.97	0.56	0.14	0.00	2.50
NNE	0.42	0.83	0.28	0.56	0.00	0.00	2.09
NE	0.56	0.56	0.28	0.00	0.00	0.00	1.40
ENE	0.00	0.14	0.00	0.00	0.00	0.00	0.14
E	0.28	0.00	0.00	0.00	0.00	0.00	0.28
ESE	0.28	0.14	0.00	0.00	0.00	0.00	0.42
SE	0.00	0.00	0.00	0.00	0.00	0.00	0.00
SSE	0.14	0.14	0.00	0.00	0.00	0.00	0.28
S	0.14	0.56	0.14	0.00	0.00	0.00	0.84



SSW	0.42	0.42	0.56	0.42	0.00	0.00	1.82
SW	0.00	0.28	0.14	1.11	1.39	0.00	2.92
WSW	0.00	0.14	0.69	0.56	0.69	0.28	2.36
W	0.00	0.42	0.28	0.28	0.00	0.00	0.98
WNW	0.42	0.00	0.28	0.00	0.00	0.00	0.70
NW	0.14	0.97	0.42	0.00	0.14	0.00	1.67
NNW	0.28	0.14	0.14	0.69	0.14	0.00	1.39
N	0.56	0.83	0.83	1.11	0.14	0.00	3.47
NNE	0.00	0.28	0.28	0.14	0.00	0.00	0.70
NE	0.00	0.00	0.83	0.14	0.00	0.00	0.97
ENE	0.14	0.28	0.00	0.00	0.00	0.00	0.42
E	0.14	0.00	0.00	0.00	0.00	0.00	0.14
ESE	0.00	0.00	0.00	0.00	0.00	0.00	0.00
SE	0.00	0.00	0.00	0.00	0.00	0.00	0.00
SSE	0.00	0.00	0.00	0.00	0.00	0.00	0.00
S	0.00	0.14	0.00	0.00	0.00	0.00	0.14
SSW	0.00	0.14	0.14	0.69	0.00	0.00	0.97
SW	0.00	0.14	0.14	0.28	0.69	0.00	1.25
WSW	0.00	0.00	0.00	0.42	0.42	0.28	1.12
W	0.00	0.00	0.14	0.14	0.00	0.00	0.28
WNW	0.00	0.56	0.00	0.00	0.00	0.00	0.56
NW	0.00	0.42	0.56	0.28	0.00	0.00	1.26
NNW	0.14	0.28	0.14	0.42	0.14	0.00	1.12
N	0.00	0.14	0.83	0.97	0.14	0.14	2.22
NNE	0.14	0.00	0.42	0.00	0.00	0.00	0.56
NE	0.00	0.14	0.42	0.00	0.00	0.00	0.56
ENE	0.00	0.00	0.00	0.00	0.00	0.00	0.00
E	0.00	0.00	0.00	0.00	0.00	0.00	0.00
ESE	0.00	0.00	0.00	0.00	0.00	0.00	0.00
SE	0.14	0.00	0.00	0.00	0.00	0.00	0.14
SSE	0.14	0.00	0.00	0.00	0.00	0.00	0.14
S	0.00	0.00	0.00	0.00	0.00	0.00	0.00
SSW	0.00	0.14	0.00	0.42	0.14	0.00	0.70
SW	0.00	0.14	0.14	0.42	0.69	0.00	1.39
WSW	0.00	0.14	0.28	0.14	0.42	0.00	0.98
W	0.00	0.14	0.00	0.14	0.14	0.00	0.42
WNW	0.00	0.14	0.28	0.00	0.00	0.00	0.42
NW	0.00	0.28	0.00	0.00	0.00	0.00	0.28
NNW	0.00	0.14	0.14	0.28	0.00	0.00	0.56
N	0.42	1.53	3.47	3.75	1.81	0.00	10.98
NNE	0.14	0.28	0.42	0.14	0.14	0.00	1.12
NE	0.69	1.11	2.08	0.00	0.00	0.00	3.88
ENE	0.42	0.28	0.42	0.00	0.00	0.00	1.12
E	0.00	0.28	0.00	0.00	0.00	0.00	0.28
ESE	0.14	0.14	0.00	0.00	0.00	0.00	0.28
SE	0.00	0.00	0.14	0.00	0.00	0.00	0.14
SSE	0.00	0.28	0.00	0.00	0.00	0.00	0.28
S	0.56	0.28	0.00	0.28	0.14	0.00	1.26
SSW	0.14	0.14	0.97	2.22	0.83	0.00	4.30
SW	0.28	0.14	0.69	1.25	1.11	0.00	3.47
WSW	0.56	0.14	0.28	1.67	0.69	0.00	3.34
W	0.14	0.00	0.42	0.14	0.28	0.00	0.98
WNW	0.14	0.42	0.14	0.00	0.00	0.00	0.70
NW	0.00	0.42	0.83	0.14	0.00	0.00	1.39
NNW	0.14	0.69	0.56	0.83	0.00	0.00	2.22
N	0.00	0.00	1.81	2.92	0.56	0.00	5.29
NNE	0.14	0.14	0.28	0.28	0.14	0.00	0.98
NE	0.14	0.14	0.69	0.14	0.00	0.00	1.11
ENE	0.00	0.56	0.56	0.00	0.00	0.00	1.12
E	0.14	0.42	0.14	0.00	0.00	0.00	0.70
ESE	0.28	0.00	0.00	0.00	0.00	0.00	0.28
SE	0.14	0.97	0.00	0.00	0.00	0.00	1.11
SSE	0.00	0.14	0.00	0.00	0.00	0.00	0.14
S	0.00	0.14	0.00	0.14	0.00	0.00	0.28
SSW	0.14	0.00	0.69	0.56	0.00	0.00	1.39
SW	0.00	0.28	0.28	1.11	0.14	0.00	1.81

WSW	0.28	0.42	0.69	0.69	0.00	0.00	2.08
W	0.14	0.14	0.14	0.00	0.00	0.00	0.42
WNW	0.14	0.28	0.00	0.00	0.00	0.00	0.42
WW	0.00	0.14	0.00	0.00	0.00	0.00	0.14
WNW	0.00	0.00	0.28	0.42	0.00	0.00	0.70
W	0.00	0.00	0.97	0.00	0.00	0.00	0.97
WNE	0.00	0.00	0.56	0.00	0.00	0.00	0.56
NE	0.00	0.00	0.14	0.14	0.00	0.00	0.28
ENE	0.14	0.28	0.28	0.00	0.00	0.00	0.70
E	0.00	0.28	0.00	0.00	0.00	0.00	0.28
ESE	0.14	0.28	0.00	0.00	0.00	0.00	0.42
SE	0.00	0.14	0.00	0.00	0.00	0.00	0.14
SSE	0.42	0.14	0.00	0.00	0.00	0.00	0.56
S	0.00	0.00	0.28	0.00	0.00	0.00	0.28
SSW	0.00	0.56	0.00	0.00	0.00	0.00	0.56
SW	0.00	0.00	0.00	0.00	0.00	0.00	0.00
WSW	0.00	0.00	0.00	0.00	0.00	0.00	0.00
W	0.00	0.00	0.00	0.00	0.00	0.00	0.00
WNW	0.00	0.00	0.00	0.00	0.00	0.00	0.00
WW	0.00	0.00	0.00	0.00	0.00	0.00	0.00
WNW	0.00	0.00	0.00	0.00	0.00	0.00	0.00
W	0.00	0.00	0.14	0.00	0.00	0.00	0.14
WNE	0.00	0.00	0.28	0.00	0.00	0.00	0.28
NE	0.00	0.00	0.00	0.00	0.00	0.00	0.00
ENE	0.00	0.00	0.00	0.00	0.00	0.00	0.00
E	0.00	0.00	0.00	0.00	0.00	0.00	0.00
ESE	0.00	0.00	0.00	0.00	0.00	0.00	0.00
SE	0.00	0.00	0.00	0.00	0.00	0.00	0.00
SSE	0.00	0.14	0.00	0.00	0.00	0.00	0.14
S	0.00	0.14	0.00	0.00	0.00	0.00	0.14
SSW	0.00	0.14	0.00	0.00	0.00	0.00	0.14
SW	0.00	0.00	0.00	0.00	0.00	0.00	0.00
WSW	0.00	0.00	0.00	0.00	0.00	0.00	0.00
W	0.00	0.00	0.00	0.00	0.00	0.00	0.00
WNW	0.00	0.00	0.00	0.00	0.00	0.00	0.00
WW	0.00	0.00	0.00	0.00	0.00	0.00	0.00
WNW	0.00	0.00	0.00	0.00	0.00	0.00	0.00
W	0.42	1.11	0.69	2.22	0.00	0.00	4.44
WNE	0.00	0.69	0.42	0.00	0.00	0.00	1.11
NE	0.00	0.14	0.00	0.00	0.00	0.00	0.14
ENE	0.14	0.00	0.00	0.00	0.00	0.00	0.14
E	0.00	0.00	0.00	0.00	0.00	0.00	0.00
ESE	0.00	0.00	0.00	0.00	0.00	0.00	0.00
SE	0.00	0.00	0.00	0.00	0.00	0.00	0.00
SSE	0.00	0.00	0.00	0.00	0.00	0.00	0.00
S	0.00	0.00	0.00	0.00	0.00	0.00	0.00
SSW	0.14	0.14	0.42	0.97	0.14	0.00	1.81
SW	0.14	1.39	2.08	0.28	0.42	0.00	4.31
WSW	0.00	0.14	0.69	0.69	0.14	0.00	1.66
W	0.00	0.14	0.56	0.69	0.14	0.00	1.53
WNW	0.00	0.00	0.14	0.28	0.00	0.00	0.42
WW	0.28	0.14	0.00	0.00	0.00	0.00	0.42
WNW	0.00	0.28	0.00	0.28	0.00	0.00	0.56
W	0.00	0.14	0.56	0.69	0.00	0.00	1.39
WNE	0.28	0.00	0.14	0.00	0.00	0.00	0.42
NE	0.00	0.00	0.14	0.00	0.00	0.00	0.14
ENE	0.00	0.00	0.00	0.00	0.00	0.00	0.00
E	0.00	0.00	0.00	0.00	0.00	0.00	0.00
ESE	0.00	0.00	0.00	0.00	0.00	0.00	0.00
SE	0.00	0.00	0.00	0.00	0.00	0.00	0.00
SSE	0.00	0.00	0.00	0.00	0.00	0.00	0.00
S	0.28	0.00	0.00	0.00	0.00	0.00	0.28
SSW	0.00	0.00	0.00	0.28	0.42	0.14	0.84
SW	0.00	0.42	0.28	0.56	0.14	0.14	1.54
WSW	0.00	0.00	0.42	0.28	0.00	0.00	0.70
W	0.00	0.00	0.00	0.14	0.14	0.14	0.42

WNW	0.00	0.00	0.00	0.42	0.14	0.00	0.56
WW	0.14	0.00	0.14	0.00	0.00	0.00	0.28
WNW	0.00	0.14	0.28	0.00	0.00	0.00	0.42
N	0.28	0.28	0.42	0.56	0.14	0.00	1.68
NNE	0.00	0.00	0.42	0.00	0.14	0.00	0.56
NE	0.14	0.00	0.00	0.00	0.00	0.00	0.14
ENE	0.14	0.00	0.00	0.00	0.00	0.00	0.14
E	0.00	0.00	0.00	0.00	0.00	0.00	0.00
ESE	0.00	0.00	0.00	0.00	0.00	0.00	0.00
SE	0.00	0.00	0.00	0.00	0.00	0.00	0.00
SSE	0.00	0.00	0.00	0.00	0.00	0.00	0.00
S	0.00	0.00	0.00	0.00	0.00	0.00	0.00
SSW	0.00	0.00	0.00	0.28	0.14	0.00	0.42
SW	0.00	0.42	0.56	0.14	0.14	0.00	1.26
WSW	0.00	0.28	0.14	0.28	0.14	0.00	0.84
W	0.00	0.00	0.00	0.00	0.14	0.00	0.14
WNW	0.00	0.00	0.00	0.00	0.00	0.00	0.00
WW	0.00	0.00	0.14	0.00	0.00	0.00	0.14
WNW	0.00	0.28	0.14	0.14	0.00	0.00	0.56
N	0.69	1.67	2.64	2.36	1.11	0.00	8.47
NNE	0.14	0.28	2.78	3.33	0.28	0.00	6.81
NE	0.14	0.14	0.14	0.14	0.00	0.00	0.56
ENE	0.00	0.28	0.00	0.00	0.00	0.00	0.28
E	0.14	0.00	0.00	0.00	0.00	0.00	0.14
ESE	0.14	0.14	0.14	0.00	0.00	0.00	0.42
SE	0.00	0.00	0.00	0.00	0.00	0.00	0.00
SSE	0.00	0.00	0.00	0.00	0.00	0.00	0.00
S	0.14	0.14	0.00	0.00	0.14	0.00	0.42
SSW	0.14	0.28	0.42	0.56	1.11	0.00	2.51
SW	0.28	1.25	2.50	2.22	0.97	0.00	7.22
WSW	0.14	0.42	1.25	2.64	0.69	0.00	5.14
W	0.00	0.00	0.56	0.42	0.00	0.00	0.98
WNW	0.00	0.56	0.28	0.28	0.00	0.00	1.12
WW	0.00	0.14	0.42	0.56	0.00	0.00	1.12
WNW	0.42	0.14	0.69	0.14	0.00	0.00	1.39
W	0.56	0.83	0.83	1.39	0.69	0.28	4.58
NNE	0.28	0.28	0.83	1.81	0.00	0.00	3.20
NE	0.00	0.00	0.28	0.28	0.00	0.00	0.56
ENE	0.00	1.25	0.14	0.00	0.00	0.00	1.39
E	0.14	0.14	0.00	0.00	0.00	0.00	0.28
ESE	0.14	0.00	0.00	0.00	0.00	0.00	0.14
SE	0.00	0.28	0.00	0.00	0.00	0.00	0.28
SSE	0.14	0.14	0.00	0.00	0.00	0.00	0.28
S	0.28	0.14	0.00	0.00	0.00	0.00	0.42
SSW	0.28	0.28	0.56	0.14	0.56	0.00	1.82
SW	0.14	0.42	1.94	3.75	1.25	0.00	7.50
WSW	0.42	0.69	1.53	1.81	0.28	0.00	4.73
W	0.00	0.28	0.00	0.00	0.00	0.00	0.28
WNW	0.14	0.00	0.00	0.14	0.00	0.00	0.28
WW	0.28	0.28	0.00	0.14	0.00	0.00	0.70
WNW	0.00	0.00	0.00	0.00	0.00	0.00	0.00
W	0.28	0.69	0.00	0.00	0.00	0.00	0.97
NNE	0.00	0.00	0.00	0.00	0.00	0.00	0.00
NE	0.00	0.14	0.00	0.00	0.00	0.00	0.14
ENE	0.00	0.28	0.00	0.00	0.00	0.00	0.28
E	0.00	0.28	0.28	0.00	0.00	0.00	0.56
ESE	0.00	0.56	0.00	0.00	0.00	0.00	0.56
SE	0.14	0.42	0.00	0.00	0.00	0.00	0.56
SSE	0.00	0.14	0.00	0.00	0.00	0.00	0.14
S	0.00	0.00	0.00	0.00	0.00	0.00	0.00
SSW	0.00	0.00	0.00	0.00	0.00	0.00	0.00
SW	0.00	0.56	0.42	0.56	0.56	0.00	2.10
WSW	0.00	0.28	0.56	0.69	0.00	0.00	1.53
W	0.00	0.14	0.00	0.00	0.00	0.00	0.14
WNW	0.14	0.00	0.00	0.00	0.00	0.00	0.14
WW	0.00	0.00	0.00	0.00	0.00	0.00	0.00



NNW	0.00	0.00	0.00	0.00	0.00	0.00	0.00
N	0.14	0.00	0.00	0.00	0.00	0.00	0.14
NNE	0.00	0.00	0.00	0.00	0.00	0.00	0.00
NE	0.00	0.00	0.00	0.00	0.00	0.00	0.00
ENE	0.00	0.00	0.00	0.00	0.00	0.00	0.00
E	0.14	0.00	0.00	0.00	0.00	0.00	0.14
ESE	0.00	0.00	0.00	0.00	0.00	0.00	0.00
SE	0.00	0.00	0.00	0.00	0.00	0.00	0.00
SSE	0.00	0.00	0.00	0.00	0.00	0.00	0.00
S	0.00	0.00	0.00	0.00	0.00	0.00	0.00
SSW	0.00	0.00	0.00	0.00	0.00	0.00	0.00
SW	0.00	0.00	0.00	0.00	0.00	0.00	0.00
WSW	0.00	0.00	0.00	0.00	0.00	0.00	0.00
W	0.00	0.00	0.00	0.00	0.00	0.00	0.00
WNW	0.00	0.00	0.00	0.00	0.00	0.00	0.00
WW	0.00	0.00	0.00	0.00	0.00	0.00	0.00
NNW	0.00	0.00	0.00	0.00	0.00	0.00	0.00
N	0.56	0.56	0.42	0.00	0.00	0.00	1.54
NNE	0.28	0.42	0.14	0.00	0.00	0.00	0.84
NE	0.28	0.14	0.00	0.00	0.00	0.00	0.42
ENE	0.00	0.14	0.00	0.00	0.00	0.00	0.14
E	0.28	0.00	0.00	0.00	0.00	0.00	0.28
ESE	0.14	0.00	0.00	0.00	0.00	0.00	0.14
SE	0.00	0.00	0.00	0.00	0.00	0.00	0.00
SSE	0.00	0.00	0.00	0.00	0.00	0.00	0.00
S	0.00	0.00	0.00	0.00	0.00	0.00	0.00
SSW	0.00	0.00	0.14	0.00	0.00	0.00	0.14
SW	0.00	0.00	0.28	0.14	0.00	0.00	0.42
WSW	0.00	0.28	0.28	0.56	0.00	0.00	1.12
W	0.00	0.14	0.14	0.00	0.00	0.00	0.28
WNW	0.00	0.00	0.00	0.14	0.00	0.00	0.14
WW	0.14	0.00	0.00	0.00	0.00	0.00	0.14
NNW	0.00	0.00	0.00	0.00	0.00	0.00	0.00
N	0.14	0.28	0.14	0.14	0.00	0.14	0.84
NNE	0.00	0.00	0.56	0.14	0.00	0.00	0.70
NE	0.00	0.00	0.00	0.00	0.00	0.00	0.00
ENE	0.00	0.00	0.00	0.00	0.00	0.00	0.00
E	0.00	0.00	0.00	0.00	0.00	0.00	0.00
ESE	0.00	0.00	0.00	0.00	0.00	0.00	0.00
SE	0.00	0.00	0.00	0.00	0.00	0.00	0.00
SSE	0.00	0.00	0.00	0.00	0.00	0.00	0.00
S	0.00	0.00	0.00	0.00	0.00	0.00	0.00
SSW	0.00	0.00	0.00	0.00	0.00	0.00	0.00
SW	0.00	0.00	0.14	0.00	0.14	0.00	0.28
WSW	0.00	0.00	0.00	0.28	0.00	0.00	0.28
W	0.00	0.00	0.00	0.00	0.00	0.00	0.00
WNW	0.00	0.00	0.00	0.14	0.00	0.00	0.14
WW	0.00	0.00	0.00	0.00	0.00	0.00	0.00
NNW	0.00	0.00	0.00	0.00	0.00	0.00	0.00
N	0.00	0.28	0.14	0.00	0.14	0.14	0.70
NNE	0.00	0.28	0.00	0.28	0.14	0.00	0.70
NE	0.00	0.14	0.14	0.00	0.00	0.00	0.28
ENE	0.14	0.14	0.00	0.14	0.00	0.00	0.42
E	0.00	0.00	0.00	0.00	0.00	0.00	0.00
ESE	0.00	0.00	0.00	0.00	0.00	0.00	0.00
SE	0.00	0.00	0.00	0.00	0.00	0.00	0.00
SSE	0.00	0.00	0.00	0.00	0.00	0.00	0.00
S	0.00	0.00	0.00	0.00	0.00	0.00	0.00
SSW	0.00	0.00	0.00	0.00	0.00	0.00	0.00
SW	0.00	0.00	0.00	0.00	0.00	0.00	0.00
WSW	0.00	0.00	0.00	0.00	0.14	0.00	0.14
W	0.14	0.00	0.14	0.28	0.14	0.00	0.70
WNW	0.00	0.00	0.00	0.00	0.00	0.14	0.14
WW	0.00	0.00	0.00	0.14	0.00	0.00	0.14
NNW	0.14	0.00	0.00	0.00	0.00	0.00	0.14
N	0.84	0.98	1.97	2.25	1.55	1.13	8.72

NNE	0.00	1.13	2.67	6.47	0.98	0.00	11.25
NE	0.00	0.70	0.84	0.70	0.42	0.00	2.66
ENE	0.00	0.42	0.42	0.28	0.14	0.00	1.26
E	0.28	0.28	0.14	0.00	0.00	0.00	0.70
ESE	0.14	0.00	0.14	0.00	0.00	0.00	0.28
SE	0.00	0.00	0.00	0.00	0.00	0.00	0.00
SSE	0.00	0.00	0.00	0.00	0.00	0.00	0.00
S	0.00	0.00	0.00	0.00	0.00	0.00	0.00
SSW	0.00	0.00	0.00	0.00	0.00	0.00	0.00
SW	0.00	0.00	0.98	0.28	0.84	0.00	2.10
WSW	0.14	0.00	1.13	1.69	0.84	0.28	4.08
W	0.00	0.28	0.42	0.98	0.70	0.42	2.80
WNW	0.14	0.00	0.14	0.00	0.42	0.14	0.84
WW	0.14	0.00	0.00	0.00	0.00	0.00	0.14
WNW	0.14	0.00	0.00	0.14	0.14	0.00	0.42
W	1.27	1.13	1.55	2.39	1.97	1.41	9.72
NNE	0.00	0.42	1.69	4.08	0.28	0.00	6.47
NE	0.00	0.56	1.69	0.70	0.84	0.00	3.79
ENE	0.70	0.84	1.69	0.28	0.70	0.00	4.21
E	0.14	0.42	0.42	0.56	0.00	0.00	1.54
ESE	0.14	0.14	0.42	0.00	0.00	0.00	0.70
SE	0.14	0.00	0.14	0.00	0.00	0.00	0.28
SSE	0.14	0.00	0.00	0.00	0.00	0.00	0.14
S	0.00	0.00	0.00	0.00	0.00	0.00	0.00
SSW	0.00	0.00	0.00	0.00	0.00	0.00	0.00
SW	0.00	0.00	1.27	0.14	0.28	0.14	1.83
WSW	0.00	0.42	0.28	1.27	1.27	0.00	3.24
W	0.14	0.56	0.70	1.13	0.56	0.14	3.23
WNW	0.00	0.00	0.42	0.98	0.42	0.00	1.82
WW	0.00	0.00	0.00	0.00	0.00	0.00	0.00
WNW	0.00	0.00	0.00	0.14	0.00	0.00	0.14
W	0.42	0.98	0.14	0.42	0.14	0.00	2.10
NNE	0.00	0.42	0.14	0.14	0.00	0.00	0.70
NE	0.00	0.00	0.00	0.70	0.00	0.00	0.70
ENE	0.00	0.28	0.42	0.14	0.00	0.00	0.84
E	0.14	0.14	0.00	0.14	0.00	0.00	0.42
ESE	0.00	0.28	0.00	0.00	0.00	0.00	0.28
SE	0.00	0.14	0.00	0.00	0.00	0.00	0.14
SSE	0.00	0.00	0.00	0.00	0.00	0.00	0.00
S	0.00	0.14	0.00	0.00	0.00	0.00	0.14
SSW	0.14	0.28	0.00	0.00	0.00	0.00	0.42
SW	0.14	0.00	0.14	0.00	0.00	0.00	0.28
WSW	0.00	0.00	0.56	0.56	0.00	0.00	1.12
W	0.00	0.14	0.70	0.84	0.00	0.00	1.68
WNW	0.00	0.28	0.28	0.00	0.00	0.00	0.56
WW	0.00	0.00	0.00	0.00	0.00	0.00	0.00
WNW	0.00	0.00	0.00	0.00	0.00	0.00	0.00
W	0.70	1.97	0.56	0.14	0.00	0.00	3.37
NNE	0.00	0.14	0.00	0.00	0.00	0.00	0.14
NE	0.00	0.00	0.00	0.00	0.00	0.00	0.00
ENE	0.00	0.00	0.00	0.28	0.00	0.00	0.28
E	0.00	0.28	0.28	0.00	0.00	0.00	0.56
ESE	0.00	0.14	0.00	0.00	0.00	0.00	0.14
SE	0.00	0.14	0.00	0.00	0.00	0.00	0.14
SSE	0.14	0.00	0.00	0.00	0.00	0.00	0.14
S	0.00	0.00	0.00	0.00	0.00	0.00	0.00
SSW	0.00	0.00	0.00	0.00	0.00	0.00	0.00
SW	0.00	0.00	0.00	0.00	0.00	0.00	0.00
WSW	0.00	0.00	0.70	0.00	0.00	0.00	0.70
W	0.00	0.14	0.42	0.28	0.00	0.00	0.84
WNW	0.14	0.00	0.00	0.00	0.00	0.00	0.14
WW	0.00	0.00	0.00	0.00	0.00	0.00	0.00
WNW	0.00	0.00	0.00	0.00	0.00	0.00	0.00
W	0.00	0.00	0.00	0.00	0.00	0.00	0.00
NNE	0.16	0.00	0.16	0.00	0.00	0.00	0.32
NR	0.00	0.16	0.16	0.00	0.00	0.00	0.32

ENE	0.32	0.49	0.00	0.00	0.00	0.00	0.81
E	0.32	0.49	0.00	0.00	0.00	0.00	0.81
ESE	0.00	0.16	0.00	0.00	0.00	0.00	0.16
SE	0.32	0.00	0.00	0.00	0.00	0.00	0.32
SSE	0.00	0.16	0.00	0.00	0.00	0.00	0.16
S	0.16	0.16	0.00	0.00	0.00	0.00	0.32
SSW	0.16	0.32	0.65	0.00	0.00	0.00	1.13
SW	0.00	1.79	0.65	0.00	0.00	0.00	2.44
WSW	0.00	0.49	0.16	0.16	0.00	0.00	0.81
W	0.00	0.32	0.81	0.32	0.00	0.00	1.45
WNW	0.00	0.00	0.00	0.32	0.16	0.00	0.48
NW	0.00	0.00	0.00	0.00	0.00	0.00	0.00
NNW	0.00	0.00	0.00	0.00	0.00	0.00	0.00
N	0.00	0.00	0.00	0.00	0.00	0.16	0.16
NNE	0.00	0.00	0.00	0.00	0.00	0.16	0.16
NE	0.00	0.16	0.00	0.00	0.00	0.00	0.16
ENE	0.00	0.16	0.00	0.16	0.00	0.00	0.32
E	0.00	0.00	0.00	0.00	0.00	0.00	0.00
ESE	0.00	0.00	0.00	0.00	0.00	0.00	0.00
SE	0.00	0.00	0.00	0.00	0.00	0.00	0.00
SSE	0.00	0.00	0.00	0.00	0.00	0.00	0.00
S	0.00	0.00	0.00	0.00	0.00	0.00	0.00
SSW	0.00	0.16	0.16	0.00	0.00	0.00	0.32
SW	0.00	0.81	0.16	0.00	0.00	0.00	0.97
WSW	0.00	0.16	0.16	0.16	0.00	0.00	0.48
W	0.00	0.00	0.16	0.16	0.00	0.00	0.32
WNW	0.00	0.00	0.00	0.65	0.00	0.00	0.65
NW	0.00	0.00	0.00	0.00	0.00	0.00	0.00
NNW	0.00	0.00	0.00	0.00	0.00	0.00	0.00
N	0.00	0.00	0.00	0.16	0.00	0.00	0.16
NNE	0.00	0.00	0.16	0.00	0.00	0.00	0.16
NE	0.00	0.16	0.16	0.49	0.16	0.00	0.97
ENE	0.00	0.00	0.00	0.00	0.00	0.00	0.00
E	0.00	0.16	0.00	0.00	0.00	0.00	0.16
ESE	0.00	0.00	0.00	0.00	0.00	0.00	0.00
SE	0.00	0.00	0.00	0.00	0.00	0.00	0.00
SSE	0.00	0.00	0.00	0.00	0.00	0.00	0.00
S	0.00	0.00	0.00	0.00	0.00	0.00	0.00
SSW	0.00	0.00	0.00	0.00	0.00	0.00	0.00
SW	0.00	0.49	0.65	0.16	0.00	0.00	1.30
WSW	0.00	0.00	0.16	0.00	0.00	0.00	0.16
W	0.00	0.00	0.00	0.16	0.00	0.00	0.16
WNW	0.00	0.00	0.00	0.16	0.16	0.00	0.32
NW	0.00	0.00	0.00	0.00	0.00	0.16	0.16
NNW	0.00	0.00	0.00	0.00	0.00	0.00	0.00
N	0.00	0.16	0.81	1.95	0.49	0.00	3.41
NNE	0.00	0.00	0.49	1.14	1.62	0.49	3.74
NE	0.00	1.46	1.79	2.44	2.27	0.32	8.28
ENE	0.00	0.32	0.16	0.16	0.00	0.00	0.64
E	0.16	0.16	0.16	0.00	0.00	0.00	0.48
ESE	0.00	0.16	0.00	0.00	0.00	0.00	0.16
SE	0.00	0.16	0.00	0.00	0.00	0.00	0.16
SSE	0.16	0.00	0.00	0.00	0.00	0.00	0.16
S	0.00	0.16	0.00	0.00	0.00	0.00	0.16
SSW	0.16	0.00	0.00	0.00	0.00	0.00	0.16
SW	0.00	0.32	0.81	0.81	0.00	0.00	1.94
WSW	0.00	0.00	0.16	1.14	0.16	0.00	1.46
W	0.00	0.00	1.14	2.27	0.81	0.00	4.22
WNW	0.00	0.00	0.32	0.65	1.30	0.32	2.59
NW	0.00	0.16	0.16	0.32	0.00	0.16	0.80
NNW	0.00	0.32	0.16	0.81	0.16	0.00	1.45
N	0.00	0.32	0.81	1.14	0.16	0.00	2.43
NNE	0.00	0.65	0.97	0.81	1.14	0.32	3.89
NE	0.00	0.97	1.79	1.30	1.95	0.00	6.01
ENE	0.00	0.32	1.14	0.65	0.00	0.00	2.11
E	0.00	0.65	0.97	0.00	0.00	0.00	1.62



ES E	0.16	0.97	0.32	0.00	0.00	0.00	1.45
SE	0.16	0.16	0.00	0.00	0.00	0.00	0.32
SS E	0.16	0.00	0.16	0.00	0.00	0.00	0.32
S	0.00	0.32	0.00	0.00	0.00	0.00	0.32
SS W	0.00	0.49	0.00	0.00	0.00	0.00	0.49
SW	0.00	0.32	0.97	0.49	0.00	0.00	1.78
WS W	0.00	1.14	2.27	2.76	0.49	0.00	6.66
W	0.16	0.49	1.46	2.11	0.97	0.00	5.19
WN W	0.16	0.16	0.16	0.32	0.16	0.00	0.96
NW	0.00	0.16	0.32	0.81	0.00	0.00	1.29
NN W	0.00	0.49	0.32	0.65	0.16	0.00	1.62
N	0.00	0.16	0.00	0.00	0.00	0.00	0.16
NNE	0.00	0.16	0.00	0.00	0.00	0.00	0.16
NE	0.16	0.49	0.16	0.16	0.00	0.00	0.97
ENE	0.00	0.32	0.65	0.16	0.00	0.00	1.13
E	0.16	0.32	0.81	0.16	0.00	0.00	1.45
ES E	0.00	0.16	0.32	0.00	0.00	0.00	0.48
SE	0.16	0.49	0.00	0.00	0.00	0.00	0.65
SSE	0.32	0.16	0.00	0.00	0.00	0.00	0.48
S	0.16	0.16	0.00	0.00	0.00	0.00	0.32
SS W	0.16	0.32	0.00	0.00	0.00	0.00	0.48
SW	0.32	0.00	0.81	0.49	0.00	0.00	1.62
WS W	0.32	0.16	0.97	0.65	0.00	0.00	2.10
W	0.00	0.49	0.49	0.00	0.00	0.00	0.98
WN W	0.00	0.00	0.00	0.00	0.00	0.00	0.00
NW	0.00	0.16	0.00	0.00	0.00	0.00	0.16
NN W	0.00	0.00	0.00	0.00	0.00	0.00	0.00
N	0.00	0.00	0.00	0.00	0.00	0.00	0.00
NNE	0.00	0.00	0.00	0.00	0.00	0.00	0.00
NE	0.16	0.00	0.32	0.00	0.00	0.00	0.48
ENE	0.00	0.32	0.65	0.00	0.00	0.00	0.97
E	0.00	0.81	0.16	0.00	0.00	0.00	0.97
ES E	0.00	1.14	0.00	0.00	0.00	0.00	1.14
SE	0.00	0.00	0.00	0.00	0.00	0.00	0.00
SSE	0.16	0.16	0.00	0.00	0.00	0.00	0.32
S	0.00	0.00	0.00	0.00	0.00	0.00	0.00
SS W	0.00	0.16	0.16	0.00	0.00	0.00	0.32
SW	0.00	0.00	0.32	0.16	0.00	0.00	0.48
WS W	0.32	0.16	0.00	0.00	0.00	0.00	0.48
W	0.16	0.00	0.00	0.00	0.00	0.00	0.16
WN W	0.00	0.00	0.00	0.00	0.00	0.00	0.00
NW	0.00	0.00	0.00	0.00	0.00	0.00	0.00
NN W	0.16	0.00	0.00	0.00	0.00	0.00	0.16
N	0.00	0.00	0.00	0.00	0.00	0.00	0.00
NNE	0.14	0.00	0.00	0.00	0.00	0.00	0.14
NE	0.42	0.28	0.14	0.00	0.00	0.00	0.84
ENE	0.14	0.28	0.00	0.00	0.00	0.00	0.42
E	0.14	0.14	0.00	0.00	0.00	0.00	0.28
ES E	0.00	0.00	0.00	0.00	0.00	0.00	0.00
SE	0.00	0.00	0.00	0.00	0.00	0.00	0.00
SSE	0.14	0.14	0.00	0.00	0.00	0.00	0.28
S	0.00	0.00	0.00	0.14	0.00	0.00	0.14
SS W	0.00	0.28	0.14	0.00	0.00	0.00	0.42
SW	0.00	0.70	0.84	0.00	0.00	0.14	1.68
WS W	0.28	0.28	0.14	0.00	0.00	0.00	0.70
W	0.00	0.00	0.28	0.00	0.56	0.00	0.84
WN W	0.00	0.00	0.00	0.00	0.42	0.14	0.56
NW	0.00	0.00	0.00	0.00	0.00	0.00	0.00
NN W	0.14	0.00	0.00	0.00	0.00	0.00	0.14
N	0.00	0.00	0.00	0.00	0.00	0.00	0.00
NNE	0.00	0.14	0.00	0.00	0.00	0.00	0.14
NE	0.00	0.14	0.00	0.00	0.00	0.00	0.14
ENE	0.00	0.00	0.00	0.00	0.00	0.00	0.00
E	0.00	0.14	0.00	0.00	0.00	0.00	0.14
ES E	0.14	0.00	0.00	0.00	0.00	0.00	0.14
SE	0.00	0.28	0.00	0.00	0.00	0.00	0.28

SS E	0.00	0.00	0.00	0.00	0.00	0.00	0.00
S	0.00	0.00	0.14	0.00	0.00	0.00	0.14
SS W	0.00	0.00	0.14	0.00	0.00	0.00	0.14
SW	0.00	0.00	0.28	0.00	0.14	0.00	0.42
WS W	0.00	0.00	0.28	0.14	0.14	0.00	0.56
W	0.00	0.00	0.00	0.14	0.00	0.14	0.28
WN W	0.00	0.00	0.00	0.14	0.28	0.42	0.84
WW	0.00	0.00	0.00	0.00	0.00	0.00	0.00
WN W	0.00	0.00	0.00	0.00	0.00	0.00	0.00
N	0.00	0.00	0.00	0.00	0.00	0.00	0.00
NNE	0.00	0.00	0.14	0.00	0.00	0.00	0.14
NE	0.00	0.00	0.14	0.00	0.00	0.00	0.14
ENE	0.00	0.00	0.28	0.00	0.00	0.00	0.28
E	0.14	0.00	0.14	0.00	0.00	0.00	0.28
ESE	0.00	0.00	0.00	0.00	0.00	0.00	0.00
SE	0.00	0.14	0.14	0.00	0.00	0.00	0.28
SS E	0.00	0.00	0.00	0.14	0.00	0.00	0.14
S	0.00	0.00	0.00	0.14	0.00	0.00	0.14
SS W	0.00	0.00	0.00	0.14	0.00	0.00	0.14
SW	0.00	0.00	0.42	0.00	0.00	0.00	0.42
WS W	0.00	0.00	0.14	0.14	0.00	0.00	0.28
W	0.00	0.14	0.00	0.00	0.14	0.14	0.42
WN W	0.00	0.14	0.00	0.00	0.00	0.00	0.14
WW	0.00	0.00	0.00	0.00	0.00	0.00	0.00
WN W	0.00	0.00	0.00	0.00	0.00	0.00	0.00
N	0.28	0.14	0.14	0.70	0.14	0.00	1.40
NNE	0.00	0.56	0.14	0.00	0.00	0.00	0.70
NE	0.00	0.70	1.39	0.56	0.00	0.00	2.65
ENE	0.00	0.14	0.84	0.28	0.00	0.00	1.26
E	0.00	1.12	0.56	0.28	0.00	0.00	1.96
ESE	0.00	0.56	0.14	0.00	0.28	0.00	0.98
SE	0.00	0.42	0.28	0.00	0.00	0.00	0.70
SS E	0.14	0.42	0.14	0.00	0.00	0.00	0.70
S	0.00	0.14	0.70	0.28	0.00	0.00	1.12
SS W	0.00	0.56	0.56	0.84	0.14	0.28	2.38
SW	0.00	0.28	1.39	0.98	0.98	0.28	3.91
WS W	0.00	0.28	1.26	0.56	0.42	0.28	2.80
W	0.14	0.28	0.42	0.28	0.84	1.39	3.35
WN W	0.00	0.00	0.00	0.14	0.14	0.70	0.98
WW	0.00	0.00	0.00	0.00	0.14	0.00	0.14
WN W	0.00	0.00	0.00	0.00	0.00	0.00	0.00
N	0.00	0.14	0.28	0.14	0.00	0.00	0.56
NNE	0.28	0.28	0.56	0.14	0.14	0.00	1.40
NE	0.42	0.42	1.81	0.98	0.28	0.00	3.91
ENE	0.42	0.28	2.37	1.81	0.00	0.00	4.88
E	0.28	1.39	2.93	0.70	0.14	0.00	5.44
ESE	0.14	0.84	0.56	0.14	0.00	0.00	1.68
SE	0.42	0.84	0.28	0.28	0.14	0.00	1.96
SS E	0.28	0.56	0.28	0.00	0.14	0.00	1.26
S	0.14	0.42	1.12	0.42	0.14	0.00	2.24
SS W	0.28	0.42	0.98	1.67	0.84	0.00	4.19
SW	0.00	0.00	0.98	2.51	1.12	0.14	4.75
WS W	0.14	0.42	0.84	1.67	0.70	0.00	3.77
W	0.14	0.14	1.12	1.12	0.00	0.14	2.66
WN W	0.28	0.28	0.28	1.39	0.28	0.00	2.51
WW	0.28	0.28	0.14	0.56	0.00	0.00	1.26
WN W	0.00	0.14	0.56	0.14	0.00	0.00	0.84
N	0.00	0.28	0.00	0.00	0.00	0.00	0.28
NNE	0.00	0.00	0.28	0.14	0.00	0.00	0.42
NE	0.00	0.56	1.39	0.28	0.00	0.00	2.23
ENE	0.00	0.42	2.93	1.12	0.00	0.00	4.47
E	0.00	0.56	0.42	0.14	0.00	0.00	1.12
ESE	0.14	0.98	0.28	0.00	0.00	0.00	1.40
SE	0.00	0.42	0.14	0.00	0.00	0.00	0.56
SS E	0.00	0.28	0.14	0.00	0.00	0.00	0.42
S	0.00	0.00	0.00	0.00	0.00	0.00	0.00

SSW	0.00	0.14	0.42	0.42	0.00	0.00	0.98
SW	0.00	0.56	0.42	0.42	0.42	0.00	1.82
WSW	0.00	0.70	0.70	0.00	0.00	0.00	1.40
W	0.14	0.14	0.14	0.14	0.00	0.00	0.56
WNW	0.00	0.42	0.00	0.00	0.00	0.00	0.42
WW	0.14	0.14	0.00	0.14	0.00	0.00	0.42
WNW	0.00	0.00	0.14	0.00	0.00	0.00	0.14
W	0.00	0.00	0.00	0.00	0.00	0.00	0.00
WNW	0.00	0.00	0.28	0.00	0.00	0.00	0.28
WE	0.00	0.00	0.28	0.14	0.00	0.00	0.42
ENE	0.00	0.00	0.00	0.28	0.00	0.00	0.28
E	0.00	0.00	0.28	0.00	0.00	0.00	0.28
ESE	0.00	0.00	0.00	0.00	0.00	0.00	0.00
SE	0.00	0.00	0.00	0.00	0.00	0.00	0.00
SSE	0.00	0.00	0.00	0.00	0.00	0.00	0.00
S	0.14	0.00	0.00	0.00	0.00	0.00	0.14
SSW	0.14	0.14	0.00	0.00	0.00	0.00	0.28
SW	0.00	0.00	0.14	0.14	0.00	0.00	0.28
WSW	0.00	0.14	0.42	0.00	0.00	0.00	0.56
W	0.00	0.00	0.28	0.00	0.00	0.00	0.28
WNW	0.00	0.00	0.00	0.00	0.00	0.00	0.00
WW	0.00	0.00	0.00	0.00	0.00	0.00	0.00
WNW	0.00	0.00	0.00	0.00	0.00	0.00	0.00
W	0.00	0.00	0.00	0.00	0.00	0.00	0.00
WNW	0.00	0.00	0.00	0.00	0.00	0.00	0.00
WE	0.00	0.00	0.14	0.00	0.00	0.00	0.14
ENE	0.00	0.28	0.00	0.00	0.00	0.00	0.28
E	0.14	0.14	0.00	0.00	0.00	0.00	0.28
ESE	0.14	0.00	0.00	0.00	0.00	0.00	0.14
SE	0.00	0.14	0.00	0.00	0.00	0.00	0.14
SSE	0.00	0.00	0.00	0.00	0.00	0.00	0.00
S	0.00	0.00	0.00	0.00	0.00	0.00	0.00
SSW	0.00	0.14	0.85	0.14	0.00	0.00	1.13
SW	0.00	1.42	1.71	0.28	0.00	0.28	3.69
WSW	0.14	0.28	0.71	0.57	0.28	0.00	1.98
W	0.14	0.43	0.85	0.00	0.00	0.28	1.70
WNW	0.00	0.28	0.43	1.14	0.14	0.43	2.42
WW	0.00	0.00	0.28	0.43	0.00	0.00	0.71
WNW	0.00	0.00	0.00	0.00	0.00	0.00	0.00
W	0.00	0.00	0.00	0.00	0.00	0.00	0.00
WNW	0.00	0.00	0.00	0.00	0.00	0.00	0.00
WE	0.00	0.00	0.14	0.14	0.00	0.00	0.28
ENE	0.00	0.00	0.00	0.00	0.00	0.00	0.00
E	0.00	0.00	0.00	0.00	0.00	0.00	0.00
ESE	0.00	0.00	0.00	0.00	0.00	0.00	0.00
SE	0.00	0.00	0.00	0.00	0.00	0.00	0.00
SSE	0.00	0.00	0.00	0.00	0.00	0.00	0.00
S	0.00	0.00	0.00	0.00	0.00	0.00	0.00
SSW	0.00	0.00	0.14	0.00	0.00	0.14	0.28
SW	0.00	0.43	0.28	0.14	0.14	0.00	0.99
WSW	0.00	0.00	0.00	0.28	0.14	0.00	0.42
W	0.00	0.00	0.00	0.14	0.28	0.43	0.85
WNW	0.00	0.00	0.00	0.14	0.28	0.14	0.56
WW	0.14	0.00	0.00	0.00	0.00	0.00	0.14
WNW	0.00	0.00	0.00	0.00	0.00	0.00	0.00
W	0.00	0.00	0.00	0.00	0.00	0.00	0.00
WNW	0.00	0.00	0.00	0.00	0.00	0.00	0.00
WE	0.00	0.00	0.14	0.00	0.00	0.00	0.14
ENE	0.00	0.00	0.00	0.00	0.00	0.00	0.00
E	0.00	0.14	0.00	0.00	0.00	0.00	0.14
ESE	0.00	0.00	0.00	0.00	0.00	0.00	0.00
SE	0.14	0.28	0.00	0.00	0.00	0.00	0.42
SSE	0.00	0.00	0.00	0.00	0.00	0.00	0.00
S	0.00	0.00	0.00	0.14	0.00	0.00	0.14
SSW	0.14	0.00	0.00	0.00	0.00	0.00	0.14
SW	0.00	0.00	0.28	0.43	0.00	0.28	0.99



WSW	0.00	0.14	0.00	0.00	0.28	0.00	0.42
W	0.00	0.43	0.14	0.00	0.14	0.57	1.28
WWW	0.00	0.00	0.00	0.00	0.43	0.00	0.43
WW	0.00	0.00	0.14	0.00	0.00	0.00	0.14
WWW	0.00	0.00	0.00	0.00	0.00	0.00	0.00
W	0.00	0.14	0.14	0.00	0.14	0.00	0.42
WWE	0.00	0.00	0.43	0.14	0.28	0.00	0.85
WE	0.00	0.00	1.00	0.57	0.14	0.00	1.71
WWE	0.00	0.14	0.43	0.43	0.00	0.14	1.14
E	0.00	0.28	0.00	0.00	0.00	0.00	0.28
ESE	0.14	0.14	0.00	0.00	0.00	0.00	0.28
SE	0.00	0.14	0.00	0.00	0.00	0.00	0.14
SSE	0.14	0.00	0.00	0.00	0.00	0.00	0.14
S	0.00	0.14	0.43	0.57	0.00	0.00	1.14
SSW	0.00	0.57	0.28	0.14	0.14	0.28	1.41
SW	0.14	0.28	0.71	2.28	1.28	0.57	5.26
WSW	0.00	0.00	0.43	0.57	1.00	0.43	2.43
W	0.00	0.14	0.28	1.14	1.14	2.28	4.98
WWW	0.00	0.00	0.71	1.99	0.85	0.28	3.83
WW	0.00	0.00	0.28	0.57	0.14	0.00	0.99
WWW	0.00	0.00	0.28	0.43	0.43	0.00	1.14
W	0.14	0.00	0.14	0.00	0.00	0.00	0.28
WWE	0.14	0.14	0.71	0.57	0.28	0.00	1.84
WE	0.00	0.57	1.42	1.71	0.28	0.00	3.98
WWE	0.00	0.85	0.71	0.28	0.28	0.00	2.12
E	0.14	0.43	1.14	0.28	0.00	0.00	1.99
ESE	0.00	0.71	0.28	0.00	0.00	0.00	0.99
SE	0.14	1.28	0.00	0.00	0.00	0.00	1.42
SSE	0.28	0.14	0.28	0.00	0.00	0.00	0.70
S	0.28	0.57	0.28	0.57	0.28	0.00	1.98
SSW	0.14	0.14	1.42	1.00	0.85	0.00	3.55
SW	0.14	1.00	0.85	2.14	2.28	0.28	6.69
WSW	0.14	0.28	1.28	2.42	1.42	0.57	6.11
W	0.00	0.43	1.00	0.57	1.00	0.14	3.14
WWW	0.00	0.14	0.85	1.42	0.00	0.00	2.41
WW	0.00	0.57	0.28	0.28	0.00	0.00	1.13
WWW	0.14	0.14	0.28	1.42	0.43	0.00	2.41
W	0.00	0.00	0.00	0.00	0.00	0.00	0.00
WWE	0.00	0.00	0.00	0.14	0.00	0.00	0.14
WE	0.00	0.00	0.00	0.57	0.14	0.00	0.71
WWE	0.00	0.14	0.00	0.00	0.00	0.00	0.14
E	0.00	0.00	0.00	0.00	0.00	0.00	0.00
ESE	0.00	0.14	0.00	0.00	0.00	0.00	0.14
SE	0.00	0.57	0.43	0.00	0.00	0.00	1.00
SSE	0.00	0.14	0.85	0.00	0.00	0.00	0.99
S	0.00	0.14	0.28	0.14	0.00	0.00	0.56
SSW	0.00	0.14	0.00	0.43	0.00	0.00	0.57
SW	0.14	0.14	0.85	0.28	0.43	0.00	1.84
WSW	0.00	0.28	0.71	0.71	0.14	0.00	1.84
W	0.28	0.00	0.14	0.00	0.14	0.00	0.56
WWW	0.14	0.00	0.00	0.00	0.00	0.00	0.14
WW	0.00	0.14	0.28	0.00	0.00	0.00	0.42
WWW	0.00	0.00	0.00	0.00	0.00	0.00	0.00
W	0.00	0.14	0.00	0.00	0.00	0.00	0.14
WWE	0.00	0.00	0.00	0.00	0.00	0.00	0.00
WE	0.00	0.00	0.00	0.00	0.00	0.00	0.00
WWE	0.00	0.00	0.00	0.00	0.00	0.00	0.00
E	0.00	0.00	0.00	0.00	0.00	0.00	0.00
ESE	0.00	0.28	0.00	0.00	0.00	0.00	0.28
SE	0.00	0.00	0.14	0.00	0.00	0.00	0.14
SSE	0.00	0.14	0.14	0.00	0.00	0.00	0.28
S	0.14	0.14	0.00	0.00	0.00	0.00	0.28
SSW	0.00	0.00	0.00	0.00	0.00	0.00	0.00
SW	0.00	0.14	0.14	0.14	0.00	0.00	0.42
WSW	0.28	0.14	0.14	0.14	0.00	0.00	0.70
W	0.14	0.00	0.00	0.00	0.00	0.00	0.14

NNW	0.14	0.28	0.00	0.00	0.00	0.00	0.42
NW	0.14	0.00	0.00	0.00	0.00	0.00	0.14
NNW	0.00	0.00	0.00	0.00	0.00	0.00	0.00
N	0.68	0.41	0.14	0.00	0.00	0.00	1.23
NNE	0.41	0.00	0.14	0.00	0.00	0.00	0.55
NE	0.00	0.14	0.00	0.00	0.00	0.00	0.14
NNE	0.68	0.14	0.14	0.00	0.00	0.00	0.96
E	0.00	0.14	0.00	0.00	0.00	0.00	0.14
ESE	0.14	0.14	0.00	0.00	0.00	0.00	0.28
SE	0.14	0.00	0.00	0.00	0.00	0.00	0.14
SSE	0.14	0.00	0.00	0.00	0.00	0.00	0.14
S	0.14	0.14	0.00	0.00	0.00	0.00	0.28
SSW	0.54	0.68	0.27	0.00	0.00	0.00	1.49
SW	0.68	1.36	1.09	0.41	0.27	0.00	3.81
WSW	0.14	0.81	1.09	0.68	0.00	0.00	2.72
W	0.00	0.68	0.41	0.14	0.00	0.00	1.23
NNW	0.00	0.41	0.00	0.00	0.00	0.00	0.41
NW	0.00	0.00	0.27	0.00	0.00	0.00	0.27
NNW	0.27	0.41	0.27	0.00	0.00	0.00	0.95
N	0.00	0.14	0.00	0.00	0.00	0.00	0.14
NNE	0.14	0.14	0.00	0.00	0.00	0.00	0.28
NE	0.00	0.14	0.14	0.00	0.00	0.00	0.28
NNE	0.00	0.27	0.00	0.00	0.00	0.00	0.27
E	0.14	0.14	0.00	0.00	0.00	0.00	0.28
ESE	0.27	0.00	0.00	0.00	0.00	0.00	0.27
SE	0.27	0.14	0.00	0.00	0.00	0.00	0.41
SSE	0.00	0.00	0.00	0.00	0.00	0.00	0.00
S	0.00	0.00	0.00	0.00	0.00	0.00	0.00
SSW	0.00	0.00	0.14	0.00	0.00	0.00	0.14
SW	0.00	0.00	0.41	0.27	0.00	0.41	1.09
WSW	0.14	0.14	0.14	0.27	0.00	0.00	0.69
W	0.00	0.14	0.00	0.00	0.00	0.00	0.14
NNW	0.00	0.00	0.27	0.14	0.00	0.00	0.41
NW	0.00	0.00	0.00	0.00	0.00	0.00	0.00
NNW	0.00	0.00	0.14	0.00	0.14	0.00	0.28
N	0.00	0.00	0.14	0.00	0.00	0.00	0.14
NNE	0.00	0.14	0.14	0.00	0.00	0.00	0.28
NE	0.00	0.14	0.00	0.14	0.00	0.00	0.28
NNE	0.00	0.00	0.14	0.00	0.00	0.00	0.14
E	0.14	0.00	0.00	0.00	0.00	0.00	0.14
ESE	0.00	0.14	0.00	0.00	0.00	0.00	0.14
SE	0.00	0.00	0.00	0.00	0.00	0.00	0.00
SSE	0.00	0.00	0.00	0.00	0.00	0.00	0.00
S	0.00	0.00	0.14	0.00	0.00	0.00	0.14
SSW	0.00	0.00	0.14	0.00	0.27	0.00	0.41
SW	0.00	0.00	0.27	0.41	0.14	0.14	0.96
WSW	0.00	0.00	0.27	0.00	0.00	0.00	0.27
W	0.00	0.00	0.00	0.00	0.00	0.00	0.00
NNW	0.00	0.00	0.00	0.00	0.00	0.00	0.00
NW	0.00	0.00	0.00	0.00	0.00	0.00	0.00
NNW	0.00	0.27	0.14	0.00	0.00	0.00	0.41
N	0.14	0.41	0.41	0.27	0.00	0.00	1.23
NNE	0.14	0.14	0.00	0.27	0.00	0.00	0.55
NE	0.00	0.68	0.95	0.27	0.00	0.00	1.90
NNE	0.00	0.27	0.00	0.00	0.00	0.00	0.27
E	0.00	0.14	0.00	0.14	0.00	0.00	0.28
ESE	0.14	0.00	0.00	0.00	0.00	0.00	0.14
SE	0.14	0.14	0.00	0.00	0.00	0.00	0.28
SSE	0.27	0.27	0.00	0.00	0.00	0.00	0.54
S	0.14	0.14	0.00	0.14	0.14	0.00	0.56
SSW	0.00	0.00	0.68	0.14	0.00	0.14	0.96
SW	0.00	0.81	0.95	1.49	1.22	0.41	4.88
WSW	0.00	0.00	0.41	0.95	0.27	0.27	1.90
W	0.27	0.41	0.54	0.54	0.41	0.00	2.17
NNW	0.00	0.14	0.14	0.14	0.00	0.00	0.42
NW	0.00	0.00	0.14	0.00	0.00	0.00	0.14

NH	0.00	0.27	0.68	0.14	0.14	0.00	1.23
N	0.14	0.54	1.90	0.81	0.14	0.14	3.67
NNE	0.00	0.54	1.49	0.54	0.00	0.00	2.57
NE	0.14	0.54	0.81	0.41	0.14	0.00	2.04
NNE	0.00	0.54	0.00	0.27	0.00	0.00	0.81
E	0.41	0.00	0.14	0.00	0.00	0.00	0.55
ESE	0.14	0.27	0.27	0.14	0.00	0.00	0.82
SE	0.00	0.00	0.00	0.00	0.00	0.00	0.00
SSE	0.00	0.41	0.00	0.14	0.00	0.00	0.55
S	0.00	0.27	0.68	0.27	0.27	0.00	1.49
SSW	0.14	0.54	0.95	1.09	0.41	0.14	3.27
SW	0.54	0.81	1.36	2.31	2.04	0.27	7.33
WSW	0.14	0.81	2.85	1.49	0.27	0.14	5.70
W	0.00	0.54	0.95	0.81	0.41	0.00	2.71
WWW	0.00	0.27	0.54	0.14	0.00	0.27	1.22
WW	0.00	0.14	0.27	0.14	0.00	0.00	0.55
NH	0.27	0.27	1.36	0.27	0.00	0.00	2.17
N	0.00	0.14	0.54	0.00	0.00	0.00	0.68
NNE	0.14	0.54	0.95	0.14	0.00	0.00	1.77
NE	0.27	0.54	0.27	0.27	0.00	0.00	1.35
NNE	0.14	0.14	0.27	0.14	0.00	0.00	0.69
E	0.14	0.14	0.00	0.00	0.00	0.00	0.28
ESE	0.00	0.00	0.00	0.00	0.00	0.00	0.00
SE	0.00	0.27	0.00	0.00	0.00	0.00	0.27
SSE	0.00	0.27	0.14	0.14	0.00	0.00	0.55
S	0.27	0.54	0.00	0.00	0.00	0.00	0.81
SSW	0.54	0.27	0.27	0.00	0.00	0.00	1.08
SW	0.27	0.68	0.81	0.68	0.14	0.14	2.72
WSW	0.00	1.90	0.41	0.68	0.14	0.00	3.13
W	0.27	0.81	0.68	0.14	0.00	0.00	1.90
WWW	0.00	0.41	0.81	0.14	0.00	0.00	1.36
WW	0.14	0.14	0.41	0.00	0.00	0.00	0.69
NH	0.00	0.14	0.27	0.00	0.00	0.00	0.41
N	0.00	0.14	0.00	0.00	0.00	0.00	0.14
NNE	0.14	0.27	0.27	0.14	0.00	0.00	0.82
NE	0.00	0.41	0.81	0.54	0.14	0.00	1.90
NNE	0.00	0.14	0.00	0.00	0.00	0.00	0.14
E	0.14	0.00	0.00	0.00	0.00	0.00	0.14
ESE	0.27	0.00	0.00	0.00	0.00	0.00	0.27
SE	0.14	0.00	0.00	0.00	0.00	0.00	0.14
SSE	0.00	0.00	0.00	0.00	0.00	0.00	0.00
S	0.00	0.27	0.00	0.00	0.00	0.00	0.27
SSW	0.00	0.00	0.00	0.00	0.00	0.00	0.00
SW	0.14	0.00	0.14	0.00	0.00	0.00	0.28
WSW	0.14	0.68	0.41	0.00	0.00	0.00	1.23
W	0.27	0.14	0.00	0.00	0.00	0.00	0.41
WWW	0.00	0.27	0.27	0.00	0.00	0.00	0.54
WW	0.00	0.27	0.14	0.00	0.00	0.00	0.41
NH	0.00	0.14	0.00	0.00	0.00	0.00	0.14
N	0.14	0.00	0.00	0.00	0.00	0.00	0.14
NNE	0.56	0.00	0.00	0.00	0.00	0.00	0.56
NE	0.97	0.28	0.00	0.00	0.00	0.00	1.25
NNE	0.56	0.00	0.00	0.00	0.00	0.00	0.56
E	0.70	0.00	0.00	0.00	0.00	0.00	0.70
ESE	0.83	0.00	0.00	0.00	0.00	0.00	0.83
SE	1.11	0.14	0.00	0.00	0.00	0.00	1.25
SSE	0.70	0.00	0.00	0.00	0.00	0.00	0.70
S	0.70	0.00	0.00	0.00	0.00	0.00	0.70
SSW	0.70	0.83	0.28	0.00	0.00	0.00	1.81
SW	2.36	2.92	1.53	0.00	0.00	0.00	6.81
WSW	1.11	1.25	0.42	0.00	0.00	0.00	2.78
W	0.83	0.28	0.00	0.00	0.00	0.00	1.11
WWW	0.00	0.00	0.00	0.00	0.00	0.00	0.00
WW	0.00	0.00	0.00	0.00	0.00	0.00	0.00
NH	0.28	0.00	0.00	0.00	0.00	0.00	0.28
N	0.14	0.00	0.00	0.00	0.00	0.00	0.14



NNE	0.00	0.00	0.00	0.00	0.00	0.00	0.00
NE	0.28	0.00	0.00	0.00	0.00	0.00	0.28
ENE	0.14	0.14	0.00	0.00	0.00	0.00	0.28
E	0.14	0.14	0.00	0.00	0.00	0.00	0.28
ESE	0.28	0.00	0.00	0.00	0.00	0.00	0.28
SE	0.28	0.00	0.00	0.00	0.00	0.00	0.28
SSE	0.14	0.00	0.00	0.00	0.00	0.00	0.14
S	0.00	0.00	0.14	0.00	0.00	0.00	0.14
SSW	0.00	0.00	0.00	0.00	0.00	0.00	0.00
SW	0.00	0.14	0.70	0.00	0.00	0.00	0.84
WSW	0.14	0.00	0.14	0.00	0.00	0.00	0.28
W	0.00	0.00	0.00	0.00	0.00	0.00	0.00
WNW	0.14	0.00	0.00	0.00	0.00	0.00	0.14
WW	0.28	0.00	0.00	0.00	0.00	0.00	0.28
WNW	0.14	0.00	0.00	0.00	0.00	0.00	0.14
W	0.00	0.00	0.00	0.00	0.00	0.00	0.00
WNE	0.14	0.00	0.00	0.00	0.00	0.00	0.14
NE	0.00	0.14	0.00	0.00	0.00	0.00	0.14
ENE	0.00	0.14	0.00	0.00	0.00	0.00	0.14
E	0.00	0.00	0.00	0.00	0.00	0.00	0.00
ESE	0.00	0.00	0.00	0.00	0.00	0.00	0.00
SE	0.14	0.00	0.00	0.00	0.00	0.00	0.14
SSE	0.00	0.00	0.00	0.00	0.00	0.00	0.00
S	0.00	0.00	0.14	0.00	0.00	0.00	0.14
SSW	0.00	0.14	0.00	0.00	0.00	0.00	0.14
SW	0.14	0.28	0.42	0.00	0.00	0.00	0.84
WSW	0.00	0.42	0.00	0.14	0.00	0.00	0.56
W	0.00	0.14	0.00	0.00	0.00	0.00	0.14
WNW	0.00	0.00	0.00	0.00	0.00	0.00	0.00
WW	0.00	0.00	0.00	0.00	0.00	0.00	0.00
WNW	0.14	0.00	0.00	0.00	0.00	0.00	0.14
W	0.56	0.56	0.00	0.00	0.00	0.00	1.12
WNE	0.00	0.42	0.00	0.00	0.00	0.00	0.42
NE	0.00	0.42	0.14	0.00	0.00	0.00	0.56
ENE	0.97	0.56	0.00	0.00	0.00	0.00	1.53
E	0.70	0.56	0.00	0.00	0.00	0.00	1.26
ESE	0.56	0.00	0.00	0.00	0.00	0.00	0.56
SE	0.28	0.00	0.00	0.00	0.00	0.00	0.28
SSE	0.00	0.00	0.00	0.00	0.00	0.00	0.00
S	0.14	0.14	0.14	0.00	0.00	0.00	0.42
SSW	0.00	0.42	0.83	0.00	0.00	0.00	1.25
SW	0.00	0.56	1.95	0.00	0.00	0.00	2.51
WSW	0.14	0.56	0.56	0.00	0.00	0.00	1.26
W	0.00	0.14	0.14	0.00	0.00	0.00	0.28
WNW	0.14	0.14	0.00	0.14	0.00	0.00	0.42
WW	0.14	0.42	0.14	0.00	0.00	0.00	0.70
WNW	0.42	0.14	0.00	0.00	0.00	0.00	0.56
W	0.97	0.14	0.56	0.14	0.00	0.00	1.81
WNE	0.56	0.83	0.14	0.00	0.00	0.00	1.53
NE	0.97	0.70	0.42	0.00	0.00	0.00	2.09
ENE	1.25	1.39	0.00	0.00	0.00	0.00	2.64
E	0.14	0.14	0.00	0.00	0.00	0.00	0.28
ESE	0.28	0.14	0.00	0.00	0.00	0.00	0.42
SE	0.14	0.00	0.00	0.00	0.00	0.00	0.14
SSE	0.28	0.42	0.14	0.00	0.00	0.00	0.84
S	0.42	1.67	1.11	0.00	0.00	0.00	3.20
SSW	0.56	1.39	0.56	0.42	0.00	0.00	2.93
SW	1.81	1.53	2.78	0.56	0.00	0.00	6.68
WSW	0.28	1.67	2.23	0.42	0.00	0.00	4.60
W	0.70	0.42	0.83	0.14	0.00	0.00	2.09
WNW	0.42	0.42	0.42	0.28	0.00	0.00	1.54
WW	0.14	0.42	0.28	0.00	0.00	0.00	0.84
WNW	0.28	0.14	0.00	0.00	0.00	0.00	0.42
W	0.00	0.14	0.14	0.00	0.00	0.00	0.28
WNE	0.42	0.14	0.14	0.00	0.00	0.00	0.70
NE	0.56	0.70	0.14	0.00	0.00	0.00	1.40

EWE	0.70	0.83	0.00	0.00	0.00	0.00	1.53
E	0.56	0.42	0.00	0.00	0.00	0.00	0.98
ESE	0.83	0.42	0.00	0.00	0.00	0.00	1.25
SE	0.14	0.00	0.00	0.00	0.00	0.00	0.14
SSE	0.56	0.00	0.00	0.00	0.00	0.00	0.56
S	0.42	0.42	0.28	0.00	0.00	0.00	1.12
SSW	0.56	0.97	0.42	0.14	0.00	0.00	2.09
SW	0.28	0.83	1.11	0.28	0.14	0.00	2.64
WSW	1.11	1.39	1.25	0.28	0.14	0.00	4.17
W	0.14	1.11	1.25	0.00	0.00	0.00	2.50
WNW	0.28	0.70	0.14	0.00	0.14	0.00	1.26
WW	0.28	0.42	0.00	0.00	0.00	0.00	0.70
WWW	0.70	0.14	0.00	0.00	0.00	0.00	0.84
W	0.14	0.56	0.00	0.00	0.00	0.00	0.70
WNE	0.56	0.00	0.00	0.00	0.00	0.00	0.56
WE	0.42	0.14	0.00	0.00	0.00	0.00	0.56
EWE	0.28	0.14	0.00	0.00	0.00	0.00	0.42
E	0.56	0.14	0.00	0.00	0.00	0.00	0.70
ESE	0.00	0.00	0.00	0.00	0.00	0.00	0.00
SE	0.28	0.00	0.00	0.00	0.00	0.00	0.28
SSE	0.28	0.00	0.00	0.00	0.00	0.00	0.28
S	0.70	0.56	0.00	0.00	0.00	0.00	1.26
SSW	0.00	0.00	0.00	0.00	0.00	0.00	0.00
SW	0.00	0.14	0.28	0.00	0.00	0.00	0.42
WSW	0.28	0.00	0.00	0.00	0.00	0.00	0.28
W	0.14	0.00	0.00	0.00	0.00	0.00	0.14
WNW	0.00	0.00	0.00	0.00	0.00	0.00	0.00
WW	0.00	0.00	0.00	0.00	0.00	0.00	0.00
WWW	0.00	0.14	0.00	0.00	0.00	0.00	0.14
W	0.00	0.00	0.00	0.00	0.00	0.00	0.00
WNE	0.28	0.00	0.00	0.00	0.00	0.00	0.28
WE	0.28	0.28	0.00	0.00	0.00	0.00	0.56
EWE	1.12	0.14	0.00	0.00	0.00	0.00	1.26
E	0.00	0.00	0.00	0.00	0.00	0.00	0.00
ESE	0.56	0.00	0.00	0.00	0.00	0.00	0.56
SE	0.28	0.00	0.00	0.00	0.00	0.00	0.28
SSE	0.00	0.00	0.00	0.00	0.00	0.00	0.00
S	0.70	0.14	0.00	0.00	0.00	0.00	0.84
SSW	0.42	1.26	0.00	0.00	0.00	0.00	1.68
SW	1.26	3.36	0.14	0.00	0.00	0.00	4.76
WSW	0.70	1.12	0.00	0.00	0.00	0.00	1.82
W	0.00	0.14	0.00	0.00	0.00	0.00	0.14
WNW	0.28	0.00	0.00	0.00	0.00	0.00	0.28
WW	0.00	0.00	0.00	0.00	0.00	0.00	0.00
WWW	0.28	0.00	0.00	0.00	0.00	0.00	0.28
W	0.14	0.00	0.00	0.00	0.00	0.00	0.14
WNE	0.00	0.00	0.00	0.00	0.00	0.00	0.00
WE	0.00	0.00	0.00	0.00	0.00	0.00	0.00
EWE	0.28	0.00	0.00	0.00	0.00	0.00	0.28
E	0.00	0.00	0.00	0.00	0.00	0.00	0.00
ESE	0.14	0.00	0.00	0.00	0.00	0.00	0.14
SE	0.14	0.00	0.00	0.00	0.00	0.00	0.14
SSE	0.14	0.00	0.00	0.00	0.00	0.00	0.14
S	0.00	0.14	0.00	0.00	0.00	0.00	0.14
SSW	0.00	0.28	0.14	0.00	0.00	0.00	0.42
SW	0.14	0.28	0.00	0.00	0.00	0.00	0.42
WSW	0.00	0.28	0.14	0.00	0.00	0.00	0.42
W	0.00	0.00	0.14	0.00	0.00	0.00	0.14
WNW	0.00	0.00	0.00	0.00	0.00	0.00	0.00
WW	0.00	0.00	0.00	0.00	0.00	0.00	0.00
WWW	0.14	0.00	0.00	0.00	0.00	0.00	0.14
W	0.14	0.00	0.00	0.00	0.00	0.00	0.14
WNE	0.00	0.00	0.00	0.00	0.00	0.00	0.00
WE	0.14	0.00	0.14	0.00	0.00	0.00	0.28
EWE	0.14	0.00	0.00	0.00	0.00	0.00	0.14
E	0.14	0.14	0.00	0.00	0.00	0.00	0.28



ES E	0.00	0.00	0.00	0.00	0.00	0.00	0.00
SE	0.00	0.00	0.00	0.00	0.00	0.00	0.00
SS E	0.00	0.00	0.00	0.00	0.00	0.00	0.00
S	0.00	0.00	0.00	0.00	0.00	0.00	0.00
SSW	0.14	0.14	0.14	0.00	0.00	0.00	0.42
SW	0.14	0.98	0.42	0.00	0.00	0.00	1.54
WSW	0.14	0.28	0.00	0.00	0.00	0.00	0.42
W	0.28	0.14	0.00	0.00	0.00	0.00	0.42
WNW	0.00	0.00	0.00	0.00	0.00	0.00	0.00
NW	0.00	0.00	0.00	0.00	0.00	0.00	0.00
NNW	0.00	0.00	0.00	0.00	0.00	0.00	0.00
N	0.42	0.14	0.14	0.00	0.00	0.00	0.70
NNE	0.14	0.70	0.00	0.28	0.00	0.00	1.12
NE	0.00	1.40	1.12	0.14	0.00	0.00	2.66
ENE	0.28	0.28	0.14	0.00	0.00	0.00	0.70
E	0.28	0.42	0.00	0.00	0.00	0.00	0.70
ESE	0.14	0.00	0.00	0.00	0.00	0.00	0.14
SE	0.14	0.00	0.14	0.00	0.00	0.00	0.28
SSE	0.00	0.00	0.00	0.00	0.00	0.00	0.00
S	0.28	0.00	0.00	0.00	0.00	0.00	0.28
SSW	0.42	0.42	0.28	0.00	0.00	0.00	1.12
SW	0.28	0.98	0.84	0.14	0.00	0.00	2.24
WSW	0.14	1.26	0.56	0.00	0.00	0.00	1.96
W	0.42	0.56	0.28	0.00	0.00	0.00	1.26
WNW	0.14	0.14	0.00	0.00	0.00	0.00	0.28
NW	0.14	0.00	0.14	0.00	0.00	0.00	0.28
NNW	0.14	0.00	0.00	0.00	0.00	0.00	0.14
N	0.42	0.28	0.28	0.00	0.00	0.00	0.98
NNE	0.28	0.98	1.12	1.26	0.00	0.00	3.64
NE	0.42	0.42	1.68	0.56	0.00	0.00	3.08
ENE	0.00	0.70	0.28	0.00	0.00	0.00	0.98
E	0.28	0.56	0.00	0.00	0.00	0.00	0.84
ESE	0.14	0.28	0.00	0.00	0.00	0.00	0.42
SE	0.42	0.00	0.00	0.00	0.00	0.00	0.42
SSE	0.00	0.00	0.00	0.00	0.00	0.00	0.00
S	0.42	0.14	0.00	0.00	0.00	0.00	0.56
SSW	0.70	0.98	0.14	0.14	0.00	0.00	1.96
SW	0.84	3.08	2.24	0.14	0.00	0.00	6.30
WSW	1.54	4.48	3.64	0.42	0.00	0.00	10.08
W	0.70	3.22	1.96	0.28	0.00	0.00	6.16
WNW	0.14	0.42	0.14	0.00	0.00	0.00	0.70
NW	0.28	0.00	0.00	0.00	0.00	0.00	0.28
NNW	0.56	0.14	0.00	0.00	0.00	0.00	0.70
N	0.14	0.00	0.28	0.00	0.00	0.00	0.42
NNE	0.14	0.70	0.28	0.56	0.14	0.00	1.82
NE	0.56	0.98	1.54	0.84	0.14	0.00	4.06
ENE	0.28	1.12	0.14	0.00	0.00	0.00	1.54
E	0.56	0.98	0.00	0.00	0.00	0.00	1.54
ESE	0.14	0.00	0.00	0.00	0.00	0.00	0.14
SE	0.28	0.00	0.00	0.00	0.00	0.00	0.28
SSE	0.28	0.28	0.00	0.00	0.00	0.00	0.56
S	0.00	0.42	0.00	0.00	0.00	0.00	0.42
SSW	0.14	0.42	0.14	0.00	0.00	0.00	0.70
SW	0.56	1.82	1.26	0.28	0.00	0.00	3.92
WSW	0.70	2.24	0.84	0.42	0.00	0.00	4.20
W	0.70	1.82	0.84	0.00	0.00	0.00	3.36
WNW	0.42	1.12	0.14	0.00	0.00	0.00	1.68
NW	0.28	0.28	0.00	0.00	0.00	0.00	0.56
NNW	0.28	0.00	0.00	0.00	0.00	0.00	0.28
N	0.28	0.28	0.00	0.00	0.00	0.00	0.56
NNE	0.00	0.14	0.00	0.00	0.00	0.00	0.14
NE	0.00	0.70	0.00	0.14	0.00	0.00	0.84
ENE	0.28	0.70	0.00	0.00	0.00	0.00	0.98
E	0.00	0.14	0.00	0.00	0.00	0.00	0.14
ESE	0.00	0.00	0.00	0.00	0.00	0.00	0.00
SE	0.00	0.00	0.00	0.00	0.00	0.00	0.00



SSE	0.14	0.00	0.00	0.00	0.00	0.00	0.14
S	0.00	0.00	0.00	0.00	0.00	0.00	0.00
SSW	0.00	0.00	0.00	0.00	0.00	0.00	0.00
SW	0.00	0.14	0.00	0.00	0.00	0.00	0.14
WSW	0.14	0.00	0.00	0.00	0.00	0.00	0.14
W	0.14	0.00	0.14	0.00	0.00	0.00	0.28
WNW	0.14	0.00	0.00	0.00	0.00	0.00	0.14
WW	0.14	0.00	0.00	0.00	0.00	0.00	0.14
WNW	0.00	0.00	0.00	0.00	0.00	0.00	0.00
N	0.44	0.00	0.00	0.00	0.00	0.00	0.44
NNE	0.44	0.00	0.00	0.00	0.00	0.00	0.44
NE	0.87	0.00	0.00	0.00	0.00	0.00	0.87
ENE	0.44	0.15	0.00	0.00	0.00	0.00	0.59
E	0.44	0.15	0.00	0.00	0.00	0.00	0.59
ESE	0.44	0.00	0.00	0.00	0.00	0.00	0.44
SE	0.15	0.00	0.00	0.00	0.00	0.00	0.15
SSE	0.00	0.00	0.00	0.00	0.00	0.00	0.00
S	2.48	0.29	0.00	0.00	0.00	0.15	2.92
SSW	0.29	1.17	0.00	0.00	0.00	0.00	1.46
SW	0.87	1.46	0.15	0.00	0.00	0.00	2.48
WSW	0.58	0.00	0.15	0.00	0.00	0.00	0.73
W	0.15	0.00	0.00	0.00	0.00	0.00	0.15
WNW	0.00	0.00	0.00	0.00	0.00	0.00	0.00
WW	0.15	0.00	0.00	0.00	0.00	0.00	0.15
WNW	0.29	0.00	0.00	0.00	0.00	0.00	0.29
N	0.15	0.00	0.00	0.00	0.00	0.00	0.15
NNE	0.00	0.00	0.00	0.00	0.00	0.00	0.00
NE	0.15	0.00	0.00	0.00	0.00	0.00	0.15
ENE	0.15	0.29	0.00	0.00	0.00	0.00	0.44
E	0.15	0.15	0.00	0.00	0.00	0.00	0.30
ESE	0.15	0.00	0.00	0.00	0.00	0.00	0.15
SE	0.00	0.00	0.00	0.00	0.00	0.00	0.00
SSE	0.00	0.00	0.00	0.00	0.00	0.00	0.00
S	0.44	0.15	0.00	0.00	0.00	0.00	0.59
SSW	0.00	0.00	0.00	0.00	0.00	0.00	0.00
SW	0.29	0.29	0.00	0.00	0.00	0.00	0.58
WSW	0.15	0.00	0.00	0.00	0.00	0.00	0.15
W	0.00	0.00	0.00	0.00	0.00	0.00	0.00
WNW	0.00	0.00	0.00	0.00	0.00	0.00	0.00
WW	0.15	0.00	0.00	0.00	0.00	0.00	0.15
WNW	0.00	0.00	0.00	0.00	0.00	0.00	0.00
N	0.00	0.15	0.00	0.00	0.00	0.00	0.15
NNE	0.00	0.00	0.00	0.00	0.00	0.00	0.00
NE	0.15	0.00	0.00	0.00	0.00	0.00	0.15
ENE	0.15	0.00	0.00	0.00	0.00	0.00	0.15
E	0.29	0.00	0.00	0.00	0.00	0.00	0.29
ESE	0.15	0.00	0.00	0.00	0.00	0.00	0.15
SE	0.15	0.00	0.00	0.00	0.00	0.00	0.15
SSE	0.00	0.00	0.00	0.00	0.00	0.00	0.00
S	0.15	0.00	0.00	0.00	0.00	0.00	0.15
SSW	0.15	0.00	0.00	0.00	0.00	0.00	0.15
SW	0.29	0.29	0.29	0.00	0.00	0.00	0.87
WSW	0.00	0.15	0.00	0.00	0.00	0.00	0.15
W	0.15	0.15	0.00	0.00	0.00	0.00	0.30
WNW	0.00	0.00	0.00	0.00	0.00	0.00	0.00
WW	0.00	0.00	0.00	0.00	0.00	0.00	0.00
WNW	0.15	0.00	0.00	0.00	0.00	0.00	0.15
N	0.15	0.00	0.15	0.00	0.00	0.00	0.30
NNE	0.15	0.73	0.00	0.00	0.00	0.00	0.88
NE	0.44	0.87	1.75	0.29	0.00	0.00	3.35
ENE	0.29	1.02	0.58	0.00	0.00	0.00	1.89
E	0.44	0.73	0.15	0.00	0.00	0.00	1.32
ESE	0.00	0.00	0.00	0.00	0.00	0.00	0.00
SE	0.15	0.15	0.00	0.00	0.00	0.00	0.30
SSE	0.15	0.15	0.00	0.00	0.00	0.00	0.30
S	0.29	0.15	0.00	0.00	0.00	0.00	0.44

SSW	0.58	0.44	0.00	0.00	0.00	0.00	1.02
SW	0.44	0.44	0.15	0.15	0.00	0.00	1.18
WSW	0.44	0.15	0.58	0.15	0.00	0.00	1.32
W	0.00	0.15	0.00	0.00	0.00	0.00	0.15
WWW	0.00	0.00	0.00	0.00	0.00	0.00	0.00
WW	0.15	0.00	0.00	0.00	0.00	0.00	0.15
NWW	0.00	0.00	0.00	0.00	0.00	0.00	0.00
N	0.44	0.73	0.29	0.15	0.00	0.00	1.61
NNE	0.44	1.17	1.31	1.02	0.00	0.00	3.94
NE	0.58	1.75	1.90	2.92	0.00	0.00	7.15
ENE	0.15	1.75	1.02	0.15	0.00	0.00	3.07
E	0.58	0.73	0.29	0.00	0.00	0.00	1.60
ESE	0.44	0.15	0.15	0.00	0.00	0.00	0.74
SE	0.29	0.15	0.15	0.00	0.00	0.00	0.59
SSE	0.15	0.15	0.29	0.00	0.00	0.00	0.59
S	0.87	0.58	0.29	0.15	0.00	0.00	1.89
SSW	0.44	0.44	0.15	0.00	0.00	0.00	1.03
SW	0.15	1.46	2.19	0.00	0.00	0.00	3.80
WSW	0.00	0.29	1.46	0.00	0.00	0.00	1.75
W	0.15	0.44	0.58	0.00	0.00	0.00	1.17
WWW	0.15	0.00	0.00	0.00	0.00	0.00	0.15
WW	0.00	0.00	0.00	0.00	0.00	0.00	0.00
WWW	0.00	0.15	0.00	0.00	0.00	0.00	0.15
W	0.00	0.15	0.00	0.00	0.00	0.00	0.15
NWW	0.44	0.15	1.17	0.87	0.00	0.00	2.63
NNE	0.44	1.02	1.60	1.02	0.00	0.00	4.08
ENE	0.29	0.58	2.48	1.17	0.00	0.00	4.52
E	0.15	0.58	0.15	0.00	0.00	0.00	0.88
ESE	0.15	0.58	0.00	0.00	0.00	0.00	0.73
SE	0.00	0.00	0.00	0.00	0.00	0.00	0.00
SSE	0.00	0.00	0.00	0.00	0.00	0.00	0.00
S	0.87	0.87	0.00	0.00	0.00	0.00	1.74
SSW	2.19	1.60	0.44	0.00	0.00	0.00	4.23
SW	0.58	1.60	0.44	0.00	0.00	0.00	2.62
WSW	0.29	1.31	0.15	0.00	0.00	0.00	1.75
W	0.29	0.73	0.29	0.00	0.00	0.00	1.31
WWW	0.73	0.73	1.02	0.00	0.00	0.00	2.48
WW	0.15	0.00	0.00	0.00	0.00	0.00	0.15
WWW	0.00	0.00	0.00	0.00	0.00	0.00	0.00
W	0.00	0.00	0.00	0.00	0.00	0.00	0.00
NWE	0.00	0.00	0.15	0.15	0.00	0.00	0.30
NE	0.15	0.15	0.15	0.00	0.00	0.00	0.45
ENE	0.29	0.87	0.87	0.00	0.00	0.00	2.03
E	0.00	0.15	0.00	0.00	0.00	0.00	0.15
ESE	0.15	0.00	0.00	0.00	0.00	0.00	0.15
SE	0.15	0.00	0.00	0.00	0.00	0.00	0.15
SSE	0.00	0.15	0.00	0.00	0.00	0.00	0.15
S	0.58	0.15	0.00	0.00	0.00	0.00	0.73
SSW	0.58	1.17	0.00	0.00	0.00	0.00	1.75
SW	0.15	0.29	0.00	0.00	0.00	0.00	0.44
WSW	0.15	0.15	0.00	0.00	0.00	0.00	0.30
W	0.00	0.00	0.00	0.00	0.00	0.00	0.00
WWW	0.00	0.44	0.15	0.00	0.00	0.00	0.59
WW	0.00	0.15	0.00	0.00	0.00	0.00	0.15
WWW	0.00	0.15	0.00	0.00	0.00	0.00	0.15

IBC002I STOP 0

	6	4	7	0	0							
	F	F	T	T	T	T						
	F	F	F	F	F	F	F	F	F	F	F	F
35.	57.			23.		84.	16.	34.				WBB
36.	01.			55.		84.	07.	08.				GAGE 2
36.	00.			02.		84.	32.	42.				GAGE 3
35.	56.			00.		84.	16.	00.				GAGE 4
35.	52.			47.		84.	30.	00.				GAGE 5
36.	01.			02.		84.	14.	47.				GAGE 6
36.	0.			51.		84.	9.	32.				BULL RUN
35.	53.			47.		84.	31.	0.				KINGSTON
35.	57.			26.		83.	55.	46.				ALCOA
35.	59.			46.		84.	15.	44.				Y-12
36.	5.			21.		84.	16.	57.				AREA 1
35.	57.			26.		83.	55.	46.				AREA 2
35.	48.			0.		84.	33.	54.				AREA 3
35.	43.			43.		84.	21.	12.				AREA 4
36.	7.			17.		84.	38.	56.				AREA 5
36.	24.			39.		84.	29.	8.				AREA 6
36.	22.			17.		84.	7.	25.				AREA 7
	0.884E+09	0.137E+10	0.100E+10	0.645E+09	0.140E+10	0.142E+10	0.121E+10	0.121E+10	0.121E+10	0.121E+10	0.121E+10	AREAS
244.	84.	80.	80.	80.	80.	80.	80.	80.	80.	80.	80.	HEIGHTS (P)
	0.289E+04	0.106E+04	0.168E+03	0.407E+03	0.407E+03	0.407E+03	0.407E+03	0.407E+03	0.407E+03	0.407E+03	0.407E+03	
	0.459E+03	0.263E+03	0.104E+03	0.155E+03	0.155E+03	0.155E+03	0.155E+03	0.155E+03	0.155E+03	0.155E+03	0.155E+03	
10.	10.	10.	10.	10.	10.	10.	10.	10.	10.	10.	10.	HGA
1	9											
F												
2	0.0012	0.00001	S02									
	826.0	784.0	761.0	803.0	767.0	783.0	708.0	708.0	708.0	708.0	708.0	BULL RUN
	784.0	608.0	711.0	517.0	0.0	63.0	0.0	0.0	0.0	0.0	0.0	KINGSTON
	2753.0	2801.0	2447.0	2405.0	2508.0	2276.0	2467.0	2467.0	2467.0	2467.0	2467.0	
	2543.0	2200.0	2455.0	2314.0	2560.0	2755.0	2864.0	2864.0	2864.0	2864.0	2864.0	
	42.0	42.0	42.0	42.0	42.0	42.0	42.0	42.0	42.0	42.0	42.0	ALCOA
	42.0	42.0	42.0	42.0	42.0	42.0	42.0	42.0	42.0	42.0	42.0	
	0.0	1.2	0.7	17.2	83.0	105.7	117.9	117.9	117.9	117.9	117.9	Y-12
	120.0	83.3	48.6	3.2	3.2	5.5	0.8	0.8	0.8	0.8	0.8	
	0.000E-01	0.000E-01	2.092E-09	1.779E-08	4.329E-08	6.804E-08	7.539E-08	7.539E-08	7.539E-08	7.539E-08	7.539E-08	AREA 1
	6.238E-08	4.665E-08	1.722E-08	5.932E-09	2.509E-10	0.000E-01	0.000E-01	0.000E-01	0.000E-01	0.000E-01	0.000E-01	
	0.000E-01	0.000E-01	5.189E-09	4.398E-08	1.074E-07	1.688E-07	1.870E-07	1.870E-07	1.870E-07	1.870E-07	1.870E-07	AREA 2
	1.547E-07	1.157E-07	4.272E-08	1.472E-08	6.223E-10	0.000E-01	0.000E-01	0.000E-01	0.000E-01	0.000E-01	0.000E-01	
	0.000E-01	0.000E-01	1.179E-09	9.989E-09	2.439E-08	3.833E-08	4.248E-08	4.248E-08	4.248E-08	4.248E-08	4.248E-08	AREA 3
	3.514E-08	2.628E-08	9.703E-09	3.342E-09	1.413E-10	0.000E-01	0.000E-01	0.000E-01	0.000E-01	0.000E-01	0.000E-01	
	0.000E-01	0.000E-01	8.638E-10	7.322E-09	1.788E-08	2.810E-08	3.114E-08	3.114E-08	3.114E-08	3.114E-08	3.114E-08	AREA 4
	2.576E-08	1.926E-08	7.112E-09	2.450E-09	1.036E-10	0.000E-01	0.000E-01	0.000E-01	0.000E-01	0.000E-01	0.000E-01	
	0.000E-01	0.000E-01	8.761E-10	7.427E-09	1.813E-08	2.850E-08	3.158E-08	3.158E-08	3.158E-08	3.158E-08	3.158E-08	AREA 5
	2.613E-08	1.954E-08	7.214E-09	2.485E-09	1.051E-10	0.000E-01	0.000E-01	0.000E-01	0.000E-01	0.000E-01	0.000E-01	
	0.000E-01	0.000E-01	8.144E-10	6.904E-09	1.686E-08	2.649E-08	2.936E-08	2.936E-08	2.936E-08	2.936E-08	2.936E-08	AREA 6
	2.429E-08	1.816E-08	6.706E-09	2.310E-09	9.768E-11	0.000E-01	0.000E-01	0.000E-01	0.000E-01	0.000E-01	0.000E-01	
	0.000E-01	0.000E-01	2.011E-09	1.705E-08	4.163E-08	6.543E-08	7.250E-08	7.250E-08	7.250E-08	7.250E-08	7.250E-08	AREA 7
	5.998E-08	4.486E-08	1.656E-08	5.705E-09	2.412E-10	0.000E-01	0.000E-01	0.000E-01	0.000E-01	0.000E-01	0.000E-01	

IHC002I STOP 0



#### APPENDIX D. OUTPUT DATA

# WALKER BRANCH CALCULATIONS, JULY 72 THRU AUG 73

PASQUILL STABILITIES NOT USED--STABILITIES FOUND IN SUBROUTINE SIGMA

ROUGHNESS= 0.350E 01 METERS

NUMBER OF WIND SPEEDS= 6  
 NUMBER OF WIND DIRECTIONS= 16  
 NUMBER OF WIND STABILITIES= 7  
 STABILITIES USED--- 1 2 3 4 5 6 7

SIGMA FOR EACH STABILITY IN THE TABLE= 0.320E 04 0.160E 04 0.800E 03 0.500E 03 0.200E 03 0.100E 03

WIND SPEED FOR WIND CLASSES

1 0.894

WIND SPEED FOR WIND CLASSES

2 2.420

WIND SPEED FOR WIND CLASSES

3 4.420

WIND SPEED FOR WIND CLASSES

4 6.870

WIND SPEED FOR WIND CLASSES

5 9.530

WIND SPEED FOR WIND CLASSES

6 14.000

LATITUDE AND LONGITUDE OF GAGE SAMPLING POINTS

ID NUMBER	NAME	LATITUDE DEGREES	LATITUDE MINUTES	SECONDS	LONGITUDE DEGREES	LONGITUDE MINUTES	SECONDS
1	BBW	35.00	57.00	23.00	84.00	16.00	34.00
2	GAGE 2	36.00	1.00	55.00	84.00	7.00	8.00

LATITUDE AND LONGITUDE OF POINT SOURCES

ID NUMBER	NAME	LATITUDE DEGREES	LATITUDE MINUTES	SECONDS	LONGITUDE DEGREES	LONGITUDE MINUTES	SECONDS
1	BULL RUN	36.00	0.0	51.00	84.00	9.00	32.00
2	KINGSTON	35.00	53.00	47.00	84.00	31.00	0.0
3	ALCOA	35.00	57.00	26.00	83.00	55.00	46.00
4	T-12	35.00	59.00	46.00	84.00	15.00	44.00

LATITUDE AND LONGITUDE OF AREA SOURCE CENTROIDS

ID NUMBER	NAME	LATITUDE DEGREES	LATITUDE MINUTES	SECONDS	LONGITUDE DEGREES	LONGITUDE MINUTES	SECONDS
1	AREA 1	36.00	5.00	21.00	84.00	16.00	57.00
2	AREA 2	35.00	57.00	26.00	83.00	55.00	46.00
3	AREA 3	35.00	48.00	0.0	84.00	33.00	54.00
4	AREA 4	35.00	43.00	43.00	84.00	21.00	12.00
5	AREA 5	36.00	7.00	17.00	84.00	38.00	56.00
6	AREA 6	36.00	28.00	39.00	84.00	29.00	8.00
7	AREA 7	36.00	22.00	17.00	84.00	7.00	25.00

AREA SOURCE AREAS IN METERS\*\*2  
 AREA SOURCE 1 AREA 1 8.840E 08  
 AREA SOURCE 2 AREA 2 1.370E 09  
 AREA SOURCE 3 AREA 3 1.000E 09  
 AREA SOURCE 4 AREA 4 6.850E 08  
 AREA SOURCE 5 AREA 5 1.800E 09  
 AREA SOURCE 6 AREA 6 1.420E 09  
 AREA SOURCE 7 AREA 7 1.210E 09

SOURCE	NAME	HEIGHT	PKAPPA	QKAPPA
POINT 1	BULL RUN	2.440E 02	2.890E 03	4.590E 02
POINT 2	KINGSTON	8.400E 01	1.060E 03	2.630E 02
POINT 3	ALCOA	8.000E 01	1.680E 02	1.040E 02
POINT 4	Y-12	8.000E 01	4.070E 02	1.550E 02
AREA 1	AREA 1	1.000E 01		
AREA 2	AREA 2	1.000E 01		
AREA 3	AREA 3	1.000E 01		
AREA 4	AREA 4	1.000E 01		
AREA 5	AREA 5	1.000E 01		
AREA 6	AREA 6	1.000E 01		
AREA 7	AREA 7	1.000E 01		
FOREST COVER				

DATA FOR POLLUTANT 1 SO2 (A GAS)  
 BOUNDARY LAYER THICKNESS= 0.120E-02 METERS  
 DIFFUSION CONSTANT FOR WASHOUT= 0.100E-04 METR\*\*2/SEC



POINT SOURCE EMISSIONS FOR PERIODS

1	2	3	4	5	6	7	8
JUL 72	AUG 72	SEP 72	OCT 72	NOV 72	DEC 72	JAN 73	FEB 73
10	11	12	13	14	15	16	17
MAR 73	APR 73	MAY 73	JUN 73	JUL 73	AUG 73	SEP 73	OCT 73
EMISSION RATE FROM POINT SOURCE							
1	2	3	4	5	6	7	8
7.2600E-02	7.4400E-02	7.6100E-02	7.8000E-02	8.0000E-02	8.2000E-02	8.4000E-02	8.6000E-02
6.0800E-02	6.2800E-02	6.4800E-02	6.6800E-02	6.8800E-02	7.0800E-02	7.2800E-02	7.4800E-02
EMISSION RATE FROM POINT SOURCE							
1	2	3	4	5	6	7	8
2.7530E-03	2.8010E-03	2.8490E-03	2.8970E-03	2.9450E-03	2.9930E-03	3.0410E-03	3.0890E-03
2.2000E-03	2.2480E-03	2.2960E-03	2.3440E-03	2.3920E-03	2.4400E-03	2.4880E-03	2.5360E-03
EMISSION RATE FROM POINT SOURCE							
1	2	3	4	5	6	7	8
4.2000E-01	4.2000E-01	4.2000E-01	4.2000E-01	4.2000E-01	4.2000E-01	4.2000E-01	4.2000E-01
4.2000E-01	4.2000E-01	4.2000E-01	4.2000E-01	4.2000E-01	4.2000E-01	4.2000E-01	4.2000E-01
EMISSION RATE FROM POINT SOURCE							
1	2	3	4	5	6	7	8
0.0	0.0	0.0	0.0	0.0	0.0	0.0	0.0
8.3300E-01	8.3300E-01	8.3300E-01	8.3300E-01	8.3300E-01	8.3300E-01	8.3300E-01	8.3300E-01
AREA SOURCE EMISSIONS FOR PERIODS							
1	2	3	4	5	6	7	8
JUL 72	AUG 72	SEP 72	OCT 72	NOV 72	DEC 72	JAN 73	FEB 73
10	11	12	13	14	15	16	17
MAR 73	APR 73	MAY 73	JUN 73	JUL 73	AUG 73	SEP 73	OCT 73
EMISSION RATE FROM AREA SOURCE							
1	2	3	4	5	6	7	8
0.0	0.0	0.0	0.0	0.0	0.0	0.0	0.0
4.6650E-08	4.6650E-08	4.6650E-08	4.6650E-08	4.6650E-08	4.6650E-08	4.6650E-08	4.6650E-08
EMISSION RATE FROM AREA SOURCE							
1	2	3	4	5	6	7	8
1.1570E-07	1.1570E-07	1.1570E-07	1.1570E-07	1.1570E-07	1.1570E-07	1.1570E-07	1.1570E-07
EMISSION RATE FROM AREA SOURCE							
1	2	3	4	5	6	7	8
0.0	0.0	0.0	0.0	0.0	0.0	0.0	0.0
2.6280E-08	2.6280E-08	2.6280E-08	2.6280E-08	2.6280E-08	2.6280E-08	2.6280E-08	2.6280E-08
EMISSION RATE FROM AREA SOURCE							
1	2	3	4	5	6	7	8
1.9260E-08	1.9260E-08	1.9260E-08	1.9260E-08	1.9260E-08	1.9260E-08	1.9260E-08	1.9260E-08
EMISSION RATE FROM AREA SOURCE							
1	2	3	4	5	6	7	8
0.0	0.0	0.0	0.0	0.0	0.0	0.0	0.0
1.9540E-08	1.9540E-08	1.9540E-08	1.9540E-08	1.9540E-08	1.9540E-08	1.9540E-08	1.9540E-08
EMISSION RATE FROM AREA SOURCE							
1	2	3	4	5	6	7	8
0.0	0.0	0.0	0.0	0.0	0.0	0.0	0.0
1.8160E-08	1.8160E-08	1.8160E-08	1.8160E-08	1.8160E-08	1.8160E-08	1.8160E-08	1.8160E-08
EMISSION RATE FROM AREA SOURCE							
1	2	3	4	5	6	7	8
0.0	0.0	0.0	0.0	0.0	0.0	0.0	0.0
4.4860E-08	4.4860E-08	4.4860E-08	4.4860E-08	4.4860E-08	4.4860E-08	4.4860E-08	4.4860E-08

POLLUTANT 1, SO2		POINT SOURCE DEPOSITION RATE (GM**2/SEC)											
GAGE	POL	JUL 72	AUG 72	SEP 72	OCT 72	NOV 72	DEC 72	JAN 73	FEB 73	MAR 73	APR 73	MAY 73	JUN 73
1	1	9.017E-07	5.474E-07	6.045E-07	4.608E-07	4.129E-07	7.934E-07	8.577E-07	7.159E-07	4.279E-07	5.173E-07	5.400E-07	5.604E-07
2	1	6.102E-07	3.585E-07	4.575E-07	3.550E-07	3.280E-07	4.216E-07	2.873E-07	3.616E-07	2.513E-07	3.682E-07	3.419E-07	1.896E-07
POINT SOURCE INCREMENT TO CONCENTRATION (G/M**3)													
1	1	1.025E-05	6.153E-06	6.801E-06	5.065E-06	4.621E-06	9.079E-06	9.745E-06	8.124E-06	4.728E-06	5.862E-06	6.087E-06	6.381E-06
2	1	4.551E-06	3.160E-06	3.814E-06	3.186E-06	3.130E-06	3.860E-06	2.763E-06	3.255E-06	2.317E-06	3.481E-06	3.101E-06	2.190E-06
POINT SOURCE INCREMENT TO CONCENTRATION (G/M**3)													
1	1	0.0	0.0	0.0	0.0	0.0	0.0	0.0	0.0	0.0	0.0	0.0	0.0
2	1	0.0	0.0	0.0	0.0	0.0	0.0	0.0	0.0	0.0	0.0	0.0	0.0
AREA SOURCE DEPOSITION RATE (GM**2/SEC)													
1	1	0.0	0.0	0.0	0.0	0.0	0.0	0.0	0.0	0.0	0.0	0.0	0.0
2	1	0.0	0.0	0.0	0.0	0.0	0.0	0.0	0.0	0.0	0.0	0.0	0.0
AREA SOURCE INCREMENT TO CONCENTRATION (G/M**3)													
1	1	0.0	0.0	0.0	0.0	0.0	0.0	0.0	0.0	0.0	0.0	0.0	0.0
2	1	0.0	0.0	0.0	0.0	0.0	0.0	0.0	0.0	0.0	0.0	0.0	0.0

WALKER BRANCH CALCULATIONS, JULY 72 THRU AUG 73

POLLUTANT 1, SO2

GAGE	POL	PERIOD	DRYDEP G/H**2/SEC	WETDEP G/H**2/SEC	TOTAL DEP G/H**2/SEC	CONC G/H**3
1	1	1	8.576E-07	4.405E-08	9.017E-07	1.025E-05
1	1	2	5.150E-07	3.240E-08	5.474E-07	6.153E-06
1	1	3	5.695E-07	3.525E-08	6.048E-07	6.805E-06
1	1	4	4.279E-07	3.698E-08	4.649E-07	5.112E-06
1	1	5	3.967E-07	2.645E-08	4.232E-07	4.740E-06
1	1	6	7.734E-07	3.388E-08	8.073E-07	9.240E-06
1	1	7	8.363E-07	4.243E-08	8.788E-07	9.992E-06
1	1	8	6.928E-07	3.624E-08	7.291E-07	8.277E-06
1	1	9	4.022E-07	3.227E-08	4.349E-07	4.805E-06
1	1	10	4.931E-07	2.664E-08	5.197E-07	5.891E-06
1	1	11	5.103E-07	3.052E-08	5.409E-07	6.097E-06
1	1	12	5.341E-07	2.630E-08	5.604E-07	6.381E-06
1	1	13	1.012E-06	3.828E-08	1.050E-06	1.209E-05
1	1	14	2.578E-07	1.447E-08	2.723E-07	3.080E-06
2	1	1	3.809E-07	2.293E-07	6.102E-07	4.551E-06
2	1	2	2.645E-07	9.408E-08	3.585E-07	3.160E-06
2	1	3	3.195E-07	1.383E-07	4.577E-07	3.817E-06
2	1	4	2.700E-07	8.848E-08	3.585E-07	3.226E-06
2	1	5	2.683E-07	6.624E-08	3.346E-07	3.206E-06
2	1	6	3.316E-07	9.881E-08	4.305E-07	3.962E-06
2	1	7	2.451E-07	5.632E-08	3.015E-07	2.929E-06
2	1	8	2.852E-07	9.143E-08	3.766E-07	3.407E-06
2	1	9	2.068E-07	5.757E-08	2.644E-07	2.471E-06
2	1	10	2.952E-07	7.696E-08	3.722E-07	3.527E-06
2	1	11	2.604E-07	8.237E-08	3.428E-07	3.111E-06
2	1	12	1.833E-07	6.344E-08	1.897E-07	2.190E-06
2	1	13	3.074E-07	2.558E-08	3.329E-07	3.672E-06
2	1	14	9.621E-08	3.395E-09	9.960E-08	1.149E-06

0

IHC002I STOP



# INTERNAL DISTRIBUTION

- |                       |  |
|-----------------------|--|
| 1. S. I. Auerbach     | 36. R. J. Luxmoore                     |
| 2. C. L. Begovich     | 37. J. B. Mankin                       |
| 3. A. A. Brooks       | 38. R. D. McCulloch                    |
| 4. R. L. Burgess      | 39. H. F. McDuffie                     |
| 5. H. P. Carter       | 40. J. K. Munro                        |
| 6. E. D. Copenhaver   | 41. B. D. Murphy                       |
| 7-16. W. M. Culkowski | 42. C. J. Nappo, Jr.                   |
| 17. F. L. Culler      | 43. J. S. Olson                        |
| 18. K. R. Dixon       | 44. R. V. O'Neill                      |
| 19. R. C. Dahlman     | 45-54. M. R. Patterson                 |
| 20. J. W. Elwood      | 55. S. K. Penny                        |
| 21. D. E. Fields      | 56. H. Postma                          |
| 22. C. W. Francis     | 57. R. J. Raridon                      |
| 23. R. H. Fowler      | 58. M. Reeves                          |
| 24. W. Fulkerson      | 59. D. E. Reichle                      |
| 25. S. R. Hanna       | 60. C. Richmond                        |
| 26. W. F. Harris      | 61. W. D. Shults                       |
| 27. G. S. Henderson   | 62-121. R. I. Van Hook                 |
| 28. R. F. Hibbs       | 122. P. R. Vanstrum                    |
| 29. H. R. Hicks       | 123-124. Central Research Library      |
| 30. J. T. Holdeman    | 125-134. CSD Library, 4500N            |
| 31. D. D. Huff        | 135. Document Reference Section - Y-12 |
| 32. D. R. Jackson     | 136-139. Laboratory Records            |
| 33. S. V. Kaye        | 140. Laboratory Records - Record Copy  |
| 34. N. M. Larson      | 141. ORNL Patent Office                |
| 35. S. E. Lindberg    |  |

# EXTERNAL DISTRIBUTION

142. Jay Bloomfield, Research Scientist, New York State, Department of Environmental Conservation, 50 Wolf Road, Albany, NY 12233
143. R. P. Betson, Head, Hydrologic Research and Analysis Staff TVA, 331 Evans Building, Knoxville, TN 37902
144. Andrew W. Breidenbach, Director, National Environmental Research Center, Environmental Protection Agency, Cincinnati, OH 45268

145. A. V. Brill, Division of Nuclear Medicine and Biomedicine, Vanderbilt University, School of Medicine, Nashville, TN 37232
146. Richard Carrigan, Division of Advanced Environmental Research and Technology, National Science Foundation, 1800 G Street, NW, Washington, DC 20550
147. Barry Commoner, Center for Biology, Washington University, Box 1126, Saint Louis, MO 63130
148. N. H. Crawford, Hydrocomp, 1502 Page Mill Road, Palo Alto, CA 94304
149. James W. Curlin, Environmental Policy Division, Congressional Research Service, Library of Congress, Washington, DC 20540
150. Paul B. Dunaway, Office of Effect Evaluation, U.S. Energy Research and Development Administration, Nevada Operations Office, P. O. Box 1400, Las Vegas, NV 89114
151. Harry W. Edwards, Department of Mechanical Engineering, B107 - Engineering Research Center, Colorado State University, Fort Collins, CO 80521
152. Farley Fisher, Environmental Protection Agency, Office of Toxic Substances, 401 M Street, SW, Washington, DC 20460
153. Delbert D. Hemphill, Environmental Health Center, 426 Clark Hall, University of Missouri, Columbia, MO 65201
154. Jack Hollander, Director, Energy and Environment Division, Lawrence Berkeley Laboratory, University of California, Berkeley, CA 94720
155. Hal Hollister, Chief, Technical Analysis Branch, Division of Biomedical and Environmental Research, U.S. Energy Research and Development Administration, Washington, DC 20545
156. Robert J. M. Horton, Special Studies Staff, National Environmental Research Center, Environmental Protection Agency, Research Triangle Park, NC 27711
157. Joseph A. Lenhard, P. O. Box E, U.S. Energy Research and Development Administration, Oak Ridge, TN 37830
158. J. I. Liverman, Director, Division of Biomedical and Environmental Research, U.S. Energy Research and Development Administration, Washington, DC 20545
159. William Lower, Environmental Trace Substances. Research Center, University of Missouri-Columbia, Rural Route 3, Columbia, MO 65201
160. Don Lynam, Assistant Manager, Environmental Health International Lead Zinc Research Organization, 292 Madison Avenue, NY 10017
161. Charles Malone, Environmental Studies Board, National Research Council, 2101 Constitution Avenue, Washington, DC 20418
162. M. T. Mills, Geophysics Corporation of America, Technology Division, Burlington Road, Bedford, MA 01730
163. Armond Georges Nassongne, Information Technology Division, Scientific and Technical Information and Information Management, Commission of The European Communities, Aldringen, Luxembourg
164. John Neuhold, Ecology Center, Utah State University, Logan, UT 97321
165. R. M. Perhac, Division of Environmental Systems and Resources, National Science Foundation, 1800 G Street, NW, Washington, DC 20550
166. Robert Rabin, Division of Biomedical and Environmental Sciences, U.S. Energy Research and Development Administration, Washington, DC 20545
167. Gary L. Rolfe, 396 Fevier, University of Illinois, Urbana, IL 61801



168. Milton E. Rose, Mathematical and Computer Sciences Program, Molecular Sciences and Energy Research, Division of Physical Research, U.S. Energy Research and Development Administration, Washington, DC 20545
169. Walter Sanders, III, Southeast Water Quality Laboratory, Water Quality Office, Environmental Protection Agency, Athens, GA 30601
170. Ivan Smith, Midwest Research Institute, 425 Volker Boulevard, Kansas City, MO 64110
171. Marvin Stephenson, Division of Advanced Research and Technology, National Science Foundation, 1800 G Street, Washington, DC 20550
172. C. H. Thompson, Chief, Hazardous Materials Branch, Division of Oil and Hazardous Materials, Office of Water Programs, Environmental Protection Agency, Washington, DC 20460
173. Jack E. Thompson, Deputy Director, National Environmental Research Center, Environmental Protection Agency, Research Triangle Park, NC 27711
174. J. E. Watkin, Environmental Secretariat, Division of Biology, National Research Council of Canada, Ottawa, Ontario K1A 0R6, Canada
175. Herbert Wiser, Director, Division of Process and Effects Research, Environmental Protection Agency, 401 M Street, SW, Washington, DC 20460
176. Bobby G. Wixson, Professor of Environmental Health, Department of Civil Engineering, University of Missouri, Rolla, 115 Engineering Research Building, Rolla, MO 65401
177. K. J. Yost, Department of Bionucleonics, Pharmacy Building, Purdue University, Lafayette, IN 47901
- 178-204. Technical Information Center, Oak Ridge, TN 37830
205. Research and Technical Support Division, ORO



**- PROCEEDINGS -**  
**CONTROLLING AIRBORNE EFFLUENTS**  
**FROM FUEL CYCLE PLANTS**



**SUN VALLEY, IDAHO August 5—6, 1976**



ATDL Contribution File No. 76/3

TOPICAL MEETING

CONTROLLING AIRBORNE EFFLUENTS FROM FUEL CYCLE PLANTS

Sun Valley, Idaho  
August 5-6, 1976

MEETING SPONSORS

AMERICAN NUCLEAR SOCIETY

Nuclear Fuel Cycle Division  
Environmental Division  
Eastern Idaho Section

AMERICAN INSTITUTE OF CHEMICAL ENGINEERS

Nuclear Engineering Division  
Environmental Division

MEETING OFFICIALS

General Chairman

Charles E. Stevenson

Assistant General Chairman

Bert R. Wheeler

Registration Chairman

Don E. Black

Hotel Liaison

David M. Paige

Finance Chairman

Robert J. Schultz

Technical Program

Cyril M. Slansky, Chairman  
Matthew C. Barrett  
Robert T. Jaske  
Martin J. Steindler  
Ralph M. Wilde  
Ray G. Wymer

Ladies Program

Bernice E. Paige

Public Information

Eugene H. Smith  
George K. Cederberg

# Environmental Research Laboratories

Air Resources

Atmospheric Turbulence and Diffusion Laboratory

Oak Ridge, Tennessee

JUNE 1976

LOCAL AND GLOBAL TRANSPORT AND DISPERSION OF AIRBORNE EFFLUENTS

S. R. HANNA

U. S. DEPARTMENT OF COMMERCE  
NATIONAL OCEANIC AND ATMOSPHERIC ADMINISTRATION

ATDL CONTRIBUTION NO. 76/3



CONTROLLING AIR-BORNE EFFLUENTS FROM FUEL CYCLE PLANTS  
ANS-AICHE Meeting, Aug. 5-6, 1976

LOCAL AND GLOBAL TRANSPORT AND DISPERSION OF AIRBORNE EFFLUENTS

Steven R. Hanna  
Atmospheric Turbulence and Diffusion Laboratory  
National Oceanic and Atmospheric Administration  
Oak Ridge, Tennessee

1. INTRODUCTION

Like most subject areas covered in these proceedings, the area of transport and dispersion in the atmosphere is much too broad to be treated thoroughly in these few pages. Therefore I will emphasize the scientific advances in this area that have taken place in the past three years, since the time of the IAEA symposium entitled "Physical Behavior of Radioactive Contaminants in the Atmosphere," held in Vienna in 1973. Good reviews of progress up until the time of that symposium are given by VOGT<sup>1</sup> and REITER.<sup>2</sup>

At many air pollution sources, such as nuclear reactor buildings or reprocessing plants, the material is not released from a tall stack but is released from vents or small stacks. In this case the pollutant is often mixed into the turbulent wake downwind of the building, and conventional plume rise and diffusion formulas are not valid. During the past three years several wind tunnel and field tests of this phenomenon have taken place and a model of mixing in the wake developed by JOHNSON et al.<sup>3</sup>

For conventional sources, where the crosswind distribution of pollutant concentrations is Gaussian, GIFFORD<sup>4</sup> has recently reviewed the extensive literature on  $\sigma_y$  and  $\sigma_z$  curves and made recommendations for the graphical and analytical techniques which give the best results. However, these methods have been tested with observations only out to distances of about ten kilometers. The special problem of short range dispersion under stable, light-wind conditions has been studied by means of several experiments, and the results summarized by VAN DER HOVEN.<sup>5</sup>

There are many transformation processes which act on pollutants at all scales. As a first step, studies are concerned with the simpler problems on small scales. For example, HORST<sup>6</sup> has developed a more physically realistic "surface depletion" method of estimating dry deposition that should prove more effective than the currently used "source depletion" method. He and SEHMEI et al.<sup>7</sup> are also developing new ways for estimating the rate of resuspension of pollutant particles lying on the surface. Chemical transformations and precipitation scavenging are being studied by the group at Pacific Northwest Laboratory also.<sup>8</sup>

In the fall of 1975, a workshop on air pollution and environmental impact analysis was held by the American Meteorological Society and the lectures were recently published. A lecture by EGAN<sup>9</sup> describes a series of recent experiments on diffusion in mountainous terrain. These experiments are important because of the increasing tendency to build power plants in rural areas near the source of the raw materials. There are also many new plants being built on shorelines, and LYON's<sup>10</sup> lecture and RAYNOR et al.'s<sup>11</sup> experiments on diffusion in shoreline environments discuss progress in these areas.

Diffusion on middle or meso-scales (length scales from 10 km to 1000 km) has been studied very little because of the large expense of observation programs and the complications introduced by non-uniform wind fields. But during the past few years it has become necessary to estimate the transport and dispersion of substances such as sulfates and radioactive gasses on these scales. HEFFTER et al.<sup>12</sup> and DICKERSON et al.<sup>13</sup> suggest methods by which the trajectories of pollutant clouds can be estimated based on observed winds. WATSON and BARR<sup>14</sup> show how a Monte Carlo estimate of diffusion can be combined with a trajectory model to predict concentrations due to nuclear explosions.

At global scales, transport and diffusion must be estimated on the basis of observations of the spread of tracer materials such as volcanic or nuclear cloud debris. The model by MACHTA<sup>15</sup> is

oversimplified, but is capable of reproducing some of the long-term characteristics of the mixing of pollutants on a global scale.

The next few pages will outline in more detail the new developments mentioned in this introduction.

## 2. INTERFERENCE OF SOURCE BUILDING ON LOCAL DIFFUSION

It is well known that for high wind speeds, if the height of a smoke stack is less than about twice the height of the source building, then the plume from the stack will often enter the turbulent wake of the building. Consequently high ground level concentrations of pollutant just downwind of the building may result. An early suggestion for accounting for the influence of both building interference and ordinary diffusion is the following equation:

$$X/Q = ((\pi\sigma_y\sigma_z + cA)U)^{-1} \quad (1)$$

where  $X$  is the concentration,  $Q$  is the source strength,  $U$  is the wind speed,  $\sigma_y$  and  $\sigma_z$  are the standard deviations of the crosswind components of the concentration distribution,  $A$  is the area of the building cross section normal to the flow and  $c$  is a constant whose most recent value is  $1/2$ .<sup>4</sup>

JOHNSON et al.<sup>3</sup> recently reported a series of measurements at the Millstone Nuclear Power Plant in which the diffusion of a tracer material released at the top of the reactor building was measured. Similar field studies are underway at the National Reactor Testing Station and wind tunnel studies are being performed at Colorado State University. JOHNSON et al.<sup>3</sup> observed that the extreme modes of plume diffusion, complete entrainment and no entrainment, rarely occurred, leading them to propose a model in which downwash occurs a fraction of the time. They call their model the "split H" model, for the effective plume rise  $H$  can assume two distinctly different values. The first plume rise value  $H_1$  is that which would occur with no building interference. The second plume rise value  $H_2$  is zero; i.e., that which would occur if the plume were completely drawn into the building wake. The split H model is assumed to apply when the ratio of plume effluent speed  $U_e$  to wind speed  $U$  is between 0.9 and 5.0. For  $U_e/U > 5.0$  there is assumed to be no entrainment, and for  $U_e/U < 0.9$  there is complete entrainment.

They further assume that the fraction of time that entrainment occurs is  $M$ . Then the average concentration is given by the formula:

$$S/Q = (1-M)(X/Q)_1 + M(X/Q)_2 \quad (2)$$

where subscripts 1 and 2 refer to concentrations estimated assuming no entrainment and complete entrainment, respectively. The equations for ground level concentrations during the two regimes are the following:

$$(X/Q)_1 = (\pi\sigma_y\sigma_z U)^{-1} \exp(-(y^2/2\sigma_y^2 + H_1^2/2\sigma_z^2)) \quad (3)$$

$$(X/Q)_2 = (\pi\beta_y\beta_z U)^{-1} \exp(-y^2/2\beta_y^2) \quad (4)$$

The contribution  $(X/Q)_1$  is given by the standard Gaussian plume formula, using the effective source height  $H_1$ . The contribution  $(X/Q)_2$  uses the Gaussian plume formula, but with plume rise equal to zero and crosswind standard deviations  $\beta_y$  and  $\beta_z$  given by

$$\beta_y = (\sigma_y^2 + cA/\pi)^{1/2} \quad (5)$$

$$\beta_z = (\sigma_z^2 + cA/\pi)^{1/2} \quad (6)$$

where  $\sigma_y$  and  $\sigma_z$  are the standard values (discussed in section 3) and  $c$  and  $A$  are defined as in equation (1). The fraction  $M$  is defined on the basis of measurements at Millstone to be given by the relations:

$$M = 2.2 - 1.33(U_e/U) \text{ for } .9 < U_e/U < 1.5 \quad (7)$$

$$M = .286 - .0571(U_e/U) \text{ for } 1.5 < U_e/U < 5 \quad (8)$$

This model was tested at Millstone using  $SF_6$  and freon tracers released at the roof vents on



the reactor building and turbine building. The correlations between predicted and observed concentrations are about .80. The predicted concentrations are generally within a factor of two of the observations.

### 3. DIFFUSION AT SHORT DISTANCES WITH NO SOURCE INTERFERENCE

The Gaussian plume formula, as described by GIFFORD<sup>16</sup> in *Meteorology and Atomic Energy*, is the most widely used method of estimating diffusion at short distances (downwind distance  $x$  less than about 10 km). It has been verified by countless diffusion experiments. For a continuous point source of strength  $Q$ (gm/sec) at effective source height  $H$ (m), the formula is:

$$X = (Q/(2\pi U \sigma_y \sigma_z)) \exp(-y^2/2\sigma_y^2) \exp(-(z-H)^2/2\sigma_z^2) \exp(-(z+H)^2/2\sigma_z^2) \quad (9)$$

where  $X$ (gm/m<sup>3</sup>) is the concentration at point  $(x, y, z)$ ,  $U$ (m/s) is the wind speed, and  $\sigma_y$ (m) and  $\sigma_z$ (m) are the crosswind lateral and vertical standard deviations of the concentration distribution. The lateral crosswind distance  $y$  is reckoned from the mean axis of the plume. The last exponential term accounts for perfect reflectivity of the material at the ground surface. In practice the parameters  $\sigma_y$  and  $\sigma_z$  are obtained from graphs, tables, or analytical expressions based on actual measurements, as a function of downwind distance,  $x$ , and atmospheric stability.

Equation (9) is similar to a solution of the so-called diffusion equation only for greatly simplified conditions; i.e., constant wind speed and eddy diffusivity coefficient and homogeneous turbulence. It is therefore largely an empirical equation, and it is used so often only because it works! Yet recently it has been applied to a variety of problems that are outside of its range of applicability. For instance, the empirical  $\sigma_y$  and  $\sigma_z$  graphs were originally derived from observations over "open country" at distances much less than 10 km from the source. Yet they have been applied to estimate diffusion over mountainous terrain or at distances more than 100 km from the source. It is therefore not surprising that the diffusion estimated using the standard  $\sigma_y$  and  $\sigma_z$  curves sometimes differs significantly from the observed diffusion. This is not the fault of the Gaussian plume model, but of the person making the application. To help clarify this situation, GIFFORD<sup>4</sup> presented a review of turbulent diffusion typing schemes, in which a historical survey of  $\sigma_y$  and  $\sigma_z$  measurements and estimation schemes is given and recommendations made for more precise expressions for  $\sigma_y$  and  $\sigma_z$ .

Gifford shows that the three major schemes in use now (Pasquill-Gifford (PG), Brookhaven National Laboratory (BNL), and Tennessee Valley Authority (TVA)) apply at different downwind distances from the source. For instance, the PG schemes are based on ground level releases of non buoyant material and are valid only for distance  $x$  less than 800 m. The BNL schemes are based on releases at a height of 110 m of a non-buoyant material and measurements are made at downwind distances between about 1 and 10 km. The TVA schemes are based on observations of large, elevated, buoyant plumes and are valid at downwind distances of several kilometers. BRIGGS<sup>17</sup> developed analytical expressions for  $\sigma_y$  and  $\sigma_z$ , given in Table 1, which agree with the PG curves at small distances and the BNL and TVA curves at large distances. Because of the lack of observations at downwind distances greater than 10 km, these expressions are intended for use only at  $x$  less than 10 km.

Table 1: Formulas Recommended by Briggs for  $\sigma_y(x)$  and  $\sigma_z(x)$ ;  $10^2 < x < 10^4$  m, Open-Country Conditions

Pasquill type	$\sigma_y, m$	$\sigma_z, m$
A	$0.22x(1 + 0.0001x)^{-1/2}$	$0.20x$
B	$0.16x(1 + 0.0001x)^{-1/2}$	$0.12x$
C	$0.11x(1 + 0.0001x)^{-1/2}$	$0.08x(1 + 0.0002x)^{-1/2}$
D	$0.08x(1 + 0.0001x)^{-1/2}$	$0.06x(1 + 0.0015x)^{-1/2}$
E	$0.06x(1 + 0.0001x)^{-1/2}$	$0.03x(1 + 0.0003x)^{-1}$
F	$0.04x(1 + 0.0001x)^{-1/2}$	$0.016x(1 + 0.0003x)^{-1}$



In order to ease the problem of cross referencing between the various schemes for estimating the turbulence type, Gifford recommends the relations given in Table 2.

Table 2: Relations Among Turbulence Typing Methods

Stability Description	Pasquill	Turner	BNL	$\sigma_A$ , deg
Very stable	A	1	B <sub>2</sub>	25
Moderately unstable	B	2	B <sub>1</sub>	20
Slightly unstable	C	3	B <sub>1</sub>	15
Neutral	D	4	C	10
Moderately stable	E	6		5
Very stable	F	7	D	2.5

The symbol  $\sigma_A$  represents the standard deviation of wind direction fluctuations. These relations are valid in general for open country. F. B. Smith, of the British Meteorological Office, is estimating  $\sigma_z$  values at downwind distances to 100 km over a variety of terrain, by obtaining numerical solutions to the diffusion equation using wind speeds and diffusivities estimated from observations. Therefore  $\sigma_z$  can be predicted knowing the downwind distance, the roughness length, the incoming solar radiation, the heat flux, the mixing depth, and the stability. This study is still underway.

Gifford also proposes methods for estimating  $\sigma_y$  and  $\sigma_z$  over urban areas and over water. He briefly discusses the problem of estimating diffusion under light wind, stable conditions (Pasquill category G). This latter problem was more thoroughly surveyed by VAN DER HOVEN<sup>5</sup> emphasizing recent observation programs. Category G is a problem because the Nuclear Regulatory Commission has been recommending a diffusion rate for category G that is even less than that for category F.<sup>18</sup> In contrast, casual plume observations suggest considerable plume meander during light wind, stable conditions.

To settle this disagreement five diffusion experiments during category G conditions were analyzed. The experimental sites were: the flat, arid interior valleys of Washington and Idaho, a flat forested area of the lower Mississippi valley, a wooded island in the Susquehanna River valley, and a forested, hilly site in Tennessee. Normalized ground level concentrations for G stability conditions are plotted as a function of downwind distance from the source in Figure 1, based on experiments performed at these sites. The lines I, II, and III are best fit lines for flat desert terrain, flat wooded terrain, and hilly wooded terrain, respectively. It is seen that concentrations are one to three orders of magnitude less at the various sites than the NRC curve for G conditions. Clearly the meandering of the plume has an important effect on ground level concentrations during stable conditions. Van der Hoven plotted similar figures for E and F stability conditions, and while the discrepancy between the observations and the standard curves was less than that for G conditions, there was still an order of magnitude difference over the flat wooded and hilly wooded terrains.

The work by Gifford and Van der Hoven is very important in that it emphasizes that the standard  $\sigma_y$  and  $\sigma_z$  curves are derived from observations over special kinds of terrain and at certain distances from the source. The curves are not expected to be correct when applied to sites where roughnesses, downwind distances, etc. are outside of the range of conditions used in the derivation of the curves. For these special cases experiments must be performed to produce new  $\sigma_y$  and  $\sigma_z$  curves. Furthermore, the application of the so-called diffusion equation does not get around these difficulties, for the empirical diffusivities,  $K_y$  and  $K_z$ , are even more elusive than  $\sigma_y$  and  $\sigma_z$ .

#### 4. REMOVAL AND TRANSFORMATION MECHANISMS

Pollutant material in the atmosphere is continually being removed by precipitation scavenging, dry deposition, and chemical transformations. During periods of high wind speed, material on the ground can be resuspended and thus increase atmospheric concentrations.



#### 4.1 DRY DEPOSITION

In *Meteorology and Atomic Energy*, VAN DER HOVEN<sup>19</sup> recommends the so-called source-depletion model for handling dry deposition. The dry deposition at the surface is postulated to be equal to the product of the ground level atmospheric concentration (given by the Gaussian plume model) and an empirical dry deposition speed  $v_d$ . As the plume material is depleted, the plume retains its Gaussian or normal shape in the vertical, but the magnitude of the concentration is reduced by an amount given by integration of the plume formula (see pp 202-208 of the reference for details).

HORST<sup>6</sup> points out that it is unrealistic to expect dry deposition at the surface to result in an instantaneous removal of material from the full depth of the plume. Consequently he proposes a so-called surface-depletion model in which the vertical distribution of material in the plume is not constrained to a Gaussian shape. Instead, the deposition flux at a point is represented as a material sink and treated as a source for downwind diffusion of a material deficit. Thus, the air concentration equals the "sum of the nondeposition diffusion from the primary source plus the diffusion from all the upwind surface sources which account for deposition":

$$X(x,y,z) = Q_0 D(x,y,z,H) - \int_{-\infty}^x \int_0^x v_d X(\xi,\eta,0) D(x-\xi,y-\eta,z,0) d\xi d\eta \quad (10)$$

where  $D$  is a diffusion function which can be equal to the concentration  $X$  given in equation (9) divided by the source strength  $Q$ . The last variable inside the parentheses in the  $D$  function is the effective source height.

While the surface-depletion model is more realistic than the source-depletion model, it can be seen from equation (10) that the mathematics involved in the surface-depletion model is not easy. The integrations must be done by a computer in nearly all practical applications. A few people are attempting to find analytical solutions to equation (10), but with no success. The problem may be simplified by noting that the diffusion function  $D$  does not necessarily have to be Gaussian. As yet, the source and surface deposition models have not been tested against a common set of observations of dry deposition.

#### 4.2 Resuspension

Most of the recent work on resuspension of material from the surface has been done by Sehmel and his colleagues at Battelle Pacific Northwest Laboratory. For a comprehensive review see SEHMET, and LLOYD,<sup>7</sup> and for a description of recent experiments see the BPNL 1975 annual report to ERDA.<sup>20</sup>

In a typical experiment, a known quantity of tracer material is sprinkled on the ground and during the next few months the rate at which this material is transferred to the air is measured by means of air samplers mounted on nearby arrays of towers. It is found that the resuspension rates (defined as the fraction of the total material on the ground resuspended per second) due to wind stresses are of the order of  $10^{-10}$  to  $10^{-8}$  fraction per second for lightly vegetated desert soil. In other words, the residence time on the surface for the particle is a year or more. These figures are highly variable depending on many factors, such as the particle size and soil type. As expected, the resuspension rate is a strong function of wind speed, increasing with the fourth or fifth power of wind speed. Experiments in which the resuspension is mainly a function of man's activities, such as truck traffic, are also underway.

Theoretical investigations of the resuspension from a generalized area source are being conducted by Horst (see pp 79-82 of the BPNL 1975 annual report). He finds that if the source strength of the resuspended material is assumed to equal the resuspension rate times the mass of material per unit area of the surface, then the resulting ground-level concentration approaches a constant factor times the source strength divided by the wind speed. This result is analogous to the result obtained by HANNA<sup>21</sup> for ground-level air concentrations over cities due to area sources of inert gasses or suspended particles.

#### 4.3 Precipitation Scavenging

In HALES<sup>18</sup> review of atmospheric transformation processes, he states that experiments have shown that aerosol tracers released into precipitating cloud systems are often brought to the ground with high efficiency in time periods of an hour or less. In a few experiments, on the other hand, very



little tracer material can be found in the rain gauge network. We know that precipitation scavenging is very important but do not understand the physical processes very well. Hales lists the following basic processes involved:

- transport of pollutant into the cloud system.
- mixing of pollutant within the cloud system.
- capture of pollutant by the cloud hydrometeors.
- delivery of precipitation-bound pollutant to ground level.

Detailed analyses of some of these problems are given by SLINN,<sup>22</sup> who derives theoretical formulas for processes such as the interception, impaction, and diffusion collection efficiencies of raindrops. The success of these methods depends on verification of the experimental predictions in actual cloud systems.

#### 4.4 Chemical Transformations

The reader is referred to the review article by HALE<sup>8</sup> for a good summary of this subject area. There has recently been a great deal of interest in atmospheric transformations related to the production of sulfates from fossil fuel burning, the destruction of the ozone layer in the stratosphere by freons from aerosol spray cans, and the production of ozone near the surface due to emissions of nitrogen oxides and hydrocarbons from motor vehicles. There are disagreements among the experts on the chemical mechanisms involved in each of these areas. At the present time, there are as many hypotheses as there are researchers on the question of the causes of high ozone concentrations in rural areas (e.g., see GRADEL et al<sup>23</sup> or HANNA<sup>24</sup>).

Chemists have devised lists of dozens of chemical reactions that are involved in, for example, the urban ozone problem or the SO<sub>2</sub>-sulfate problem. Typically, the rates of simple reactions can be expressed in the form

$$r_A = k_A X_A^\alpha X_B^\beta \quad (11)$$

where  $r_A$  is the reaction rate,  $k_A$  is the reaction rate constant,  $X_A$  and  $X_B$  are the concentrations of substances A and B, and  $\alpha$  and  $\beta$  are the stoichiometric constants for substances A and B in that reaction. Term (11) is added to the right hand side of the diffusion equation in practical applications. Unfortunately the rate constants  $k_A$  are often determined in laboratory experiments rather than in atmospheric experiments. As with all the problems mentioned in this section, the accuracy of the models is highly dependent on the results of difficult and expensive field experiments.

#### 5. INFLUENCES OF TOPOGRAPHY ON LOCAL PLUME DIFFUSION

A thorough discussion of turbulent diffusion in complex terrain is given by EGAN.<sup>9</sup> It is obvious that the terrain around any pollutant source is unique and that it is difficult to generalize from experiments conducted at these sources. However, it is possible to come to some tentative conclusions based on the results of recent experiments. During neutral and unstable conditions, plume centerline concentrations are observed to be a factor of two to twenty less than those over level terrain. During stable conditions, plumes will attempt to flow around an obstacle such as a hill rather than striking the hill point blank. The latter assumption was used in the Southwest Energy Study<sup>25</sup> and was severely criticized by the utilities involved, since it led to very high predicted SO<sub>2</sub> concentration on the sides of mesas in Arizona and New Mexico, and consequently stringent air pollution control requirements. At the point the plume struck the side of the mesa, it was assumed that the ground level concentration equaled the plume centerline concentration. Final resolution of this controversy will depend on further field measurements.

The experiment by START et al<sup>26</sup> in Huntington Canyon, Utah, is typical of the recent series of diffusion experiments in complex terrain. Oil fog and sulfur hexafluoride were released on the floor and walls of a steep walled canyon and at the top of a 183 m stack being built in the canyon. Concentrations of tracer material were measured by ground-based and helicopter-mounted samplers. An example of their results for class D stability conditions is given in Figure 2. The observed quantity  $XU/Q$  is a factor of four or five less than that predicted by the Pasquill-Gifford method. But, as mentioned earlier, there is no reason to expect that the Pasquill-Gifford curves, which are based on measurements over smooth terrain, would apply to rugged topography at Huntington Canyon.



The problem of diffusion around obstacles has been treated theoretically by HUNT and MULHEARN<sup>27</sup> who assume that the mean flow can be obtained from potential flow theory. A hill is represented by a semicircle and the diffusivity coefficient,  $K$ , is assumed constant. The predicted ratio of the maximum ground level concentrations due to a line source located a distance  $x$  upwind of the center of the hill, with and without the hill is:

$$\frac{X_{\max}(\text{hill})}{X_{\max}(\text{no hill})} = 1/(1-a^2/(x^2 + h^2)) \quad (12)$$

where  $a$  is the height of the hill and  $h$  is the height of the source. For  $a$ ,  $h$ , and  $x$  equal to 1 km, .1 km, and 1 km, respectively, the ratio of the concentrations is about 100. This formula is clearly restricted by its assumption of constant  $K$ , for it is well known that  $K$  can vary by several orders of magnitude in the boundary layers of obstacles. Nevertheless, in spite of the shortcomings of the theories and experiments, we are much closer to the truth now than we were three years ago.

## 6. DIFFUSION NEAR SHORELINES

Many air pollution sources are located near shorelines because of the tendency to settle urban areas near bodies of water. The differing surface characteristics (temperature, reflectivity, roughness, etc.) of the adjacent land and water bodies give rise to phenomena such as sea breezes and extreme stabilities or instabilities. Important recent literature in the subject area of diffusion in the shoreline environment include a review by LYONS<sup>9</sup> and specific studies by RAYNOR et al.<sup>11</sup> and HOSKER.<sup>28</sup>

LYONS<sup>9</sup> concentrates on measurements of diffusion near the western shore of Lake Michigan. He presents observations of lake and land surface temperatures which show that the lake surface temperature can be as much as 20 to 30°C warmer or colder than the land. This difference leads to great instability over the lake in the early winter during cold air outbreaks, and great stability over the lake in the early summer. Photographs of smoke plumes which are visible for tens of miles in the stable layer are shown. For the case of onshore air flow during the daytime when a stable layer exists over the water, the warm land surface causes the formation of a well-mixed layer near the surface which grows in height as the air moves inland. Lyons calls the boundary between the well-mixed air near the surface and the stable air aloft the thermal internal boundary layer (TIBL). Plumes from tall stacks at the shoreline diffuse very slowly in the stable layer until some distance inland when the TIBL intersects the plume. At this point, the plume mixes quickly to the ground, giving relatively high ground level concentrations. Lyons and his colleagues have successfully modeled this situation by assuming a typical stable Gaussian plume at first, and then instantaneously mixing the plume to the ground when the TIBL is intercepted. In these calculations, the slope of the TIBL is based on measurements at a specific location, and no general method for calculating the slope of the TIBL is given.

The ocean shoreline on the southern coast of Long Island, N. Y., has been the site for a series of diffusion experiments performed by Brookhaven National Laboratory. This research was prompted by recent plans for floating nuclear power reactors off the Atlantic Coast. RAYNOR et al.<sup>10</sup> discuss a set of experiments in which oil fog is released at a height above the water of about 7 m from a boat anchored from one to three miles offshore. Photographs from an aircraft and densitometer measurements from another boat and a van along the shore are used to measure the size of the plume. They find that diffusion over the ocean is largely governed by the air-water temperature difference. When stable lapse rates occur, diffusion is much less than over land under similar wind speed and insolation conditions. Pictures of pencil-thin plumes are shown. During unstable lapse rates, much diffusion occurs, similar to what is observed over land.

HOSKER<sup>28</sup> attempts to relate the above observations and other observations of diffusion over water to a theoretical model. He fits several observations of the crosswind diffusion standard deviation  $\sigma_y$  using the formula:

$$\sigma_y = \sigma_A x_r (x/x_r)^p \quad (13)$$

where  $\sigma_A$  is the standard deviation of the horizontal wind angle,  $x_r$  is a reference length, and  $p$  depends on stability. This formula was originally suggested by CRAMER et al.<sup>29</sup> It is found that the best fit to observations is obtained with  $p$  equal to .85 and  $x_r$  equal to 500 m. Over water, observed values of  $\sigma_A$  during neutral conditions are typically 3° to 5°, or a factor of two or three less than values observed over land during similar stability conditions. Methods of estimating  $\sigma_A$  based on wind speed, stability, and surface roughness are suggested.



## 7. REGIONAL TRANSPORT AND DISPERSION

The preceding sections have been concerned with transport and dispersion at distances less than about 10 km from the source. Regional length scales range from about 10 km to about 1000 km, thus including most urban and industrial region sizes. Conversion of  $\text{SO}_2$  to sulfates is important at these scales. Usually the wind speed and direction vary with space and time in a regional problem. Unfortunately, there are very few diffusion experiments at these scales that we can use to derive empirical relations. Standard meteorological reporting stations are also sparse on these scales, having an average spacing of about 200 km. But still there are problems at these scales that require answers right now; e.g.: the sulfate or ozone problems, or the problem of the radioactive dose from an accident at a nuclear fuel reprocessing plant.

Current models of regional transport and diffusion have separate modules for transport and diffusion. The center of a puff of material is assumed to ride with the mean wind speed. In one scheme developed by HEFFTER et al.<sup>12</sup> the transport module depends on the availability of computer tapes of observed winds at as many stations as possible within the region of interest. Heffter possesses many such tapes, obtained from the U. S. Air Force, and has calculated many trajectories from them. He follows a parcel from its origin to end point using winds estimated every three hours and interpolated from nearby reporting stations. The wind velocity of the parcel is assumed to equal the average of the wind velocities at all stations within a 300 km radius, weighting each velocity by  $(1 - 0.5 \sin D_1)/R_1^2$ , where  $R_1$  is the distance to the station from the parcel, and  $D_1$  is the angle between the most recent wind direction of the parcel and the direction of the vector connecting the parcel position and the reporting station position. Either winds at a given level or average winds through a layer can be calculated. For sources in the surface layer, the observed average wind from the ground to the top of the mixing layer is assumed to correspond to the mean transport wind. Heffter's computer program has several options for calculating and displaying the trajectories, depending on the needs of the users. As expected, trajectories calculated over a period of several days or distances of 1000 km do not generally approximate straight lines, and often execute loops and other reversal phenomena.

The accuracy of trajectories generated from a network of wind stations was tested in the Eastern Tennessee Trajectory Experiment (ETTEX),<sup>30</sup> where tetroons (constant level balloons) were tracked through a wind station grid and estimated and actual trajectories were compared. It is found that agreement is the best for nearly neutral conditions, when the trajectory range is accurate within about 15% and the direction is accurate within a few degrees. During convective afternoons, the range and direction differences increase to 30% and 30°, respectively, due to the increased turbulence generated by the large thermals. During stable nighttime conditions agreement is good if both the tetroons and the pibal observations are high enough that they are out of the influence of local drainage flows. If the trajectory is calculated for a low height of, say, 100 m, during the night, then the calculated and observed trajectories could go in opposite directions. These comparisons will be reported by C. J. Nappo at the AMS Symposium on Atmospheric Turbulence, Diffusion, and Air Quality, to be held in Raleigh, N. C. in October.

HEFFTER et al.<sup>12</sup> also suggest methods by which dispersion, dry deposition, and precipitation scavenging can be accounted for along the parcel trajectory. A Gaussian plume is assumed, which means that dispersion parameters  $\sigma_y$  and  $\sigma_z$  must be estimated. For most applications,  $\sigma_z$  is not important, since the pollutant becomes uniformly distributed in the vertical in the mixed layer within a few tens of kilometers of the source. The parameter  $\sigma_y$  is estimated from:

$$\sigma_y(\text{meters}) = .5t(\text{seconds}), \quad (14)$$

where  $t$  is travel time in seconds. This one formula is used in all of the applications by HEFFTER et al.<sup>12</sup> It would be more desirable to develop a formula which accounted for changes in meteorological conditions. For example, the relation

$$d\sigma_y/dt = \sigma_v, \quad (15)$$

at least accounts for changes in turbulence level.

Dry deposition is calculated in the regional model using the source depletion model discussed in section 4.1. Precipitation scavenging is estimated from the formula



$$D_w = \bar{X}_a EP \quad (16)$$

where  $D_w$  is wet deposition per unit area per unit time,  $\bar{X}_a$  is the vertically averaged concentration of material in the air column from the ground to the top of the cloud,  $P$  is the precipitation rate, and  $E$  is the average scavenging ratio  $X_w/\bar{X}_a$ . The parameter  $X_w$  refers to the concentration in rainwater. The model is currently being run using the values  $V_d = 3 \times 10^{-3}$  m/s,  $E = 4.2 \times 10^3$  (by volume),  $P = 3.2 \times 10^{-8}$  m/s, and the depth of the rain layer is 4000 m. Clearly these parameters are highly arbitrary and much work needs to be done to better define them for regional scale calculations.

Another practical approach to the regional transport and diffusion problem is reported by DICKERSON and ORPHAN.<sup>13</sup> They describe the Atmospheric Release Advisory Capability (ARAC), which was developed for ERDA facilities that require a real time method of estimating concentrations of radioactive substances produced by routine or accidental releases on scales out to 1000 km. So far this program is in operation only at LLL, but installation of equipment is also underway at Savannah River Plant and Rocky Flats Plant. The central facility, where all data are stored and detailed models are run, is located at Lawrence Livermore Laboratory (LLL).

Air Force and National Weather Service upper air observations, and meteorological observations from towers and surface stations at the local facilities will be received by the central facility at LLL on a routine basis. The local facilities will have capabilities for storing some of these data and making short time forecasts of transport and diffusion. However, a variety of forecast models will be on hand at LLL, so that when an accidental release occurs, several options can be exercised by the user. The user chooses whether he wants, for example, normalized Gaussian diffusion calculations out to 5 km from the source, or regional calculations using a particle-in-cell technique out to 100 km from the source. The predicted concentration maps are graphically displayed on the user's viewing screen, thus permitting immediate decision as to which areas should be evacuated, for example. From the time of the accidental release to the time of the prediction of concentration patterns, only a few minutes have elapsed.

For detailed regional calculations, a three dimensional numerical model is used by LLL. The observed winds are adjusted so that they are mass-consistent (non-divergent), thus assuring that unrealistic accumulations of material will not occur. Diffusion is estimated using a particle-in-cell code, which reduces the possibility of unrealistic artificial diffusion. However, it is necessary that the three dimensional field of the eddy diffusivity coefficient,  $K$ , be known. The specification of  $K$  is always a problem.

Validation tests were run against the observed diffusion of an  $Ar^{41}$  plume out to distances of 80 km from the source at SRP.<sup>31</sup> Predicted and observed concentrations were within a factor of two 60% of the time. Considering the uncertainties in  $K$  and in removal processes, this is good agreement.

## 8. MONTE CARLO SIMULATION OF DIFFUSION ON REGIONAL SCALES

In the Monte Carlo method of estimating diffusion, trajectories of hundreds or thousands of individual particles are calculated, based on a mean transport by the measured average wind field and a turbulent transport by turbulent fluctuations chosen randomly from the known distribution of turbulent speeds. The final distribution of material is reconstructed from the end points of the thousands of particles.

Of course, the rule that you can't get something for nothing also applies to regional-scale diffusion. In each of the models described so far, information is required that is not well known: the Gaussian plume model requires  $\sigma_y$  and  $\sigma_z$ ; the diffusion equation requires eddy diffusivities  $K$ , and the Monte Carlo model requires the spectrum of the turbulent components of the wind speed. All of these parameters are elusive at the regional scales, primarily due to the lack of meteorological and diffusion observations at these scales.

The Monte Carlo method is interesting because it directly links diffusion to turbulence. The bomb-cloud dispersion model recently described by WATSON and BARR<sup>4</sup> assumes that the speed of an individual particle is made up of three components: a mean transport wind speed, given by 12 hour radiosonde observations; an intermediate scale fluctuating speed representing time scales between 6 min. and 12 hr., obtained from the turbulent energy spectrum; and a small scale



fluctuating speed representing time scales less than 6 min., obtained by random sampling from the turbulent energy at the tail of the turbulent energy spectrum.

The first difficulty with this model is that the radiosonde winds are not averaged over 12 hours, but instead represent a nearly instantaneous speed obtained every 12 hours. Second, as the time step of the trajectory calculation is reduced, the random contribution to the speed fluctuations also is reduced, approaching zero. Consequently for vanishing time steps, the trajectories of all particles become the same. Finally, there is the fundamental problem that the diffusion of a bomb cloud, or a puff, is a relative diffusion problem (see PASQUILL,<sup>32</sup> pp 211-223) which should be treated by looking at the relative spread of two particles released simultaneously a short distance apart, rather than the trajectories of single particles released serially.

Many of the suggestions of WATSON and BARR<sup>14</sup> are being used by the Atmospheric Turbulence and Diffusion Laboratory in Oak Ridge in order to analyze the relative dispersion of tetroons.<sup>33</sup> For example, Watson and Barr suggest a recursion relation for the turbulent fluctuation  $U'_j$  at the time step  $j$  in terms of turbulent fluctuations  $U'_i$  at the previous  $j-1$  time steps:

$$U'_j = \sum_{i=1}^{j-1} \beta_{j,i} U'_i + \Delta U'_j, \quad (17)$$

where  $\Delta U'_j$  is the randomly selected contribution from eddies whose time scale is less than the time step. The coefficients  $\beta_{j,i}$  are functions of the turbulent velocity autocorrelation curve. The formulas for  $\beta_{j,i}$  are simple, but long, and are given on pp 6-7 of WATSON and BARR's report.<sup>14</sup> The velocity autocorrelation curve is obtained from a Fourier transform of the turbulent energy spectrum, corrected for finite travel time of the particle (see PASQUILL,<sup>32</sup> pp 11-16).

The improvement that we recommend is that the  $\beta_{j,i}$  coefficients should be obtained not from the mean autocorrelation curve, but by random sampling from the known distribution of  $U'(t)U'(t + \tau)$  at time lag  $\tau$ . Analyses of tetroon velocity fluctuations suggest that, during the afternoon, the standard deviation of fluctuations of  $U'(t)U'(t + \tau)$  equals about  $.5\sigma_u^2$  at time lags  $\tau$  between 2 minutes and one hour. With this method, as the time step approaches zero, the random nature of the trajectory is retained.

To apply this method, a good knowledge of the spectrum of atmospheric turbulence at the time and location of the diffusion is required. WATSON and BARR<sup>14</sup> use three arbitrary spectra (high, medium, and low energy) in their calculations. Methods should be developed for estimating spectra based on measurements of parameters such as wind speed, turbulence intensity, height, time of day, and stability. Otherwise we have a detailed diffusion model based on very crude turbulence information.

## 9. CONTINENTAL AND GLOBAL SCALE TRANSPORT AND DIFFUSION

The first work concerning transport and diffusion at large scales was related to the atomic energy program. Now, there is also interest in global dispersion of non-radioactive substances, such as sulfates, carbon dioxide, lead, and freons. It is apparent that the products of man's technology can be dispersed to all parts of the earth, and models are needed so that we can determine the world wide concentration patterns due to known releases of material.

Because a network of upper air weather stations exists throughout the world, with spacings of about 200 km over land areas, there are sufficient wind velocity and stability observations available for operation of a global scale transport and diffusion model. However, our knowledge of diffusivity coefficients applying at scales smaller than 200 km is not adequate. Furthermore, artificial diffusion due to errors in numerical approximations will eventually swamp the real diffusion in a computer model of global dispersion having a horizontal grid distance of 200 km and several vertical levels. For these reasons, large computer models employing observed or predicted winds and subgrid scale diffusivity coefficients to estimate global dispersion have not displaced the simpler zonally-averaged models.

MACHTA<sup>15</sup> has made several advances in understanding global dispersion using a simple zonally-averaged model in which variations in pollutant concentration occur only in the meridional (y) and vertical (z) directions. The average value of the diffusivity  $K_y$  is  $3 \times 10^6 \text{ m}^2/\text{s}$ , and the diffusivity  $K_z$  is  $5 \text{ m}^2/\text{s}$  in the troposphere and  $.3 \text{ m}^2/\text{s}$  in the stratosphere. The distributions of diffusivities with latitude are given in previous reports by Machta.



2

The diffusivities are generally chosen so as to give the best agreement between predictions and observations of the concentrations of some tracer. Several tracers have been studied, but most suffer from at least one major difficulty, such as imperfectly known source strength, inadequate observations of concentrations, or too-rapid removal rate. For example, radon is emitted fairly uniformly from the earth's surface. But its short half life (3.8 days) and variabilities in emissions limit its usefulness as a tracer. Machta's model predicts a much more rapid decrease of radon with height than is observed. As another example, Argon-37 is produced cosmogenically and by nuclear tests. Despite obvious uncertainties in the source strength of Argon-37, Machta's model is shown to successfully predict the mean concentration during a three month period when anthropogenic sources were at a minimum. A purely anthropogenic tracer, Freon-11, has also been studied as a possible tracer, since it is nearly inert and its source strength can be estimated based on sales of aerosol spray cans. Recently it has been accused of reacting with substances in the stratosphere to decrease the naturally-occurring concentrations of ozone at levels of about 20 km. Machta's model can simulate the observed latitudinal distribution of Freon-11 only if the magnitudes of the predicted concentrations are reduced by a factor of .75.

A paper by COWAN et al.<sup>34</sup> discusses the possible uses of heavy methanes (20 or 21) as tracers for testing atmospheric transport and diffusion models on global scales. Concentrations as low as 1 part in  $2 \times 10^{16}$  parts (by volume) in the air can be detected by a mass spectrometer. A release of 84 grams of methane-21 was detected at downwind distances of 1500 to 2500 km. The advantages of this tracer are that it is relatively inert, there are practically no natural sources, it can be detected by a proven measuring instrument, and it is non-toxic.

The major applications of Machta's model have been to carbon dioxide and krypton-85. There is much interest in carbon dioxide because of its observed slow build-up in the atmosphere due to the burning of fossil fuels. However, the sources and sinks of carbon dioxide in the biosphere are not well known. By using the latest available observations of carbon dioxide release to and uptake from the surface, MACHTA<sup>15</sup> finds that his model can simulate fairly well the observed annual amplitude of carbon dioxide concentration variation in the northern hemisphere.

Krypton-85 is released by man's activities at nuclear-fuel reprocessing plants. It is useful as a tracer because of its relatively long half life (10.8 yrs.) and its inert behavior. Unfortunately the source information is classified. MACHTA et al.<sup>35</sup> assumed a hypothetical point source release of Krypton-85 at a processing plant in Illinois and traced its dispersion around the globe. The dispersion is assumed to proceed in four phases. During the first six hours, a local wind rose is used to calculate the concentrations in pie-shaped sectors around the source. From the end point of these calculations to 3 days, a climatology of wind trajectories is used (in the application described by MACHTA et al.<sup>35</sup> the required climatology was not yet complete and a simpler method was used). From 3 to 30 days, a Gaussian plume is assumed, whose centerline follows the mean low-level flow and whose cross wind standard deviation,  $\sigma_y$ , is set equal to  $(2K_y t)^{1/2}$ . Thereafter, the concentration patterns are assumed to be zonally uniform and the model described previously is applied. Unfortunately there are no observations to verify this model.

Clearly, present models of global transport and diffusion are very crude. But as Machta has shown, many characteristics of the observations of the spread of global tracers can be simulated by a crude model. In the future, transport and diffusion models will use the results of global circulation models as input. The artificial diffusion problem associated with computer models may be overcome through use of the particle-in-cell technique which is being rapidly developed by several laboratories. Subgrid scale parameterizations of mixing and adequate observations of tracer concentrations will be the major challenges of the future.

#### 9. FINAL COMMENT

Because of the emphasis on research conducted during the past two or three years, there are omissions of important work conducted before this period. The reader is asked to consult the list of references at the end of this paper for excellent reviews of the history of many of the subject areas that have been covered.

Acknowledgements: I wish to thank L. Machta, I. Van der Hoven, T. Crawford, J. Knox, C. Elderkin, S. Barr, P. Barry, and W. Johnson for sending me draft copies of their latest studies.

# REFERENCES

1. VOGT, K. J., 1974: Dispersion of airborne radioactivity released from nuclear installations; population exposure in local and regional environment. Physical Behaviour of Radioactive Contaminants in the Atmosphere, Proceedings of a Symposium, Vienna, 12-16 Nov. 1973 jointly organized by the LAEA and WMO, 3-34.
2. REITER, E. R., 1974: Dispersion of radioactive material on small, meso- and global scales. Loc. Cit., 35-64.
3. JOHNSON, W. B., SINGH, H. B., CAVANAGH, L. A. and SMITH, J. H., 1975: General Field-Test Plan for Evaluation of Roof-Vent Effluent Diffusion from Reactor and Turbine Buildings, prepared for Atomic Industrial Forum, Inc. by Stanford Res. Instit., 333 Ravenswood Ave., Menlo Park, Ca. 94025, 110 pp.
4. GIFFORD, F. A., 1976: Turbulent diffusion typing schemes--a review, Nuclear Safety, 17, 68-87.
5. VAN DER HOVEN, I., 1976: A survey of field measurements of atmospheric diffusion under low wind speed inversion conditions, to be published in May-June issue of Nuclear Safety.
6. HORST, T. W., 1974: A surface depletion model for deposition from a Gaussian plume. Proceedings of Atmospheric-surface Exchange of Particulate and Gaseous Pollutants-1974 Symposium, CONF-740921, ERDA Symp. Series, Nat. Tech. Inf. Service, U. S. Dept. of Commerce, Springfield, Va.
7. SEHMEL, G. A. and LLOYD, F. D., 1974: Particle resuspension rates. Loc. Cit.
8. HALES, J. M., 1975: Atmospheric transformation of pollutants, Lectures on Air Pollution and Environmental Impact Analysis (D. A. Haugen, coordinator), Am. Meteorol. Soc., 45 Beacon St., Boston, Mass., 02108, pp 228-242.
9. EGAN, B. A., 1975: Turbulent diffusion in complex terrain. Loc. Cit., pp 112-135.
10. LYONS, W. A., 1975: Turbulent diffusion and pollutant transport in shoreline environments. Loc. Cit., pp 136-208.
11. RAYNOR, G. S., MICHAEL, P., BROWN, R. M., and SETHURAMAN, S., 1974: A research program on atmospheric diffusion from an oceanic site. Proceedings, Symposium on Atmospheric Diffusion and Air Pollution, American Meteorol. Soc., 45 Beacon St., Boston, Mass., 02108, pp 281-288.
12. HEFFTER, J. L., A. D. TAYLOR, and G. J. FERBER, 1975: A regional-continental scale transport, diffusion, and deposition model. NOAA Tech. Memo ERL ARL 50, Air Resources Lab., Silver Spring, Md., 27 pp.
13. DICKERSON, M. H. and R. C. ORPHAN, 1975: Atmospheric Release Advisory Capability (ARAC), submitted to Nuclear Safety, Lawrence Livermore Laboratory, Livermore, Ca. 27 pp.
14. WATSON, C. W. and S. BARR, 1976: Monte Carlo Simulation of the Turbulent Transport of Airborne Contaminants. LA-6013, Los Alamos Scientific Laboratory, Los Alamos, N. M. 87545, 28 pp.
15. MACHTA, L., 1974: Global scale atmospheric mixing. Advances in Geophysics, 18B, Academic Press, San Francisco, 33-56.
16. GIFFORD, F. A., 1968: An outline of theories of diffusion in the lower layers of the atmosphere. Meteorology and Atomic Energy-1968 (D. Slade, ed.), TID-24190, National Technical Inform. Service, U. S. Dept. of Commerce, Springfield, Va. 22151, 66-116.
17. BRIGGS, G. A., 1973: Diffusion estimates for small emissions, in Environ. Res. Lab., Air Resources Atmos. Turb. and Diff. Lab. 1973 Annual Rept., ATDL-106, USDOC-NOAA.



18. YANSKY, G. R., MARKEE, E. H. and RICHTER, A. P., 1966: Climatology of the National Reactor Testing Station, USAEC, Idaho Operations Office, Rep. IDO-12048.
19. VAN DER HOVEN, I., 1968: Deposition of particles and gasses. Meteorology and Atomic Energy-1968 (D. Slade, ed.), TID-24190 National Technical Inform. Service, U. S. Dept. of Commerce, Springfield, Va. 22151, 202-207.
20. SIMPSON, C. L., 1976: Pacific Northwest Laboratory Annual Report for 1975 to the USAEC Division of Biological and Environmental Research. Part III Atmospheric Sciences, Battelle Pacific Northwest Lab., Richland, Wash., 99352. See pp 83-118 for the contributions of Sehmel and colleagues.
21. HANNA, S. R., 1971: A simple model of calculating dispersion from urban area sources. J. Air Poll. Control Assoc., 21, 774-777.
22. SLINN, W. G. N., 1974: Precipitation scavenging: some problems, approximate solutions, and suggestions for further research, in Precipitation Scavenging-1974, R. W. Beadle and R. G. Semonin, eds., ERDA Symposium Series, in press.
23. CLEVELAND, W. S., B. KLEINER, J. E. MCRAE, and J. L. WARNER, 1976: Photochemical air pollution: transport from the New York City area into Connecticut and Massachusetts, Science, 191, 16 Jan., 179-181.
24. HANNA, S. R., 1975: Modeling smog along the Los Angeles-Palm Springs trajectory, presented at Am. Chem. Soc. Meeting, Philadelphia, April 7, to be published in Advances in Environ. Sci. and Tech. (I. Suffet, ed.), John Wiley & Sons, New York.
25. VAN DER HOVEN, I., et al., 1972: Southwest Energy Study, Report of the Meteorology Work Group, U. S. Dept. of Interior, Draft Report, 113 pp.
26. START, G. E., C. R. DICKSON, and L. L. WENDELL, 1975: Diffusion in a canyon within rough mountainous terrain, J. Appl. Meteorol., 14, 333-346.
27. HUNT, J. C. R. and P. J. MULHEARN, 1973: Turbulent dispersion from sources near two-dimensional obstacles. J. Fluid Mech., 61, 245-274.
28. HOSKER, R. P., 1974: A comparison of estimation procedures for over-water plume dispersion. Proceedings, Symposium on Atmospheric Diffusion and Air Pollution, American Meteorol. Soc., 45 Beacon St., Boston, Mass., 02108, pp 281-288.
29. CRAMER, H. E., G. M. DESANTO, K. R. DUMBAULD, P. MORGENSTERN, R. N. SWANSON, 1964: Meteorological Prediction Techniques and Data Systems. GCA Tech. Rept. No. 64-3-G.
30. HANNA, S. R., C. J. NAPPO, R. P. HOSKER, and G. A. BRIGGS, 1974: Description of the Eastern Tennessee Trajectory Experiment, presented at AMS Conference on Regional and Mesoscale Modeling, Analysis, and Prediction, Las Vegas, available as report no. 103 from ATDL, P. O. Box E, Oak Ridge, Tennessee, 37830, 26 pp.
31. KERN, C. D., 1975: Real time prediction and verification of Argon-41 concentrations--a joint effort with the Lawrence Livermore Laboratory, in Savannah River Laboratory Environ. Transport and Effects Research-1974, E. I. du Pont de Nemours & Co., Savannah River Lab., Aiken, S. C., 29801, pp 11-1 to 11-18.
32. PASQUILL, F., 1974: Atmospheric Diffusion, second edition, Halsted Press, John Wiley and Sons, Inc., New York, 429 pp.
33. HANNA, S. R., 1976: Relative diffusion of tetroon pairs during convective conditions, to be published in J. Appl. Meteorol.
34. COWAN, G. A., D. G. OTT, A. TURKEVICH, L. MACHTA, G. J. FERBER, and N. R. DALY, 1976: Heavy methanes as atmospheric tracers. Science, 191, 1048-1050.
35. MACHTA, L., G. J. FERBER, and J. L. HEFFTER, 1974: Regional and global scale dispersion of <sup>85</sup>Kr for population dose calculations, Physical Behaviour of Radioactive Contaminants in the Atmosphere, Proceedings of a Symposium, Vienna, 12-16 Nov. 1973 jointly organized by the IAEA and WMO, 411-424.

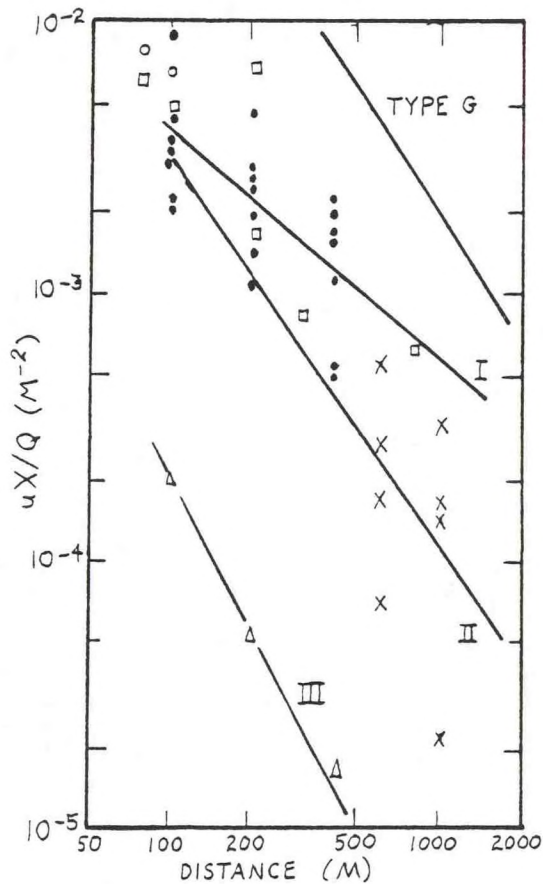


Figure 1: Normalized peak concentration ( $UX/Q$ ) as a function of distance downwind for Type G diffusion ( $\square$  Washington,  $\bullet$  Idaho,  $\times$  Louisiana,  $\circ$  Pennsylvania,  $\Delta$  Tennessee) (from VAN DER HOVEN<sup>5</sup>). The top line is the curve that was recommended for G conditions before this study was undertaken. The curves labeled I, II, and III are the best fit lines for smooth desert-like terrain, wooded flat terrain, and wooded hilly terrain, respectively.

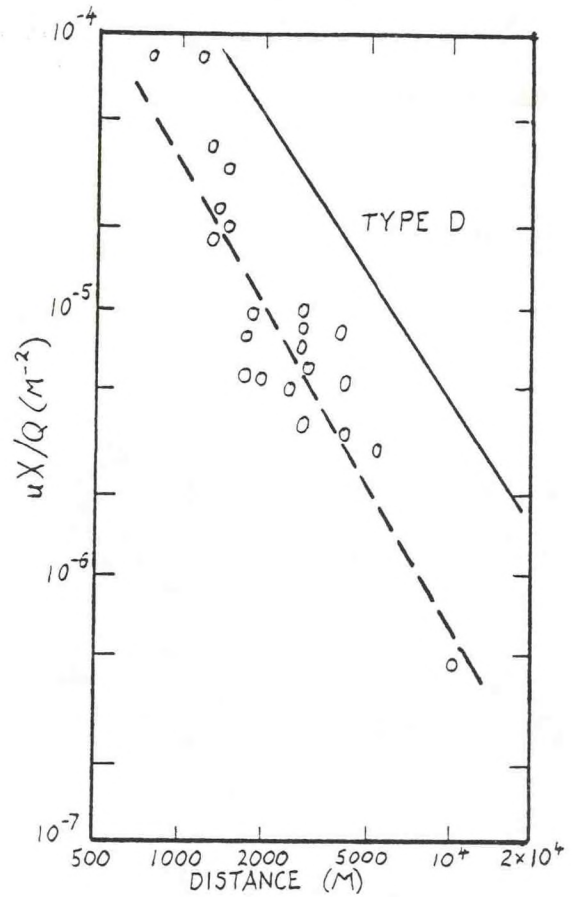


Figure 2: Helicopter samples of axial concentrations of  $SF_6$  tracer gas at Huntington Canyon, D stability (from START ET AL.<sup>26</sup>). The solid line is the PG curve for D stability. The dashed line is the straight line that best fits the observations.





# Environmental Research Laboratories

## Air Resources

### Atmospheric Turbulence and Diffusion Laboratory

#### Oak Ridge, Tennessee

OCTOBER 1976

FOREST METEOROLOGY RESEARCH WITHIN THE OAK RIDGE SITE,  
EASTERN DECIDUOUS FOREST BIOME, USIBP<sup>1,2</sup>

B. A. Hutchison  
D. R. Matt

U. S. DEPARTMENT OF COMMERCE  
NATIONAL OCEANIC AND ATMOSPHERIC ADMINISTRATION

ATDL Contribution File No. 76/

FOREST METEOROLOGY RESEARCH WITHIN THE OAK RIDGE SITE,  
EASTERN DECIDUOUS FOREST BIOME, USIBP<sup>1,2</sup>

by

B. A. Hutchison

D. R. Matt

Atmospheric Turbulence and Diffusion Laboratory  
National Oceanic and Atmospheric Administration  
Oak Ridge, Tennessee

October, 1976

---

<sup>1</sup>This research supported in part by the Eastern Deciduous Forest Biome, US-IBP, funded by the National Science Foundation under Interagency Agreement AG-199, BMS76-00761 with the U.S. Energy Research and Development Agency, Oak Ridge National Laboratory, and in part by the Division of Biomedical and Environmental Research, ERDA.

<sup>2</sup>ATDL Contribution File No. 76/4.

## PREFACE

An abridged version of this paper is to appear in a forthcoming volume describing results of research conducted at the Oak Ridge Site, Eastern Deciduous Forest Biome of the U.S. International Biological Program. This volume is to be published by Dowden, Hutchinson, and Ross, Inc. of Stroudsburg, Pa. 18360. Since a publication date has not yet been established, we are publishing this version independently in order to make the information available more quickly.



## INTRODUCTION

Microclimatic conditions within a forest are defined by interactions among synoptic climate, forest structure, forest physiology, soil moisture (and, to a lesser degree, fertility) conditions, and feedback mechanisms that exist between the set of controlling parameters and forest microclimate. Among the many implications of this definition is the fact that knowledge of ecosystem structure and function implies understanding of this complex of interactions. For this reason, the fundamental objective of our research is to identify and quantify these interactions.

Because of the obvious importance of solar radiation to ecosystem structure and function, our initial research efforts were directed toward studies of solar radiation within a deciduous forest composed predominantly of tulip poplar (Liriodendron tulipifera L.). The temporal and spatial variation of solar radiation within and above this stand have been documented (Hutchison and Matt, in press). An attempt to relate this variation to forest structure was less successful but provides direction for further research (Hutchison, 1975).

Beyond the space and time variation in solar radiation distributions within the forest, the subsequent partitioning of this energy, which is effected mainly by the autotrophs by virtue of their dominance in ecosystem structure, also has profound implications upon ecosystem functioning. Conversely, the functioning of the forest has important effects upon energy partitioning. Despite its importance to ecosystem structure and function, resource limitation prevented serious research efforts on our part in this area of forest micrometeorology. Studies, by McConathy (1976), of the water relations of this stand and their effects upon leaf energy budgets provide good preliminary information of the energy partitioning in the fully leafed forest however.

The most intractable area of forest micrometeorology, in our view, remains the quantification of forest structure. The situation is complicated by the fact that different variables are likely to be affected by different structural characteristics. For example, the penetration of radiation into a forest seems to be a function of the amount and spatial distribution of biomass in the forest as well as its optical characteristics whereas the penetration of wind is probably a function of canopy roughness and biomass flexibility, as well as space density.

Much work has been done in agricultural crops relative to the radiation penetration problem and several studies have been made of forests (e.g. Anderson, 1964, Horn, 1971, Miller and Norman, 1971, Norman, et al., 1971, and Norman and Jarvis, 1975). Less study has been made of the interrelations between forest structure and other micrometeorologic variables. Further study of this area is needed.

This chapter describes results of our forest micrometeorologic research efforts within the Eastern Deciduous Forest Biome, USIBP. We consider the vertical and temporal variation in the forest radiation budget along with a few other micrometeorologic variables and the annual radiation regime of this deciduous forest.

#### SITE DESCRIPTION

The forest under study is a seral, deciduous forest in which tulip poplar is the predominant species. The stand is around 50 years old and is situated in a moist limestone sink within a small stream valley on the USERDA reservation some 10 km south of the town of Oak Ridge. Because the sink is mesic, the stand has a different species composition, a greater density and diversity, and a more highly developed understory than is typical of the oak-hickory forests of the Appalachian region. Figure 1 shows a general view of the stand in its fully leafed phase of midsummer.



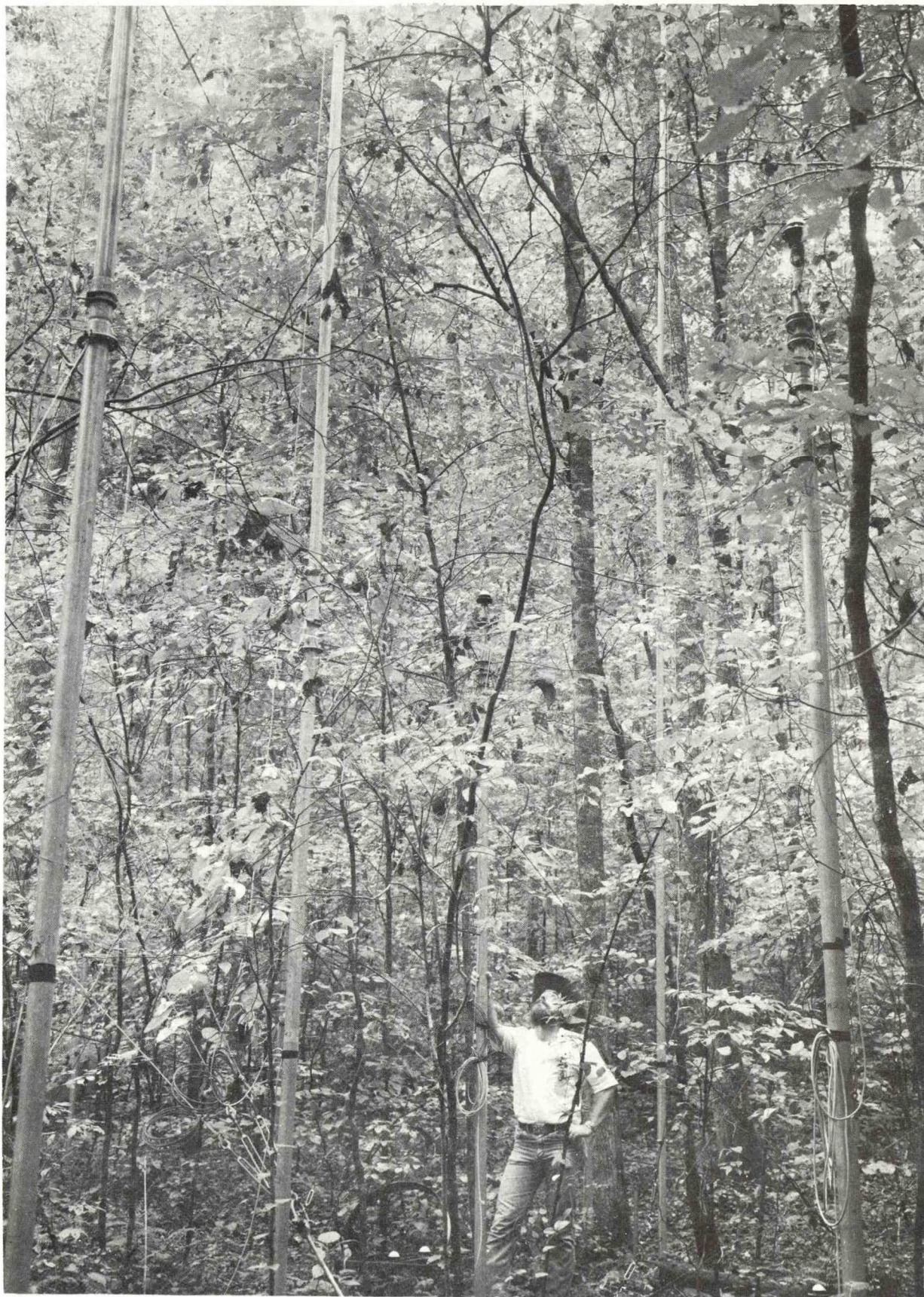


Figure 1. General view of the tulip poplar stand in midsummer showing method of deployment of elevated solarimeters.



The overstory canopy is nearly pure tulip poplar although numerous other species are present in small numbers as indicated in Table 1. The overstory canopy extends down past the zone of crown closure (at about 25 meters height) to the base of the live crown which is well defined at about 16 m height. Between 16 and 10 m, there are a few crowns of suppressed trees but in general, this stratum is devoid of biomass other than the boles of the codominant overstory trees. Between 10 and 3 m, there is a rather distinct secondary canopy composed mainly of flowering dogwood and redbud while below 3 m are found numerous tree saplings as well as shrubs of various species, mostly woody hydrangea (Hydrangea arborescens), and an herbaceous layer predominantly composed of Christmas fern (Polystichum acrostichoides). Many other herbaceous species are present especially in the spring but their contribution to the herbaceous biomass is small.

The pertinent mensurational data for this forest stand are shown in Table 2. As indicated, the overall basal area of this forest at the time of these studies was about  $28 \text{ m}^2 \text{ ha}^{-1}$  and the total stem density exceeded  $5500 \text{ stems ha}^{-1}$ . The total leaf area index of the fully leafed forest was reported as  $6 \text{ m}^2 \text{ m}^{-2}$  (Burgess and O'Neill, 1975).

Table 1: Species composition of canopy strata in Liriodendron forest

<u>Stratum</u>	<u>Species</u>	<u>Percent Composition</u>
Upper Canopy (above 16 m)	tulip poplar ( <u>Liriodendron tulipifera</u> )	72.3
	red maple ( <u>Acer rubrum</u> )	9.2
	Shortleaf pine ( <u>Pinus echinata</u> )	4.6
	ash ( <u>Fraxinus spp.</u> )	3.2
	oak ( <u>Quercus spp.</u> )	3.1
	hickory ( <u>Carya spp.</u> )	3.1
	black locust ( <u>Robinia pseudoacacia</u> )	1.5
	black gum ( <u>Nyssa sylvatica</u> )	1.5
	sourwood ( <u>Oxydendron arboreum</u> )	1.5
		100.0
Mid Canopy (10 to 16 m)	red bud ( <u>Cercis canadensis</u> )	30.6
	oak ( <u>Quercus spp.</u> )	25.0
	sourwood ( <u>Oxydendron arboreum</u> )	16.7
	tulip poplar ( <u>Liriodendron tulipifera</u> )	11.1
	hickory ( <u>Carya spp.</u> )	8.3
	red maple ( <u>Acer rubrum</u> )	5.6
	shortleaf pine ( <u>Pinus echinata</u> )	2.7
		100.0
Lower Canopy (0 to 10 m)	flowering dogwood ( <u>Cornus florida</u> )	46.2
	hickory ( <u>Carya spp.</u> )	13.2
	red bud ( <u>Cercis canadensis</u> )	9.5
	ash ( <u>Fraxinus spp.</u> )	7.8
	sourwood ( <u>Oxydendron arboreum</u> )	5.0
	oak ( <u>Quercus spp.</u> )	4.3
	red maple ( <u>Acer rubrum</u> )	4.3
	tulip poplar ( <u>Liriodendron tulipifera</u> )	3.0
	slippery elm ( <u>Ulmus rubra</u> )	1.7
	ironwood ( <u>Carpinus caroliniana</u> )	1.3
	black walnut ( <u>Juglans nigra</u> )	0.4
	hawthorn ( <u>Crataegus spp.</u> )	0.4
	mulberry ( <u>Morus rubra</u> )	0.4
	sassafras ( <u>Sassafras albidum</u> )	0.4
	hophornbeam ( <u>Ostrya virginiana</u> )	0.2
	eastern red cedar ( <u>Juniperus virginiana</u> )	0.2
	other species	1.7
		100.0



Table 2. Mensurational Data and Diversity of the Cesium Tagged Liriodendron Forest at the Oak Ridge Site

Canopy Level	Height (m)	Average DBH (cm)	Basal Area (m <sup>2</sup> hectare <sup>-1</sup> )	Density (stems hectare <sup>-1</sup> )	Shannon-Weaver Species Diversity Index
Upper	16-30	23.8	24.0	520	1.11
Mid	10-15	8.6	1.7	290	1.42
Forest floor	1.5-9	2.3	3.0	4770	1.78
Overall	Range 1.5-30	-	Total 28.7	Total 5580	Overall Index 2.06

The climate of the region is characteristically warm and humid. Winters are mild and wet with frontal storm systems dominating the weather patterns. Summers are hot and humid with convective thunderstorms developing almost daily yielding erratic, intense precipitation events over the region. Average annual precipitation is around  $125 \text{ cm yr}^{-1}$  and nearly all occurs as rain. Heavy radiative ground fog develops frequently throughout the year at this site and because of the topography and proximity to a TVA reservoir, this fog cover often persists until midday.

The access road to the study area is in the zone of influence of an unshielded research reactor of the Oak Ridge National Laboratory. As a result, access to the site was severely restricted and hence, maintenance and repair of the monitoring system and the associated data acquisition equipment was a continuing problem.

#### METHODS

Components of the radiation balance above and within the forest were measured using a variety of radiometers. Incoming solar radiation and its spatial variation was measured using an array of Lintronic Dome Solarimeters, a commercially available modification of a field solarimeter designed by Monteith (1959).

Solar Radiation incident upon the forest was measured initially with a Lintronic sensor and later, with a Kipp and Zonen solarimeter. We planned to measure the outgoing solar radiation along with net all wave radiation by a moving sensor technique that would allow determinations of the spatial variation in these terms as well. Implementation of this plan was never realized and as a result, the shortwave and all-wave balances presented here were obtained from instruments mounted along a single tower. Shortwave balances were determined using upright and inverted Kipp and Zonen solarimeters while net all-wave balances were obtained with Funk type radiometers as manufactured by Solar Radiation Instruments of Altona, Victoria, Australia. Net radiometer domes were kept inflated with bottled nitrogen gas and condensation on the domes prevented by the use of heating rings. The diffuse shortwave radiative component was measured using a Kipp and Zonen solarimeter above and Lintronic sensors within the forest shaded by shadow bands as designed by Horowitz (1969).

Incoming shortwave solar radiation measurements were replicated 10 times in horizontal space at 3 levels in the forest: on the forest floor, at 3 m at the base of the secondary canopy, and at 16 m at the base of the overstory line crown. Measurements



of diffuse radiation were replicated twice at each level. The above canopy incident radiation measurements as well as the short- and all-wave balance measurements were not replicated in horizontal space as noted above. Balance measurements were made at 3, 16, and 33m level. The spectral response of the solarimeters used ranged from 0.3 to 3  $\mu$  while that of the net all-wave radiometer was from 0.3 to 60  $\mu$ .

Two towers were instrumented with bead thermistors at 0.3, 1, 3, 6.5, 10, 13, 16, 20, 23, 26.5, and 33 m heights. Thermistors were enclosed in non-aspirated flat-plate radiation shields to minimize heating affects of beam solar radiation. Output signals from these thermistors as well as from the various radiometers were scanned at preselected intervals and recorded on punch paper tape.

Wind speed measurements were not automated owing to a lack of suitable instrumentation. Because of this, wind data are available for portions of only a few days. For winds within the forest, Thornthwaite sensitive cup anemometers were used and the mechanical counter readout, recorded at fixed intervals of time. These anemometers have a threshold starting speed of about 10 cm sec<sup>-1</sup>, a speed somewhat above that of a considerable portion of the forest wind. Hence, the profiles shown here must be considered as indicative of forest wind conditions rather than as absolute measures of these conditions. Above canopy wind speeds

were measured using a standard cup anemometer having a threshold starting speed of around  $40 \text{ cm sec}^{-1}$ . Output from this sensor was recorded on strip charts.

## RESULTS AND DISCUSSIONS

### Diurnal Variation in Forest Microclimate:

To illustrate the diurnal variation in the microclimate of the fully leafed forest, we present data from a clear day in early September. The shortwave radiation balance for the within and above canopy levels are shown in figure 2. As shown in figure 2a, the above canopy record, this day was quite clear although some haze or thin clouds apparently developed just after solar noon causing the slight asymmetry in the record of incident radiation. The amounts of radiation reflected from the forest canopy vary directly as the levels of incident radiation but owing to the low reflectivity of such a canopy, the reflected amounts are a small fraction of the radiation incident.

Within the forest, amounts of radiation received at the 16 m and 3 m levels on the triangular tower (fig. 2b and c) are much reduced by virtue of the attenuation of radiation by forest biomass. (Results of replicated forest solar radiation measurements are discussed below). The curves showing the downward or incoming component are also much less smooth as a result of the variable penetration of beam radiation.

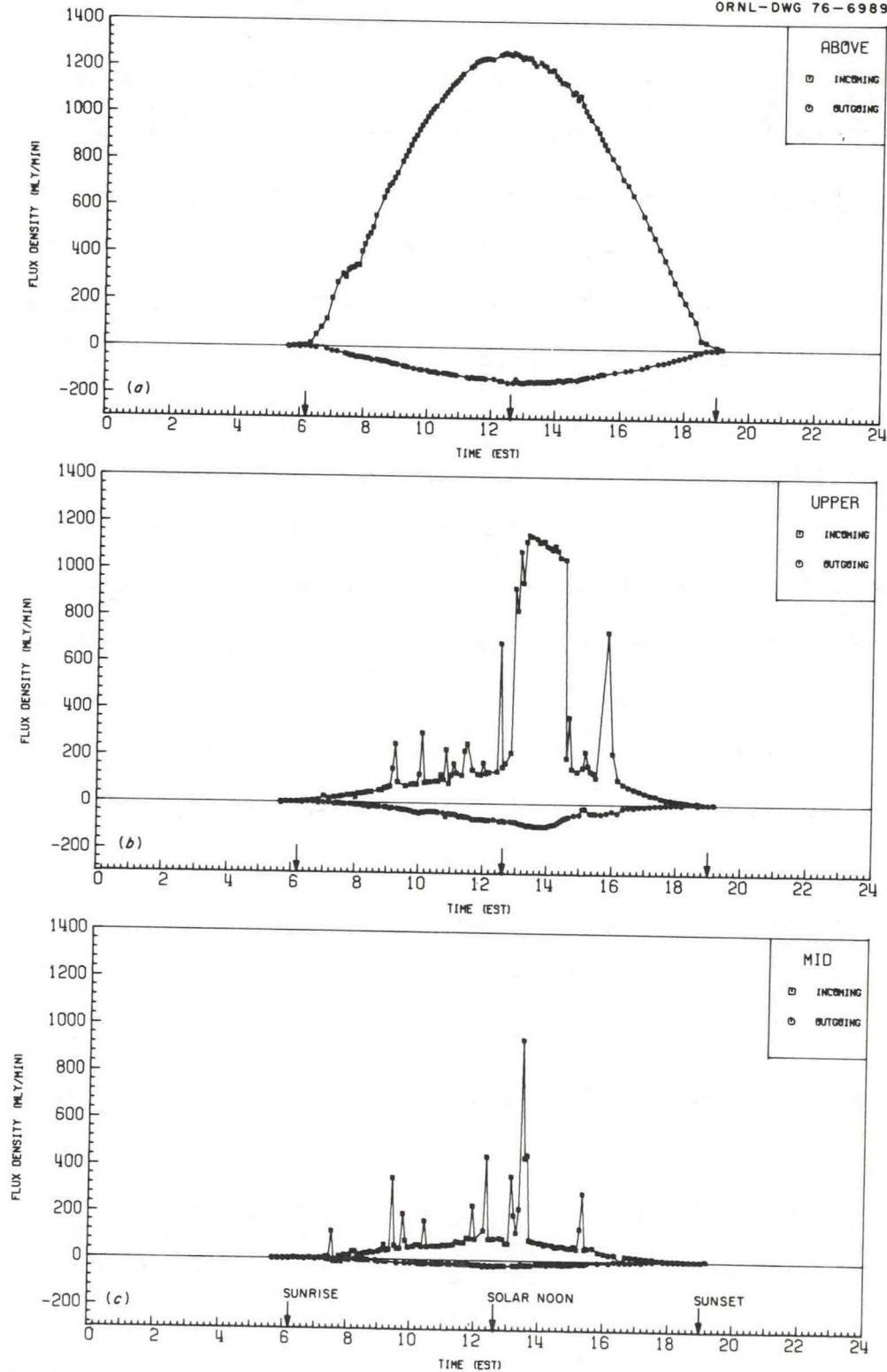


Figure 2. Shortwave radiation balances within and above a fully leafed *Liriodendron* forest.



Peaks in these curves on Figures 2b and c represent sunflecks created by beam radiation penetrating canopy gaps. The minimum values of these curves show much less variability in time and represent, as Gay et al. (1971) have pointed out, the amount of diffuse radiation received at these 2 points. A major problem associated with nonreplicated measurements of highly varying quantities is also shown on figures 2b and c. A large canopy opening existed to the west of the tower from which these measurements were made. Because of this, beam radiation along with additional diffuse sky radiation penetrated this opening and reached the 16 m sensor for several hours soon after solar noon. Total radiation received at this point during this time nearly equalled that incident upon the forest. (The amount was slightly reduced from that incident on the forest since the opening was not sufficiently large to allow radiation from the entire sky to reach the 16 m sensors.) Although the duration and amount of increase were less at 3 m (fig. 2a), the effect of this canopy opening is still quite evident in the 3 m record. Since this opening was much larger than those typically present throughout the stand, these peak values are not representative of average conditions within the stand. However, since our reflected measurements were not replicated, we show the incoming values measured at the same points for these comparisons.

The outgoing or reflected radiation as measured by the inverted sensors show much less variation through time as shown on figures 2b and c. Since the Kipp and Zonen sensors have a hemispherical field of view, the amounts of radiation indicated on these figures are integrations of the amounts of radiation reflected from forest floor and from biomass in the  $2\pi$  steradian solid angle below these inverted sensors. Since the reflected values change slowly and smoothly through time, the total area and intensity of sunflecks below these sensors must also change only slowly and smoothly through time. Even the 16 m sunfleck (or sunlit area) of several hours duration produced by the large canopy opening results in only a slight increase in reflected radiation (fig. 2b). At 3 m (fig. 2c), effects of the large canopy opening is not evident in the record of reflected radiation flux densities. Amounts of radiation reflected are considerably reduced from those observed at the above canopy level as a result of the reduced amounts of radiation reaching the interior of the forest.

Subtracting the reflected shortwave radiation amounts from the incoming amounts shown in figure 2 yields the net shortwave or solar radiation balance as plotted in figure 3 along with the net allwave balance. Above the canopy (figure 3a), the net shortwave exceeds the net allwave radiation amounts throughout the 24 hour period indicating that the longwave balance of the fully leafed

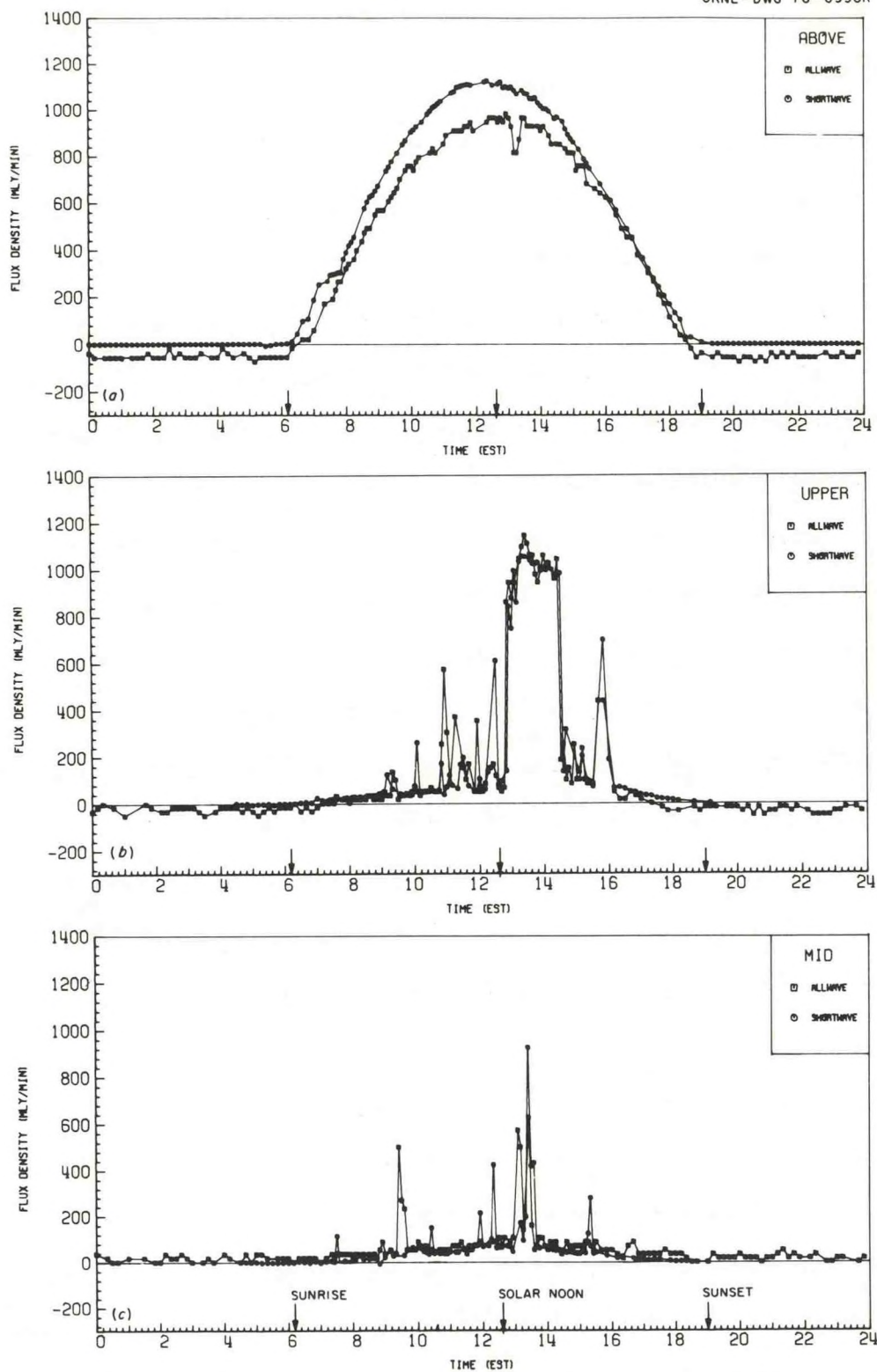


Figure 3. Net all-wave and shortwave radiation balances within and above a fully leafed Liriodendron forest.



forest is consistently negative or outward. Within the canopy, much less difference is found between the net shortwave and allwave radiation balances. At the 16 m level of figure 3b, the net shortwave radiation generally exceeds the net allwave radiation although the situation becomes confused at midday because of sunflecks that do not always impinge upon both the shortwave and allwave sensors at the same time. At any rate, the general trend in the upper canopy appears to be one of net longwave radiation loss throughout both day and night. At 3 m (fig. 3c), on the other hand, the situation is reversed. Net allwave radiation fluxes are positive through the night and since no shortwave radiation is present then, the net longwave radiation flux must be positive. During the daylight hours, the net allwave radiation consistently exceeds the net shortwave radiation indicating a positive longwave radiation balance then as well. If this is true, the forest floor and the biomass below 3 m constantly gain heat energy which must be mostly dissipated through convective heat exchange or evapotranspiration since the materials within this stratum do not typically increase in temperature throughout the duration of the fully leafed forest phenoseasons. Data from Baumgartner(1969) show similar positive longwave balances within a high spruce forest in Germany on a clear August day. Hence, our data appear reasonable.

Plotting the spatially averaged total incoming solar radiation as measured by the Lintronic Dome Solarimeter array as isopleths of radiant flux densities in a height-time dimensional system for this clear September day results in figure 4. This and subsequent figures of this type must be interpreted with caution since the values between the measurement points in space and in time are necessarily, interpolations. While our time grid is quite dense, our height grid is limited as indicated in figure 4. Thus, the radiation isopleths indicated between the measurement levels are known to be there from the data but their positions as shown on this figure are merely our estimates of their actual locations in this frame of reference. Nevertheless, we feel that this figure exhibits the salient features of the radiation climate of the fully leafed forest quite well. It is obvious from figure 4 that most of the incident solar radiation is attenuated by the overstory canopy and never reaches the 16 m level. As a result, the radiation amounts received throughout the interior of the forest are but small fractions of that incident upon the canopy.

The spatially averaged diffuse radiation component is plotted in similar fashion in figure 5. In this case, around half the incident diffuse component is attenuated by the overstory canopy. While this is a highly significant amount, it is nowhere near the magnitude of the attenuation of the direct beam component as

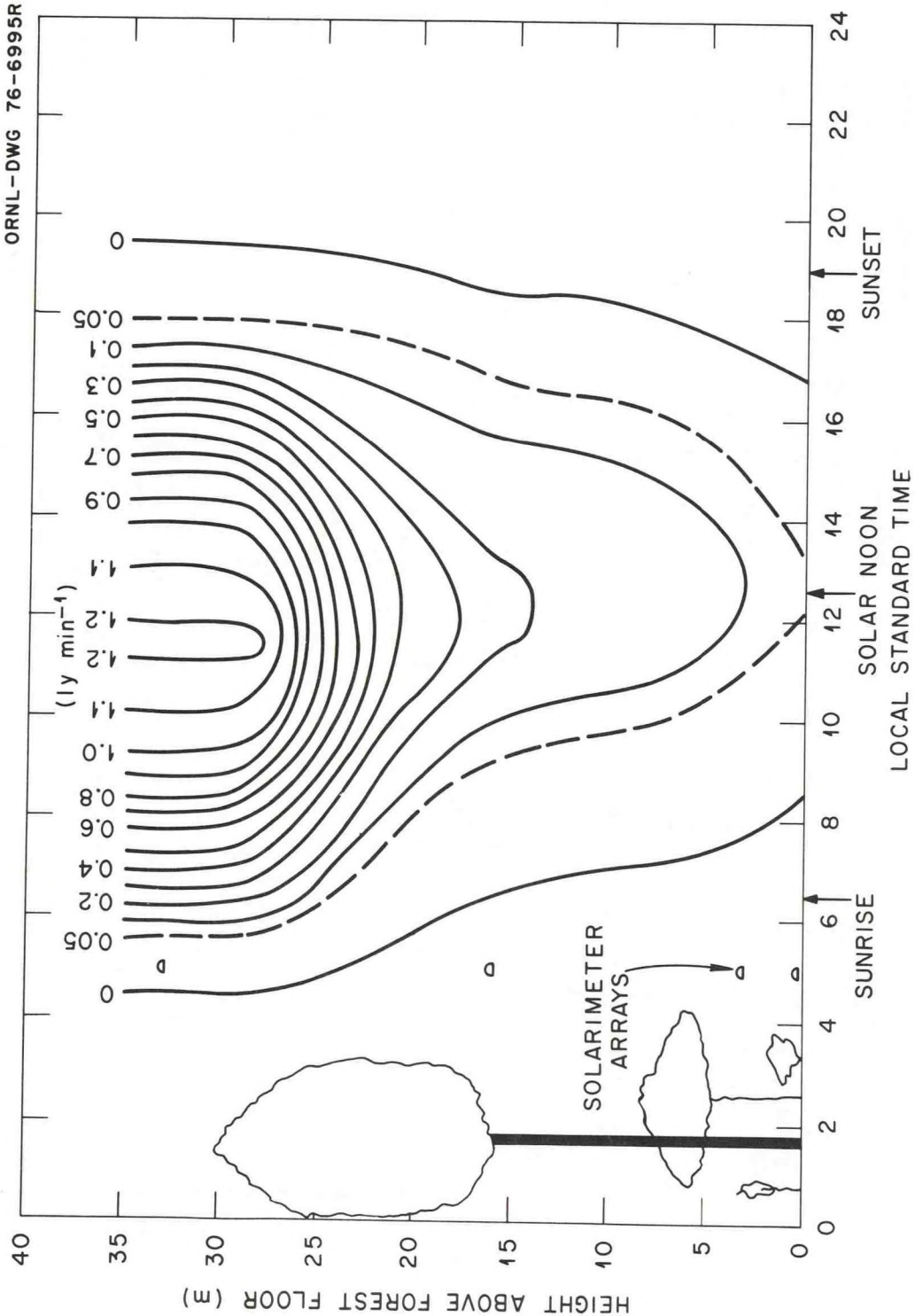


Figure 4. Space average total solar radiation within and above a fully leafed *Liriodendron* forest.



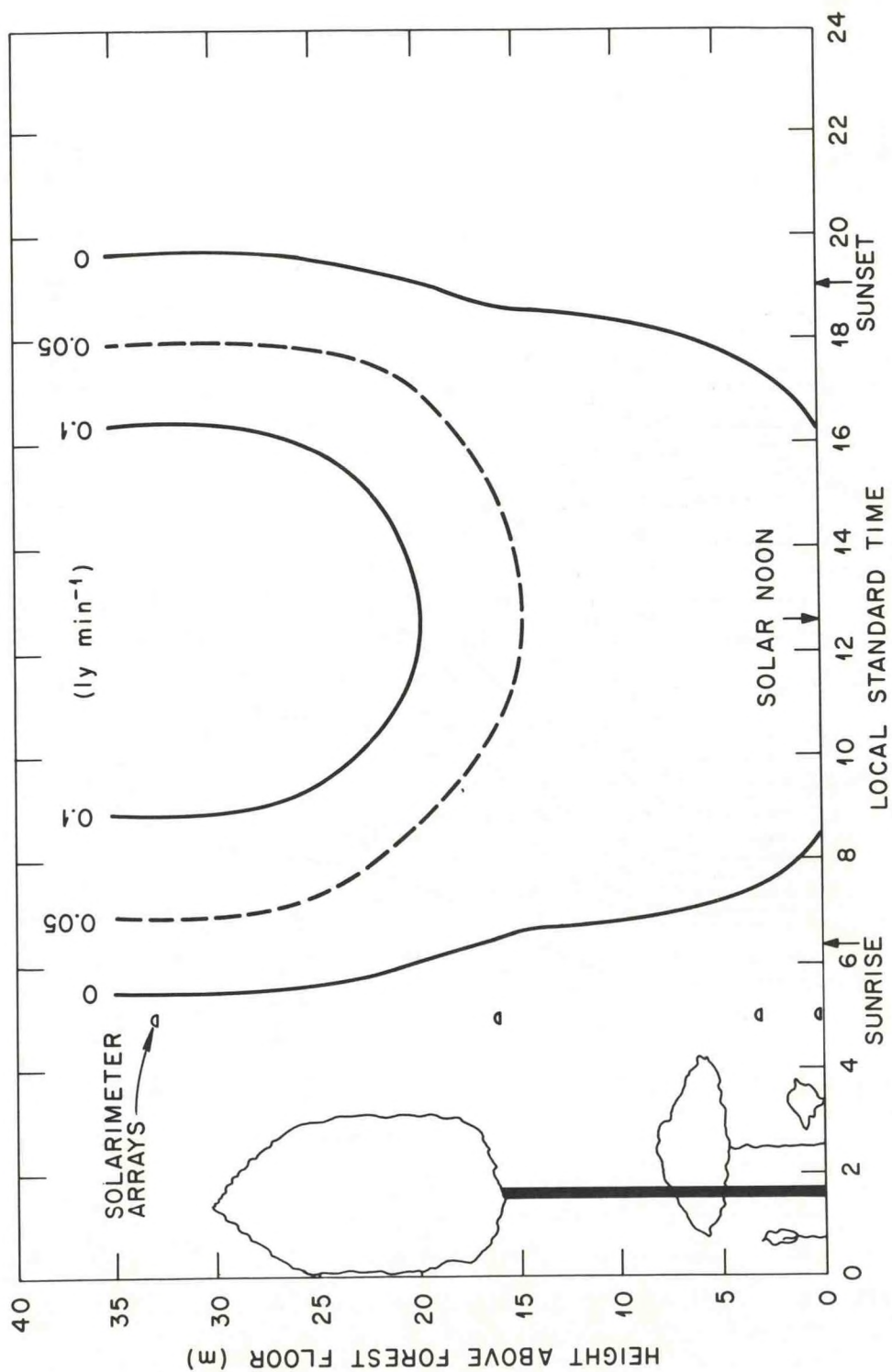


Figure 5. Space average diffuse solar radiation within and above a fully leafed Liriodendron forest.

shown in figure 6. As we pointed out in an earlier paper (Hutchison and Matt, in press) this attenuation of diffuse radiation by the forest biomass is somewhat offset by the conversion of beam radiation to diffuse radiation by reflection from or transmission through leaf tissue. Hence, the uniformity of attenuation of diffuse radiation amounts through the length of the forest cannot be extended to radiation quality. The spectrally selective absorption, reflection, and transmission properties of leaves imply that the radiation field within the forest becomes increasingly dominated by green and near infrared wavelengths with increasing depth in the forest.

It is evident from a comparison of figures 4, 5, and 6 that, of the two components making up the total, the beam radiative component suffers the greatest attenuation by the forest biomass. Since beam radiation arises from the nearly point source sun (as viewed from earth), the penetration of this component to points in the forest requires openings aligned with the solar beam, a not particularly frequent occurrence.

Diffuse radiation, on the other hand, emanates from the entire vault of sky and thus, some diffuse radiation penetrates any canopy opening, no matter what its orientation.

The distribution of net allwave radiation flux densities is shown in figure 7. Again, the effect of the large canopy opening to the west of the tower is strongly evident. The daylight hours net radiation regime is quite similar to that of the average solar radiation (excepting the enhanced penetration

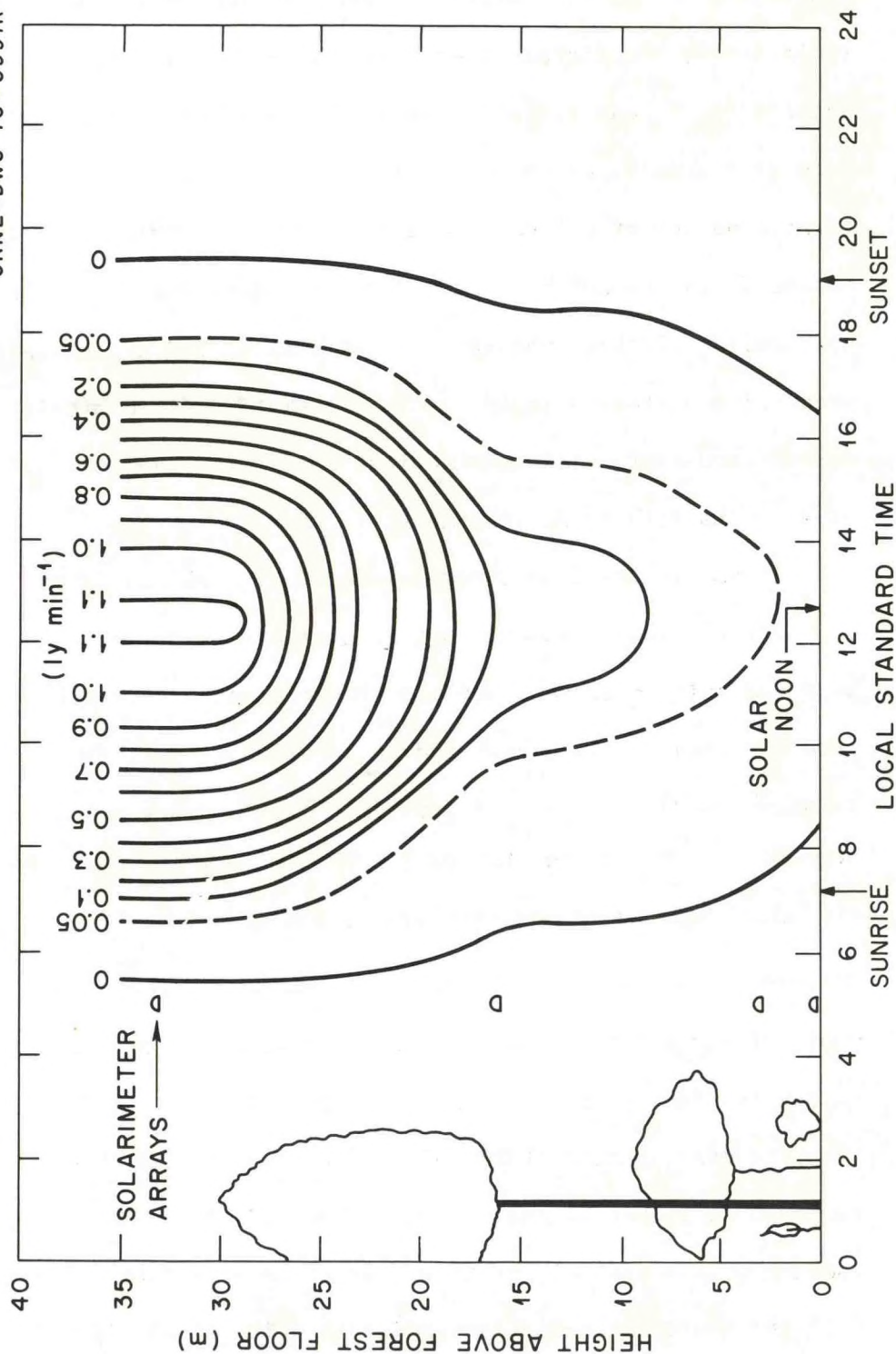


Figure 6. Space average direct beam solar radiation within and above a fully leafed Liriodendron forest.





Figure 7.

through the large canopy gap) indicating the dominant role of radiation of solar wavelengths in the daytime net all-wave balance. At night, with zero shortwave radiation, only the longwave radiative exchanges are operative and the shift from net upward to net downward fluxes between the 3 and 16 m levels is clearly shown on this figure. The oscillatory nature of the above canopy net all-wave radiation fluxes in the early morning on figure 7 is probably the result of broken clouds passing overhead.

Because of the strong absorption of solar radiation in the overstory canopy, leaf temperatures, and hence, air temperatures in that canopy should be higher than those either above or below the canopy. Figure 8 shows that throughout the daylight hours, air temperatures are higher in the overstory canopy and decrease with increasing depth in the forest. At night, there is some indication that the canopy remains slightly warmer into the early morning hours when radiative cooling apparently reverses this trend and results in a cold spot in the overstory canopy.

Comparison of figures 7 and 8 indicates an impossible situation near the forest floor during the early morning of this day. Figure 7 shows that net all-wave flux densities at this time are positive at the forest floor but figure 8 indicates that the air near the forest floor is warmer than

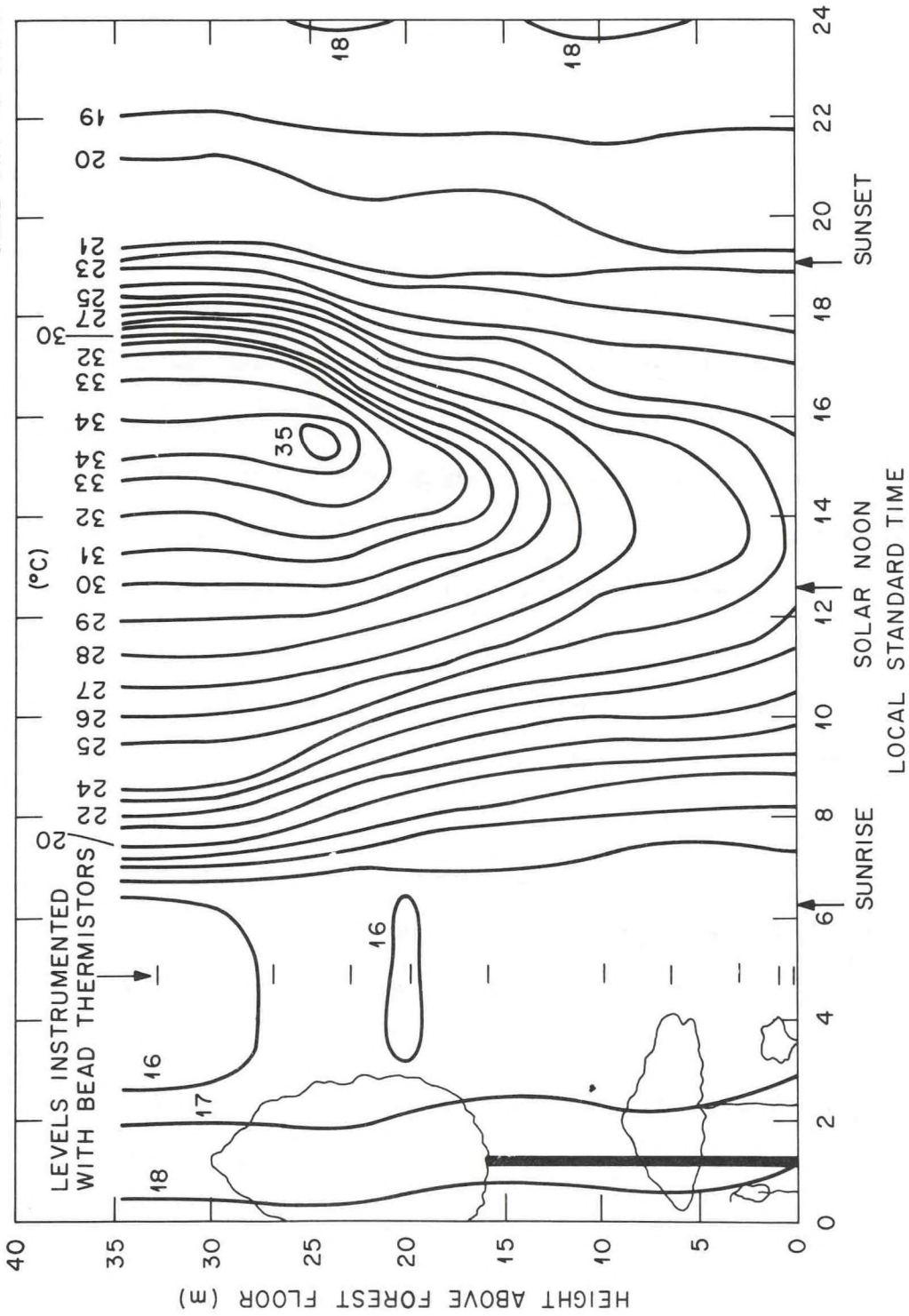


Figure 8. Space average air temperature within and above a fully leafed Liriodendron forest.



that above at this time. This discrepancy most likely arises as a result of differences between replication of net all-wave flux measurements and measurement of air temperatures. Net radiation was measured along a single tower whereas the air temperatures of figure 8 represent averages of measurements made along 2 separate towers. It seems likely, in view of the small differences indicated, that the forest floor may have been cooler beneath the net radiometer profile but sufficiently warmer at the other tower to yield an elevated mean temperature. On the other hand, instrument errors cannot be ruled out.

The distribution of windspeeds above and within this forest around midday on a clear September day is shown in figure 9. The characteristic reduction of wind speeds within the forest is highly evident on this figure. While no evidence of complete decoupling of the flow within and above the forest is apparent, the number of measurements in vertical space were insufficient to rule out that possibility.

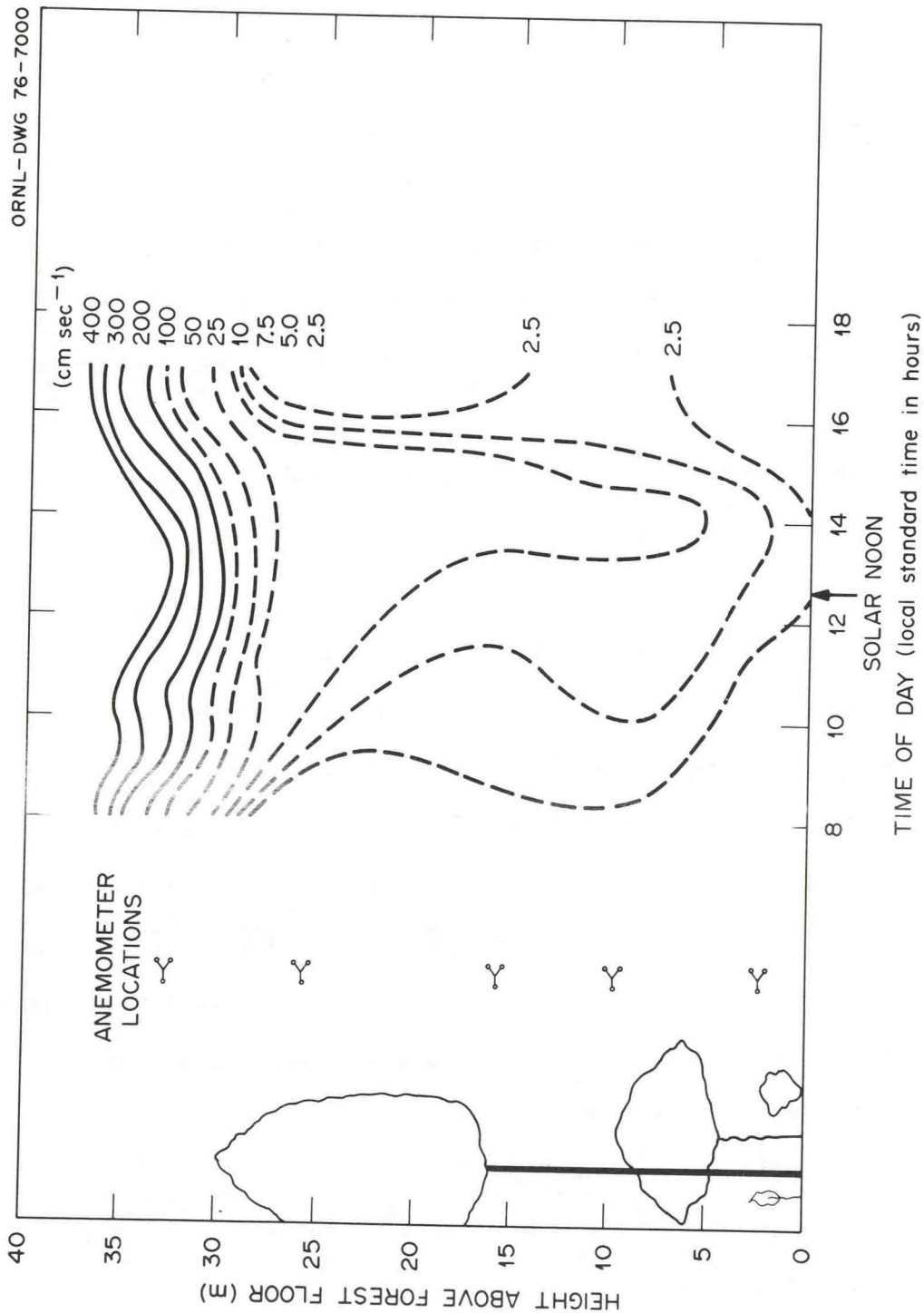


Figure 9. Distribution of hourly average wind speeds within and above a Liriodendron forest.

Turning now to a clear November day, the daily course of incident shortwave radiation on the leafless forest is shown in figure 10. Amounts of incident radiation are much reduced on figure 10a from those of September of figure 2a because of the increasingly shorter daylengths and lower solar elevations as the winter solstice approaches. Because of a sensor malfunction, we were unable to obtain any records of reflected radiation at the above canopy level for the leafless forest.

Radiation amounts received within the forest as shown in figures 10b and c are increased over those received in the autumnal fully leafed forest despite the reduced amounts of radiation incident upon the forest. The loss of leaves more than offsets this reduction in incident amounts. Reflected radiation amounts are also larger because of the greater penetration of radiation into the forest and, probably, because of an increased albedo resulting from leaf loss. Greater numbers of sunflecks are present within the leafless forest but the attenuation of shortwave radiation remains significant. Once again, effects of the large canopy opening are strongly evident in the 16 m record but these effects mostly disappear before the 3 m level is reached.

As a result of reduced insolation in winter, the daytime net allwave radiation at the top of the canopy (figure 11a) is also



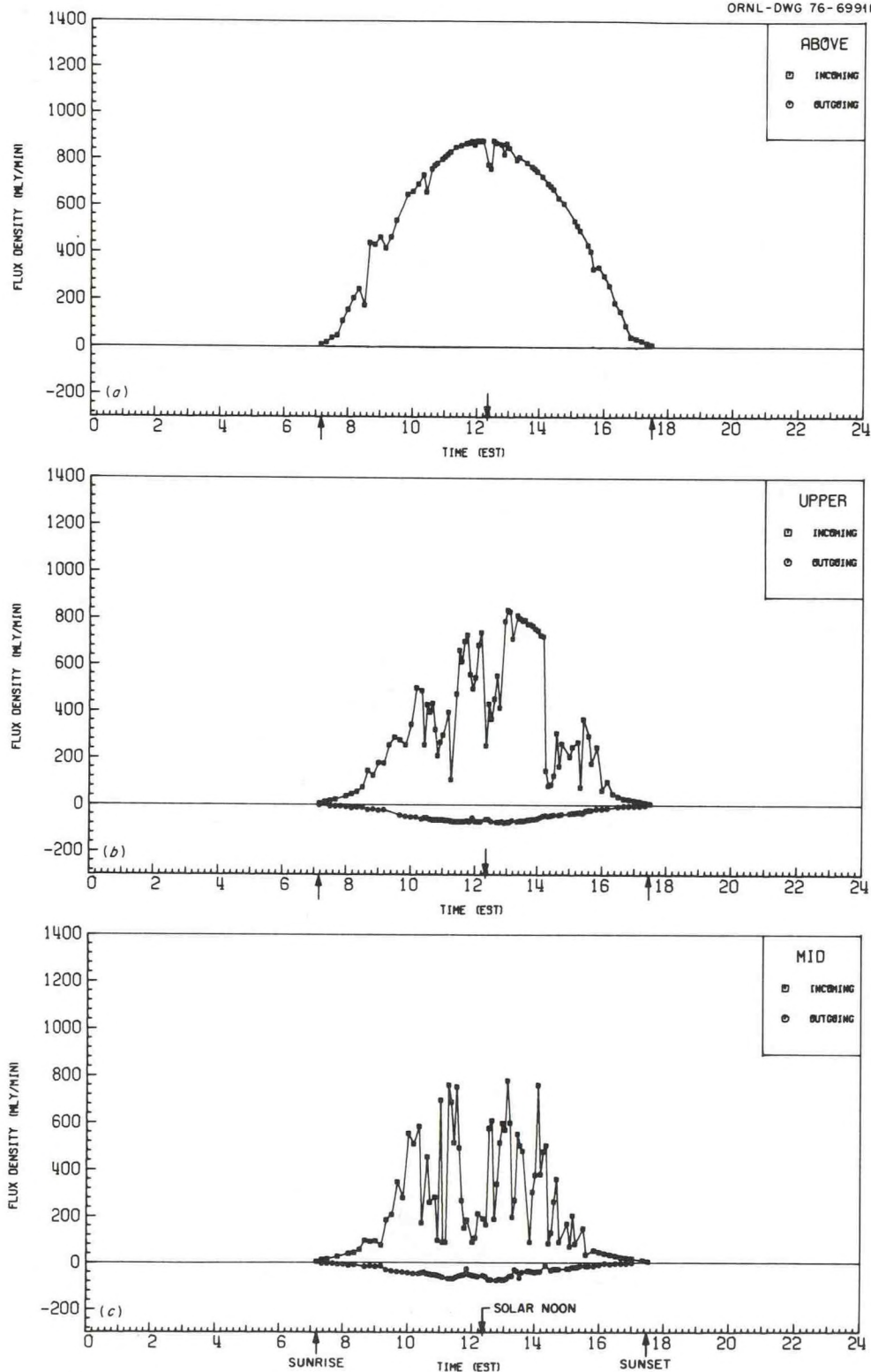


Figure 10. Shortwave radiation balances within and above a leafless Liriodendron forest.

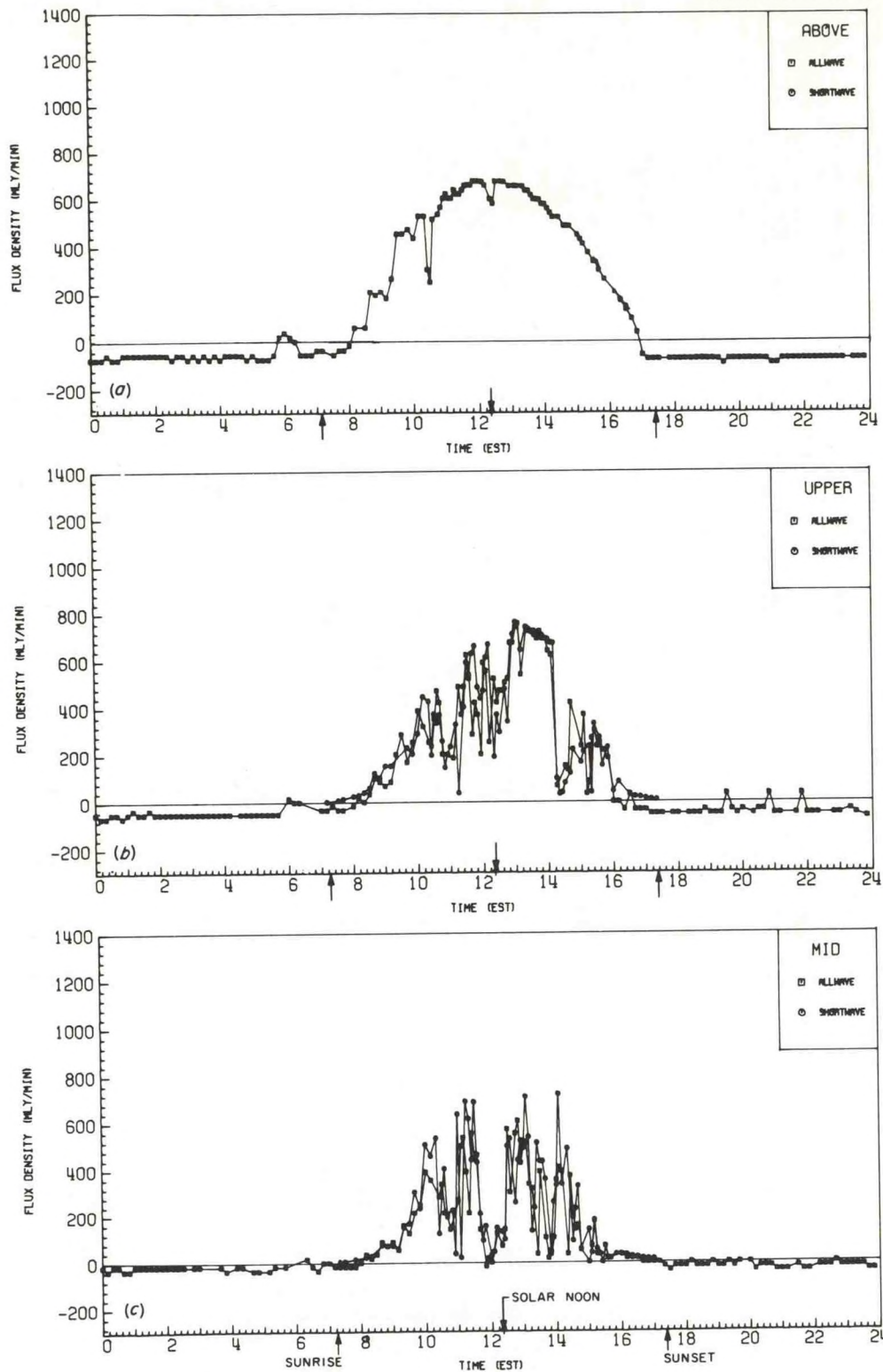


Figure 11. Net all-wave and shortwave radiation balance within and above a Liriodendron forest.

reduced. At night, the net allwave loss is somewhat greater than from the fully leafed forest, however. This probably reflects the drier air masses present over the east Tennessee region during the winter which implies greater atmospheric transparency to radiation of terrestrial wavelengths. Thus, less longwave radiation is radiated downward by the atmosphere.

Figures 11b and c show the net shortwave and allwave radiation flux densities observed within the leafless forest. Because of the increased penetration of solar radiation into the leafless forest, both these quantities are somewhat increased during daylight over those received within the fully leafed forest. The nighttime longwave radiation balance is consistently negative throughout the leafless forest.

The distribution of average total solar radiation in and above the leafless forest is shown in figure 12. Despite the leafless canopy, the lower solar elevations of winter and the consequent longer optical paths of beam radiation result in significant attenuation of such radiation by the woody biomass of the overstory canopy. As before, the diffuse component, shown on figure 13, penetrates the forest more freely. The beam radiation distribution is shown on figure 14. Although increased penetration of the beam component is shown to occur around solar noon, the flux densities incident upon the forest at this time are so reduced from those earlier in the year and the attenuation by the overstory canopy remains sufficiently great that increases in radiation amounts at the lower forest levels are not at all striking (compare figures 6 and 14).



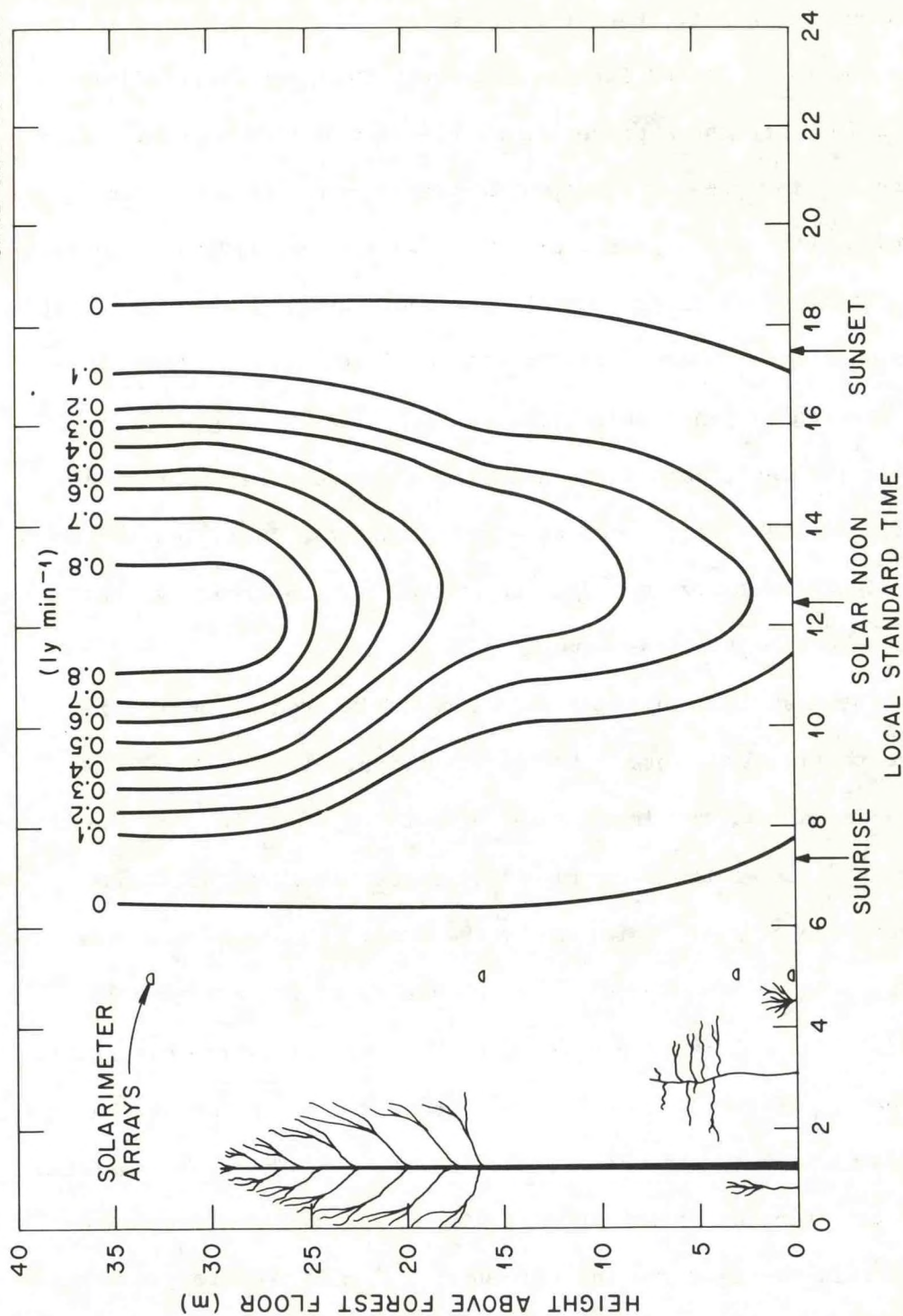


Figure 12. Space average total solar radiation within and above a leafless Liriodendron forest.

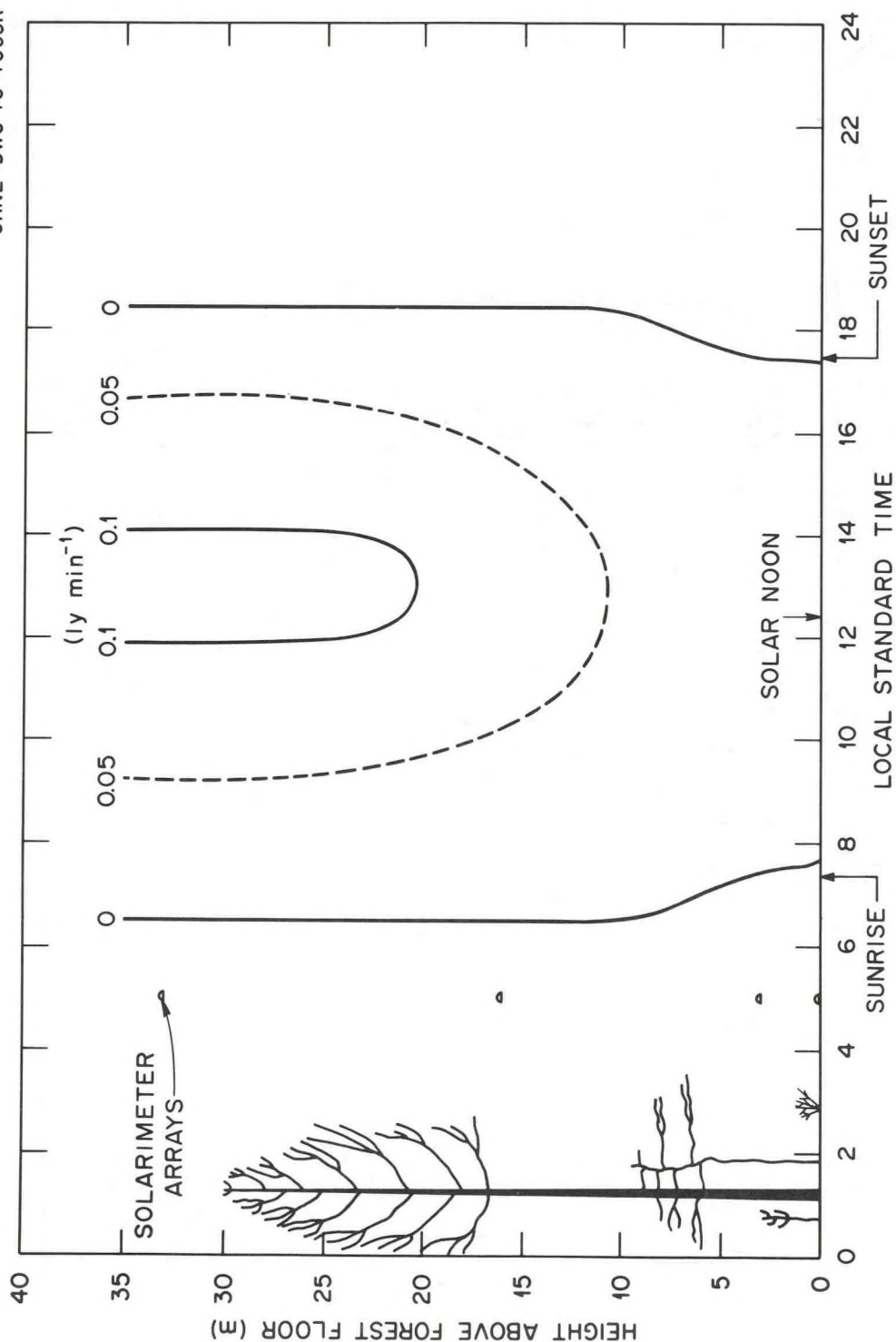


Figure 13. Space average diffuse solar radiation within and above a leafless Liriodendron forest.

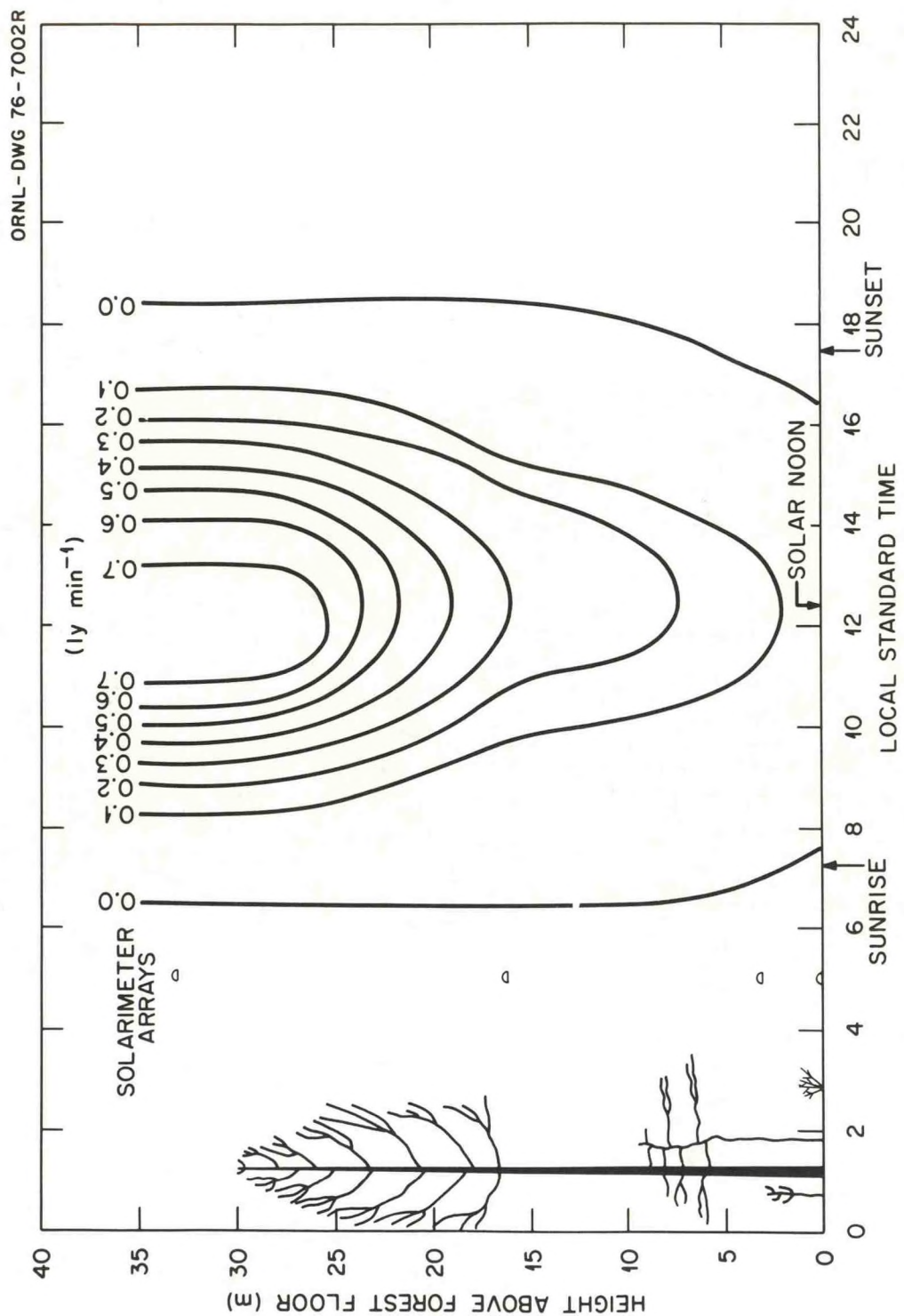


Figure 14. Space average direct beam solar radiation within and above a leafless Liriodendron forest.



Figure 15 shows the distribution of net allwave flux densities on this winter day in the leafless forest. As with the shortwave portion, the highest positive allwave values occur with the maximal daily solar elevations of midday. Vertical distribution in the morning and afternoon approach uniformity while nighttime values are more strongly negative at higher levels in the forest.

The temperature regime of the leafless forest is shown in figure 16. Despite the absence of leaves, the overstory canopy remains the active stratum in terms of radiation and temperature. As in the fully leafed case, the leafless overstory canopy is warmer during the day and most of the night, and colder in the very early morning than higher or lower strata. Minimum nighttime temperatures are found near the forest floor in the early morning, probably as a result of cold air drainage downslope and into the sink in which this stand is situated.

The wind speed distribution for midday hours of a similar clear day closer to the winter solstice is shown in figure 17. Although the forest is bare of leaves, little of the above canopy wind penetrates into the forest. Despite the highly porous appearance of the leafless forest, the woody biomass effects sufficient drag to substantially reduce wind speeds within the canopy.

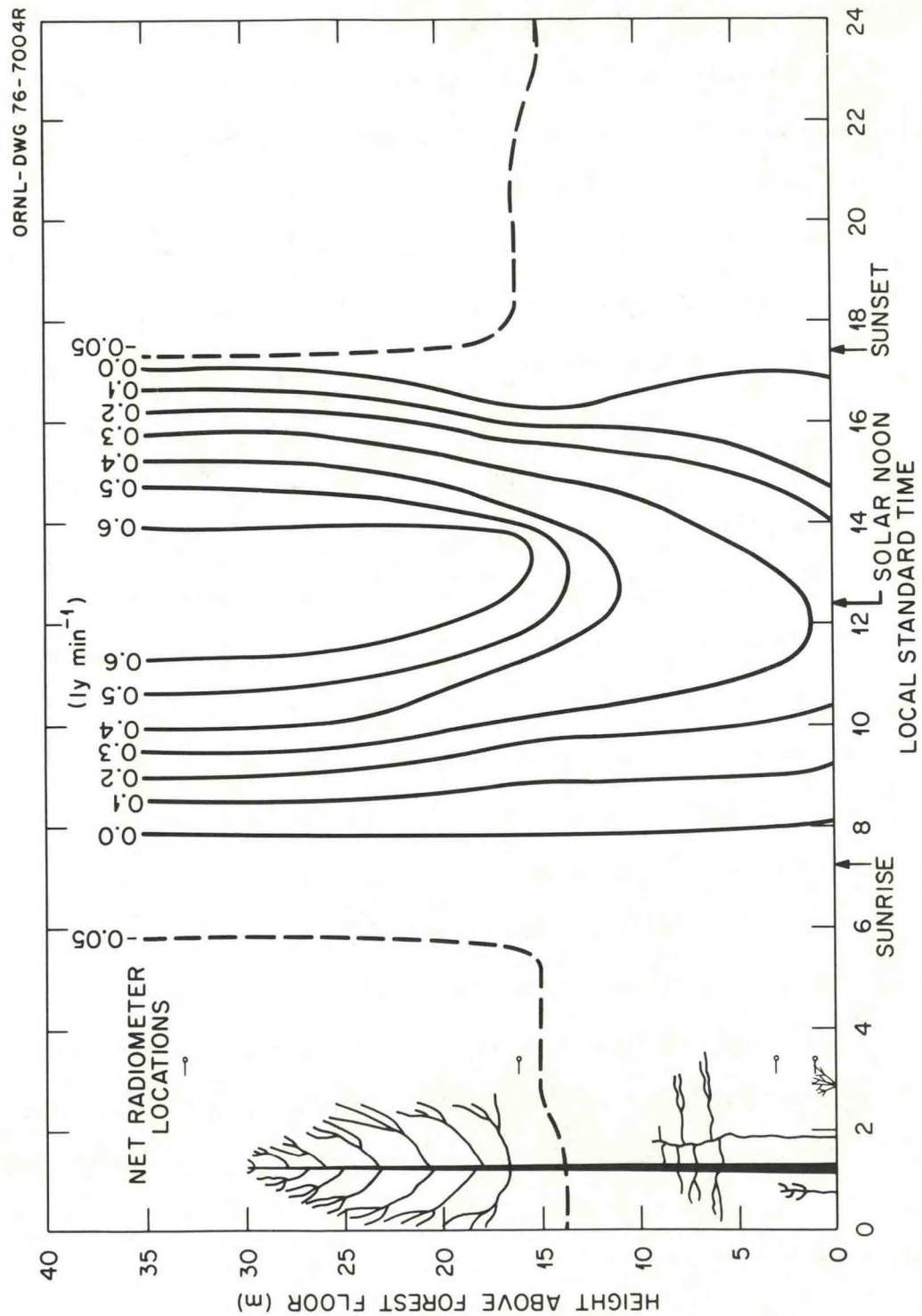


Figure 15. Net all-wave radiation within and above a leafless Liriodendron forest.

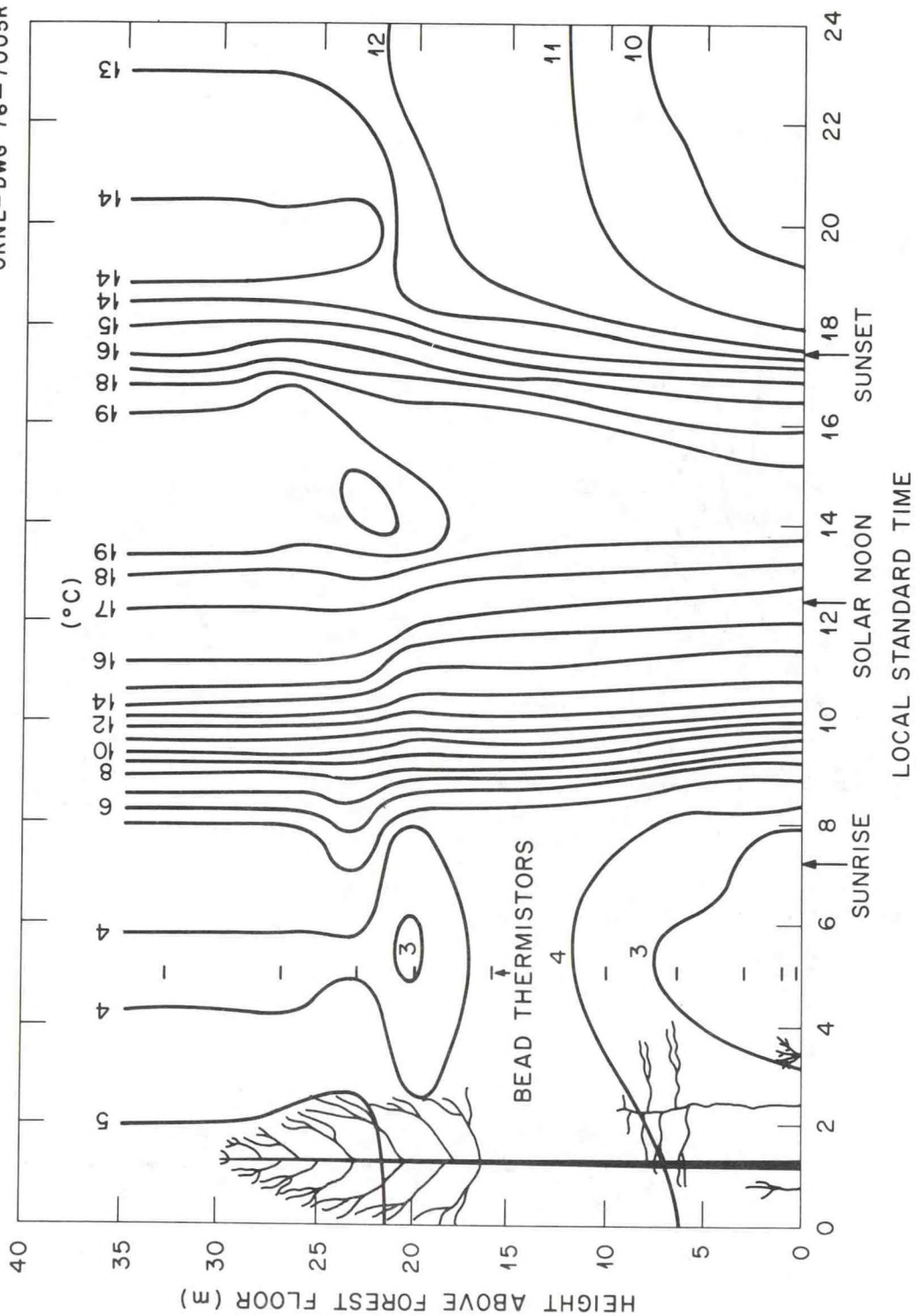


Figure 16. Space average air temperatures within and above a leafless *Liriodendron* forest.



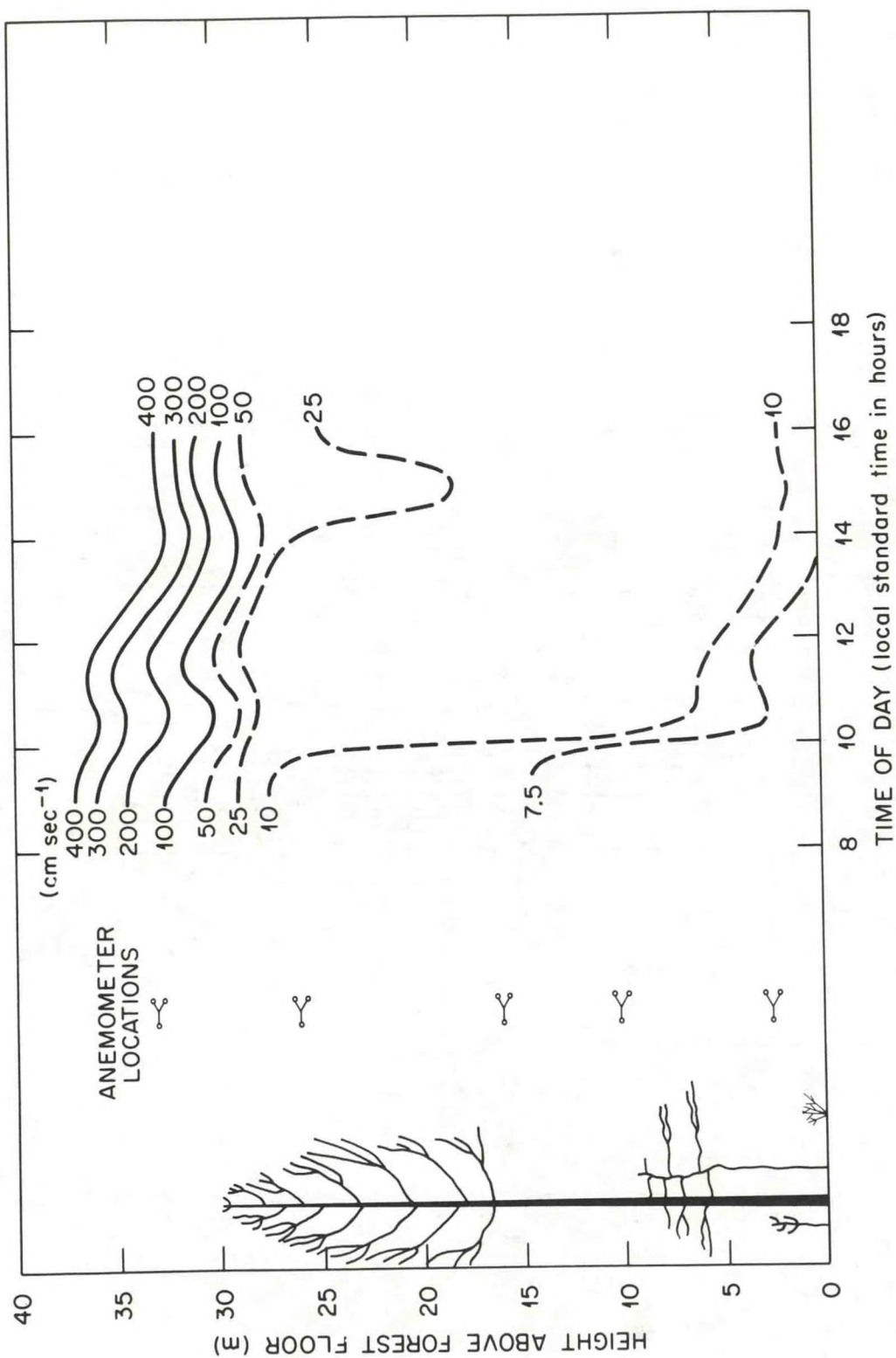


Figure 17. Distribution of hourly average wind speeds within and above a *Liriodendron* forest.

## SEASONAL VARIATION IN FOREST MICROCLIMATE

While the diurnal trends of most of the data presented in figures 2 through 17 strongly reflect the temporal pattern of incident solar radiation, the absolute values are functions of the prevailing synoptic conditions and of forest structure. These absolute values also reflect, to a lesser degree, the physiological state of the forest and the soil moisture regime but our data are neither sufficiently precise nor complete to illustrate such interactions.

These data do show, however, that the presence or absence of leaves and the seasonal change in solar elevations are highly important factors in the observed forest microclimate. The leafless forest allows radiation to penetrate the canopy more freely but because solar elevations are lower around the winter solstice when the forest is leafless, optical paths for beam radiation are longer and, despite the absence of leaves, the woody forest biomass effects considerable attenuation of beam radiation. As we have noted above, comparison of figures 2 and 10 show that despite the reduction in incident radiation amounts from September to November, the loss of leaves from the forest more than compensates for this reduction and higher flux density radiation is received within the November leafless forest. Similarly, comparison of figure 3 and 11 indicate that the loss of leaves generally increases both the net shortwave and allwave radiation amounts within the forest during daylight hours.

At night, the loss of the absorptive and radiative surfaces offered by the leaves allows the positive net longwave radiation gain at the floor of the fully leafed forest to become negative in the leafless forest.

The effects of the interactions between reduced solar elevations and the change in forest structure from early autumn to early winter upon forest radiation regimes are illustrated by a comparison of figures 4, 5 and 6 with figures 12, 13, and 14. Daylengths are considerably shortened and amounts of total radiation are substantially reduced during this time. Since the maximum midday diffuse flux densities of these early autumn and early winter days are nearly equal, it is apparent that the greatest reductions have occurred in the direct beam radiative component incident upon the forest.

On both days, greatest amounts of all components penetrate the forest around midday by virtue of the maximum solar elevations of that time period and of the maximum amounts of radiation incident. Because these maximum solar elevations are so much lower in early winter than in early autumn, the absolute quantities of radiation received within the leafless forest of early winter, although around twice those received in early autumn, are not large relative to the amounts of radiation incident upon the leafless forest.



Comparison of figures 7 and 15, the distributions of net allwave radiation in and above the forest on the 2 days under consideration, indicates a much more isotropic vertical distribution of net allwave radiation in the leafless forest than in the fully leafed forest. Only at midday in the leafless forest do strong vertical gradients in these values develop as a result of the attenuation of the beam shortwave radiative component by the forest biomass. Similarly, the daytime distributions of air temperatures shown on figures 8 and 16 tend more toward isothermal in the leafless forest. At night, the loss of leaves, along with other seasonal changes in synoptic climate, results in the reverse. The nearly isothermal nighttime vertical temperature conditions of the fully leafed forest are replaced by strong inversions in the leafless forest (under clear skies).

Comparing the wind speed distributions of the fully leafed and leafless forest of figures 9 and 17 respectively, the similarity between the two days is striking. Despite a major change in forest structure, the penetration of wind into the forest remains slight. Nevertheless, wind speeds within the forest are increased by factors of 2 to 3, a substantial relative change. Plotting the average of these data for the period solar noon and 3 hours on these two days of figures 9 and 17 as a height distribution yields figure 18. Here again the similarity between the 2 curves is striking. The greatest within forest differences between fully leafed and leafless conditions are indicated for the closed overstory

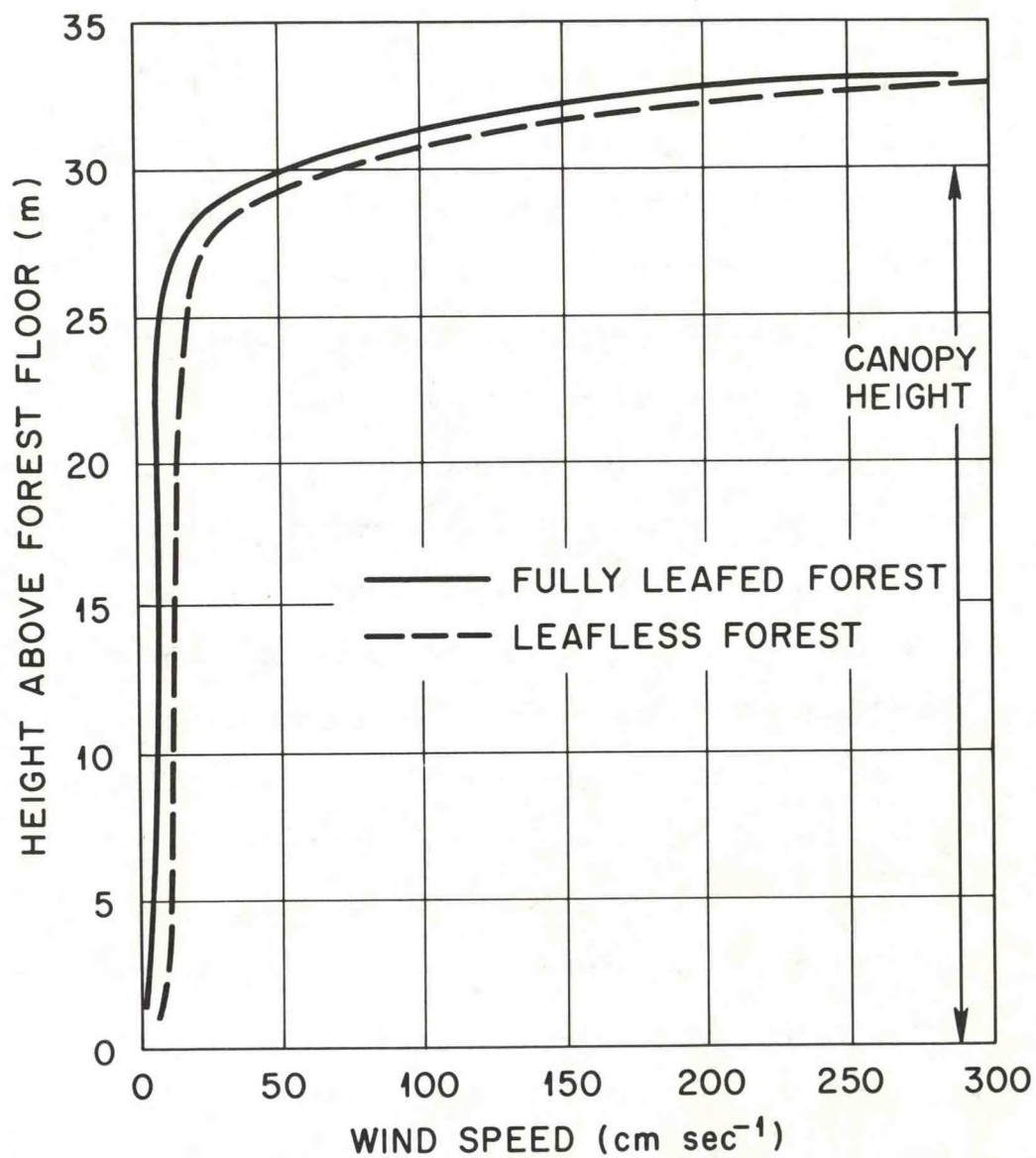


Figure 18. Average wind speeds within and above a Liriodendron forest during the period solar noon  $\pm 3$  hours in the fully leafed and leafless phases.

canopy stratum as would be expected since that is the stratum of greatest biomass density change from the fully leafed to leafless states. Even larger differences are indicated above the canopy (30-33 m height) but since the curves through this stratum are interpolations of measurements at 26 and 33 m, the existence of these differences is questionable.

A number of investigators have noted that, for many purposes, space or time mean radiation values are less than satisfactory because of the nonnormality of the flux density frequency distributions induced by the presence of beam radiation (Ramann, 1911, Alekseev, 1963, Gay et al, 1971). As Norman et al (1971) point out, the mean of a nonnormal radiation flux density distribution is an especially poor characterization of radiation climate for processes such as photosynthesis or evaporation which vary nonlinearly with radiation amounts. Our early results indicated that flux density frequency distributions in this forest in late spring were bimodal between the projecting tips of tree crowns above crown closure and unimodal but highly skewed within the forest (Hutchison, 1971). Plotting the radiation data for this September day as a frequency distribution yields figure 19. Despite the numerous sunflecks indicated on figures 2b and c, this figure shows that very little high flux density radiation penetrates the overstory canopy. As noted earlier, beam radiation is strongly attenuated by the forest biomass. That radiation that does penetrate canopy openings is further reduced by penumbral



# FLUX DENSITY FREQUENCY DISTRIBUTION

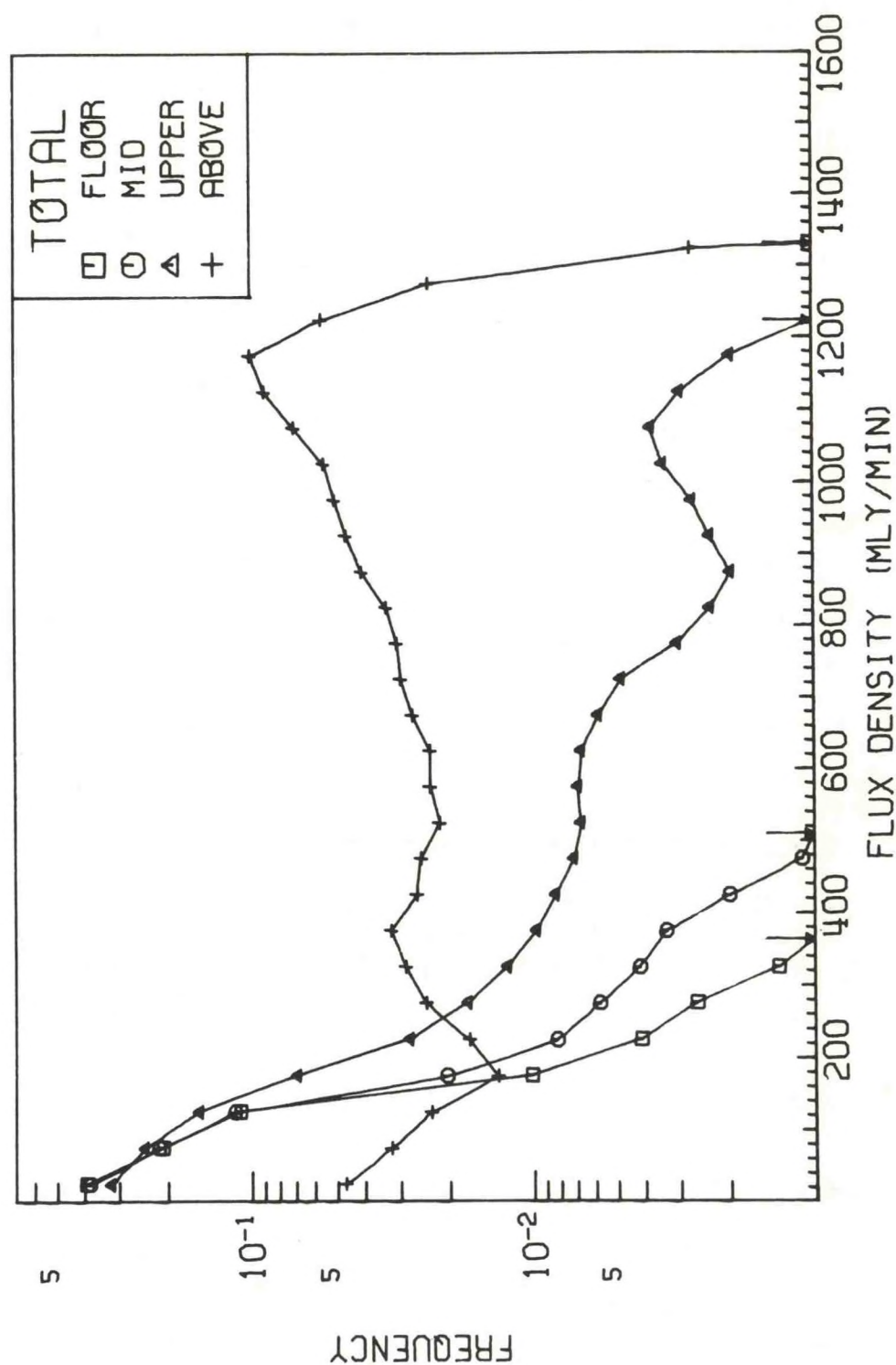


Figure 19. Distribution of total shortwave radiant flux densities within and above a fully leafed Liriodendron forest.

effects arising because of the small but finite sized solar disk (Norman, et al 1971). Thus, despite the high frequency of high flux density radiation incident upon the forest canopy, little high flux density radiation is found within the forest. Despite the severe reductions in both total amounts of radiation and in the frequency of high flux density radiation, figure 19 indicates that most of the radiation reaching a level in the forest is received at flux densities exceeding  $40 \text{ mly min}^{-1}$ , the photosynthetic compensation points for tulip poplar (Burgess and O'Neill, 1975). Because of the spectral selectivity of canopy transmission however, the quality of radiation within the forest may be limiting for photosynthesis even though total quantities are not.

The frequency distributions of radiant flux densities for the winter day are shown in figure 20. The amount of higher flux density radiation incident upon the forest is, of course, reduced in winter but despite this reduction, increases in the frequency of occurrence of higher radiant flux densities within the forest are evident from a comparison of figures 19 and 20. Because the frequency values are plotted to a log scale on these two figures however, the indicated increases in penetration of higher flux density radiation are, in actuality, rather small.

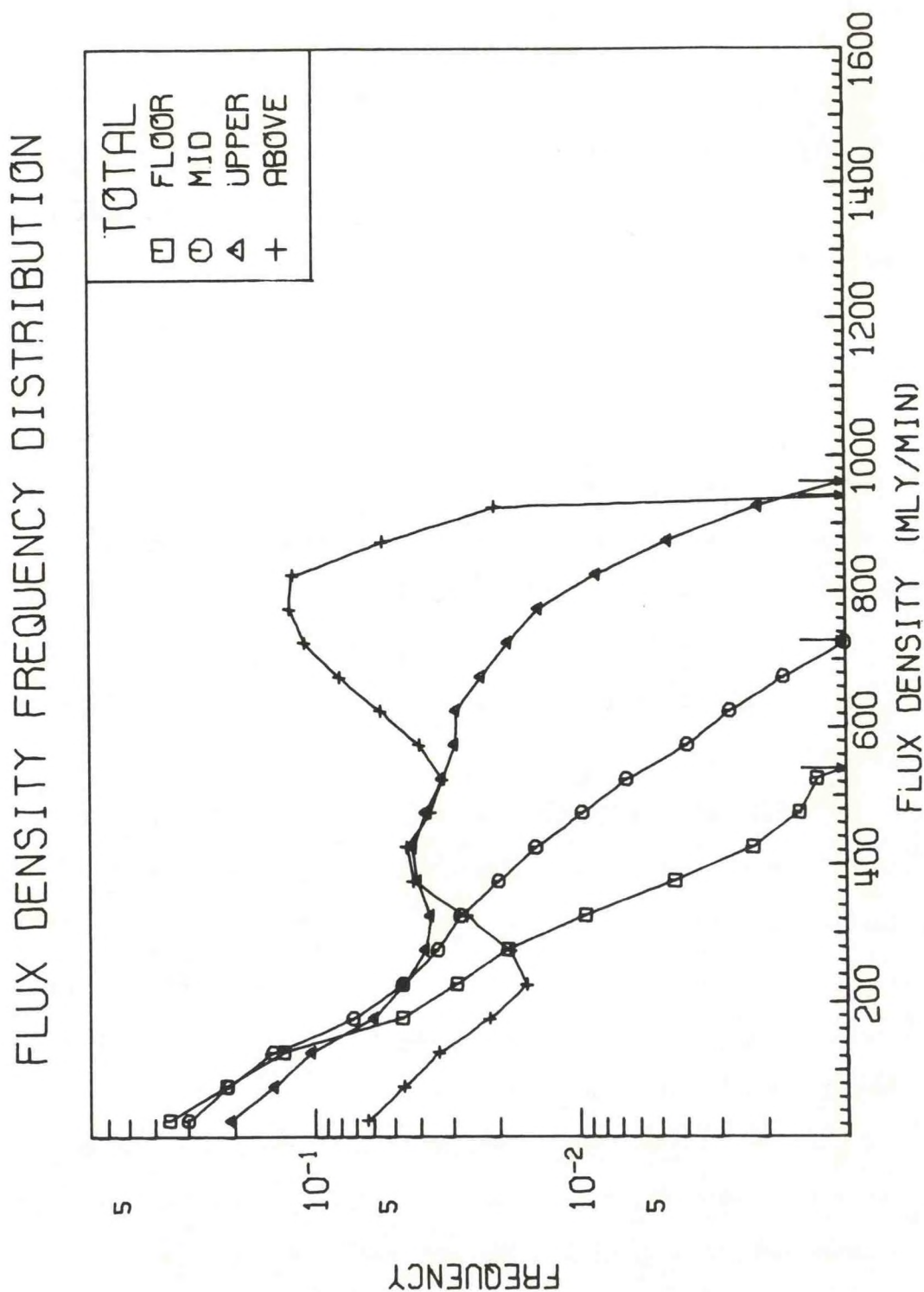


Figure 20. Distribution of total shortwave radiant flux densities within and above a leafless Liriodendron forest.



To further illustrate the effects of the interaction of solar elevation and forest phenology upon forest radiation climate, we derive the annual course of average daily total solar radiation received in and above the forest. Since our data collection was discontinuous through time, the annual forest radiation regime was approximated by calculating the average fraction of radiation penetrating to each of the 3 forest levels for morning periods and for afternoon periods for each of 7 phenoseasons which characterize the changes in solar beam geometry and in forest structure throughout the annual circuit of the earth about the sun. The data were segregated into morning or afternoon periods in order to account for the different penetration of radiation during the foggy mornings that are frequently present. The data were also segregated according to 3 cloudiness classes: clear, partly cloudy, or overcast. The 7 phenoseasons were defined as in figure 21 using the dates of the 2 solstices and the 2 equinoxes along with phenological data for this forest reported by Taylor (1974).

Thus, the average fractional penetration of radiation into the forest was determined for 2 time classes x 3 cloudiness categories x 7 phenoseason for a total of 42 possible penetration fractions to each of the 3 forest levels. Segregating the continuous record of radiation collected at the Oak Ridge weather station some 10 km to the north in the same manner, the phenoseasonal incident radiation totals for each cloudiness-time category were determined.

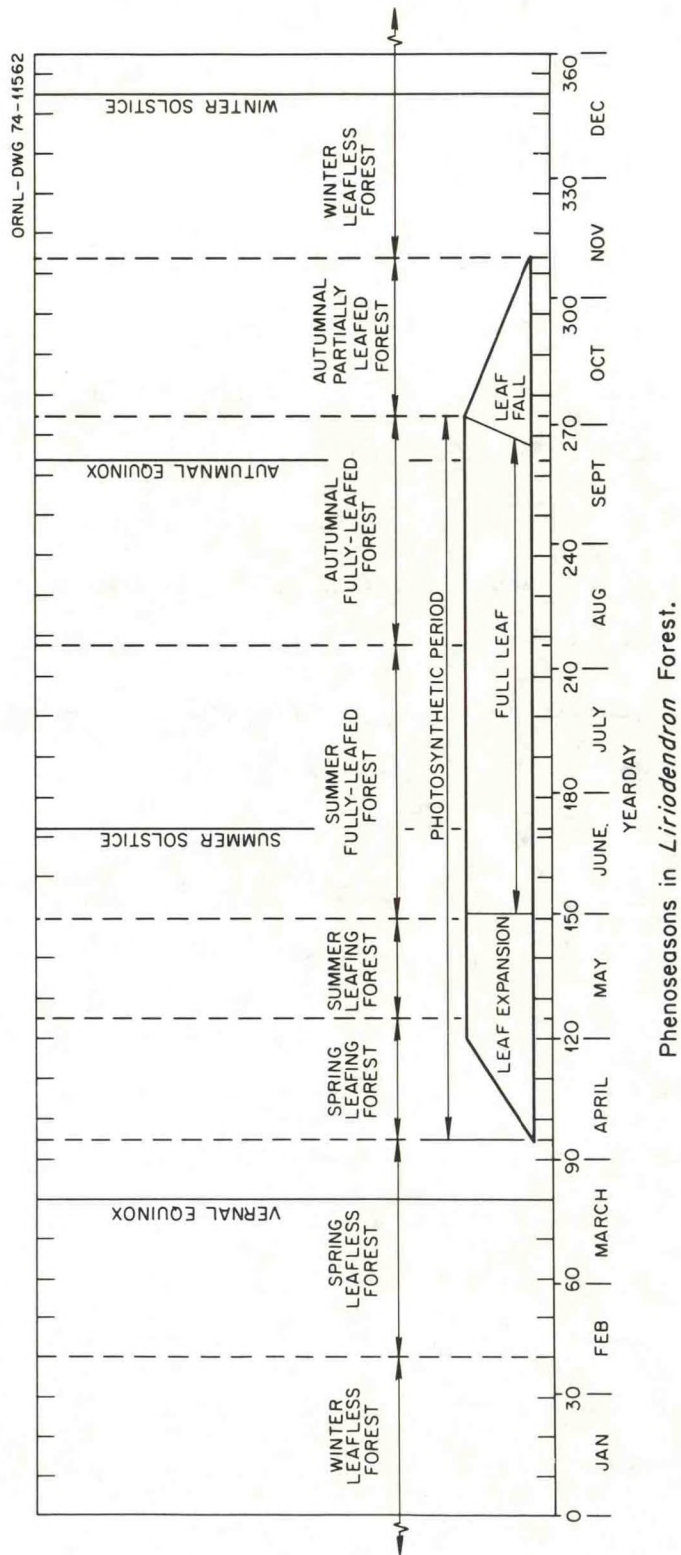


Figure 21. Phenoseasons of an east Tennessee *Liriodendron* forest  
(Phenological data due to Taylor, 1974).

Multiplying each phenoseasonal total by the appropriate fractional penetration then yielded an estimate of the amount of radiation received at each forest level during each time-cloudiness category in each phenoseason. Summing these amounts within the 7 phenoseasons yields table 3, the radiation climate summary for this stand. In this table, the period from bud break, which marks the beginning of the spring leafing forest phenoseason, to the start of leaf abscission, which marks the end of the autumnal fully leafed forest phenoseason, is considered the photosynthetically active period. The remainder of the year is considered photosynthetically dormant.

As shown in table 3, more radiation is received within the forest during the photosynthetically dormant period than during the photosynthetically active period in spite of the fact that the total radiation incident upon the dormant forest is only slightly over half that incident upon the forest during the active portion of the year. It is evident that the amounts of radiation received within the forest during the leafing and fully leafed phenoseasons are quite low in comparison to the amounts of radiation incident during those phenoseasons.

Dividing the data of table 3 by the number of days in each phenoseason yields an estimate of the average daily total radiation received within and above the forest in each phenoseason. Plotting these average daily totals in a height-phenoseason coordinate system yields figure 22, an approximation of the annual



Table 3. Approximation of radiation received within the Liriodendron forest throughout the year

Phenoseason	Duration (days)	Total Solar Radiation Received [Langley's (percent of yearly total)]			
		Above (32 m)	Upper Canopy (16 m)	Midcanopy (3 m)	Forest Floor (0 m)
Winter leafless	91	13,300 (11.5%)	5,400 (17.5%)	2,400 (16.9%)	1,500 (16.5%)
Spring leafless	55	15,000 (13.0%)	7,600 (24.6%)	4,900 (34.5%)	4,100 (45.0%)
*Spring leafing	30	10,200 ( 8.8%)	4,000 (12.9%)	2,500 (17.6%)	1,800 (19.8%)
*Summer leafing	26	11,700 (10.1%)	2,400 ( 7.8%)	800 ( 5.6%)	300 ( 3.3%)
*Summer fully leafed	67	31,500 (27.2%)	5,100 (16.5%)	1,500 (10.6%)	700 ( 7.7%)
*Autumn fully leafed	57	21,100 (18.2%)	3,300 (10.7%)	1,000 ( 7.0%)	200 ( 2.2%)
Autumn partially leafed	39	12,900 (11.2%)	3,100 (10.0%)	1,100 ( 7.8%)	500 ( 5.5%)
*Photosynthetically active period total	180	74,500 (64.4%)	14,800 (47.9%)	5,800 (40.8%)	3,000 (33.0%)
Photosynthetically dormant period total	185	41,200 (35.6%)	16,100 (52.1%)	8,400 (59.2%)	6,100 (67.0%)
Yearly total	365	115,700	30,900	14,200	9,100

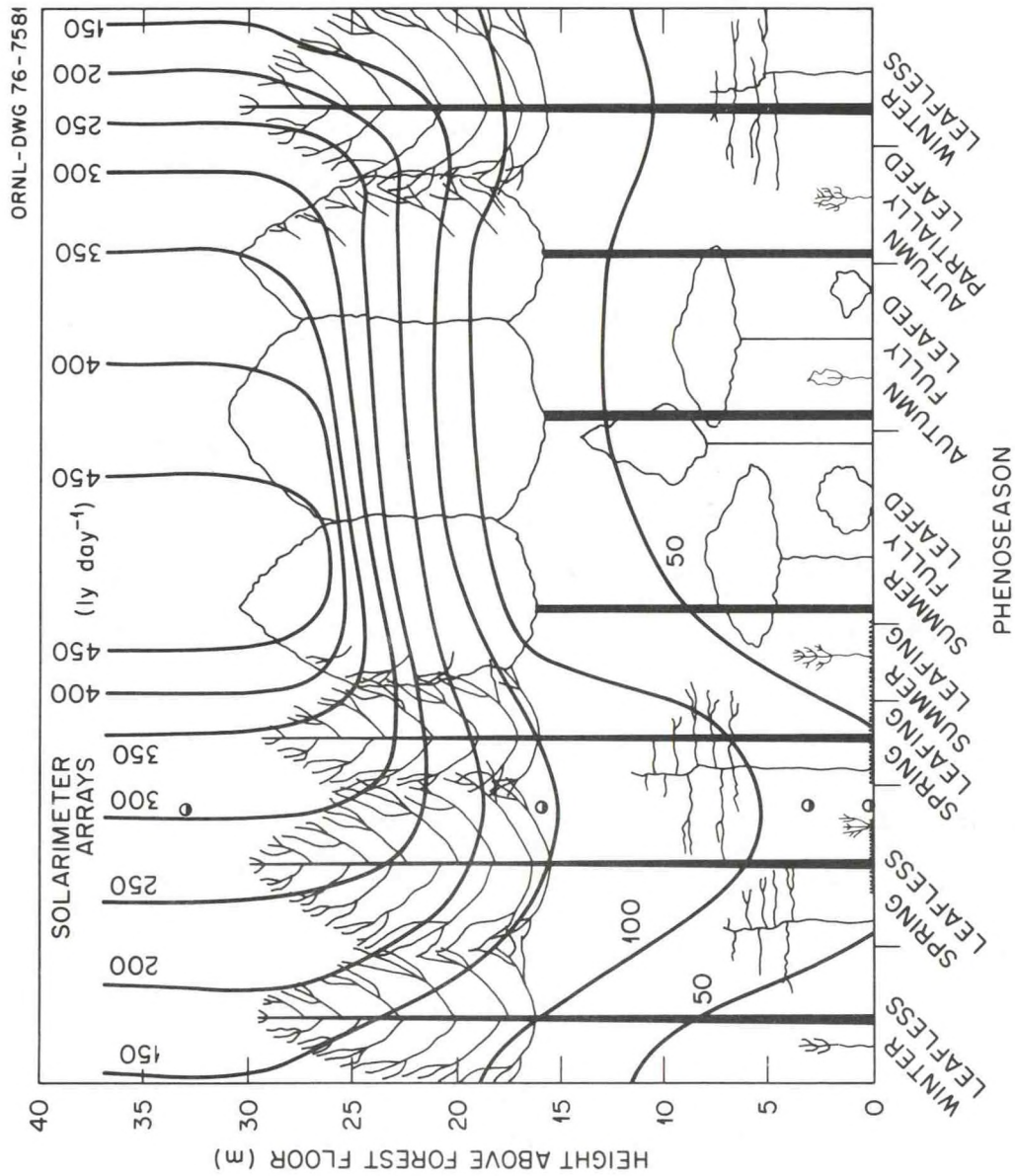


Figure 22. Approximation of the annual course of average daily total solar radiation received within and above a Liriodendron forest.

radiation regime of this tulip poplar forest. This figure illustrates the phenologically and seasonally induced changes in forest radiation climate. Again we caution that the continuous data of this figure are interpolations of discreet observations. As such, the spacing of the radiation isopleths are, to a large degree, estimates.

Following the winter solstice, solar elevations increase daily with the apparent northward march of solar paths. As a result, amounts of radiation penetrating the leafless forest increase rapidly. With the increasing radiation levels at the forest floor, the herbaceous vegetation of early spring begins its annual cycle of growth and reproduction. In early April however, bud break occurs and leaves begin to expand in the forest canopies. Hence, radiation levels within the forest abruptly decrease in the spring leafing forest. With closure of the canopy in the summer leafing forest, the rates of decrease in radiation penetration slow somewhat. Then in early June, the forest attains full leaf and little change in forest structure occurs until the onset of leaf abscission in late September. Despite a relatively static forest structure during this period, figure 22 shows that radiation amounts continue to decline very slowly throughout the summer and autumn fully leafed forest phenoseasons. This slow decline is the result of the southward



march of solar paths following the summer solstice which causes decreasing solar elevations and daylengths. Then, with the advent of leaf abscission and subsequent leaf fall, forest structure again changes from fully leafed to leafless and slight increases in forest radiation result. The continued decline in solar elevations and daylengths offset this increase in early winter and radiation amounts received within the forest again decline toward the winter solstice.

#### SUMMARY AND CONCLUSIONS

The data presented here indicate that the diurnal trends in forest microclimate are dominated by the diurnal trend in incident solar radiation amounts and the diurnal changes in solar elevations. Absolute values of these microclimatic variables, on the other hand, reflect strongly, the synoptic climatic conditions present and, to a lesser degree, the interactions among synoptic climatic parameters, forest structure, forest physiology, and soil moisture conditions. The seasonal changes in forest microclimate are the result of changes in incident radiation amounts, earth-sun geometry, and phenological change in forest structure along with seasonal changes in synoptic climatic parameters.

As many others have reported, the beam radiative component is strongly attenuated by the forest biomass throughout the year. The diffuse component is attenuated less but even in the leafless forest, amounts of attenuation effected by the woody forest biomass significantly reduce the amounts of diffuse radiation received within the forest. The greatest attenuation of beam radiation occurs in the overstory canopy stratum throughout the year. Because of the lower solar elevations of winter and early spring, around half of the incident beam radiation is attenuated by the leafless overstory canopy stratum of this forest. With the decreasing solar elevations of autumn, beam radiation attenuation in the fully leafed overstory stratum approaches 85 percent. The attenuation of the diffuse component appears more uniform throughout the vertical extent of the forest in all forest phenoseasons but the variable conversion of beam radiation to diffuse radiation confuses this issue.

The greatest amounts of total radiation are received within the leafless forest with the rising solar elevations of early spring. Least amounts are received in early autumn when the forest is still fully leafed and solar elevations are decreasing toward the minimum of the winter solstice. On these clear days, net allwave radiation tends to be positive during daylight hours as a result of the incoming solar radiation

and negative at night because of the net longwave radiation loss to space. Within the fully leafed forest however, a stratum near the forest floor in which the net longwave radiation is always positive is found. With the loss of leaves, this positive net longwave radiation layer is destroyed and the vertical structure of net longwave radiation balances approaches isotropic in the leafless forest.

Amounts of solar radiation reflected by the various forest strata vary only slowly through clear days. This implies that fewer replications of measurements of this variable are needed for determination of space or time averages than for highly varying quantities such as beam radiation.

The active surface of the forest is shown to be the overstory canopy, whether fully leafed or leafless, in terms of radiation, air temperatures, and wind speeds. Maximum attenuation of solar radiation occurs in this stratum causing maximum air temperatures to be found there throughout much of the day. Greatest nighttime longwave losses are experienced in the overstory resulting in minimum night air temperatures there. Aerodynamically, the forest constitutes an extremely rough surface situated at some level within the overstory canopy.



It is unfortunate that our attempts to quantify forest structures have been less than successful in view of the degree of control exerted by changes in this structure upon forest microclimate exhibited by the data presented here. Studies of the interactions which effect the observed forest microclimate are continuing however, and emphasis upon quantification of forest structure and physiological response will increase in future work.

#### LITERATURE CITED

- Alekseev, V. A. 1963. Light measurements under a forest canopy. Soviet Plant Phys. 10; 109-201.
- Anderson, M. C. 1964. Light relations of terrestrial plants communities and their measurements, Biol. Rev. 39; 425-486.
- Baumgartner, A. 1969. Meteorological approach to the exchange of CO<sub>2</sub> between the atmosphere and vegetation, particularly forest stands. Photosynthetica 3; 127-149.
- Burgess, R. L. and R. V. O'Neill (ed.) 1975. Eastern Deciduous Forest Biome Progress Report, Sept. 1, 1973 - Aug. 31, 1974. Environmental Sciences Division, Oak Ridge National Lab. Pub. No. 757. Oak Ridge, Tn. 252 p.
- Gay, L. W., K. R. Knoerr, and M. O. Braaten 1971. Solar radiation variability on the floor of a pine plantation. Agr. Met. 3; 39-50.
- Horn, H. W. 1971. The Adaptive Geometry of Trees. Princeton Univ. Press, Princeton, N.J. 144p.
- Horowitz, J. L. 1969. An easily constructed shadow band for separating direct and diffuse radiation. Solar Energy 12; 543-545.
- Hutchison, B. A. 1971. Spatial and Temporal variation in the distribution and partitioning of solar energy in a deciduous forest ecosystem. ATDL, NOAA Contribution No. 54. Oak Ridge, Tn. 40 p.
- Hutchison, B. A. 1975. Photographic assessment of deciduous forest radiation regimes. PhD. Thesis, Yale University and ATDL, NOAA Contribution No. 75/3, Oak Ridge, Tn. 164 p.
- Hutchison, B. A. and D. R. Matt. 1976. Beam enrichment of diffuse radiation in a deciduous forest. Agric. Met. 17: 93-110.
- Hutchison, B. A. and D. R. Matt, in press. The distribution of solar radiation within a deciduous forest. Ecol. Mono.

- McConathy, R. K. 1976. Leaf energy balance and transpirational relationships of tulip poplar (*Liriodendron tulipifera*). M.S. Thesis, University of Tennessee, Knoxville, 110 p.
- Miller, E. E. and J. M. Norman 1971. A sunfleck theory for plant canopies II. Penumbra effects: Intensity distributions along sunflect segments. Agron. J. 63; 739-743.
- Monteith, J. L. 1959. Solarimeter for field use. J. Scient. Inst. 36; 341-346.
- Norman, J. M., E. E. Miller, and C. B. Tanner 1971. Light intensity and sunfleck-size distributions in plant canopies. Agron. J. 63; 743-748.
- Norman, J. M. and P. G. Jarvis 1975. Photosynthesis in spruce (*Picea sitchensis* (Bong.) Carr.). V. Radiation penetration theory and a test case. J. Appl. Ecol. 12; 839-878.
- Ramann, E. 1911. Lichtmessungen in Fichtenbestanden. Allg. Forst.-u. Jazdztz. 87; 401-406.
- Taylor, F. G. 1974. Phenodynamics of production in a mesic deciduous forest. In Phenology and Seasonality Modeling. H. Leith (ed.) Springer Verlag, New York, pp. 237-254.



EFFECTS OF SKY BRIGHTNESS DISTRIBUTION UPON DIFFUSE  
RADIATION WITHIN A DECIDUOUS FOREST<sup>1,2</sup>

B. A. Hutchison

D. R. Matt

Atmospheric Turbulence and Diffusion Laboratory  
National Oceanic and Atmospheric Administration  
Oak Ridge, Tennessee  
July, 1976

(to be submitted to Agricultural Meteorology)

---

<sup>1</sup> This research supported in part by the Eastern Deciduous Forest Biome, US-IBP, funded by the National Science Foundation under Interagency Agreement AG-199, BMS76-00761 with the U. S. Energy Research and Development Oak Ridge National Laboratory, and in part by the Division of Biomedical and Environmental Research, ERDA.

<sup>2</sup> Contribution No. \_\_\_\_\_, Eastern Deciduous Forest Biome, US-IBP ATDL Contribution File No. 76/5.

(WITHDRAWN)

---



THIRD SYMPOSIUM  
ON  
ATMOSPHERIC TURBULENCE, DIFFUSION, AND AIR QUALITY

Sponsored by the  
AMERICAN METEOROLOGICAL SOCIETY

OCTOBER 19-22, 1976  
RALEIGH, NORTH CAROLINA

The manuscripts reproduced in this collection of preprints are unrefereed papers presented at the Third Symposium on Atmospheric Turbulence, Diffusion, and Air Quality; their appearance in this collection does not constitute formal publication.

AMERICAN METEOROLOGICAL SOCIETY  
45 Beacon Street, Boston, Massachusetts, 02108, U.S.A.

ATDL Contribution File No. 76/6



OBSERVED AND PREDICTED COOLING TOWER PLUME RISE  
AT THE JOHN E. AMOS POWER PLANT, WEST VIRGINIA

Steven R. Hanna  
Air Resources  
Atmospheric Turbulence and Diffusion Laboratory  
National Oceanic and Atmospheric Administration  
Oak Ridge, Tennessee 37830

1. INTRODUCTION

There is much current interest in cooling tower plume rise because of its importance in determining the environmental impact of cooling towers at planned power plants and industrial facilities. Some of the possible environmental problems related to heat and water emissions from cooling towers are drift deposition, ground level fog, cloud formation, and precipitation enhancement (see the conference proceedings *Cooling Tower Environment - 1974*.) An important factor in all of these problems is the calculation of the plume trajectory, which is often complicated by the presence of multiple sources and water phase changes in the plume. As Briggs (1975) shows, the latent heat does not strongly influence plume rise if there is no cloud present at the top of the plume. His simple formulas for plume rise can be expected to work quite well on most days for cooling tower plumes. However, if a cloud forms at the top of the plume, the final cloud height will depend partly on cloud physics process. A one dimensional plume and cloud growth model was developed to study these effects (Hanna, 1976). In this paper, the predictions of the model are compared with observations of cooling tower plume rise at the John E. Amos, W. Va. power plant (2900 MWe), reported by Kramer, *et al.* (1975).

2. PLUME AND CLOUD GROWTH MODEL

The numerical model uses Weinstein's (1970) one-dimensional cloud growth model as a basis but alters its entrainment assumption so that it agrees with known relations for the rise of buoyant stack plumes (Briggs, 1975). The cloud microphysics processes are parameterized using suggestions by Kessler (1969). Current measurements by Norman, *et al.* (1975) at the Keystone cooling towers and Woffinden, *et al.* (1976) at the Chalk Point cooling tower should help determine whether Kessler's parameterizations are valid for cloud physics processes in cooling tower clouds.

A detailed description of the model would be too lengthy to include in this short summary, but is given elsewhere (see Hanna, 1976) in a form such that it can be studied or used by others. The computer program is operational (e.g., it is being used at Argonne National Laboratory by A. Policastro) and copies of the program and its description can be obtained by writing the present author.

There are four aspects of this model that can be regarded as improvements over previous versions. First, it incorporates Briggs' (1975) suggestion that the ratio of the total effective momentum flux to the momentum flux within the plume boundary approaches 2.25, due to the fact that the ambient air above the rising plume is also accelerating. Second, based on determinations of visible plume length by Slawson, *et al.* (1974), and Meyer, *et al.* (1974), it is assumed that saturation occurs in the plume when the excess water vapor content is greater than 50% of the saturation deficit in the ambient air. Third, the effects of ambient wind speed shears are included in the equation for continuity of plume volume flux. Finally, an arbitrary assumption is made to account for the merging of multiple plumes: when the plume radius grows to one-half of the distance between the towers, the cross sectional area of the model plume increases so that it is equal to the sum of the previous areas of all the plumes.

3. MODEL INPUTS

During the winter of 1974-1975, Smith-Singer Meteorologists, Inc. flew a light aircraft around the three cooling tower plumes at the John E. Amos, W. Va. Power Plant (see Kramer, *et al.*, 1975). Vertical profiles of ambient temperature, dew-point, and wind speed to heights of about 1500m were obtained, and photographs of the plume were taken. Runs were purposely made on cold, humid days when a long visible plume was expected. In all the runs analyzed in this paper, the plume was visible through its point of leveling-off, so that plume rise could easily be estimated. Consequently, all of the information needed for input to the plume and cloud growth model was available.

The three natural draft cooling towers are in a line, 200m apart. Two have a height of 132m, top radius,  $R_0$ , of 29m, initial vertical speed,  $w_0$ , of 4.6 m/s, and are each capable of servicing a generator of 800 MWe. The third tower has a height of 150m, top radius of 40m, initial vertical speed of 4.2 m/s, and is capable of servicing a generator of 1300 MWe. For this study, the plume from the third tower is modeled initially. When its radius equals 100m, it is assumed that the plumes merge and the radius automatically increases by a factor of 1.5. The plume is assumed to be initially saturated, and initial cloud and rainwater concentrations are arbitrarily assumed to be 1 g/kg. The optimum initial plume temperature  $T'_p$  is calculated

from the manufacturer's specifications discussed by Kramer, et al. (1975):

$$T'_{po} = (297.4 + .635 (T_d - 273)) (1 + .01 (1 - RH)) \quad (1)$$

where  $T_d$  and RH are ambient dewpoint and relative humidity, and temperatures have the units °K. To account for differences in plant load, the following relation is used to calculate the actual initial plume temperature:

$$T_{po} - T_{eo} = C \cdot (T'_{po} - T_{eo}) \quad (2)$$

where  $T_{eo}$  is the ambient temperature at tower top and C is the ratio of actual plant load to full load (2900 MWe). For bent over plumes (wind speed, U, less than 1 m/s), an effective initial plume radius,  $R_{eff}$ , is used in order to maintain continuity of the momentum flux (Hanna, 1972):

$$R_{eff} = R_o (w_o/U)^{1/2} \quad (3)$$

#### 4. RESULTS

Input conditions for three typical runs are given in Table 1. These input data and results are given in detail so that they can be used by others for model comparison.

TABLE 1

Input conditions for runs 1, 10, and 15. Height z refers to height above tower top

z(m)	Run 1			Run 10			Run 15		
	T <sub>e</sub> (°K)	T <sub>d</sub> (°K)	U( $\frac{m}{s}$ )	T <sub>e</sub> (°K)	T <sub>d</sub> (°K)	U( $\frac{m}{s}$ )	T <sub>e</sub> (°K)	T <sub>d</sub> (°K)	U( $\frac{m}{s}$ )
0	268.6	264.2	13.5	268.0	264.7	2.2	261.3	261.3	0
91	267.4	264.1	13.5	267.5	264.2	4.9	265.7	259.6	0
213	269.1	262.4	13.5	266.3	264.1	4.9	265.2	258.5	0
304	269.1	260.0	13.5	265.2	263.5	4.9	267.7	257.4	0
456	269.1	257.4	13.5	264.1	263.0	4.9	265.2	256.3	0
578	270.2	245.2	16.	263.0	262.5	6.7	264.7	254.6	2.5
669	270.8	247.5	16.	262.5	262.5	8.9	264.7	249.7	5.5
821	271.3	252.4	16.	264.7	256.4	8.9	264.7	249.7	5.5
942	272.4	254.1	16.	265.8	251.9	8.9	264.1	247.4	5.5
1064	271.3	259.1	16.	266.9	248.6	8.9	263.0	246.9	6.0
C = .98			C = .98			C = .98			
T <sub>po</sub> = 292.3			T <sub>po</sub> = 292.6			T <sub>po</sub> = 289.4			
Observed Rise = 560m			Observed Rise = 820m			Observed Rise = 1120m			



The predicted profiles of vertical speed,  $w$ , plume-ambient temperature difference,  $(T_p - T_e)$ , and cloud water content,  $Q_c$ , for these three runs are plotted in Figures 1 through 3.

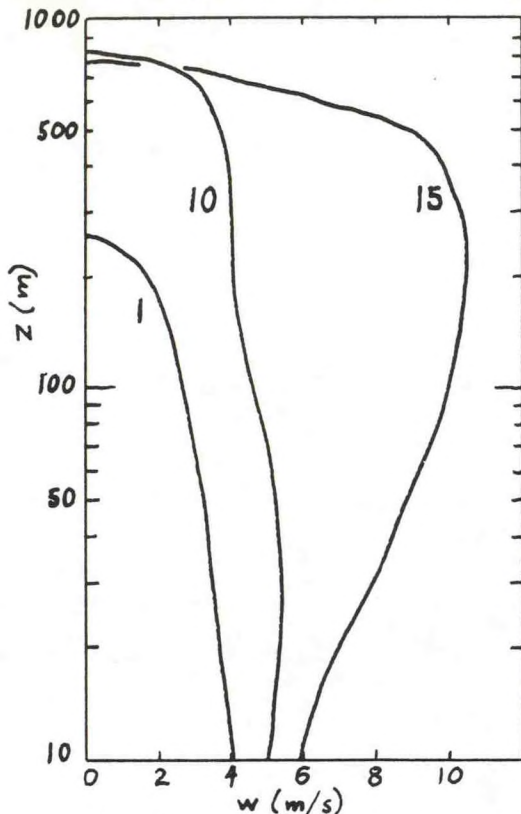


Figure 1: Variation of calculated vertical speed,  $w$ , with height for runs 1, 10, and 15.

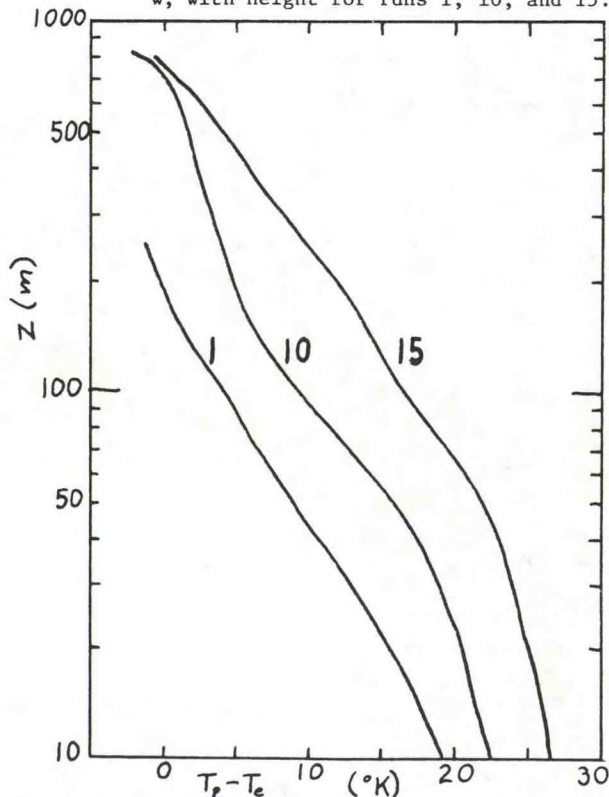


Figure 2: Variation of calculated temperature difference,  $(T_p - T_e)$  with height for runs 1, 10, and 15.

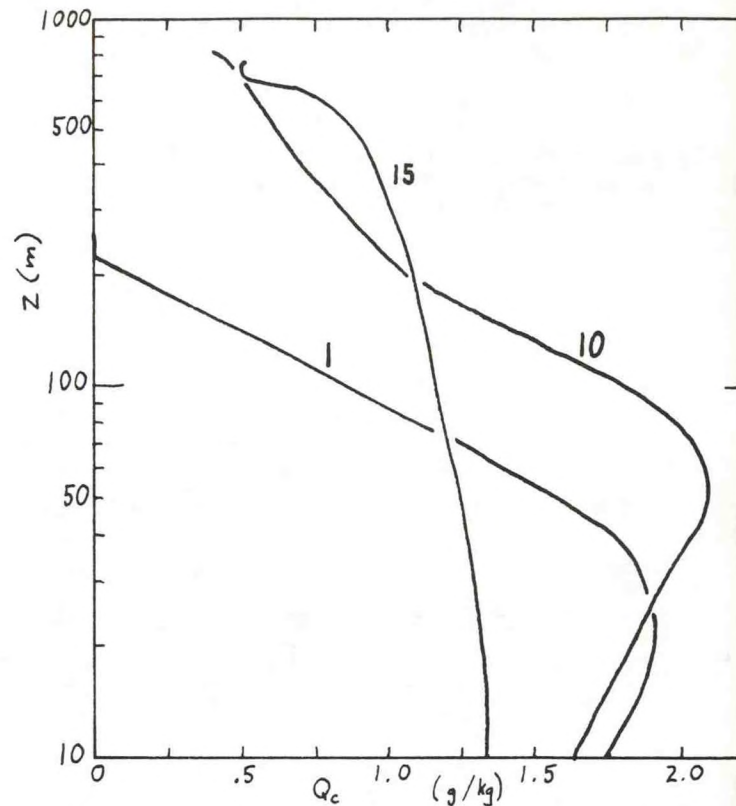


Figure 3: Variation of calculated cloud water content,  $Q_c$ , with height for runs 1, 10, and 15.

Runs 1 and 10 are bent over plumes and run 15 is a vertical plume which bends over above a height of about 600m. Because of the reduced entrainment rate for the vertical plume, its temperature difference and vertical speed do not decrease with height as fast as those for the bent over plumes. However, because the ambient air is drier for the vertical plume than for the two bent over plumes, the cloud water content  $Q_c$  of the vertical plume is not much different from that of the bent over plumes. As the wind speed increases above 1 m/s at a height of about 500 m in run 15, the entrainment coefficients switch from those applying to a vertical plume to those applying to a bent over plume. The visible plume in run 1 is predicted to evaporate just below the height of final plume rise, while the observed visible plume on that day extended through the height of maximum plume rise. Cloud water content at the top of the plumes in runs 10 and 15 is about .5 g/kg, a value within the range of measured cloud water content in natural clouds. Measurements of the cloud water content of the plume during these runs would have been useful, but unfortunately in-plume measurements were not part of this program.

The plumes in the bent over runs are predicted to merge at a height of about 200m, in agreement with the observations. The plumes in run 15 do not merge until a height of about 500m is reached due to the reduced entrainment. This is also in rough



agreement with observations, although the prediction of a constriction in the plumes just above the tower top for vertical plumes is not verified by the Amos photographs.

A summary of observed and predicted plume rise for all of the runs analyzed in this program is given in Table 2.

TABLE 2  
Observed and Calculated Plume Rise

Run	$\bar{U}$ (m/s)	Inversion height above tower (m)	Observed plume rise (m)	Model plume rise (m)	Analytical plume rise, sensible, one unit (m)
1	14		560	260	250
6	11		850	820	430
8	9		370	350	250
10	6	720	820	820	590
11	0	660	880	900	980
12	6	1140	1060	1200	720
15	3		1120	790	780
16	6	1200	1160	700	380
17	8	360	360	430	410
18	6		910	720	410
19	0	840	800	970	910
24	6	750	760	630	500
28	5		360	400	310
31	0		500	900	780
35	3	390	360	590	480
44	8	960	910	420	510
45	7	1200	910	370	390
47	0	900	800	1020	910
48	7	750	670	360	340
Avg.	5.6	820	750	670	540

The average model and observed plume rises are 670m and 750m, respectively, and the correlation coefficient is 0.49. It can be concluded that the plume and cloud growth model can be satisfactorily used to estimate the plume characteristics and the development of clouds due to cooling tower emissions.

The plume rise predicted by Briggs' (1975) well-known analytical formulas is included in the last column of Table 2. In the application of this formula, the initial buoyancy flux is assumed to equal the sensible heat flux from the largest tower. It is seen that the average predicted plume rise is 540m and the correlation with observations is .37.

The height of the base of the capping inversion or the "mixing layer" is also listed in Table 2. Brennan, et al. (1976) have analyzed these data and find that, when a capping inversion is present, the plume will generally rise to this height and level off. For the data in Table 2 the correlation between capping inversion height and observed plume rise is 0.90. A good general rule might be that, when an inversion caps a mixed layer, and the base of this inversion is at a height of less than about 1 km, then the final plume rise from cooling towers as large as those at the Amos plant will equal the inversion height. By the nature of the Amos experiments (cold winter mornings) low mixing heights could be expected. But during other seasons of the year the mixing heights will increase and it will be much less likely that the plume will reach the capping inversion.

Acknowledgements. The cooperation of Smith-Singer Meteorologists, Inc. and the American Electric Power Service Corporation in providing the Amos data is greatly appreciated. This work was performed under an agreement between the National Oceanic and Atmospheric Administration and the Energy Research and Development Administration.

#### References

Brennan, P. T., D. E. Seymour, M. J. Butler, M. L. Kramer, M. E. Smith and T. T. Frankenburg, 1976: The observed rise of visible plumes from hyperbolic natural draft cooling towers. Atmos. Environ., in press.

Briggs, G. A., 1975: Plume rise predictions. Lectures on Air Pollution and Environmental Impact Analyses. American Meteorol. Soc., 45 Beacon St., Boston, Mass., 59-111.

Cooling Tower Environment - 1974, ERDA Symposium Series, CONF-740302, Nat. Tech. Information Service, U. S. Dept. of Commerce, Springfield, Va., 22161, (\$13.60), 638 pp.

Hanna, S. R., 1972: Rise and condensation of large cooling tower plumes. J. Appl. Meteorol., 11, 793-799.

Hanna, S. R., 1976: Predicted and observed cooling tower plume rise and visible plume length at the John E. Amos power plant. To be published in Atmos. Environ., available as No. 75/25 from ATDL, P. O. Box E, Oak Ridge, Tn. 37830; 39 pp plus 5 figures.

Kessler, E., 1969: On the distribution and continuity of water substance in atmospheric circulations. Meteorol. Monographs, 10, 84 + ixpp, published by the Amer. Meteorol. Soc., 45 Beacon St., Boston.

Kramer, M. L., D. E. Seymour, M. J. Butler, R. N. Kempton, P. J. Brennan, J. J. Conte and R. G. Thomson, 1975: John E. Amos Cooling Tower Flight Program Data, December 1974-March 1975. Smith-Singer Meteorologists, Inc., 134 Broadway, Amityville, N. Y. 11701 for American Electric Power Service Corp., P. O. Box 487, Canton, Ohio 44701.

Meyer, J. H., T. W. Eagles, L. C. Kohlenstein, J. A. Kagan and W. D. Stanbro, 1974: Mechanical draft cooling tower visible plume behavior: Measurements, models, predictions. In Cooling Tower Environment - 1974, ERDA Symposium Series, CONF-740302, pp 307-352.

Norman, J. M., D. W. Thomson, J. Pena and R. Miller, 1975: Aircraft turbulence and drift water measurements in evaporative cooling tower plumes. Dept. of Meteor., Penn. State Univ., University Park, Pa. 16802.

Slawson, P. R., J. H. Coleman and J. W. Frey, 1974: Some observations on cooling-tower plume behavior at the Paradise Steam Plant. In Cooling Tower Environment - 1974, ERDA Symposium Series, CONF-740302, pp 147-160.

Weinstein, A. I., 1970: A numerical model of cumulus dynamics and microphysics. J. Atmos. Sci., 27, 246-255.

Woffinden, G. J., J. A. Anderson and P. R. Harrison, 1976: Aircraft Survey, Chalk Point Cooling Tower Plume, Dec. 1975. Rep. No. 76R-1410 by MRI, Altadena, Cal. 91001 for the Maryland Power Plant Siting Program, 33 pp + appendices.

**SULCAL**  
**A MODEL of SULFUR CHEMISTRY in a PLUME**

C. F. Baes, Jr.

J. T. Holdeman

W. M. Culkowski

OAK RIDGE NATIONAL LABORATORY

ATDL Contribution File No. 76/7



Printed in the United States of America. Available from  
National Technical Information Service  
U.S. Department of Commerce  
5285 Port Royal Road, Springfield, Virginia 22161  
Price: Printed Copy \$5.00; Microfiche \$2.25

This report was prepared as an account of work sponsored by the United States Government. Neither the United States nor the Energy Research and Development Administration, nor any of their employees, nor any of their contractors, subcontractors, or their employees, makes any warranty, express or implied, or assumes any legal liability or responsibility for the accuracy, completeness or usefulness of any information, apparatus, product or process disclosed, or represents that its use would not infringe privately owned rights.

# TABLE OF CONTENTS

	PAGE
Abstract . . . . .	1
1. Introduction . . . . .	2
1.1 The Rapid Reactions of Sulfur . . . . .	2
1.2 The Slow Oxidation of SO <sub>2</sub> . . . . .	7
1.3 Other Reactions . . . . .	9
2. The Model . . . . .	11
2.1 The Plume Components . . . . .	14
2.2 Effective Concentrations and Plume Volume . . . . .	14
2.3 The Rate of Change of Component Concentration . . . . .	20
2.4 The Composition of the Plume . . . . .	21
3. Test Calculations . . . . .	25
References . . . . .	33
Appendices	
Appendix A Program SULCAL . . . . .	35
1. Partial List of Symbols . . . . .	36
2. Program Listing . . . . .	38
3. Sample Input and Output . . . . .	53
Appendix B Effective Volume of Free Plume . . . . .	57
1. Mean Concentration When Plume Touches the Ground . .	60
2. Plume Depletion Due to Washout . . . . .	62
3. Plume Depletion Due to Dry Deposition . . . . .	62
4. Choice of Sigma . . . . .	63

	PAGE
Appendix C Activity Coefficients, The Water Activity and Initial Values . . . . .	67
1. The Estimation of Ion Activity Coefficients and the Osmotic Coefficient . . . . .	68
2. Initial Estimate of Quantities Needed for the Calculation of the Plume Composition . . . . .	71



# LIST OF FIGURES

	PAGE
1. Program SULCAL .....	12
2. Quantities Calculated by SULCAL for the Reference Case ....	28
3. The Effect of the Relative Humidity and the Extent of Acid Neutralization on the Ratio of the Rates of SO <sub>2</sub> Oxidation by Ozone (R <sub>OZ</sub> ) and by Hydroxyl Radical (R <sub>OH</sub> ) at 25°C .....	31
4. Variation of the Concentration of Aerosol Droplets with the Activity of Water a <sub>w</sub> (the Relative Humidity/100) at 25°C...	69
5. The Sulfuric Acid - Ammonium Sulfate - Water System at 25°C .....	72

# LIST OF TABLES

	PAGE
Table I     Equilibrium Constants .....	4
Table II    Rate Expressions for S(IV) Oxidation .....	8
Table III   Input Data .....	15
Table IV    Calculation of Dispersion Coefficients .....	19
Table V     Sensitivity of Values Calculated by SULCAL to Variation of Input Values .....	26

Contract No. W-7405-eng-26

SULCAL: A MODEL OF SULFUR CHEMISTRY IN A PLUME

C. F. Baes, Jr.  
Chemistry Division

J. T. Holdeman  
Computer Sciences Division

W. M. Culkowski  
Atmospheric Turbulence and Diffusion Laboratory

APRIL 1976

Work supported by the National Science Foundation RANN  
Program under NSF Interagency Agreement No. AG-389

OAK RIDGE NATIONAL LABORATORY  
Oak Ridge, Tennessee 37830  
operated by  
UNION CARBIDE CORPORATION  
for the  
ENERGY RESEARCH AND DEVELOPMENT ADMINISTRATION



# ABSTRACT

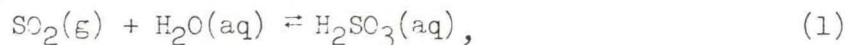
A computer program has been written that models the following features of the chemical behavior of sulfur emitted to the atmosphere from fossil-fuel burning power plants: (1) the rapid reactions of  $\text{SO}_2$  with aerosol droplets to produce the dissolved sulfite species  $\text{H}_2\text{SO}_3$ ,  $\text{HSO}_3^-$  and  $\text{SO}_3^{2-}$ ; (2) the rapid reactions of  $\text{SO}_3$  to produce the dissolved sulfate species  $\text{HSO}_4^-$  and  $\text{SO}_4^{2-}$ ; (3) the neutralization of the acid thus produced by atmospheric ammonia and (4) the eventual formation of particulate ammonium sulfate; (5) the slow oxidation of  $\text{SO}_2$  to sulfate species by hydroxyl radical, and (6) the slow oxidation of species of  $\text{SO}_2$  in aerosol droplets to sulfate species by dissolved ozone and oxygen. The model employs averaged concentrations based on the Gaussian plume and can calculate deposition rates for gaseous and particulate material as a function of such variables as distance from the source, wind speed, meteorological stability class, temperature, relative humidity, and the ambient concentrations of OH radical, ozone, and ammonia.

## 1. INTRODUCTION

Industrially produced sulfur enters the atmosphere in reactive forms, primarily  $\text{SO}_2$  and  $\text{SO}_3$ , that cannot be treated as inert substances while they remain in the atmosphere. This report describes a stand-alone model of atmospheric transport which includes the effects of (1) rapid chemical reactions that produce new species and (2) slow reactions by which  $\text{SO}_2$  or its products from rapid reactions are oxidized to sulfates in various forms. As shall be seen, the most important consequence of these reactions is the production of an aerosol of liquid acidic droplets; hence, one object of the calculation is to estimate the amount and composition of the aerosol in a unit volume of the plume and its deposition rate. The model was developed for use as a sub-model in the Air Transport Model (ATM).<sup>1</sup>

### 1.1 The Rapid Reactions of Sulfur

Both gaseous  $\text{SO}_2$  and  $\text{SO}_3$  can undergo rapid chemical reactions with constituents of the atmosphere. Gaseous  $\text{SO}_2$  can dissolve in aerosol droplets producing the following products in solution:\*



These reactions are reversible as well as rapid and as a result the concentration of the species involved are related to one another by

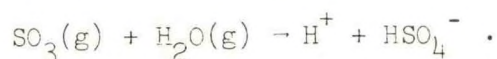
---

\*The abbreviations (g), (aq), and (c) used in chemical reactions denote species in the gaseous, aqueous, or solid states, respectively.



equilibrium constants (i.e.,  $K_1$ ,  $K_2$ , and  $K_3$  in Table I) that have known values<sup>2</sup> as a function of temperature. These, and the other equilibrium constants in Table I, include in their expressions a quotient of so-called activity coefficients ( $g_i$ ) which, as shall be seen, are functions of the composition of the solution involved. (The activity coefficients reflect the non-ideal behavior of the individual ions in the solution.) The tendency of  $\text{SO}_2$  to form the aqueous species  $\text{H}_2\text{SO}_3$ ,  $\text{HSO}_3^-$ , and  $\text{SO}_3^{2-}$  is weak and at the low concentrations of  $\text{SO}_2$  in the atmosphere (usually  $<0.1$  ppm) reaction occurs only if condensed water is already present.

In contrast, gaseous  $\text{SO}_3$  reacts vigorously and completely with water, even in the gaseous form, to produce acid droplets



The bisulfate ion  $\text{HSO}_4^-$  undergoes rapid and reversible dissociation,



As a result, no trace of  $\text{SO}_3$  gas is found in the atmosphere. If it is introduced, it is converted completely to acid droplets containing the ions  $\text{H}^+$ ,  $\text{HSO}_4^-$  and  $\text{SO}_4^{2-}$ , the concentrations of which are related to one another by  $K_4$  (Table I).

The acid ( $\text{H}^+$ ) produced by the solution of  $\text{SO}_2$  and  $\text{SO}_3$  in water can be neutralized by atmospheric ammonia in another set of rapid and reversible reactions, producing the aqueous ammonium ion,



and  $K_5$  and  $K_6$  apply. These reactions can lead to the formation of particles of ammonium sulfate,  $(\text{NH}_4)_2\text{SO}_4$ , if they proceed far enough and the relative humidity is less than  $\sim 83\%$ . When both liquid and solid are



Table I Equilibrium Constants<sup>a</sup>

Text <sup>b</sup> Symbol	Definition <sup>b</sup>	Log K(25°C)	Log K=A+B/T(K)		Program Name
			A	B	
K <sub>1</sub>	$\frac{[\text{H}_2\text{SO}_3]}{P_{\text{SO}_2} a_w}$	0.090	-4.4912	1365.9	EKS
K <sub>2</sub>	$\frac{[\text{H}^+][\text{HSO}_3^-]}{[\text{H}_2\text{SO}_3]} \cdot \left( \frac{g_{\text{H}^+} g_{\text{HSO}_3^-}}{g_{\text{H}_2\text{SO}_3}} \right)$	-1.765	-4.815	909.4	EKLS
K <sub>3</sub>	$\frac{[\text{H}^+][\text{SO}_3^{2-}]}{[\text{HSO}_3^-]} \cdot \left( \frac{g_{\text{H}^+} g_{\text{SO}_3^{2-}}}{g_{\text{HSO}_3^-}} \right)$	-7.220	-8.8549	487.36	EK2S
K <sub>4</sub>	$\frac{[\text{H}^+][\text{SO}_4^{2-}]}{[\text{HSO}_4^-]} \cdot \left( \frac{g_{\text{H}^+} g_{\text{SO}_4^{2-}}}{g_{\text{HSO}_4^-}} \right)$	-1.994	-5.8348	1145.2	EK3S
K <sub>5</sub>	$\frac{[\text{NH}_3]}{P_{\text{NH}_3}}$	1.756	-4.233	1785.5	EKN
K <sub>6</sub>	$\frac{[\text{NH}_4^+]}{[\text{NH}_3][\text{H}^+]} \cdot \left( \frac{g_{\text{NH}_4^+}}{g_{\text{H}^+}} \right)$	9.251	0.1026	2727.5	EKLN

Table I (continued)

Text <sup>b</sup> Symbol	Definition <sup>b</sup>	Log K(25°C)	Log K=A+B/T(K)		Program Name
			A	B	
$K_7$	$= \frac{[\text{NH}_4^+]^2[\text{SO}_4^{2-}]}{[\text{NH}_4^+ \text{gSO}_4^{2-}]}$	-0.221 <sup>c</sup>	0.929 <sup>c</sup>	-343.1	EKSS
$K_8$	$= \frac{[\text{H}_2\text{CO}_3]}{P_{\text{CO}_2} a_w}$	-1.462	-5.0160	1059.74	EKC
$K_9$	$= \frac{[\text{H}^+][\text{HCO}_3^-]}{[\text{H}_2\text{CO}_3]} (\text{g}_\text{H} + \text{g}_{\text{HCO}_3^-})$	-6.368	-5.0300	-398.85	EK1C
$K_{10}$	$= \frac{[\text{H}^+][\text{CO}_3^{2-}]}{[\text{HCO}_3^-]} (\text{g}_\text{H} + \text{g}_{\text{CO}_3^{2-}})$	-10.328	-7.7260	-775.85	EK2C
$K_{13}$	$= \frac{[\text{O}_3]}{P_{\text{O}_3}}$	-2.146 <sup>d</sup>	-8.488 <sup>d</sup>	1891 <sup>d</sup>	EKOZ
$K_w$	$= \frac{[\text{H}^+][\text{OH}^-]}{a_w}$	-14.00	-4.2134	-2916.54	EKW
$P_{\text{H}_2\text{O}}^\circ$	$= \frac{P_{\text{H}_2\text{O}}}{a_w}$	-1.505	6.2057	-2298.9	PWO

<sup>a</sup>Numerical values are based on NBS Technical Note 270-3, et seq<sup>2</sup> unless otherwise indicated and should represent K values with adequate accuracy from 0 to 40°C.

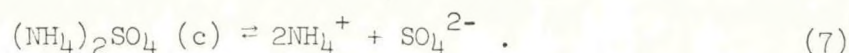
<sup>b</sup>Subscript on K refers to Eq. No. in text; concentrations of species in solution [i] are in molal units (mmol/g H<sub>2</sub>O); gas pressures P<sub>i</sub> are in atmospheres; activity coefficients of ions g<sub>i</sub> are calculated as described in Appendix C.1.

<sup>c</sup>Adjusted to give the observed solubility of (NH<sub>4</sub>)<sub>2</sub>SO<sub>4</sub> in water.

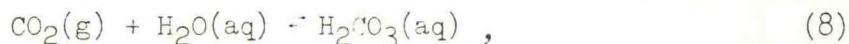
<sup>d</sup>Based on data of Rowson quoted in Seidell,<sup>17</sup> Vol. II, p 1240.



present, the following equilibrium (and  $K_7$ ) applies,



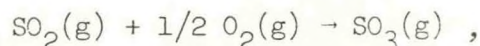
Another atmospheric gas that can affect the acidity (pH) of aerosol droplets is  $\text{CO}_2$ .



All three reactions are rapid and reversible and the concentrations of the species involved are related by  $K_8$ ,  $K_9$ ,  $K_{10}$ .

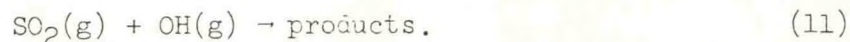
## 1.2 The Slow Oxidation of $\text{SO}_2$

The slower reactions to be considered are those by which  $\text{SO}_2$  and some of the products of its rapid reactions (all of which are species of tetravalent sulfur) are oxidized to sulfate (hexavalent sulfur) species in the atmosphere. The direct oxidation of  $\text{SO}_2$  by atmospheric oxygen



(followed instantly by reaction of  $\text{SO}_3$  with  $\text{H}_2\text{O}$ ) is slow and proceeds by a photochemical path. More rapid oxidation can occur by at least three other paths.

Recently Castleman et al<sup>3</sup> and Davis and Klauber<sup>4</sup> have concluded that the most rapid reaction involving a gaseous oxidant is that with the hydroxyl (OH) radical,



The rate expression and rate constant ( $k_{11}$ ) are given in Table II. The concentration of OH radical, an intermediate in other reactions, is found by Wang et al<sup>5</sup> to be in the range  $<2 \cdot 10^{-13}$  to  $2 \cdot 10^{-12}$  atm, and

Table II Rate Expressions for S(IV) Oxidation

Rate Expression	k <sup>a</sup> (25°C)	Log k=A+B/T(K)		Pro-gram Name
		A	B	
(1) Oxidation of SO <sub>2</sub> (g) by OH(g), <sup>(b)</sup> $-\frac{dP_{SO_2}}{dt} = k_{11} P_{SO_2} P_{OH}$	k <sub>11</sub> = 1.83 · 10 <sup>7</sup>	7.26	(0) <sup>e</sup>	RK4
(2) Oxidation of HSO <sub>3</sub> <sup>-</sup> by O <sub>3</sub> , <sup>(c)</sup> $-\frac{d[HSO_3^-]}{dt} = k_{12} [HSO_3^-] g_X [O_3]$	k <sub>12</sub> = 9.8 · 10 <sup>5</sup>	14.61	-2570 <sup>e</sup>	RK3
(3) Oxidation of SO <sub>3</sub> <sup>2-</sup> by O <sub>2</sub> , <sup>(d)</sup> $-\frac{d[SO_3^{2-}]}{dt} = [K'_{14} + K''_{14} ([H^+] g_{H^+})^{1/2}] [SO_3^{2-}] g_X^{2-}$	k' <sub>14</sub> = 0.013 k'' <sub>14</sub> = 59	11.438 15.095	-3973 -3973	RK1 RK2

<sup>a</sup>Subscript on k refers to the Eq. No. in text. Concentration and pressure units are as in Table I, footnote b. Time is in sec.

<sup>b</sup>Castleman et al,<sup>3</sup> Davis and Klauber.<sup>4</sup>

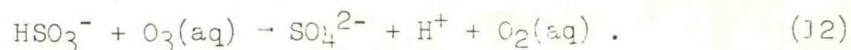
<sup>c</sup>Penkett<sup>6</sup> measured k<sub>12</sub> at 9.6°C.

<sup>d</sup>McKay,<sup>7</sup> Fuller and Crist.<sup>8</sup>

<sup>e</sup>Our estimate.

hence the half-time for reaction 11 could be as short as a few hours.

Of the reactions that occur in solution, the oxidation of  $\text{HSO}_3^-$  by ozone ( $\text{O}_3$ ) may be the fastest,<sup>6</sup>

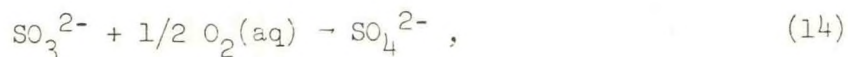


This reaction is preceded by



With an atmospheric concentration of ozone of  $10^{-7}$  atm, we estimate from  $k_{12}$  and  $K_{13}$  (Tables I and II) a half life of 2 min. for  $\text{HSO}_3^-$  in solution.

Another reaction which is known to occur in solution involves the oxidation of  $\text{SO}_3^{2-}$  by dissolved oxygen.<sup>7,8</sup> While the overall reaction is



the mechanism is apparently complex and is not known in detail. The reaction can be catalyzed by some metal ions and retarded by others. In pure solutions the kinetics are described by the equations and constants in Table II.

### 1.3 Other Reactions

There are, of course, other reactions that could affect the behavior of sulfur in the atmosphere, including reversible equilibria such as the solution of  $\text{NO}_2$  in aerosol droplets and slow reactions such as the dissolution of a flyash particle in an acid droplet or the catalytic oxidation of  $\text{SO}_2$  at particle surfaces. There are numerous other constituents of a plume which could react with  $\text{SO}_2$  or which certainly will affect the concentrations of ozone and hydroxyl radical. Such other reactions are not included in the present model, either because they are poorly



understood at present, or because they would greatly complicate the model and its validation.

## 2. THE MODEL

From the foregoing the essential features of the chemistry of sulfur in the atmosphere which might be included in a model are (1) the slow oxidation of  $\text{SO}_2$  to produce acidic aerosol droplets in which (2) various rapidly attained and shifting chemical equilibria are established (Table I) including (3) progressive neutralization by ammonia, which-- if the aerosol remains in the atmosphere long enough--can ultimately produce a relatively innocuous solid,  $(\text{NH}_4)_2\text{SO}_4$ . The computations performed by SULCAL to accomplish this may be summarized as follows (Fig. 1):\*

1. M. SULCAL, the main program, first calculates the emission rate of plume components from the source.
2. S. SIG is called to obtain the effective volume of the plume for the calculation of component concentrations at a starting point a short distance (x) from the source.
3. M. SULCAL then calls S. KUTTA<sup>9</sup> to begin the calculation of the composition of the plume at increasing values of x.
4. S. KUTTA calls S. RATE repeatedly to determine the rate of change of the concentration of the plume components with x, to be used in a Runge-Kutta integration of the component concentrations vs. x.
5. Each time S. RATE is entered it first calls S. EXPCT which determines by extrapolation or interpolation on x the starting values of several quantities to be refined in the calculation of the composition of the plume.

---

\* Here and elsewhere M and S denote main and subroutine programs, respectively.

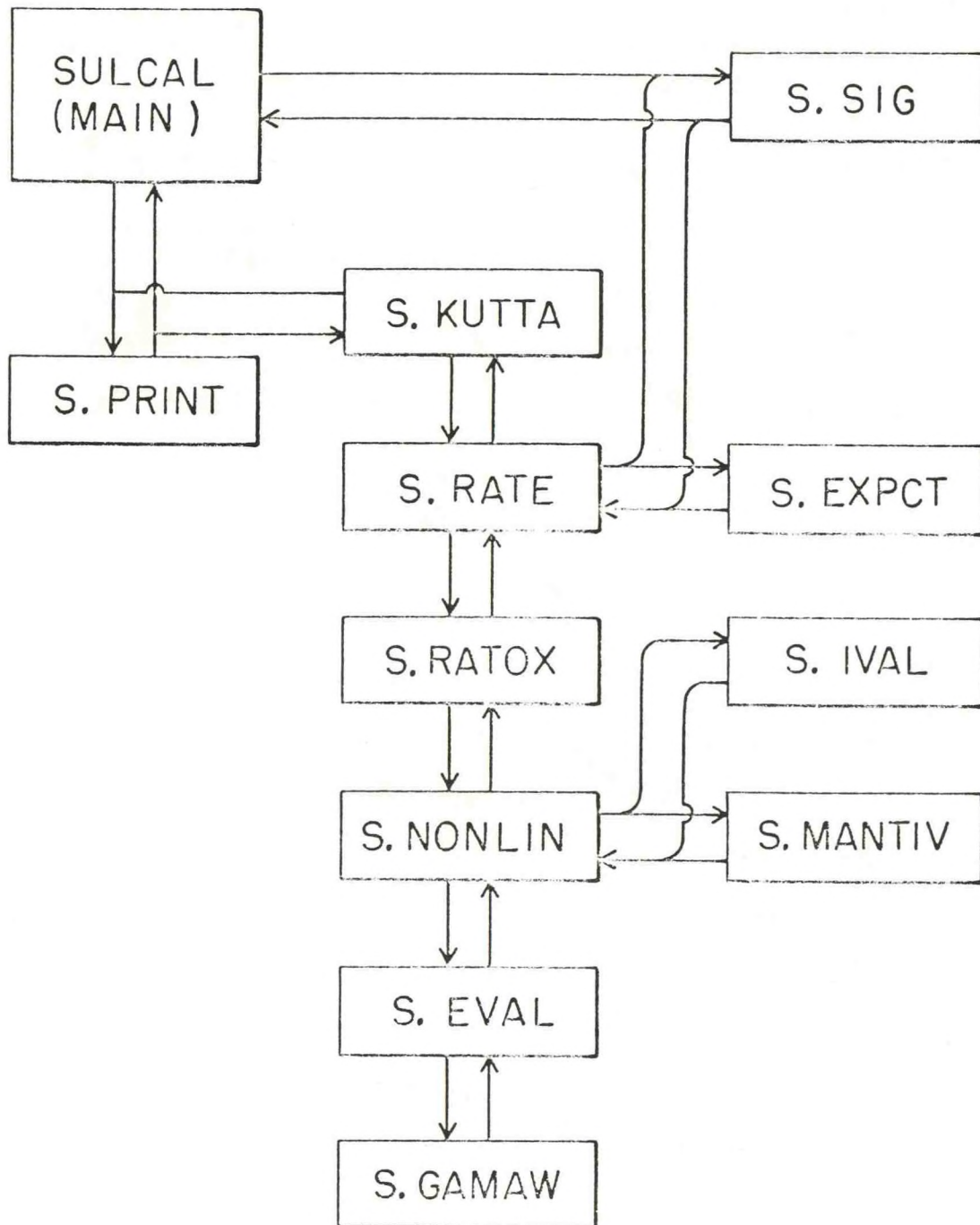


Fig. 1 Program SULCAL.



6. S. RATE next calls S. SIG to determine the effective volume of the plume at the current value of  $x$  and its rate of change with  $x$ .
7. S. RATE then calls S. RATOX to calculate the rate of S(IV) oxidation.
8. S. RATOX first calls S. NONLIN<sup>10</sup> which employs the secant method to refine quantities needed to calculate the composition of the gas and aerosol phases of the plume.
9. S. NONLIN calls S. EVAL repeatedly to calculate these compositions to test for convergence of the quantities being refined.
10. S. EVAL calls S. GAMAW repeatedly to refine values of needed ionic activity coefficients and the activity of water, quantities which are themselves dependent on the composition of the droplets.
11. With the amount and composition of each phase in the plume returned to S. RATOX, the rate of S(IV) oxidation is calculated in the gas phase and in the droplets.
12. With the oxidation rates returned to S. RATE, the rate of change of the component concentrations are calculated, including also the effects of dilution and deposition; these are returned to S. KUTTA.
13. S. KUTTA returns to M. SULCAL integrated values of the component concentrations at specified values of  $x$ .
14. S. KUTTA and M. SULCAL call S. PRINT to put out results as the calculation proceeds.

The important features of the calculation are described in the following

sections. The program is listed in Appendix A.

## 2.1 The Plume Components

There are seven chemical constituents whose concentrations specify the composition of the plume in sufficient detail for the purposes of the model. They include S(IV), S(VI),  $\text{CO}_2$ ,  $\text{H}_2\text{O}$ ,  $\text{NH}_3$ ,  $\text{O}_3$ , and OH. The first four come in part from the stack. It is assumed that S(IV) is emitted from the stack entirely as  $\text{SO}_2(\text{g})$ , and S(VI) entirely as droplets with the composition  $\text{SO}_3 \cdot n\text{H}_2\text{O}$ . The concentrations of all seven components in the surrounding air are specified as input data.

The rates ( $Q_i$ ) at which  $\text{SO}_2$ ,  $\text{SO}_3 \cdot n\text{H}_2\text{O}$ ,  $\text{CO}_2$  and  $\text{H}_2\text{O}$ --along with unreacted atmospheric gases--are emitted from the stack are calculated from input data (Table III), including the composition of the coal and the rate at which it is burned, the excess of air used, the fraction of sulfur converted to  $\text{SO}_3$ , and the moles of water ( $n$ ) condensed by a mole of  $\text{SO}_3$ . The flow rate of gas ( $V_p^\circ$ ) at the mouth of the stack is calculated from the mass flow rate and the specified exit temperature.

The total concentration ( $C_i$ ) of each of the seven components is to be calculated vs.  $x$ . A Gaussian plume is assumed for the estimation of dilution and deposition.

## 2.2 Effective Concentrations and Plume Volume

The simplest conditions under which to study chemical reactions would involve well-mixed solutions of uniform concentration and temperature. Though the conditions in a plume are far from this ideal, it is possible to define mean concentrations and temperature, and effective rate and equilibrium constants under the assumption of rapid mixing such that the net rate of oxidation to sulfur (VI) is the same



Table III Input Data

	Units	Typical Value	Text Symbol	Program Name
Carbon in coal	wt %	82.57 <sup>a</sup>		WPCTC
Hydrogen in coal	"	6.93		WPCTH
Sulfur in coal	"	1.0		WPCTS
Rate of coal combustion	kg/sec	100		QCOAL
Fraction of S converted to SO <sub>3</sub>	--	0.02		FCTS6
Fractional excess of air in combustion	--	0.25		EXAIR
Moles H <sub>2</sub> O condensed per moles SO <sub>3</sub>	--	5	n	FCON
Temperature of plume at mouth of stack	°C	177		TCP
Ambient temperature	°C	21.11		TCA
Ambient concentration of S(IV)	mmol/m <sup>3</sup>	0.004	A <sub>1</sub>	A(1)
Ambient concentration of S(VI)	"	0	A <sub>2</sub>	A(2)
Ambient concentration of O <sub>3</sub>	"	0.0032	A <sub>3</sub>	A(3)
Ambient concentration of OH	"	2·10 <sup>-8</sup>	A <sub>4</sub>	A(4)
Ambient concentration of CO <sub>2</sub>	"	12.26	A <sub>5</sub>	A(5)
Ambient concentration of NH <sub>3</sub>	"	0.0006	A <sub>6</sub>	A(6)
Ambient concentration of H <sub>2</sub> O	"	930	A <sub>7</sub>	A(7)
Effective height of stack	m	400	h	H
Meteorological stability class	--	1 to 6 <sup>b</sup>		NSC
Roughness length of terrain	--	1 to 6 <sup>b</sup>		NRL
Wind speed	m/sec	(a)	u <sub>x</sub>	UX
Deposition velocity of gas	m/sec	0.01	v <sub>d</sub> <sup>g</sup>	VDG
Deposition velocity of particle	m/sec	0.01	v <sub>d</sub> <sup>p</sup>	VDP
Initial distance from source	m	300		XNEXT
Initial trial value of Δx	m	0.1		DELX



	Units	Typical Value	Text Symbol	Program Name
Fractional error of integrated quantities	--	$3 \cdot 10^{-6}$		ERRR
No. of distance intervals	--	--		NX
Size of distance interval	m	--		XINCR (NX)

<sup>a</sup>This value is higher than is typical of power plant fuels.

<sup>b</sup>The numbers 1 to 6 denote stability classes A to F and roughness lengths of 1, 4, 10, 40, 100, and 400 m, respectively. The range of wind speeds depends on the stability class (Table IV).

for the idealized uniform case as for a real plume or for the model Gaussian distribution of concentrations. This can be achieved for reactions involving concentrations through second order in the Gaussian distributed concentrations by the artifice of an effective volume related to the Gaussian dispersion coefficients. Higher order reaction rates can be preserved if desired through appropriate scaling of the rate constants. The justification is given in Appendix B. We use the Gaussian distribution here not because we think it fits the plume distribution better than other forms, but rather because these are existing measurements of plume volume which have been expressed in terms of the Gaussian dispersion.

In terms of the effective plume volume  $V_p$ , the concentration ( $C_i$ ) of each plume component is given by

$$C_i = Q_i/V_p + A_i(1 - V_p^0/V_p), \quad (15)$$

where  $Q_i$  is the emission rate of component  $i$  (mmol/sec),  $A_i$  its ambient concentration (mmol/m<sup>3</sup>), and  $V_p^0$  the initial plume volume flow rate (m<sup>3</sup>/sec). Thus the effective plume volume is a volume flow rate (m<sup>3</sup>/sec) at a given  $x$ , or, a volume (m<sup>3</sup>) of a length of plume  $u_x$  where  $u_x$  is the wind velocity (m/sec).

The effective plume volume  $V_p$  is related to the dispersion coefficients  $\sigma_y$  and  $\sigma_z$  (m) of the Gaussian distribution by the expression (see Appendix B)

$$V_p = 4\pi \sigma_y \sigma_z u_x \beta \quad (\text{m}^3/\text{sec}), \quad (16)$$

where  $\beta$  is a correction factor which accounts for the change in the concentration distribution due to the interaction with (or "reflection"

from) the ground. The factor  $\beta$  is given by the expression (Appendix B)

$$\beta = \left[ 1 + \frac{1}{\sqrt{2}} \exp(-h^2/\sigma_z^2) \right]^{-1}, \quad (17)$$

where  $h$  is the effective stack height (m). Note that when  $\sigma_z \ll h$  then  $\beta = 1$  and when  $\sigma_z \gg h$  then  $\beta = .59$ . The value of  $\beta$  changes smoothly as the ratio  $h/\sigma_z$  passes through unity.

The dispersion coefficients used in the effective reaction volume determination are instantaneous or short-time averaged coefficients ( $\sigma_s$ ), and are smaller than the long-time averaged dispersion coefficients ( $\sigma_\ell$ ) described by Hosker<sup>11</sup> (Table IV) which are used to calculate ground level concentrations and depositions. Both coefficients are a function of the meteorological stability class, the distance  $x$  from the stack, and a roughness length characteristic of the terrain. To these dispersion coefficients we have added a small correction  $\sigma^\circ$

$$\sigma^\circ = \sqrt{V_p^\circ / 4\pi u_x}, \quad (18)$$

which keeps the plume volume finite at the source, preventing infinite concentrations and reaction rates.

The rate of change of average component concentration with distance due to surface deposition is given by

$$\frac{dC_i}{dx} = -C_i V_d \gamma / u_x, \quad (19)$$

where  $V_d$  is the conventionally defined deposition velocity and  $\gamma$  is

$$\gamma = (\sqrt{2/\pi}/\sigma_z) \exp(-h^2/2\sigma_z^2). \quad (20)$$

$\gamma$  and  $V_p$  are calculated for each specified value of  $x$  in S. SIG;  $\sigma_z$  is the conventional long-time averaged dispersion coefficient.

The short-time dispersion coefficient  $\sigma_s$  can be related to the long-



Table IV Calculation of Dispersion Coefficients<sup>a</sup>

$$\sigma_y(x) = C_3 x / \sqrt{1 + 0.001x} + \sigma^\circ$$

$$\sigma_z(x) = \ln(c_1 x^{d_1}) \cdot \frac{a_1 x^{b_1}}{1 + a_2 x^{b_2}} + \sigma^\circ$$

$$(\sigma^\circ = \sqrt{V_p^\circ / (4\pi u_x)})$$

Stability Class	$u_x$ (m/sec)	$a_1$	$b_1$	$a_2$	$b_2$	$c_3$
A (1) <sup>b</sup>	1 - 2.5	0.112	1.06	$5.38 \cdot 10^{-4}$	0.815	0.22
B (2)	1.5 - 5	0.130	0.950	$6.52 \cdot 10^{-4}$	0.750	0.16
C (3)	2 - >6	0.112	0.920	$9.05 \cdot 10^{-4}$	0.718	0.11
D (4)	5 - >10	0.098	0.889	$1.35 \cdot 10^{-3}$	0.688	0.08
E (5)	2 - 5	0.0609	0.895	$1.96 \cdot 10^{-3}$	0.684	0.06
F (6)	2 - 3	0.0638	0.783	$1.36 \cdot 10^{-3}$	0.672	0.04

Roughness Length (cm)		$c_1$	$d_1$
1	(1) <sup>b</sup>	1.56	0.0480
4	(2)	2.02	0.0269
10	(3)	2.718	0
40	(4)	5.16	-0.060
100	(5)	7.37	-0.0957
400	(6)	11.7	-0.128

<sup>a</sup>From Hosker<sup>11</sup>; these are long-time averaged ( $\sigma_\theta$ ) values. A factor has been omitted from the expression for  $\sigma_z$  since it differs little from unity (< 10%) for the distances of interest (< 30 km).

<sup>b</sup>Numbers are values of NSC and NRL supplied as input data (Table III).

term coefficients  $\sigma_\ell$  by

$$\sigma_s = f \sigma_\ell . \quad (21)$$

The form of  $f$  is given in Appendix B.

In equation 15, additivity of gas volumes is assumed. By the assumption of the ideal gas law, the mean absolute temperature of the plume is then given as

$$T = \frac{T_a}{1 - (1 - T_a/T_p) (V_p^0/V_p)} , \quad (22)$$

where  $T_p$  and  $T_a$  are respectively the absolute temperature of the plume at the mouth of the stack and of the ambient air.

### 2.3 The Rate of Change of Component Concentrations

The seven derivatives  $dC_i/dx$  are evaluated at a given  $x$  in S. RATE each time it is called by S. KUTTA. There are three possible contributions to each derivative which arise from (1) dilution, (2) deposition, and (3) oxidation,

$$\frac{d C(i)}{dx} = R_1(i) + R_2(i) + R_3(i) . \quad (23)$$

The terms due to dilution are of the form

$$R_1(i) = - [C(i) - A(i)] \frac{d \ln V_p}{dx} , \quad (24)$$

obtained by differentiation of eq 15.

For the terms arising from deposition two deposition velocities are specified  $V_d^g$  for gases and  $V_d^p$  for aerosol particles. For the components S(VI) and  $H_2O$  only particulate deposition is involved

$$R_2(S(VI)) = - C(S(VI)) \cdot V_d^p \gamma/u_x , \quad (25)$$

$$R_2(H_2O) = - (g_w/0.018) \cdot V_d^p \gamma/u_x . \quad (26)$$

(Here  $g_w$  is the amount of condensed water in  $g/m^3$ .) For the components S(IV) and  $NH_3$  the expressions are of the form

$$R_2(i) = - \left\{ [P(i)/RT] v_d^g + [C(i) - P(i)/RT] v_d^p \right\} v/u_x . \quad (27)$$

$P(i)$  is the pressure of the gaseous species. For the other components ( $CO_2$ ,  $O_3$ , and  $OH$ ) the deposition rates are assumed to be zero.

The rates of oxidation of S(IV), calculated in and returned from S. RATOX are used in the following  $R_3$  terms:

$$R_3(S(IV)) = - R_T/u_x , \quad (28)$$

$$R_3(S(VI)) = R_T/u_x , \quad (29)$$

$$R_3(O_3) = -R_{OZ}/u_x , \quad (30)$$

where  $R_T$  is the total oxidation rate and  $R_{OZ}$  is the oxidation rate from reaction of  $HSO_3^-$  with ozone in the droplets (both in  $mmol\ m^{-3}\ sec^{-1}$ ). The depletion of  $OH$  by reaction with  $SO_2$  is neglected since its concentration is controlled by other reactions not included in the model.

#### 2.4 The Composition of the Plume

The remainder of the calculation is concerned mainly with determining for a given set of component concentrations the partial pressures of gases, the amount and composition of the aerosol droplets, and the amount--if any--of particulate ammonium sulfate in order that the oxidation rates of the various species of S(IV) (eqs 11, 12, and 14) can be calculated.

Given the concentrations of the components S(IV), S(VI),  $NH_3$ ,  $CO_2$ , and  $H_2O$ , the following material balance equations may be written:



$$C(S(IV)) = P_{SO_2}/RT + ([H_2SO_3] + [HSO_3^-] + [SO_3^{2-}])g_w , \quad (31)$$

$$C(S(VI)) = ([HSO_4^-] + [SO_4^{2-}])g_w + C_s , \quad (32)$$

$$C(CO_2) = P_{CO_2}/RT + ([H_2CO_3] + [HCO_3^-] + [CO_3^{2-}])g_w , \quad (33)$$

$$C(NH_3) = P_{NH_3}/RT + ([NH_3] + [NH_4^+])g_w + 2C_s , \quad (34)$$

$$C(H_2O) = P_{H_2O}/RT + g_w/0.018 . \quad (35)$$

(The pressures  $P_i$  are in atm, all solution concentrations  $[i]$  are in mmol/gH<sub>2</sub>O--i.e., molal units--and  $C_s$  is the amount of (NH<sub>4</sub>)<sub>2</sub>SO<sub>4</sub> solid in mmol/m<sup>3</sup>.) Upon appropriate substitution of equilibrium constants (Table I) in these equations, the unknown quantities which remain are  $[H^+]$ ,  $g_w$ ,  $C_s$ , and the ionic activity coefficients.

Only four activity coefficients are distinguished (see Appendix C.1),

$$\epsilon_{H^+}, \epsilon_{NH_4^+}, \epsilon_{X^-}, \epsilon_{X^{2-}} ,$$

the activity coefficients of all singly charged anions being assumed to be the same and similarly for doubly charged anions. The activity coefficients, and the osmotic coefficient ( $\phi$ ) needed for the calculation of the activity of water, are rather complicated but not too sensitive functions of the corresponding ion concentrations  $[H^+]$ ,  $[NH_4^+]$ ,  $[X^-]$ , and  $[X^{2-}]$  (Appendix C.1). They are refined each time S. EVAL is entered with trial values of  $[H^+]$ ,  $g_w$ , and  $C_s$  by repeated cycling between S. EVAL and S. GAMAW.

The quantities  $[H^+]$ ,  $g_w$ , and  $C_s$  (if >0) are refined by cycling between S. NONLIN and S. EVAL until the following conditions are met:

(1) Charge Balance

$$[H^+] + [NH_4^+] = [X^-] + 2[X^{2-}] \quad (36)$$

(2) Water Activity Balance

$$P_{H_2O}/P_{H_2O}^\circ = a_w \quad (37)$$

Here  $P_{H_2O}^\circ$  is the saturation partial pressure of water in the atmosphere and  $a_w$  is calculated from the composition of the solution (i.e., from  $\phi$ ). This condition specifies that the vapor pressure of the droplets as defined by their composition and the temperature will equal the partial pressure of water in the atmosphere.

(3) Ammonium Sulfate Saturation (only if  $C_s > 0$ )

$$K_7 = [NH_4^+]^2 [SO_4^{2-}] g_{NH_4^+}^2 g_{X^{2-}} \quad (38)$$

The residual deviations from these conditions are defined to equal or to approximate the fractional discrepancy in the concentration of ions in the droplets

$$y_1 = ([H^+] + [NH_4^+] - [X^-] - 2[X^{2-}]) / \Sigma[i] \quad (39)$$

$$y_2 = (P_{H_2O}/P_{H_2O}^\circ - 1/a_w) / (0.018 \cdot \Sigma[i]) \quad (40)$$

$$y_3 = \left( \frac{[NH_4^+]^2 [SO_4^{2-}] \cdot g_{NH_4^+}^2 g_{X^{2-}}}{K_7} \right)^{1/3} - 1 \quad (41)$$

This appears to give an appropriate weight to each.

Initial estimates of  $g_w$ ,  $[H^+]$ ,  $[NH_4^+]$ ,  $[X^-]$  and  $[SO_4^{2-}]$  are made the first time S. RATOX is entered as described in Appendix C.2. The initial estimate of  $C_s$  is made if and when the droplets become supersaturated with ammonium sulfate ( $y_3 > 0$ ), otherwise  $C_s = 0$ . Subsequent estimates of these quantities are made in S. EXPCT before entry into

S. FATOX (Fig. 1).

The quantities  $[H^+]$  and  $g_w$  are refined in S. NONLIN in logarithmic form since both can adopt widely ranging values and have either a first power or higher effect on the concentration of species in solution.

The quantity  $g_w$  can go to zero if the concentration ratio  $[NH_4^+]/[SO_4^{2-}]$  reaches 2 and the solution is saturated with  $(NH_4)_2SO_4$ . If significant amounts of acid remain unreacted, however, the drops cannot dry out.\*

The value of  $g_w$  is monitored and if it becomes lower than  $10^{-8} \text{ g/m}^3$  the computation of solution composition is discontinued and only the oxidation of  $SO_2$  by OH (Eq. 11) is calculated.

The quantity  $C_s$  differs from  $[H^+]$  and  $g_w$  in its effect on the calculations. When it is small it has a small effect on the composition of the droplets, but when it approaches half the amount of the  $NH_3$  component present the difference  $C(NH_3) - 2C_s$  becomes important in determining the amount of the droplets. Because of these considerations, the variable  $C_s$  is refined in S. NONLIN in the form

$$X_3 = \log[C(NH_3)/(C(NH_3) - 2C_s)] . \quad (42)$$

---

\*While there is evidence that under these conditions an acid salt  $[(NH_4)_2SO_4]_3 \cdot H_2SO_4$  can form, for simplicity we consider only the formation of  $(NH_4)_2SO_4$ .



### 3. TEST CALCULATIONS

A series of calculations, summarized in Table V, were carried out to determine the sensitivity of the various output quantities to what are thought to be typical ranges of the input quantities. The under-scored values are reference values. Some of the output quantities for the reference case are plotted versus the distance from the source in Fig. 2. The other output quantities in the table result by varying each input quantity from its reference value while holding all other inputs at the reference values. For example, entries in the first row were generated using 2.5 wt. % sulfur in coal, stability class C, wind speed 2 m/sec, OH concentration  $2 \cdot 10^{-8}$  mmol/m<sup>3</sup>, NH<sub>3</sub> concentration  $6 \cdot 10^{-4}$  mmol/m<sup>3</sup>, and temperature 21.11°C.

In all calculations ERRR, the error limit parameter in S. KUTTA, was set at  $3 \cdot 10^{-6}$ . In test calculations this produced output values differing by < 0.2% from the limiting values obtained as ERRR was further decreased. In the calculation of the reference case: S. KUTTA called S. RATE 1345 times in performing the integration from X = 0.3 to 25 km; S. NONLIN called S. EVAL an average of 5.7 times per step of the integration; each time S. EVAL was called, it called S. GAMAW an average of 6.1 times. The computation time for the reference case on the IBM-360-91 computer was 16 sec.

Under the conditions tested, the aerosol droplets contain mostly sulfuric acid with a relatively small amount of ammonium sulfate, the latter being limited by and equivalent to the supply of ambient ammonia. The concentration of the droplets is strongly dependent on the ambient

Table V Sensitivity of Values Calculated by SULCAL to Variation of Input Values

Input Values <sup>a,b</sup>		Output Values at 25 km From Stack <sup>c</sup>					
		SO <sub>2</sub> (10 <sup>-2</sup> mmol/m <sup>3</sup> )	Sulfate (10 <sup>-3</sup> mmol/m <sup>3</sup> )	SO <sub>2</sub> Ox. Rate (%/hr)	Liq Water (10 <sup>-3</sup> g/m <sup>3</sup> )	H <sub>2</sub> SO <sub>4</sub> in Droplets (mmol/g H <sub>2</sub> O)	(NH <sub>4</sub> ) <sub>2</sub> SO <sub>4</sub> in Droplets (mmol/g H <sub>2</sub> O)
Sulphur in Coal (Wt %)	2.5	14.3	19.3	3.2	7.7	2.5	0.039
	1.0	6.0	7.9	3.2	3.1	2.4	0.096
	0.5	3.2	4.0	3.2	1.6	2.4	0.189
Meteorological Stability Class	A	4.8	6.3	3.2	2.6	2.4	0.12
	C	6.0	7.9	3.2	3.1	2.4	0.096
	F	14.8	19.7	3.2	6.5	3.0	0.046
Wind Speed (m/sec)	1	9.8	25.3	3.2	9.0	2.8	0.033
	2	6.0	7.9	3.2	3.1	2.4	0.096
	4	3.5	2.5	3.2	1.0	2.2	0.29
	8	2.0	0.84	3.2	0.32	1.7	0.93
Ambient OH (10 <sup>-8</sup> mmol/m <sup>3</sup> )	10	3.9	28.2	16.0	11.2	2.5	0.027
	2	6.0	7.9	3.2	3.1	2.4	0.096
	0.5	6.4	3.0	0.8	1.2	2.3	0.26
	0.1	6.6	1.6	0.16	0.60	2.1	0.50
Ambient NH <sub>3</sub> (10 <sup>-4</sup> mmol/m <sup>3</sup> )	20	6.0	7.9	3.2	3.0	2.3	0.33
	6	6.0	7.9	3.2	3.1	2.4	0.096
Ambient Temp. (°C)	18.33	6.0	7.9	3.2	740	0.010	0.00040
	19.44	6.0	7.9	3.2	14	0.54	0.021
	21.11	6.0	7.9	3.2	3.1	2.4	0.096



Table V (continued)

Input Values <sup>a, b</sup>	Output Values at 25 km From Stack <sup>c</sup>					
	SO <sub>2</sub> (10 <sup>-2</sup> mmol/m <sup>3</sup> )	Sulfate (10 <sup>-3</sup> mmol/m <sup>3</sup> )	SO <sub>2</sub> Ox. Rate (%/hr)	Liq Water (10 <sup>-3</sup> g/m <sup>3</sup> )	H <sub>2</sub> SO <sub>4</sub> in Droplets (mmol/g H <sub>2</sub> O)	(NH <sub>4</sub> ) SO <sub>4</sub> in Droplets (mmol/g H <sub>2</sub> O)
Ambient Temp.	23.89	7.9	3.2	1.6	4.7	0.18
(°C)	26.67	7.9	3.2	1.2	6.5	0.25
	29.44	7.9	3.2	0.95	7.9	0.31

<sup>a</sup>Underscored numbers are the reference values. Each alternate value was taken while all other input values at the reference values.

<sup>b</sup>Other input values were: Wt % carbon in coal = 82.6; Wt % Hydrogen in coal 6.9%; Combustion rate = 100 Kg coal/sec; Effective stack height = 400 m; Deposition velocity = 0.01 m/sec; ambient water concentration = 930 mmol/m<sup>3</sup>.

<sup>c</sup>Concentrations are averages across the plume (See Appendix B).



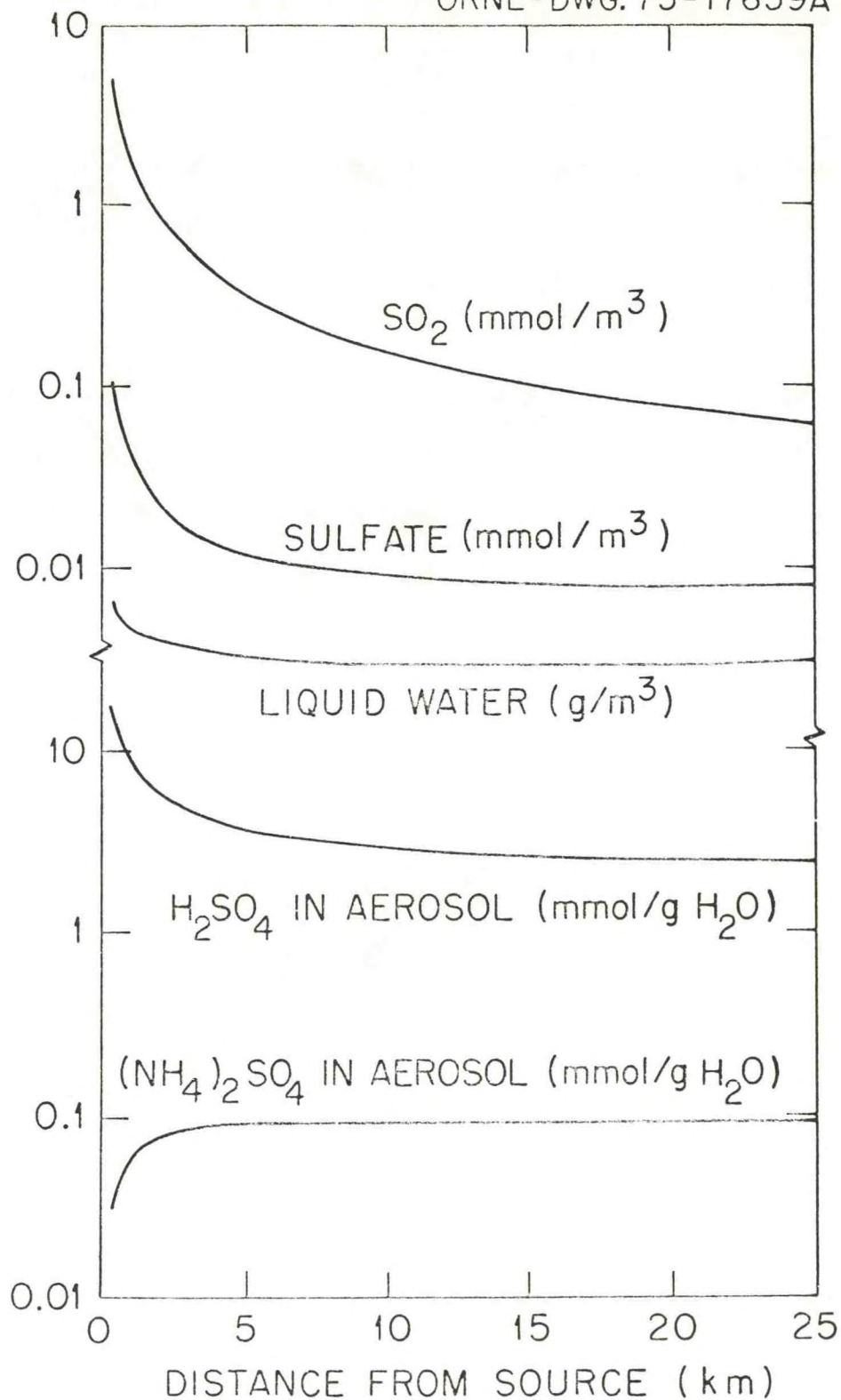


Fig. 2 Quantities calculated by SULCAL for the reference case.

temperature because of the strong inverse effect of the temperature on the relative humidity (the total concentration of water in the ambient air was not varied). The amounts of  $\text{SO}_2$ , sulfuric acid and condensed water in the plume change directly as the sulfur emission rate, which here is varied by changing the sulfur content in the coal. Increased wind speed strongly decreases the concentrations of  $\text{SO}_2$ , sulfuric acid and liquid water.

Under all the conditions tested in Table V, only the OH radical is important in the oxidation of  $\text{SO}_2$  and the percentage of  $\text{SO}_2$  oxidized per hour depends almost entirely on the ambient concentration of the OH radical. This concentration is controlled at the assumed values by unspecified chemical reactions. The conditions under which the oxidation of  $\text{SO}_2$  species in the droplets (reactions 12 and 14) becomes significant may be determined as follows: The ratio of the rate of oxidation of  $\text{HSO}_3^-$  in solution by ozone ( $R_{\text{Oz}}$ ) to the rate of oxidation of gaseous  $\text{SO}_2$  by OH radical ( $R_{\text{OH}}$ ) is given approximately by

$$\frac{R_{\text{Oz}}}{R_{\text{OH}}} = (K_1 K_2 K_{13} k_{12}/k_{11}) \cdot RT \cdot \left( \frac{g_w P_{\text{O}_3}}{[\text{H}^+] P_{\text{OH}}} \right). \quad (43)$$

The ratio of the rates in solution of  $\text{SO}_3^{2-}$  oxidation by oxygen  $R_0$  to  $\text{HSO}_3^-$  oxidation by ozone is given by

$$\frac{R_0}{R_{\text{Oz}}} = \frac{K_3}{K_{13}} \left( \frac{k_{14}' + k_{14}'' [\text{H}^+]}{k_{12}} \right) / [\text{H}^+] P_{\text{O}_3}. \quad (44)$$

(Both these expressions are approximations because activity coefficients have been neglected.) With  $P_{\text{O}_3}$  and  $P_{\text{OH}}$  at their reference values ( $8 \cdot 10^{-8}$  and  $5 \cdot 10^{-13}$  atm, respectively) these ratios of rates at  $25^\circ\text{C}$

become

$$\frac{R_{Oz}}{R_{OH}} \approx 3 \cdot 10^{-5} \frac{g_w}{[H^+]} \quad (45)$$

and

$$\frac{R_O}{R_{OH}} \approx \frac{1 \cdot 10^{-6}}{[H^+]} + \frac{5 \cdot 10^{-3}}{[H^+]^{1/2}} \quad (46)$$

Thus the oxidation of  $HSO_3^-$  by ozone should become significant when the ratio  $g_w/[H^+]$  exceeds  $\sim 10^4$ . The rate of  $SO_3^{2-}$  oxidation by dissolved oxygen should then become significant when the pH exceeds  $\sim 4$ . Since  $g_w$  and  $[H^+]$  change in opposite directions and almost logarithmically with the relative humidity, the rate of oxidation of  $SO_2$  species in aerosol droplets increase rapidly in importance as the relative humidity increases (Fig. 3). This rate is also favored by conditions that produce a more complete neutralization of the acid droplets. In general, neutralization is favored by a lower sulfur emission rate and a lower OH radical concentration, both tending to reduce the rate of production of the acid  $SO_3$ . It is favored as well by a high ambient concentration of ammonia and a high wind speed, both tending to deliver more ammonia to the acid droplets.

We emphasize that, in addition to the approximations in the present model arising from the use of averaged concentrations in the plume, the oxidation mechanisms are oversimplified and incomplete. The concentration of OH radical, which may often determine the rate of the most rapid oxidation reaction, is controlled by other chemical reactions not included in the model. The species of  $SO_2$  in solution oxidized by ozone may include others in addition to (or perhaps instead of)  $HSO_3^-$ .



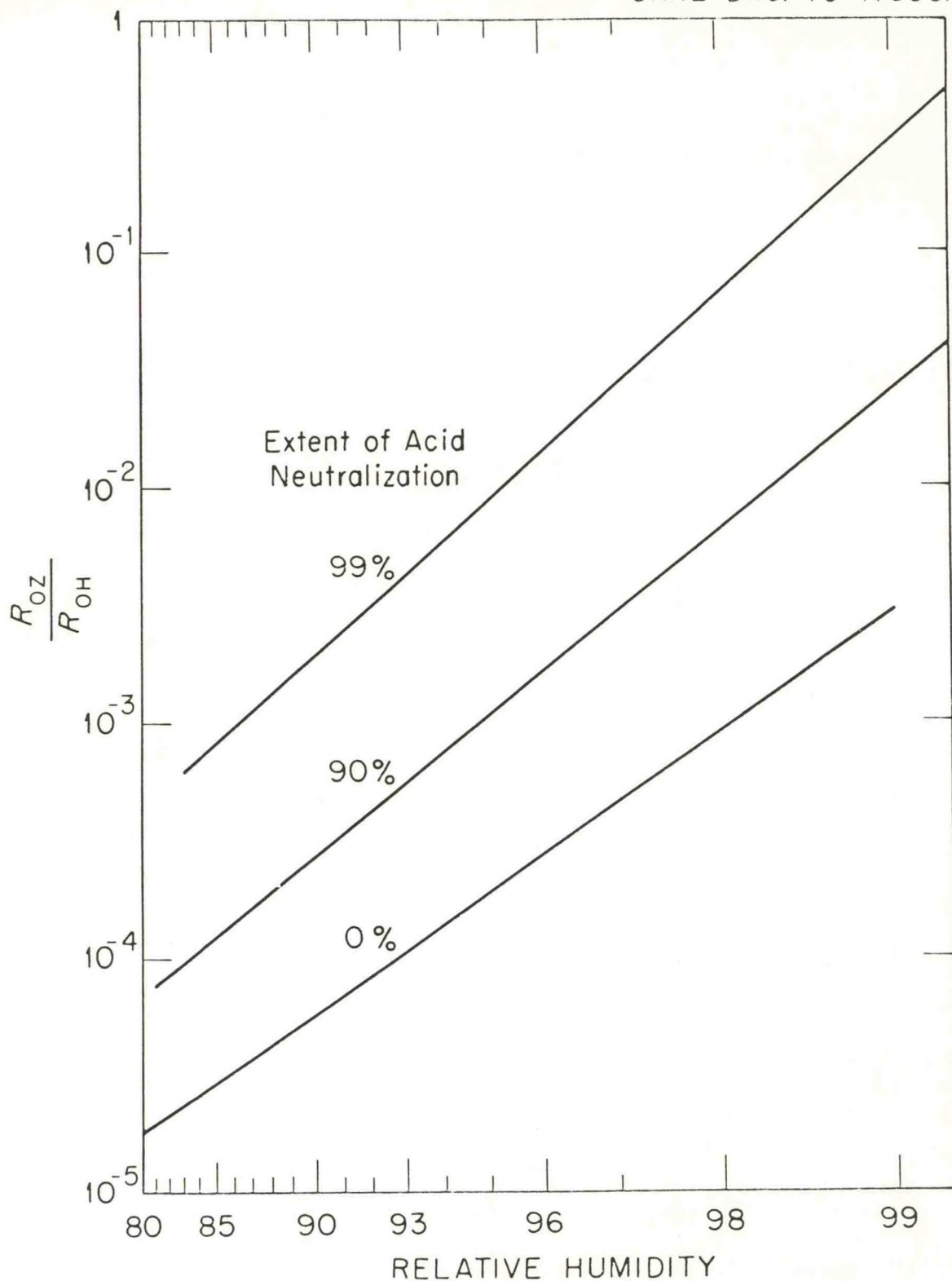


Fig. 3 The effect of the relative humidity and the extent of acid neutralization on the ratio of the rates of  $SO_2$  oxidation by ozone ( $R_{Oz}$ ) and by hydroxyl radical ( $R_{OH}$ ) at  $25^\circ C$ .

The oxidation of  $\text{SO}_3^{2-}$  by oxygen can be catalyzed or poisoned by certain metal ions in solution. Finally, possible catalytic oxidation of  $\text{SO}_2$  at the surface of solid particles and droplets has not been included. It does not seem worthwhile to include all such effects at present, nor may it be so even when sufficient knowledge has been gained. As more information does become available, however, it will be relatively easy to modify the rate expressions in the S. RATOX and to add others as may be desired.

#### ACKNOWLEDGEMENT

We are indebted to M. R. Patterson for many useful discussions during the course of this work.

## REFERENCES

1. (a) M. T. Mills and M. Reeves, "A Multi-Source Atmospheric Transport Model for Deposition of Trace Contaminants", ORNL/NSF/EATC-2 (1973); (b) W. M. Culkowski and M. R. Patterson, "A Comprehensive Atmospheric Transport and Diffusion Model", ORNL/NSF/EATC-17 (1976).
2. "Selected Values of Chemical Thermodynamic Properties", NBS Technical Note 270-3, 1968.
3. A. W. Castleman, Jr., R. E. Davis, H. R. Munkelwitz, I. N. Tang, and William P. Wood, "Kinetics of Association Reactions Pertaining to  $\text{H}_2\text{SO}_4$  Aerosol Formation", in International J. of Chemical Kinetics, Chem. Kinetics Symposium No. 1, S. W. Benson, D. N. Golden, and J. R. Baker, Eds., Interscience, New York, 1975, p. 543.
4. D. D. Davis and G. Klauber, "Atmospheric Gas-Phase Oxidation Mechanism for the Molecule  $\text{SO}_2$ ", in International J. of Chemical Kinetics, Chem. Kinetics Symposium No. 1, S. W. Benson, D. N. Golden and J. R. Baker, Eds., Interscience, New York, 1975, p. 629.
5. C. C. Wang, L. I. Davis, Jr., C. H. Wu, S. Japar, H. Niki, and B. Weinstock, Science, 189, 797 (1975).
6. S. A. Penkett, Nature Physical Science, 240, 105 (1972).
7. H. A. C. McKay, Atmospheric Environment, 5, 7 (1971).
8. E. C. Fuller and R. H. Crist, J. Am. Chemical Soc., 63, 1644 (1941).
9. A subroutine for performing a Runge-Kutta Integration of simultaneous first order differential equations, written by F. D. Hammerling, Computer Technology Center, Union Carbide Corp., Nuclear Div., Oak Ridge, Tn.



10. A subroutine for solving a system of simultaneous equations by the secant method, written by R. E. Funderlic and J. Rinzel, Computer Technology Center, Union Carbide Corp., Nuclear Div., Oak Ridge, Tn.
11. R. P. Hosker, Jr., "Estimates of Dry Deposition and Plume Depletion Over Forests and Grassland", Environmental Research Laboratories, Air Resources. Atmospheric Turbulence and Diffusion Laboratory, Oak Ridge, Tn., IAEA-SM-181/19.
12. R. A. Scriven, "Properties of the Probable Ground Level Concentration from an Elevated Source", Laboratory Note No. RD111N-61/65, Central Electric Research Laboratory, Oct. 13, 1975.
13. K. S. Pitzer and L. Brewer, revised ed., "Thermodynamics", by G. N. Lewis and M. Randall, McGraw Hill, New York, 1961.
14. K. S. Pitzer, J. Phys. Chem., 77 (2), 268 (1973).
15. R. A. Robinson and R. H. Stokes, "Electrolyte Solutions", 2nd ed., rev., Butterworths, London, 1965.
16. T. F. Young, L. F. Maranville, and H. M. Smith, "Raman Spectral Investigations of Ionic Equilibria in Solutions of Strong Electrolytes" in The Structure of Electrolyte Solutions, W. J. Hamer, Ed., John Wiley & Sons, Inc., New York, 1959.
17. A. Seidell, "Solubilities", 4th ed., rev. by W. F. Linke, Amer. Chem. Soc., 1965.

APPENDIX A

Program SULCAL

## 1. Partial List of Symbols

<u>In Text</u>	<u>Definition</u>	<u>In Program</u>
$a_w$	Activity of water	AWI
$B_{JK}^0, B_{JK}^1$	Parameters for calculating interaction coefficients between cation J and anion K $B_{JK}^0 = B(1,J,K)$ $B_{JK}^1 = B(2,J,K)$	B(I,J,K)
B	Correction factors (Eq. 17) for reflection of plume from ground, for short-time (BETAS) and time-averaged (BETAL) plumes	BETAS, BETAL
$C_i$ or C(i)	Total concentration of component; (mmol/m <sup>3</sup> )	QC(I)
$C_s$	Concentration of (NH <sub>4</sub> ) <sub>2</sub> SO <sub>4</sub> particles in plume (mmol/m <sup>3</sup> )	CSS
ERRR	Error limit employed in S. KUTTA	ERRR
f	Factor relating short-time and long-time sigmas (Eq. 22, App. B)	FLS
$g_i$	Activity coefficient of an ion; $G(1,1) = g_{H^+}, G(1,2) = g_{NH_4^+},$ $G(2,1) = g_{X^-}, G(2,2) = g_{X^{2-}}$	G(I,J)
$g_w$	Concentration of condensed water in plume (g H <sub>2</sub> O/m <sup>3</sup> )	CGW
Y	Factor (Eq. 20) which corrects effective plume concentration to ground level concentrations	GAMMA
$P_j$	Pressure of a gaseous constituent (atm)	P(J)
$P_w^0$	Vapor pressure of pure water (atm)	PWO
$\phi$	Osmotic coefficient of aerosol droplets (Eq. 4, App. C)	P
$Q_i$	Emission rate of component: (mmol/sec)	Q(I)
R	The gas constant (m <sup>3</sup> mmol <sup>-1</sup> °K <sup>-1</sup> )	R



<u>In Text</u>	<u>Definition</u>	<u>In Program</u>
$\frac{1}{RT}$	Factor for conversion of pressure (atm) to concentration (mmol/m <sup>3</sup> )	CONST
$\sigma_{l,y}^*, \sigma_{l,z}^*$	Time-averaged dispersion coefficients for a point source	SGPY, SGPZ
$c^o$	Correction which makes $\sigma_y$ and $\sigma_z$ finite at $x = 0$ (Eq. 18)	SGO
$\sigma_{l,y}, \sigma_{l,z}$	Time-averaged dispersion coefficient (m)	SGLY, SGLZ
$\sigma_{s,y}, \sigma_{s,z}$	Short-time dispersion coefficient (m)	SGSY, SGSZ
T	Absolute temperature of plume (°K)	T
$u_x$	Wind velocity (m/sec)	UX
$v_d^g, v_d^p$	Disposition velocity for gases and particles (m/sec)	VDG, VDP
$v_p$	Effective volume (m <sup>3</sup> /sec) (the effective volume of a length of plume equal to $u_x$ , the wind velocity in m/sec). VRG is calculated using short-time dispersion coefficients and VLG is calculated with time-averaged dispersion coefficients	VRG, VLG
$v_p^o$	Gas flow rate at mouth of stack (m <sup>3</sup> /sec)	VRGO
x	Distance (m) from source in wind direction	X

## 2. Program Listing

```

C PROGRAM FOR CALCULATION OF CHEMICAL FORMS OF SULFUR IN AND THEIR      BLCK
C DEPOSITION FROM A PLUME                                                BLCK
    BLOCK DATA                                                            BLCK
        IMPLICIT REAL*8 (A-H,O-Z)                                         BLCK
C R = GAS CONSTANT (M**3/ATM/K,MMOL)                                     BLCK
C PI = 3.1416, FLN = LN(10), FMW = GMS H2O/MMOL                         BLCK
C R(I,J,K) = INTERACTION COEF'S. OF CATION I WITH ANION J, TWO        BLCK
C PARAMETERS FOR EACH IJ PAIR                                           BLCK
C Z = ION CHARGE (FIRST SUBSCRIPT IS 1 FOR CATIONS AND 2 FOR ANIONS)    BLCK
        COMMON/PLK/R,PI,FLN,FMW,B(4,4,2),Z(2,4)                          BLCK
        DATA B(1,1,1),B(1,1,2),B(1,2,1),B(1,2,2),B(2,1,1),          BLCK
        &B(2,1,2),B(2,2,1),B(2,2,2)                                       BLCK
        &C(1,2722D+0,3.0803D+0,0.0502D+0,-4.0054D+0,0.0D+0,C.319D+C,    BLCK
        &-0.04873D+0,-1.18580D+0/                                           BLCK
        DATA PI,FLN,R,FMW/3.1415927D+0,2.302585D+0,82.0597D-9,18.0153D-3/ BLCK
        &Z(1,1),Z(1,2),Z(2,1),Z(2,2)/1.0D+C,1.0D+C,-1.0D+C,-2.0D+0/    BLCK
        END                                                                BLCK
C
C MAIN PROGRAM                                                            MAIN
    IMPLICIT REAL*8 (A-H,O-Z)                                             MAIN
    EXTERNAL RATE                                                         MAIN
    COMMON/BLK/R,PI,FLN,FMW,B(4,4,2),Z(2,4)                             MAIN
C NOX = TOTAL NUMBER OF TIMES S. RATE IS ENTERED FOR A GIVEN CASE      MAIN
    COMMON/CASE/NOX                                                       MAIN
    COMMON/RTX/NSC,NRL,VRG0,TP,H,UX,A(7),TA,DELX,VDG,VDP               MAIN
    COMMON/SIGMA/SG0,SGPY,SGPZ,SGLY,SGLZ,SGSY,SGSZ,BEIAL,BETAS          MAIN
    COMMON/ARG/CGW,PH,CSS,C(2,4),T,RTT,RTOH,RTOZ,RTO,NCAL,NITN          MAIN
    COMMON/EQK/EKN,EK1N,EKC,EK1C,EK2C,EKS,EK1S,EK2S,EK3S,EKSS,EKW       MAIN
    COMMON/CON/CMH,CMN,CM1N,CMC,CM1C,CM2C,CMS,CM1S,CM2S,CM3S,CM4S,      MAIN
    &PN,PC,PS                                                             MAIN
    COMMON/ACT/DHA,G(2,4),P,PWO,CONST                                    MAIN
    COMMON/GIVN/WPCTC,WPCTH,WPCTS,QCOAL,FCTS6,EXAIR,FCON,TCP,TCA,       MAIN
    &XLAST,XNEXT,ERRR                                                    MAIN
    COMMON/VAP/QC(7)                                                      MAIN
    DIMENSION Q(7),FDMY(7),XINCR(50)                                     MAIN
C WPCTI=WT. % OF ELEMENT I IN COAL                                       MAIN
C QCOAL=COMBUSTION RATE IN KG/SEC                                         MAIN
C PCTS6=FRAC OF S CONVERTED TO S(VI),EXAIR=FACTION OF EXCESS AIR USED   MAIN
C FCON=NO.OF MOLES OF WATER CONDENSED/MOLE SO3, TCP=TEMP OF EXIT GAS (C)  MAIN
C H=APPARENT STACK HEIGHT IN METERS                                       MAIN
    1 READ(20,100) WPCTC,WPCTH,QCOAL,FCTS6,EXAIR,FCON,TCP,H            MAIN
C STABILITY CLASS,ROUGHNESS LENGTH,WIND SPEED (M/SEC)                   MAIN
C AND AMBIENT CONCENTRATIONS (MMOL/M**3) AND TEMPERATURE (C)            MAIN
    2 READ(20,100) NSC,NRL,UX,VDG,VDP,(A(I),I=1,7),TCA,WPCTS           MAIN
C CALCULATE MOLES OF GASES PER KG OF COAL BURNED                         MAIN
    RMLC=WPCTC/1.200115                                                  MAIN
    RMLW=0.5*WPCTH/0.100797                                              MAIN
    RMLS4=(WPCTS/3.2064)*(1.0-PCTS6)                                     MAIN
    RMLS6=(WPCTS/3.2064)*PCTS6                                           MAIN
C CALCULATE MOLES OF OXYGEN CONSUMED PER KG OF COAL BURNED              MAIN
    CMLO2=RMLC+0.5*RMLW+RMLS4+1.5*RMLS6                                  MAIN
C CALCULATE TOTAL MOLES OF EFFLUENT GAS PER KG OF COAL BURNED           MAIN
    RMLGAS=RMLC+RMLW+RMLS4+((79.05/20.95)*(1.0+EXAIR)+EXAIR)*CMLO2    MAIN
    &-FCON*RMLS6                                                         MAIN
    TP=TCP+273.15                                                         MAIN
    TA=TCA+273.15                                                         MAIN
C CALCULATE RATE OF EMISSION OF GAS (M**3/SEC)                           MAIN
    VRG0=RMLGAS*QCOAL*(82.0597D-6)*TP                                    MAIN

```



C CALCULATE EMISSION RATES OF COMPONENTS IN MMOLS/SEC	MAIN
BNFCT=1000.0*QCCAL	MAIN
Q(1)=RMLS4*BNFCT	MAIN
Q(2)=RMLS6*BNFCT	MAIN
Q(3)=0.0	MAIN
Q(4)=0.0	MAIN
Q(5)=RMLC*BNFCT	MAIN
Q(6)=0.0	MAIN
Q(7)=RMIW*BNFCT	MAIN
NOX=1	MAIN
C READ FIRST VALUE OF X (*), DELTA X AND ERROR LIMIT	MAIN
READ(20,100) XNEXT,DELX,ERRR	MAIN
C READ NO. OF STEPS IN X AND THE SIZE OF EACH	MAIN
READ(20,100) NX,(XINCR(I),I=1,NX)	MAIN
NCAL=0	MAIN
NITN=0	MAIN
C CALCULATE CONCENTRATIONS AT STARTING VALUE OF X (MMOLS/M**3)	MAIN
CALL SIG(XNEXT,VRG,FEX)	MAIN
DO 10 I=1,7	MAIN
QC(I)=Q(I)/VRG+A(I)*(1.0-VRG0/VRG)	MAIN
10 CONTINUE	MAIN
CALL PRINT(1)	MAIN
C START CALCULATION OF QC(I) VS. X	MAIN
DO 20 I=1,NX	MAIN
XLAST=XNEXT	MAIN
XNEXT=XNEXT+XINCR(I)	MAIN
CALL KUTTA(XLAST,XNEXT,QC,7,DELX,ERRR,40,FATE)	MAIN
20 CONTINUE	MAIN
C CALL RATE FOR FINAL CALCULATION OF PLUME COMPOSITION	MAIN
CALL RATE(XNEXT,QC,PDMY,1)	MAIN
XLAST=XNEXT	MAIN
CALL PRINT(2)	MAIN
GO TO 2	MAIN
100 FORMAT(7G10.0)	MAIN
END	MAIN
C	
C SUBROUTINE TO CALCULATE EFFECTIVE VOLUME OF PLUME (VRG)	SIG
C AND THE DEPOSITION FACTOR (FEXD)	SIG
C CALCULATION OF SIGMA(Y) AND SIGMA(Z) ACCORDING TO HOSKER	SIG
SUBROUTINE SIG(X,VRG,FEXD)	SIG
IMPLICIT REAL*8(A-H,O-Z)	SIG
DIMENSION GC3(6),GA1(6),GB1(6),GA2(6),GB2(6),GC1(6),GD1(6),FCTL(6)	SIG
COMMON/CASE/NOX	SIG
COMMON/PTE/NSC,NRL,VRG0,TP,H,UX,A(7),TA,DELX,VDG,VEP	SIG
COMMON/SIGMA/SG0,SGPY,SGPZ,SGLY,SGLZ,SGSY,SGSZ,BETAL,BETAS	SIG
DATA GC3/0.22D+0,0.16D+0,0.11D+0,0.08D+0,0.06D+0,	SIG
80.04D+0/	SIG
DATA GA1/0.112D+0,0.130D+0,0.112D+0,0.098D+0,	SIG
80.0609D+0,0.0638D+0/	SIG
DATA GB1/1.06D+0,0.950D+0,0.920D+0,0.889D+0,0.895D+0,	SIG
80.783D+0/	SIG
DATA GA2/0.000538D+0,0.000652D+0,0.000905D+0,	SIG
80.00135D+0,0.00196D+0,0.00136D+0/	SIG
DATA GB2/0.815D+0,0.750D+0,0.718D+0,0.688D+0,0.684D+0,	SIG
80.672D+0/	SIG
DATA GC1/1.56D+0,2.02D+0,2.71828D+0,5.16D+0,7.37D+0,	SIG
811.7D+0/	SIG
DATA GD1/0.048CD+0,0.0269D+0,0.0D+0,-0.06D+0,-0.0957D+C	SIG



E, -0.128D+0/	SIG
DATA FCTL/5.0D+2, 2.5D+2, 1.0D+2, 0.5D+2, 0.2D+2, 0.1D+2/	SIG
C UPON FIRST ENTRY ASSIGN VALUES TO PARAMETERS THAT DEPEND ON STABILITY	SIG
C CLASS, ROUGHNESS LENGTH, AND WIND SPEED	SIG
IF (NOX.GT.1) GO TO 1	SIG
PI=3.1415927	SIG
C3=GC3 (NSC)	SIG
A1=GA1 (NSC)	SIG
B1=GB1 (NSC)	SIG
A2=GA2 (NSC)	SIG
B2=GB2 (NSC)	SIG
C1=GC1 (NRL)	SIG
D1=GD1 (NRL)	SIG
RL=FCTL (NSC)	SIG
PLS=DSQRT (X/(X+50.0*RI))	SIG
SGO=DSQRT (VRGO/(4.0*PI*UX))	SIG
C CALCULATE POINT-SOURCE TIME-AVERAGED SIGMA (Y)	SIG
1 DTY=1.0+0.001*X	SIG
SGPY=C3*X/DSQRT (DTY)	SIG
F=DLOG (C1*X**D1)	SIG
G=A1*X**B1/(1.0+C+A2*X**B2)	SIG
C CALCULATE POINT-SOURCE TIME-AVERAGED SIGMA (Z)	SIG
SGPZ=F*G	SIG
C CALCULATE TIME-AVERAGED SIGMA (Y) AND SIGMA (Z) FOR REAL SOURCE	SIG
SGLY=SGPY+SGO	SIG
SGLZ=SGPZ+SGO	SIG
C CALCULATE SHORT-TIME SIGMA (Y) AND SIGMA (Z) FOR REAL SOURCE	SIG
SGSY=PLS*SGPY+SGO	SIG
SGSZ=PLS*SGPZ+SGO	SIG
C EVALUATE CORRECTION FACTOR BETA	SIG
EXFS=-(H/SGSZ)**2	SIG
IF (EXFS.LT.-25.0) EXFS=-25.0	SIG
EXFL=-(H/SGLZ)**2	SIG
IF (EXFL.LT.-25.0) EXFL=-25.0	SIG
BETAL=1.0/(1.0+0.70711*DEXP (EXFL))	SIG
BETAS=1.0/(1.0+0.70711*DEXP (EXFS))	SIG
C CALCULATE EFFECTIVE REACTION VOLUME VRG (M**3)	SIG
C AND EFFECTIVE DEPOSITION VOLUME VLG (M**3)	SIG
VRG=4.0*PI*SGSY*SGSZ*UX*BETAS	SIG
VLG=4.0*PI*SGLY*SGLZ*UX*BETAL	SIG
C CALCULATE FACTOR RELATED TO DRY DEPOSITION	SIG
GAMA=DSQRT (2.0/PI)/SGLZ*DEXP (EXFL/2.0)	SIG
FFXD= (VRG/VLG)*GAMA	SIG
RETURN	SIG
END	SIG
C	
C SUBROUTINE CALLED BY KUTTA TO CALCULATE RATE OF CHANGE OF COMPONENT	RATE
C CONCENTRATIONS YI(I) WITH DISTANCE X (DYDX)	RATE
C IN = INTEGER WHICH (WHEN 1) SIGNALS CALCULATION OF DYDX AT X	RATE
SUBROUTINE RATE (X, YI, DYDX, IN)	RATE
IMPLICIT REAL*8 (A-H, O-Z)	RATE
DIMENSION YI (7), DYDX (7)	RATE
COMMON/BLK/R, PI, PLN, FMW, B (4, 4, 2), Z (2, 4)	RATE
COMMON/CASE/NOX	RATE
COMMON/RTE/NSC, NRL, VRGO, TP, H, UX, A (7), TA, DELX, VDG, VDP	RATE
COMMON/ARG/CGW, PH, CSS, C (2, 4), T, RTT, RTOH, RTOZ, RTO, NCAL, NITN	RATE
COMMON/CON/CMH, CMN, CM1N, CM1C, CM2C, CM3S, CM1S, CM2S, CM3S, CM4S,	RATE
EPN, PC, PS	RATE

```

COMMON/ACT/DHA,G(2,4),P,PW0,CONST
COMMON/VAR/Y(7)
DO 10 I=1,7
Y(I)=YI(I)
10 CONTINUE
C HAVE DROPLETS DRIED UP?
IF(CGW.LE.0.0) GO TO 2
C ESTIMATE STARTING VALUES OF CGW,PH,CSS, AND ACTIVITY COEFFICIENTS
CALL EXPCT(NOX,IN,X,CGW,PH,CSS,C(1,2),C(2,1),C(2,2))
C EVALUATE DLN(V)/D(X) NUMERICALLY
2 X1=X+DELX/2.0
X2=X-DFLX/2.0
CALL SIG(X,VRG,FEXD)
CALL SIG(X1,VRG1,FEX)
CALL SIG(X2,VRG2,PEX)
DLVDX=2.0*(VRG1-VRG2)/(DELX*(VRG1+VRG2))
C CALCULATE TEMPERATURE IN PLUME (K)
T=TA/(1.0-(1.0-TA/TP)*VRG0/VRG)
CONST=1.0/(R*T)
C CALCULATE RATE OF OXIDATION OF S(IV)
CALL RATOX
NOX=NOX+1
C CALCULATE DYDX(I)
DYDX(1)=-(RTT*(PS*CONST*(VDG-VDP)+Y(1)*VDP)*FEXD)/UX
DYDX(2)=(RTT-Y(2)*VDP*FEXD)/UX
DYDX(3)=-RTOZ/UX
DYDX(4)=0.0
DYDX(5)=0.0
DYDX(6)=-(PN*CONST*(VDG-VDP)+Y(6)*VDP)*FEXD/UX
DYDX(7)=-CGW/FMW*VDP*FEXD/UX
DO 1 I=1,7
DYDX(I)=DYDX(I)-(Y(I)-A(I))*DLVDX
1 CONTINUE
RETURN
END
C
C SUBROUTINE TO CALCULATE RATE OF S(IV) OXIDATION
SUBROUTINE RATOX
IMPLICIT REAL*8(A-H,O-Z)
EXTERNAL IVAL
EXTERNAL EVAL
DIMENSION X(10)
COMMON/BLK/R,PI,FLN,FMW,B(4,4,2),Z(2,4)
COMMON/CASE/NOX
COMMON/ARG/CGW,PH,CSS,C(2,4),T,RTT,RTOH,RTOZ,PTO,NCAL,NITN
COMMON/FQK/FKN,EK1N,EKC,EK1C,EK2C,EKS,EK1S,EK2S,EK3S,EKSS,EKW
COMMON/CON/CMH,CMN,CM1N,CMC,CM1C,CM2C,CMS,CM1S,CM2S,CM3S,CM4S,
6FN,PC,PS
COMMON/ACT/DHA,G(2,4),P,PW0,CONST
COMMON/VAR/C4,C6,COZ,COH,CC,CN,CW
C CONSTANTS FOR THE CALCULATION OF RATE AND EQUILIBRIUM CONSTANTS
C AS A FUNCTION OF THE TEMPERATURE
DATA EKN0,EKNT,EKC0,EKCT,EKS0,EKST,EK1N0,EK1NT,
6EK1S0,EK1ST,EK2S0,EK2ST,EK1C0,EK1CT,EK2C0,EK2CT,EK3S0,
6EK3ST,EKSS0,EKSS1,EKW0,EKWT,EKOZ0,EKOZT,RK10,RK1T,RK20,RK2T,
6RK30,RK3T,RK40,RK4T,EPW0,EPWT
6/-4.233D+0,1.7855D+0,-5.016D+0,1.05974D+0,-4.4912D+0,1.3659D+0,
60.1026D+0,2.7275D+0,-4.815D+0,0.9054D+0,-8.8549D+0,0.48736D+0,

```



```

6-5.030D+0,-0.39885D+0,-7.7260D+0,-0.77585D+C,-5.8348D+0,1.1452D+0,
80.929D+0,-0.3431D+0,-4.2134D+0,-2.91654D+C,-8.488D+0,1.891D+C,
811.4378D+0,-3.9725D+0,15.0947D+0,-3.9725D+0,14.61D+0,-2.57D+0,
52.65D+0,0.0D+0,6.2057D+0,-2.2989D+0/
C ALL CONCENTRATIONS ARE IN MMOL/L/METER**3 OR MMOL/G
C CALCULATE TEMPERATURE DEPENDENT PARAMETERS
PT=1000.0/T
DPA=(4.91D-1+8.0D-4*(T-273.15))*FLN
EKN=DEXP((EKN0+EKNT*PT)*FLN)
EKC=DEXP((EKC0+EKCT*PT)*FLN)
EKS=DEXP((EKS0+EKST*PT)*FLN)
EK1N=DEXP((EK1N0+EK1NT*PT)*FLN)
EK1S=DEXP((EK1S0+EK1ST*PT)*FLN)
EK2S=DEXP((EK2S0+EK2ST*PT)*FLN)
EK1C=DEXP((EK1C0+EK1CT*PT)*FLN)
EK2C=DEXP((EK2C0+EK2CT*PT)*FLN)
EK3S=DEXP((EK3S0+EK3ST*PT)*FLN)
EKSS=DEXP((EKSS0+EKSST*PT)*FLN)
FKW=DEXP((EKWC+EKWT*PT)*FLN)
EKOZ=DEXP((EKOZ0+EKOZT*PT)*FLN)
RK1=DEXP((RK10+RK1T*PT)*FLN)
RK2=DEXP((RK20+RK2T*PT)*FLN)
RK3=DEXP((RK30+RK3T*PT)*FLN)
RK4=DEXP((RK40+RK4T*PT)*FLN)
PW0=DEXP((EPW0+EPWT*PT)*FLN)
C TFST TO SEE IF CGW AND PH ARE GIVEN
IF(NOX.GT.1) GO TO 1
CSS=0.0
C ESTIMATE STARTING VALUES OF CGW, ION CON'NS AND GAMAS
PNI=3.0
TB=(PW0*CONST-CW+PNI*C6)/2.0
TC=-PNI*C6*CW
CGW=FMW*(-TB+DSQRT(TB**2-TC))
X(1)=DLOG10(CGW)
G(1,1)=1.0
G(2,1)=1.0
G(2,2)=1.0
CALL NONLIN(X,1,ICONV,IVAL)
CGW=DEXP(X(1)*FLN)
PH=-DLOG10(C(1,1))
C BEGIN REFINEMENT
C HAVE DROPLETS DRIED OUT?
1 IF(CGW.LE.0.0) GO TO 10
X(1)=DLOG10(CGW)
X(2)=PH
C ARE DROPLETS UNSATURATED?
IF(CSS.LE.0.0) GO TO 2
C IS ENOUGH ACID PRESENT TO PREVENT DRYING OUT OF DROPLETS?
IF(CN/C6.LT.2.0) GO TO 4
10 CGW=0.0
CSS=C6
RTO=0.0
RTOZ=0.0
PS=C4/CONST
PN=(CN-2.0*CSS)/CONST
PC=CC/CONST
GO TO 11
2 CSS=0.0

```



CALL NONLIN(X,2,ICONV,EVAL)	RTCX
C IS SOLUTION SUPERSATURATED WITH (NH4)2SO4?	RTCX
GFS=G(1,2)**2*G(2,2)	RTOX
DSS=CM1N**2*CM4S*GFS-FKSS	RTOX
IF(DSS.LT.0.0) GO TO 6	RTCX
C IS ENOUGH ACID PRESENT TO PREVENT DRYING OUT OF DROPLETS?	RTOX
IF((CN/C6).LT.2.0.AND.CGW.GT.1.0D-8) GO TO 3	RTOX
GO TO 10	RTCX
C ESTIMATE AMOUNT OF SOLID (NH4)2SO4	RTOX
3 CSS=DSS*CGW/((CM1N+4.0*CM4S)*CM1N*GFS)	RTOX
IF((CN-2.0*CSS).GT.0.0) GO TO 4	RTCX
CSS=0.4*CN	RTOX
4 X(3)=DLOG10(CN/(CN-2.0*CSS))	RTOX
CALL NONLIN(X,3,ICONV,EVAL)	RTCX
C HAS SOLUTION BECOME UNSATURATED WITH (NH4)2SO4?	RTOX
IF(X(3).LE.0.0) GO TO 2	RTOX
C HAVE DROPLETS DRIED UP?	RTOX
IF(CGW.LE.1.0D-8) GO TO 10	RTOX
CSS=CN/2.0*(1.0-DEXP(-X(3)*FLN))	RTOX
6 CGW=DEXP(X(1)*FLN)	RTOX
PH=X(2)	RTCX
CMH=DEXP(-PH*FIN)	RTOX
C BEGIN CALCULATION OF RATE OF OXIDATION OF S(IV)	RTOX
C RATE OF OXIDATION OF SO32- BY OXYGEN IN SOLUTION (MMOL/M**3/SEC)	RTCX
RQ1=RK1*G(2,2)	RTOX
RQ2=RK2*G(1,1)**0.5*G(2,2)	RTOX
RTO=(RQ1+RQ2*CMH**0.5)*CM2S*CGW	RTCX
C RATE OF OXIDATION OF HSO3- BY OZONE IN SOLUTION (MMOL/M**3/SEC)	RTOX
RQ3=RK3*G(2,1)	RTOX
CMOZ=EKOZ*COZ/(CONST+EKOZ*CGW)	RTOX
RTOZ=RQ3*CMOZ*CM1S*CGW	RTOX
C RATE OF OXIDATION OF SO2 BY OH RADICAL IN GAS PHASE (MMOL/M**3/SEC)	RTOX
11 RTOH=RK4*COH*PS*CONST	RTOX
C TOTAL OXIDATION RATE OF S(IV) (MMOL/METER**3/SEC)	RTOX
RTT=RTOH+RTOZ+RTO	RTCX
RETURN	RTOX
END	RTCX
C	
C SUBROUTINE TO REFINE CGW, PH, CSS BY SECANT METHOD	NLIN
SUBROUTINE NONLIN(XIN,N,ICONV,EVAL)	NLIN
C PROGRAM AUTHORS R. E. PUNDERLIC AND J. RINZEL,	NLIN
C COMPUTING TECHNOLOGY CENTER, UNION CARBIDE CORP., NUCLEAR DIV.,	NLIN
C OAK RIDGE, TENN.	NLIN
C	NLIN
C CTC OPD PROGRAM NO. 9066	NLIN
IMPLICIT REAL*8 (A-H,O-Z)	NLIN
LOGICAL WRT	NLIN
COMMON/HONON/WRT	NLIN
DIMENSION XIN(N),X(20,21),XBAR(20,2),A(21,21),AINV(21,21),P(21),	NLIN
1B(21),XNORM(21),BNORM(20)	NLIN
WRT=.FALSE.	NLIN
ICONV=0	NLIN
NP1=N+1	NLIN
DO 110 J=1,NP1	NLIN
DO 120 I=1,N	NLIN
IF(J.NE.1) GO TO 130	NLIN
X(I,J)=XIN(I)	NLIN
GO TO 120	NLIN

130	X(I,J)=XIN(I)	NLIN
	IF(J-1.EQ.I) X(I,J)=0.005+X(I,J)	NLIN
120	CONTINUE	NLIN
110	CONTINUE	NLIN
	DO 1 J=1, NP1	NLIN
	B(J)=1.	NLIN
	A(NP1,J)=1.	NLIN
1	CALL EVAL(X(1,J),A(1,J))	NLIN
	DO 2 I=1, NP1	NLIN
	DO 2 J=1, NP1	NLIN
	AINV(I,J)=0.0D0	NLIN
	IF(I.EQ.J) AINV(I,J)=1.0D0	NLIN
2	CONTINUE	NLIN
	DO 4 J=1, NP1	NLIN
	SUM=0.	NLIN
	DO 3 I=1, N	NLIN
3	SUM=SUM+DABS(A(I,J))	NLIN
4	XNORM(J)=SUM	NLIN
	CALL MATINV(A,AINV,NP1)	NLIN
	DO 5 I=1, N	NLIN
5	XBAR(I,1)=X(I, NP1)	NLIN
	ITER=40	NLIN
	DO 15 K=1, ITER	NLIN
	XBNUM=0.	NLIN
	XBDEN=0.	NLIN
	DO 7 I=1, N	NLIN
	XB=0.	NLIN
	DO 6 J=1, NP1	NLIN
6	XB=XB + AINV(J, NP1) * X(I, J)	NLIN
	XBAR(I,2)=XB	NLIN
	XBNUM=XBNUM + (XBAR(I,2)-XBAR(I,1))**2	NLIN
7	XBDEN=XBDEN + XBAR(I,2)**2	NLIN
	ICONV=ICONV+1	NLIN
	IF((XBNUM/XBDEN).LT.1.D-14) GO TO 16	NLIN
	DO 8 I=1, N	NLIN
8	XBAR(I,1)=XBAR(I,2)	NLIN
	BIGNOR=0.	NLIN
	DO 9 J=1, NP1	NLIN
	BNORM(J)=XNORM(J)*DABS(B(J))	NLIN
	IF(BNORM(J).LE.BIGNOR) GO TO 9	NLIN
	BIGNOR=BNORM(J)	NLIN
	JCOL = J	NLIN
9	CONTINUE	NLIN
	CALL EVAL(XBAR,P)	NLIN
	P(NP1)=1.	NLIN
	XNORM(JCOL)=0.	NLIN
	DO 10 I=1, N	NLIN
	X(I,JCOL)=XBAR(I,1)	NLIN
10	XNORM(JCOL)=XNORM(JCOL)+DABS(P(I))	NLIN
	DO 11 I=1, NP1	NLIN
	B(I)=0.	NLIN
	DO 11 J=1, NP1	NLIN
11	B(I)=B(I)+AINV(I,J)*P(J)	NLIN
	DO 13 I=1, NP1	NLIN
	IF(I.EQ.JCOL) GO TO 13	NLIN
	DO 12 J=1, NP1	NLIN
12	AINV(I,J)=AINV(I,J)-AINV(JCOL,J)*(B(I)/B(JCOL))	NLIN
13	CONTINUE	NLIN

DO 14 I=1,NP1	NLIN
14 AINV(JCOL,I)=AINV(JCOL,I)/B(JCOL)	NLIN
15 CONTINUE	NLIN
WRITE(20,101)	NLIN
101 FORMAT('1*****THE FOLLOWING CASE DID NOT CONVERGE*****')	NLIN
16 WRT=.TRUE.	NLIN
CALL EVAL(XBAR,P)	NLIN
DO 17 I=1,N	NLIN
17 XIN(I)=XBAR(I,2)	NLIN
RETURN	NLIN
END	NLIN
C	
SUBROUTINE MATINV(A,B,III)	MINV
IMPLICIT REAL*8 (A-H,C-Z)	MINV
DIMENSION A(21,21), B(21,21)	MINV
KK=III	MINV
NV=III	MINV
KKM=KK-1	MINV
DO9I=1,KKM	MINV
S=0.0	MINV
DO1J=1,KK	MINV
R=DABS(A(J,I))	MINV
IF(R.LT.S) GO TO 1	MINV
S=R	MINV
L=J	MINV
1 CONTINUE	MINV
IF(L.EQ.I) GO TO 5	MINV
IF(L-I) 2,5,2	MINV
2 DO3J=1,KK	MINV
S=A(I,J)	MINV
A(I,J)=A(L,J)	MINV
3 A(L,J)=S	MINV
DO4J=1,NV	MINV
S=B(I,J)	MINV
B(I,J)=B(L,J)	MINV
4 B(L,J)=S	MINV
5 IF(A(I,J).EQ.0.) GO TO 9	MINV
IPO=I+1	MINV
DO8J=IPO,KK	MINV
IF(A(J,I).EQ.0.) GO TO 8	MINV
S=A(J,I)/A(I,I)	MINV
A(J,I)=0.0	MINV
DO6K=IPO,KK	MINV
6 A(J,K)=A(J,K)-A(I,K)*S	MINV
DO7K=1,NV	MINV
7 B(J,K)=B(J,K)-B(I,K)*S	MINV
8 CONTINUE	MINV
9 CONTINUE	MINV
KMC=KK-1	MINV
DO11K=1,NV	MINV
B(KK,K)=B(KK,K)/A(KK,KK)	MINV
DO11I=1,KMO	MINV
N=KK-I	MINV
DO10J=N,KMO	MINV
10 B(N,K)=B(N,K)-A(N,J+1)*B(J+1,K)	MINV
11 B(N,K)=B(N,K)/A(N,N)	MINV
RETURN	MINV
END	MINV



```

C
C SUBROUTINE CALLED BY S NONLIN TO CALCULATE ION CONCENTRATIONS C(I),
C ACTIVITY COEFFICIENTS G(I), AND THE RESIDUAL IN THE WATER
C ACTIVITY BALANCE Y(1) FOR THE CURRENT VALUE OF CGW AS GIVEN BY X(1)
SUBROUTINE IVAL(X,Y)
IMPLICIT REAL*8 (A-H,O-Z)
DIMENSION X(10),Y(21)
COMMON/BLK/R,PI,FLN,FMW,B(4,4,2),Z(2,4)
COMMON/ARG/CGW,PH,CSS,C(2,4),T,RTT,RTCH,PTOZ,RTO,NCAL,NITN
COMMON/EQK/EKN,EK1N,EKC,EK1C,EK2C,EKS,EK1S,EK2S,EK3S,EKSS,EKW
COMMON/ACT/DHA,G(2,4),P,PW0,CONST
COMMON/VAR/C4,C6,COZ,COH,CC,CN,CW
CGW=DEXP(X(1)*FLN)
GHS=G(1,1)*G(2,2)/G(2,1)
QHS=EK3S/GHS
C BEGIN REFINEMENT OF ACTIVITY COEFFICIENTS AND ION CONCENTRATIONS
C FOR CURRENT VALUE OF X(1)
DO 10 I=1,100
BT=(QHS+(CN-C6)/CGW)/2.0
CT=QHS*(CN-2.0*C6)/CGW
C(1,1)=-BT+DSQRT(BT**2-CT)
C(1,2)=CN/CGW
TERM=C6/(CGW*(C(1,1)+QHS))
C(2,1)=C(1,1)*TERM
C(2,2)=QHS*TERM
QL=QHS
CALL GAMAW(DHA,2,2,B,C,Z,G,P,AWI)
GHS=G(1,1)*G(2,2)/G(2,1)
QHS=EK3S/GHS
IF((QL-QHS)/QHS)**2.1T.1.0D-12) GO TO 20
10 CONTINUE
20 RAW=(CW-CGW/FMW)/(PW0*CONST)
C CALCULATE RESIDUAL IN WATER ACTIVITY BALANCE
Y(1)=(AWI-RAW)*FMW*(C(1,1)+C(1,2)+C(2,1)+C(2,2))
RETURN
END
C
C SUBROUTINE,CALLED BY NONLIN, CALCULATES ION CONCENTRATIONS,
C ACTIVITY COEFFICIENTS AND RESIDUALS FOR CURRENT VALUES OF
C CGW,PH AND CSS AS GIVEN BY X(1),X(2), AND X(3)
SUBROUTINE EVAL(X,Y)
IMPLICIT REAL*8 (A-H,O-Z)
DIMENSION X(10),Y(21)
COMMON/BLK/R,PI,FLN,FMW,B(4,4,2),Z(2,4)
COMMON/CASE/NOX
COMMON/ARG/CGW,PH,CSS,C(2,4),T,RTT,RTCH,PTOZ,RTO,NCAL,NITN
COMMON/EQK/EKN,EK1N,EKC,EK1C,EK2C,EKS,EK1S,EK2S,EK3S,EKSS,EKW
COMMON/CON/CMH,CMN,CM1N,CMC,CM1C,CM2C,CMS,CM1S,CM2S,CM3S,CM4S,
&PN,PC,PS
COMMON/ACT/DHA,G(2,4),P,PW0,CONST
COMMON/VAR/C4,C6,COZ,COH,CC,CN,CW
IF(CSS.EQ.0.0) GO TO 10
CSS=CN/2.0*(1.0-DEXP(-X(3)*FLN))
10 CMH=DEXP(-X(2)*FLN)
CGW=DEXP(X(1)*FLN)
C(1,1)=CMH
C BEGIN REFINEMENT OF ACTIVITY COEFFICIENTS
DO 1 J=1,100

```

CALL GAMAW(DHA,2,2,B,C,Z,G,P,AWI)	EVAL
GQ1=G(2,1)*G(1,1)	EVAL
GQ2=G(2,1)/(G(2,2)*G(1,1))	EVAL
EQ1N=EK1N*G(1,1)/G(1,2)	FVAL
EQC=EKC*AWI	EVAL
EQ1C=EK1C/GQ1	EVAL
EQ2C=EK2C*GQ2	EVAL
FQS=EKS*AWI	EVAL
EQ1S=EK1S/GQ1	EVAL
EQ2S=EK2S*GQ2	EVAL
EQ3S=EK3S*GQ2	EVAL
FQSS=EKSS/(G(1,2)**2*G(2,2))	EVAL
FQW=EKW*AWI/GQ1	EVAL
CMHSQ=CMH*CMH	EVAL
PN=(CN-2.0*CSS)/(CONST+EKN*(1.0+EQ1N*CMH)*CGW)	EVAL
CMN=PKN*PN	EVAL
CM1N=EQ1N*CMN*CMH	EVAL
PC=CC/(CONST+EQC*(1.0+EQ1C/CMH+EQ1C*EQ2C/CMHSQ)*CGW)	EVAL
CMC=EQC*PC	EVAL
CM1C=EQ1C*CMC/CMH	EVAL
CM2C=EQ2C*CM1C/CMH	EVAL
PS=C4/(CONST+FQS*(1.0+EQ1S/CMH+EQ2S*EQ1S/CMHSQ)*CGW)	EVAL
CMS=EQS*PS	EVAL
CM1S=EQ1S*CMS/CMH	EVAL
CM2S=EQ2S*CM1S/CMH	EVAL
CMOH=FQW/CMH	EVAL
CM3S=(C6-CSS)/((1.0+EQ3S/CMH)*CGW)	EVAL
CM4S=EQ3S*CM3S/CMH	EVAL
CMA1=CM1C+CM1S+CM3S+CMOH	EVAL
CMA2=CM2C+CM2S+CM4S	EVAL
DLSQI=((C(1,2)-CM1N)/CM1N)**2+((C(2,1)-CMA1)/CMA1)**2	EVAL
+((C(2,2)-CMA2)/CMA2)**2	EVAL
C(1,2)=CM1N	EVAL
C(2,1)=CMA1	EVAL
C(2,2)=CMA2	EVAL
IF(DLSQI.LT.1.0D-12) GO TO 2	EVAL
1 CONTINUE	EVAL
C CALCULATE RESIDUALS IN CHARGE BALANCE Y(1), WATER ACTIVITY BALANCE	EVAL
C Y(2), AND (NH4)2SO4 SOLUBILITY BALANCE Y(3) (IF APPLICABLE)	EVAL
2 SUMI=C(1,1)+C(1,2)+C(2,1)+C(2,2)	EVAL
Y(1)=(C(1,1)+C(1,2)-C(2,1)-2.0*C(2,2))/SUMI	EVAL
SUMN=CMN+CMS+CMC	EVAL
AWI=DEXP(-FMW*SUMI*P)	EVAL
CRAW=1.0/AWI+FMW*SUMN	EVAL
ARAW=PW0*CONST/(CW-CGW/FMW)	EVAL
Y(2)=(ARAW-CRAW)/(FMW*SUMI)	EVAL
IF(CSS.EQ.0.0) GO TO 20	EVAL
AQSS=CM1N**2*CM4S	EVAL
Y(3)=(AQSS/EQSS)**(1.0/3.0)-1.0	EVAL
20 NCAL=NCAL+1	EVAL
NITN=NITN+J	EVAL
RETURN	EVAL
END	EVAL
C	
C SUBROUTINE TO CALCULATE ACTIVITY COEFFICIENTS AND ACTIVITY OF WATER	GMAW
C DHA = DEBYE-HUCKEL CONSTANT, NC = NO. OF CATIONS	GMAW
C NA = NO. OF ANIONS, B = INTERACTION COEFFICIENTS,	GMAW
C C = ION CONCENTRATIONS (MMOL/G H2O), Z = ION CHARGE	GMAW









YLL(I)=YL(I)	XPC1
YL(I)=Y(I)	XPCT
20 DYDX(I)=(YL(I)-YIL(I))/(XL-XLL)	XPCT
8 DO 30 I=1,6	XPCT
30 Y(I)=YL(I)+DYDX(I)*(X-XL)	XPCT
RETURN	XPCT
9 DO 40 I=1,6	XPCT
40 Y(I)=YL(I)+DYDX(I)*(XL-XLL)	XPCT
RETURN	XPCT
END	XPCT
C	
C SUPPORTINE TO DETERMINE COMPONENT CONC'N BY RUNGA-KUTTA INTEGRATION	KUTA
SUBROUTINE KUTTA(XL,XU,Y,NE,DEL,ACCURC,IMAX,EQUA)	KUTA
C PROGRAM AUTHOR F. D. HAMMERLING,	KUTA
C COMPUTING TECHNOLOGY CENTER, UNION CARBIDE CORP., NUCLEAR DIV.,	KUTA
C OAK RIDGE, TENN.	KUTA
CC MODIFIED AS INDICATED FOR THIS PROGRAM	KUTA
EXTERNAL EQUA	KUTA
DIMENSION Y(10),YI(10),YN(10),K1(10),K2(10),K3(10),K4(10),K5(10),	KUTA
> F(10),F1(10),F1(10)	KUTA
DOUBLE PRECISION Y,F,E,F1,XN,XL,DEL,XU,H,TEST,ACCURC,YN,YI,K1,	KUTA
> K2,K3,K4,K5	KUTA
LOGICAL QUIT,FIRST	KUTA
ITTER=0	KUTA
N=NE	KUTA
XN=XL	KUTA
H=DEL	KUTA
FIRST=.TRUE.	KUTA
QUIT=.FALSE.	KUTA
DO 10 I=1,N	KUTA
10 YN(I)=Y(I)	KUTA
20 IF (XN+H.LT.XU) GO TO 30	KUTA
DEL=H	KUTA
H=XU-XN	KUTA
IF (FIRST) DEL=H	KUTA
QUIT=.TRUE.	KUTA
CC THE INTEGER (IN = 1 OR 0) HAS BEEN ADDED TO ARGUMENT LIST	KUTA
CC OF S. EQUA TO SIGNAL FIRST CALCULATION OF EACH INCREMENT	KUTA
30 CALL EQUA(XN,YN,F1,1)	KUTA
CC PRINT OUT RESULTS OF THIS FIRST CALCULATION AT THE BEGINNING OF	KUTA
CC EACH INTERVAL IN X SPECIFIED IN THE MAIN PROGRAM	KUTA
IF (FIRST) CALL PRINT(2)	KUTA
40 DO 50 I=1,N	KUTA
K1(I)=H*F1(I)/3.	KUTA
50 YI(I)=YN(I)+K1(I)	KUTA
CALL EQUA(XN+H/3.,YI,F,0)	KUTA
DO 60 I=1,N	KUTA
K2(I)=H*F(I)/3.	KUTA
60 YI(I)=YN(I)+K1(I)/2.+K2(I)/2.	KUTA
CALL EQUA(XN+H/3.,YI,F,0)	KUTA
DO 70 I=1,N	KUTA
K3(I)=H*F(I)/3.	KUTA
70 YI(I)=YN(I)+3.*K1(I)/8.+9.*K3(I)/8.	KUTA
CALL EQUA(XN+H/2.,YI,F,0)	KUTA
DO 80 I=1,N	KUTA
K4(I)=H*F(I)/3.	KUTA
80 YI(I)=YN(I)+3.*K1(I)/2.-9.*K3(I)/2.+6.*K4(I)	KUTA
CALL EQUA(XN+H,YI,F,0)	KUTA



TEST=0.0	KUTA
DO 90 I=1,N	KUTA
K5(I)=H*F(I)/3.	KUTA
E(I)=(K1(I)-9.*K3(I)/2.+4.*K4(I)-K5(I)/2.)/5.	KUTA
TEST=DMAX1(TEST,DABS(E(I)))	KUTA
90 CONTINUE	KUTA
IF (TEST.LT.ACCURC) GO TO 100	KUTA
ITTE=ITTE+1	KUTA
IF (ITTE.GE.IMAX) GO TO 140	KUTA
H=H/2.	KUTA
QUIT=.FALSE.	KUTA
FIRST=.FALSE.	KUTA
GO TO 40	KUTA
100 DO 110 I=1,N	KUTA
110 YN(I)=YN(I)+(K1(I)+4.*K4(I)+K5(I))/2.	KUTA
XN=XN+H	KUTA
FIRST=.FALSE.	KUTA
IF (TEST.GE.ACCURC/32.) GO TO 120	KUTA
H=2.*H	KUTA
ITTE=ITTE-1	KUTA
120 IF (.NOT.QUIT) GO TO 20	KUTA
DO 130 I=1,N	KUTA
130 Y(I)=YN(I)	KUTA
GO TO 150	KUTA
140 WRITE(21,1000)	KUTA
150 RETURN	KUTA
1000 FORMAT(1X,'IMAX EXCEEDED')	KUTA
END	KUTA
C	
C SUBROUTINE FOR PRINTING OUTPUT ON LINE PPRINTER	PRNT
SUBROUTINE PRINT(N)	PRNT
IMPLICIT REAL*8(A-H,O-Z)	PRNT
COMMON/PLK/R,PI,FLN,FMW,B(4,4,2),Z(2,4)	PRNT
COMMON/CASE/NOX	PRNT
COMMON/RTE/NSC,NRL,VRGO,TP,H,UX,A(7),TA,DELX,VDG,VDP	PRNT
COMMON/SIGMA/SGO,SGPY,SGPZ,SGLY,SGLZ,SGSY,SGSZ,BETAL,BETAS	PRNT
COMMON/ARG/CGW,PH,CSS,C(2,4),I,RIT,RTOH,RTOZ,RTO,NCAL,NITN	PRNT
COMMON/EQK/EKN,EK1N,EKC,EK1C,EK2C,EKS,EK1S,EK2S,EK3S,EKSS,EKW	PRNT
COMMON/CON/CMH,CMN,CM1N,CMC,CM1C,CM2C,CMS,CM1S,CM2S,CM3S,CM4S,	PRNT
&PN,PC,PS	PRNT
COMMON/ACT/DHA,G(2,4),P,PWO,CONST	PRNT
COMMON/GIVN/WPCTC,WPCTH,WPCTS,QCCAL,FCTS6,EXAIR,FCON,TCP,TCA,	PRNT
&XLAST,XNEXT,ERRR	PRNT
COMMON/VAR/C4,C6,COZ,CCH,CC,CN,CW	PRNT
GO TO (1,2),N	PRNT
1 WRITE(21,100) WPCTC,WPCTH,WPCTS,QCCAL,FCTS6,EXAIR,FCON,H,	PRNT
&TCE,NSC,NRL,UX,VDG,VDP,TCA	PRNT
WRITE(21,125) (A(I),I=1,7)	PRNT
WRITE(21,150) ERRR,SGO	PRNT
RETURN	PRNT
2 WRITE(21,300) XLAST,DELX,SGPY,SGLY,SGSY,SGPZ,SGLZ,SGSZ,	PRNT
&CGW,PH,CSS,T,NCX,NCAL,NITN,	PRNT
&RTT,RTOH,RTOZ,RTO,G(1,1),G(1,2),G(2,1),G(2,2)	PRNT
WRITE(21,325) C4,C6,COZ,COH,CC,CN,CW	PRNT
WRITE(21,340) PN,PC,PS	PRNT
IF (CGW.GT.0.0) GO TO 21	PRNT
WRITE(21,348)	PRNT
21 WRITE(21,350) CMN,CM1N,CMC,CM1C,CM2C,CMS,CM1S,CM2S,CM3S,CM4S	PRNT



303

### 3. Sample Input and Output

The following input values, used in the reference case (Table V), were read by the indicated READ statements in M. SULCAL:

```
[READ(20, 100)  WPCTC,WPCTH,QCOAL,FCTS6,EXAIR,FCON,TCP,H]
82.57      6.93      100.0      0.02      0.25      5.0      177.0
400.0
```

```
[READ(20, 100)  NSC,NRL,UX,VDG,VDP,(A(I), I=1, 7),TCA,WPCTS]
      3      5      2.0      0.01      0.01      0.004      0.0
0.0032  2.0E-8  12.26  6.0E-4  929.7  21.11  1.0
```

```
[READ(20, 100)  XNEXT,DELX,ERRR]
300.0      0.1  0.000003
```

```
[READ(20, 100)  NX,(XINCR(I), I=1,NX)]
      4      700.0  4000.0  5000.0  15000.0
[100 FORMAT (7G 10.0)]
```

The output produced is shown on the next two pages. The first three rows of values, mostly input, are independent of  $x$ . In row 2 are the ambient concentrations of the seven components  $S(IV)$ ,  $S(VI)$ ,  $O_3$ ,  $OH$ ,  $CO_2$ ,  $NH_3$ , and  $H_2O$ . Rows 4 through 9 are repeated for each specified value of  $x$ . Row 4 includes the current value of the increment in  $x$  (DELX) in S. KUTTA. In row 5, NOX, NCL and NITN are, respectively, the accumulated entries into S. RATE, S. EVAL and S. GAMAW. Row 6 includes the oxidation rates: total, by  $OH$ , by  $O_3$ , and by oxygen; and the activity coefficients of the aqueous ions  $H^+$ ,  $NH_4^+$ ,  $X^-$ , and  $X^{2-}$ . In row 7 are the effective concentrations of components in the plume. Row 8 includes the partial pressures of  $NH_3$ ,  $CO_2$  and  $SO_2$  gases. Finally in row 9 are the concentrations of the aqueous species  $NH_3$ ,  $NH_4^+$ ,  $H_2CO_3$ ,  $HCO_3^-$ ,  $CO_3^{2-}$ ,  $H_2SO_3$ ,  $HSO_3^-$ ,  $SO_3^{2-}$ ,  $HSO_4^-$  and  $SO_4^{2-}$ .

SULFUR CHEMISTRY IN A GAUSSIAN PLUME

WPCTC	WPCTH	WPCIS	WCOAL	FCUSP	EXAIR	PCON	H	ICP	NSC	NRL	UX	VDG	VUP	TCA
82.57	6.93	1.00	100.00	0.02	0.25	5.00	400.00	177.00	3	5	2.00	0.01	0.01	21.11
AC4	AC6	ADZ	AOH	ACC	ACN	ACW								
4.00D-03 0.0	3.20D-03 2.00D-08	1.23D 01	6.00D-04	9.30D 02										
IRRR	SGO													
3.0D-06	8.84													
X	DELY	SGPY	SGLY	SGSY	SGPZ	SGLZ	SGSZ							
300.0	0.10	28.94	37.78	15.73	29.31	38.15	15.82							
CGW	PH	CSS	T	NOX	NCL	NITN								
6.39D-03 -1.20D5	0.0	330.21	2	5	24									
RTT	RTOH	RTOZ	PTO	GH	GN	GHS	GS							
3.00D-05 3.00D-05	5.27D-16	1.32D-18	49.3771	0.3923	59.5242	0.0157								
C4	C6	COZ	COH	CC	CN	CW								
4.89D 00 9.98D-02	2.19D-03	1.37D-08	1.11D 03	4.11D-04	1.19D 03									
PN	PC	PS												
9.4D-15	3.0D-02	1.3D-04												
CMN	CM1N	CMC	CM1C	CM2C	CM5	CM1S	CM2S	CM3S	CM4S					
1.390D-13	6.4383D-02	3.6043D-05	1.0670D-15	4.3346D-25	1.0746D-05	2.0027D-12	4.0459D-19	1.5294D 01	3.1787D-01					
X	DELY	SGPY	SGLY	SGSY	SGPZ	SGLZ	SGSZ							
1000.0	12.80	77.41	86.25	27.26	75.31	84.75	26.90							
CGW	PH	CSS	T	NOX	NCL	NITN								
4.47D-03 -0.9559	0.0	305.47	595	2973	16466									
RTT	RTOH	RTOZ	PTO	GH	GN	GHS	GS							
1.32D-05 1.32D-05	1.41D-14	2.28D-17	6.0477	0.4031	9.8348	0.0165								
C4	C6	COZ	COH	CC	CN	CW								
1.65D 00 3.73D-02	2.86D-03	1.79D-08	3.82D 02	5.36D-04	1.02D 03									
PN	PC	PS												
2.0D-14	9.6D-03	4.1D-05												
CMN	CM1N	CMC	CM1C	CM2C	CM5	CM1S	CM2S	CM3S	CM4S					
8.3464D-13	1.2014D-01	1.4463D-04	1.2400D-13	7.3285D-23	2.1002D-05	5.6631D-10	3.3964D-16	7.7839D 00	6.9631D-01					
X	DELY	SGPY	SGLY	SGSY	SGPZ	SGLZ	SGSZ							
5000.0	102.40	223.19	232.03	61.94	236.07	244.92	65.00							
CGW	PH	CSS	T	NOX	NCL	NITN								
3.20D-03 -0.6134	0.0	296.23	1160	5805	35040									
RTT	RTOH	RTOZ	PTO	GH	GN	GHS	GS							
2.60D-06 2.60D-06	3.84D-14	9.02D-17	1.4106	0.4276	2.7777	0.0196								
C4	C6	COZ	COH	CC	CN	CW								



2.970-01	1.200-02	3.140-03	1.360-08	7.930-01	5.890-04	1.450-02			
PN	PC	PS							
1.00-13	1.90-03	7.20-06							
CMN	CM1N	CMC	CM1C	CM2C	CM5	CM1S	CM2S	CM3S	CM4S
6.3393D-12	1.8356D-01	5.7970D-05	1.4439D-12	1.5260D-21	7.4317D-06	8.3611D-09	1.2068D-14	2.9836D-00	7.4973D-01
	X	DELX	SGPY	SGLY	SGSY	SGPZ	SGLZ	SGSZ	
	10000.0	204.80	329.80	338.65	87.30	355.17	364.22	93.39	
	CGW	PH	CSS	T	NOX	NCL	NITN		
	3.04D-03	-0.5419	0.0	295.23	1340	6705	40674		
	ATT	PTOH	RTOZ	PTO	GH	GN	GHS	GS	
	1.28D-06	1.28D-06	2.97D-14	7.95D-17	1.1468	0.4362	2.2439	0.0211	
	C4	C6	COZ	COH	CC	CN	CW		
	1.45D-01	9.11D-03	3.17D-03	1.98D-08	4.54D-01	5.93D-04	9.37D-02		
PN	PC	PS							
1.5D-13	1.1D-03	3.5D-06							
CMN	CM1N	CMC	CM1C	CM2C	CM5	CM1S	CM2S	CM3S	CM4S
9.7110D-12	1.9500D-01	3.5642D-05	1.6543D-12	1.9528D-21	4.1551D-06	8.5414D-09	1.4235D-14	2.3121D-00	6.8261D-01
	X	DELX	SGPY	SGLY	SGSY	SGPZ	SGLZ	SGSZ	
	25000.0	819.20	534.71	543.56	136.05	552.64	561.49	140.32	
	CGW	PH	CSS	T	NOX	NCL	NITN		
	3.10D-03	-0.4734	0.0	294.67	1540	7707	46631		
	ATT	PTOH	RTOZ	PTO	GH	GN	GHS	GS	
	5.30D-07	5.30D-07	1.73D-14	5.09D-17	1.0142	0.4435	1.9694	0.0224	
	C4	C6	COZ	COH	CC	CN	CW		
	5.95D-02	7.47D-03	3.19D-03	1.99D-08	2.63D-01	5.94D-04	7.33D-02		
PN	PC	PS							
1.8D-13	6.4D-04	1.4D-06							
CMN	CM1N	CMC	CM1C	CM2C	CM5	CM1S	CM2S	CM3S	CM4S
1.2339D-11	1.9167D-01	2.1560D-05	1.5005D-12	1.9100D-21	1.7838D-06	5.6055D-09	1.0265D-14	1.9130D-00	6.2662D-01

## APPENDIX B

### EFFECTIVE VOLUME OF FREE PLUME

The reactions in a plume are complicated by the situation that the reaction rates vary across and down the plume because of variations in concentration, temperature and mixing. The detailed treatment of these varying conditions is beyond the scope of this investigation. We want to use an idealized model for this study and yet relate the result to the conditions which are obtained in the open environment. The dispersion of effluents in the atmosphere has been successfully modeled by a Gaussian distribution in which the variance or dispersion  $\sigma$  follows empirically determined relations that are functions of time, distance from source, and the prevailing meteorological and topographical conditions. We will show that when modeling reaction rates it is possible to use a simple uniform model which can yield the same reaction rates as a well mixed Gaussian distribution.

In the following treatment, let  $q_i$  be the total amount of reactant  $i$ , in a unit length of the plume in the  $x$  direction, let  $C_i$  be the density or concentration of reactant  $i$ , and let  $R$  be the total rate of production of the reaction product. Consider a binary reaction

$$\frac{\text{Rate}}{\text{Volume}} = k C_1^{\alpha_1} C_2^{\alpha_2}, \quad (1)$$

then

$$R = k \int_V C_1^{\alpha_1} C_2^{\alpha_2} dv. \quad (2)$$

Let

$$C_i = \frac{q_i}{2\pi\sigma_y\sigma_z} e^{-y^2/2\sigma_y^2} e^{-z^2/2\sigma_z^2}. \quad (3)$$

Then the rate of reaction in a volume of unit length in the x-direction and infinite in extent in the y and z direction is

$$\begin{aligned}
 R &= \int_{-\infty}^{\infty} dy \int_{-\infty}^{\infty} dz \, k \, C_1^{\alpha_1} C_2^{\alpha_2} \\
 &= \frac{k \, q_1^{\alpha_1} q_2^{\alpha_2}}{2\pi\sigma_y\sigma_z} \int_{-\infty}^{\infty} dy \int_{-\infty}^{\infty} dz \, e^{-(\alpha_1+\alpha_2)y^2/2\sigma_y^2} e^{-(\alpha_1+\alpha_2)z^2/2\sigma_z^2} \\
 &= \frac{k \, q_1^{\alpha_1} q_2^{\alpha_2}}{(2\pi\sigma_y\sigma_z)^{\alpha_1+\alpha_2}} (2\pi\sigma_y\sigma_z) \cdot \frac{1}{\alpha_1+\alpha_2} \\
 &\equiv \frac{k \, q_1^{\alpha_1} q_2^{\alpha_2}}{(4\pi\sigma_y\sigma_z)^{\alpha_1+\alpha_2-1}} (4\pi\sigma_y\sigma_z) \left( \frac{2^{\alpha_1+\alpha_2-1}}{\alpha_1+\alpha_2} \right), \quad (4)
 \end{aligned}$$

where we have assumed a uniform or effective temperature. Now suppose the same amounts of reactants were spread uniformly through a volume  $V$  such that

$$\bar{C}_i = q_i/V. \quad (5)$$

Then

$$\bar{R} = k \int_V \bar{C}_1^{\alpha_1} \bar{C}_2^{\alpha_2} dv = \frac{k q_1^{\alpha_1} q_2^{\alpha_2}}{V^{\alpha_1+\alpha_2}} \cdot V. \quad (6)$$

Now if we choose as a control volume  $V = 4\pi\sigma_y\sigma_z$  then

$$\bar{R} = \frac{\alpha_1 + \alpha_2}{2^{\alpha_1+\alpha_2-1}} R = F R. \quad (7)$$

The choice  $V = 4\pi\sigma_y\sigma_z$  yields reaction rates which are correct through second order. Note this includes the case  $\alpha_1 = 0$  with  $\alpha_2 = 1$  or 2.



Other cases can be handled by scaling the rate constants by the relation

$$\bar{k} = k \cdot \frac{2^{\alpha_1 + \alpha_2 - 1}}{\alpha_1 + \alpha_2} , \quad (8)$$

where  $\bar{k}$  is the effective rate constant. Similar results may be obtained for equilibria, and they may be extended to reactions and equilibria of the form  $kC_1^{\alpha_1} C_2^{\alpha_2} \dots C_n^{\alpha_n}$  by replacing  $(\alpha_1 + \alpha_2)$  in the equations above by  $(\alpha_1 + \alpha_2 + \dots + \alpha_n)$ .

#### 1. Mean Concentration When Plume Touches the Ground

The forgoing discussion assumes a free plume and neglects interactions with the surface. An effect of the ground is to limit the downward spread of the plume and to restrict the dilution of the effluents near the land surface. This has been successfully modeled by assuming an "image plume", i.e., a "reflection" of the plume at the ground. The effect of the "image plume" is included in the present treatment as follows:

Consider the total reaction rate

$$R = k \int_V C_1 C_2 \, dv , \quad (9)$$

where the concentrations  $C_i$  have the distribution

$$C_i(x, y, z) = \frac{q_i}{2\pi\sigma_y\sigma_z} e^{-y^2/2\sigma_y^2} \left[ e^{-(z-h)^2/2\sigma_z^2} + e^{-(z+h)^2/2\sigma_z^2} \right] , \quad (10)$$

where  $q_1$  is the total amount of material available to react in a unit length of plume. Then

$$\begin{aligned}
 R &= \frac{k q_1 q_2}{(2\pi\sigma_y\sigma_z)^2} \int_{-\infty}^{\infty} e^{-y^2/2\sigma_y^2} dy \int_{-\infty}^{\infty} \left( e^{-(z-h)^2/2\sigma_z^2} + e^{-(z+h)^2/2\sigma_z^2} \right)^2 dz \\
 &= \frac{k q_1 q_2}{(2\pi\sigma_y\sigma_z)^2} \cdot \sqrt{2\pi} \sigma_y \int_0^{\infty} dz \left[ \left( e^{-2(z-h)^2/2\sigma_z^2} \right. \right. \\
 &\quad \left. \left. + e^{-(z+h)^2/2\sigma_z^2} \right) + 2e^{-\frac{(z-h)^2}{2\sigma_z^2}} e^{-\frac{(z+h)^2}{2\sigma_z^2}} \right] \\
 &= \frac{k q_1 q_2}{(2\pi\sigma_y\sigma_z)^2} \left[ \frac{2\pi\sigma_y\sigma_z}{2} + \sqrt{2\pi} \sigma_y 2 \int_0^{\infty} e^{-(z^2-2hz+h^2+z^2+2hz+h^2)/2\sigma_z^2} dz \right] \\
 &= \frac{k q_1 q_2}{(2\pi\sigma_y\sigma_z)^2} \left[ \frac{2\pi\sigma_y\sigma_z}{2} + \sqrt{2\pi} \sigma_y e^{-h^2/\sigma_z^2} 2 \int_0^{\infty} e^{-2z^2/2\sigma_z^2} dz \right] \\
 &= \frac{k q_1 q_2}{(4\pi\sigma_y\sigma_z)^2} \cdot (4\pi\sigma_y\sigma_z) \left[ 1 + \frac{e^{-h^2/\sigma_z^2}}{\sqrt{2}} \right] = k \left( \frac{q_1}{\beta V} \right) \left( \frac{q_2}{\beta V} \right) (\beta V) \beta \left[ 1 + \frac{e^{-h^2/\sigma_z^2}}{\sqrt{2}} \right]
 \end{aligned}$$

(11)

where  $V = 4\pi\sigma_y\sigma_z$ . To give the same reaction rate assuming  $\tau = Q/V$  we must choose

$$\beta = \frac{1}{1 + \exp(-h^2/\sigma_z^2)/\sqrt{2}} \quad (12)$$

Note for point source,  $\beta(x=0) = 1$ ,  $\beta(x=\infty) = \frac{\sqrt{2}}{1 + \sqrt{2}} = .586$ .

## 2. Plume Depletion Due to Washout

According to the washout concept, the depletion from the box of the chemical model is expressed in terms of the washout coefficient  $\Lambda$  as,

$$\Delta m = \Lambda m \Delta t, \quad (13)$$

where  $m$  is the amount of (aerosol or water soluble) material in the box.

But in terms of the volume  $V$  of the box,  $C = m/V$ , hence

$$\left(\frac{dC}{dt}\right)_{\text{washout}} = -\Lambda C. \quad (14)$$

Washout occurs under conditions of higher than normal ambient humidity.

Washout is not included in the present model.

## 3. Plume Depletion Due to Dry Deposition

The ground level concentration according to the Gaussian plume model is given by

$$C(x, y, 0) = \frac{Q(x)}{2\pi\sigma_y\sigma_z u x} e^{-y^2/2\sigma_y^2} e^{-h^2/2\sigma_z^2}. \quad (15)$$



In terms of the concentration  $\bar{C}$  of the chemical box model

$$\bar{C}(x) = Q(x)/4\pi\sigma_y'\sigma_z'u_x, \quad (16)$$

or

$$C(x,y,0) = 4\bar{C} e^{-y^2/2\sigma_y'^2} e^{-h^2/2\sigma_z'^2}. \quad (17)$$

The dry deposition in time  $\Delta t$  at a distance  $x$  is

$$\begin{aligned} \Delta m &= \int_{-\infty}^{\infty} dy \int_{x-1/2}^{x+1/2} dx C(x,y,0) V_d \Delta t = 4\bar{C} V_d \Delta t \sqrt{2\pi} \sigma_y u_x e^{-h^2/2\sigma_z'^2} \\ &= - \left( \frac{d\bar{C}}{dt} \right)_{\text{dep}} (4\pi\sigma_y'\sigma_z'u_x) \Delta t, \end{aligned} \quad (18)$$

where  $V_d$  is the deposition "velocity".

Hence

$$\left( \frac{dC}{dt} \right)_{\text{dep}} = -\bar{C} 2V_d \left( \frac{e^{-h^2/2\sigma_z'^2}}{\sqrt{2\pi} \sigma_z} \right). \quad (19)$$

#### 4. Choice of Sigma

The behavior of a natural plume is far more complicated than the idealized case we have considered so far. Over a period of time convection cells move, the plume may wander, fan, fumigate, etc., so that the volume swept out is considerably larger than that which obtains in any instant. It is the larger volume which is described by the dispersion coefficients of Pasquill-Gifford and Briggs-Smith, which are

defined for a point source. For the shorter distances at least, the instantaneous plume will be considerably smaller. At very short distances a "concentration catastrophe" arises if the plume dimensions are allowed to shrink to zero. Two artifices are used to avoid this crisis. One is the concept of a "virtual (point) source" behind the stack, i.e. the distances along the plume are measured from a point behind the stack and can not go to zero. The second artifice (which we use) involves adding a constant such that  $4\pi\sigma_y\sigma_z u_x$  reduces to the initial plume volume flow rate  $V_p^\circ$  at  $x = 0$ . At small distances the additive term  $\sigma^\circ$  dominates while at large distances it can be neglected.

In defining the various dispersion coefficients below we use an asterisk to denote a point source, a subscript  $\ell$  for long-time (larger)  $\sigma$ 's and a subscript  $s$  for short-time (smaller)  $\sigma$ 's. We assume that large scale effects such as deposition are governed by these coefficients given by

$$\sigma_\ell = \sigma_\ell^* + \sigma^\circ . \quad (20)$$

The instantaneous dispersion coefficients used in determining the size of the "box" we define by

$$\sigma_s = f\sigma_\ell^* + \sigma^\circ , \quad (21)$$

where  $f$  is a function of the distance  $x$ ,  $f < 1$  and  $f$  approaches unity at large distances. The exact form of  $f$  is not crucial and we have elected to use a form due to Scriven,<sup>12</sup> which we write in the form

$$f = \sqrt{\frac{x}{x+50L}} , \quad (22)$$

where L is given in the table below.

<u>Stability Class</u>	<u>L (meters)</u>
A	500
B	250*
C	100
D	50*
E	20*
F	10

---

\*Interpolated values.



APPENDIX C

ACTIVITY COEFFICIENTS, THE WATER ACTIVITY, AND INITIAL VALUES

# 1. The Estimation of Ion Activity Coefficients and the Osmotic Coefficient

For an ideal solution, the activity coefficients of ions are unity and the activity of water is given by its mole fraction,

$$a_w = \frac{n_w}{n_w + \sum_i n_i + \sum_j n_j} = \frac{55.51}{55.51 + \sum_i [i] + \sum_j [j]} \quad (1)$$

(here i and j refer to cations and anions, respectively). Such behavior is approached as solutions become more and more dilute. The aerosol droplets in the atmosphere often are quite concentrated, however, and the deviations from ideal behavior can be considerable (Fig.4). Hence it is necessary to estimate the values of ion activity coefficients for use in the equilibrium constant expressions (Table I) and in the calculation of the activity of water. The following is based on the treatments of Pitzer and Brewer<sup>13</sup> and Pitzer.<sup>14</sup>

The activity coefficients of ions  $g_i$  and  $g_j$  in a solution and the activity of water ( $a_w$ ) are related by the Gibbs-Duhem equation,

$$\sum_i [i] d \ln([i]g_i) + \sum_j [j] d \ln([j]g_j) = -55.51 d \ln a_w. \quad (2)$$

The activity of water is usually expressed in terms of the osmotic coefficient  $\phi$ ,

$$\ln a_w = -0.018(\sum_i [i] + \sum_j [j])\phi. \quad (3)$$

The relationship between the osmotic coefficient and the activity coefficient is obtained by combining Eqs. 2 and 3 and integrating,

$$\phi = 1 + \frac{\sum_i [i] \int_0^c \frac{d \ln g_i}{[i]} + \sum_j [j] \int_0^c \frac{d \ln g_j}{[j]}}{\sum_i [i] + \sum_j [j]}. \quad (4)$$

The integrations are from 0 concentration to the individual ion concentrations in the solution for which  $\phi$  is desired.

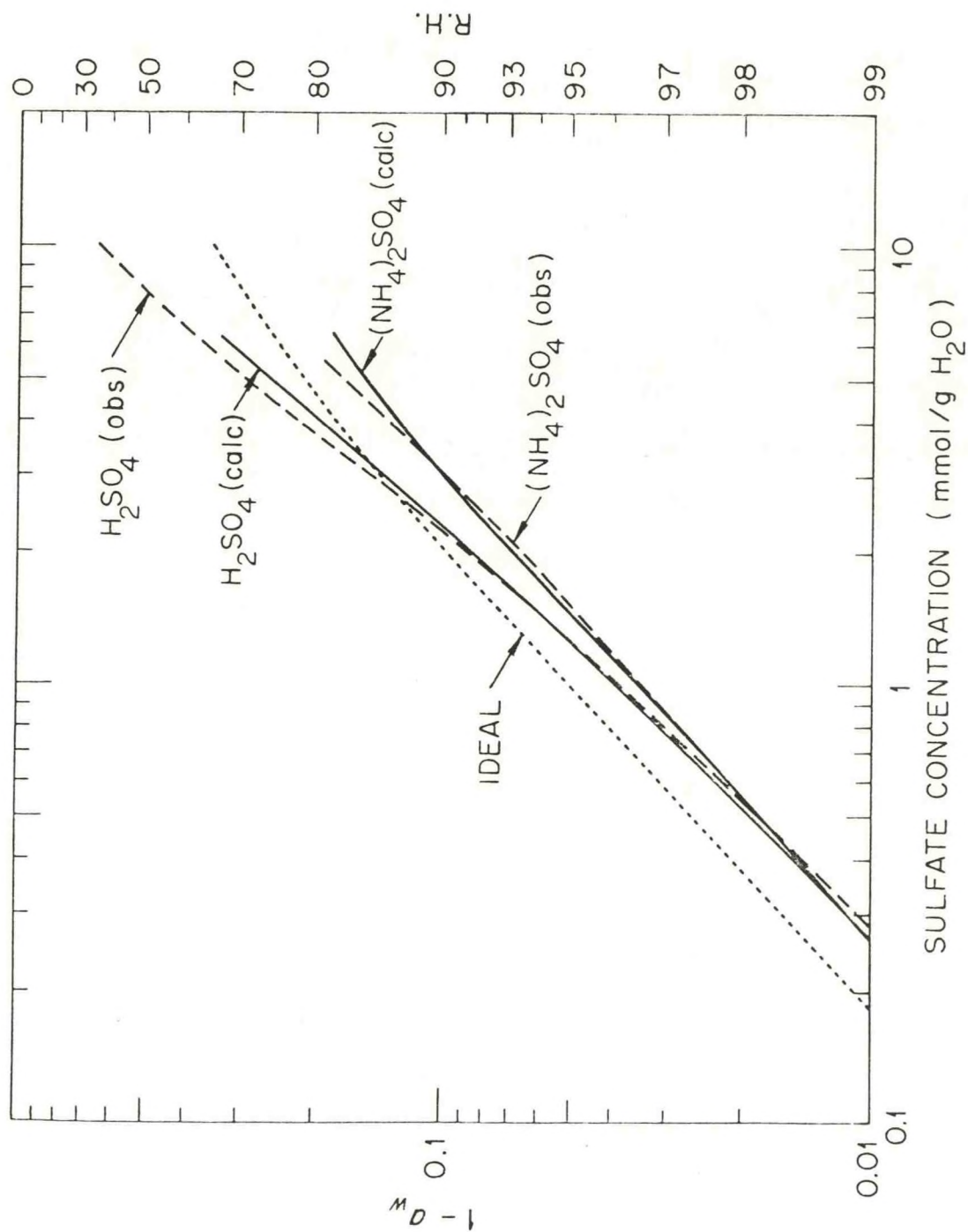


Fig. 4 Variation of the concentration of aerosol droplets with the activity of water  $a_w$  (the relative humidity/100) at 25°C.



The following expressions are assumed for the individual ionic activity coefficients;

$$\ln g_i = \frac{-Z_i^2 S I^{1/2}}{1 + I^{1/2}} + \sum_j B_{ij}^g [j] , \quad (5a)$$

$$\ln g_j = \frac{-Z_j^2 S I^{1/2}}{1 + I^{1/2}} + \sum_i B_{ij}^g [i] , \quad (5b)$$

wherein  $Z_i$  and  $Z_j$  are the ion charges,  $I$  is the ionic strength

$$I = \frac{1}{2} (\sum_i Z_i^2 [i] + \sum_j Z_j^2 [j]) , \quad (6)$$

and  $S$  is the Debye-Hückel constant, a theoretical quantity which depends only on the density and dielectric constant of the solvent and on the temperature. It is given with adequate accuracy for present purposes by the approximate expression

$$S = 1.1305 + 0.01842 t(^{\circ}\text{C}) \quad (7)$$

The coefficients  $B_{ij}^g$ , one for each pairwise combination of cations and anions is assumed to be a function only of  $I$ .

$$B_{ij}^g(I) = B_{ij}^c + B_{ij}^l F(I) \quad (8)$$

$$F(I) = [1 - (1 + 2I^{1/2} - 2I) \cdot \exp(-2I^{1/2})] / 4I . \quad (8a)$$

$B_{ij}^c$  and  $B_{ij}^l$  are adjustable constants.

The above expressions for  $g_i$  and  $g_j$  (eqs 5-8) when introduced into eq 4 give the following expression for  $\phi$

$$\phi = 1.0 + \frac{-2SG(I) + \sum_i \sum_j B_{ij}^{\phi} [i][j]}{\sum_i [i] + \sum_j [j]} , \quad (9)$$

$$G(I) = (1 + I^{1/2}) - \frac{1}{(1 + I^{1/2})} - 2 \ln(1 + I^{1/2}) , \quad (9a)$$

$$B_{ij}^{\phi} = B_{ij}^{\circ} + B_{ij}^1 \exp(-2I^{1/2}) \quad (9b)$$

Since four kinds of ions are distinguished, two cations ( $H^+$  and  $NH_4^+$ ) and two anions ( $X^-$  and  $X^{2-}$ ), there are four pairwise combinations of cations with anions and 8 adjustable parameters. Six of the following values were assigned by fitting the appropriate expressions above to the known osmotic and activity coefficients of pure  $H_2SO_4$  and  $(NH_4)_2SO_4$  solutions given by Robinson and Stokes<sup>15</sup> (Fig. 4), and the observed dissociation of  $HSO_4^-$  ion in pure sulfuric acid solutions (Young et al<sup>16</sup>).

i	j	$B_{ij}^{\circ}$	$B_{ij}^1$
$H^+$	$x^-$	0.272	3.080
$H^+$	$x^{2-}$	0.050	-4.005
$NH_4^+$	$x^-$	0.0*	0.319*
$NH_4^+$	$x^{2-}$	-0.049	-1.186

The remaining two (with asterisks) were adjusted to give approximately the observed solubility of  $(NH_4)_2SO_4$  in  $H_2SO_4$  solutions (Seidell,<sup>17</sup> Vol. II p. 756), Fig. 5.

## 2. Initial Estimate of Quantities Needed for the Calculation of the Plume Composition

The initial estimates of the amount of condensed water  $g_w$  and of the ion concentrations  $[H^+]$ ,  $[NH_4^+]$ ,  $[x^2]$  and  $[x^{2-}]$  are made by assuming that the only ions present in solution are  $H^+$ ,  $NH_4^+$ ,  $HSO_4^-$ , and  $SO_4^{2-}$  and that all the  $NH_3$  is present as  $NH_4^+$ . The following expressions then apply;

$$[NH_4^+] = C(NH_3)/g_w, \quad (10)$$

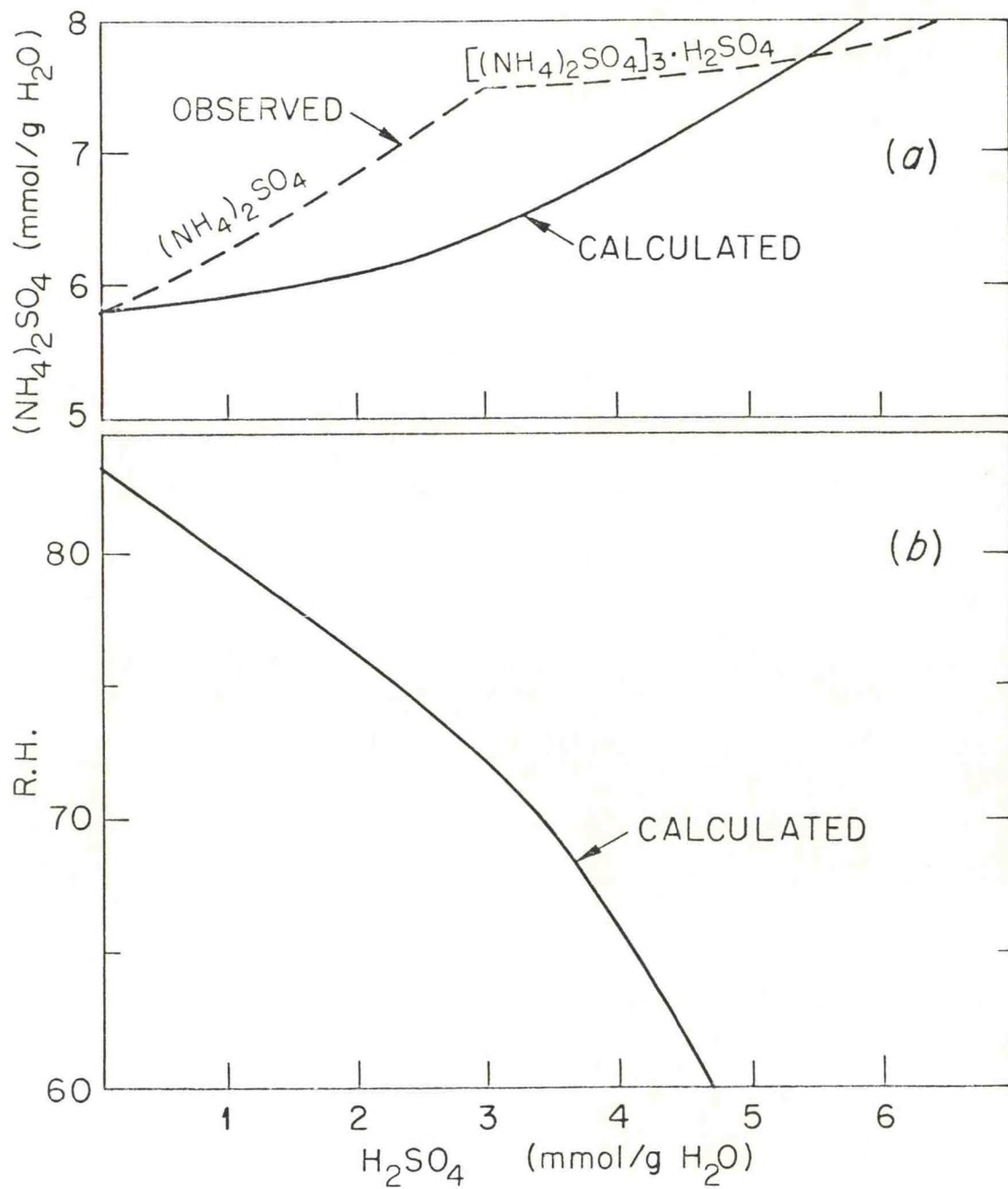


Fig. 5 The sulfuric acid - ammonium sulfate - water system at 25°C.



$$[x^-] = [HSO_4^-] = \frac{[H^+]}{[H^+] + Q_4} \cdot \frac{C(S(VI))}{\epsilon_w}, \quad (11)$$

$$[x^{2-}] = [SO_4^{2-}] = \frac{Q_4}{[H^+] + Q_4} \cdot \frac{C(S(VI))}{\epsilon_w}, \quad (12)$$

where  $Q_4$  is the concentration quotient from  $K_4$  (Table I),

$$Q_4 = \frac{[H^+][SO_4^{2-}]}{[HSO_4^-]} = K_4 \cdot \frac{\epsilon_{x^-}}{\epsilon_H + \epsilon_{x^{2-}}}. \quad (13)$$

Introducing Eqs. 10 to 13 into the charge balance equation

$$[H^+] + [NH_4^+] = [HSO_4^-] + 2[SO_4^{2-}], \quad (14)$$

a quadratic in  $[H^+]$  is obtained with the solution

$$[H^+] = -B + (B^2 - C)^{1/2}, \quad (15)$$

wherein

$$B = [Q_4 + [C(NH_3) - C(S(VI))]/\epsilon_w]/2, \quad (15a)$$

$$C = Q_4[C(NH_3) - 2C(S(VI))]/\epsilon_w. \quad (15b)$$

The only unknowns are  $\epsilon_w$  and the ion activity coefficients.

The calculation begins by solving the following equation for  $\epsilon_w$ ,

$$[C(H_2O) - \epsilon_w/0.018] \frac{RT}{P_w^\circ} = \frac{\epsilon_w}{\epsilon_w + 3 \cdot C(S(VI)) \cdot 0.018}. \quad (16)$$

Each side is an expression of the activity of water, the right side being an approximation of the mole fraction of water in solution assuming three moles of ions are produced by a mole of S(VI). The solution for  $\epsilon_w$  is

$$\epsilon_w = [-B' + (B'^2 - C')^{1/2}] \cdot 0.018, \quad (17)$$

$$B' = [P_w^\circ/RT - C(H_2O) + 3 C(S(VI))]/2, \quad (17a)$$

$$C' = -3 C(S(VI)) \cdot C(H_2O). \quad (17b)$$

The activity coefficients are set initially at unity. The ion concentrations thus obtained from Eqs. 10-15 are used to estimate activity coefficients in S. GAMAW, and the calculation is repeated by cycling between S. EVAL AND S. GAMAW until the activity coefficients become constant (only a few interactions are needed). Then the water activity given by S. GAMAW is compared with that given by the amount of gaseous water,

$$a_w = [C(H_2O) - g_w/0.018]RT/P_w^\circ \quad (18)$$

and  $g_w$  is adjusted by repeated cycling between S. NONLIN and S. EVAL until a good estimate of  $g_w$  (and ion concentrations and activity coefficients) is obtained.

INTERNAL DISTRIBUTION

- |                       |  |
|-----------------------|--|
| 1. S. I. Auerback     | 51. M. H. Lietzke                      |
| 2-11. C. F. Baes, Jr. | 52. S. E. Lindberg                     |
| 3. C. L. Begovich     | 53. R. J. Luxmoore                     |
| 4. A. A. Brooks       | 54. J. B. Mankin                       |
| 5. R. L. Burgess      | 55. W. L. Marshall                     |
| 6. S. Cantor          | 56. R. D. McCulloch                    |
| 7. H. P. Carter       | 57. H. F. McDuffie                     |
| 8. E. D. Copenhagen   | 58. R. E. Mesmer                       |
| 9-18. W. M. Culkowski | 59. J. K. Munro                        |
| 19. F. L. Culler      | 60. B. D. Murphy                       |
| 20. K. R. Dixon       | 61. C. J. Nappo, Jr.                   |
| 21. R. C. Dahlman     | 62. J. S. Olson                        |
| 22. J. W. Elwood      | 63. R. V. O'Neill                      |
| 23. D. E. Fields      | 64. M. R. Patterson                    |
| 24. R. H. Fowler      | 65. S. K. Penny                        |
| 25. C. W. Francis     | 66. H. Postma                          |
| 26. W. Fulkerson      | 67. R. J. Raridon                      |
| 27. E. L. Fuller      | 68. M. Reeves                          |
| 28. S. R. Hanna       | 69. D. E. Reichle                      |
| 29. W. F. Harris      | 70. C. Richmond                        |
| 30. G. S. Henderson   | 71. W. D. Shults                       |
| 31. R. F. Hibbs       | 72. R. A. Strehlow                     |
| 32. H. R. Hicks       | 73. I. L. Thomas                       |
| 33. C. J. Hochanadel  | 74-93. R. I. Van Hook                  |
| 34-43. J. T. Holdeman | 94. P. R. Vanstrum                     |
| 44. H. F. Holmes      | 95-96. Central Research Library        |
| 45. D. D. Huff        | 97-106. CSD Library, 4500N             |
| 46. D. R. Jackson     | 107. Document Reference Section - Y-12 |
| 47. J. S. Johnson     | 108-111. Laboratory Records            |
| 48. S. V. Kaye        | 112. Laboratory Records - Record Copy  |
| 49. O. L. Keller      | 113. ORNL Patent Office                |
| 50. N. M. Larson      |  |



#### EXTERNAL DISTRIBUTION

114. Jay Bloomfield, Research Scientist, New York State, Department of Environmental Conservation, 50 Wolf Road, Albany, NY 12233
115. R. P. Betson, Head, Hydrologic Research and Analysis Staff TVA, 331 Evans Building, Knoxville, TN 37902
116. Andrew W. Breidenbach, Director, National Environmental Research Center, Environmental Protection Agency, Cincinnati, OH 45268
117. A. V. Brill, Division of Nuclear Medicine and Biomedicine, Vanderbilt University, School of Medicine, Nashville, TN 37232
118. Richard Carrigan, Division of Advanced Environmental Research and Technology, National Science Foundation, 1800 G Street, NW, Washington, DC 20550
119. Barry Commoner, Center for Biology, Washington University, Box 1126, Saint Louis, MO 63130
120. N. H. Crawford, Hydrocomp, 1502 Page Mill Road, Palo Alto, CA 94304
121. James W. Curlin, Environmental Policy Division, Congressional Research Service, Library of Congress, Washington, DC 20540
122. Paul B. Dunaway, Office of Effect Evaluation, U.S. Energy Research and Development Administration, Nevada Operations Office, P. O. Box 1400, Las Vegas, NV 89114
123. Harry W. Edwards, Department of Mechanical Engineering, B107 - Engineering Research Center, Colorado State University, Fort Collins, CO 80521
124. Farley Fisher, Environmental Protection Agency, Office of Toxic Substances, 401 M Street, SW, Washington, DC 20460
125. Delbert D. Hemphill, Environmental Health Center, 426 Clark Hall, University of Missouri, Columbia, MO 65201
126. Jack Hollander, Director, Energy and Environment Division, Lawrence Berkeley Laboratory, University of California, Berkeley, CA 94720
127. Hal Hollister, Chief, Technical Analysis Branch, Division of Biomedical and Environmental Research, U.S. Energy Research and Development Administration, Washington, DC 20545

128. Robert J. M. Horton, Special Studies Staff, National Environmental Research Center, Environmental Protection Agency, Research Triangle Park, NC 27711
129. Joseph A. Lenhard, P. O. Box E, U.S. Energy Research and Development Administration, Oak Ridge, TN 37830
130. J. I. Liverman, Director, Division of Biomedical and Environmental Research, U.S. Energy Research and Development Administration, Washington, DC 20545
131. William Lower, Environmental Trace Substances Research Center, University of Missouri-Columbia, Rural Route 3, Columbia, MO 65201
132. Don Lynam, Assistant Manager, Environmental Health International Lead Zinc Research Organization, 292 Madison Avenue, NY 10017
133. Charles Malone, Environmental Studies Board, National Research Council, 2101 Constitution Avenue, Washington, DC 20418
134. M. T. Mills, Geophysics Corporation of America, Technology Division, Burlington Road, Bedford, MA 01730
135. Armond Georges Nassongne, Information Technology Division, Scientific and Technical Information and Information Management, Commission of The European Communities, Aldringen, Luxembourg
136. John Newhold, Ecology Center, Utah State University, Logan, UT 97321
137. R. M. Perhac, Division of Environmental Systems and Resources, National Science Foundation, 1800 G Street, NW, Washington, DC 20550
138. Robert Rabin, Division of Biomedical and Environmental Sciences, U.S. Energy Research and Development Administration, Washington, DC 20545
139. Gary L. Rolfe, 396 Fevier, University of Illinois, Urbana, IL 61801
140. Milton E. Rose, Mathematical and Computer Sciences Program, Molecular Sciences and Energy Research, Division of Physical Research, U.S. Energy Research and Development Administration, Washington, DC 20545
141. Walter Sanders, III, Southeast Water Quality Laboratory, Water Quality Office, Environmental Protection Agency, Athens, GA 30601



- 142. Ivan Smith, Midwest Research Institute, 425 Volker Boulevard, Kansas City, MO 64110
- 143. Marvin Stephenson, Division of Advanced Research and Technology, National Science Foundation, 1800 G Street, Washington, DC 20550
- 144. C. H. Thompson, Chief, Hazardous Materials Branch, Division of Oil and Hazardous Materials, Office of Water Programs, Environmental Protection Agency, Washington, DC 20460
- 145. Jack E. Thompson, Deputy Director, National Environmental Research Center, Environmental Protection Agency, Research Triangle Park, NC 27711
- 146. J. E. Watkin, Environmental Secretariat, Division of Biology, National Research Council of Canada, Ottawa, Ontario K1A 0R6, Canada
- 147. Herbert Wiser, Director, Division of Process and Effects Research, Environmental Protection Agency, 401 M Street, SW, Washington, DC 20460
- 148. Bobby G. Wixson, Professor of Environmental Health, Department of Civil Engineering, University of Missouri, Rolla, 115 Engineering Research Building, Rolla, MO 65401
- 149. K. J. Yost, Department of Bionucleonics, Pharmacy Building, Purdue University, Lafayette, IN 47901
- 150-176. Technical Information Center, Oak Ridge, TN 37830
- 177. Research and Technical Support Division, ORO
- 178. James Meagher, TVA, Air Quality Branch, River Oaks Building, Muscle Shoals, AL 35660
- 179. Vinaya Sharma, TVA, Air Quality Branch, River Oaks Building, Muscle Shoals, AL 35660



## THE ANNUAL CYCLE OF SOLAR RADIATION IN A DECIDUOUS FOREST\*

B. A. HUTCHISON and D. R. MATT

*Atmospheric Turbulence and Diffusion Laboratory, National Oceanic and Atmospheric Administration, Oak Ridge, Tennessee 37830 (U.S.A.)*

(Received November 29, 1976; accepted February 8, 1977)

### ABSTRACT

Hutchison, B. A. and Matt, D. R., 1977. The annual cycle of solar radiation in a deciduous forest. *Agric. Meteorol.*, 18: 255—265.

Periodic solar radiation measurements within and above an east Tennessee *Liriodendron* forest and continuous records of insolation from a nearby NOAA weather station were used to derive an approximation of the annual radiation regime within and above the deciduous forest. The interaction of changing solar elevations, insolation, and forest phenology are shown to control the radiation climate within the forest. Maximum radiation penetrates the forest in early spring as solar paths rise higher in the sky each day just prior to leaf expansion. After leaf expansion begins, average radiation received within the forest decreases rapidly despite continued increases in solar elevations and daily insolation. This forest attains full leaf in early June and from then until the advent of leaf abscission near the autumnal equinox, forest structure remains relatively static. Solar elevations and daily insolation decline following the summer solstice, however, and as a result, average radiation penetrating the forest slowly declines throughout the summer reaching an annual minimum in early autumn. With leaf fall, slightly increased amounts of radiation penetrate the forest but as within-forest solar paths continue to lengthen, radiation within the forest again declines. Minimum amounts of solar radiation penetrate the leafless forest around the winter solstice.

---

\* Research supported in part by the Eastern Deciduous Forest Biome, US-IBP, funded by the National Science Foundation under Interagency Agreement AG-199, BMS76-00761 with the Energy Research and Development Administration — Oak Ridge National Laboratory, and in part by the Division of Biomedical and Environmental Research, ERDA. Contribution No. 277, Eastern Deciduous Forest Biome, US-IBP. ATDL Contribution File No. 76/8. Publication No. 986, Environmental Sciences Division, ORNL. This report was prepared as an account of work sponsored by the United States Government. Neither the United States nor the Energy Research and Development Administration, nor any of their employees, nor any of their contractors, subcontractors, or their employees, makes any warranty, express or implied, or assumes any legal liability or responsibility for the accuracy, completeness or usefulness of any information, apparatus, product or process disclosed, or represents that its use would not infringe privately owned rights.



## INTRODUCTION

Seasonal variation in the radiation climates of forests (or other plant stands) is the integrated effect of interactions among seasonal changes in angle of incidence of the solar beam, in forest phenology, and in weather conditions affecting atmospheric transparency. Potential insolation at temperate latitudes varies sinusoidally as a result of the regular seasonal changes in the elevation of the solar path. Observed amounts of radiation incident upon the earth's surface depart from such a sinusoidal pattern by virtue of irregular changes in the transparency of the atmosphere to solar radiation resulting from weather conditions as well as other factors. Within a forest, yet other departures from the temporal pattern in incident radiation are manifest. These variations are largely the result of changing canopy transmissivity effected by changing solar elevations and by phenological changes in forest structures.

Conifer forests, in general, are not subject to the dramatic phenological structural changes of deciduous forests. However, phenological effects upon radiation regimes within a *Picea rubens* forest were found by Schomaker (1968). Even in the absence of such phenological change, radiation climates of conifer forests would show seasonal variation. For example, Scheer (1953), in studies in an Austrian conifer forest, found increasing canopy transmissivities in the spring and decreasing transmissivities in the autumn. In the spring, solar elevations rise higher each day toward their maximum on the summer solstice. As a result, optical path lengths through a forest canopy decrease daily during this period and with decreasing optical path lengths, radiation attenuation correspondingly decreases. In the autumn, the reverse holds. Solar elevations decrease, optical path lengths increase, and the end result is that increased attenuation of radiation by the forest canopy reduces canopy transmissivity.

In temperate-zone deciduous forests, these interactions between angles of incidence of the solar beam and forest structure are supplanted by substantial phenological change in forest canopy structure. As a result, the seasonal variation in deciduous forest radiation climates is especially pronounced. In the oak—hornbeam forests of Hertfordshire, England, Salisbury (1916) denoted the leafless period as the light phase and the leafed portion of the year as the shade phase in recognition of the profound differences in radiation climates effected by leaf expansion in the forest canopy. He studied the effects of the timing, duration, and intensity of these light and shade phases upon the development, density, and species composition of the understory vegetation, providing early documentation of the interdependent functioning of components of forest ecosystems.

Our studies of the time and space distributions of radiant flux densities in an east Tennessee deciduous forest of *Liriodendron tulipifera* provide data on the seasonal variation in radiation climate in this forest. These results emphasize the importance of solar elevation—phenology interactions in the definition of radiation climates throughout the vertical extent of the forest.



## THE FOREST

Measurements of radiant flux densities were made in a *Liriodendron tulipifera* stand about 50 years of age situated in a moist limestone sink on the ERDA reservation 10 km south of the town of Oak Ridge, Tennessee. Because of the mesic site, a more highly developed understory and a higher stand density is found in this stand than is typical of the Appalachian region. The overstory is nearly pure *Liriodendron tulipifera* (>70% by number) with some *Acer rubrum* (about 10%) and small numbers of a variety of other species. (For a more complete description, see Hutchison, 1975.) The overstory canopy extends from around 30 m down to 16 m, the well-defined lower limit of the live-crown. Between 16 and 10 m, there are a few crowns of suppressed trees along with the boles of the codominant overstory trees. A rather distinct secondary canopy, comprised mostly of *Cornus florida*, *Cercis canadensis*, and pole-sized trees of various species, is found between 10 and 3 m above the forest floor. Below 3 m, saplings of numerous tree species along with shrubs, mostly *Hydrangea arborescens*, are present. At the forest floor, a variable stand of herbaceous vegetation exists. Most of the herbaceous biomass is contributed by *Polystichum acrostichoides* and *Parthenocissus quinquefolia* but in early spring, many other species are found including *Podophyllum peltatum*, *Dentaria diphylla*, and *Phlox divaricata*.

The basal area of the tree species in this stand is about  $28 \text{ m}^2 \text{ ha}^{-1}$  while the stem density exceeds  $5500 \text{ stems ha}^{-1}$ . When fully developed, the leaf area index of this forest is about 6 (Burgess and O'Neill, 1975). Photographs of the winter leafless and summer fully leafed canopies are shown in Figs. 1 and 2, respectively.

## REGIONAL CLIMATE

The climate of the area is characteristically warm and humid. Winters are mild and wet with frontal storm systems predominating. Summers tend to be hot and humid with few frontal storm systems. Convective thunderstorms may develop almost daily yielding erratic, small areas of intense precipitation over the region. Average annual precipitation exceeds  $125 \text{ cm yr}^{-1}$ . Heavy radiative ground fog develops frequently in early mornings throughout the year. Because of the topography of the study site and its proximity to a TVA reservoir, such fog often persists in this forest until midday.

## METHODS

Amounts of global solar radiation received within and above the *Liriodendron* forest were measured with arrays of Lintronic Dome Solarimeters. These commercial modifications of Monteith's (1959) field solarimeter sense radiation in the spectral band  $0.3\text{--}3.0\mu$ , this band width accounting for some 98% of the solar radiation reaching the earth's surface (Fritz, 1958). Measure-



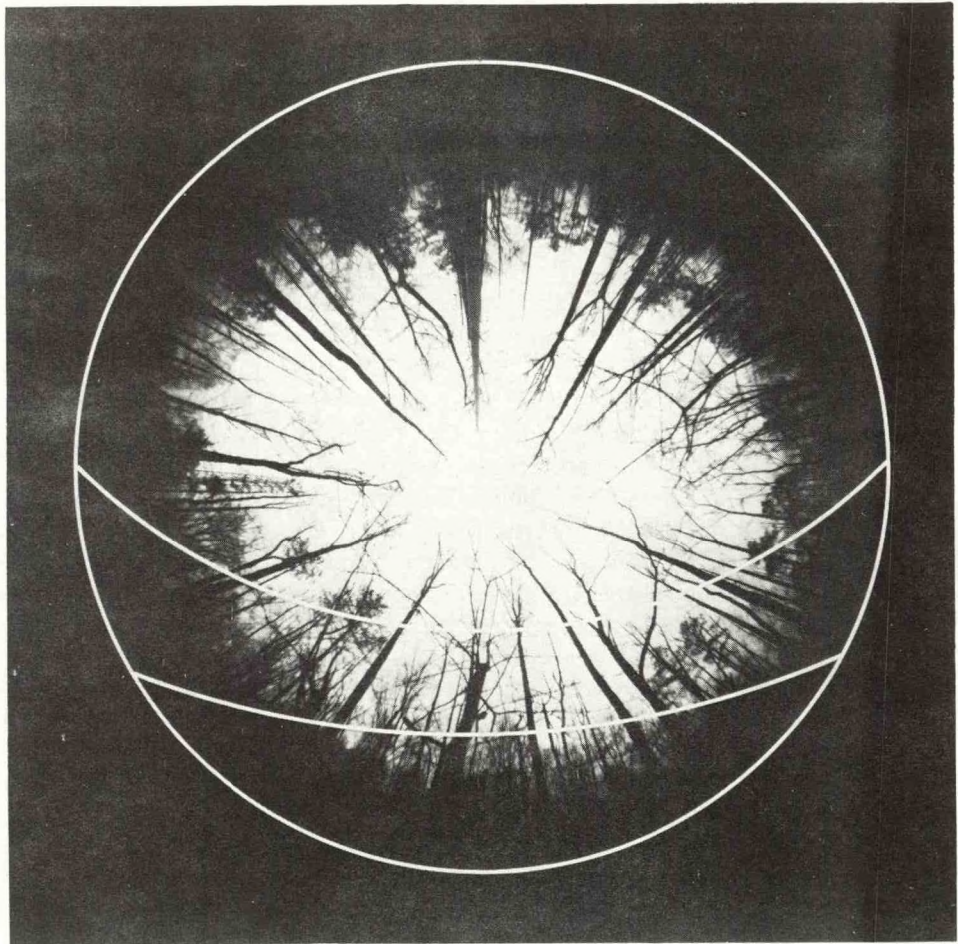


Fig.1. Hemispherical canopy photograph of the winter leafless forest taken from the forest floor. Outermost arc represents solar path on the winter solstice. Innermost arc represents solar path on the equinoxes. Photo #0060-75.

ments within the forest were replicated 10 times in horizontal space and at 3 vertical levels. Horizontal replications were randomly sited while vertical replications were made at the forest floor, at 3 m at the base of the secondary canopy, and at 16 m, the base of the overstory live-crown. Incident global radiation was initially measured with a single dome solarimeter and later, with a pair of Kipp and Zonen solarimeters situated about 2 m above the tops of the trees. Output signals from all sensors were fed into a digital data acquisition system which scanned the sensors at preselected intervals (5 or 10 min) and recorded outputs on punch paper tape. All solarimeters were periodically recalibrated against the Precision Eppley Pyramometer that we use as a shelf standard and nonlinear calibration functions were derived for each dome



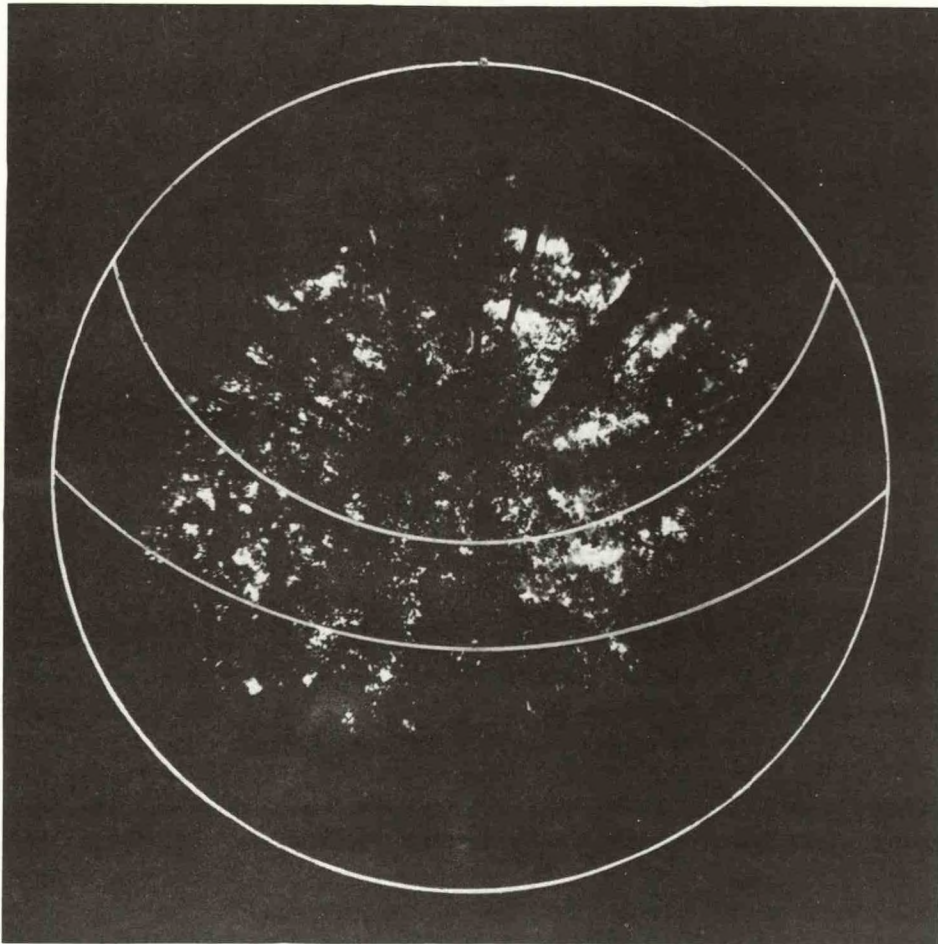


Fig.2. Hemispherical canopy photograph of the summer fully leafed forest taken from the forest floor. Outermost arc represents solar paths on the equinoxes. Innermost arc represents solar path on the summer solstice. Photo #0062-75.

solarimeter to account for the nonlinear response of these sensors to low level radiant flux densities (Matt and Hutchison, 1974). Care was taken to maintain identical orientations of sensors in the field and during calibration to minimize errors resulting from departures from flatness of the printed circuit sensing elements of these solarimeters.

Because of repeated lightning damage to the data acquisition system and of restricted access to the study site, continuous monitoring of the instrument net proved impossible. However, sufficient data were collected over a two-year period to characterize radiation regimes within the forest in all seasons of the year and in all phenological phases of the forest under a variety of weather conditions.



The annual radiation regime of this forest was reconstructed from the discontinuous observational data by calculating values of average fractional radiation penetration to each of the three forest levels for a variety of combinations of times of day, weather conditions, seasons, and phenological states of the forest and applying these fractional penetrations to the continuous solar radiation record collected at the NOAA weather station in Oak Ridge. Because of frequent morning fog, radiation observations were segregated into morning and afternoon periods. Weather conditions considered were clear, partly cloudy, and overcast skies. Seasonality and phenological changes in forest structure were considered together by separating the year into seven unequal parts (phenoseasons) which characterize both solar elevations and forest phenology conditions. Thus, we considered two time of day x three sky condition x seven phenoseason categories for each of the three levels in the forest. An average fractional penetration was calculated from the forest radiation data for each of the 42 categories. The continuous solar radiation record from the Oak Ridge weather station was similarly segregated and the total radiation received in each category was calculated. Multiplying the fractional penetration value times the radiation total appropriate for each category yielded an estimate of the amount of radiation received at each forest level in each time of day x cloudiness x phenoseason category. Summing over the time of day x cloudiness categories further yielded an estimate of the phenoseasonal total radiation received at each forest level. Since the phenoseasons are of unequal duration, these totals were normalized by the number of days in each phenoseason. Thus, we compare estimated average daily total radiation received in each of seven phenoseasons.

The seven phenoseasons were defined using the summer and winter solstices, the vernal and autumnal equinoxes, and the dates of the various forest phenological events of importance to the radiation regimes. Phenological data used for these definitions are reported by Taylor (1974).

#### TEMPORAL VARIATION IN *LIRIODENDRON* FOREST RADIATION REGIMES

The derived annual cycle of radiation regimes within and above this forest is shown in Fig. 3. Radiation amounts incident upon and penetrating the winter leafless forest are minimal but show a dramatic increase following the solstice. Since there is no phenological change in forest structure of importance to radiation penetration during the winter and the spring leafless forest phenoseasons, this increase is the result of increasing solar elevations following the winter solstice. This is emphatically illustrated in Fig. 1. The outermost arc of this figure corresponds to the solar path in the winter solstice while the innermost arc represents the path on the vernal equinox. Because of the amount of woody biomass occluding the sky along the winter solstice solar path, little beam radiation is able to penetrate the forest and, as reported by Anderson (1964), the radiation regime of the leafless forest around the winter solstice is dominated by diffuse sky radiation.



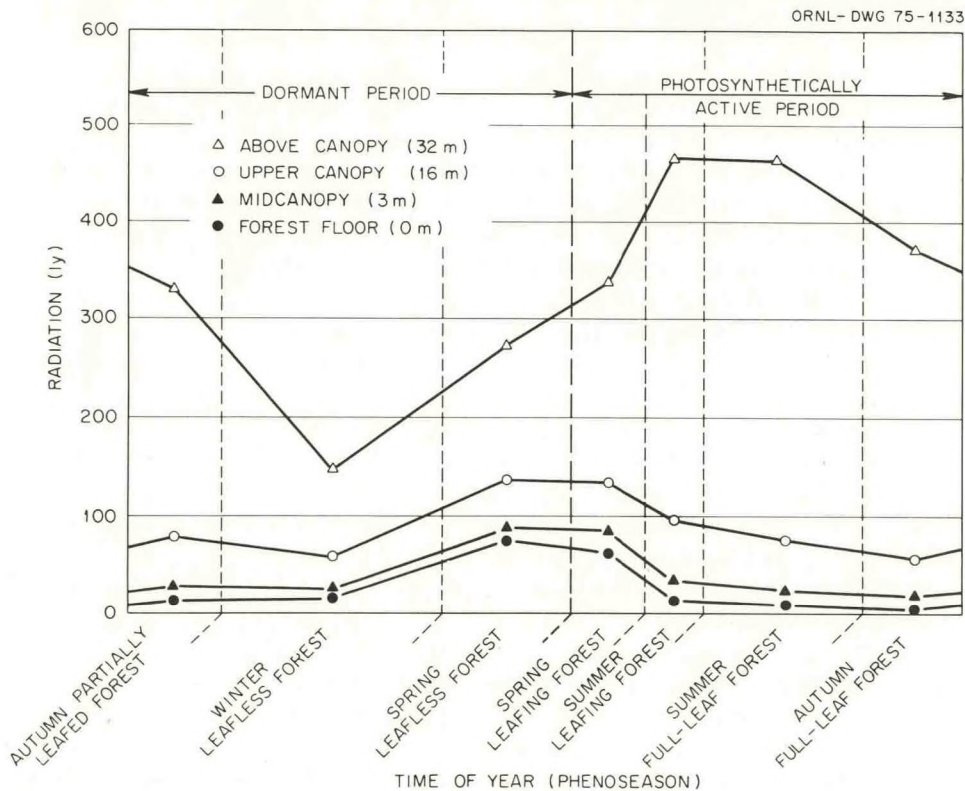


Fig.3. Approximation of the annual radiation regimes above and within the *Liriodendron* forest. ORNL DWG. 75-1133R.

With the increasingly higher solar paths following the winter solstice, more beam radiation penetrates the canopy and radiation totals within the forest rise dramatically. These increasing radiation totals slow or reverse abruptly with the onset of leaf expansion that marks the beginning of the spring leafing forest phenoseason. Despite the continued rise in solar paths and in insolation at the top of the forest, radiation received within declines quite rapidly at lower forest levels and somewhat less rapidly in the overstory. As the summer solstice approaches, leaf expansion closes the canopy and additional leaf layers continue to be added to the canopy. During the summer leafing forest phenoseason, rates of decrease in radiation received within the forest decline somewhat following closure of the canopy but remain substantial.

In early June, this forest attains full leaf and from this time until leaf abscission begins in the autumn, forest structure remains relatively static as evidenced by relative constancy of leaf area indices throughout this period. The period from attainment of full leaf to midway between the summer solstice and the autumnal equinox is termed the summer fully leafed forest phenoseason. During this phenoseason, the rates of decline in radiation received within the forest decrease but never become zero. Now, as in winter,

forest structure is essentially constant but, following the summer solstice, the altitudes of solar paths begin to decrease and as a result, amounts of radiation incident upon the forest decrease. Because the canopy density of the summer fully leafed forest (Fig.2) is much less variable over the hemisphere of sky than in the winter leafless phase, the rates of decline in radiation penetration are not pronounced. On the average, the degree of canopy opening along the summer solstice solar path (represented by the innermost arc of Fig.2) is slightly greater than that along the path of the sun at anytime following (B. A. Hutchison and D. R. Matt, unpublished). Hence, beam radiation penetration declines slowly through time and total radiation received within the forest decreases. In the autumnal fully leafed forest phenoseason, the summer forest is irradiated by an autumn sun. Solar elevations and daily insolation both continue to decline and correspondingly, radiation within the forest continues to decrease.

With the advent of leaf abscission soon after the autumnal equinox, leaf fall begins and the forest enters the autumn partially leafed forest phenoseason. During this period, the loss of leaves from the canopy temporarily offsets the declining beam radiation penetration resulting from decreased solar elevations. The reduced canopy density also allows increased penetration of diffuse sky radiation. The end result of these two factors is a slight increase in total radiation received within the forest during this phenoseason. When all leaves have fallen, the forest enters the winter leafless forest phenoseason once again. Structure remains static while insolation and solar elevations decline toward their annual minima. Radiation within the forest correspondingly declines during this portion of the winter leafless forest phenoseason.

Assuming exponential depletion of solar radiation by forest biomass throughout the year, the data of Fig.3 may be plotted as isopleths of total radiation (Fig.4). Caution must be used in the interpretation of this figure. Since we have data for discrete levels above and within the forest, we know that the isopleths of Fig.4 exist. However, their placement on this figure merely represents our estimate of their actual position. Nevertheless, this figure conveys much information regarding seasonal variation in the radiation climate of this *Liriodendron* forest or of other temperature zone deciduous forests. Anderson's (1964) caveats regarding effects of latitudinal, climatic, and phenological differences upon radiation in different forests still obtain, but we would expect differences of degree, rather than of a kind, between such forests.

Table I summarizes the phenoseasonal distribution of daily totals of radiation received within and above the forest along with the average fractional radiation penetration. Minimum radiation amounts and fractional penetration occur during the autumn fully leafed forest phenoseason while maxima in both quantities occur during the spring leafless forest phenoseason. In contrast to Anderson's (1964) results, the minimum as well as the maximum in both the absolute quantities and the relative amounts of radiation in the forest coincide in time throughout the vertical extent of the forest.



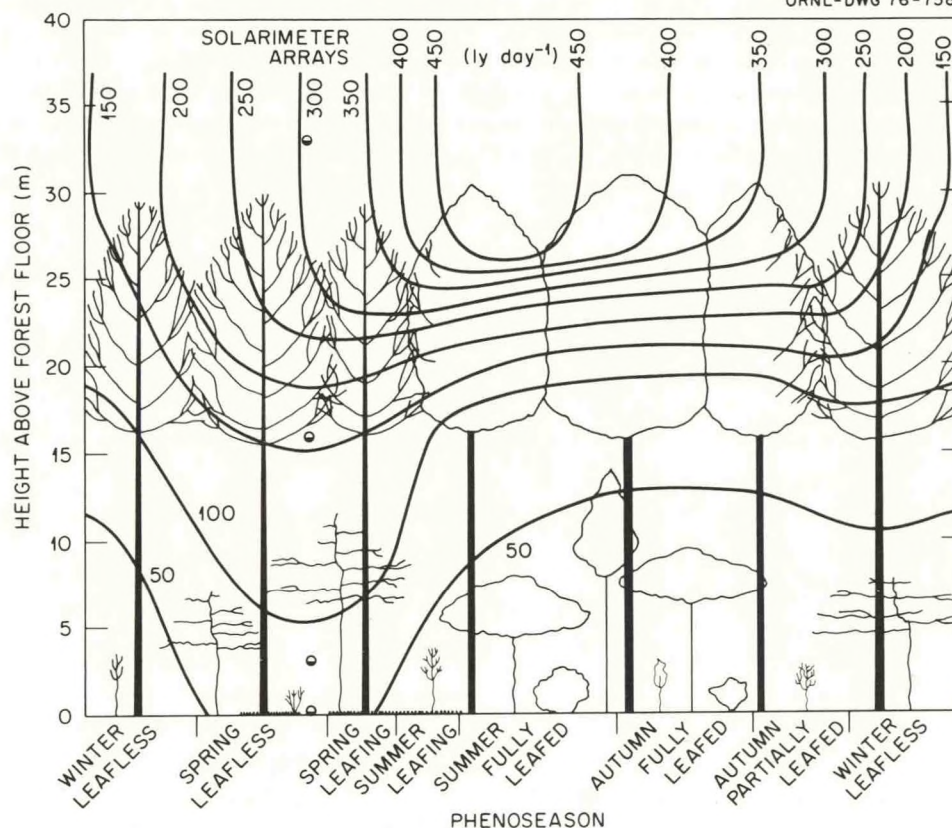


Fig. 4. Synthesized annual course of average daily total solar radiation received above and within the *Liriodendron* forest.

TABLE I

Average daily total radiation received within and above the *Liriodendron* forest

Phenoseason	Duration (days)	Average daily total radiation [ly (% of incident)] at level:			
		Above	16 m	3 m	0 m
Winter leafless	91	146	59 (40.4)	26 (17.8)	16 (11.0)
Spring leafless	55	272	139 (51.1)	89 (32.7)	75 (27.6)
Spring leafing*	30	340	134 (39.4)	85 (25.0)	61 (17.9)
Summer leafing*	26	466	95 (20.4)	33 ( 7.1)	14 ( 3.0)
Summer full leaf*	67	463	75 (16.2)	22 ( 4.8)	10 ( 2.2)
Autumn full leaf*	57	371	58 (15.6)	18 ( 4.8)	4 ( 1.1)
Autumn partially leafed	39	330	79 (24.0)	29 ( 8.8)	12 ( 3.6)

\* Photosynthetically active phenoseasons.



Table II shows the radiation totals received during the photosynthetically active and dormant portions of the year. The photosynthetically active portion of the year is considered to extend from the onset of leaf expansion to the beginning of leaf abscission. Although almost twice as much radiation is

TABLE II

Total radiation received within and above the *Liriodendron* forest during the leafed and leafless phases

Period	Duration (days)	Total radiation [ly (% of yearly total)] at level:			
		Above	16 m	3 m	0 m
Photo- synthetically active	180	74500 (64.4)	14800 (47.9)	5800 (40.8)	3000 (33.0)
Photo- synthetically dormant	185	41200 (35.6)	16100 (52.1)	8400 (59.2)	6100 (67.0)
Yearly total	365	115700	30900	14200	9100

incident on this forest during the active portion of the year, radiation within the forest is reduced from that received in the dormant phase. Only in the overstory canopy are amounts of radiation received of comparable magnitude. The disparity between active and dormant period totals increases with depth in the forest.

#### CONCLUSIONS

The radiation climates of a deciduous forest are strongly controlled by the angle of incidence of the solar beam and by phenological changes in forest structure. As a result of the interactions of these factors, the three levels within the east Tennessee *Liriodendron* forest under study receive minimum leafless phase radiation around the winter solstice and maximum radiation in early spring just prior to leaf expansion. This spring maximum is also the annual maximum and obtains at all three vertical levels in the forest where observations were made. Despite continual increases in solar elevations and in daily insolation following the onset of leaf expansion, radiation at all levels within the forest decreases rapidly. This rate of decrease slows after full leaf development but continues until leaf abscission as a result of the declining solar elevations and daily insolation following the summer solstice. Maximum fully leafed phase radiation is received in the forest around the summer solstice with minimum radiation present within the autumn fully leafed forest just prior to the onset of leaf abscission. The radiation amounts received at the forest floor during this phenoseason are lower than at any other time of year.

The maximum and minimum coincide in time at the vertical levels of the forest where measurements were made and hold for both the absolute amounts of radiation received as well as for the relative fractional amounts of incident radiation penetrating the forest.

#### REFERENCES

- Anderson, M. C., 1964. Studies of the woodland light climate, II. Seasonal variation in light climate. *J. Ecol.*, 52: 643-663.
- Burgess, R. L. and O'Neill, R. V., 1975. Eastern Deciduous Forest Biome Progress Report, Sept. 1, 1973-Aug. 31, 1974. Environmental Sciences Division, Oak Ridge National Laboratory [EDFB/IBP-75 11]. Oak Ridge, Tenn., 252 pp.
- Fritz, S., 1958. Transmission of solar energy through the earth's clear and cloudy atmosphere. *Trans. Conf. Use Solar Energy: The Scientific Basis*, E. F. Carpenter (ed.), Univ. Ariz. Press, Tucson, Ariz., Vol. 1, pp. 17-36.
- Hutchison, B. A. 1975. Photographic Assessment of Deciduous Forest Radiation Regimes. PhD Thesis, Yale Univ., New Haven, Conn., 164 pp.
- Matt, D. R., and Hutchison, B. A., 1974. Response of Lintronic Dome Solarimeters to varying solar radiation flux densities. US-IBP Eastern Deciduous Forest Biome Memo Rpt., No. 74-1, 8 pp.
- Monteith, J. L., 1959. Solarimeters for field use. *J. Sci. Inst.*, 36: 341-346.
- Salisbury, E. J., 1916. The oak-hornbeam woods of Hertfordshire, Parts I and II. *J. Ecol.*, 4: 83-117.
- Scheer, G., 1953. Über Änderung der Globalbeleuchtungsstärke durch Belaubung und Horizonteinengung. *Wetter Leben*, 5: 65-71.
- Schomaker, C. E., 1968. Solar radiation measurements under a spruce and a birch canopy during May and June. *For. Sci.*, 14: 31-38.
- Taylor, F. G., 1974. Phenodynamics of production in a mesic deciduous forest. In: H. Lieth (Editor), *Phenology and Seasonality Modeling*. Springer-Verlag, New York, N.Y., pp. 237-254.





THIRD SYMPOSIUM  
ON  
ATMOSPHERIC TURBULENCE, DIFFUSION, AND AIR QUALITY

Sponsored by the  
AMERICAN METEOROLOGICAL SOCIETY

OCTOBER 19-22, 1976  
RALEIGH, NORTH CAROLINA

The manuscripts reproduced in this collection of preprints are unrefereed papers presented at the Third Symposium on Atmospheric Turbulence, Diffusion, and Air Quality; their appearance in this collection does not constitute formal publication.

AMERICAN METEOROLOGICAL SOCIETY  
45 Beacon Street, Boston, Massachusetts, 02108, U.S.A.

# THE SIMULATION OF ATMOSPHERIC TRANSPORT USING OBSERVED AND ESTIMATED WINDS

Carmen J. Nappo, Jr.

Air Resources  
Atmospheric Turbulence and Diffusion Laboratory  
National Oceanic and Atmospheric Administration  
Oak Ridge, Tennessee 37830

## 1. INTRODUCTION

The spread of pollutants in the atmosphere is often mathematically simulated by the linear combination of transport by the mean wind and dispersion by parameterized turbulence. Recent examples of this method can be found in Heffter *et al.* (1975) and Watson & Barr (1976). In the planetary boundary layer, atmospheric transport can be simulated by trajectory analysis using winds estimated by vertically extrapolating surface winds. Examples of this method can be found in Peterson (1966) and Joynt & Blackman (1976). Several questions arise when trajectories are constructed in the planetary boundary layer. How accurately can trajectories simulate the observed positions of an air parcel along the air parcel's path? How accurate are trajectories constructed from surface winds compared with trajectories constructed from winds observed through the depth of the boundary layer? How does atmospheric stability effect the accuracy of trajectory calculations? One of the main objectives of the Eastern Tennessee Trajectory Experiment (ETTEX), Hanna *et al.* (1974), was to obtain a data base sufficient to answer these questions.

In this study, the ETTEX pilot balloon wind observations are assumed to be a best realization of the real wind field. These data will be used to simulate the trajectories of tetroons released during stable, unstable and transition periods. For each class of stability, the error of the simulation will be determined at the end of each advection step of the trajectory calculation. The average and standard deviation of these errors form the overall accuracy of the trajectory simulation. These results will then be considered to be the "best possible" simulations. This procedure will then be repeated using estimated winds derived from vertically extrapolated surface winds. We can then judge the validity of atmospheric transport calculations using observed or estimated winds.

## 2. THE DATA

The ETTEX region is shown in Figure 1. The elevation contours are in meters and the observation stations are marked with a cross. Wind observations at the ETTEX stations were made with 30 gm pilot balloons tracked by single theodolite. Readings were recorded at 30 second intervals for 10 minutes. Soundings were made at hourly intervals during steady conditions and at half-hourly intervals during transition periods.

These soundings were then vertically smoothed and interpolated to 100 meter increments in elevation from 300 to 2000 meters (MSL). Missing observations were interpolated from the time series using linear regression.

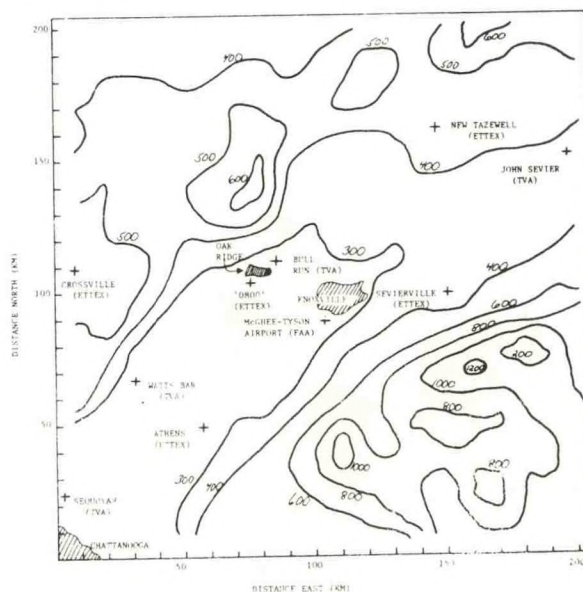


Figure 1. ETTEX Region

Surface winds were measured at the five ETTEX stations, the Sequoyah, Watts Bar, Bull Run and John Sevier TVA power generation plants, and the McGhee-Tyson airport. Observations at the ETTEX stations are 20 minute averages and the TVA observations are hourly averages. The estimated wind fields were determined from these surface winds using a power law extrapolation for the speed and a parameterized veering (clockwise turning) of the wind with height. The  $u$  and  $v$  components of the wind at height  $z$  are then given by

$$u = s_o(z/h)^n \sin(\phi_o + \beta z) \quad (1)$$

$$v = s_o(z/h)^n \cos(\phi_o + \beta z) \quad (2)$$



where  $s_0$  is the surface wind speed at height,  $h$ , above the ground surface;  $\phi_0$  is the wind direction at height  $z_0$  in degrees from north, and  $\beta$  is the parameterized veering in degrees per meter. Table I lists the various forms of  $n$  and  $\beta$  as functions of stability used in this study. Case I tests the 1/7 power law with no turning of the wind with height. Case II has been used by Gudiksen *et al.* (1975). Case III tests case II in the absence of wind veering. Case IV tests extreme values of  $n$  and  $\beta$  for stable and unstable conditions.

Table I. Power law exponent,  $n$ , and wind veering parameter,  $\beta$  ( $^\circ/100$  m)

Stability	Case							
	I		II		III		IV	
	$n$	$\beta$	$n$	$\beta$	$n$	$\beta$	$n$	$\beta$
Stable	$1/4$	0.0	0.10	1.0	0.10	0.0	0.075	1.0
Unstable	$1/4$	0.0	0.20	3.0	0.20	0.0	0.200	4.0
Transition	$1/4$	0.0	0.30	5.0	0.30	0.0	0.200	4.0

The tetron trajectories that are simulated are summarized in Table II. The tetrons were tracked with a high resolution radar provided by the NOAA ARL Field Laboratory in Idaho Falls.

### 3. THE TRAJECTORY MODEL

The trajectory model first interpolates the wind observations at each vertical level over a  $20 \times 20$  horizontal, uniform grid. The grid resolution is 10 km. The interpolating scheme uses a weighting function given by  $a^2/(a^2+r^2)$  where  $r$  is the distance from an observation point to a point on the grid and 'a' is a constant of value 16 km because it gave, in general, the most accurate trajectory calculations using the observed pilot balloon winds. The interpolation scheme takes into account the presence of solid vertical boundaries i.e. mountains by setting to zero the velocity component normal to the boundary. In this way, horizontal wind fields are constructed for each observation time at 100 m intervals from 300 to 2000 m (MSL) and time dependence between observations is introduced by linear interpolation. There is no smoothing of the time series. Trajectories are calculated by first averaging the wind field through a prescribed depth, and then advecting an hypothetical air parcel a distance  $|\vec{v}|\Delta t$  where  $\vec{v}$  is the resultant velocity at the point in space where the advection begins and  $\Delta t$  is the

Table II. Tetron flight data

Period	Date	Tetron No.	Simulation start time (EDT)	Simulation duration (min)	Mean elevation M (MSL)	Standard deviation of elevation	Stability
1	7/16/74	N1	10:10	280	947	416	Unstable
2	7/17/74	N2	11:21	280	756	292	Very unstable
	7/17/74	N3	12:00	250	836	274	
	7/17/74	N4	13:00	190	759	236	
	7/17/74	N4	13:00	190	759	236	
3	7/18/74	N5	16:00	180	1000	321	Transition
	7/18/74	N6	16:00	230	989	255	
	7/18/74	N7	16:00	260	1050	219	
4	7/19/74	N9	17:40	200	837	121	Transition
5	8/07/74	N13	05:10	100	1074	106	Stable
	8/07/74	N14	05:10	80	1079	95	
	8/07/74	N15	05:20	80	1117	137	



length of the advection step, 10 minutes. The layer thicknesses used for the trajectory calculations are summarized in Table III. The resultant velocity is determined by first locating the position of the starting point of the advection step and then interpolating to this point the velocities at the corners of the grid cell in which the point lies. This secondary interpolation uses  $1/(1+d^2)$  as a weighting function where  $d$  is the distance (km) from a cell corner to the point. This function was used to avoid computational errors if  $d$  becomes small.

Table III. Layer depths used in the trajectory calculations

Period	Date	Stability	Elevation of layer M (MSL)
1	7/16/74	Unstable	500-1000
2	7/17/74	Very unstable	500-900
3	7/18/74	Transition	600-1000
4	7/19/74	Transition	700-1000
5	8/07/74	Stable	1000-1200

#### 4. OVERALL ACCURACY. DEFINITION AND SIGNIFICANCE

At the end of each 10 minute advection step of a trajectory calculation, the errors in the range and azimuth between the observed and calculated tetron position are determined. These errors are defined as

$$\text{Range Error (\%)} = 100(|\vec{r}_c| - |\vec{r}_t|) / |\vec{r}_t|$$

$$\text{Azimuth Error (deg)} = \phi_t - \phi_c$$

where  $\vec{r}_c$  and  $\vec{r}_t$  are respectively the calculated and observed tetron positions relative to the release point and  $\phi_t$  and  $\phi_c$  are the azimuth angles measured clockwise from north for the observed and calculated tetron positions, respectively. A sample of these errors as a function of distance is shown in Figure 2. The trajectories for this case are shown in Figure 3 (The numbers on the trajectories represent elapsed time in hours from release). The similarity in the shape of the range error and azimuth error curves in Figure 2 is due to the similarity in the trajectories shown in Figure 3. From these figures, we see that a negative range error indicates an under-estimation of the transport and a negative azimuth error indicates that the calculated tetron position is to the right of the observed tetron position. Azimuth errors apparently tend to decrease with distance; however, this is generally true only when the calculated and observed tetron trajectories are similar. On the other hand, range errors, in general, decrease with distance because they are expressed as a percent of travel distance and, except in cases of light and variable winds, the difference in range,  $(|\vec{r}_c| - |\vec{r}_t|)$ , tends to remain constant.

In order to quantify the accuracy of a trajectory calculation, the average and standard deviation of the range and azimuth errors are formed using the calculated positions along

the trajectory. These quantities are taken as a measure of the overall accuracy. Of these two quantities, the overall accuracy in azimuth is the more important, since in practice one is more concerned about where an air parcel is going rather than its transport speed. This point is discussed further in Smith & Jeffrey (1975). In many cases, the standard deviation of the error is more meaningful than its average. This is because trajectory calculations using averaged wind data or single observations made at large time intervals cannot reproduce the turbulent fluctuations that act on real air parcels. A calculated trajectory may well represent the non-turbulent transport of an air parcel with the result that the average overall errors are small; however, in the presence of strong convective turbulence or terrain induced perturbations to the wind not realized by the observations, the standard deviation of these errors will be large. We can anticipate that the standard deviations will depend upon the intensity of the turbulence and on the smoothness of the topography. The measure of overall accuracy should be considered as the uncertainty in a trajectory calculation.

RANGE AND AZIMUTH ERROR AS A FUNCTION OF DISTANCE FROM RELEASE POINT

TETRON 89 TRAJECTORY SIMULATION		
OVERALL ACCURACY:	RANGE (%)	AZIMUTH (deg)
OBSERVED WINDS	-20.3 ± 7.9	5.9 ± 5.2
ESTIMATED WINDS	-66.6 ± 6.5	-1.0 ± 4.9

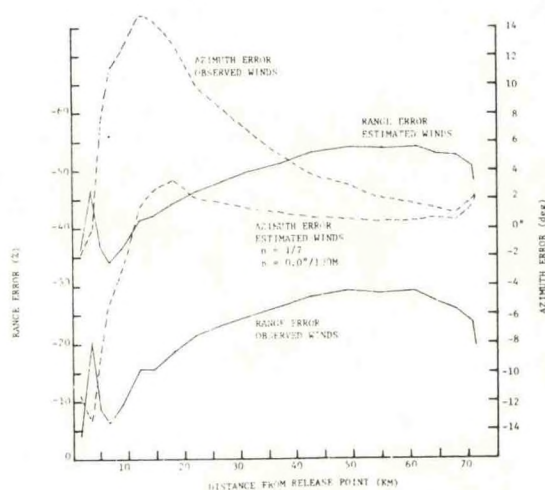


Figure 2

#### 5. THE RESULTS

The overall accuracy of the trajectory calculations for each period are listed in Table IV. The results for periods 2,3 and 5 are averages of the results for the individual trajectory calculations. To better relate these errors to the actual trajectories, four samples of the trajectory simulations are presented in Figures 3 to 6.

Table IV. Overall accuracy –  
range error (%), azimuth error (deg)

Period		Observed Winds	Estimated Winds			
			Case I	Case II	Case III	Case IV
1	Range error	$-5.3 \pm 6.2$	$-0.4 \pm 7.6$	$-15.2 \pm 5.8$	$-15.4 \pm 6.0$	$-22.9 \pm 5.0$
	Azimuth error	$-2.4 \pm 4.6$	$-0.1 \pm 3.4$	$-3.2 \pm 3.2$	$0.9 \pm 3.2$	$-2.5 \pm 3.2$
2	Range error	$114.8 \pm 217.8$	$55.3 \pm 122.1$	$44.8 \pm 117.1$	$43.9 \pm 116.6$	$40.3 \pm 116.6$
	Azimuth error	$-50.1 \pm 67.6$	$79.6 \pm 59.2$	$78.1 \pm 59.3$	$75.2 \pm 55.3$	$79.3 \pm 59.9$
3	Range error	$-5.3 \pm 5.2$	$-6.6 \pm 8.1$	$17.1 \pm 10.6$	$15.5 \pm 10.1$	$17.2 \pm 9.9$
	Azimuth error	$-3.1 \pm 3.9$	$16.2 \pm 4.8$	$4.7 \pm 4.8$	$13.7 \pm 5.1$	$-3.8 \pm 4.7$
4	Range error	$-20.3 \pm 7.9$	$-46.6 \pm 6.5$	$-33.4 \pm 7.6$	$-35.2 \pm 7.4$	$-32.0 \pm 7.4$
	Azimuth error	$5.9 \pm 5.2$	$-1.0 \pm 4.9$	$-20.2 \pm 5.2$	$-5.3 \pm 5.9$	$-25.8 \pm 4.8$
3+4	Range error	$-12.8 \pm 6.6$	$-26.6 \pm 7.3$	$-8.2 \pm 9.1$	$-9.9 \pm 8.8$	$-7.4 \pm 8.7$
	Azimuth error	$1.4 \pm 4.6$	$7.6 \pm 4.9$	$-7.8 \pm 5.0$	$4.2 \pm 5.5$	$-14.8 \pm 4.8$
5	Range error	$61.1 \pm 73.7$	$-87.4 \pm 5.7$	$-67.1 \pm 14.4$	$-76.6 \pm 10.5$	$-80.4 \pm 7.8$
	Azimuth error	$6.1 \pm 8.4$	$172.5 \pm 17.0$	$101.4 \pm 11.8$	$150.3 \pm 16.3$	$117.3 \pm 8.6$

For period 1, the estimated winds are as accurate as the observed winds. The introduction of veering, cases II and IV, results in larger azimuth error; however the increased error is not significant when compared to the azimuth error for the observed winds.

In period 2, a great difference exists between the trajectory calculations as can be seen, for example, in Figure 4. The overall accuracies in the estimated wind trajectory calculations are relatively insensitive to the value of the power law exponent and the degree of wind veering factor.

TRAJECTORY CALCULATIONS USING  
OBSERVED AND ESTIMATED WINDS

TETROON N9 TRAJECTORY SIMULATION

OVERALL ACCURACY:	RANGE (Z)	AZIMUTH (deg)
OBSERVED WINDS	$-20.3 \pm 7.9$	$5.9 \pm 5.2$
ESTIMATED WINDS	$-46.6 \pm 6.5$	$-1.0 \pm 4.9$

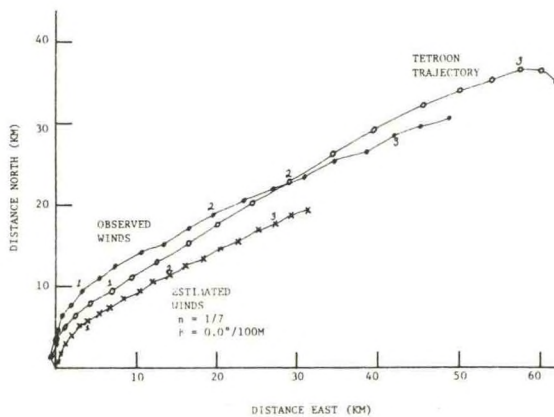


Figure 3

TRAJECTORY CALCULATIONS USING  
OBSERVED AND ESTIMATED WINDS

TETROON N2 TRAJECTORY SIMULATION

OVERALL ACCURACY:	RANGE (Z)	AZIMUTH (deg)
OBSERVED WINDS	$107.5 \pm 195.8$	$-51.5 \pm 59.1$
ESTIMATED WINDS	$12.7 \pm 148.6$	$87.3 \pm 55.6$

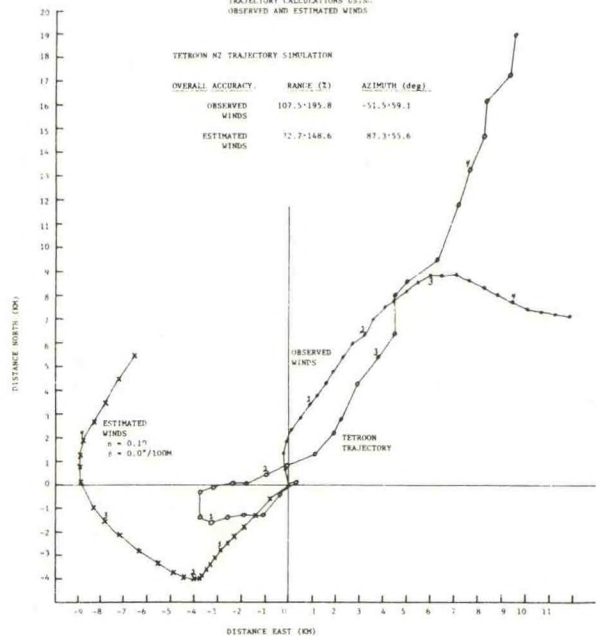


Figure 4



Because periods 3 and 4 are of the same stability type, their results can be averaged. These averages are shown in Table IV as period (3+4). From Figures 3 and 5, we see that the estimated wind and observed wind trajectories are in fair agreement with the actual tetron trajectory.

In period 5, the estimated winds are extremely poor in predicting the direction of the tetron path as is quite evident in Figure 6. Wind veering helps reduce the azimuth error, however a great deal more than  $5^\circ/100$  m is necessary.

## 6. DISCUSSION OF RESULTS

From the above results, we see that the greatest overall errors occur for the strongly stable and unstable cases. These errors are equally as great for the observed as well as the estimated winds. During period 2, there were light winds with strong convective turbulence. The hourly ETTEX observations could not resolve the mean wind structure because of its extreme variability, and as a result large errors exist in the average range and azimuth calculations. The large variability of the winds also produces large standard deviations of these errors. The estimated winds, however, do produce less average error in range because these winds are time averages and thus more truly reflect the mean transport winds.

The results for period 5 are in contrast somewhat with those of period 2, i.e. large mean errors but with small standard deviations. From Figure 5, we see that during the first two hours of the trajectory the estimated winds produce a path directed approximately down the Tennessee Valley. An analysis of the surface winds throughout the Tennessee Valley for a six week period during the ETTEX experiment, shows the apparent existence of a large scale nocturnal wind directed down the valley. It is believed that this wind is the result of drainage from the Smoky Mts. and the Cumberland Plateau. Under night-time conditions, the surface winds are evidently uncoupled from the upper level winds and cannot be expected to produce a meaningful trajectory result. An example of this valley wind is seen in Figure 7 which shows the early morning wind field over the ETTEX region at various elevations. The wind field was derived from the ETTEX observations. The wind arrows with circles at 400 m are surface observations which were not used in the interpolation. Note that between 400 and 1600 m, there exists a  $180^\circ$  wind shear. In an earlier report (Nappo 1975) it was suggested that under stable conditions the large scale terrain features produce a strong horizontal variability of the wind field. In an attempt to compensate for this variability, the estimated winds were horizontally averaged at each level and the trajectories recalculated. The result of this procedure for tetron N13 is shown in Figure 6. Horizontal averaging reduces the overall azimuth error by about  $60^\circ$ , and suggests a possible procedure to follow during stable conditions.

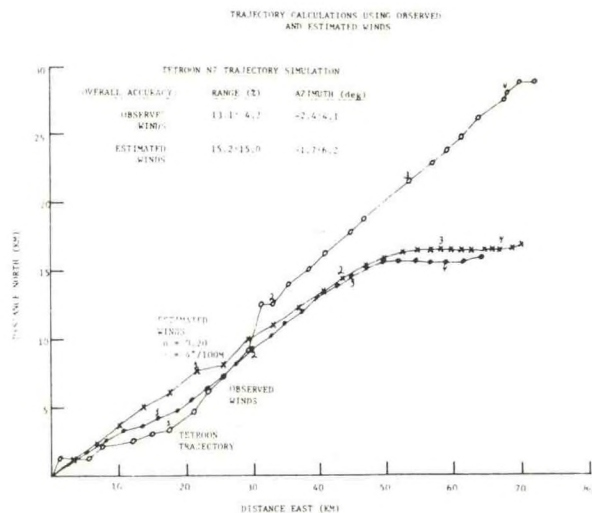


Figure 5

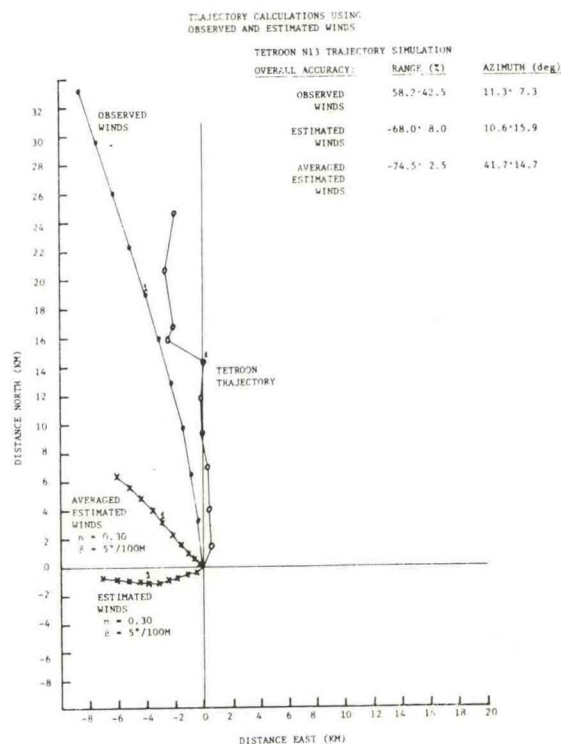
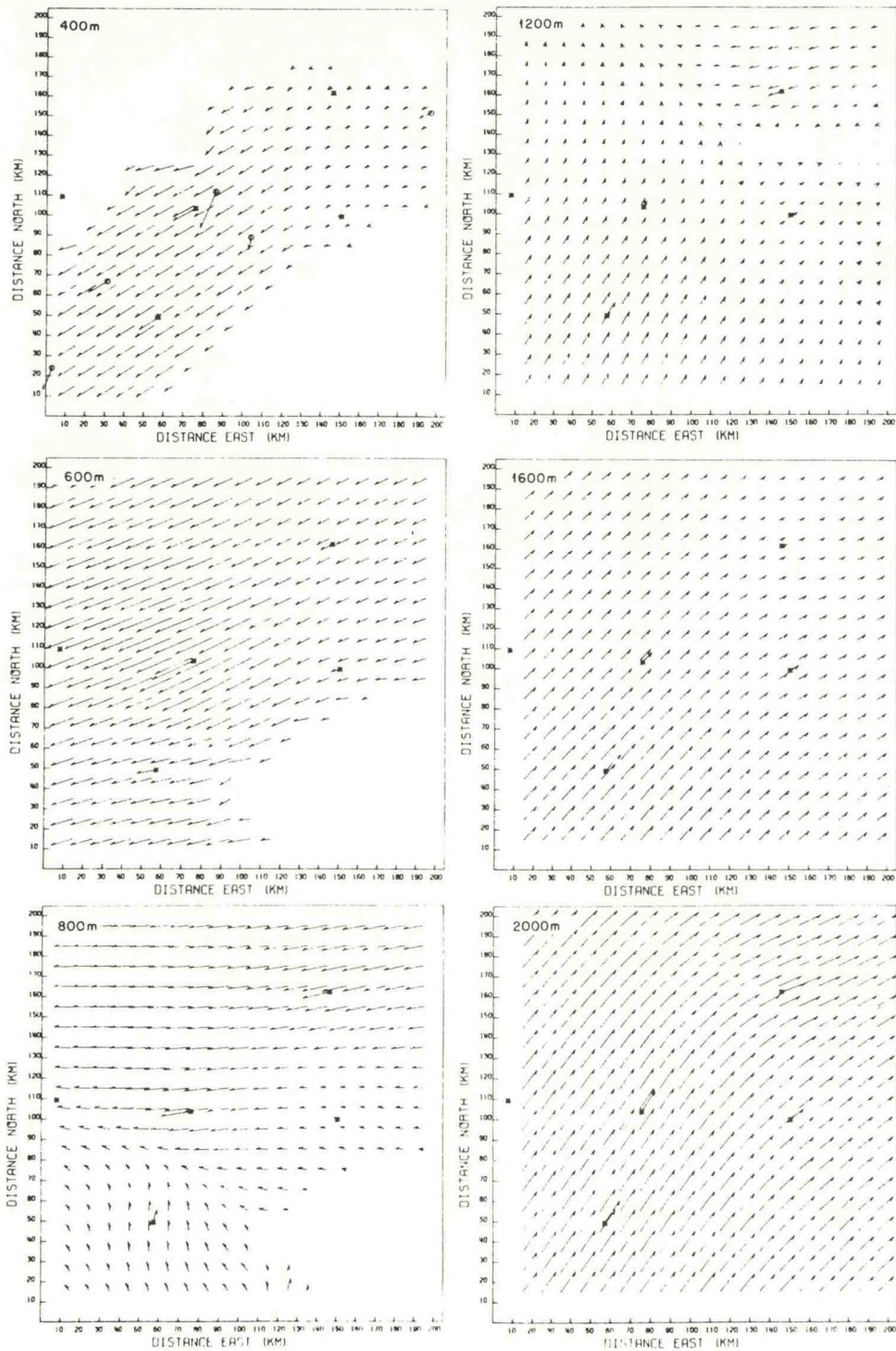


Figure 6





ETTEX Wind Field 8-06-74 at 0700EDT for Various Heights Above Sea Level.

Figure 7

## 7. CONCLUSION

The results presented here have been derived from a limited number of observations for a particular geographic region; however, this study does offer the following generalizations:

7.1 In strongly stable and unstable conditions, air parcel trajectories formed from surface wind estimates can be expected to be in large error. Under these conditions, horizontal averaging of the estimated winds can improve the overall accuracy.

7.2 For moderately unstable and transition conditions, the surface winds adjusted in the manner used by Gudiksen *et al.* (1975) offer acceptable results, i.e. overall errors in range and azimuth on the order of 10% and 10 degrees respectively.

7.3 For strongly unstable conditions, a time average of winds is necessary.

7.4 Except for unstable conditions, the observed winds are better than the estimated winds; however, only under stable conditions are the observed winds significantly better.

7.5 With appropriate adjustments, surface winds can offer reliable estimates of atmospheric transport.

## ACKNOWLEDGEMENT

This work was performed under an agreement between the National Oceanic and Atmospheric Administration and the Energy Research and Development Administration.

## REFERENCES

- Hanna, S. R., C. J. Nappo, R. P. Hosker, and G. A. Briggs, 1974: Description of the eastern Tennessee trajectory experiment (ETTEX). Air Resources Atmospheric Turbulence and Diffusion Laboratory, ATDL Contribution No. 103.
- Heffter, J. L., A. D. Taylor and G. J. Ferber, 1975: A regional-continental scale transport, diffusion, and deposition model. *NOAA Tech. Memo. ERL-ARL-50*. U. S. Dept. of Commerce, Air Resources Laboratories, Silver Spring, Maryland.
- Joynt, R. C. and D. R. Blackman, 1976: A numerical model of pollutant transport, to appear in Vol. 10, *Atmos. Environ.*
- Nappo, C. J., 1975: Time dependent mesoscale wind fields over complex terrain, Air Resources Atmospheric Turbulence and Diffusion Laboratory, ATDL Contribution No. 75/6.
- Peterson, K. R., 1966: Estimating low-level tropospheric trajectories, *J. Atmos. Sci.* 5, 553-564.
- Smith, F. B. and G. H. Jeffrey, 1975: Airborne transport of sulphur dioxide from the U.K. *Atmos. Environ.*, Vol. 9, 643-660.
- Watson, C. W. and S. Barr, 1976: Monte Carlo simulation of the turbulent transport of airborne contaminants, report no. LA-6103, Los Alamos Scientific Laboratory of the Univ. of Calif., Los Alamos, N.M.



## Tropospheric Relative Diffusion Observations

F. A. GIFFORD

*Atmospheric Turbulence and Diffusion Laboratory, NOAA, Oak Ridge, Tenn.*

10 September 1976

### ABSTRACT

Data on relative atmospheric diffusion, that is, the spreading by diffusion of puffs or particle pairs (e.g., of balloons) relative to their mutual center of mass, are reexamined. Richardson (1926) proposed his well-known law,  $K = 0.2\sigma^3$ , on the basis of an early collection of such data. More recently, much more extensive data sets have been studied which include relative diffusion data over far greater range of  $\sigma$  values. Further relative diffusion data sources are combined with these and, by classifying these data in various ways, it is shown that they suggest the relation  $\sigma \propto t^{1/3}$ , in agreement with previous results including Richardson's, over the range  $2 \leq t \leq 10^3$  s. There is good evidence of slower diffusion in the range generally corresponding to the spectral "gap." For still greater values of  $t$  the data are not inconsistent with a second accelerated diffusion regime, displaced by approximately one order of magnitude in  $\sigma$ .

It is a fundamental, characteristic feature of turbulent flows that they diffuse properties, including tracer substances, which are often introduced into these flows especially to measure turbulence effects. For many years workers have tried to study atmospheric turbulence this way by measuring the rate of diffusive spreading about their instantaneous centroid of pairs, groups, clusters, puffs or plumes of various tracer substances. Richardson (1926) assembled observations including such tracer spreading in the atmosphere, over a rather large range of times and distances, and derived his famous law of relative diffusion from these data, i.e.,  $K = 0.2\sigma^3$ ;  $K$  is eddy diffusivity and  $\sigma$  the cluster or puff size. (In these and most of the following cases  $\sigma$  is the standard deviation of the horizontal component of the tracer cloud's distribution.) Obukhov (1941) deduced from similarity considerations that  $K = A\epsilon^{1/3}\sigma^3$ , where  $\epsilon$  is the eddy-energy dissipation rate and  $A$  is a universal constant. Such a puff or cluster spreading law is expected to apply in a turbulent flow whose energy is derived from large-scale motions and is dissipated at small scales. The domain of applicability, the intermediate scales sufficiently far removed from the two extremes of large-scale energy supply and small-scale energy removal, is called the "inertial range." Batchelor (1952) showed these laws to imply, in this range, that  $\sigma \propto t^{1/3}$ . This is a practically as well as a theoretically interesting result, in that it shows that instantaneous "relative" diffusion occurs at a rate distinctly faster than that of "average" diffusion, typified by the mean spreading of plumes about a fixed axis, which is at most  $\sigma \propto t$ .

Richardson's data, which indicate dispersion as  $t^{1/3}$  over a range from 1 m to 10 km, imply a very large atmospheric energy-cascade range, far larger than is believed to exist in the planetary boundary layer. It is probable that the effect of cross-wind shear on horizontal spreading is coming into play at times corresponding to about 5 km or more of downwind travel. Corrsin (1953), Saffman (1962) and Smith (1965) have derived  $\sigma \propto t^{1/3}$  laws for horizontal relative diffusion in shear flows, as Snyder (1972) points out. Moreover, Pasquill (1974) concluded that neither Richardson's data nor the upper troposphere and stratosphere relative diffusion data summarized by Heffter (1965) contain examples of individual runs for which the spreading exceeded  $\sigma \propto t$ . On the other hand, Gifford (1957) analyzed short-range, smoke-puff spreading data from several small-scale boundary layer tracer experiments and found good evidence of  $t^{1/3}$  behavior for a few tens of seconds, presumably reflecting inertial subrange spreading.

Crawford (1966) and Hage (1964) combined data from many atmospheric relative diffusion experiments and other sources, including all the above data sets, in attempts to extend and generalize this approach. Although these plots present a somewhat scattered picture, Crawford suggested a curve of  $\sigma \propto t^{1.2}$  as generally representative over the range  $1 \leq t \leq 10^6$  seconds, approximately. A more recent collection, by Bauer (1974), further complicates the picture by adding both Okubo's (1971) ocean surface dye-spreading data, and data from various meteor-trail and rocket-trail observations high in the atmosphere, in some instances



above the lower limit of diffusive equilibrium ( $\sim 100$  km). The resulting plot of  $\sigma$  values vs  $t$  is characterized by great scatter, up to three orders of magnitude in  $\sigma$  and slightly more in  $t$ .

The difficulty with these interesting collections is that the data are too heterogeneous and confused to support any clear interpretation in terms of boundary layer/tropospheric diffusion. As it grows, a plume, puff or cluster of balloons released somewhere near the surface experiences first the boundary layer turbulence at increasing scales. After several hours it grows larger than the boundary layer depth and, after several days may spread through most of the depth of the troposphere. During this time it is being diffused by ever larger eddies, whose physical character changes markedly as the boundary layer turbulence gives way to the essentially two-dimensional turbulence characteristic of the large-scale motion. Stratospheric diffusion must generally be quite different from tropospheric because of the strongly stable thermal stratification there. And ionospheric and ocean-surface spreading are also better considered separately because they involve various physical effects not encountered in the troposphere. Thus, to improve clarity and relevance, Crawford's data have been replotted in Fig. 1, leaving out all

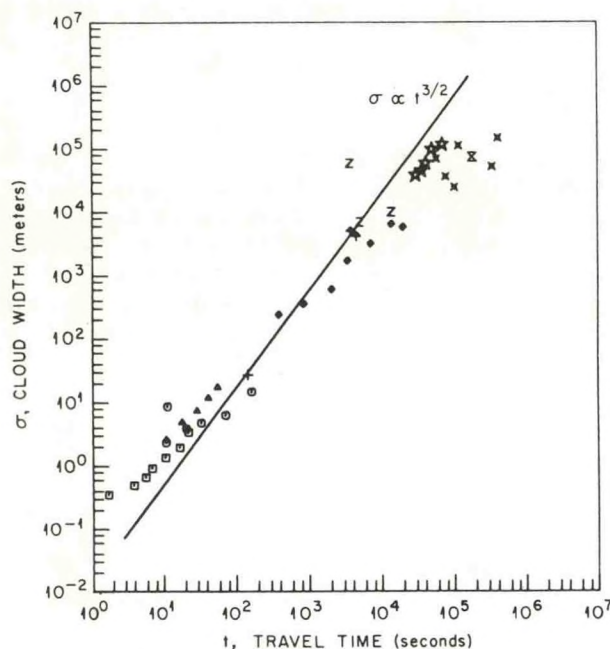


FIG. 1. Crawford's (1966) data on relative diffusion showing cloud width  $\sigma$  vs travel time  $t$ , from which purely stratospheric points have been removed. (For detailed references see Crawford's paper.)

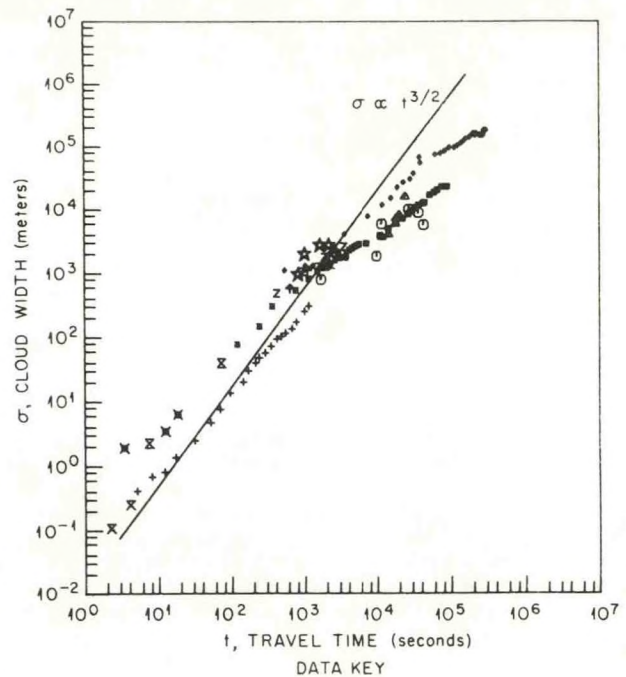


FIG. 2. Additional tropospheric relative diffusion data showing cloud width  $\sigma$  vs travel time  $t$ .

purely stratospheric points. The law  $\sigma \propto t^{3/2}$  fits the result fairly well between about 50 and 3000 s. Elsewhere the spreading is slower, and Crawford's overall fit by  $\sigma \propto t^{1.2}$  is a good compromise over the whole range.

More recently, several interesting new sets of spreading data have been reported. Byzova *et al.* (1970) observed spreading of a boundary layer smoke plume photographically. Their data indicate a clear  $t^{3/2}$  regime from 10 s to at least 500 s. Randerson (1972) analyzed the spread of a radioactive cloud which was tracked over several days. Although there may be a hint of a  $t^{3/2}$  regime in the early points ( $t < 3000$  s), the data for greater times indicate a distinctly slower rate of spread. Angell *et al.* (1971) observed the spreading of tetraon pairs in the boundary layer. Spreading was uniformly less than  $t^{3/2}$ , but all their data points are for  $t > 3000$  s. Hanna (1975) also studied boundary layer spreading of tetraon pairs. Between 100 and 400 s spreading was close to  $t^{3/2}$  but was less than that for greater times.

In Fig. 2 these new sets of spreading data have all been plotted, together with a number of sets of instantaneous plume- or puff-spreading data that have heretofore been overlooked in connection with relative diffusion study. These include the long-distance, plume-spreading data by Peterson (1968) and Smith and Heffernan (1956); Davies' (1959) tropospheric smoke-



spreading data from the Long Beach oil refinery fire; Kazanski and Monin's (1957) surface-layer, smoke-spreading data plus tropospheric tetraon spreading data by Kao and Wendell (1968); Roberts' (1923) artillery burst data; and Edinger's (1952) soap bubble data. Several more pieces of data could perhaps be added, but these are ample to support the following conclusions. For puffs or plumes released in the boundary layer there is, after the disappearance of initial source size effects, a  $t^{1/3}$  spreading regime extending to somewhere between 1000 and 3000 s, the exact point presumably depending on meteorological conditions for the particular run. Then a slower regime appears, characteristic of mesoscale diffusion in the spectral "gap." Whether there is, at yet larger scales, another accelerated diffusion regime due to an energy cascade from the synoptic-scale atmospheric disturbances is not apparent from these data. Several such distinct regimes have been reported to occur in ocean diffusion, for instance by Ozmidov (1968). Also, a schematic atmospheric energy spectrum indicating two  $k^{-5/3}$  regimes on either side of a mesometeorological minimum has recently been discussed from the theoretical point of view by Golitsyn (1973). All that can be said of the atmospheric diffusion data at present is that *they are not inconsistent with* a second accelerated diffusion regime at large time scales, displaced about an order of magnitude in  $\sigma$ .

**Acknowledgment.** This research was performed under an agreement between the Energy Research and Development Administration and the National Oceanic and Atmospheric Administration.

## REFERENCES

- Angell, J. K., P. W. Allen and E. A. Jessup, 1971: Mesoscale relative diffusion estimates from tetraon flights. *J. Appl. Meteor.*, **10**, 43–46.
- Batchelor, G. K., 1952: Diffusion in a field of homogeneous turbulence II. The relative motion of particles. *Proc. Cambridge Phil. Soc.*, **48**, 345–362.
- Bauer, E., 1974: Dispersion of tracers in the atmosphere and ocean: survey and comparison of experimental data. *J. Geophys. Res.*, **79**, 789–795.
- Byzova, N. L., Ye. K. Garger and V. N. Ivanov, 1970: Experimental estimation of the Lagrangian time scale of turbulence. *Izv. Atmos. Oceanic Phys.*, **6**, 315–320.
- Corrsin, S., 1953: Remarks on turbulent heat transfer. *Proc. First Iowa Symp.*, University of Iowa, Iowa City, 5–30.
- Crawford, T. V., 1966: A computer program for calculating the atmospheric dispersion of large clouds. University of California, Laerence Radiation Laboratory, Rep. UCRL-50179, 56 pp.
- Davies, R. W., 1959: Large-scale diffusion from an oil fire. *Advances in Geophysics*, Vol. 6, Academic Press, 413–414.
- Edinger, J. G., 1952: A technique for measuring the detailed structure of atmospheric flow. *Geophys. Res. Pap. No. 19*, AFGRD, Cambridge, Mass.
- Gifford, F., 1957: Relative atmospheric diffusion of smoke puffs. *J. Meteor.*, **14**, 410.
- Golitsyn, G. S., 1973: *Introduction to the Dynamics of Planetary Atmospheres*. Hydrometeor. Press, Leningrad, 103 pp. [Translated as NASA TT F-15, 97 pp.]
- Hage, K. D., 1964: Particle fallout and dispersion below 30 km in the atmosphere. Final Rep. SC-DC-64-1463, Sandia Corp., Albuquerque, N. M.
- Hanna, S. R., 1975: Relative diffusion of tetraon pairs during convective conditions. Paper presented at First Conf. Regional and Mesoscale Modeling, Analysis and Prediction, Las Vegas, Nev., Amer. Meteor. Soc.
- Heffter, J. J., 1965: The variation of horizontal diffusion parameters with time for travel periods of one hour or longer. *J. Appl. Meteor.*, **4**, 153.
- Kao, S. K., and L. L. Wendell, 1968: Some characteristics of relative particle dispersion in the atmosphere's boundary layer. *Atmos. Environ.*, **2**, 397–407.
- Kazanski, A. B., and A. S. Monin, 1957: The form of smoke jets. *Izv. Atmos. Oceanic Phys.*, **8**, 1020–1033.
- Obukhov, A. M., 1941: On the distribution of energy in the spectrum of turbulent flow. *Izv. Akad. Nauk Ser. Geogr. Geofiz.*, **5**, 453–456.
- Okubo, A., 1971: Oceanic diffusion diagrams. *Deep-Sea Res.*, **18**, 789–802.
- Ozmidov, R. V., 1968: Dependence of the coefficient of horizontal turbulent exchange in the ocean on the phenomenon scale. *Izv. Atmos. Oceanic Phys.*, **4**, 703–704.
- Pasquill, F., 1974: *Atmospheric Diffusion*, 2nd ed. Wiley, 429 pp.
- Peterson, K. R., 1968: Continuous point-source plume behavior out to 160 miles. *J. Appl. Meteor.*, **7**, 217–226.
- Randerson, D., 1972: Temporal changes in horizontal diffusion parameters of a single nuclear debris cloud. *J. Appl. Meteor.*, **11**, 670–673.
- Richardson, L. F., 1926: Atmospheric diffusion shown on a distance-neighbor graph. *Proc. Roy. Soc. London*, **A110**, 709–737.
- Roberts, O. F. T., 1923: The theoretical scattering of smoke in a turbulent atmosphere. *Proc. Roy. Soc. London*, **A104**, 640–654.
- Saffman, P. G., 1962: The effect of wind shear on horizontal spread from an instantaneous ground source. *Quart. J. Roy. Meteor. Soc.*, **88**, 382–393.
- Smith, F. B., 1965: The role of wind shear in horizontal diffusion of ambient particles. *Quart. J. Roy. Meteor. Soc.*, **91**, 318–329.
- Smith, E. J., and K. J. Hefferman, 1956: The decay of the ice-nucleating properties of silver iodide released from a mountain top. *Quart. J. Roy. Meteor. Soc.*, **82**, 301–309.
- Snyder, W. H., 1972: Similarity criteria for the application of fluid models to the study of air pollution meteorology. *Bound. Layer Meteor.*, **3**, 113–134.





# Environmental Research Laboratories

Air Resources

Atmospheric Turbulence and Diffusion Laboratory

Oak Ridge, Tennessee

JULY 1976

FIRST ANNUAL REPORT ON WEATHER MODIFICATION EFFECTS OF COOLING TOWERS

S. R. Hanna  
R. P. Hosker, Jr.

ATDL Contribution File No. 76/11

U. S. DEPARTMENT OF COMMERCE  
NATIONAL OCEANIC AND ATMOSPHERIC ADMINISTRATION

FIRST ANNUAL REPORT  
ON  
WEATHER MODIFICATION EFFECTS OF COOLING TOWERS

to  
U. S. Environmental Protection Agency  
and  
U. S. Energy Research and Development Administration

from  
National Oceanic and Atmospheric Administration  
Air Resources Atmospheric Turbulence and Diffusion Laboratory  
Oak Ridge, Tennessee

S. R. Hanna  
R. P. Hosker, Jr.

## TABLE OF CONTENTS

	<u>Page</u>
Chapter I: Introduction and summary	1
Chapter II: Development and applications of a cooling tower plume and cloud growth model, by S. R. Hanna	3
Chapter III: Plans for laboratory study of flow and plume behavior near single and multiple cooling towers of various types, by R. P. Hosker, Jr.	30
Chapter IV: Tentative schedule for future work	51
Chapter V: References	55
Appendix A	
Appendix B	



## CHAPTER I

### INTRODUCTION AND SUMMARY

This is the first annual report on work accomplished at the National Oceanic and Atmospheric Administration's Air Resources Atmospheric Turbulence and Diffusion Laboratory (ATDL), Oak Ridge, Tennessee, on "Weather Modification Effects of Cooling Towers." This research was carried out under an interagency agreement between the U. S. Environmental Protection Agency and the U. S. Energy Research and Development Administration under the general title "Cooling System Program," Interagency Energy Accomplishment Plan I. D. no. 77BCD, IAG I.D. no. D5-E681, program element EHA541, Task no. T/A 1.b, dated April 16, 1975. The principal investigator is F. A. Gifford, Jr., Director of ATDL. Participating ATDL scientists include G. A. Briggs, S. R. Hanna, R. P. Hosker, Jr., and K. S. Rao.

Chapter II reports on a cooling tower plume and cloud growth model developed at ATDL by S. R. Hanna. Using observed atmospheric vertical profiles of temperature, dew point and wind speed, and the source parameters for a cooling tower, the ATDL plume and cloud growth model estimates the variation with height of vertical speed, temperature, water vapor content, and liquid water content in the plume. The present model is one dimensional and steady state, but

future plans call for the development of multidimensional models. The model predictions are compared to observations of cooling tower plumes at the Rancho Seco and John E. Amos power plants and a refinery cloud. Fair agreement is obtained between estimates and observations of excess water and temperature in the plume, visible plume length, and plume rise. The model is also applied to 241 radiosonde soundings from Nashville, using four hypothetical sources ranging from a single 1000 MW cooling tower to a  $10^5$  MW power park. It is estimated that liquid water will form at the top of the plume 39% of the time for the  $10^3$  MW tower. Estimated visible plume length and plume rise are presently being compared with observations from TVA's Paradise, Kentucky, cooling tower.

Chapter III presents the plans for laboratory study of flow and plume behavior near single and multiple cooling towers of different types. An extensive survey of the laboratory simulation literature has been completed, requirements for the requisite modeling facility formulated, and equipment, including a suitable wind tunnel, purchased. Funding and construction delays in obtaining a building to house the tunnel have unavoidably postponed the start of the experimental test program. It is presently anticipated that the finished facility will be in operation before January 1, 1977, roughly six months behind the original schedule.

Chapter IV provides a new tentative schedule of accomplishment. An accelerated laboratory test program should permit meeting the original project deadline for completion with no serious difficulty.

Chapter V lists the references cited in the theoretical and experimental sections.

## CHAPTER II

### DEVELOPMENT AND APPLICATIONS OF A COOLING TOWER PLUME AND CLOUD GROWTH MODEL

by  
Steven R. Hanna

#### 1. Introduction

Single cooling towers emit as much as 1000 MW of sensible and latent heat to the atmosphere. Planned energy centers or power parks may contain clusters of cooling towers which emit a total of 100,000 MW. As shown by Hanna and Gifford (1975) heat releases of this magnitude have the potential to significantly alter local weather. Cooling towers can also alter the local environment by the production of fog and clouds, and the deposition of drift salts.

There are several models available for estimating drift deposition and visible plume length from single cooling towers (see Cooling Tower Environment - 1974 and McVehil and Heikes, 1975). However, there are no data suitable for testing the drift deposition models and very few data suitable for testing the visible plume models. Currently a drift deposition experiment is underway at Chalk Point, Maryland, (Environmental Systems Corporation, 1976) as part of a comprehensive study of the salt water natural draft cooling tower at that site. A few measurements of visible plume length are available (e.g.; Slawson et al., 1974; Meyer et al., 1974), and there are several more sets of measurements that are just being published. Three of the new sets of visible plume observations



are compared with model predictions in this report. These are the observations of cooling tower plumes at the John E. Amos fossil power plant (Kramer et al., 1975), the Rancho Seco nuclear power plant (Wolf, 1976), and a refinery plume near St. Louis (Auer, 1976).

The basic model presented in this report is a simple one-dimensional model (variables are functions only of height). Since the cooling tower emissions are usually constant with time, at least over time periods less than four or five hours, the steady-state assumption is good. Phenomena such as multiple plume merging and changes in the environmental air surrounding the plume are accounted for only by crude parameterization. According to our plan, this model is only the first in a series of models, and future models will be multidimensional and able to handle plume-environment interactions. Other members of our research group, S. Rao and C. Nappo (1976), are developing second order closure and fully turbulent models of multiple plumes.

A thorough description of the one-dimensional numerical model for plume and cloud growth that is used in the analyses in later sections is given in Section 2 of the paper by Hanna (1976a), to be published in Atmospheric Environment, appended to this report (Appendix A). Section 3 of Appendix A describes the input data that are necessary to run the model.

## 2. John E. Amos Cooling Towers

During the winter of 1974-1975, Smith-Singer Meteorologists, Inc. obtained measurements with a light aircraft around the three cooling tower plumes at the John E. Amos power plant in West Virginia (Kramer et al., 1975). Experiments were performed only on cold, humid mornings when long visible plumes were expected. The aircraft measured vertical profiles of temperature and dew point, and roughly estimated the wind speed. Photographs of the visible plume were taken, but the aircraft did not penetrate the plume. Plant personnel provided data on the load of the cooling towers.

The plant ran close to its rated capacity of 2900 MW during most of the experiments. In the model, the plume from a single tower is followed until its radius,  $R$ , equals one half of the distance,  $s$ , between the towers ( $s=200\text{m}$ ). The initial plume radius,  $R_0$ , and vertical speed,  $w_0$ , equal 40m and 4.4m/s, respectively. To insure continuity of the momentum flux, the effective initial plume radius for bent-over plumes is calculated from the equation (Hanna, 1972):

$$R_{\text{eff}} = R_0 (w_0/U)^{1/2}, \quad (1)$$

where  $U$  is the wind speed. Using the specifications given by Kramer et al (1975), the initial plume temperature,  $T_{po}$ , at full load is assumed to be given by the relation:

$$T_{po} = (297.4 + .635(T_d - 273))(1 + .01(1 - RH)), \quad (2)$$

where  $T_d$  is the ambient dew point and  $RH$  is the ambient relative humidity. For power outputs less than full load, initial plume temperature is calculated from:

$$\frac{T_{po} - T_{eo}}{T_{po}(\text{eq.2}) - T_{eo}} = \frac{\text{actual load}}{2900 \text{ mw}}, \quad (3)$$

where  $T_{eo}$  is the ambient temperature. Initial plume cloud water,  $Q_c$ , and hydrometeor water,  $Q_H$ , are arbitrarily set equal to .001 g/g, on the basis that fog or cloud is obviously present at the tower mouth. This estimate could be made more accurate if observations of liquid water at the tower mouth were taken.

About half of the sets of observations could not be used because of uncertainties in the temperature profiles or plume photographs. Of the 27 sets that were used, the input data for four are given in Appendices A and B (Hanna, 1976a and 1976b). Kramer et al. (1975) give complete listings of all the data.



## 2.1 Plume Rise at Amos

In 19 of the runs studied, the observed visible plume passed through the point of maximum plume rise. A comparison of observed and predicted plume rise is given in Table 1, showing that the average predicted plume rise (670m) is close to the average observed rise (750m). The correlation coefficient is 0.49, which is only fair. The last column of the table contains Briggs (1975) analytical plume rise prediction, where the initial buoyancy flux is assumed to equal the sensible heat flux from the largest tower. The average predicted rise is 540m and the correlation with observations is 0.37. Column five in the table contains the observed height of the base of the capping inversion or mixing layer, which is seen to be well-correlated (0.90) with the observed plume rise. Brennan et al., (1976) have analyzed these data and find that when a capping inversion is present the plume will level off after striking it. This rule is probably not valid in the summer when the height of the capping inversion is much higher and the plume is likely to reach final rise before striking the inversion.

Some examples of predicted vertical profiles of  $Q_c$ ,  $w$ , and  $(T_p - T_e)$  are given in Figures 1-3 of Appendix B. The predicted cloud water content,  $Q_c$ , is generally about .5 to 1.5 g/kg, which agrees with observations in natural cumulus clouds. The maximum vertical speed,

Table 1

Observed and Calculated Plume Rise at John E. Amos Power Plant

Run	$\bar{u}$ (m/s)	Ambient tower top saturation deficit (g/kg)	$\Delta\theta/\Delta Z$ over depth of plume ( $^{\circ}\text{C}/\text{mx}10^3$ )	Inversion height above tower (m)	Observed plume rise (m)	Model plume rise (m)	Analytical plume rise sensible one unit (m)
1	14	.43	13.5		560	260	250
6	11	.13	3.0		850	820	430
8a	9	0	9.8		370	350	250
10a	5	.60	2.1	720	820	820	590
11	0	1.34	6.1	660	880	900	980
12	6	1.25	1.2	1140	1060	1200	720
15	3	.28	10.7		1120	790	780
16	6	.41	7.2	1200	1160	700	380
17a	8	.29	6.7	360	360	430	410
18	6	.78	5.6		910	720	410
19	0	1.07	6.9	840	800	970	910
24	6	.60	4.0	750	760	630	500
28a	5	.52	21.8		360	400	310
31	0	1.02	11.6		500	900	780
35a	3	.87	9.8	390	360	590	480
44	8	1.16	1.9	960	910	420	510
45	7	1.16	5.6	1200	910	370	390
47	0	1.44	3.8	900	800	1020	910
48a	7	1.46	7.6	750	670	360	340
Avg.	5.6	.76	7.4	820	750	670	540

w, is between 4 and 10 m/s. The temperature excess,  $(T_p - T_e)$  is seen to decrease almost linearly with  $\log z$  for the runs plotted. Unfortunately there were no in-plume measurements during this experiment that could be used to test these predictions.

## 2.2 Visible Plume Length at Amos

There are seven runs in which the visible plume is moderately long but does not reach the point of maximum plume rise. These runs are summarized in Table 2. The results of a simple analytical model (Hanna, 1974) are also given, where it is assumed that the tip of the visible plume occurs when the initial flux of excess water,  $w_o R_o^2 Q_{po}$ , in the plume equals the saturation deficit flux,  $UR^2(Q_{eos} - Q_{eo})$ :

$$h = 2R_o (w_o/U)^{1/2} [(2Q_{po}/(Q_{eos} - Q_{eo}))^{1/2} - 1] \quad (4)$$

$$\ell = 1.4(R_o^{3/2} U^{3/4} w_o^{3/4} / F^{1/2}) [(2Q_{po}/(Q_{eos} - Q_{eo}))^{1/2} - 1]^{3/2} \quad (5)$$

In these equations  $h$  is visible plume height,  $\ell$  is visible plume length, subscripts p, e, o, and s refer to plume, environmental, initial, and saturated variables, respectively, and  $F$  is the initial buoyancy flux:

$$F = (g/T_{po}) w_o R_o^2 (T_{po} - T_{eo}) \quad (6)$$



Table 2.

## Visible Plume Dimensions for Plumes whose Visible Portion

does not Reach the Point of Maximum Rise, for John E. Amos Power Plant

Run	$\bar{U}$ (m/s)	ambient saturation deficit (g/Kg)		observed		numerical model		analytical model		ambient RH at plume level
		tower top	plume level	visible plume height (m)	visible plume length (m)	visible plume height (m)	visible plume length (m)	visible plume height (m)	visible plume length (m)	
2	13	3.0	3.9	100	200	75	290	100	370	.4
3	10	2.6	2.7	150	500	120	350	140	400	.65
13	10	.86	1.8	100	300	150	480	210	730	.6
20	10	2.8	3.9	200	400	70	250	120	290	.45
27	20	1.5	2.0	390	600	120	450	110	800	.55
39	15	2.9	3.6	240	450	140	240	100	430	.45
41	16	3.5	3.2	50	300	55	290	80	360	.35
Avg.	13	2.5	3.0	180	390	100	340	120	450	.50

The factor 2 in front of  $Q_{po}$  in equations (4) and (5) is the so-called "peak factor," accounting for the observation that a visible plume can persist past the point at which the average plume becomes unsaturated. Saturated parcels of air persist in the midst of unsaturated air. The empirical peak factor was first used in the analyses by Meyer et al. (1974), Slawson et al. (1974), and Briggs (1975).

It is seen in Table 2 that the numerical and analytical models are equally capable of estimating the visible plume height and length. The average observed and estimated visible plume length and height agree within 20% and 80%, respectively. More detailed discussions of these comparisons are given in Appendices A and B.

### 3. St. Louis Refinery Cloud

While measuring cumulus clouds in the vicinity of St. Louis with an instrumented light aircraft, Auer (1976) noticed a cumulus cloud that was obviously forming in the plume from a refinery complex. He made several passes through the cloud, measuring temperature excess, vertical speed, and excess water. He also obtained vertical soundings of dry bulb temperature, dew point, and wind speed. Unfortunately, the source details are sketchy in his report, and it is necessary to arbitrarily choose parameters such as the initial plume radius. Auer states that the refinery gives off  $7 \times 10^{11} \text{ cal h}^{-1}$  (about 800 MW), divided about equally

between sensible and latent heat. For the model calculations the initial plume temperature, relative humidity, radius, and vertical speed are assumed to equal 302.3 K, humidity 76%, 250 m, and 1 m/s, respectively. Initial values of cloud and rainwater content are set equal to zero. The environment profiles are given in Table 3.

Table 3

Profiles of Temperature, Dewpoint, and Windspeed for the St. Louis Refinery Cloud on 10 August 1973 (after Auer, 1976)

z(m)	Temperature (°K)	Dewpoint (°K)	U(m/s)
0.	300.5	296.0	1.1
250.	298.0	295.5	1.1
450.	296.5	295.0	1.3
600.	295.0	294.5	1.8
750.	293.5	292.8	1.9
900.	292.5	291.0	3.0
1050.	291.8	285.0	2.5
1200.	290.6	288.5	2.0
1350.	289.4	288.5	2.0
1500.	288.5	286.5	1.1
1650.	287.5	286.5	2.0
1850.	286.0	284.2	3.8
2000.	285.0	282.0	3.8
2100.	284.8	278.0	3.8
2250.	284.0	277.5	3.8
2350.	283.3	277.8	3.8



The comparison of observations with model output are summarized in Table 4 below (all heights are in meters above the surface):

Table 4

Comparison of Observations and Predictions for St. Louis Refinery

	Observed	Predicted
Cloud base	700m	650m
Cloud top	2050m	2350m
<u>z(m)</u>	Liquid Water Content Observed (g/m <sup>3</sup> )	Liquid Water Content Predicted (g/m <sup>3</sup> )
930	.046	.56
1270	.10	.75
1860	.44	1.30
<u>z(m)</u>	Observed w(m/s)	Predicted w(m/s)
500	3	2.0
1500	4	2.0
2000	3	2.3
<u>z(m)</u>	Observed (T <sub>p</sub> -T <sub>e</sub> ) (°K)	Predicted (T <sub>p</sub> -T <sub>e</sub> ) °K
500	.2	.1
1500	-.5	.3
2000	-.2	.5

The height of the cloud base and top are quite well predicted by the model. There is a slight inversion above about 2100 m which causes the plume to level off. The predicted vertical speed  $w$  is about a factor of two too low at all heights and the predicted liquid water content is a factor of three to ten too high. The observed and predicted temperature

differences are within 1°K of each other. Because of the differences in water vapor content between the plume and the environment, the virtual temperature difference ( $T_{pv} - T_{ev}$ ) is positive even though the observed actual temperature difference is negative at heights of 1500 and 2000m.

Auer calculated the entrainment rate based on his measurements of temperature in the cloud. He finds that the entrainment rate is between 33 and 91%/km for eight different passes through the cloud. In the numerical model the entrainment rate  $(1/V)(dV/dz)$  equals  $0.8/R$ , where  $V$  is the volume flux,  $UR^2$ . Thus the theoretical entrainment rate is about 160% at cloud base and about 75% at a height of 2000 m (using  $R = R_0 + 0.4z$ ). There is a great deal of uncertainty among the cloud modelers with respect to their recommendations of entrainment rate for cumulus clouds (see Cotton, 1975). It is measurements such as Auer's which will allow modelers to better specify the entrainment rate.

#### 4. Rancho Seco Cooling Towers

The plumes from the two natural draft cooling towers at the Rancho Seco, California, nuclear power plant were sampled by Wolf (1976a) using a light aircraft. Environmental data from the three days of measurements are listed in Table 5.

The two towers have radii of 30 m and their centers are separated by 140 m. In the model, a single plume is followed to a height where its radius equals 70 m, or one half of the distance between the towers. Beyond this point, the plumes are assumed to merge and the fluxes of all parameters increase by a factor of two. The measured initial velocities,  $w_0$ , on the three days

Height above tower (m)	2/17/75		U <sup>(3)</sup>	2/18/75		2/20/75	
	T <sub>e</sub> <sup>(1)</sup>	T <sub>d</sub> <sup>(2)</sup>		T <sub>e</sub>	T <sub>d</sub>	T <sub>e</sub>	T <sub>d</sub>
0	280.0	270.9	5.0	283.0	274.4	283.2	275.4
44	279.5	270.6	5.0	—	—	282.8	274.8
120	278.8	270.9	5.0	281.5	273.7	282.0	274.7
197	278.2	270.0	5.0	—	—	—	—
273	278.9	268.9	5.6	280.4	272.3	280.6	273.4
425	279.2	265.3	7.2	279.5	269.9	279.2	271.2
578	278.4	266.8	9.4	278.5	267.1	277.9	271.3
654	—	—	—	277.8	267.2	—	—
730	278.0	264.7	11.0	278.0	268.6	276.6	270.1
807	—	—	—	278.1	267.7	—	—
883	—	—	—	278.0	266.5	276.1	269.0

(1) Dry bulb temperature, °K.

(2) Dewpoint, °K.

(3) Wind Speed, from pilot balloons (m/s)



2/17, 2/18, and 2/20, are 4.4, 3.6, and 3.9 m/s, respectively.

Wolf suggests that the initial liquid water content should be less than we have been using previously, since he has measured liquid water concentrations no greater than .0001 g/g at a distance of 125 m from the tower exits. Therefore, for these three runs, it is assumed that  $Q_{CO}$  equals .0005 and  $Q_{HO} = .0001$  g/g. Equations (2) and (3), based on the John E. Amos towers, were used to estimate the initial plume temperatures.

The estimated visible plume length and height are compared with observations in Table 6.

Table 6

Observed and Estimated Visible Plume Length  
and Height at Rancho Seco

	Feb 17		Feb 18		Feb 20	
	<u>obs.</u>	<u>model</u>	<u>obs.</u>	<u>model</u>	<u>obs.</u>	<u>model</u>
Plume length (m)	vert.	170	500	130	1000	250
Plume height (m)	350	110	800	160	420	75

It is seen that the model underestimates visible plume length and height by a factor of three to five. However, Wolf reports that he observed visible plumes when the average plume relative humidity was as low as 60%. Either the plume is far lumpier than we think, or the measured relative humidities are too low. If the former is true, the model could be improved by increasing the peak factor.

The observed and estimated excess temperature and excess water content are in better agreement than the visible plume parameters, as seen in Table 7. The observed temperature excess is about twice the estimated excess, on the average. The observed and estimated excess water content are generally quite close. The paradox exists that visible plume length is not estimated very well, while excess water content is estimated quite well. Adjustments in the peak factor cannot simultaneously improve predictions of visible plume length and excess water content at Rancho Seco.

#### 5. Climatology of Plume Types

Since the plume and cloud growth model is relatively simple and each computer run costs only a few cents, it is feasible to apply the model to large numbers of input data. The statistics of the resulting plume predictions can be calculated and a climatology of plume types developed. The average plume rise and visible plume length and height for a year and for various seasons can be included in the climatology. Plume characteristics for weather categories ranging from clear to precipitation can be estimated.

Upper air and surface observations from the Nashville weather service office for the months January, April, July, and October, 1974, were obtained. Since observations are taken twice each day

Table 7

Observed and Estimated Temperature and Water Content  
Excesses at Rancho Seco

Date	Height above tower (m)	$(T_p - T_e) (^{\circ}\text{K})$		$(q_p + Q_c + Q_H - q_e) (\text{g/kg})$	
		obs.	model	obs.	model
Feb 17	120m	7.2 $^{\circ}\text{K}$	2.3 $^{\circ}\text{K}$	5.1 g/kg	3.3 g/kg
	136	5.6	2.0	3.6	3.1
	151	5.0	1.6	3.1	2.8
	181	1.9	1.2	1.8	2.5
	273	2.3	-.3	2.1	1.8
	349	0.7	top at 340m	1.1	
Feb 18	197m	2.2 $^{\circ}\text{K}$	1.3 $^{\circ}\text{K}$	2.2 g/kg	3.2 g/kg
	273	2.1	0.7	2.4	2.4
	425	0.8	-0.1	1.8	1.9
	578	-0.3	-0.5	0.8	1.7
	730	-0.5	top at 610m	0.4	
	883	-2.1		0.4	
	974	-3.8		0	
Feb 20	120m	3.0 $^{\circ}\text{K}$	1.3 $^{\circ}\text{K}$	1.9g/kg	2.6g/kg
	151	3.0	0.9	2.0	2.0
	181	1.4	0.7	0.8	1.7
	273	0.9	0.4	0.6	1.2
	425	0	0.1	0.4	1.1
	486	1.0	0	0.7	0.9
	730	-0.4	top at 720m	-0.1	



(morning and evening), a total of 241 sets of input data are used. The Nashville station was chosen because of its proximity to the proposed TVA Hartsville power park, the surrogate nuclear energy center site at Land-Between-the Lakes, and the existing TVA Paradise steam plant.

The four different types of sources used as input to the model are listed in Table 8.

Table 8

Source Input for Plume Climatology Study

Approximate power	Number of cooling towers	$w_o$ (m/s)	$T_o$ (°K)	$R_o$ (m)	Characteristics
1000 MW	1	4.4	(eq 2)	30	Typical natural draft tower.
10000 MW	1	4.4	(eq 2)	92	Same, but larger diameter.
100000 MW	1	4.4	(eq 2)	300	Same, but much larger diameter.
100000 MW	100	4.4	(eq 2)	30	Square grid. Groups of four towers, with the towers spaced 200m apart. Groups are spaced 1 km apart.

Because the model is one dimensional, plume merging in the 100000 MW power park with 100 cooling towers must be completely parameterized.

It is assumed that the four plumes in a group merge if the plume radius equals 100m (one half of the distance between the towers) and the groups merge if the plume radius equals 500m (one half of the distance between the groups). The other source types in the

table are treated as if all the heat were from one cooling tower. This is unrealistic for the 10000 and 100000 MW sources, but will provide estimates of the worst possible cases of weather modification.

### 5.1 Plume Rise

Final plume rise is defined as the height at which the vertical speed of the plume,  $w$ , reaches zero. In about one-third of the runs for the single 1000 MW tower, a cloud exists ( $Q_C + Q_H > 0$ ) at the height of final plume rise. This fraction increases to 95% for the single  $10^5$  MW tower. The average plume rise for the four different months and four different sources are listed in Table 9. The numbers in parentheses are the range of plume rise for that class.

The increase in plume rise with increase in source strength for the first three types of sources is in approximate agreement with Briggs' (1975) theory for plume rise, which predicts that the plume rise for bent over plumes is proportional to source strength raised to the one third power. The figures for average annual plume rise show that the ratio of the  $10^4$  MW plume rise to the  $10^3$  MW plume rise is 2.04 and the ratio of the  $10^5$  MW plume rise to the  $10^3$  MW plume rise is 4.25. Briggs' theory predicts that these ratios will be  $10^{1/3}$ , or 2.15, and  $100^{1/3}$ , or 4.65, respectively.



Table 9

Average Plume Rise Estimated Using Nashville Radiosonde Observations.  
The Range in Plume Rise for that Class is Given in Parentheses.

Month (all 1974)	Morning Rise (m)				Evening Rise (m)				Average Rise (m)			
	$10^3$ MW	$10^4$ MW	$10^5$ MW	$10^5$ MW spaced	$10^3$ MW	$10^4$ MW	$10^5$ MW	$10^5$ MW spaced	$10^3$ MW	$10^4$ MW	$10^5$ MW	$10^5$ MW spaced
Jan.	500 (160- 1340)	880 (320- 1450)	1470 (650- 3600)	610 (160- 1390)	660 (240- 1360)	970 (400- 1690)	1590 (750- 4010)	740 (240- 1530)	580 (160- 1360)	920 (320- 1690)	1530 (650- 4010)	670 (160- 1530)
Apr.	490 (170- 1430)	1030 (300- 1920)	2340 (780- 4500)	610 (170- 1740)	890 (120- 1600)	1410 (190- 2160)	2550 (420- 4300)	1090 (120- 1880)	690 (120- 1600)	1220 (190- 2160)	2440 (420- 4500)	850 (120- 1880)
July	470 (200- 1590)	1530 (340- 3110)	3130 (1260- 4950)	890 (210- 3620)	730 (240- 1800)	1590 (520- 2710)	3570 (1690- 5460)	1130 (240- 2980)	600 (200- 1800)	1500 (340- 3110)	3250 (1260- 5460)	1010 (210- 3620)
Oct.	360 (190- 990)	850 (320- 3160)	2410 (850- 4790)	420 (230- 1200)	550 (260- 1140)	1140 (500- 2160)	2610 (1500- 4600)	770 (210- 2300)	450 (190- 1140)	1000 (320- 3160)	2510 (850- 4790)	600 (210- 2300)
Avg. annual	450 (160- 1590)	1030 (300- 3160)	2340 (650- 4950)	630 (160- 3620)	710 (120- 1800)	1280 (190- 2710)	2580 (420- 5460)	930 (120- 2980)	580 (120- 1800)	1180 (190- 3160)	2460 (420- 5460)	780 (120- 3620)



The spaced  $10^5$  MW energy center yields an average plume rise between those for the single  $10^3$  MW tower and the single  $10^4$  MW tower. Occasionally, the plumes will combine and yield a plume rise close to that for the single  $10^5$  MW tower. In about 90% of the runs, the four towers in a group merge, and in about 15% of the runs, the 25 groups merge. But since merger generally occurs near the top of the plume, it doesn't give the plume much additional boost. A general rule for avoiding plume merger is to space the cooling towers a distance apart equal to the average plume rise from a single tower. In this way, the plume radii, which grow roughly as  $.4z$ , do not reach the critical value for plume merger (one-half the distance between the towers).

The enhancement of plume rise due to the merging of multiple plumes has been predicted theoretically by Briggs (1974). The ratio of the enhanced plume rise from  $N$  sources to the plume rise from one source, which is denoted by  $E_N$ , is a function of the number of sources,  $N$ , the plume rise from one source,  $H$ , and the distance between the sources,  $s$ .

$$E_N = ((N + S)/(1 + S))^{1/3} \quad (7)$$

where  $S = ((N-1)s/N^{1/3}H)^{3/2}$

From the results in Table 9, it can be assumed that  $H$  is 580 m. For the small groups in our hypothetical power park ( $N = 4$  and  $s = 200\text{m}$ ),  $E_N$  equals 1.43. For the entire power park ( $N = 100$  and  $s = 1000\text{m}$ ),  $E_N$  equals 1.14. In this case the enhancement factors for the groups of four and the entire power park should probably be multiplied together. Thus the theoretical enhancement  $E_N$  is predicted to be about 1.4 or 1.5 for our hypothetical power park. The plume and cloud growth model yields the result that the average annual ratio of plume rise for the  $10^5$  MW spaced power park to the plume rise for the single  $10^3$  MW cooling tower is  $780\text{m}/580\text{m}$ , or 1.35.

The seasonal variation of plume rise in Table 9 is what would be expected intuitively, with the lowest plume rise usually occurring during the winter when the lower atmosphere is more stable. Similarly, the afternoon plume rises are 10 to 80% greater than the morning plume rises. The diurnal variation is less for the large sources, since the morning inversion is usually limited to a layer about 100 to 200 m deep near the ground. However, the annual variation is greatest for the large sources, presumably due to the influence of the deep isothermal or inversion layers which exist during the winter. Also, it should be stressed that this "climatology" is based on observations during only four months. Ideally, observations during at least ten years should be used to establish a stable climatology.



## 5.2 Cloud at Top of Plume

In many model calculations, liquid water exists in the plume at the height of final rise. Either a cloud persists from the tower opening through the entire depth of the plume, or it forms just above the lifting condensation level, with clear air beneath it. The frequencies of cloud occurrence for the six weather classes are given in Table 10, where the source is the single 1000 MW, 30 m radius tower. On the average, a cloud is predicted at the top of the plume 39% of the time. During precipitation, fog, or cases when the cloud height is less than 10,000 ft., a cloud is predicted about 60% of the time. Clouds are very unlikely during afternoons which are clear or have high clouds. The reason that such high occurrence of clouds are not reported from operating cooling towers is that on foggy days or days with precipitation it is hard to see the plume. The model calculates plumes on all days, instead of just sunny days when the observer can easily see the plume.

Table 10

Frequency of Cloud Occurrence (QCO + QHO>0 at Height of Final Rise)  
for 1000 MW Tower at Nashville

Weather Class	Observed class freq.		Frequency of cloud occurrence within class	
	am	pm	am	pm
1. Clear	.09	.15	.32	0
2. Precipitation	.18		.60	
3. Cloud height $\geq$ 20,000 ft. (no prec.)	.05	.07	.23	0
4. $10,000 \leq$ cloud height < 20,000 ft. (no prec.)	.09		.14	
5. Cloud height < 10,000 ft. (no prec.)	.24		.53	
6. Fog (no prec.)	.13		.65	
All	1.00		.39	



The frequency of cloud occurrence is predicted to increase as source size increases, as shown in Table 11.

Table 11

Frequency of Cloud Occurrence Estimated  
Using Nashville Radiosonde Observations

Month (all 1974)	$10^3$ MW	$10^4$ MW	$10^5$ MW	$10^5$ MW spaced
Jan.	.41	.70	.97	.59
Apr.	.34	.59	.96	.43
July	.51	.76	.97	.59
Oct.	.31	.54	.89	.39
Total	.39	.64	.95	.50

For the  $10^5$  MW spaced power park the frequency of cloud occurrence is roughly halfway between those for single  $10^3$  MW and  $10^4$  MW cooling towers. As seen in Table 9, the plume rise for the spaced power park occupies the same relative position between that for the single  $10^3$  MW and  $10^4$  MW towers. A cloud forms nearly all the time (frequency .95) over the single  $10^5$  MW cooling tower. This is a good argument against clustering the waste heat sources as close together as possible. This model predicts that a cloud averaging 2500 m deep would exist nearly continuously over an area with radius 300 m dissipating  $10^5$  MW of heat.

### 5.3 Liquid Water Content of Cloud Formed by Cooling Tower

The liquid water content of a cloud determines the visibility in the cloud and the rainfall rate from the cloud. The removal of large raindrops from the plume is calculated using a scheme developed by Simpson and Wiggert (1969), but it is uncertain whether the estimated rainfall rate at the ground is realistic. A cooling tower cloud is unlike a natural cloud in that its base is stationary rather than drifting with the wind.

The average liquid water contents listed in Table 12 refer to only those cases when a cloud formed at the top of the plume. The average liquid water contents range between .29 and .63, in agreement with typical values reported by Fletcher (1962) of the liquid water content in natural clouds. The peak liquid water content is 1.49 g/kg. It is seen that the average liquid water content for the larger sources is significantly greater than that for the  $10^3$  MW source, but that there is no significant seasonal variation. In most cases the liquid water content at the top of the plume is less than that in the middle sections of the cloud.

Table 12

Average and Peak Concentration of Cloud Water at the Top of Plumes  
Which are Condensed at the Height of Final Rise, Estimated  
Using Nashville Radiosonde Observations.

Month (all 1974)	Average Concentration (g/kg)				Peak Concentration (g/kg)			
	$10^3$ MW	$10^4$ MW	$10^5$ MW	$10^5$ MW spaced	$10^3$ MW	$10^4$ MW	$10^5$ MW	$10^5$ MW spaced
Jan.	.40	.54	.62	.47	.72	.96	1.49	.98
Apr.	.44	.60	.61	.54	.82	1.15	1.19	1.00
July	.29	.63	.44	.49	.91	1.03	.77	1.25
Oct.	.33	.39	.44	.36	.62	1.02	1.09	.90
Total	.36	.54	.53	.47	.91	1.15	1.49	1.25



#### 5.4 Relation of Plume Rise to Inversion Height

Based on observations of cooling tower plume rise on cold winter mornings at the John E. Amos power plant Brennan et al. (1975) state that the capping inversion height, or mixing layer depth, determines the final plume rise. In Section 2 and in Hanna (1976a), it is pointed out that this conclusion is not likely to be valid during the summer, when the capping inversion is much higher than it is in the winter. Consequently the 241 Nashville runs were analyzed to determine the relation between plume rise from the 1000 MW cooling tower and inversion height.

A well-defined capping inversion is found in 89 of the runs, with the average plume rise and inversion height during these conditions equal to 690 m and 1250 m, respectively. All the runs are summarized in Table 13. The correlation coefficients between plume rise and inversion height are seen to be very high for the group of runs where the estimated plume rise is greater than or equal to the inversion height. If the plume has enough buoyancy to bring it to the capping inversion, it will in all likelihood stop there.

Table 13

Plume Rise and Capping Inversion Height for the 1974 Nashville Soundings. The Number of Runs in Each Category is Given in Parenthesis.

Month	Avg. Capping inversion height	Avg. Model plume rise	Correlation Coefficient between Capping Inversion Height and Plume Rise	
			All runs with inversion	Runs with plume rise $\geq$ inversion height
Jan.	920m	640m	.31(39)	.989(14)
Apr.	1640	760	.20(25)	.998(5)
July	1700	1250	.78(5)	(0)
Oct.	1280	570	.15(20)	(2)
Total	1250	690	.33(89)	.993(21)



### 5.5 Visible Plume Length

The model calculations stop after the vertical speed of the plume falls to zero. Downwind of this point, where passive diffusion governs the distribution of excess water, very little is known about cooling tower plumes. It is better to wait for the results of measurement programs than to go ahead with a completely arbitrary model of passive diffusion. Consequently, this section on visible plumes is concerned only with plumes which evaporate before they reach the height of final rise. With this restriction, for the single 1000 MW source, the average annual visible plume height is 150 m and the average annual visible plume length is 190 m. These estimates are about a factor of two less than the observations of visible plume geometry at the Paradise cooling towers, where the average annual visible plume height is 280 m and the average annual visible plume length is 390 m. At Paradise there are three cooling towers with a total energy output of more than 2000 MW. Our analysis of the daily Paradise observations is continuing in order to compare the model predictions of plume rise and visible plume length with the observations for the classes of weather conditions listed in Table 10.

Seasonal variations of predicted visible plume length and height are given in Table 14. It is seen that the average resultant visible plume length is about 40% to 75% longer in January than in July, and that the morning length is about twice as long as the afternoon length. Furthermore, the angle of the plume with the horizontal is about  $30^\circ$  less in the winter than in the summer,

presumably due to the greater wind speeds in the winter (8.0 m/s in January compared to 3.4 m/s in July). The shortest plumes occur on hot dry days in July, when the visible plume length is only about 50 m, or about one tower diameter.

Table 14

Visible Plume Length and Height Predicted Using Nashville Radiosonde Observations, for Plumes which are not Visible at their Final Height of Rise. The Resultant Plume Length is the Hypotenuse formed by the Visible Plume Length and Height.

Month	Height(m)		Length(m)		Resultant(m)	
	am	pm	am	pm	am	pm
Jan.	230	130	430	170	490	210
Apr.	180	90	330	130	380	160
July	240	120	140	90	280	150
Oct.	240	80	210	110	310	140
Average	220	100	280	130	360	160

### CHAPTER III

#### PLANS FOR LABORATORY STUDY OF FLOW AND PLUME BEHAVIOR NEAR SINGLE AND MULTIPLE COOLING TOWERS OF VARIOUS TYPES

by  
R.P. Hosker, Jr.

##### 1. Introduction

In order to realistically mathematically model and predict the behavior and environmental interactions of cooling towers and their plumes, a certain amount of physical insight into the details of the associated phenomena is essential. Laboratory and field studies, as well as providing this requisite understanding of the physics, can also provide the data needed for validation of the resulting mathematical models. From an engineering point of view, such empirical studies can also furnish a great deal of information on phenomena which can significantly affect cooling tower performance (and hence overall power plant efficiency), such as plume downwash, reingestion, and mutual interference effects within tower clusters.

The reporting of such experimentally-derived information is relatively recent in the open literature. Aynsley and Carson (1973) remark, for example, that only twelve papers devoted to cooling tower plumes had been published prior to 1969. Since then, however, research interest in cooling towers has grown enormously. Most of the references to major field and laboratory programs both within the U.S. and abroad can be found in the proceedings of a 1974 symposium (Cooling Tower Environment-1974), and in an excellent critical



review by McVehil and Heikes (1975). The paper of Meyer et al. (1974) is particularly noteworthy because of its very detailed field observations of plume behavior. More recent field studies have been reported by Kramer et al. (1975), Brennan et al. (1976), Norman et al. (1976), and Wolf (1976a).

Few reports on laboratory modeling of cooling towers and their plumes have appeared in the open literature until recently. The contributions of Kennedy and his colleagues (Kennedy and Fordyce, 1974; Bugler and Tatinclaux, 1974) and of Onishi and Trent (1976) are of considerable interest. A study by Symes and Meroney (1970), though not originally intended for cooling tower use, has important implications for near-tower plume behavior.

A review of the above publications indicates several research topics important for the development of realistic mathematical models for cooling tower and plume behavior. In particular, McVehil and Heikes (1975) suggest that, as a practical matter, the most significant cooling tower effects may very often be highly localized problems associated with aerodynamic interactions between the tower, its surroundings, the plume, and the atmosphere. Similarly, in a discussion of Meyer et al. (1974)'s data, Briggs (1974) remarked that "building effects" seemed to be the strongest influences on plume behavior other than those taken into account by relatively simple plume rise models. And Carson (1974), in a discussion of research

required for evaluation of both mechanical and natural draft cooling tower effects, commented on the need for plume models which can include the effects of relative tower orientation, aerodynamic downwash, and other such interactions. Criteria for the atmospheric conditions under which downwash and recirculation may be expected are also necessary, especially for cases involving arrays of towers; such information may provide guidance for avoiding or minimizing these problems by proper design and operation practices.

Experimental work on these unresolved near-tower problems is probably most easily accomplished by laboratory modeling, and this is the primary approach to be taken at ATDL. In the following sections, the requirements for reasonably accurate laboratory simulation of cooling tower and plume behavior will be briefly examined and used to establish the general size and operating conditions of the necessary flow facility. A detailed description of equipment already purchased or about to be procured is given. A list and a tentative timetable are presented for the sequence of cooling tower experiments planned for this facility in Chapter IV.

## 2. Similarity Criteria

### 2.1 General Background

A number of authors (Cermak et al., 1966; McVehil et al., 1967; Ludwig et al., 1971; Snyder, 1972; Lin et al., 1974; Kennedy and Fordyce, 1974; among others) have considered the conditions under

which a fluid (either gas or liquid) model of a given flow situation can provide physically realistic results. These similarity conditions are conveniently obtained by a dimensional analysis of the governing equations (Navier-Stokes, or an approximation of them) together with the proper initial and boundary conditions on the flow.

The procedure, which will only be summarized here, first requires writing out the conservation equations applicable to the atmospheric boundary layer. Mass, momentum, and energy are to be conserved. Viscous, rotational, and gravitational effects must be taken into account. Equations describing the dispersion of (possibly reactive) contaminants within the main fluid must also be given. In addition, the initial and boundary conditions of the real flow must also be explicitly formulated.

The resulting set of coupled, nonlinear, partial differential equations together with the boundary and initial conditions must then be nondimensionalized. This is often done by choosing characteristic values for the dependent variables, such as velocity, temperature, and effluent concentration, so that their nondimensional values are unity or less over the entire flow field. Convenient characteristic values of length and time can be chosen so that either the nondimensional independent variables (time and the spatial coordinates) are of order unity or less, or the nondimensional gradients of these variables are of order unity or less. If the



scales of certain phenomena are very dissimilar--eg, mean velocity and turbulent fluctuations--then two characteristic values may be appropriate. For example, the mean velocity may be scaled by the geostrophic wind speed, while the turbulent velocity components may be normalized with a typical root-mean-square value for one of the components.

In the new set of nondimensional equations and boundary conditions, certain terms are preceded by nondimensional coefficients. A model of the atmospheric boundary layer must, to be physically realistic, obey the same equations as does the natural flow. In particular, the nondimensional coefficients appearing in the governing equations and boundary conditions should be equal in both the model and the atmosphere. In practice it is impossible to obtain such equality of parameters, and so the model is not an exact simulation of the real flow. The question of just how closely the various parameters must be duplicated to produce a reasonable amount of accuracy in a practical model has been the subject of considerable work and discussion (see the authors listed above). Many of their conclusions are utilized in the discussion below.

The nondimensional parameters which arise from the conservation equations for mass, momentum, and energy are the Reynolds number, the bulk Richardson number (the inverse square of the overall densimetric Froude number), the Rossby number, the Prandtl number, and the Eckert number. The equation describing diffusion of a

passive effluent within the main fluid gives rise to the Schmidt number.

The Prandtl and Schmidt numbers occur in the equations as products with the Reynolds number. These products can be physically interpreted as the ratio of the heat or effluent, respectively, transferred per unit area in unit time by advection to that quantity transferred by molecular diffusion. The Eckert number appears in the energy equation divided by the Reynolds number; this expression indicates the ratio of the heat generated over a unit area in unit time by viscous forces to that transferred by advection. In the atmospheric boundary layer, molecular-scale diffusion processes are nearly always negligible compared to turbulent diffusion. As long as the model flow is also highly turbulent, similarity of the Prandtl, Schmidt, and Eckert numbers should not be necessary for good model accuracy.

The Rossby number is a measure of the relative importance of inertial and Coriolis forces. The Coriolis force is responsible for the gradual turning of the wind vector with height (the so-called "Ekman spiral"). Near the surface, however, this turning is not significant. An estimate of the thickness of the surface layer within which the Coriolis effect is negligible to within, say, 10% can be made using Lettau's (1962) model for the wind spiral.

This height is about 50m except in low winds, at high latitudes, or over rough terrain; for moderate to strong winds over most surfaces the layer of negligible Coriolis effect should be 100m or more in thickness. For diffusion modeling within the surface layer one should therefore be able to neglect the Rossby similarity requirement. For elevated sources or for diffusion over great distances, however, the effect may become important. Snyder (1972) has surveyed the diffusion literature and concluded that the Coriolis force significantly affects dispersion results when the horizontal distance of travel is more than 5 km for elevated releases, and more than 12 km for ground-level sources.

The bulk Richardson number expresses the ratio of buoyant to inertial forces for the overall flow field, and is especially significant, therefore, at low wind speeds. Since it is a measure of atmospheric stability and hence of the degree of mixing possible, it can be expected to be an important parameter in model studies involving diffusion.

The Reynolds number represents the relative importance of inertial and viscous forces in the flow. A large Reynolds number suggests that viscous effects should be negligible; this is largely true within the bulk of the fluid. However, in regions (e.g., near obstacles) where large velocity gradients are present, viscous shear profoundly affects the overall flow patterns through its influence on boundary layer development, transition and separation, and wake behavior. Since these phenomena can introduce very large perturbations of the flow field which would exist in



the absence of viscosity, the Reynolds number is an important parameter in any modeling effort.

The nondimensional conditions imposed at the various fluid boundaries impose further constraints on the model flow (see, for example, Ludwig et al., 1971; Snyder, 1972; Kennedy and Fordyce, 1974). Geometric similarity is perhaps the most obvious requirement; all stack and building dimensions and distances must be correctly scaled. The nondimensional wind speed and temperature spatial distributions must be duplicated at the upwind boundary of the region of modeling interest; both the mean and the fluctuating portions of these quantities should be reproduced in the model. The buoyancy of effluents emitted into the modeled region must be taken into account by matching the effluent densimetric Froude numbers to those of the prototype. Similarly, initial momentum effects in plumes can be properly simulated only if the prototype ratios of efflux velocity to ambient wind speed are reproduced in the model.

## 2.2 Application to Cooling Tower Modeling

If the situations to be modeled concern only the near-field behavior of cooling towers and their plumes, then a number of the above-mentioned similarity requirements are unimportant and may be neglected in the modeling effort. Others may be relaxed.

For example, since the horizontal region of interest will extend less than a kilometer or so, the earth's rotation will have no significant effect on the plume, and the Rossby number criterion may be omitted.

A chief concern of this modeling study will be the interaction between plumes and cooling towers. Phenomena such as strongly bent over plumes, downwash, recirculation, and mutual interference between tower arrays are produced mainly by the aerodynamic flow fields around the towers themselves. Such effects are especially important during periods of strong winds, which commonly occur during conditions of neutral or near-neutral atmospheric stability. The present investigation will therefore be confined to such circumstances, during which the bulk Richardson number is nearly zero. A model flow with no corrections for ambient atmospheric stability should hence be adequate.

The Reynolds number in the atmosphere is typically very large-- $10^5/m$  to  $10^6/m$  of characteristic length  $L$ . Its definition,  $Re \equiv UL/\nu$ , suggests that a reduction in  $L$  might be properly compensated by an increase in characteristic wind speed  $U$  and/or a decrease in the fluid kinematic viscosity  $\nu$ . However, sizeable scale reductions, on the order of 1/100 or more are necessary to reduce large structures such as cooling towers to reasonable laboratory dimensions. Furthermore, buoyant plume modeling requirements restrict  $U$  to as small a value as practicable, as discussed below. Hence it will in general not be possible to match Reynolds numbers in the model and prototype flows. This difficulty is sidestepped by an appeal to the concept of "Reynolds number independence" introduced by Townsend (1956). McVehil et al. (1967) and Snyder (1972) have reviewed some of the pertinent ideas; the situation may be summarized as follows.

In the nondimensional momentum equations of fluid flow, the terms describing viscous effects are preceded by the coefficient  $1/Re$ , indicating that in the atmosphere, where  $Re$  is large, the flow must be nearly viscosity independent away from zones of strong velocity gradients. Furthermore, atmospheric flows are nearly always "fully aerodynamically rough" (Sutton, 1953); that is, the surface irregularities and the flow speeds are both sufficiently large that no laminar boundary sublayer exists at the surface (Sutton, 1953; Schlichting, 1960). Consequently even the flow close to the surface is nearly viscosity-independent. As regards the turbulent structure of the flow, all of the large energy-containing eddies and probably most of the intermediate-sized eddies are also independent of viscosity (Townsend, 1956). The smallest eddies present in the flow, however, dissipate kinetic energy by viscous action and must necessarily be Reynolds number dependent (Landau and Lifshitz, 1959). In other words, at large Reynolds numbers both the mean flow and most of the turbulent structure will be invariant with changes in  $Re$ ; only the small-scale structure in which energy dissipation occurs varies with  $Re$ . The latter feature is relatively unimportant for structural and diffusion modeling.

The key to successful modeling of neutrally stable atmospheric flow phenomena (excluding those in the energy dissipation scale) is thus to insure that the model flow is likewise independent of Reynolds number--ie, that a "critical" Reynolds number is exceeded



in the model. This critical value, at which the flow becomes fully rough over the various surfaces, can be determined from the criterion (Sutton, 1953)  $u_* z_0 / \nu \geq 2.5$ , where  $z_0$  is the surface's aerodynamic roughness length and  $u_* \equiv \sqrt{\tau_w / \rho}$  is the friction velocity determined from the wall shear stress  $\tau_w$ . The critical value may also be empirically determined by observing larger scale flow phenomena such as boundary layer separation and reattachment points, and wake behavior; these will cease to change when the critical Reynolds number is reached. For sharp-edged structures these features may be largely fixed by the geometry, leading to relatively small values for  $Re$  critical; for example, Golden's (1961) experiments suggest  $Re$  critical  $\approx 11,000$  for a cube. Rounded structures, on the other hand, must rely on the flow itself to establish separation points, and the critical values will hence be larger. Halitsky et al. (1963) found  $Re$  critical  $> 79,000$  for a typical smooth reactor shell model. Increased roughness of the model surfaces, as well as devices such as boundary layer trips could lower these values (Schlichting, 1960; Halitsky, 1968). Premature separation can also be artificially controlled by means such as boundary layer suction or blowing (Goldstein, 1965).

As an example, consider a hypothetical mechanical draft cooling tower consisting of a box-like structure 20m x 20m x 12m high, surmounted by a pair of roughly cylindrical stacks 10m in diameter x 7m high. The characteristic length  $L$  for the box is taken as the square root of its projected area, while that for a stack is taken as its diameter. For a model scale of 1/150, in air, a characteristic

speed  $U \approx 1.6$  m/sec yields  $Re \approx 11,000$ , which would satisfy Golden's (1961) lower bound for cubical structures. However,  $Re$  for one of the stacks under these conditions is only a bit over 7,000--probably far too small for naturally induced separation to occur at a location similar to that in the prototype. Roughening of the stack surface and other such "tricks" would probably be needed to produce a realistic separation point on this model.

The parameters associated with the boundary conditions must now be considered. For the neutrally stable atmospheric flows of interest, the mean velocity profile approaching the modeled zone should be nearly logarithmic in height if the upwind terrain is approximately homogeneous (Pasquill, 1971, for example). In practice this logarithmic profile is often approximated by a power law whose exponent depends on the upwind surface roughness (Davenport, 1963).

It is also necessary to model the turbulence structure of the approaching flow. Since the components of this profile are randomly fluctuating quantities, one can only hope to duplicate the statistics of the turbulence. Townsend (1956) notes that a statistical description of such a turbulent field requires a knowledge of the joint probability distribution function for the components at all spatial points. Once this has been specified, an infinite set of joint moments (i.e., the mean values of products of powers of the various fluctuating components) can be calculated. Conversely, supplying a complete set of measured moments is

equivalent to specifying the distribution function (Lumley and Panofsky, 1964). Hence an accurate model of a turbulent profile should reproduce all the joint moments of the prototype profile. These include, for example, the double, triple, and higher order Eulerian velocity correlation coefficients.

In view of the difficulty, cited by Brodkey (1967), of measuring even triple correlation coefficients, modelers are usually content to match the turbulence intensity profiles for each of the velocity components and the profiles of the various double correlation coefficients, or equivalently, the various spectra. Such matching should not be considered to be a full duplication of the atmosphere's turbulence structure; only the intensity and, in some sense, the size of the turbulent eddies have been reproduced. A number of such attempts have been reported (Davenport and Isyumov, 1967; Sundaram et al. 1972; Peterka and Cermak, 1974; and others). Typical atmospheric data have been reported by, for example, Busch and Panofsky (1968), Gault, Jones, Monson, and their colleagues (1967, 1969, 1970), Izumi (1971), and Izumi and Caughey (1976).

An important similarity parameter for cooling tower modeling is the densimetric Froude number of the effluent, defined as

$$Fr = W_p / (gd|\Delta\rho/\rho_a|)^{1/2}, \text{ where } W_p \text{ is the plume efflux velocity,}$$



$d$  is the exit diameter, and  $\Delta\rho = \rho_a - \rho_p$  is the difference in density between the atmosphere and the emerging plume. If  $Fr$  is small, buoyancy effects will be significant in the modeling. For a mechanical draft cooling tower, Kennedy and Fordyce (1974) found that  $2 \leq Fr \leq 7$  for most prototype situations. The data of Slawson et al. (1974) for the natural draft towers at Paradise, KY., give  $0.28 \leq Fr \leq 0.60$ . Evidently buoyancy effects are more important for natural draft towers, as could be intuitively expected.

Another important cooling tower parameter is the ratio of plume efflux velocity to the ambient windspeed at the exit,  $W_p/U_a$ . For mechanical draft towers Kennedy and Fordyce (1974) use  $0.4 \leq W_p/U_a \leq 12$ , while Slawson et al. (1974) give  $0.22 \leq W_p/U_a \leq 0.76$  for natural draft towers. Larger values are likely for both types in near-calm atmospheric conditions.

As Hoult et al. (1975) pointed out, the need to duplicate both of these parameters in a cooling tower model bounds the scale reduction which can be used at a specified flow speed or, alternately, limits the flow speed if the model size is prescribed. This can be seen as follows. Combine the expression requiring  $Fr$  and  $W_p/U_a$  to be equal in both model and field to obtain

$$U_m = Fr(W_p/U_a)_f^{-1} (gd_m |\Delta\rho/\rho_a|_m)^{1/2} \quad (1)$$

where the subscripts denote model or field values. The density difference term can be much larger in the laboratory than in the

field if, say, a helium-air mixture is used for the model plume. However, it appears that  $|\Delta\rho/\rho_a|_m \leq 0.4$  should be maintained to avoid altering the plume entrainment mechanisms (Hoult and Weil, 1972; Hoult et al., 1975). That is,

$$U_m \leq 1.98 Fr(W_p/U_a)^{-1} (d_f)^{1/2} (d_m/d_f)^{1/2}, \quad (2)$$

where the ratio  $d_m/d_f$  is the scale reduction. The flow speed is also bounded from below by the Reynolds number requirement discussed earlier. Hence for a given model scale reduction, there is only a limited range of tower operating conditions, described by  $Fr(W_p/U_a)^{-1}$ , that can be successfully modeled. For example, consider a mechanical draft tower whose exit diameter is approximately 8m. Suppose that, for a scale of 1/100, the lowest flow speed for which the external flow is independent of Reynolds number is 1 m/sec. Subject to the restriction (2), this model could be used to simulate tower behavior only for  $Fr(W_p/U_a)^{-1} \geq 1.8$ .

One last requirement should be placed on the model flow. The effluent plume should be fully turbulent, just as in the prototype. This may occur naturally for sufficiently large exit velocities, or can be induced by roughness elements inside the stack.

### 3. The Modeling Facility

#### 3.1 General Considerations

The test facility design was determined partly by the modeling restrictions pointed out above, and partly by the desire to obtain

a moderately versatile easily-used device. Air was selected as the modeling fluid because of our previous experience and the extensive literature available on testing structures in simulated atmospheric flows.

Size evolved from a compromise between the large test section area needed for high Reynolds numbers at low flow speeds, and cost limitations on the wind tunnel and the building required to house it. As discussed above,  $Re \approx 20,000$  or more should provide a fairly accurate simulation of the flow about a sharp-edged obstruction such as a mechanical draft cooling tower. To permit testing over a wide range of values of  $Fr(W_p/U_a)^{-1}$ , a low flow speed is needed. If  $U_m \approx 1 \text{ m/sec}$ , then the characteristic dimension of the model tower must be 30 cm or more, so that the model's projected area is roughly  $0.1 \text{ m}^2$ . Blockage effects due to the presence of the tunnel walls will be small if the test section area is at least ten times larger (Pope and Harper, 1966); that is, a test section area of  $1 \text{ m}^2$  would be suitable for this example. This is about the largest test section available in prefabricated wind tunnel units at moderate prices; larger tunnels require special shipping arrangements or on-site construction.

Special techniques are needed to produce the simulated velocity profiles and turbulence characteristics in a wind tunnel of modest length. Many such methods have been tried within the last ten years. A review of the pertinent literature (Lloyd, 1967;



Templin, 1969; Campbell and Standen, 1969; Counihan, 1969; Counihan, 1970; Ludwig et al., 1971; Peterka and Cermak, 1974; and others) suggested that at least 3m of the test section should be reserved for flow "processing". Since only near-field measurements out to a distance of 6 or 8 model heights are planned, a total test section length of about 6m was considered adequate.

Speed requirements were rather simple: a range from less than 1 m/sec to 20 m/sec or more. The mean speed profile in the as-delivered (unmodified) test section was required to be highly uniform everywhere in the test section. Similarly, the turbulence levels in this "clean" test section were required to be very low. The flow speed was required to be easily set, repeatable, and stable to within 1% over periods of ten minutes or more.

Large, door-mounted windows were specified on each side for easy access to the model and for photography. Flow visualization studies are anticipated to be an important part of this research. Fixed windows were therefore specified for the test section ceiling to facilitate overhead photography. Removable floor panels were required to allow rapid changes of flow processing devices such as roughness elements, and to permit easy model changes. A turntable will be installed in one such panel to allow testing at various angles of wind incidence.

### 3.2 Wind Tunnel Specifications

The above requirements are met by a Wirecomb, Inc. model 1391 wind tunnel equipped with an extra test section module. The major

specifications of this tunnel are listed in table 15, and a sketch of the tunnel is provided in Figure 1.

The wind tunnel arrived in Oak Ridge on May 21, 1976, and is presently stored in the Oak Ridge Associated Universities warehouse until the ERDA-funded building to house it has been constructed at ATDL.

TABLE 15

Wind Tunnel Specifications

<u>Type:</u>	Open-circuit, low speed, enclosed test section.
<u>Test section size:</u>	Two modules, useable separately or in tandem, each 1mx1mx3m long. Total test section length = 6m.
<u>Flow speed:</u>	1 m/sec or less to 22 m/sec or more. Speed "infinitely" resolvable.
<u>Turbulence level:</u>	Longitudinal turbulence intensity <1% with one inlet screen, and <0.5% with three inlet screens.
<u>Velocity profile:</u>	Flat within $\pm 1\%$ everywhere in test section except in thin wall boundary layers.
<u>Flow stability:</u>	Flow speed constant within $\pm 1\%$ over periods of ten minutes or more.
<u>Power and drive:</u>	30 HP SCR-controlled DC motor driving a 7-blade adjustable pitch fan by V-belts and pulleys.
<u>General construction:</u>	Plywood on steel frame modules. Each module caster-mounted. Plexiglas viewing windows.
<u>Overall size:</u>	Inlet approximately 2.6m square; overall length approximately 13.2m.

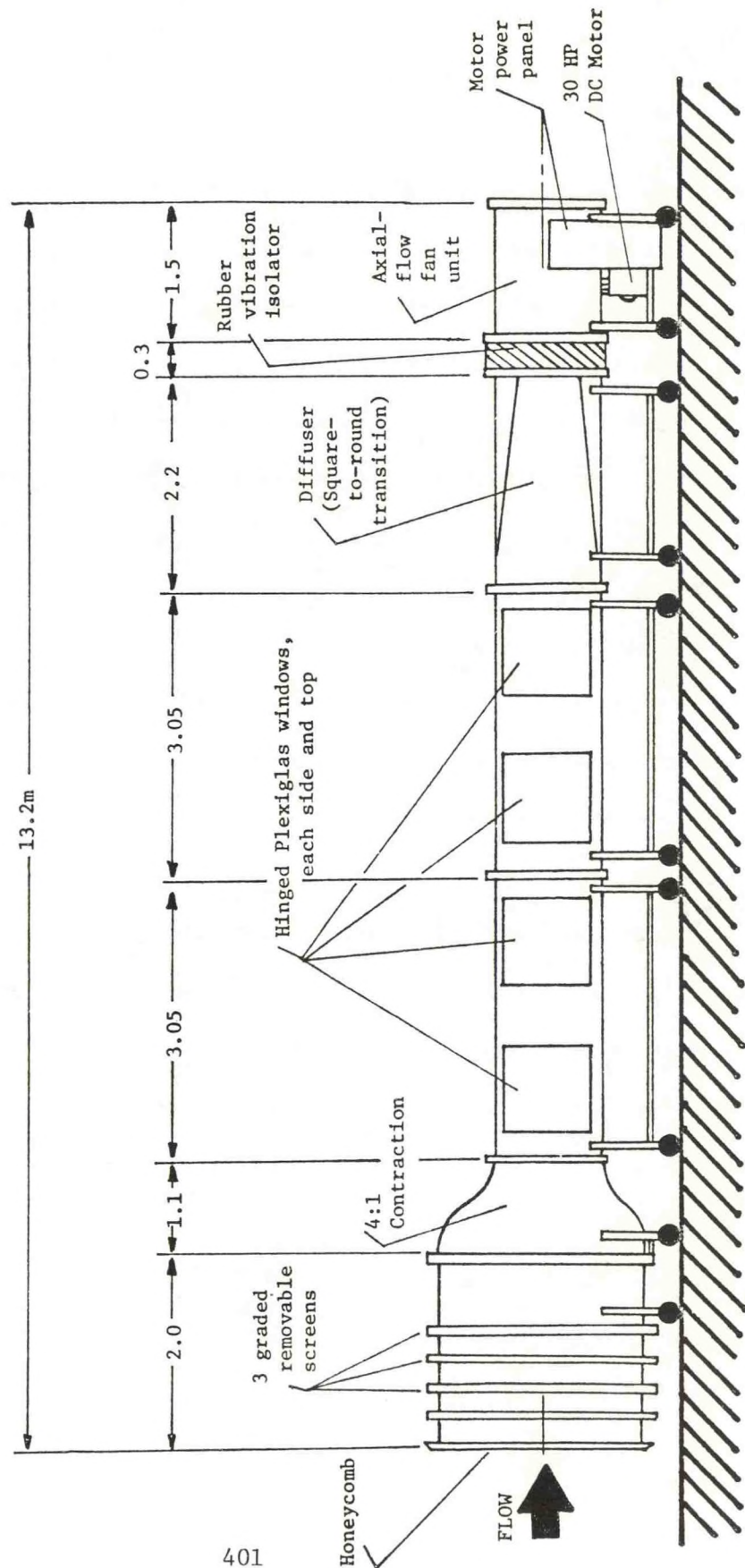


Figure 1: ATDL wind tunnel, to be used for laboratory studies of cooling towers immersed in a simulated atmospheric boundary layer. Test section 1 m. square inside. Flow speed 0-22 m/sec. Modified Wirecomb (Kenney) model 1391.



### 3.3 Additional Equipment

Measurements of flow speed and turbulence levels will be accomplished with standard constant-temperature anemometry techniques. Three channels of linearized Flow Corporation model 750-1 hot wire anemometers are presently on hand; these will probably be supplemented with a Thermo-Systems model 1050 system using hot-film probes for improved ruggedness. At very low flow speeds special techniques such as measuring the eddy-shedding frequency of small cylinders may be necessary; in this method, the velocity is obtained from the known Strouhal number dependence on Reynolds number.

Flow visualization will be accomplished by standard methods including smoke, surface-mounted tufts and flags, grids of tufts, and surface "paints" to reveal eddy structure. A 35 mm motor-driven Canon F-1 camera with a 250 frame film back and several lenses has been purchased; a 16 mm Kodak K-100 movie camera is also available. A small darkroom facility will be set up to permit rapid, on-site processing of exposed film.

Equipment for concentration measurements within the model plumes has not yet been purchased; several of these instruments are under consideration.

The wind tunnel, darkroom, and a model storage area will be housed in a prefabricated steel building 9.1mWx30.5mLx4.3mH. The interior will be temperature-controlled to within  $\pm 1^{\circ}\text{C}$ , and

humidity controlled to  $\pm 2\%$  RH. Funds for this building and its HVAC equipment have been provided by ERDA. The building will be located immediately behind the existing ATDL building, within 50m of the ATDL workshop.

## CHAPTER IV

### TENTATIVE SCHEDULE FOR FUTURE WORK

#### 1. Mathematical Modeling of Cooling Tower Plumes

Review of the literature is planned to continue through the end of the present study to insure recent ideas and data are incorporated in the final model. An initial model of cloud growth has already been completed, and is described in Chapter 2, above. Validation of this model against field data will continue until the end of 1976. Work to develop a second generation cloud growth model has already begun; ATDL staff working on this model include S. R. Hanna, C. J. Nappo, and K. S. Rao. Construction of this more sophisticated theory is expected to require about one year. Early validation attempts will begin in about six months, and will aid significantly in developing the model. Final validation will continue until the end of 1977. A sensitivity study of this second-generation plume model will begin in mid-1977, and will continue until the end of the study. Results will be reported in the literature at various stages of the work. The tentative schedule for completion of the various tasks is indicated in Table 16.

#### 2. Physical Modeling of Cooling Towers, Plumes, and Interactions

A preliminary literature survey has been completed; review of the literature will continue until the end of the study to take advantage of newly reported results. Equipment requirements have





been largely compiled and orders placed; virtually all the necessary instrumentation will be either on hand or on order by late fall of 1976. The building to house the wind tunnel should be complete about December 1, 1976. The tunnel will be set up and tested by a factory engineer before final acceptance. A complete check of the wind tunnel's flow behavior and installation of instruments such as probe traversing mechanisms, hot wire probes and recorders, etc. will continue until April, 1977. Efforts to properly simulate neutrally stable atmospheric boundary layer flows will then begin, using the most favorable techniques reported in the literature. Study of individual cooling towers should begin by July, 1977. A range of upwind roughnesses, tower Froude numbers, and tower efflux velocity ratios will be examined. Modifications of tower shape will be considered. Arrays of towers will be studied in 1978; downwash, recirculation, and other interference effects will be treated. ATDL staff engaged in this work will include R. P. Hosker and K. S. Rao. A report summarizing and analyzing the data will be published at the completion of the project. The tentative schedule for these tasks is listed in Table 16.

Other research of interest in evaluating possible weather modification effects of cooling towers will be conducted by G. A. Briggs of ATDL at the U. S. EPA's Fluid Modeling Facility, Research Triangle Park, N. C., from Sept., 1976 to Sept., 1977. Generalized studies are planned of multiple plume merger, the effects of ambient turbulence on strongly buoyant plumes, and the generation and/or concentration

of vorticity near bent-over plumes. The lift-off of an initially wake-entrained buoyant plume will also be examined. The schedule for accomplishment is presently uncertain because of the fairly large number of people expected to be using the EPA facilities during this period, and so has not been listed in Table 16. Results will be reported in the literature.

TABLE 16: Tentative schedule for task accomplishment in study of "Weather Modification Effects of Cooling Towers"

TASK	TIME PERIOD					
	7/75-12/75	1/76-6/76	7/76-12/76	1/77-6/77	7/77-12/77	1/78-6/78
Lit. survey of cloud growth models						
Develop initial cloud growth model						
Validation of initial cloud growth model						
Develop second generation cloud growth model						
Validation of final cloud growth model						
Sensitivity study of final cloud growth model						
Lit. survey of physical modeling of cooling towers						
Develop equipment requirements and purchase						
Installation and test of wind tunnel and related equipment						
Atmospheric boundary layer simulation for approach flow						
Wind tunnel study of single cooling towers, various shapes						
Wind tunnel study of cooling tower arrays and plume interactions						

 - COMPLETED
  - SCHEDULED



## CHAPTER V

### REFERENCES

- Auer, A. H., Jr. (1976) "Observations of an industrial cumulus." J. Appl. Meteorol., 15, 406-413.
- Aynsley, E., and Carson J. E. (1973) "Atmospheric effects of water cooling facilities, a summary," presented at the Cooling Tower Institute Annual Meeting, Jan. 29-31, Houston, Tx.
- Brennan, P. T., Seymour D. E., Butler M. J., Kramer M. L., Smith M. E., and Frankenburg T. T. (1976) "The observed rise of visible plumes from hyperbolic natural draft cooling towers." Atmos. Environ., 10, no. 6, 425-431.
- Briggs, G. A. (1974) "Plume rise from multiple sources," in Cooling Tower Environment-1974, National Technical Information Service, U. S. Department of Commerce, Springfield, Va., 22161, 161-179.
- Briggs, G. A. (1974) Discussion following Meyer, et al.'s paper in Cooling Tower Environment-1974, ed. by Hanna and Pell, ERDA-TIC, NTIS CONF-740302, 1975, 352.
- Briggs, G. A. (1975) Plume rise predictions. Lectures on Air Pollution and Environmental Impact Analyses. American Meteorol. Soc., 45 Beacon St., Boston, Mass., 59-111.
- Brodkey, R. S. (1967) The Phenomena of Fluid Motions (Addison-Wesley Publishing Co., Reading, Massachusetts).
- Bugler, T. W., and Tatinclaux J. C. (1974) Scale Effects on Cooling Tower Model Studies, Iowa Institute of Hydraulic Research report no. 168, Univ. of Iowa, September.
- Busch, N.E. and Panofsky H. A. (1968) "Recent spectra of atmospheric turbulence," Quart. J. of Roy. Meteor. Soc., 94, no. 400 (April), 132-148.
- Campbell, G. S. and Standen N. M. (1969) Progress Report II on Simulation of Earth's Surface Winds by Artificially Thickened Wind Tunnel Boundary Layers, National Aeronautical Establishment tech. rept. LTR-LA-37, National Research Council of Canada, Ottawa, July.
- Carson, J. E. (1974) "Meteorological consequences of thermal discharges from nuclear power plants--research needs," in Cooling Tower Environment-1974, ed. by Hanna and Pell, ERDA-TIC, NTIS CONF-740302, 1975, 221-238.

- Cermak, J. E., Sandborn V. A., Plate E. J., Binder G. H., Chuang H., Meroney R. N., and Ito S. (1966) Simulation of Atmospheric Motion by Wind Tunnel Flows, Fluid Dynamics and Diffusion Laboratory Tech. Report no. CER66JEC-VAS-EJP-GJB-HC-RNM-S117, Colorado State University, Ft. Collins, Colorado, May.
- Cooling Tower Environment-1974, ERDA Symposium Series, CONF-740302, Nat. Tech. Information Service, U. S. Dept. of Commerce, Springfield, Va., 22161, 638 pp.
- Cotton, W. R. (1975) Theoretical cumulus dynamics. Reviews of Geophysics and Space Physics, 13, 419-447.
- Counihan, J. (1969) "An improved method of simulating an atmospheric boundary layer in a wind tunnel" Atmospheric Environment 3, no. 2 (March), 197-214.
- Counihan, J. (1970) "Further measurements in a simulated atmospheric boundary layer," Atmospheric Environment 4, no. 3 (May), 259-275.
- Davenport, A. G. (1963) "The relationship of wind structure to wind loading," in Wind Effects on Buildings and Structures, proceedings of conf. at Nat. Physical Laboratory, Teddington, Middlesex, England, June 26-28 (Her Majesty's Stationery Office, London, 1965), 54-101.
- Davenport, A. G. and Isyumov N. (1967) "The application of the Boundary Layer Wind Tunnel to the prediction of wind loading," in Wind Effects on Buildings and structures, proc. of International Research Seminar at the Nat. Research Council, Ottawa, Canada, Sept. 11-15 (Univ. of Toronto Press, 1968), vol. I, 201-225.
- Environmental Systems Corporation (1976) Chalk Point Cooling Tower Project Seasonal Test Data for the period December 15-19, 1975, Report no. PPSP-CPCTP-8, Prepared by ESC, Knoxville, Tn. for the Md. Power Plant Siting Program, Chalk Point Cooling Tower Project, 157 pp.
- Fletcher, N. H. (1962) The Physics of Rainclouds. Cambridge Univ. Press, London, 386 pp.
- Gault, J. D. (1967) Low Altitude Atmospheric Turbulence LO-LOCAT Mid-Term Technical Data Analysis, U.S.A.F. Aeron. Systems Div. Tech. Rept. SEG-TR-67-35, Wright-Patterson AFB, Ohio, August.
- Golden, J. (1961) Scale Model Techniques, M. A. thesis, Dept. of Meteor. and Oceanography, New York Univ.



- Goldstein, S., editor (1965) Modern Developments in Fluid Dynamics, vols. I and II (Dover Publications, Inc., New York).
- Halitsky, J. (1968) "Gas diffusion near buildings," chapter 5-5 in Meteorology and Atomic Energy 1968 (D. H. Slade, ed.), U. S. AEC TID-24190, 221-255.
- Halitsky, J., Golden J., Halpern P., and Wu P. (1963) Wind Tunnel Tests of Gas Diffusion from a Leak in the Shell of a Nuclear Power Reactor and from a Nearby Stack, Geophys. Sci. Lab. report 63-2, Dept. of Meteor. and Oceanography, New York Univ.
- Hanna, S. R. (1972) "Rise and condensation of large cooling tower plumes." J. Appl. Meteorol., 11, 793-799.
- Hanna, S. R. (1974) "Meteorological effects of the mechanical draft cooling towers of the Oak Ridge Gaseous Diffusion Plant," in Cooling Tower Environment-1974, ERDA Symposium Series, CONF-740302, Nat. Tech. Information Service, U. S. Dept. of Commerce, Springfield, Va., 22161, 291-306.
- Hanna, S. R. (1976a) "Predicted and observed cooling tower plume rise and visible plume length at the John E. Amos power plant." To be published in Atmos. Environ.
- Hanna, S. R. (1976b) "Observed and predicted cooling tower plume rise at the John E. Amos power plant, West Virginia," Proceedings of the Third Symposium on Atmospheric Turbulence Diffusion, and Air Quality, American Meteorological Society, Raleigh, North Carolina.
- Hanna, S. R. and Gifford F. A. (1975) "Meteorological Effects of Energy Dissipation at Large Power Plants." Bull. Am. Meteorol. Soc., 56, 1069-1076.
- Hoult, D. P., O'Dea S. R., Touchton G. L., and Ketterer R. J., (1975) "Turbulent plume in a turbulent cross flow: comparison of wind tunnel tests with field observations," paper #75-49.1 presented at 68th Annual Meeting of the Air Pollution Control Assoc., Boston, Mass., June 15-20.
- Hoult, D. P. and Weil J. C. (1972) "Turbulent plume in a laminar cross flow," Atmospheric Environment, 6, no. 8 (August), 513-531.
- Isumi, Y., editor (1971) Kansas 1968 Field Program Data Report, USAF Cambridge Research Lab. environmental research paper 379, AFCRL-72-0041, December 27.



- Izumi, Y. and Caughey J. S. (1976) Minnesota 1973 Atmospheric Boundary Layer Experiment Data Report, USAF Cambridge Research Lab. environmental research paper 547, AFCRL-TR-76-0038, January 21.
- Jones, G. W., Jones, J. W. and Monson K. R. (1969) Interim Analysis of Low Altitude Atmospheric Turbulence (LO-LOCAT) Data, USAF Aeron. Systems Div. Tech. Rept. ASD-TR-69-7, Wright-Patterson AFB, Ohio, February.
- Jones, J. W., Mielke R. H., Jones G. W., et al. (1970) Low Altitude Atmospheric Turbulence LO-LOCAT Phase III, USAF Flight Dynamics Laboratory Tech. Rept. AFFDL-TR-70-10, vol. I, part I, Wright-Patterson AFB, Ohio, November.
- Kennedy, J. F., and Fordyce H. (1974) "Plume recirculation and interference in mechanical-draft cooling towers," in Cooling Tower Environment-1974, ed. by Hanna and Pell, ERDA-TIC, NTIS CONF-740302, 1975, 58-87.
- Kramer, M. L., Seymour D. E., Butler M. J., Kempton R. N., Brennan P. J., Conte J. J. and Thomson R. G. (1975) John E. Amos Cooling Tower Flight Program Data, December 1974-March 1975, by Smith-Singer Meteorologists, Inc., 134 Broadway, Amityville, N.Y., 11701 for American Electric Power Service Corp., P.O. Box 487, Canton, Ohio, 44701.
- Kramer, M. L., Smith M. E., Butler M. J., Seymour D. E., and Frankenberg T. T. (1975) "Cooling towers and the environment," paper 75-17.3 presented at the 68th Annual Meeting of the Air Poll. Control Assoc., Boston, Mass., June 15-20.
- Landau, L. D., and Lifshitz E. M. (1959) Fluid Mechanics, vol. 6 of Course of Theoretical Physics (Addison-Wesley Publishing Co., Reading, Massachusetts).
- Lettau, H. H. (1962) "Theoretical wind spirals in the boundary layer of a barotropic atmosphere," Beiträge zur Physik den Atmosphäre, 35, 195-212.
- Lin, J. T., Lin H. T., and Pao Y. H. (1974) Laboratory Simulation of Plume Dispersion in Stably Stratified Flows Over a Complex Terrain, Flow Research, Inc. report no. 29 to the U. S. E.P.A. under contract 68-02-0800, February.
- Lloyd, A. (1967) "The generation of shear flow in a wind tunnel," Quart. J. of Roy. Meteor. Soc., 93, no. 395 (January) 79-96.

- Ludwig, G. R., Sundaram T. R., and Skinner G. T. (1971) Laboratory Modeling of the Atmospheric Surface Layer with Emphasis on Diffusion, Cornell Aeronautical Laboratory report no. VC-2740-S-2 to the Fallout Studies Branch, Division of Biology and Medicine, U.S. AEC, AEC no. NYO-4038-2, under contract AT(30-1)-4038, July.
- Lumley, J. L. and Panofsky H. A. (1964) The Structure of Atmospheric Turbulence (Interscience Publishers, New York).
- McVehil, G. E., Ludwig G. R., and Sundaram T. R. (1967) On the Feasibility of Modeling Small Scale Atmospheric Motions, Cornell Aeronautical Laboratory report no. ZB-2328-P-1, April 22.
- McVehil, G. E. and Heikes K. E. (1975) Cooling Tower Plume Modeling and Drift Measurement. A Review of the State-of-the-Art, prepared for ASME (Contract G-131-1) by Aerospace Division, Ball Brothers Research Corporation, Boulder, Colorado, 80302.
- Meyer, J. H., Eagles T. W., Kohlenstein L. C., Kagan J. A., and Stanbro W. D. (1974) "Mechanical draft cooling tower visible plume behavior: measurements, models, predictions," in Cooling Tower Environment-1974, ERDA Symposium Series, CONF-740302 Nat. Tech. Information Service, U. S. Dept. of Commerce, Springfield, Va., 22161, 307-352.
- Monson, K. R., Jones G. W., Mielke R. H., et al., (1969) Low Altitude Atmospheric Turbulence LO-LOCAT Phase III Interim Report, U.S.A.F. Flight Dynamics Laboratory Tech. Rept. AFFDL-TR-69-63, vol. I, Wright-Patterson AFB, Ohio, October.
- Nappo, C. J. (1976) "The detailed numerical simulation of vorticity concentration downwind of large heat sources," in ATDL Annual Report to the Atmospheric Effects of Nuclear Energy Centers Program, ATDL-NOAA, Oak Ridge, TN.
- Norman, J. M., Thomson D. W., Pena J., and Miller R. (1976) Aircraft Turbulence and Drift Water Measurements in Evaporative Cooling Tower Plumes, Penn. State Univ., Meteorology Dept. research report (draft).
- Onishi, Y. and Trent D. S. (1976) Mathematical and Experimental Investigations on Dispersion and Recirculation of Plumes from Dry Cooling Towers at Wyodak Power Plant in Wyoming, Battelle Pacific Northwest Laboratory report BNWL-1982, prepared for ERDA under contract E(45-1):1830, February.



- Pasquill, R. (1971) "Wind structure in the atmospheric boundary layer," in A Discussion on Architectural Aerodynamics, Phil. Trans. Roy. Soc. Lond. A. 269, 439-456.
- Peterka, J. A. and Cermak J. E. (1974) Simulation of Atmospheric Flows in Short Wind Tunnel Test Sections, Fluid Dynamics and Diffusion Laboratory report CER73-74JAP-JEC32, Colorado State Univ., Ft. Collins, June.
- Pope, A and Harper J. J. (1966) Low-Speed Wind Tunnel Testing (John Wiley and Sons, New York).
- Rao, K. S. (1976) "3-D subgrid turbulence enclosure models- a critical review," in ATDL Annual Report to the Atmospheric Effects of Nuclear Energy Center Program, ATDL-NOAA, Oak Ridge, Tennessee.
- Schlichting, H. (1960) Boundary Layer Theory, 4th Edition, (McGraw Hill Book Company, New York).
- Simpson J. and Wiggert V. (1970) "Models of precipitating cumulus towers." Mon. Wea. Rev., 97, 471-489.
- Slawson, P. R., Coleman J. H., and Frey J. W. (1974) "Some observations on cooling-tower plume behavior at the Paradise Steam Plant," in Cooling Tower Environment-1974, ERDA Symposium Series, CONF-740302, Nat. Tech. Information Service, U. S. Dept. of Commerce, Springfield, Va., 22161, 147-160.
- Snyder, W. H. (1972) "Similarity criteria for the application of fluid models to the study of air pollution meteorology," Boundary-Layer Meteor., 3, no. 1 (Sept.), 113-134.
- Sundaram, T. R., Ludwig G. R., and Skinner G. T. (1972) "Modeling of the turbulence structure of the atmospheric surface layer," AIAA Journal 10, no. 6 (June), 743-750.
- Sutton, O. G. (1953) Micrometeorology (McGraw-Hill Book Co., New York).
- Symes, C. R., and Meroney R. N. (1970) Cone Frustrums in a Shear Layer, Fluid Dynamics and Diffusion Laboratory Tech. Report no. CER70-71CRS-RNM11, Colorado State University, Ft. Collins, Colorado, August.



Templin, R. J. (1969) Interim Progress Note on Simulation of Earth's Surface Winds by Artificially Thickened Wind Tunnel Boundary Layers, National Aeronautical Establishment tech. rept. LTR-LA-22, National Research Council of Canada, Ottawa, February 26.

Townsend, A. A. (1956) The Structure of Turbulent Shear Flow (Cambridge Univ. Press).

Wolf, M. A. (1976a) "Natural draft cooling tower plume characteristics determined with airborne instrumentation." Pac. Northwest Lab. Annual Rep. for 1975 to the USERDA DBER. Part 3 Atmospheric Sciences, BNWL-2000 PT3, 281-288.

Wolf, M. A. (1976b) Private communication dated 10 May 1976.

APPENDIX A

PREDICTED AND OBSERVED COOLING TOWER PLUME RISE AND  
VISIBLE PLUME LENGTH AT THE JOHN E. AMOS POWER PLANT

by

Steven R. Hanna

Air Resources

Atmospheric Turbulence and Diffusion Laboratory  
National Oceanic and Atmospheric Administration  
Oak Ridge, Tennessee 37830

June, 1976

ATDL Contribution File No. 75/21.

# ABSTRACT

A one-dimensional numerical cloud growth model and several empirical models for plume rise and cloud growth are compared with twenty seven sets of observations of cooling tower plumes from the 2900 MW John E. Amos power plant in West Virginia. The three natural draft cooling towers are 200m apart. In a cross wind, the plumes begin to merge at a distance of about 500m downwind. In calm conditions, with reduced entrainment, the plumes often do not merge until heights of 1000m. The average plume rise, 750m, is predicted well by the models, but day-to-day variations are simulated with a correlation coefficient of about .5. Model predictions of visible plume length agree, on the average, with observations for visible plumes of short to moderate length (less than about 1km). The prediction of longer plumes is hampered by our lack of knowledge of plume spreading after the plumes level off. Cloud water concentrations predicted by the numerical model agree with those measured in natural cumulus clouds (about .1g/kg to 1g/kg).



## 1. Introduction

In the assessment of atmospheric effects of energy centers, a crucial problem is the calculation of visible plume and cloud growth caused by emissions from cooling towers. At a power plant, for example, cooling towers emit as much as twice the energy generated for electricity. Typically, more than half of this "waste" energy is in the form of latent heat. Many current power plants use from one to four large natural draft cooling towers, which have the following physical characteristics:

top diameter:	~70m
height:	~150m
vertical plume speed:	~5m/sec
difference between plume and ambient T;	~20°C

Some power plants use mechanical draft cooling towers, which rely on fans to force the air flow and are not as tall (a typical height is 20 or 30m). Arrays of mechanical draft towers have historically been built in lines, but recent construction includes disc and doughnut shaped systems.

Proposed energy centers, if constructed, will dissipate about 100,000MW of waste heat from a surface area of about  $100\text{km}^2$ . Energy fluxes of this magnitude put energy centers on the same scale as large geophysical phenomena such as bushfires, volcanoes, and thunderstorms (Hanna and Gifford, 1975). Clearly it is very important that we study the possible environmental effects of energy centers before they are built, in order to determine the spacing, tower type, and so on, that will minimize environmental impact.

Unfortunately, the models and observations necessary for these assessments do not exist. The state of art of this area of research is summarized in the conference proceedings entitled Cooling Tower Environment - 1974 and in the critical review by McVehil and Heikes (1975). A few models for estimating visible plume are presented in these publications, but there is very little discussion of cloud growth models. The only published attempts at modeling the cloud physics processes in cooling tower plumes are so-called "one-dimensional models", where plume parameters are a function only of height, as reported by EG&G (1971) and Hanna (1971). In both of these models, Weinstein's (1970) cloud growth model is used as a basis.

In determining the atmospheric effects of energy centers, it is reasonable to begin with simple one dimensional models. Then, after the capabilities of these models are assessed, the research can proceed to two or three dimensional models.

The model by Hanna (1971) was revived, encouraged by recent developments in the area of aircraft measurements of cooling tower plumes. For example, M. Wolf (1976), of Battelle Pacific Northwest Laboratory, is using an aircraft-mounted cloud droplet spectrometer to measure water drop characteristics in cooling tower plumes

at the Rancho Seco Plant in California. Norman et al. (1975) of Penn State University are making a nearly complete series of cloud physics and turbulence measurements from their aircraft at the Keystone, Pa., cooling towers. Similar measurements are being made by Woffinden et al. (1976) of Meteorology Research, Inc. as part of the Chalk Point Project.

The observations that are used to test our model were obtained by Kramer et al. (1975) at the John E. Amos, West Virginia, power plant of the American Electric Power Service Corporation. Observations were made on 54 separate occasions during the winter of 1974-1975, aiming for periods when the plume would be as long as possible. Ambient profiles of temperature, dew point, and wind speed were obtained by aircraft; and many photographs of the plume were taken. These measurements are particularly valuable, since in many cases the visible plume obviously extended beyond the point of maximum plume rise, and therefore final plume rise could be obtained. Unfortunately, no in-plume observations were made.

The Amos measurements were analyzed statistically by Brennan et al. (1976), who found very little relationship between plume rise and wind speed, but a good relationship between plume rise and haze layer or inversion height. It is expected that the relationship with haze layer height will deteriorate for measurements made during the warmer seasons of the year, when the haze layer is much deeper.



## 2. Numerical Model Description

The numerical model has been constructed so that it agrees with known relationships for the rise of buoyant stack plumes at small heights and the growth of natural continental cumulus clouds at large heights. It is based on theories of plume rise developed by Briggs (1969), cloud growth developed by Weinstein (1970), and cloud microphysics developed by Kessler (1969). Since the model is one-dimensional (i.e., plume parameters are a function of height only), it cannot be expected to portray cloud growth as well as two or three dimensional models which account for cross-plume gradients. But one-dimensional models have been shown to work quite well for stack plumes and for many cumulus clouds, and are a necessary first step in the analysis of atmospheric effects of energy

The framework of this model was first reported by Hanna (1971), but testing of the model had to wait until sufficient observations of cooling tower plumes were made. A few modifications to the 1971 model were made, based on recent developments in plume rise theory. The first change reflects a suggestion by Briggs (1975) which resolves the paradox that, for a given entrainment rate for bent over plumes, the final plume rise and the rate of change of plume radius with height cannot simultaneously agree with observations. This problem is solved using the knowledge that the rate of

change of the momentum flux with height depends partly on the fact that ambient air above the rising plume must also be accelerated. The effective radius of the "momentum plume" is therefore larger than the radius as determined from temperature differences. Briggs finds that agreement with observations is reached when the following relations are used:

$$\text{For bent over plumes: } \begin{cases} \partial R_m / \partial z = .6 \text{ (momentum plume)} & (1) \\ \partial R_t / \partial z = .4 \text{ (temperature plume)} & (2) \end{cases}$$

where  $R_m$  is the radius of the momentum plume and  $R_t$  is the radius of the temperature plume. Consequently the ratio,  $E_m$ , of the effective momentum flux to the momentum flux within the temperature plume approaches  $(.6/.4)^2$ , or 2.25.

The second modification to the model reflects observations by Slawson et al. (1974) and Meyer et al (1974), that visible plume lengths are consistently underpredicted by basic plume models, due to the fact that inhomogeneities in the plume can result in locally saturated spots, even though the plume is unsaturated on the average. Meyer et al (1974) resolve this problem through the use of a peak factor, explaining that: "it was simply assumed that the excess water-vapor content at the plume center is higher than the average excess water-vapor content predicted in the plume by an empirically

determined constant that is referred to as the peak factor." They suggest that the peak factor equals 1.86. Briggs (1975) has reanalyzed their data and other data, and finds that the peak factor equals 2.0. This factor is incorporated into the present model by assuming that the ratio,  $E_w$ , of the cross-sectional area of the moisture plume to the temperature plume approaches 1/2. In terms of the rate of change of the radius with height, this assumption can be written:

$$\partial R_w / \partial z = .71 \partial R_t / \partial z, \quad (3)$$

where  $R_w$  is the radius of the moisture plume. Note that the constant .71 is the inverse of the square root of the peak factor. Equation (3) applies to both vertical and bent over plumes.

The third modification to the model accounts for the stretching of the plume as it rises through layers of wind shear. In order to maintain continuity in the volume flux, the term  $(R_t/2U) \partial U / \partial z$  is subtracted from the right hand side of equation (1). Since the wind shear is usually positive in the boundary layer, the rate of growth of the plume radius is not as great as it would be in a region of constant wind speed. Murthy (1970) gives solutions to the plume rise equations for a wind profile which satisfies a power law.

The final basic modification to the model is made to account for merging of multiple cooling tower plumes. This states simply that, when the radius of the plume equals one half of the distance between the centers of the towers, the plumes merge and the cross-sectional area of the single merged plume equals the cross-sectional areas of the two or more individual plumes at the time of the merger.



Photographs of the Amos plumes in the report by Kramer et al. (1975) suggest that for bent-over plumes, merger begins at a distance of 300 to 500m downwind. For vertical plumes, where entrainment is less, merger does not begin until heights of 500 to 1000m are reached. It is also interesting that the observed plumes in calm conditions do not constrict, as predicted by plume rise theory, but in all cases steadily increase their radius as height increases. From the plume photographs, it appears that the plume diameter doubles or triples after it rises one tower height (150m).

The following equations are used in the model:

Equation of Motion:

$$\partial(w^2/2)/\partial z = (g/E_m) [(T_p(1 + .61E_w Q_p) - T_e(1 + .61E_w Q_e)) / (T_p(1 + .61E_w Q_p)) - E_w(Q_c + Q_h)] - (O_m w^2 / R_m) \quad (4)$$

where  $w$ (m/s) is the vertical speed,  $g$ (m/s<sup>2</sup>) is the acceleration of gravity,  $T$ (°K) is temperature, and the  $Q$ 's (g/g) are specific water densities. The entrainment coefficient for the momentum plume,  $O_m$ , is defined by  $(1/V)dV/dz = O_m/R_m$ , where the volume flux,  $V$ , equals  $UR_m^2$  for a bent over plume and  $wR_m^2$  for a vertical plume. Subscripts p, e, c, and h refer to plume variables, environmental variables, cloud water content, and hydrometeor water content, respectively. The term on the left is the vertical acceleration of the plume. The terms on the right are the buoyancy force and the drag or entrainment force.

Equation for Temperature Change:

$$\begin{aligned} \partial T_p / \partial z = & \{ -(LE_w / c_p) \partial Q_{ps} / \partial z \} - g / c_p - O(T_p - T_e) / R + \{ (L_i E_w / c_p) (Q_h + Q_c) / \Delta z \} \\ & - \{ (LE_w / c_p) O_w (Q_p - Q_e) / R_w \} \end{aligned} \quad (5)$$

The terms in curly brackets apply only when the plume is saturated. The subscript s refers to a saturated variable. The parameters  $L$  (j/g),  $L_i$  (j/g), and  $c_p$  (j/g $^{\circ}$ K) are the latent heats for vapor-water and water-ice transitions, and the specific heat of air at constant pressure. The entrainment rates  $O$  and  $O_w$  refer to the temperature and water plumes, respectively.  $\Delta z$  is the height increment of the numerical integration. The terms on the right are the heat gained due to condensation, the heat lost due to dry adiabatic expansion, the entrainment rate or heat required to warm entrained air, the heat gained due to freezing of liquid water, and the heat lost as liquid water is evaporated in order to saturate the entrained air. A term suggested by Weinstein (1970) which accounts for the evaporation of liquid water at the plume's edge, was originally included in equation (5). Since the contribution of this term was found to be insignificant, it was removed from the equation.

Equation for Water Vapor Change:

$$\text{Unsaturated } \partial Q_p / \partial z = -O_w (Q_p - Q_e) / R_w \quad (6)$$

$$\text{Saturated } \partial Q_p / \partial z = \partial Q_{ps} / \partial z \quad (7)$$

In equation (6), for an unsaturated plume,  $Q_p$  changes only because of entrainment. In equation (7), for a saturated plume, the loss is due to condensation of liquid water in the rising plume.

Equation for Cloudwater Change:

$$\frac{\partial Q_c}{\partial z} = -\frac{\partial Q_{ps}}{\partial z} - 10^{-3}(Q_c - .0005)/w - .00522Q_c(1000Q_h)^{.875}/w - \frac{0}{w}(Q_p + Q_c - Q_e)/R_w \quad (8)$$

The first term on the right hand side is the gain due to condensation in the rising plume. The second and third terms are losses due to conversion and coalescence of cloudwater into hydrometeor water (after Kessler, 1969). The last term is a decrease due to entrainment. Note that cloud water is used first to saturate the entrained air.



Equation for Hydrometeor Water Change:

$$\partial Q_h / \partial z = 10^{-3} (Q_c - .0005) / w + .00522 Q_c (1000 Q_h)^{.875} / w - 4.5 Q_h (1000 Q_h)^{.125} / (w R_w \cdot \cos(\arctan(w/U))) - Q_h / R_w + K_2 / \Delta z \quad (9)$$

Terms one and two are the gains due to conversion and coalescence of cloudwater into hydrometeor water. Term three is the loss due to rainout. Term four is the decrease due to entrainment. The last term ( $K_2$ ) is the saturation deficit of the plume if all of the cloud water has been evaporated into the entrained air after a given height increment,  $\Delta z$ , but the entrained air is still not saturated. Then if all of the hydrometeor water is evaporated after a given height increment and the entrained air is still not saturated, the whole plume must become unsaturated.

Entrainment:

Vertical Plume:

$$\begin{aligned} O_m &= 0 = .15 & O_w &= .107 \\ \partial R_m / \partial z &= \partial R / \partial z = .15 - R(g/T_p)(T_p - T_e) / 2w^2 \\ \partial R_w / \partial z &= .71 \partial R / \partial z \end{aligned} \quad (10)$$

Bent Over Plume:

$$\begin{aligned} O_w &= .57 & O &= .8 & O_m &= 1.2 \\ \partial R / \partial z &= .4 - (R/2U) \partial U / \partial z \\ \partial R_w / \partial z &= .71 \partial R / \partial z \\ \partial R_m / \partial z &= 1.5 \partial R / \partial z \end{aligned} \quad (11)$$

The entrainment relations are based on Briggs (1975) latest guidelines. They are in rough agreement with Cotton's (1975) review of entrainment rates used in cumulus cloud models. He finds that various investigators use entrainment coefficients, 0, ranging from zero to unity, depending on which value gives predicted cloud heights in agreement with a particular set of observations.

The entrainment formulas for bent over plumes are used when the local wind speed,  $U$ , exceeds 1 m/s. Consequently, the entrainment constants may switch from those appropriate for bent over plumes to those appropriate for vertical plumes at different heights in the same run.

Saturation Specific Humidity:

a)  $T_1 = 273.16^\circ\text{K} < T < 373^\circ\text{K}$

$$\begin{aligned} \ln Q_{ps} = & 2.303(10.79574(1-T_1/T) + 1.50475 \times 10^{-4}(1-10^{-8.2969(T/T_1-1)}) \\ & + .42873 \times 10^{-3}(10^{4.76955(1-T_1/T)-1}) - 5.028 \ln T/T_1 - \ln p + 1.335 \end{aligned} \quad (12)$$

b)  $T < T_1 = 273.16^\circ\text{K}$

$$\begin{aligned} \ln Q_{ps} = & 2.303(-9.09685(T_1/T-1) + .87682(1-T/T_1)) \\ & - 3.56654 \ln T_1/T - \ln p + 1.335 \end{aligned} \quad (13)$$

where  $p$  is pressure in millibars, calculated by means of the hydrostatic equation. These two empirical equations are the "Goff-Gratch" formulas, as given by the World Meteorological Organization (1966). Any equation relating  $T$  and  $Q_{ps}$ , such as the Clausius-Clapeyron equation, could be used in place of equations (12) and (13).

Equations (12) and (13) are plotted in Figure 1, for  $p = 1000\text{mb}$ , forming the psychrometric curve which is the basis of several published methods for determining the vapor content and temperature of plumes (e.g., Wigley and Slawson, 1971). The technique is illustrated by plotting the initial saturated plume position  $(T_{po}, Q_{po})$  and the unsaturated environment position  $(T_e, Q_e)$ . Depending on the relative amounts of plume air and environment air in the resulting mixture, the rising plume can be predicted to be somewhere along the line between these two points. However, if the resulting mixing ratio,  $Q_{pl}$ , is greater than the saturation mixing ratio,  $Q_{pls}(T_{pl})$ , then some of the water vapor must condense, and the actual position  $(T'_{pl}, Q'_{pl})$  is approached. The slope of the dotted line,  $\Delta Q/\Delta T$ , or  $L/c_p$ , equals  $-.8$  on this figure. If there were no initial liquid water, then the concentration of liquid water at position  $(T'_{pl}, Q'_{pl})$  would be  $(Q_{pl} - Q'_{pl})$ . The end of the visible plume is the point at which the straight line crosses the curved line near the bottom of figure 1.



Unfortunately, the psychrometric technique is not so handy for plumes from natural draft cooling towers, which rise several hundred meters. The saturation curve shifts as height (i.e., pressure) changes. Furthermore, the environmental position ( $T_e$ ,  $Q_e$ ) may vary considerably over the depth of the plume. It is still possible to use the psychrometric chart for a well-mixed adiabatic environment (see Briggs, 1975) where the straight line in Figure 1 can be shifted uniformly to the left by the amount  $zg/c_p$  in order to account for temperature changes with height. The psychrometric chart technique has been applied most successfully to short plumes from mechanical draft cooling towers (see McVehil and Heikes, 1975).

Equations (1) through (13) are a complete set, and are solved on a high-speed digital computer using height steps of .01m, .1m, and 1m for heights less than 10m, between 10 and 100m, and above 100m, respectively. As may be expected, the possibility of a phase change requires detailed logical steps in the computer program. For example, if the calculated vapor content  $Q_p$  happens to be greater than the saturated vapor content  $Q_{ps}$  after a single height step is taken, it is necessary to condense some of the excess vapor. The condensation takes place in such a way that the energy released by condensation just balances the heat gained due to a temperature increase.

Several of the parameterizations in this model are based on measurements in natural clouds rather than cooling tower clouds. For example, rainout is included in the program (eq. 9, term 3), using a mechanism suggested by Simpson and Wiggert (1969). This mechanism is based on the assumption that the relative rate of loss of hydrometeor water in a given time interval is proportional to the distance that the water drops would fall in that interval, divided by the vertical component of the plume radius. Because this relation was first developed for large cumulus clouds, it is questionable whether the rainfall rates that it yields in our application are realistic. Unfortunately, there are not yet sufficient observations in cooling tower plumes to derive empirical relationships for cloud physics processes. Some of this information is beginning to come from the Penn State program (Norman et al, 1975), but much more needs to be done.

### 3. Input Data

All of the observation periods were during the winter of 1974-1975, and were deliberately chosen by Kramer et al (1975) so that a long visible plume would be present. Low temperatures, high relative humidities, low wind speeds and stable conditions all increase the chances of a long visible plume. The first two conditions lower the saturation deficit ( $Q_{es} - Q_e$ ) of the ambient air, while the last two conditions increase the concentration of excess water in the plume. During a run, the aircraft would obtain vertical profiles of dry bulb temperature, dew point, and wind speed in the lowest 2000m. Several photographs of the plume were taken, and the visible plume height and length were noted. At the same time, power plant personnel provided information on the net load of the three cooling towers. These data have been summarized in a very complete fashion, including drawings of the visible plume, by Kramer et al (1975). About half of the runs could not be used in this study, because of problems such as the disappearance of the plume in a cloud deck or insufficient ambient profile data. Of the 27 runs which are analyzed, seven have bent over plumes in which the visible plume does not extend to the point



of maximum plume rise, seven have vertical plumes, and 13 have bent over plumes in which the visible plume does extend to the point of maximum plume rise.

The three cooling towers at the Amos plant have the characteristics listed in Table 1.

Table 1

Specifications for Amos Cooling Towers (from Kramer et al (1975))

	<u>height</u>	<u>top radius</u>	<u>w<sub>0</sub></u>	<u>Capacity</u>
Towers 1 & 2	132m	29m	4.6m/s	800MW(each)
Tower 3	150m	40m	4.2m/s	1300MW

The towers are in a line, spaced 200m apart. During the observation periods, the plant ran close to its generating capacity of 2900MW. The initial heat flux used in the model is

modified based on the actual energy output for each observation period. Also, prior to plume merger (which is assumed to occur when plume radius equals  $\frac{1}{2}$  tower spacing, or 100m), only the plume from tower 3 is modeled. The initial plume radius,  $R_0$ , is taken as 40m, and the initial plume vertical speed,  $w_0$ , is assumed to be 4.4m/s (the average over the towers).

The initial plume temperature is estimated by an empirical relation derived from the specifications in Kramer et al. (1975):

$$T_{po} = (297.4 + .635(T_d - 273))(1 + .01(1 - RH)), \quad (14)$$

where  $T_d$  and RH are the ambient dew point and relative humidity. Since the Amos plant does not always operate at full capacity, the ratio of actual to full power is also input for each run. This ratio is used to revise the plume temperature calculated by equation (14) by assuming that the actual difference between the plume and environment temperatures equals the power ratio times the temperature difference calculated using equation (14). These assumptions were not tested, since no measurements of initial plume temperature were made at the Amos plant.

To insure continuity of the momentum flux, the effective initial plume radius for bent over plumes is calculated from the equation (Hanna, 1972):

$$R_{eff} = R_o (w_o/U)^{1/2} \quad (15)$$

The mixing ratio of the initial cloud water,  $Q_c$ , and hydrometeor water,  $Q_h$ , are also required as input to the model. Both have arbitrarily been set equal to .001, on the basis that fog or cloud is obviously present at the tower mouth; and the sum of the two, .002g/g, is typical for vigorous natural cumulus clouds (Fletcher, 1962). If the plume evaporates, however, buoyancy will be reduced slightly due to the energy that must be taken from the air to evaporate the liquid drops. For example, if the initial liquid water content, .002g/g, were to evaporate at the tower mouth, plume temperature would be reduced by  $(L/c_p)(.002\text{g/g})$ , or  $5^\circ\text{C}$ .

Because of the possibility that errors would be introduced by the arbitrary specification of  $Q_c$  and  $Q_h$ , a sensitivity test was run in which  $Q_c$  (which equals  $Q_h$ ) was set equal to .00001, .0001, .001, and .01 g/g. It was found that, when the visible plume is large and a cloud forms in its upper reaches, the initial values of  $Q_c$  and  $Q_h$  have little effect on final plume rise and cloud water concentration. But for dry ambient conditions when the plume evaporates at a height of about 50m, the initial values of  $Q_c$  and  $Q_h$  can have a significant effect on plume length and plume rise. The results of running the model for an isothermal ambient atmosphere ( $10^\circ\text{C}$ ) with 50% relative humidity are given in Table 2.



Table 2

Model Output for Isothermal Atmosphere ( $10^{\circ}\text{C}$ )

with 50% RH and  $U = 10\text{m/s}$ .

Initial $Q_h$ and $Q_c$ (g/g)	Plume Rise (m)	Visible Plume Height (m)	Visible Plume Length (m)	$Q_c$ at max	$z(\text{m})$
.00001	249	52	165	.00057	15
.0001	248	52	165	.00063	15
.001	232	67	230	.00129	10
.01	138	138	610	.01000	0

It is seen from this table that when the initial  $Q_c$  equals  $10^{-5}$  or  $10^{-4}$ , plume parameters are not significantly affected. But when  $Q_c$  equals  $10^{-3}$ , the value used in analyzing the Amos data, plume rise decreases by 7% and visible plume height increases by 29% above that for plumes which begin with essentially no liquid water. When  $Q_c$  equals  $10^{-2}$ , which is a concentration at least an order of magnitude greater than that observed in natural clouds, plume rise is nearly halved and the plume is visible through its point of maximum rise. It can be concluded that the possibility of errors in our choice of initial  $Q_h$  and  $Q_c$  introduces an uncertainty of about 10 to 20% in calculations of visible plume length for plumes on dry days, but has little effect for plumes on humid or cold days, when the initial liquid water never has a chance to evaporate.

There is not room here to include all of the 27 sets of Amos data used in this analysis. But as an example of the input data, the observations by Kramer et al. (1975) during run 6 are listed in Table 3. These data were used to generate the output in Figure 2, which is discussed in a later section.

Table 3

Observations at John E. Amos power plant  
(Kramer et al., 1975), for 18 Dec. 1974 (Run 6).

Height Above Tower (m)	Ambient Dry Bulb °K	Ambient Dew Point °K	Wind Speed m/s
0	268.0	266.9	
122	266.9	266.9	9
243	265.2	265.2	
365	264.1	264.1	
426	263.6	263.6	
578	263.0	263.0	
700	262.4	262.4	
821	261.9	261.9	
942	260.8	260.8	
1064	259.7	259.7	
1186	259.1	259.1	12

Ratio of actual power to maximum power = .83  
Initial plume temperature (from equation 14) = 290°K  
Observed plume rise = 850m  
Observed visible plume length = 9.6km

#### 4. Results

The computer model was run for each of the 27 test cases, and values of total plume rise and visible plume height and length were noted. Also, some simple formulas for estimating plume rise and visible plume parameters were tested.

##### 4.1 Final plume rise

In nineteen of the observation periods analyzed, the visible plume extends through the point of maximum plume rise. The average wind speed and vertical potential temperature gradient through the layer in which plume rise took place are given in Table 4. In addition, the saturation deficit in the ambient air at the tower top is given. The observed plume rise listed in the table refers to the final equilibrium height of the plume centerline. All heights are in meters above the tower top.

In column five of the table, the height of the base of the lowest significant inversion in the temperature sounding is given. This height might also be called the mixing height. For the observations when an inversion is present, the average inversion height is 820m and the average observed plume height is 790m. The correlation coefficient between inversion height and observed plume height is .90. This good agreement has led Brennan et al. (1976),



Table 4

## Observed and Calculated Plume Rise

Run	$\bar{U}$ (m/s)	Ambient tower top saturation deficit (g/kg)	$\Delta\theta/\Delta Z$ over depth of plume ( $^{\circ}\text{C}/\text{mx}10^3$ )	Inversion height above tower (m)	Observed plume rise (m)	Model plume rise (m)	Analytical Plume rise sensible one unit (m)	sensible + latent all units (m)	$E_N$ applied to sensible one unit (m)
1	14	.43	13.5		560	260	250	450	270
6	11	.13	3.0		850	820	430	770	490
8a	9	0	9.8		370	350	250	450	270
10a	5	.60	2.1	720	820	820	590	1060	700
11	0	1.34	6.1	660	880	900	980	1500	
12	6	1.25	1.2	1140	1060	1200	720	1280	870
15	3	.28	10.7		1120	790	780	1200	
16	6	.41	7.2	1200	1160	700	380	680	430
17a	8	.29	6.7	360	360	430	410	730	460
18	6	.78	5.6		910	720	410	730	460
19	0	1.07	6.9	840	800	970	910	1400	
24	6	.60	4.0	750	760	630	500	900	580
28a	5	.52	21.8		360	400	310	570	340
31	0	1.02	11.6		500	900	780	1200	
35a	3	.87	9.8	390	360	590	480	880	550
44	8	1.16	1.9	960	910	420	510	910	590
45	7	1.16	5.6	1200	910	370	390	700	440
47	0	1.44	3.8	900	800	1020	910	1400	
48a	7	1.46	7.6	750	670	360	340	610	380
Avg.	5.6	.76	7.4	820	750	670	540	920	

in an independent assessment of these observations, to conclude that, when an inversion lid is present, the plume will rise to this lid and stop. The inversion lids are formed by the natural buoyant and mechanical mixing actions in the boundary layer. Apparently the energy fluxes in the cooling tower plumes are similar to those in natural convective elements during the winter in West Virginia, and the plumes, like the natural convective elements, rise to the base of the inversion lid. But since these inversion layers are often shallow and weak, it is difficult to measure them accurately with the aircraft probe. Consequently, the detailed structure of the inversion lid cannot be included in the numerical plume and cloud growth model. During the summer, when the height of the inversion layer is greatly increased due to the increased surface heat fluxes, the cooling tower plume is less likely to reach the top of the mixed layer.

The output of a typical computer run is given in Figure 2, based on the input data in Table 3. A slight change in curvature of the predicted  $\Delta T$ ,  $w$ , and  $Q_c$  profiles is evident at a height of about 200m. This is the height at which the three plumes merge in this run, and the buoyancy flux increases by

a factor of about 2.3. Since the ambient atmosphere in this run is nearly saturated pseudoadiabatic, the plume rises quite high and contains a moderate amount of cloud water through its entire trajectory.

The estimates of plume rise from the numerical model for each run are in column 7 of Table 4. The difference between average observed (750m) and estimated (670m) plume rise is about 12%. The correlation coefficient is .49, which can be considered fair. The observed and predicted plume rises are plotted in Figure 3.

Maximum cloud water concentration,  $Q_c$ , predicted by the numerical model ranges from .0010 to .0016 g/g, in agreement with typical values reported by Fletcher (1962) for natural cumulus clouds. Unfortunately, the aircraft did not obtain any measurements of liquid water concentrations for comparison with these predictions.

The last three columns in Table 4 contain analytical estimates of plume rise. The formulas suggested by Briggs (1969)



for plume rise, H, are used:

$$H = 5.0F^{1/4}s^{-3/8} \quad \text{Vertical} \quad (16)$$

$$H = 2.9(F/Us)^{1/3} \quad \text{Bent-over} \quad (17)$$

where the buoyancy flux, F, and stability parameter, s, are defined by the relations:

$$F = w_o R_o^2 (g/T_{vpo}) (T_{vpo} - T_{veo}) \quad (18)$$

$$s = (g/T_{eo}) (\partial \theta_e / \partial z) \quad (19)$$

In these relations the subscript v refers to virtual temperature.

If the sensible heat from a single tower unit is used in estimating the buoyancy flux, F, then the estimated plume rises in column 8 of Table 4 are obtained. The average estimated plume rise is 540m, or 28% lower than observed. The correlation coefficient between estimated and observed plume rise is .37. One reason for this low correlation is that average temperature gradients are used in calculating the stability parameter, s. The effects of small inversion layers are smoothed out by the analytic technique, but have a great influence on the observed plumes.

Note that the correlation between estimates of the analytical and numerical models is .82. In otherwords, the numerical model is not much different from or better than the simple analytical model for estimating plume rise.

Another estimate of plume rise can be obtained by redefining the buoyancy parameter to include the latent heat (Hanna, 1972):

$$F = w_o R_o^2 g [(T_{vpo} - T_{veo}) / T_{vpo} + (L / c_p T_{vp}) (Q_{po} - Q_{eo})] \quad (20)$$

If the sensible plus latent fluxes from the three cooling towers are added together to form F, the predictions are obtained which are listed in column 9 of Table 4. The average plume rise using the maximum F is 920m, or 23% greater than observed. Clearly the actual effective buoyancy flux is somewhere between the sensible flux from a single tower and the total heat fluxes from all towers.

The empirical technique suggested by Briggs (1974) for estimating the plume rise from multiple sources was also applied, and the results are in the last column of Table 4. He derived his formula from observations of plume rise from multiple stacks at TVA power plants. The plume rise from N stacks equals the plume rise from a single stack, H, multiplied by an enhancement factor,  $E_N$ , defined by:

$$E_N = ((N + S)/(1 + S))^{1/3}$$

where  $S = ((N-1) \Delta x / N^{1/3} H)^{3/2}$

The distance  $\Delta x$  is the spacing between towers, which equals 200m at Amos. It is seen from the last column of Table 4 that the enhancement factor for these data, assuming that H is the plume rise due to sensible heat only from a single tower, ranges from 1.08 to 1.21. This additional rise brings the magnitudes of the plume rise estimates closer to the observations, but does not increase the correlation coefficient.

#### 4.2 Visible plume dimensions

In addition to the runs analyzed above, there were also seven runs in which the visible plume was moderately long but did not extend through the point of maximum plume rise. Since visible plume length is not well defined for plumes occurring in calm conditions, analysis will be limited to the bent over cases. Observed visible plume lengths are obtained using the photographs published by Kramer et al. (1975) for the short plumes in Table 5, and from aircraft observers' notes supplied by Conte (private letter, 1975) for the longer plumes in Table 6. The aircraft observers' notes were not used for the shorter plumes because the accuracy of the visible plume length listed by the aircraft observers is  $\pm \frac{1}{4}$  mile.



Table 5

## Visible Plume Dimensions for Plumes whose Visible Portion

does not Reach the Point of Maximum Rise

Run	$\bar{U}$ (m/s)	ambient saturation deficit (g/Kg)		observed		numerical model		analytical model		ambient RH at plume level
		tower top	plume level	visible plume height (m)	visible plume length (m)	visible plume height (m)	visible plume length (m)	visible plume height (m)	visible plume length (m)	
2	13	3.0	3.9	100	200	75	290	100	370	.4
3	10	2.6	2.7	150	500	120	350	140	400	.65
13	10	.86	1.8	100	300	150	480	210	730	.6
20	10	2.8	3.9	200	400	70	250	120	290	.45
27	20	1.5	2.0	390	600	120	450	110	800	.55
39	15	2.9	3.6	240	450	140	240	100	430	.45
41	16	3.5	3.2	50	300	55	290	80	360	.35
Avg.	13	2.5	3.0	180	390	100	340	120	450	.50

Table 6

Visible Plume Dimensions for Plumes where the Visible Plume  
Extends through the Point of Maximum Rise

Run	$\bar{U}$ (m/s)	ambient tower top saturation deficit g/kg	saturation deficit at plume elev. g/kg	observed visible plume length (m)	ambient RH at plume level
1	14	.43	2.2	1600	.4
6	11	.13	0	9600	1.
8a	9	0	.65	4800	.9
10a	5	.60	0	25600	1.
12	6	1.2	0	4800+	1.
16	6	.41	1.3	2400	.8
17a	8	.29	.29	8000	.9
18	6	.78	1.1	1600	.7
21	9	.43	1.8	1600	.6
24	6	.60	.55	16000+	.85
44	8	1.2	.29	9000	.9
45	7	1.2	1.5	1600	.6
48a	7	1.5	1.2	32000+	.8
Avg.	8	.67	.84	4800m (median)	.80

In Table 5 the observed relative humidity, wind speed, visible plume height and length, and ambient saturation deficits at tower top and plume height are given for the set of plumes of moderate length. The average visible plume height and length predicted by the numerical model are seen to agree with the average of the observations fairly well. But the correlation between variations in observed and predicted lengths is poor. This poor correlation can be explained by the fact that weather conditions ( $U$ ,  $T$ ,  $\Delta Q$ ,  $RH$ ) are quite similar for each of the runs in Table 5, and consequently we are dealing with comparatively small differences among fairly large numbers. It can be concluded that, for wind speeds of about 13 m/s and saturation deficits of about 3g/kg, visible plume length at the Amos Plant is about 400m.

The results of a simple analytical model suggested by Hanna (1974) are given in columns nine and ten of Table 5. Formulas for visible plume height,  $h$ , and length,  $\ell$ , of bent over plumes are based in this model on the hypothesis that the tip of the visible plume occurs when the initial flux of excess water,  $V_o Q_{po}$ , in the plume just balances the saturation deficit flux,  $V(Q_{eos} - Q_{eo})$ :

$$h = 2R_o (w_o/U)^{1/2} [(2Q_{po}/(Q_{eos} - Q_{eo}))^{1/2} - 1] \quad (23)$$

$$\ell = 1.4 (R_o^{3/2} U^{3/4} w_o^{3/4} / F^{1/2}) [(2Q_{po}/(Q_{eos} - Q_{eo}))^{1/2} - 1]^{3/2} \quad (24)$$



Note the occurrence of the peak factor, set equal to 2, inside the brackets of these equations. As expected, the analytical predictions of  $h$  and  $l$  agree fairly well with the predictions of the numerical model, but offer no significant improvement in accounting for the variability of the observed parameters.

Observations and predictions for the longer plumes are in Table 6. Note that for these longer plumes, extending beyond the point of maximum plume rise, average saturation deficit has dropped to .7 g/kg, average wind speed has dropped to 8 m/s, and average relative humidity increased to 80%, when compared with the shorter plumes in Table 5. The plus sign after three of the observed visible plume lengths indicates that the plume merged with existing clouds at that distance.

In Figure 4, observed plume length is plotted versus  $(1-RH)$  for all the observations in Tables 5 and 6. The ambient relative humidity at plume height is used for  $RH$ . The correlation coefficient is  $-.58$  for these data. The line on the figure is given by the formula

$$l = (2.15 \times 10^4 \text{ m}) e^{-7.6(1-RH)} \quad (25)$$

and is valid only for the Amos location during the winter. During the summer, when a given relative humidity implies a much larger saturation deficit, the line in Figure 4 can be expected to shift downwards considerable.

It is expected that the chances for a long plume would increase as wind speed,  $U$ , decreases and as saturation deficit,  $Q_{es} - Q_e$ , decreases. This relationship is tested in Figure 5, where observed plume length is plotted versus  $U(Q_{es} - Q_e)$ . The saturation deficit is measured at plume level. If the data followed by a + are not included, then the correlation coefficient is  $-.51$ .

The analytical model, equation (24), was not applied to the data in Table 6 because there is no information available on the increase in radius of cooling tower plumes after they have leveled off. Gifford (1975) reports TVA data on the observed spread of stack plumes, but they have a much smaller initial size and less plume rise than cooling tower plumes. Since most of the Amos plumes analyzed here terminate in stable layers, the passive diffusion should be very slight. This question cannot be satisfactorily resolved until further measurements are made.

## 6. Acknowledgements

This work was performed under an agreement between the National Oceanic and Atmospheric Administration and the Energy Research and Development Administration. Discussions with G. A. Briggs were very helpful. I would not have been able to obtain the observations so quickly without the assistance of M. E. Smith, P. T. Brennan, M. L. Kramer, and J. J. Conte of Smith-Singer Meteorologists, Inc. and D. L. Mazzitti of the American Electric Power Service Corporation. V. Quinn of the Air Resources Laboratory in Las Vegas contributed many valuable suggestions in his review of this manuscript.



## REFERENCES

- Brennan P. T., Seymour D.E., Butler M.J., Kramer M. L., Smith M.E., and Frankenburg T. T. (1976) The observed rise of visible plumes from hyperbolic natural draft cooling towers. Atmos. Environ., in press.
- Briggs G. A. (1969) Plume Rise. AEC Critical Review Series, TID-25075 from Clearinghouse for Fed. Scient. and Tech. Inf., U.S. Dept. of Comm., Springfield, Va., 82 pp.
- Briggs G. A. (1974) Plume rise from multiple sources, in Cooling Tower Environment-1974, National Technical Information Service, U. S. Department of Commerce, Springfield, VA., 22161, 161-179.
- Briggs G. A. (1975) Plume rise predictions. Lectures on Air Pollution and Environmental Impact Analyses. American Meteorol. Soc., 45 Beacon St., Boston, Mass., 59-111.
- Cooling Tower Environment-1974, ERDA Symposium Series, CONF-740302, Nat. Tech. Information Service, U. S. Dept. of Commerce, Springfield, Va., 22161, (\$13.60), 638 pp.
- Cotton W. R. (1975) Theoretical cumulus dynamics. Reviews of Geophysics and Space Physics, 13, 419-447.
- E. G. & G., Inc. (1971) Potential environmental modifications produced by large evaporative cooling towers, prepared for Water Quality Office, EPA, Cont. no. 14-12-542 by E. G. & G. Environmental Services Operation, Boulder, Colo., 75 pp.
- Fletcher N. H. (1962) The Physics of Rainclouds. Cambridge Univ. Press, London, 386 pp.
- Gifford F. A. (1975) Turbulent diffusion typing schemes: a review. Nuclear Safety, 17, 68-86.
- Hanna S. R. (1971) Meteorological effects of cooling tower plumes. presented at Cooling Tower Inst. Meeting, Houston, 25 Jan., 17 pp., available as report no. 48 from ATDL, P.O. Box E, Oak Ridge, Tenn., 37830.
- Hanna S. R. (1972) Rise and condensation of large cooling tower plumes. J. Appl. Meteorol., 11, 793-799.

- Hanna S. R. (1974) Meteorological effects of the mechanical draft cooling towers of the Oak Ridge Gaseous Diffusion Plant, in Cooling Tower Environment-1974, ERDA Symposium Series, CONF-740302, Nat. Tech. Information Service, U.S. Dept. of Commerce, Springfield, Va., 22161, (\$13.60), pp 291-306.
- Hanna S. R. and Gifford F. A. (1975) Meteorological Effects of Energy Dissipation at Large Power Parks. Bull. Am. Meteorol. Soc., 56, 1069-1076.
- Kessler E. (1969) On the Distribution and Continuity of Water Substance in Atmospheric Circulations Meteorol. Monographs, 10, 84 + ixpp, published by the Am. Meteorol. Soc., 45 Beacon St., Boston.
- Kramer M.L., Seymour D. E., Butler M. J., Kempton R. N., Brennan P. J., Conte J. J. and Thomson R. G. (1975) John E. Amos Cooling Tower Flight Program Data, December 1974-March 1975, by Smith-Singer Meteorologists, Inc., 134 Broadway, Amityville, N.Y., 11701 for American Electric Power Service Corp., P.O. Box 487, Canton, Ohio, 44701.
- McVehil G. E. and Heikes K. E. (1975) Cooling Tower Plume Modeling and Drift Measurement. A Review of the State-of-the-Art, prepared for ASME (Contract G-131-1) by Aerospace Division, Ball Brothers Research Corporation, Boulder, Colorado, 80302.
- Meyer J. H., Eagles T. W., Kohlenstein L. C., Kagan J. A., and Stanbro W. D. (1974) Mechanical draft cooling tower visible plume behavior: measurements, models, predictions, in Cooling Tower Environment-1974, ERDA Symposium Series, CONF-740302 Nat. Tech. Information Service, U. S. Dept. of Commerce, Springfield, Va., 22161, (\$13.60), 307-352.
- Murthy C. R. (1970) On the mean path of a buoyant chimney plume in non-uniform wind. J. Appl. Meteorol., 9, 603-611.
- Norman J. M., Thomson D. W., Pena J., and Miller R. (1975) Aircraft turbulence and drift water measurements in evaporative cooling tower plumes. Dept. of Meteorol., Penn. State Univ., University Park, PA., 16802.
- Simpson J. and Wiggert V. (1970) Models of precipitating cumulus towers. Mon. Wea. Rev., 97, 471-489.

- Slawson P. R., Coleman J. H., and Frey J. W. (1974) Some observations on cooling-tower plume behavior at the Paradise Steam Plant, in Cooling Tower Environment-1974, ERDA Symposium Series, CONF-740302, Nat. Tech. Information Service, U.S. Dept. of Commerce, Springfield, Va., 22161, (\$13.60), 147-160.
- Wigley T.M.L. and Slawson P. R. (1971) On the condensation of buoyant, moist, bent-over plumes. J. Appl. Meteorol., 10, 259-263.
- Weinstein A. I. (1970) A numerical model of cumulus dynamics and microphysics. J. Atmos. Sci., 27, 246-255.
- Woffinden, G. J., Anderson, J. A., and Harrison, P. R. (1976) Aircraft Survey, Chalk Point Cooling Tower Plume, Dec. 1975, Rept. no. 76R-1910 by MRI, Altadena, Calif. 91001 for the Md. Power Plant Siting Program. 32 pp + appendices.
- Wolf, M. A., (1976) Natural draft cooling tower plume characteristics determined with airborne instrumentation. Pac. Northwest Lab. Annual Rep. for 1975 to the USERDA DBER. Part 3 Atmospheric Sciences, BNWL-2000 PT3, 281-288.
- World Meteorol. Org., 1966: International Meteorological Tables, WMO-188-TP-94, introd. to tables 4.6 and 4.7.



## APPENDIX B

### OBSERVED AND PREDICTED COOLING TOWER PLUME RISE AT THE JOHN E. AMOS POWER PLANT, WEST VIRGINIA

Steven R. Hanna  
Air Resources  
Atmospheric Turbulence and Diffusion Laboratory  
National Oceanic and Atmospheric Administration  
Oak Ridge, Tennessee 37830

#### 1. INTRODUCTION

There is much current interest in cooling tower plume rise because of its importance in determining the environmental impact of cooling towers at planned power plants and industrial facilities. Some of the possible environmental problems related to heat and water emissions from cooling towers are drift deposition, ground level fog, cloud formation, and precipitation enhancement (see the conference proceedings Cooling Tower Environment - 1974.) An important factor in all of these problems is the calculation of the plume trajectory, which is often complicated by the presence of multiple sources and water phase changes in the plume. As Briggs (1975) shows, the latent heat does not strongly influence plume rise if there is no cloud present at the top of the plume. His simple formulas for plume rise can be expected to work quite well on most days for cooling tower plumes. However, if a cloud forms at the top of the plume, the final cloud height will depend partly on cloud physics process. A one dimensional plume and cloud growth model was developed to study these effects (Hanna, 1976). In this paper, the predictions of the model are compared with observations of cooling tower plume rise at the John E. Amos, W. Va. power plant (2900 MWe), reported by Kramer, *et al.* (1975).

#### 2. PLUME AND CLOUD GROWTH MODEL

The numerical model uses Weinstein's (1970) one-dimensional cloud growth model as a basis but alters its entrainment assumption so that it agrees with known relations for the rise of buoyant stack plumes (Briggs, 1975). The cloud microphysics processes are parameterized using suggestions by Kessler (1969). Current measurements by Norman, *et al.* (1975) at the Keystone cooling towers and Woffinden, *et al.* (1976) at the Chalk Point cooling tower should help determine whether Kessler's parameterizations are valid for cloud physics processes in cooling tower clouds.

A detailed description of the model would be too lengthy to include in this short summary, but is given elsewhere (see Hanna, 1976) in a form such that it can be studied or used by others. The computer program is operational (e.g., it is being used at Argonne National Laboratory by A. Policastro) and copies of the program and its description can be obtained by writing the present author.

There are four aspects of this model that can be regarded as improvements over previous versions. First, it incorporates Briggs' (1975) suggestion that the ratio of the total effective momentum flux to the momentum flux within the plume boundary approaches 2.25, due to the fact that the ambient air above the rising plume is also accelerating. Second, based on determinations of visible plume length by Slawson, *et al.* (1974), and Meyer, *et al.* (1974), it is assumed that saturation occurs in the plume when the excess water vapor content is greater than 50% of the saturation deficit in the ambient air. Third, the effects of ambient wind speed shears are included in the equation for continuity of plume volume flux. Finally, an arbitrary assumption is made to account for the merging of multiple plumes: when the plume radius grows to one-half of the distance between the towers, the cross sectional area of the model plume increases so that it is equal to the sum of the previous areas of all the plumes.

#### 3. MODEL INPUTS

During the winter of 1974-1975, Smith-Singer Meteorologists, Inc. flew a light aircraft around the three cooling tower plumes at the John E. Amos, W. Va. Power Plant (see Kramer, *et al.*, 1975). Vertical profiles of ambient temperature, dew-point, and wind speed to heights of about 1500m were obtained, and photographs of the plume were taken. Runs were purposely made on cold, humid days when a long visible plume was expected. In all the runs analyzed in this paper, the plume was visible through its point of leveling-off, so that plume rise could easily be estimated. Consequently, all of the information needed for input to the plume and cloud growth model was available.

The three natural draft cooling towers are in a line, 200m apart. Two have a height of 132m, top radius,  $R_0$ , of 29m, initial vertical speed,  $w_0$ , of 4.6 m/s, and are each capable of servicing a generator of 800 MWe. The third tower has a height of 150m, top radius of 40m, initial vertical speed of 4.2 m/s, and is capable of servicing a generator of 1300 MWe. For this study, the plume from the third tower is modeled initially. When its radius equals 100m, it is assumed that the plumes merge and the radius automatically increases by a factor of 1.5. The plume is assumed to be initially saturated, and initial cloud and rainwater concentrations are arbitrarily assumed to be 1 g/kg. The optimum initial plume temperature  $T'_{p0}$  is calculated

from the manufacturer's specifications discussed by Kramer, et al. (1975):

$$T'_{po} = (297.4 + .635 (T_d - 273)) (1 + .01 (1 - RH)) \quad (1)$$

where  $T_d$  and RH are ambient dewpoint and relative humidity, and temperatures have the units °K. To account for differences in plant load, the following relation is used to calculate the actual initial plume temperature:

$$T_{po} - T_{eo} = C \cdot (T'_{po} - T_{eo}) \quad (2)$$

where  $T_{eo}$  is the ambient temperature at tower top and C is the ratio of actual plant load to full load (2900 MWe). For bent over plumes (wind speed, U, less than 1 m/s), an effective initial plume radius,  $R_{eff}$ , is used in order to maintain continuity of the momentum flux (Hanna, 1972):

$$R_{eff} = R_o (w_o/U)^{1/2} \quad (3)$$

#### 4. RESULTS

Input conditions for three typical runs are given in Table 1. These input data and results are given in detail so that they can be used by others for model comparison.

TABLE 1

Input conditions for runs 1, 10, and 15. Height z refers to height above tower top

z(m)	Run 1			Run 10			Run 15		
	$T_e$ (°K)	$T_d$ (°K)	$U$ ( $\frac{m}{s}$ )	$T_e$ (°K)	$T_d$ (°K)	$U$ ( $\frac{m}{s}$ )	$T_e$ (°K)	$T_d$ (°K)	$U$ ( $\frac{m}{s}$ )
0	268.6	264.2	13.5	268.0	264.7	2.2	261.3	261.3	0
91	267.4	264.1	13.5	267.5	264.2	4.9	265.7	259.6	0
213	269.1	262.4	13.5	266.3	264.1	4.9	265.2	258.5	0
304	269.1	260.0	13.5	265.2	263.5	4.9	267.7	257.4	0
456	269.1	257.4	13.5	264.1	263.0	4.9	265.2	256.3	0
578	270.2	245.2	16.	263.0	262.5	6.7	264.7	254.6	2.5
669	270.8	247.5	16.	262.5	262.5	8.9	264.7	249.7	5.5
821	271.3	252.4	16.	264.7	256.4	8.9	264.7	249.7	5.5
942	272.4	254.1	16.	265.8	251.9	8.9	264.1	247.4	5.5
1064	271.3	259.1	16.	266.9	248.6	8.9	263.0	246.9	6.0
	C = .98			C = .98			C = .98		
	$T_{po} = 292.3$			$T_{po} = 292.6$			$T_{po} = 289.4$		
	Observed Rise = 560m			Observed Rise = 820m			Observed Rise = 1120m		



The predicted profiles of vertical speed,  $w$ , plume-ambient temperature difference,  $(T_p - T_e)$ , and cloud water content,  $Q_c$ , for these three runs are plotted in Figures 1 through 3.

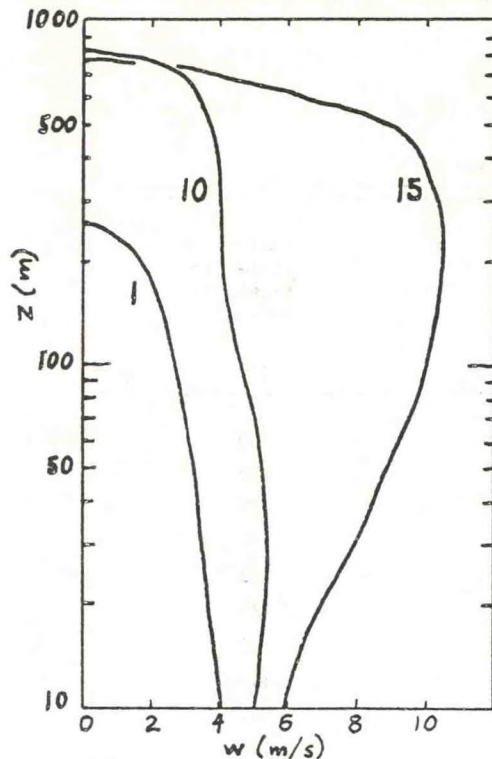


Figure 1: Variation of calculated vertical speed,  $w$ , with height for runs 1, 10, and 15.

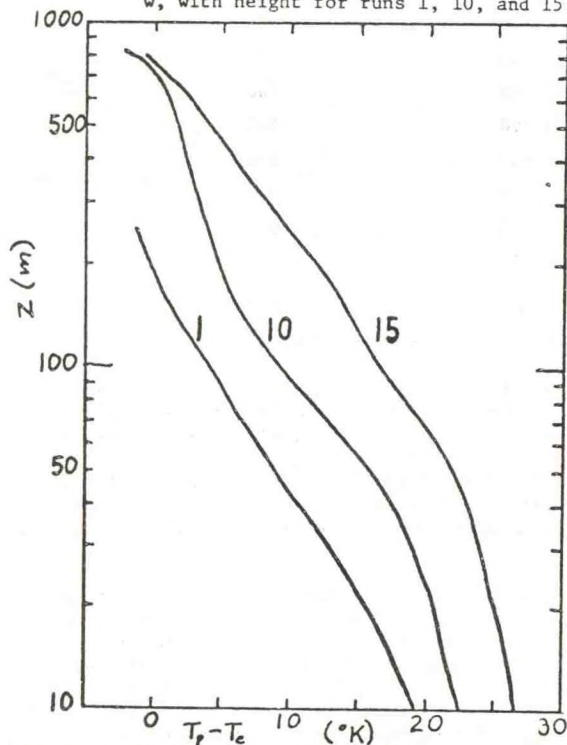


Figure 2: Variation of calculated temperature difference,  $(T_p - T_e)$  with height for runs 1, 10, and 15.

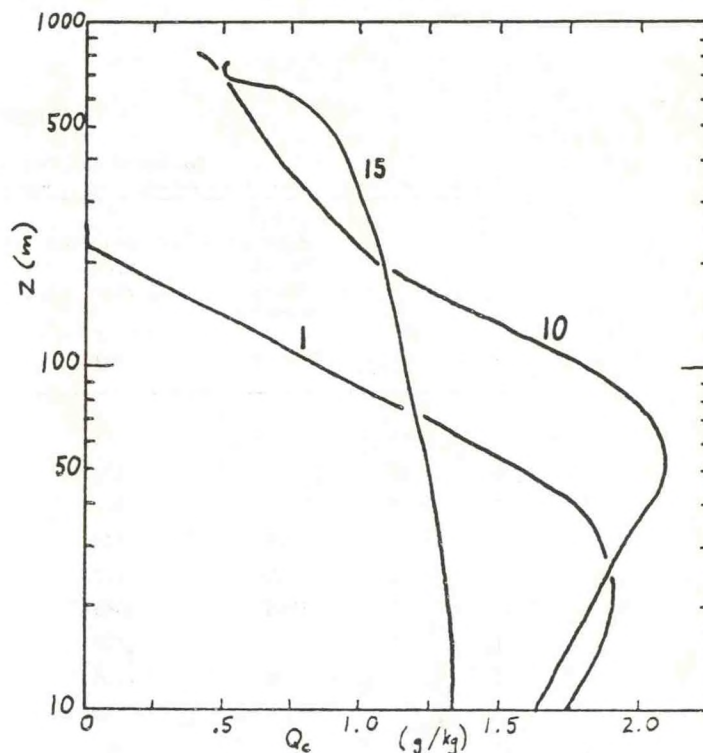


Figure 3: Variation of calculated cloud water content,  $Q_c$ , with height for runs 1, 10, and 15.

Runs 1 and 10 are bent over plumes and run 15 is a vertical plume which bends over above a height of about 600m. Because of the reduced entrainment rate for the vertical plume, its temperature difference and vertical speed do not decrease with height as fast as those for the bent over plumes. However, because the ambient air is drier for the vertical plume than for the two bent over plumes, the cloud water content  $Q_c$  of the vertical plume is not much different from that of the bent over plumes. As the wind speed increases above 1 m/s at a height of about 500 m in run 15, the entrainment coefficients switch from those applying to a vertical plume to those applying to a bent over plume. The visible plume in run 1 is predicted to evaporate just below the height of final plume rise, while the observed visible plume on that day extended through the height of maximum plume rise. Cloud water content at the top of the plumes in runs 10 and 15 is about .5 g/kg, a value within the range of measured cloud water content in natural clouds. Measurements of the cloud water content of the plume during these runs would have been useful, but unfortunately in-plume measurements were not part of this program.

The plumes in the bent over runs are predicted to merge at a height of about 200m, in agreement with the observations. The plumes in run 15 do not merge until a height of about 500m is reached due to the reduced entrainment. This is also in rough



agreement with observations, although the prediction of a constriction in the plumes just above the tower top for vertical plumes is not verified by the Amos photographs.

A summary of observed and predicted plume rise for all of the runs analyzed in this program is given in Table 2.

TABLE 2  
Observed and Calculated Plume Rise

Run	$\bar{U}$ (m/s)	Inversion height above tower (m)	Observed plume rise (m)	Model plume rise (m)	Analytical plume rise, sensible, one unit (m)
1	14		560	260	250
6	11		850	820	430
8	9		370	350	250
10	6	720	820	820	590
11	0	660	880	900	980
12	6	1140	1060	1200	720
15	3		1120	790	780
16	6	1200	1160	700	380
17	8	360	360	430	410
18	6		910	720	410
19	0	840	800	970	910
24	6	750	760	630	500
28	5		360	400	310
31	0		500	900	780
35	3	390	360	590	480
44	8	960	910	420	510
45	7	1200	910	370	390
47	0	900	800	1020	910
48	7	750	670	360	340
Avg.	5.6	820	750	670	540

The average model and observed plume rises are 670m and 750m, respectively, and the correlation coefficient is 0.49. It can be concluded that the plume and cloud growth model can be satisfactorily used to estimate the plume characteristics and the development of clouds due to cooling tower emissions.

The plume rise predicted by Briggs' (1975) well-known analytical formulas is included in the last column of Table 2. In the application of this formula, the initial buoyancy flux is assumed to equal the sensible heat flux from the largest tower. It is seen that the average predicted plume rise is 540m and the correlation with observations is .37.

The height of the base of the capping inversion or the "mixing layer" is also listed in Table 2. Brennan, et al. (1976) have analyzed these data and find that, when a capping inversion is present the plume will generally rise to this height and level off. For the data in Table 2 the correlation between capping inversion height and observed plume rise is 0.90. A good general rule might be that, when an inversion caps a mixed layer, and the base of this inversion is at a height of less than about 1 km, then the final plume rise from cooling towers as large as those at the Amos plant will equal the inversion height. By the nature of the Amos experiments (cold winter mornings) low mixing heights could be expected. But during other seasons of the year the mixing heights will increase and it will be much less likely that the plume will reach the capping inversion.

Acknowledgements. The cooperation of Smith-Singer Meteorologists, Inc. and the American Electric Power Service Corporation in providing the Amos data is greatly appreciated. This work was performed under an agreement between the National Oceanic and Atmospheric Administration and the Energy Research and Development Administration.

#### References

- Brennan, P. T., D. E. Seymour, M. J. Butler, M. L. Kramer, M. E. Smith and T. T. Frankenburg, 1976: The observed rise of visible plumes from hyperbolic natural draft cooling towers. Atmos. Environ., in press.
- Briggs, G. A., 1975: Plume rise predictions. Lectures on Air Pollution and Environmental Impact Analyses. American Meteorol. Soc., 45 Beacon St., Boston, Mass., 59-111.
- Cooling Tower Environment - 1974, ERDA Symposium Series, CONF-740302, Nat. Tech. Information Service, U.S. Dept. of Commerce, Springfield, Va., 22161, (\$13.60), 638 pp.
- Hanna, S. R., 1972: Rise and condensation of large cooling tower plumes. J. Appl. Meteorol., 11, 793-799.
- Hanna, S. R., 1976: Predicted and observed cooling tower plume rise and visible plume length at the John E. Amos power plant. To be published in Atmos. Environ., available as No. 75/25 from ATDL, P. O. Box E, Oak Ridge, Tn. 37830; 39 pp plus 5 figures.
- Kessler, E., 1969: On the distribution and continuity of water substance in atmospheric circulations. Meteorol. Monographs, 10, 84 + ixpp, published by the Amer. Meteorol. Soc., 45 Beacon St., Boston.
- Kramer, M. L., D. E. Seymour, M. J. Butler, R. N. Kempton, P. J. Brennan, J. J. Conte and R. G. Thomson, 1975: John E. Amos Cooling Tower Flight Program Data, December 1974-March 1975. Smith-Singer Meteorologists, Inc., 134 Broadway, Amityville, N. Y. 11701 for American Electric Power Service Corp., P. O. Box 487, Canton, Ohio 44701.
- Meyer, J. H., T. W. Eagles, L. C. Kohlenstein, J. A. Kagan and W. D. Stanbro, 1974: Mechanical draft cooling tower visible plume behavior: Measurements, models, predictions. In Cooling Tower Environment - 1974, ERDA Symposium Series, CONF-740302, pp 307-352.
- Norman, J. M., D. W. Thomson, J. Pena and R. Miller, 1975: Aircraft turbulence and drift water measurements in evaporative cooling tower plumes. Dept. of Meteor., Penn. State Univ., University Park, Pa. 16802.
- Slawson, P. R., J. H. Coleman and J. W. Frey, 1974: Some observations on cooling-tower plume behavior at the Paradise Steam Plant. In Cooling Tower Environment - 1974, ERDA Symposium Series, CONF-740302, pp 147-160.
- Weinstein, A. I., 1970: A numerical model of cumulus dynamics and microphysics. J. Atmos. Sci., 27, 246-255.
- Woffinden, G. J., J. A. Anderson and P. R. Harrison, 1976: Aircraft Survey, Chalk Point Cooling Tower Plume, Dec. 1975. Rep. No. 76R-1410 by MRI, Altadena, Cal. 91001 for the Maryland Power Plant Siting Program, 33 pp + appendices.





## Comments on "Observations of an Industrial Cumulus"

STEVEN R. HANNA

*Atmospheric Turbulence and Diffusion Laboratory, NOAA, Oak Ridge, Tenn. 37830*

2 August 1976

In a note entitled "Observations of an Industrial Cumulus," Auer (1976) stated that his observations may find utility in evaluation of numerical cloud models. The purpose of this brief note is to compare the results of a one-dimensional, steady-state cloud model with Auer's observations. The model is based on Weinstein's (1970) one-dimensional cloud model, but is forced at low heights to agree with the theories of stack plume rise proposed by Briggs (1975). Its purpose is to estimate the environmental effects of cooling tower plumes. A complete description of the model and its application to the cooling tower plumes at the John E. Amos, West Virginia, power plant is given by Hanna (1976). Currently the model is being applied to simulate observations of cooling tower plumes at the Rancho Seco, California, power plant (Wolf, 1976). As input the model requires ambient vertical profiles of temperature, dew point and wind speed. The radius, temperature, vertical speed and mixing ratios of water vapor, cloud water and hydrometeor water of the plume at the source are also required.

Auer's observations were taken with an instrumented light aircraft which was engaged in measuring cumulus clouds in the vicinity of St. Louis under the auspices of Project METROMEX. During one of the METROMEX runs, a cumulus cloud was noticed that was obviously forming in the plume from a refinery complex. Several passes through the cloud were made, and a nearly complete set of cloud data, including temperature excess, turbulence intensity, vertical speed, cloud droplet spectra, CCN, Aitken nuclei and excess water were obtained. Ambient vertical profiles of temperature and dew point were also measured by a slow spiral descent of the aircraft and the vertical wind profiles were measured using pilot balloons.

The surface temperature used in this model application, 300.5 K, is estimated by dry adiabatic extrapolation from the temperature at the lowest aircraft measurement level. The surface dew point, 296.0 K, is estimated by linear extrapolation from the dew points measured by the aircraft in the layer between 250 and 600 m above the ground. Since the source details are

sketchy in Auer's paper, it is necessary to arbitrarily choose parameters such as the initial plume radius. In subsequent discussions with Auer, it was decided that the values of 250 m for the initial plume radius and  $1 \text{ m s}^{-1}$  for the initial plume vertical speed are reasonable. It is assumed that all emissions are at ground level. In Footnote 1 of Auer's (1976) paper, it is stated that the total energy emission is  $7 \times 10^{11} \text{ cal h}^{-1}$  ( $\sim 800 \text{ MW}$ ), divided about equally between sensible and latent heats. These conditions are satisfied by an initial plume temperature of 302.3 K and a relative humidity of

TABLE 1. Comparisons of observations and predictions for the St. Louis refinery cloud. (All heights are in meters above the surface.)

	Observed	Predicted
Cloud base (m)	700	650
Cloud top (m)	2050	2350
$z$ (m)	Observed liquid water content ( $\text{g m}^{-3}$ )	Predicted liquid water content ( $\text{g m}^{-3}$ )
930	0.046	0.56
1260	0.10	0.74
1860	0.44	1.30
$z$ (m)	Observed vertical speed ( $\text{m s}^{-1}$ )	Predicted vertical speed ( $\text{m s}^{-1}$ )
500	3	2.0
1500	4	2.0
2000	3	2.3
$z$ (m)	Observed temperature excess (K)	Predicted temperature excess (K)
500	0.2	0.1
1500	-0.5	0.3
2000	-0.2	0.5

76.5%. Initial cloud water and hydrometeor mixing ratios are set equal to zero.

The comparisons of Auer's observations and the model output are given in the Table 1. The cloud cross sections presented by Auer were used to estimate averages across the entire width of the cloud at a given height. The observations of temperature excess were obtained by averaging the temperatures in the cloud cross sections sent to the author by Auer in a letter dated 7 July 1976.

It is seen in the table that the heights of the cloud base and top are predicted quite well by the model. There is a slight inversion above about 2100 m which causes the plume to level off. The predicted vertical speed is about 20–50% too low and the predicted liquid water content is a factor of 3–10 too high. The observed and predicted temperature excesses are within 0.8 K of each other.

Auer also calculated the entrainment rate based on his measurements of temperature in the cloud. He finds that the entrainment rate is between 33 and 91%  $\text{km}^{-1}$  for eight different passes through the cloud. In the numerical model the entrainment rate  $(1/V)(dV/dz)$  can be approximated by  $0.8/R$ , where  $V$  is the volume flux  $UR^2$ , and  $U$  and  $R$  are the wind speed and the plume radius, respectively. Thus the model entrainment rate is about 160%  $\text{km}^{-1}$  at cloud base and about 75%  $\text{km}^{-1}$  at a height of 2000 m (using  $R=R_0+0.4z$ ).

It can be concluded that this model does a fair job of simulating the observed temperature excess, vertical

speed and cloud base and top. The predicted entrainment rate is about a factor of 2 too high and the predicted liquid water content is a factor of 3–10 too high. Auer also measured turbulent energy, cloud droplet spectra, CCN and Aitken nuclei, but none of these variables is used in the present model. It would be interesting to see if a two- or three-dimensional model with more detailed cloud microphysics could improve on these predictions.

*Acknowledgment.* This research was performed under an agreement between the National Oceanic and Atmospheric Administration, the Energy Research and Development Administration, and the Environmental Protection Agency.

#### REFERENCES

- Auer, A. H., Jr., 1976: Observations of an industrial cumulus. *J. Appl. Meteor.*, **15**, 406–413.
- Briggs, G. A., 1975: Plume rise predictions. *Preprints, Lectures on Air Pollution and Environmental Impact Analyses*, Amer. Meteor. Soc., 59–111.
- Hanna, S. R., 1976: Predicted and observed cooling tower plume rise and visible plume length at the John E. Amos power plant. *Atmos. Environ.* (in press).
- Weinstein, A. I., 1970: A numerical model of cumulus dynamics and microphysics. *J. Atmos. Sci.*, **27**, 246–255.
- Wolf, M. A., 1976: Natural draft cooling tower plume characteristics determined with airborne instrumentation. Batelle Northwest Lab., Annual Rep. for 1975 to the USERDA DBER, Part 3 Atmospheric Sciences, BNWL-2000 PT3, 281–288.



# Environmental Research Laboratories

Air Resources

Atmospheric Turbulence and Diffusion Laboratory

Oak Ridge, Tennessee

June 1976

REGIONAL TRANSPORT MODEL OF ATMOSPHERIC SULFATES

K. S. Rao  
I. Thomson  
B. A. Egan

ATDL Contribution File No. 76/13

U. S. DEPARTMENT OF COMMERCE  
NATIONAL OCEANIC AND ATMOSPHERIC ADMINISTRATION



REGIONAL TRANSPORT MODEL OF ATMOSPHERIC SULFATES

K. S. RAO

NOAA-ARL ATMOSPHERIC TURBULENCE &  
DIFFUSION LABORATORY  
OAK RIDGE, TENNESSEE

I. THOMSON AND B. A. EGAN

ENVIRONMENTAL RESEARCH & TECHNOLOGY  
CONCORD, MASSACHUSETTS



For Presentation at the 69th Annual Meeting of the  
Air Pollution Control Association  
Portland, Oregon                      June 27-July 1, 1976

## REGIONAL TRANSPORT MODEL OF ATMOSPHERIC SULFATES

K. S. Rao\*, I. Thomson and B. A. Egan  
Environmental Research & Technology, Concord, Mass. 01742

### ABSTRACT

In recent years, there has been substantial evidence that particulate sulfate in the presence of sulfur oxide gases is a major contributor to the health hazards of air pollution, and there is considerable interest in developing a strategy for controlling the atmospheric sulfate concentration levels. This requires a systematic modeling program supported by observations aimed at understanding the relation between the emissions, chemical transformation, deposition, transport, and dispersion of sulfur oxides over distances of hundreds of kilometers from major sources.

As part of the Sulfate Regional Experiment (SURE) Design Project, a regional transport model of atmospheric sulfates has been developed. This quasi-Lagrangian three-dimensional grid numerical model uses a detailed  $\text{SO}_2$  emission inventory of major anthropogenic sources in the eastern U.S. region, and observed meteorological data during an episode as inputs. The model accounts for advective transport and turbulent diffusion of the pollutants. The chemical transformation of  $\text{SO}_2$  and  $\text{SO}_4^{2-}$  and the deposition of the species at the earth's surface are assumed to be linear processes at specified constant rates.

The numerical model can predict the daily average concentrations of  $\text{SO}_2$  and  $\text{SO}_4^{2-}$  at all receptor locations in the grid region during the episode. Because of the spatial resolution of the grid, this model is particularly suited to investigate the effect of tall stacks in reducing the ambient concentration levels of sulfur pollutants. This paper presents the formulations and assumptions of the regional sulfate transport model. The model inputs and results are discussed. Isopleths of predicted  $\text{SO}_2$  and  $\text{SO}_4^{2-}$  concentrations are compared with the observed ground level values.

The bulk of the information in this paper is directed to air pollution meteorologists and environmental engineers interested in the atmospheric transport modeling studies of sulfur oxide pollutants.

### INTRODUCTION

Recent experimental evidence suggests that particulate sulfates in the atmosphere contribute significantly to the health hazards of air pollution, adverse ecological effects due to increased acidity in lakes, corrosion and degradation of materials, and a general reduction in visibility. Current studies in the U.S. and Europe indicate that the exposure to sulfate particulates resulting from anthropogenic  $\text{SO}_2$  emissions covers large regions extending for hundreds of kilometers downwind from major urban sources. Numerical model calculations supported by observations play an important role in understanding the relation between  $\text{SO}_2$  emissions and atmospheric concentrations of  $\text{SO}_2$  and  $\text{SO}_4^{2-}$ .

A three-dimensional grid cell numerical model developed to investigate the regional transport of atmospheric sulfates is outlined in this paper. This model is an adaptation of the advection-diffusion transport model of Egan and Mahoney<sup>(1)</sup> based on a forward time explicit computational scheme which conserves not only the mass in each cell, but also certain statistical features of the mass distribution. The total mass in each grid cell is replaced by an equivalent rectangular pulse with the same mass, the same center of mass, and the same radius of gyration. This method suppresses the pseudo-diffusion errors that occur in the conventional finite difference procedures.

The numerical transport model essentially solves the mass conservation (tracer) equation which includes terms describing the horizontal advection transport, turbulent diffusion, emission, chemical transformation, and deposition processes.

#### Model Description and Formulations

This quasi-Lagrangian numerical model accounts not only for the advective transport in the horizontal by the mean wind, but the turbulent diffusion of the species as well. The masses are advected and dispersed each time step in the Lagrangian sense, and immediately afterwards a mass decomposition to the stationary Eulerian grid is performed. The horizontal emission grid has 26x17 cells covering a region of 2080 km (E-W) X 1360 km (N-S) in the eastern U.S. and southern Canada. To accomplish the turbulent diffusion calculations, the model has three air layers in the vertical, each of uniform depth over the grid region: 0-300m, 300-700m, 700-1500m. This allows the emissions to be introduced into one of the three layers depending on the effective effluent release height (stack height + plume rise) for elevated point sources. All ground-level point and area source emissions are introduced into the lowest layer next to the ground. Thus, this model is particularly suited to investigate the effects of tall stacks in reducing the atmospheric concentration levels of  $SO_x$  pollutants.

The mean wind field is assumed to be two-dimensional and the actual observed mean wind speeds (U and V components) at each horizontal grid cell are specified as model inputs at three or more vertical levels from the synoptic wind charts available at 12-hour intervals for the duration of the episode. For each time step, integration of the species conservation equations yields the instantaneous concentration distributions over the entire three-dimensional grid region consisting of 26x17x3 cells. The instantaneous concentrations in each cell are summed up and averaged over a 24-hour integration time period, to calculate the daily average concentrations which are then compared with the observed values at the receptor for that particular day. Thus, the three-dimensional numerical model can simultaneously predict the 24-hour average concentrations at all receptor locations in the grid region. The integration time period can be easily adjusted to be longer or shorter than 24 hours depending on the modeler's specific requirements.

The mass conservation equations of the pollutant species in a non-divergent flow field are given by:

$$\frac{\partial C_1}{\partial t} = -U \frac{\partial C_1}{\partial x} - V \frac{\partial C_1}{\partial y} + \frac{\partial}{\partial z} \left( K \frac{\partial C_1}{\partial z} \right) + \frac{Q}{h_i} - k_t C_1 \quad (1)$$

$$\frac{\partial C_2}{\partial t} = -U \frac{\partial C_2}{\partial x} - V \frac{\partial C_2}{\partial y} + \frac{\partial}{\partial z} \left( K \frac{\partial C_2}{\partial z} \right) + \frac{3}{2} k_t C_1 \quad (2)$$

where subscripts 1 and 2 denote  $SO_2$  and  $SO_4^{\equiv}$  species respectively, C is the concentration, K is the vertical eddy diffusivity, Q is the  $SO_2$  area-emission rate in the grid cell of height  $h_i$ , and  $k_t$  is the transformation rate of  $SO_2$  to  $SO_4^{\equiv}$ .

The deposition of the species at the earth's surface is described by the boundary condition:

$$\left[ K \frac{\partial C}{\partial z} \right]_{z=0} = (1 - r) \bar{K} C_o / \bar{h} \quad (3)$$



where  $r$  is a reflection coefficient defined by

$$r = 1 - V_d \bar{h} / \bar{K}, \quad 0 \leq r \leq 1 \quad (4)$$

In Eqs. (3) and (4),  $\bar{h}$  and  $\bar{K}$  are the mean depth and the mean eddy diffusivity of the lowest two vertical layers,  $C_0$  is the ground-level concentration, and  $V_d$  is the deposition velocity of the pollutant. The latter is dependent upon the type of pollutant material, the type of deposition substrate, and the meteorological conditions. The measured deposition velocities for  $SO_2$ , generally range from 0.5 to 2.5 cm/s and for  $SO_4^{2-}$  from 0.1 to 0.5 cm/s<sup>(2)</sup>. By adopting representative values<sup>(3)</sup> of  $V_{d1} = 1$  cm/s and  $V_{d2} = 0.1$  cm/s for the species, the deposition loss of material at the earth's surface can be simulated. The grid top boundary is assumed to be perfectly reflecting ( $r=1$ ).

For wide area sources, the lateral spread of the plume by horizontal diffusion is negligible compared to the horizontal transport by mean wind and vertical turbulent diffusion<sup>(1)</sup>. Therefore, the governing equations of the model do not include the horizontal diffusion terms.

#### Model Inputs

The total anthropogenic  $SO_2$  emission rates ( $Q$ ) are fixed by the emission inventory based on NEDS data, and specified in  $gms/m^2/sec$  in each cell. The emissions are classified by the effective height of emission, season, and species, and stored on a computer disc for link-up with the computer program. A nominal wind speed of 5 m/sec is used in the plume rise calculations using Briggs' standard plume rise formula<sup>(4)</sup> for near-neutral stability conditions.

For the duration of the episode, the observed mean wind speed and direction are available at each 1000 ft above the mean sea level at 12-hour intervals from the National Weather Service radiosonde data. The latter are plotted as U and V isotachs over the horizontal grid region of 26x17 cells for each vertical level and the winds are assigned numerical values at the center of each cell. These winds are corrected for the local topography and interpolated in the program to calculate the U and V components at the center of each vertical layer for each grid cell.

The model has the capability of incorporating temporally and spatially varying mixing depth (H) input data. In the present study, observed mixing depth data for the episode period modeled were not readily available, and a constant  $H(x,y,t) = 1500m = \sum_{i=1}^3 h_i$  was assumed.

The K-profile specified as input to the model has the correct asymptotic behavior to simulate the diurnal and spatial variation of the eddy diffusivity. For simplicity, however, near-neutral stability conditions are assumed for the calculation of eddy diffusivity profile in this study from which discrete values of  $K$  are specified at the centers of the three vertical air layers.

#### Numerical Solution, Results and Discussion

The Egan-Mahoney numerical method, which conserves the zeroth, first, and second moments of mass distribution, is used to calculate the 3-D concentration of field  $SO_2$  and  $SO_4^{2-}$  species from Eqs. (1) to (4). Details and discussion of this method can be found in References 1, 5 and 6.

The tracer equations are integrated with respect to time over a 24-hour period (October 5, 1974) selected for modeling. An integration time step  $\Delta t = 1$  hour is determined such that it satisfies the criteria for convergence and stability of the numerical solution:

$$K_1 \Delta t / h_1^2 \leq 0.5 \quad (5)$$

For each time step, the 3-D grid comprised of  $26 \times 17 \times 3$  cells is swept twice to solve the two coupled tracer equations by calculating the three moments for each species. New wind inputs are specified every 12 hours. In spite of the complexity of the program, the computing times for a 24-hour integration are very reasonable (under five minutes) in the present study.

The calculated concentrations in level-1 are compared with the daily-average ground-level concentrations measured at ERT's AIRMAP<sup>®</sup> Network receptors for this sampling period. The available  $\text{SO}_4^{2-}$  data from filter analyses are plotted against the predicted  $\text{SO}_4^{2-}$  concentrations for two different values of the transformation rate as shown in Figure 1. The plot shows a good correlation between predictions and observations, and suggests a value of  $k_t = 1$  to 2 percent per hour as appropriate for the model. A similar plot for the ground-level  $\text{SO}_2$  concentrations is shown in Figure 2. Here also the agreement between observations and predictions is satisfactory. The comparatively small change between the predicted  $\text{SO}_2$  concentrations for the two transformation rates indicates that the chemical sink term in Eq. (1) is not important.

For  $k_t = 1$  percent per hour, the isopleths of the predicted daily average  $\text{SO}_4^{2-}$  and  $\text{SO}_2$  concentrations over the horizontal grid region in level-1 are shown in Figures 3 and 4, respectively. Similar isopleths for vertical levels 2 and 3 are shown in Figures 5 to 8. A qualitative comparison between the isopleths shows reasonable consistency with the emissions distributions. The ground level  $\text{SO}_2$  distribution is strongly influenced by the surface and mid-level emissions localized over spatial scales of 0-100 km. The ground level  $\text{SO}_4^{2-}$  distribution is more difficult to interpret in the light of the  $\text{SO}_2$  emission inventory. The results suggest that the mid-level emissions strongly influence the estimated ground-level  $\text{SO}_4^{2-}$  concentrations. It appears that intensive contributions to the latter occur from sources within an influence zone of 100-300 km, which justifies the regional scale model treatment of the atmospheric sulfate transport.

#### Conclusions

Numerical advection-diffusion models are useful tools to investigate the effect of meteorological conditions of air pollution interest on concentration distributions of sulfur pollutants in the atmosphere. Regional transport models, relating spatially and temporally varying  $\text{SO}_2$  emissions to atmospheric  $\text{SO}_x$  concentrations are fundamental to the rational adoption of both short and long-term control strategies.

The results of the numerical model described in this paper suggest that advection of pollutants may be a dominant consideration on regional scale problems for slowly reactive pollutants. The Egan-Mahoney moment method was adopted primarily to reduce pseudo-diffusive errors in modeling advection. The model has the flexibility to incorporate variable inputs such as mean wind and turbulent diffusivity profiles and observed mixing depth data for sub-grid scale detail. Further, the chemical transformation and removal processes can be easily modeled as indicated in this paper.

The emphasis in this study was on adapting and developing the existing modeling tools to gain valuable insights into the regional transport of atmospheric sulfates. Viewed in this light, many of the simplifying assumptions of the model are justified. The satisfactory agreement between the calculated and observed concentrations is encouraging. However, more extensive observed concentration data are needed to fully calibrate and validate the model.

#### Acknowledgments

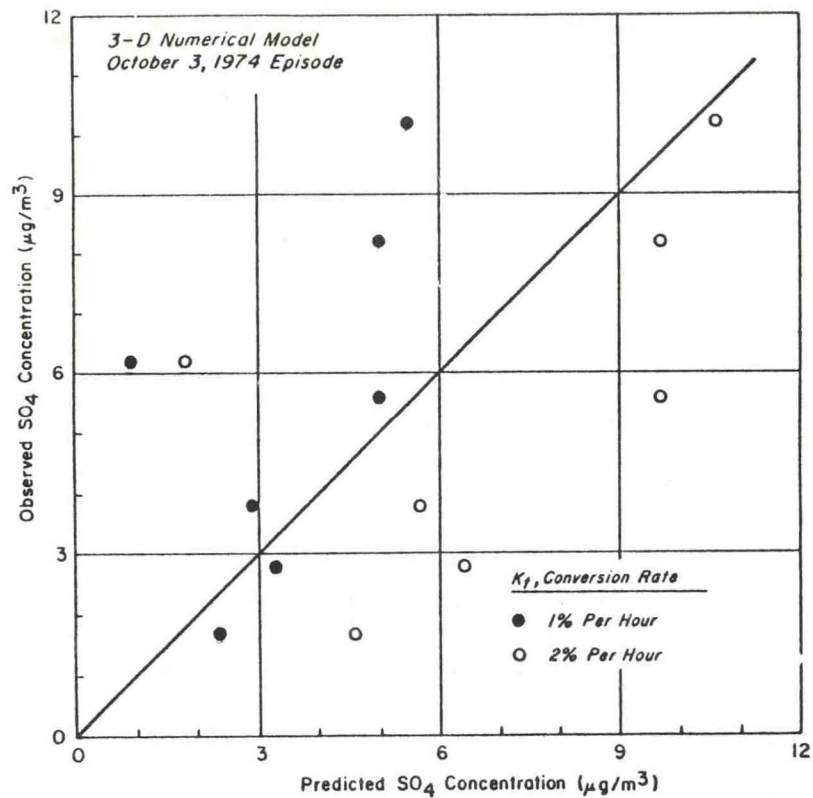
The work reported in this paper is part of the Sulfate Regional Experiment (SURE) Design Project sponsored by the Electric Power Research Institute (EPRI). The authors wish to acknowledge the assistance of Mrs. C. Ingersoll and Mr. D. McNaughton in the preparation of inputs to the model.

#### References

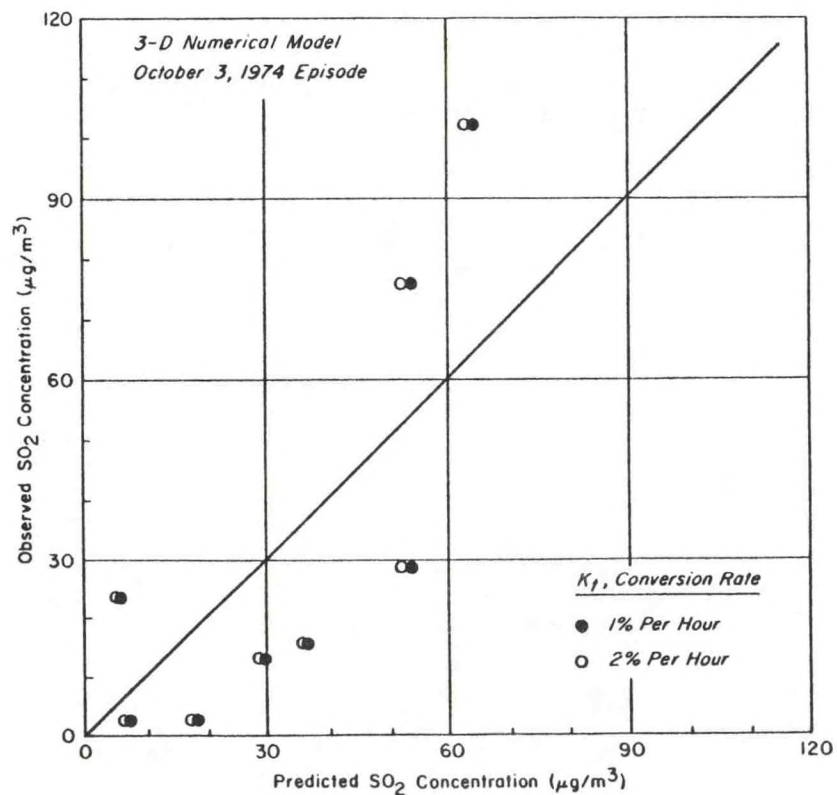
1. Egan, B.A. and J.R. Mahoney, Applications of a numerical air pollution transport model to dispersion in the atmospheric boundary layer, *J. Appl. Meteorol.*, **11**, pp.1023-1039, 1972.
2. SURE: Sulfate Regional Experiment Design Project. Report P-1386, Environmental Research & Technology, Inc., Concord, Mass. 01742, 1976, 500 pp.
3. Hidy, G.M., Removal processes of gaseous and particulate pollutants, Chap.III, *Chemistry of the Lower Atmosphere*, S.I. Rasool, ed., Plenum Press, New York, 1973, pp.121-173.
4. Briggs, G.A., Plume Rise, TID-25075, Clearinghouse for EFTI, Springfield, Va. 22151, 1969, 82 pp.
5. Egan, B.A., and J. R. Mahoney, Numerical Modeling of Advection and Diffusion of Urban Area Source Pollutants, *J. Appl. Meteor.*, **11**, 312-322.
6. Pedersen, L.B. and L.P. Prahm, A method for numerical solution of the advection equation, *Tellus*, **26**, No. 5, pp. 594-602, 1974.

\*Present affiliation: NOAA-ARL Atmospheric Turbulence & Diffusion Laboratory, P. O. Box E, Oak Ridge, Tennessee 37830.





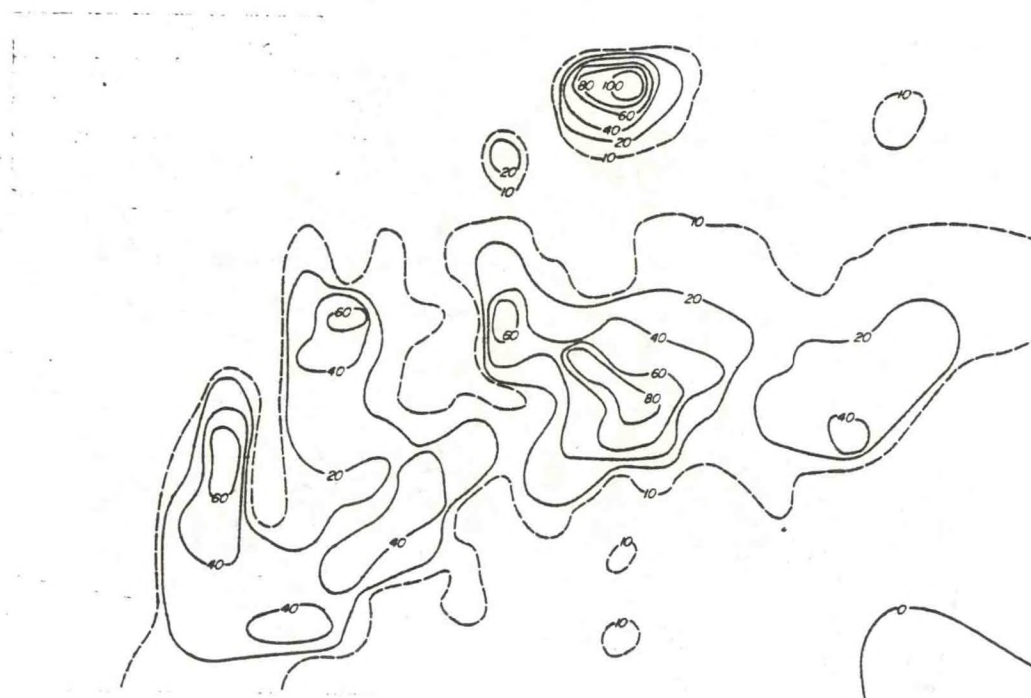
1. Comparison of predicted and observed ground level  $\text{SO}_4^{\text{m}}$  concentrations.



2. Comparison of predicted and observed ground level  $\text{SO}_2$  concentrations.



3. Isopleths of calculated  $\text{SO}_4^{2-}$  concentrations ( $\mu\text{g}/\text{m}^3$ ) in grid vertical level-1 for October 3, 1974.



4. Isopleths of calculated  $\text{SO}_2$  concentrations ( $\mu\text{g}/\text{m}^3$ ) in grid vertical level-1 for October 3, 1974.

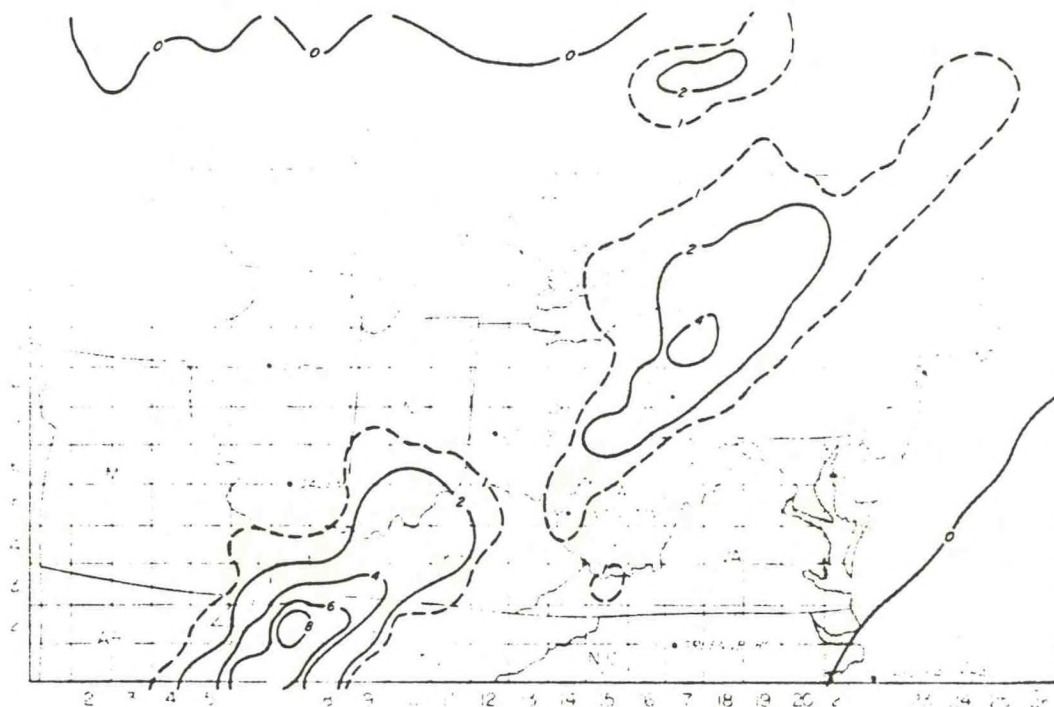


5. Isopleths of calculated  $\text{SO}_4$  concentrations ( $\mu\text{g}/\text{m}^3$ ) in grid vertical level-2 for October 3, 1974.



6. Isopleths of calculated  $\text{SO}_2$  concentrations ( $\mu\text{g}/\text{m}^3$ ) in grid vertical level-2 for October 3, 1974.





7. Isopleths of calculated  $\text{SO}_4^=$  concentrations ( $\mu\text{g}/\text{m}^3$ ) in grid vertical level-3 for October 3, 1974.



8. Isopleths of calculated  $\text{SO}_2$  concentrations ( $\mu\text{g}/\text{m}^3$ ) in grid vertical level-3 for October 3, 1974.



# **Environmental Research Laboratories**

**Air Resources**

**Atmospheric Turbulence and Diffusion Laboratory**

**Oak Ridge, Tennessee**

**September 1976**

## **1975 ANNUAL REPORT**





## PHYSICS OF THE BIOSPHERE

The microclimate within a stand of vegetation is affected by interactions among synoptic climate, stand structure, stand physiology, and soil moisture status and fertility. As such, studies of the micrometeorology of plant stands require expertise in a number of diverse disciplines. The exceptional quality of two recent additions to the literature of mass, heat, and momentum transfers in the soil-plant-atmosphere continuum is as much a result of the disciplinary breadth of the contributors as of their individual competence.

The proceedings of the Dubrovnik seminar<sup>1</sup> on heat and mass transfer in the environment of plants is an impressive collection of lectures which gives a broad overview of the status of knowledge of specific processes, and of shorter contributions describing recent research efforts and results. As such, it provides both background material and insights of problem areas needing further research. Part I deals with the basic transfer processes and methods for their study in the soil, lower atmosphere, and plants. Part II, titled "Applications," covers various aspects of microclimatic manipulation for increased yields as well as the problem of pollution in the plant environment. In all, this book contains 40 papers representing state-of-the-art summaries of current knowledge of heat and mass transfer in terrestrial ecosystems. The body of the book is reproduced from typescript which probably explains how a 594 page book can be sold for less than \$30.00.

The two-volume series edited by Monteith<sup>2</sup> is, in many ways, similar to the above volume, although discussion of transfers in soil are omitted. Volume 1 deals with the processes involved in heat, mass, and momentum transfers in vegetation along with methods of modeling these processes and techniques of observation. Volume 2 contains 13 case studies of different kinds of ecosystems: six agricultural crops, four forests, and three other major types of terrestrial ecosystems. An impressive feature of these two volumes is the use of uniform symbols throughout. Thus, the generally excellent quality of individual chapters is enhanced by the use of consistent symbols from chapter to chapter.

In general, these volumes seem better suited for the non-specialist in that more details of the derivation of mathematical equations are included and the development of the various subjects is more thorough. The chapter by Ross on "Radiative Transfer in Plant Communities" is the best English language summary available of the work by Ross and his colleagues at the Institute of Astrophysics and Atmospheric Physics in

Toravere, Tartu, USSR. Until Ross's book [Ross, Ju. K. 1975. *Radiatsionyi Rezhim i Arkhitektonika Rastitelnogo Pokrova* (Radiation Regime and Architecture of the Vegetation Canopy) Gidrometeoizdat, Leningrad. 342 pp.] is translated into English, this chapter will serve

admirably, for those of us unable to read Russian, to describe the elegant models of radiation in vegetation developed by Ross and his associates. Similarly the chapter by A. S. Thom on momentum, mass, and heat exchanges in plant stands is very well done and will serve as a good starting point for the non-meteorologist working in this area of ecology. The hydrologic cycle in plant stands is surveyed by Rutter while Chamberlain discusses the special case of mass transfer in vegetation associated with the movement of particles, e.g. pollen, pollutants. Waggoner shows how the principles developed in earlier chapters may be synthesized into models of plant stands at various levels (single leaf to entire stand) and for different processes (heat and water transfer, photosynthesis, transfer of harmful gases and disease vectors). The concluding chapter of volume 1 by Szeicz deals with micrometeorologic instruments and their exposure.

In volume 2, case studies of temperate cereals, maize and rice, sugar beets and potatoes, sunflowers, cotton, and Townsville stylo are presented under agricultural crops; coniferous forests, deciduous forests, tropical rain forests, and citrus orchards under forests; and swamps, grasslands, and tundra under other ecosystems. The quality of these chapters is less uniform than those of volume 1. Nevertheless, most of those included are well worth reading. While I am admittedly biased toward forest meteorology, I feel that the chapter on coniferous forests by Jarvis, James, and Landsberg is outstanding and worth the price of this volume alone. On the other hand, the deciduous forest chapter by Rauner is merely a cursory summary of results from his research on this subject. I found this chapter disappointing.

While processes are not treated as thoroughly in the DeVries and Afgan volume, the shorter length of most chapters allowed for the inclusion of a greater variety of material. Thus, while Ross's treatment of radiative transfer in vegetation is admittedly elegant, the measurement of stand structural parameters required to drive this model would probably require greater effort than directly measuring the radiation. Hence the chapter by Norman describing simpler methods of approximating canopy structures and their radiation regimes is more immediately applicable than the treatment by Ross and Nilson in this volume or by Ross in the volume edited by Monteith. For reasons such as these, it is difficult to recommend either of these volumes over the other. I believe that ecologists, whether micrometeorological specialists or not, will benefit from study of either or both of these works.

B. A. HUTCHISON

ATMOSPHERIC TURBULENCE AND DIFFUSION

LABORATORY, NOAA

Oak Ridge, TN 37830

<sup>1</sup> DeVries, D. A. and N. H. Afgan (eds.). 1975. *Heat and mass transfer in the biosphere, Part I: Transfer processes in the plant environment*. Scripta Book Company, Halsted Press, John Wiley and Sons, New York. vii + 594 pp. \$24.95.

<sup>2</sup> Monteith, J. L. (ed.). 1976. *Vegetation and the Atmosphere, Vol. 1: Principles*. Academic Press, London. xx + 278 pp. \$26.00. *Vol. 2: Case Studies*. Academic Press, London. xix + 439 pp. \$38.75.





## THE DISTRIBUTION OF SOLAR RADIATION WITHIN A DECIDUOUS FOREST<sup>1</sup>

BOYD A. HUTCHISON  
AND

DETLEF R. MATT

*Atmospheric Turbulence and Diffusion Laboratory, National Oceanic and Atmospheric  
Administration, P.O. Box E, Oak Ridge, Tennessee 37830 USA*

**Abstract.** Solar radiation was measured within and above an east Tennessee deciduous forest over a 2-yr period. Diurnal patterns of within-forest radiation follow the temporal variation in incident radiation but become more irregular with depth in the forest because of the highly variable penetration of beam radiation in space and in time. Seasonally, radiation in the forest increases substantially from winter to its annual maximum in early spring as solar elevations increase. Although solar elevations continue to rise each day until the summer solstice, amounts of total radiation and its beam component drop sharply in the forest with the advent of leaf expansion. Diffuse radiation in the forest continues to increase slowly following the onset of leaf expansion but reverses as the forest approaches a fully leafed state. Following the summer solstice, forest structure remains essentially static until abscission while solar elevations decrease. In summer and early autumn, total radiation and both its beam and diffuse components decrease slowly in the forest to their annual minimum in autumn. With leaf abscission and subsequent fall, radiation increases slightly in the forest but soon declines again as solar elevations approach their annual minimum of the winter solstice.

**Key words:** *Deciduous forest; diffuse radiation; direct beam radiation; diurnal variation; fractional penetration; radiation penetration; seasonal variation; solar radiation; spatial variation; temperate forest; Tennessee.*

### INTRODUCTION

Solar energy is the driving force for essentially all processes occurring within ecosystems. Because of the dependence of ecosystem functioning upon solar energy, evolution has resulted in ecosystems that tend to be dominated by the primary producer trophic level. In terrestrial ecosystems, green plants are nearly always the ecological dominants. By virtue of the architecture of forest ecosystems, the canopy of photosynthetic tissue largely governs both abiotic and biotic energy flows within these ecosystems. The canopy controls abiotic energy flow through the combined effects of biomass distribution, geometry, and optical characteristics upon the penetration of solar radiation into the forest and upon the partitioning of radiant energy within the forest. Since forest canopies shade the ground beneath, the bulk of photosynthetic production of forests occurs in the overstory canopy, therefore the biotic energy flow in the system is strongly controlled as well.

As part of the ecosystem analysis effort at the Oak Ridge site, Eastern Deciduous Forest Biome, U.S. International Biological Program, we have studied the space and time distribution of solar radiation within a deciduous forest dominated by tulip poplar (*Liriodendron tulipifera*). The objectives of this

study were: (1) to determine the variation of solar radiation in space and time in the forest and (2) to relate this variation to the structure and phenological state of the forest. In this paper we deal with these objectives rather qualitatively. Subsequent papers will attempt to quantify the relationships between forest radiation regimes and forest structure.

Forest radiation regimes are highly variable because of the interactions of a variety of external and internal factors. Amounts of radiation incident upon the forest vary regularly owing to diurnal and seasonal changes in earth-sun geometry and irregularly because of varying atmospheric turbidity and cloudiness. Optical characteristics of forests change through time with phenological changes in forest structure and with forest tree growth. Superimposed upon the variation produced by these factors is that variability resulting from horizontal and vertical heterogeneity in forest structure.

In this paper we illustrate the effects of the earth's daily rotation upon forest radiation regimes by considering full-day radiation records above and within the forest. The effects of seasonal changes in earth-sun geometry and of phenological changes in forest structure are shown by comparing clear-day radiation totals in each of seven phenoseasons which characterize the forest in terms of season and phenological state. A phenoseason is a segment of the year during which the prevailing earth-sun geometry and pheno-

<sup>1</sup> Manuscript received 31 October 1975; accepted 28 December 1976.



TABLE 1. Mensurational data and diversity of the cesium-tagged *Liriodendron* forest at the Oak Ridge site

Canopy level	Height (m)	Average dbh (cm)	Basal area (m <sup>2</sup> /hectare)	Density (stems/hectare)	Shannon-Weaver species diversity index
Upper	16-30	23.8	24.0	520	1.11
Mid	10-15	8.6	1.7	290	1.42
Forest floor	1.5- 9	2.3	3.0	4770	1.78
Overall	Range 1.5-30	----	Total 28.7	Total 5580	Overall index 2.06

logical state of the forest create a unique set of conditions which determine forest radiation regimes. We present data from clear days to prevent confounding the effects of these sources of variation by changing cloudiness. Nevertheless, some variation is included resulting from the differing amounts of atmospheric turbidity present on these clear days. Since we have no measure of this factor, we are unable to separate out its effect upon forest radiation other than by selecting data from the clearest days of record for analysis. To show the effect of cloud cover, we include data from a heavily overcast day in winter and in summer for comparison. Since partly cloudy days are difficult to characterize for comparative purposes, we ignore data from such days except in the derivation of the annual radiation budget for the forest under study. Finally, the effects of horizontal and vertical heterogeneity in forest structure are quantified through replication of measurements of forest radiation in horizontal and vertical space.

To further illustrate the effects of seasonality and phenological changes in forest structure, average phenoseasonal penetration rates were calculated and applied to phenoseasonal total incident radiation measured at the NOAA weather station in Oak Ridge,  $\approx 10$  km to the north. As described below, the method of derivation of the seasonal budget attempts to account for the variation arising from differing degrees of cloudiness and morning fog that is frequently present in east Tennessee. All data from this study are written on magnetic tape and may be obtained for further analysis from the authors.

#### SITE DESCRIPTION

The forest in which this study of radiation climate was made is a seral, deciduous forest composed predominantly of tulip poplar, *Liriodendron tulipifera* L. The stand is  $\approx 50$  yr of age and is situated in a moist limestone sink on the ERDA reservation  $\approx 10$  km south of the town of Oak Ridge. Because of the mesic nature of the sink, this stand has a higher density and a more highly developed understory than is typical of the Appalachian region.

The overstory canopy is nearly pure tulip poplar although numerous other species are present in small numbers. The overstory canopy extends down past the zone of crown closure ( $\approx 20$  m above the floor) to about 16 m elevation. The lower limit of the overstory is rather well defined since the live crown generally ends at 16 m. Between 16 and 10 m there are a few crowns of suppressed trees, but in general this stratum is devoid of biomass other than the boles of codominant overstory trees. Below 10 m, however, is a rather distinct secondary canopy composed principally of flowering dogwood (*Cornus florida*) and redbud (*Cercis canadensis*). This secondary canopy extends down to about 3 m above the forest floor. Below 3 m are the crowns of numerous saplings and shrubs of various species.

The pertinent mensurational data for this forest are shown in Table 1, along with the Shannon-Weaver diversity indexes for tree species in the various canopy strata. The overall basal area of this forest at the time of this study was  $\approx 28$  m<sup>2</sup>/ha, while the total stem density exceeded 5,500 stems/hectare. The leaf area index of this forest when fully leafed was 6.0 (Dinger et al. 1972). Figure 1 shows a general view of the forest under study in summer full-leaf.

The climate of the region in which the study site is situated is characteristically warm and humid. Winters are mild and wet with frontal storm systems predominating. Summers are hot and humid with convective thunderstorms developing almost daily, yielding scattered areas of intense precipitation. Because of the high humidity and nearby reservoirs in the Tennessee River system, heavy radiative ground fog is frequently present in mornings throughout the year. Hence, fog at this site often persists well into the day.

The study is within the zone of influence of an unshielded research reactor at the Oak Ridge National Laboratory. Because of this, we could enter the site only during periods when the reactor was not in operation. As a result, instruments and the data acquisition system could not be checked frequently, hence, maintenance and repair of the monitoring





FIG. 1. General view of the tulip poplar stand in midsummer showing method of deployment of elevated solarimeters. ORNL Photo #2155-73.



system was a continuing problem which created difficulties in data analysis.

#### METHODS

Radiation reaching the earth's surface is of two forms: radiation in a collimated beam directly from the sun (beam radiation), and radiation diffused by its passage through the earth's atmosphere (diffuse or sky radiation). These two radiative components interact differently with vegetation and so must be measured separately if the relationships between stand structure and radiation climate are of interest (Anderson 1964b). Total radiation was measured using open sensors, while the diffuse component was measured using sensors equipped with shadow bands as designed by Horowitz (1969). (A shadow band is visible on the forest floor in Fig. 1.) Subtracting the diffuse radiation amount from the simultaneous total radiation yields an estimate of the direct beam radiation received at that time.

The penetration of beam radiation into a forest depends upon the flux density of the solar beam incident upon the stand and upon the number, size, and space distribution of canopy openings (Anderson 1964c, Anderson and Denmead 1969, Horn 1971, Reifsnyder et al. 1971). On the other hand, diffuse radiation penetration depends upon the distribution and amount of sky brightness, the number, the size, and the space distribution of canopy openings, and the geometry, space distribution, and optical characteristics of the forest biomass (Verhagen et al. 1963, Anderson 1964b,c, Anderson and Denmead 1969, Horn 1971, Miller and Norman 1971). Since the sun's apparent position changes through the day and from day to day, and since canopy opening distributions tend to be highly variable, the amount of beam radiation penetrating a forest canopy is highly variable in space and time. In contrast, the factors governing the penetration of diffuse radiation are not highly variable, therefore diffuse radiation within a forest is more uniform in space and time. As a result, different sampling schemes are necessary for measurements of the two radiative components if comparable statistical accuracy of the two quantities is required (Gay et al. 1971, Reifsnyder et al. 1971). Reifsnyder et al. (1971) found that 18 replicate measurements of total radiation at the floor of a Connecticut deciduous forest were necessary to obtain space means having standard errors of the means of  $\pm 10$  millilangleys per minute (mly/min) [ $\approx 418$  joules  $m^{-2}$ ] or less. Only two replications of the diffuse measurement were necessary to attain this level of precision.

Radiant flux densities were measured within and above the forest with an array of Lintronic Dome Solarimeters<sup>®</sup>, a commercial modification of Mon-

teith's (1959) field solarimeter. These instruments sense radiation in the spectral band 0.3 to 3  $\mu m$ , this band accounting for some 98% of the solar energy reaching the earth's surface (Fritz 1958). Horizontal space variation in total radiation received within the forest was assessed through replication of observations at a given level. Vertical variation was similarly determined by replicating the horizontal arrays at three levels in the forest. All sensors were randomly situated in horizontal space with 11 replications at the 16-m level and 12 at the 3- and 0-m levels. Elevated sensors were mounted on the tops of telescoping steel masts extended to the desired height (see Fig. 1).

The levels of vertical replications of measurement were selected such that the attenuation of radiation by major canopy strata could be determined. The sensors at 16 m were at the base of the overstory canopy while those at 3 m were at the base of the secondary canopy. The sensors on the forest floor were elevated above the general level of herbaceous vegetation and thus sensed that radiation penetrating the three-canopy strata: the overstory canopy, the secondary understory canopy, and the shrub layer.

Incoming diffuse radiation was also measured at each of these levels. Following Reifsnyder et al. (1971), the diffuse measurements were replicated twice at the 0- and 3-m levels. Only one measurement of this variable was possible at 16 m throughout 1972 and early 1973. In late 1973, the diffuse measurement was replicated twice at 16 m as at other levels.

The total and diffuse radiation incident upon the forest was measured using single open and shaded sensors located 32 m above the forest floor, 1 to 2 m above the tops of the tallest trees. Although Drummond (1956) developed a method for correcting measurements of diffuse radiation for that radiation originating in the area of sky occluded by the shadow band, all diffuse data are presented here uncorrected. We feel that the distribution of brightness in the forest canopy is likely to be considerably different from that in the sky owing to the conversion of beam radiation to diffuse radiation by multiple reflections and transmissions from and through leaves. Hence application of corrections such as those proposed by Drummond (1956) is probably inappropriate for measurements within plant stands and thus all diffuse data are presented in their uncorrected form.

All sensors were periodically recalibrated against an Eppley Precision Pyranometer<sup>®</sup> that we use as a local standard. Owing to the nonlinear response of the Lintronic sensors, nonlinear calibration functions were empirically derived for each sensor used in this study (Matt and Hutchison 1974). These functions were used to convert the millivolt output signals from the Lintronic solarimeters to engineering units. Care was taken to orient all sensors the same during cali-



bration and during field measurements to minimize errors arising from departures from flatness of the printed-circuit sensing elements.

The output signals from all sensors were fed into a data acquisition system, scanned periodically (10-min intervals on weekdays in 1972, 5-min intervals on weekdays in 1973, and 20-min intervals on weekends), converted to digital form, and recorded on punch paper tape. Subsequently these paper tapes were read, the data converted to engineering units, edited, and summarized.

As noted above, horizontal space variation in total and diffuse radiation was assessed through simultaneous, horizontally replicated measurements. The space average direct beam radiation can then be derived by subtracting the space mean diffuse radiation from the space mean total. Vertical variation was assessed through comparison of space means from the three different levels. Temporal variation within days was characterized by analyzing radiation measurements made periodically through full days. All curves of smoothed data were smoothed using a five-point smoothing technique.

Seasonal variation in radiation incident upon the earth's surface increases with increasing latitude owing to the combined effects of the earth's tilted axis of rotation and its annual revolution about the sun. Superimposed upon this regular, annual cycle of radiation received within plant stands is another, less regular variation produced by phenological changes in stand structure. Even in temperate zone conifer forests, seasonal changes in radiation climates have been reported which are ascribed to phenological changes in the canopy structure (e.g., Schomaker 1968).

In deciduous forests, the effects of phenological change upon radiation climates within the forests rival those effects of changing celestial geometry. Salisbury (1916) referred to two different radiation climates in the deciduous woodlands in which he worked. The radiation regime in the leafless winter forest was termed the light phase, while the radiation climate of the fully-leaved summer forest was termed the shade phase. While these relative phases are clearcut, they do not coincide with absolute amounts of radiation penetrating deciduous forests because of the great variation in incident insolation from day to day and from season to season (Anderson 1964b).

To account for the seasonally and phenologically induced changes in forest radiation regimes, we define seven phenoseasons as shown in Fig. 2, using the solstices, the equinoxes, and dates of phenological events in this forest of importance to radiation penetration. Phenological data were obtained from Taylor (1974). Data from a single clear day in each phenoseason were summarized and plotted over time of

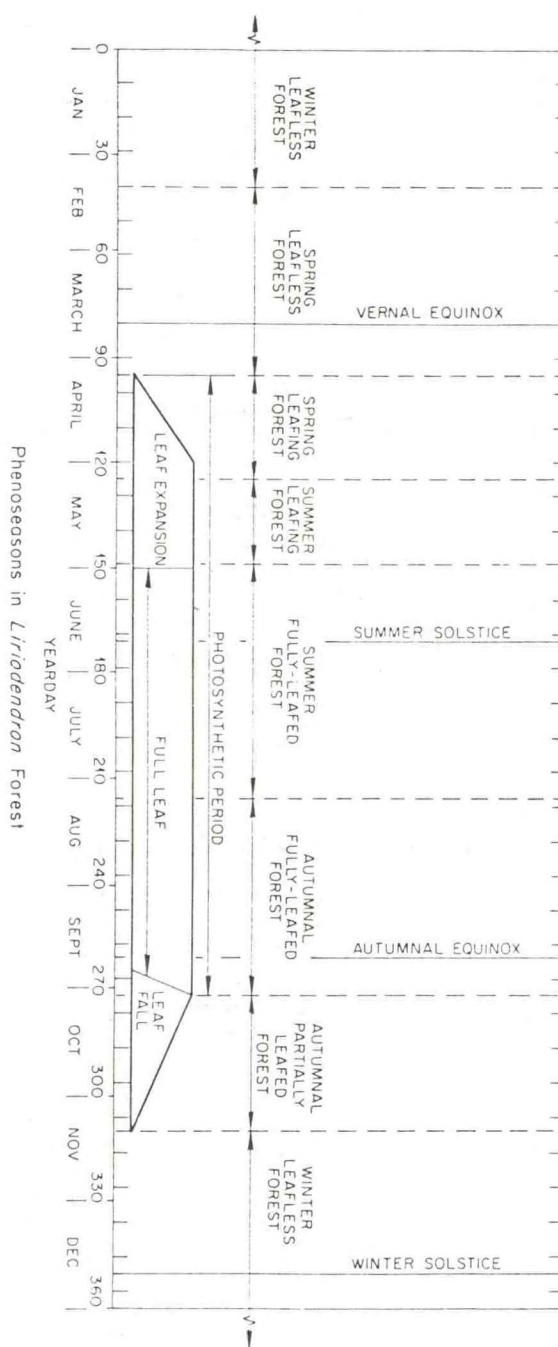


FIG. 2. Phenoseasons in the tulip poplar forest. ORNL Dwg. 74-11562.

year to illustrate the changes in forest radiation climates resulting from changing earth-sun geometry and phenological state.

To further illustrate seasonal differences, average phenoseasonal penetration rates were calculated and applied to the continuous radiation record from the NOAA weather station in Oak Ridge. In this way, the annual radiation regime above and within this

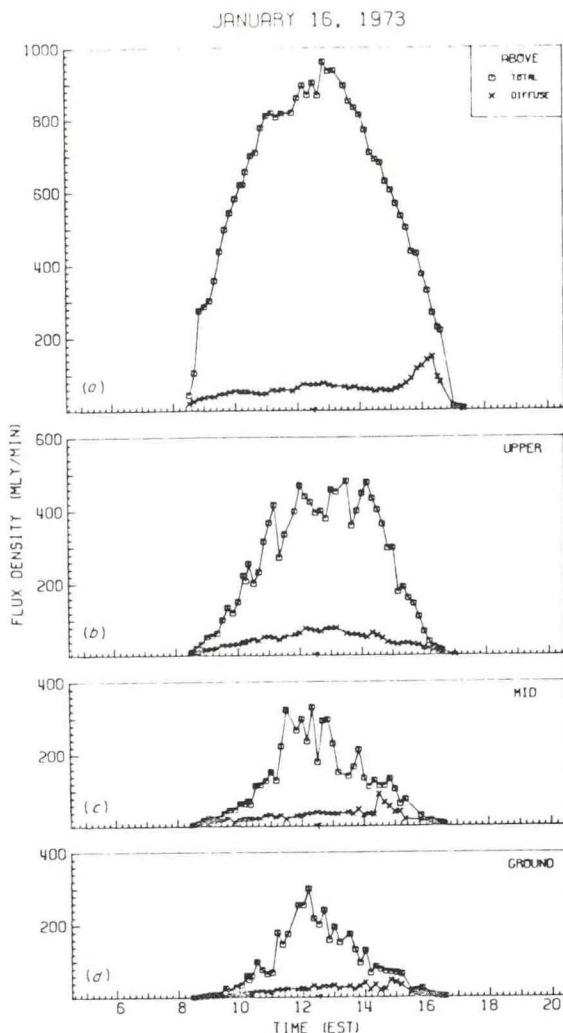


FIG. 3. Diurnal course of average radiation on a clear day in the winter leafless forest: (a) above canopy total and diffuse radiation, (b) 16 m total and diffuse radiation, (c) 3 m total and diffuse radiation, and (d) 0 m total and diffuse radiation. The arrows on the abscissae (time axis) of this and subsequent figures denote solar noon. Afternoon peaks in diffuse radiation curves are spurious and result from beam radiation passing beneath the shadow band and striking the shaded sensor. To convert millilangleys (mly) to joules per square metre ( $\text{J m}^{-2}$ ), multiply by 41.84. ORNL Dwg. 76-15807.

forest was derived. For this approximation, data from partly cloudy days had to be included since partly cloudy skies are far more common than either clear or heavily overcast skies. To incorporate the effects of varying cloudiness, the continuous radiation record from the Oak Ridge weather station was segregated into clear, partly cloudy, and overcast mornings and afternoons and the half-day totals of radiation calculated for each of the six cloudiness time period categories. The separation of morning and

afternoon data was necessary because of the frequent, heavy morning fog that is present in this region on clear to partly cloudy days.

Similarly, the forest radiation data were segregated as above as well as by phenoseason. Average phenoseasonal penetration rates were then calculated for each cloudiness-time period category for each of the three levels in the forest. Summing the appropriate half-day radiation totals from the Oak Ridge station over the phenoseason and multiplying by the corresponding fractional penetration for each forest level yielded an estimate of the total radiation received at each level in the forest for each kind of half-day cloudiness category in each phenoseason. Summing these estimates over all cloudiness classes and half-days in each phenoseason yielded an estimate of the total radiation received during each of seven phenoseasons at each of the three levels in the forest. From these derived totals, gross phenoseasonal mean penetration rates were calculated, as well as photosynthetically active and leafless seasonal totals and percentages.

## RESULTS AND DISCUSSION

### *Clear day forest radiation regimes*

Radiation regimes above and within the winter leafless forest on a representative January day are shown in Fig. 3. Since total radiation represents the sum of the beam and diffuse radiation components, the differences between the total and diffuse radiation curves on this and subsequent similar figures represent the flux densities of beam radiation received. As is evident from Fig. 3a, skies on this winter day were clear except for the 2-h period just prior to solar noon. During this time, thin clouds or haze developed which were sufficiently dense to reduce beam radiation inputs slightly, but not so dense as to significantly increase the incident diffuse radiation. The brief plateau at 0900 h in the total radiation record of Fig. 3a results from melting of frost on the solarimeter dome. Peaks in the diffuse radiation records at around 1600 h are spurious and result from beam radiation passing beneath the shadow bands and striking the shaded sensors. The equivalent morning peaks are absent because of topographic shading by a low ridge to the southeast of the study site on this midwinter day.

The rapid morning rise and equivalent rapid afternoon decrease in total radiant flux densities of Fig. 3a are characteristic of reasonably clear day records. Within the leafless forest however (Fig. 3b,c, and d), when solar elevations are low the slopes of the total radiation curves are much reduced from those above the forest. Then at some time nearer solar noon, the slopes of the within-forest curves increase. Through-



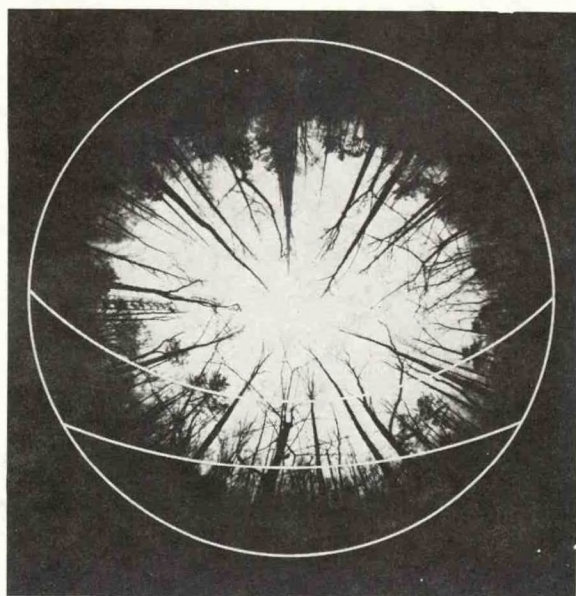


FIG. 4. Canopy photograph of winter leafless forest taken from the forest floor, showing solar paths on the winter solstice and on the vernal equinox. Note that the canopy density is much higher along the winter solstice solar path throughout most of the day than on the vernal equinox, represented by the innermost solar path on this figure. ORNL Photo # 0060-75.

out the day, the slopes of diffuse radiation curves are quite low and change only slowly with time. Hence it is the beam radiative component that is responsible for the changing slopes and temporal irregularity of the total radiation curves.

Figure 4 explains this well. Throughout most of the winter day, the solar path (outermost arc) is obscured by woody forest biomass. Only around midday is sky along the solar path visible from the forest floor. Hence the beam radiation is strongly attenuated by the woody biomass and only at midday can such radiation penetrate to the forest floor. Diffuse radiation, on the other hand, originates from the entire hemisphere of sky and therefore can penetrate into the forest more freely. Note too that as the solar paths rise in the sky from winter to spring, the amount of sky obscured by woody biomass along these paths decreases. Furthermore, the midday period during which the sun is above the completely occluded regions near the horizon lengthens. This has great significance to the seasonal variation in the radiation climates of this forest as is discussed in the seasonal variation section.

While the above canopy record of total radiation appears fairly symmetric about solar noon, the within-forest records show considerable asymmetry. Despite the random siting of replicated sensors in the forest, the heterogeneity of the forest structure is

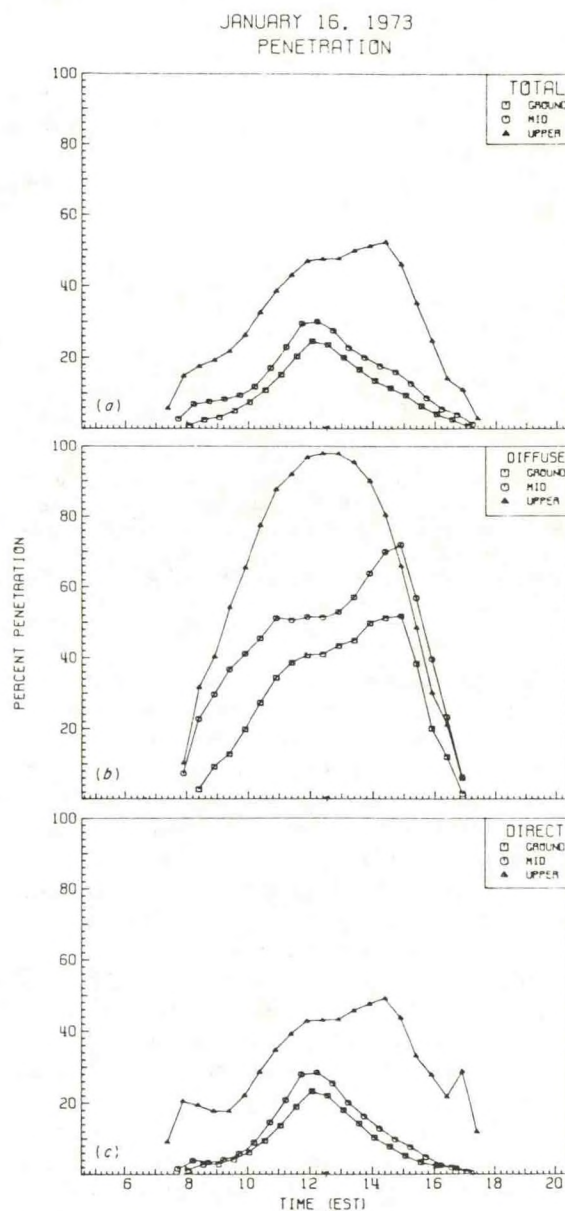


FIG. 5. Smoothed daily course of average fractional penetration of solar radiation in the winter leafless forest under clear skies: (a) total radiation, (b) diffuse radiation, and (c) direct beam radiation. A five-point smoothing technique was used to reduce noise in all smoothed curves. ORNL Dwg. 76-16854.

still manifest in these data. At 16 m, somewhat greater canopy opening is indicated to the west of the sensors at that level. At the 3- and 0-m levels, more canopy openings fall to the east of the sensors than to the west resulting in greater morning penetration of beam radiation. Figure 5 gives further evidence of this. While the fractional diffuse penetrations along with the fractional penetrations of the



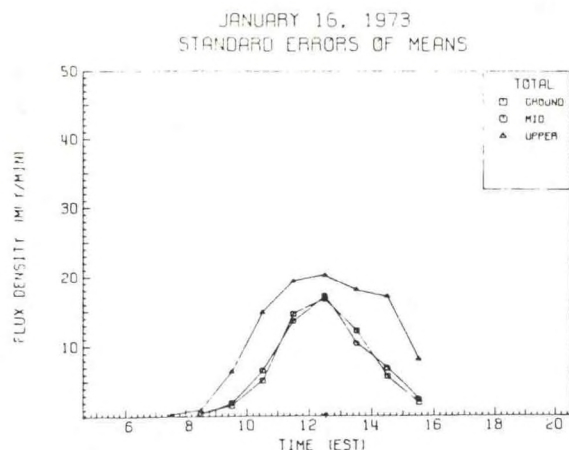


FIG. 6. Smoothed daily course of spatial variability of total radiation received within the winter leafless forest as measured by the half-hour time averaged instantaneous standard error of the space mean total radiation. To convert millilangleys to joules  $m^2$ , multiply by 41.84. ORNL Dwg. 76-158000.

derived beam radiative component are in error after about 1500 h because of the spurious peaks in the diffuse records of Fig. 3, considerable asymmetry is still evident in Fig. 5 prior to this time. Peak direct beam penetration occurs in midafternoon at 16 m and in late morning at 3- and 0-m levels (Fig. 5c). Since the beam radiation component dominates the total radiation received in the winter forest, the fractional penetration of total radiation (Fig. 5a) follows that of the beam radiation closely.

The penetration of diffuse radiation into the forest exceeds that of the beam component throughout much of the day (Fig. 5b). This would be expected in view of the canopy structure shown in Fig. 4. Greatest attenuation of the beam component occurs in the overstory canopy (Fig. 5c) with much less but still significant attenuation between 16 and 3 m. Little further attenuation between 3 m and the forest floor is indicated. Attenuation of the diffuse component is more even throughout the vertical extent of the forest (Fig. 5b).

Spatial variation in total radiation flux densities within the forest follow the temporal pattern of beam radiation closely (Fig. 6). The space variation is greatest at 16 m and similar in magnitude at the lower levels. Midday variations at all levels greatly exceed the  $\pm 10$ -mly/min variation desirable for most energy budget determinations (Reifsnyder et al. 1971).

Beyond the problem of characterizing radiation climates of vegetative stands engendered by the extreme variability of beam radiation in space and time, is the further problem of defining such climates in a biologically meaningful manner. Ramann (1911)

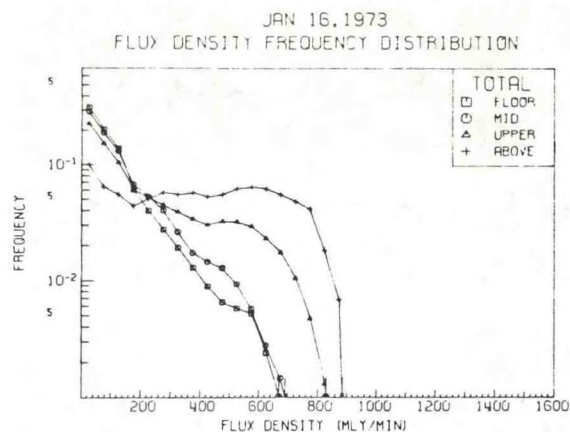


FIG. 7. Smoothed frequency distributions of total radiation flux densities observed within and above the winter leafless forest on a clear midwinter day. Millilangleys  $\times 41.84 =$  joules  $m^2$ . ORNL Dwg. 76-15803.

pointed out that the presence of beam radiation in plant stands produces nonnormal frequency distributions of radiant flux densities, thereby making the use of mean values less than satisfactory for many purposes. Mean radiation values are especially poor characterizations of radiation climates in terms of processes such as photosynthesis and transpiration which vary nonlinearly with radiant flux density (Norman et al. 1971).

Typically, radiant flux density frequency distributions are bimodal in the upper reaches of fully leafed plant canopies (Niilisk et al. 1970, Hutchison 1971) and are unimodal and tend to be skewed at greater canopy depths (Ovington and Madgwick 1975, Hutchison 1971, Hutchison and Matt 1973). Using a 50-mly/min  $[= 2.092 \text{ kJ}/(m^2 \text{ min})]$  class interval and a 5-point smoothing procedure to reduce noise, we construct the distributions of Fig. 7 for this winter day. The above-canopy distribution is roughly rectangular while within-forest distributions are unimodal and skewed as previously reported. Modal frequencies at all levels in the forest are in the 0- to 50-mly/min class and the modal frequencies are shown to increase with depth. According to these data,  $<2\%$  of the radiation received within the winter leafless forest occurs at flux densities exceeding 200 mly/min  $[= 8.368 \text{ kJ}/(m^2 \text{ min})]$  despite incident midday flux densities of the order of 900 mly/min  $[= 37.656 \text{ kJ}/(m^2 \text{ min})]$ . Because of penumbral effects, radiant flux densities in the leafless forest are severely reduced below those incident. Despite the accentuation of the skewness of these distributions effected by the plotting of the ordinate to a log scale, it is evident from Fig. 7 that mean daily radiation values are poor characterizations of leafless forest radiation regimes. Since the kurtosis of these distributions decreases and

JUNE 14, 1972

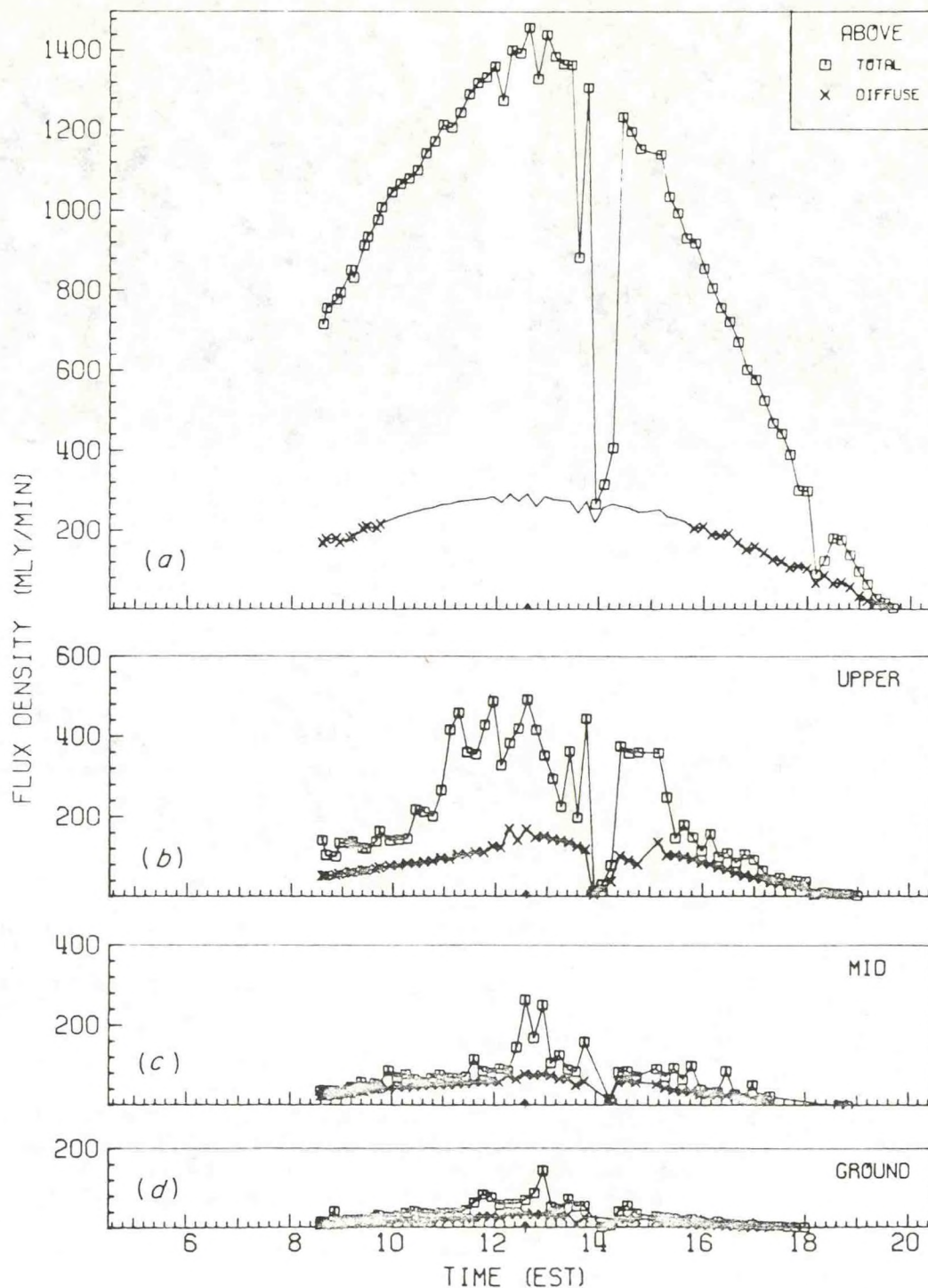


FIG. 8. Diurnal course of average radiation on a mostly clear day in the summer fully leafed forest: (a) above canopy, (b) 16 m, (c) 3 m, and (d) 0 m average total and diffuse radiation records. The portion of the above canopy diffuse radiation curve lacking symbols is estimated. See text for details. Millilangleys  $\times 41.84 = \text{joules/m}^2$ . ORNL Dwg. 76-16171.



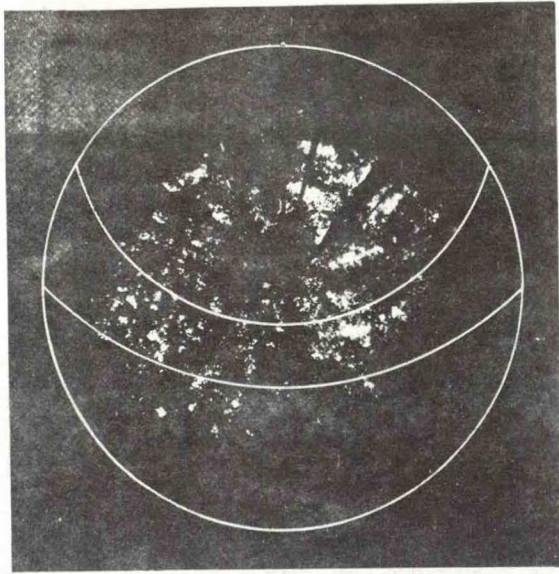


FIG. 9. Fully leafed forest canopy photograph from the forest floor. Innermost arc represents solar path on the summer solstice while the outer arc represents the path of the sun on the equinoxes. ORNL Photo #0062-75.

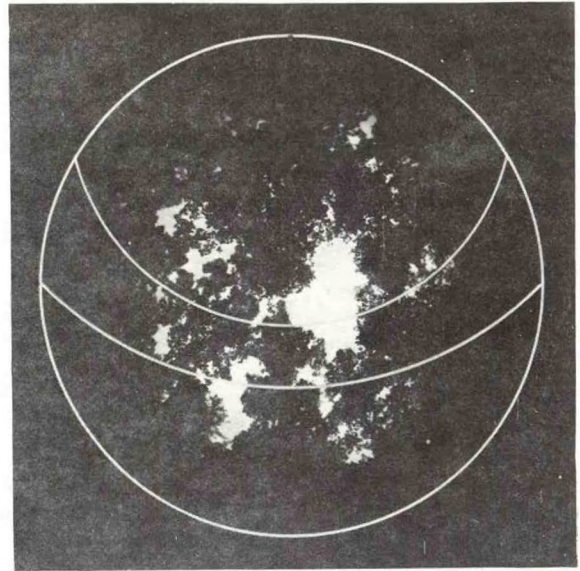


FIG. 10. Fully leafed forest canopy photograph from the upper canopy (16 m) level. Innermost arc represents the solar path on the summer solstice while the outer arc represents the path of the sun on the equinoxes. ORNL Photo #0061-75.

the skewness increases with height in this forest, mean radiation becomes an increasingly poor indicator of radiation regimes with increasing height in the leafless forest.

In contrast to the low solar elevations and leafless state found in the winter forest, Fig. 8 shows the forest radiation regimes for a fairly clear day in the fully leafed forest of June. Since this day is near the summer solstice, solar elevations throughout this day approach their annual maximum. At this time the leaf area index of the forest was stabilized at about six. Because convective afternoon clouds develop nearly daily and atmospheric humidity remains high, truly clear days are rare. The clearest summer day for which we have data is 14 June 1972, but as shown on Fig. 8a, heavy clouds obscured the sun for much of a 2-h period in the early afternoon of this day. Furthermore, the above-canopy shadow band was improperly set on this day resulting in erroneous midday diffuse radiation values. The segment of the diffuse curve of Fig. 8a without symbols represents our estimates of the actual values for this period. These estimated values were derived from analysis of clear midday segments of diffuse radiation records from other June days and by selecting values which yield the smooth midday segment shown here. Since these values are estimates however, the midday values presented of fractional diffuse penetration and of fractional beam penetration derived using the estimated diffuse flux densities are suspect.

The characteristic convex upward morning and

afternoon total incident radiation curve segments of winter are replaced, in summer, by the more linear ascending and descending curve segments of Fig. 8a. This phenomenon reflects the higher atmospheric humidity and turbidity of the east Tennessee summer which reduces incident beam flux densities early and late in the day. The incident diffuse radiation flux density values are also substantially increased over those incident upon the winter forest. This results from greater amounts of total radiation incident as well as from higher atmospheric turbidity which increases the conversion of beam to diffuse radiation in the atmosphere.

Within the forest, peak values of total radiation in the upper canopy (16 m) are not dissimilar from those of winter, however, at greater depths in the forest, these peak values are substantially reduced (Figs. 8c,d). The lengths of the morning and afternoon periods of slowly increasing total radiation are greatly increased over those of winter as a result of the increased day length. Effects of the greatly increased midday solar elevations from winter minimum to summer maximum upon the penetration of radiation into this forest are negated by the addition of leafy biomass in the forest canopy. Because of the greater amounts of incident diffuse radiation in summer and of greater amounts of beam enrichment of diffuse radiation in the fully leafed forest (Hutchison and Matt 1976), diffuse radiation flux densities are increased at the three forest levels under study with smaller increases found at greater forest depths. As



before, the asymmetry of the within-forest curves about solar noon reflects that insufficient measurement replications were made to account for the spatial heterogeneity in structure in this forest.

Views of the fully leafed forest canopy at 0 and 16 m are shown in Figs. 9 and 10. As indicated by these photos, the sky in the region just above the horizon is completely occluded at both levels. At higher angular elevations, more canopy opening is present, but even at 16 m most openings are small and irregularly distributed. Since the distance to which beam radiation can penetrate undiminished through an opening in an opaque surface is a function of the diameter of the opening (Horn 1971), the greatly diminished sizes of canopy openings from winter (Fig. 4) to summer implies greatly decreased beam radiation penetration by virtue of increased penumbral effects (Miller and Norman 1971). Hence, despite the greatly increased amount of beam radiation incident upon the summer forest, greater absorption and attenuation of this radiation is effected by the fully leafed canopy, and the fraction of radiation penetrating the canopy decreases.

Figure 11 emphasizes this reduction. The fractional penetration of total radiation and both its components are reduced from those of winter, especially at midday. Since these midday values for beam and diffuse radiation are suspect by virtue of the use of estimated incident diffuse radiant flux densities, we will not consider them further. However, values for the penetration of total radiation are derived from observed data and should be reasonable. The change in shape of the morning and afternoon portions of the curves of Fig. 11 from those of winter (Fig. 5) are also of interest. Since there is no abrupt change from occluded to unoccluded sky in the fully leafed canopy (Figs. 9 and 10), the fractional penetration of radiation in general and of diffuse radiation in particular increases much more gradually in summer (Fig. 11b) than in winter (Fig. 5b).

Despite the reduction in beam radiation penetration into the fully leafed forest, Fig. 12 shows that midday spatial variabilities are larger at 16 m in summer than in winter (Fig. 6). Variability at 3 m is somewhat decreased while that at the forest floor is strongly reduced. Peak values occur only at midday when significant beam penetration can occur. Earlier and later in the day, space variation is much lower at all three levels. The increased upper canopy space variation with a fully leafed canopy reflects increased heterogeneity in the upper canopy when leaves are present.

As in winter, the summer clear day flux density frequency distributions approach rectangular above and are unimodal and highly skewed within the forest

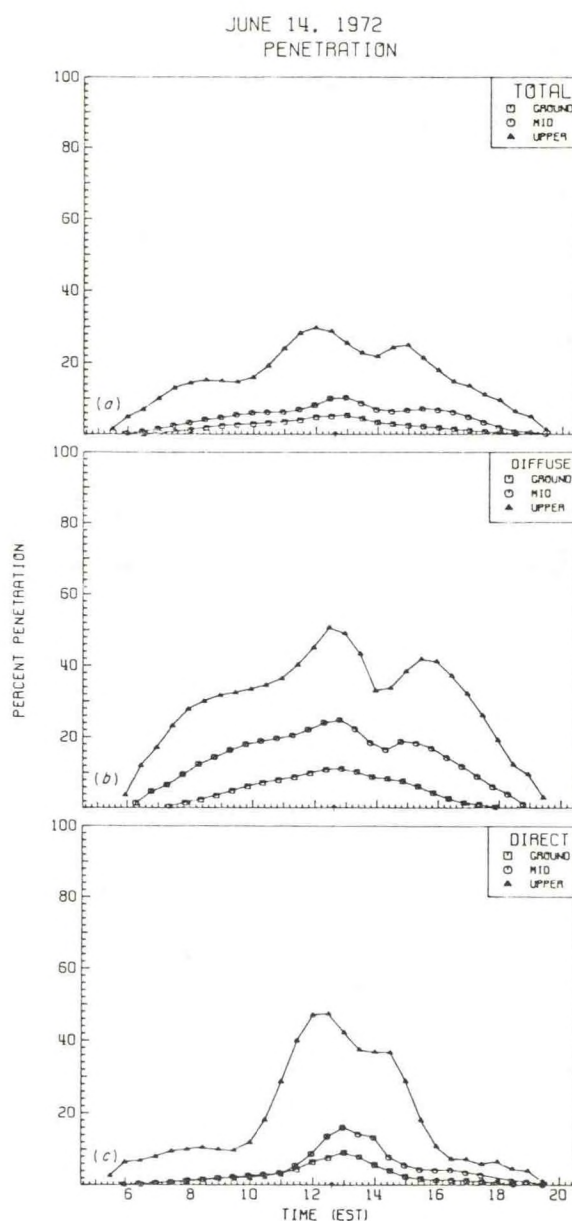


FIG. 11. Smoothed course of average fractional penetration of solar radiation in the summer fully leafed forest under clear skies: (a) total, (b) diffuse, and (c) direct beam radiation. ORNL Dwg. 76-16857.

(Fig. 13). Much higher flux densities are received by the forest in summer by virtue of the greatly increased midday solar elevations. Nevertheless, the incidence of radiation at flux densities  $>200$  mly/min are decreased at the lower levels in the summer forest because of the increased penumbral overlap in the sunflecks formed by the much smaller canopy openings (Figs. 7 and 13). At 16 m, incidence of higher flux density sunflecks increases somewhat (since the incident diffuse is estimated to peak at around 200

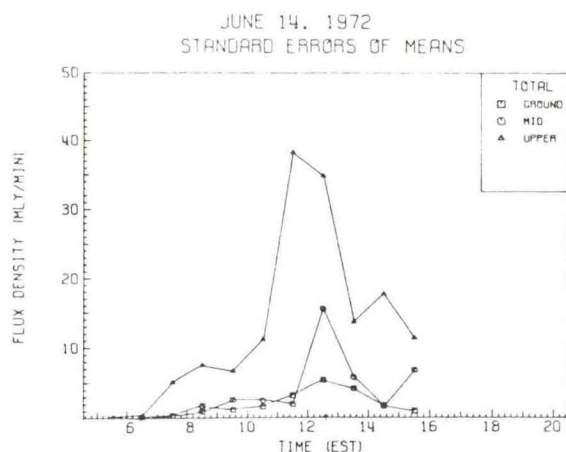


FIG. 12. Smoothed course of spatial variability of total radiation received within the summer fully leafed forest as measured by the half-hour time averaged instantaneous standard error of the space mean total radiation. Millilangleys  $\times 41.84 = \text{J/m}^2$ . ORNL Dwg. 76-15795.

mly min at midday on 14 June, all flux densities in excess of this amount probably stem from beam radiation) but still drops to insignificant frequencies at rather low flux densities compared to those incident upon the forest. Essentially no radiation reaches 0 or 3 m at flux densities  $> 200$  mly/min, while only about half of that received at 16 m exceeds this flux density.

To give biological perspective for these data, Dinger (1971) has reported that light saturation in *Liriodendron tulipifera* occurs at flux densities of about 400 mly/min [ $= 16.736 \text{ kJ}/(\text{m}^2 \text{ min})$ ], while the compensation point for this intolerant species occurs at about 40 mly/min [ $\approx 1.674 \text{ kJ}/(\text{m}^2 \text{ min})$ ]. Hence, despite the great attenuation of radiation and the severe reduction of incidence of higher flux density radiation by the fully leafed forest, few leaves in this forest received insufficient quantities of radiation for photosynthetic compensation on clear summer days. However, since leaves transmit green and near infrared wavelengths preferentially, much of the radiation present within the summer forest may be photosynthetically inactive.

#### Overcast day forest radiation regimes

With overcast skies, amounts of radiation reaching the surface of the earth or of a plant community are reduced from those present on clear days because of absorption and back-reflection of radiation by and from the cloud cover. Furthermore, direct beam radiation is diffused by the process of transmission through clouds, and consequently that radiation incident upon a forest on overcast days is nearly entirely diffuse. This is evident in Fig. 14a.

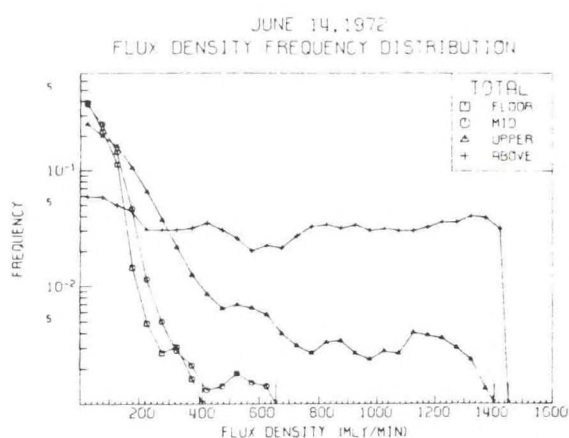


FIG. 13. Smoothed frequency distributions of total radiation flux densities within and above the summer fully leafed forest on a mostly clear summer day. Millilangleys  $\times 41.84 = \text{J/m}^2$ . ORNL Dwg. 76-15796.

Throughout the morning and early afternoon of this January day, skies were heavily overcast; total and diffuse flux densities are nearly equal. That difference that is present is most likely the result of the presence of the shadow band since our diffuse values are uncorrected for radiation stemming from the portion of the sky occluded by the band. In mid-afternoon the sky cleared partially, resulting in a sharp rise in incident total radiation.

During the overcast portion of this day, the records of total radiation above and within the leafless forest of Fig. 14 are quite similar to the equivalent diffuse records on the clear day of 16 January (see Fig. 3). Total radiation within the forest on the overcast day exceeds the amount of diffuse radiation received there on the clear January day because of the greater amounts of diffuse radiation incident on the forest on the overcast day. Otherwise the diurnal trends are similar.

Comparison of Figs. 15 and 5a for the overcast and clear winter days, respectively, shows that more of the incident radiation penetrates the forest on the overcast day than on the clear day. However, comparison of Fig. 15 with Fig. 5b shows that the proportion of radiation from overcast skies that penetrates the forest is less than that of the diffuse that penetrates on a clear day. This indicates that the enrichment of diffuse radiation within the forest on clear days by down-reflected direct beam radiation may be significant even in the leafless winter forest.

Because of the absence of direct beam radiation, the forest is much more uniformly illuminated on this overcast day. The space variation in total radiation is around  $\pm 1$  mly/min [ $\approx 41.8 \text{ J} \cdot \text{m}^{-2} \cdot \text{min}^{-1}$ ] or less at all levels in the forest. With the clearing skies in midafternoon, the space variation



JANUARY 30, 1973

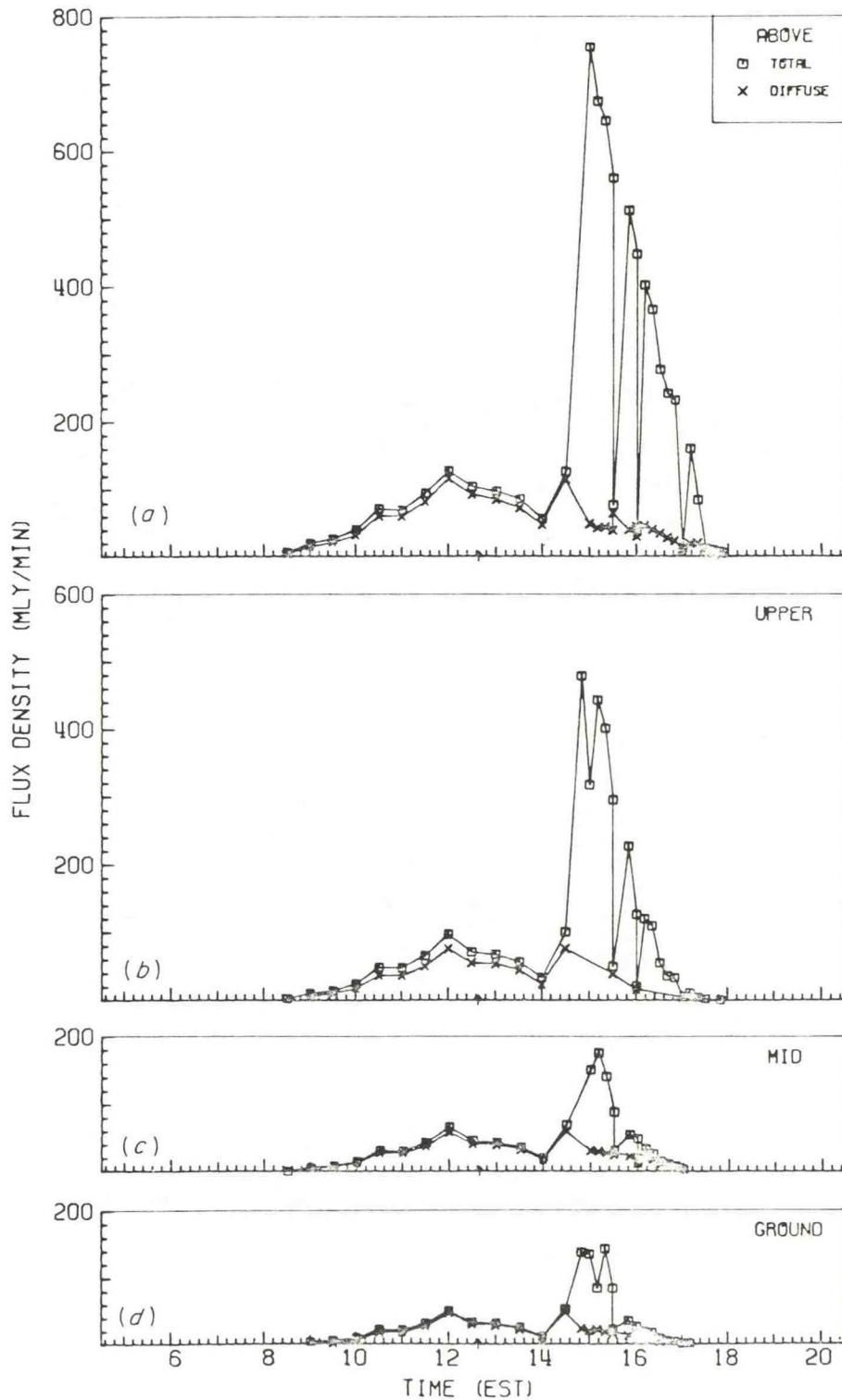


FIG. 14. Diurnal course of average radiation on an overcast day in the winter leafless forest: (a) above canopy, (b) 16 m, (c) 3 m, and (d) 0 m. Millilangleys  $\times 41.84 = \text{J m}^2$ . ORNL Dwg. 76-15808.

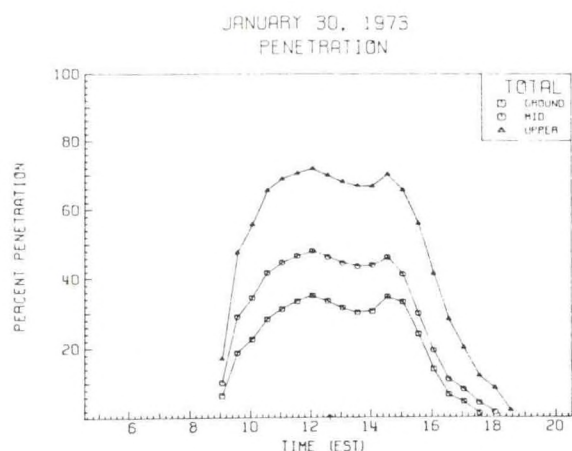


FIG. 15. Smoothed daily course of average fractional penetration of solar radiation from an overcast sky in the winter leafless forest. ORNL Dwg. 76-16784.

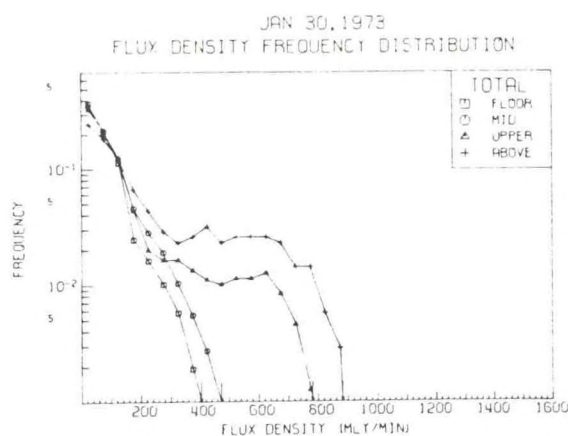


FIG. 16. Smoothed frequency distributions of total radiant flux densities observed within and above the winter leafless forest on an overcast day. Millilangleys  $\times 41.84 = \text{J/m}^2$ . ORNL Dwg. 76-15801.

risers dramatically to values comparable to those of the clear winter day shown in Fig. 6.

As shown on Fig. 16, no radiation was incident on the forest at flux densities  $>900$  mly/min. Within the forest, the woody biomass is shown to effect considerable change in the frequency distributions of radiant flux densities from that incident. Only at the 16-m level are there significant amounts of radiation present at flux densities exceeding 200 mly/min.

Radiation received within and above the summer fully leafed forest on a heavily overcast day is shown in Fig. 17. The irregularity of these curves indicates that the density of the cloud cover on this June day was not as uniform in time as on the overcast January day. Nevertheless, the density of cloud cover was sufficiently high to reduce incident direct beam flux densities to very low values.

As would be expected with reduced insolation, the radiation within the forest is much reduced from that received on the clear day of 14 June (see Figs. 8 and 17). Almost no radiation penetrates to the 3- or 0-m levels. The amounts of diffuse radiation penetrating the forest shown in Figs. 17c and d are substantially reduced from those penetrating the forest on the clear June day of Figs. 8b and c despite comparable magnitudes of incident diffuse radiation on these two days. This further illustrates the importance of direct beam enrichment of diffuse radiation within the forest through transmission and down-reflection processes.

Comparison of the winter and summer overcast day penetration of Figs. 15 and 18 shows that the fully leafed forest canopy effects a considerable reduction in the penetration of diffuse radiation from overcast skies. Furthermore, whereas in winter the proportion of radiation penetrating the forest is in-

creased with overcast skies, the reverse is true in the summer leafed forest. Comparison of Figs. 18 and 11a shows that the fraction of total incident radiation penetrating to all forest levels is reduced by the cloud cover when the forest is fully leafed. This finding is in disagreement with results of studies by Brecheen (1951) and by Tsel'Niker (1968). As Anderson (1964a) has pointed out, forests in general show decreasing canopy density from the horizon to the zenith. This is especially true in conifer forests and is increasingly true of deciduous forests at higher latitudes. Since uniformly overcast skies usually have brightness distributions that increase from horizon to zenith (Moon and Spencer 1942), in contrast to clear skies where the brightest area of the sky is immediately adjacent to the solar disk (Dorno 1919, Kimball and Hand 1921, Pokrowski 1929), a forest whose canopy density decreases toward the zenith will admit a greater proportion of incident radiation on overcast days than on clear days. As the canopy photograph of our forest in winter shows (Fig. 4), the leafless forest does have minimal canopy density at the zenith and the penetration of radiation into the forest in this phenologic phase agrees with results reported in the literature. However, measurements of canopy opening distributions on replicated canopy photos from this forest in full leaf indicate maximum sky area visible at midelevation angles (Fig. 19). Hence, our results for the summer overcast day are in disagreement with those of Brecheen (1951) who worked in western conifer forests and of Tsel'Niker (1968) who studied radiation in an oak forest near Moscow.

Comparison of clear day diffuse radiation (Figs. 8b,c, and d) with overcast day total (Figs. 17b,c, and d) shows that more diffuse radiation is received

JUNE 20, 1972

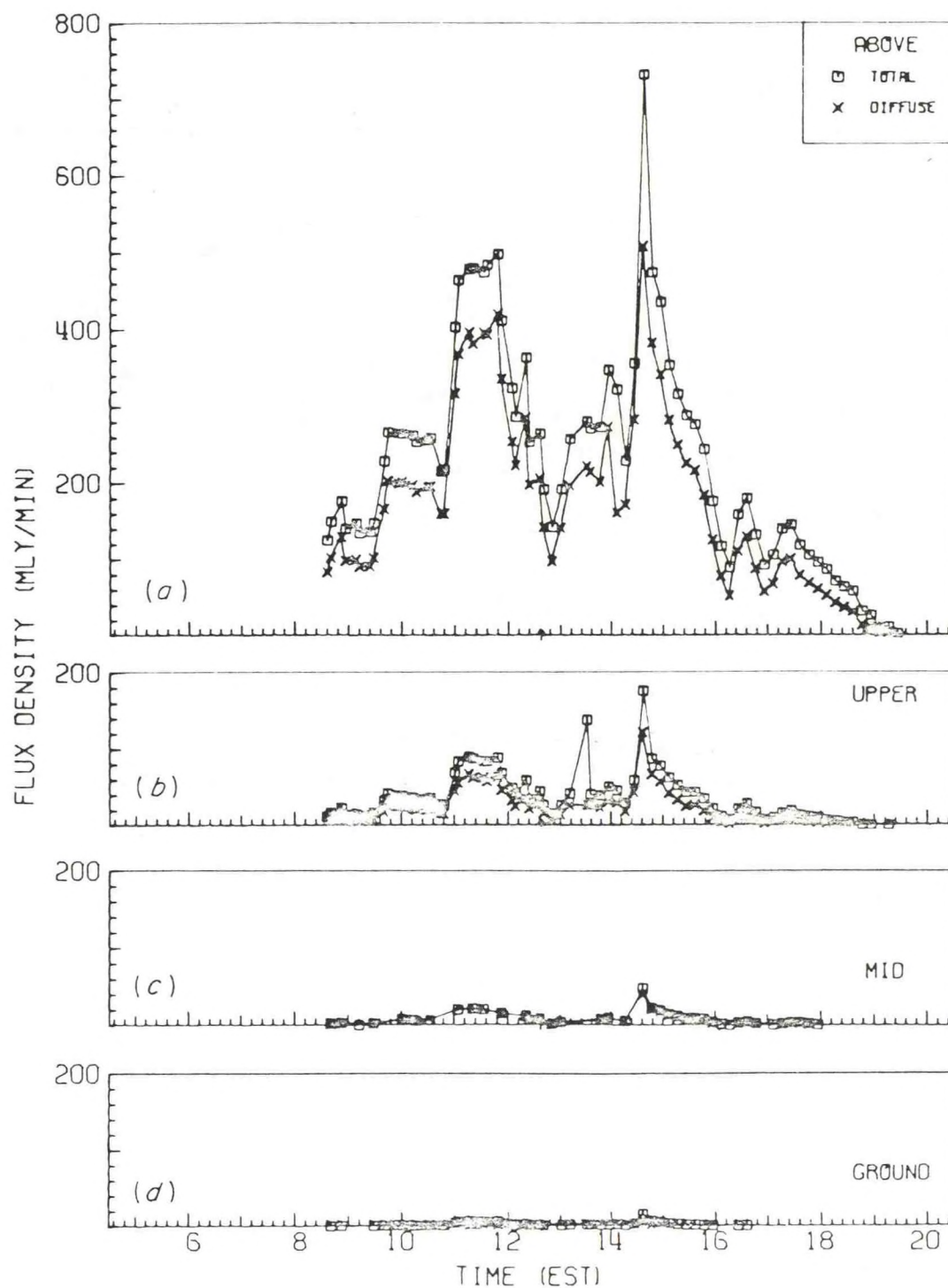


FIG. 17. Diurnal course of average radiation on an overcast day within and above the summer fully leafed forest: (a) above canopy, (b) 16 m, (c) 3 m, and (d) 0 m. While the detail of the radiation records at 3 and 0 m is lost when plotted to this scale, the reduction of radiant flux densities to very low levels is obvious. Milliangleys  $\times 41.84 = \text{J/m}^2$ . ORNL Dwg. 76-15809.



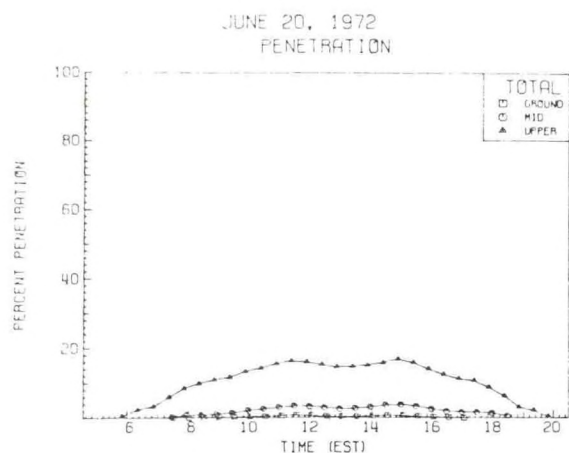


FIG. 18. Smoothed daily course of average fractional penetration of solar radiation from an overcast sky in the summer fully leafed forest. ORNL Dwg. 76-16783.

within the fully leafed forest on a clear day than total radiation on this overcast day. On clear days, significant enrichment of diffuse radiation within the forest occurs because of the down-reflection and

transmission of direct beam radiation from and through leaf tissues, which has the effect of increasing the apparent proportion of incident diffuse radiation that penetrates the canopy (Hutchison and Matt 1976). Thus, in the fully leafed forest, fractional clear day diffuse penetration and absolute quantities of diffuse radiation exceed overcast day fractional radiation penetration and amounts.

As in the winter leafless forest, overcast day illumination within the summer fully leafed forest is quite uniform in space and in time. Variabilities at the lower levels are  $< \pm 1$  mly/min throughout the overcast day. In the upper canopy (16 m), this variation ranges from  $\pm 1$  to  $\pm 5$  mly/min. The cloud cover effects a considerable reduction in spatial and temporal variability in radiation through its elimination of the direct beam component.

Because of the lack of high flux density radiation incident upon the forest on this day (Fig. 20), skewness in the flux density distributions within the forest practically disappears. Modal frequencies in the 0- to 20-mly/min flux density class are increased and the frequencies drop to insignificant values at quite low flux densities at all levels in the forest.

### OPENING AS FRACTION OF SKY AREA

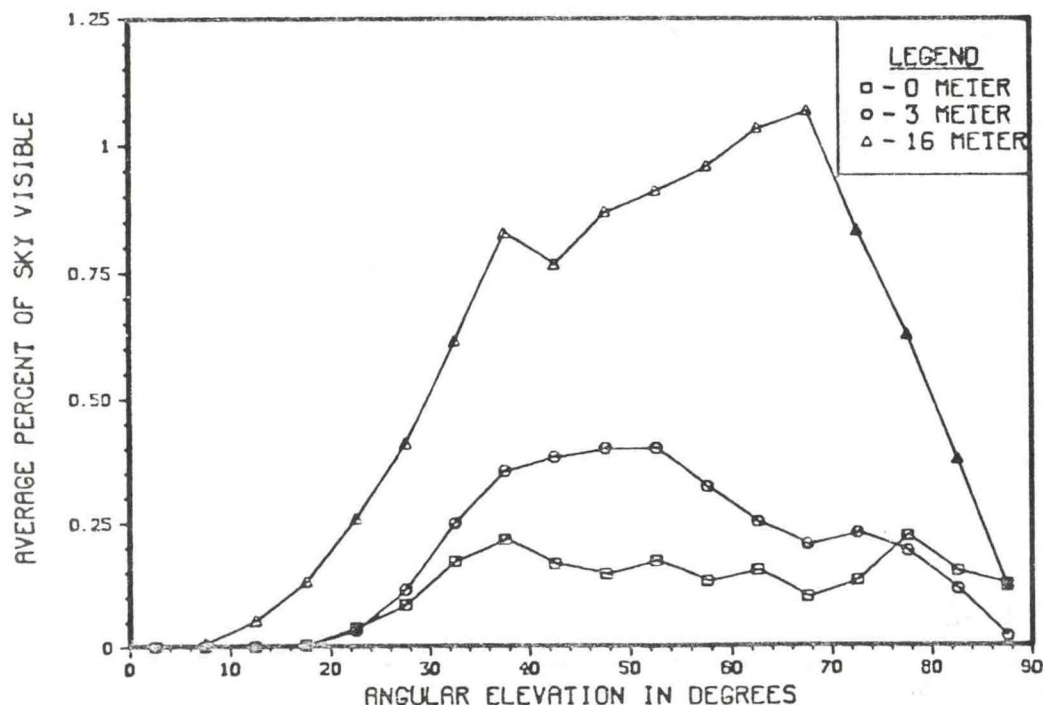


FIG. 19. Distribution of canopy opening expressed as a percent of the total projected area of sky over angular elevation. ORNL Dwg. 77-9655.

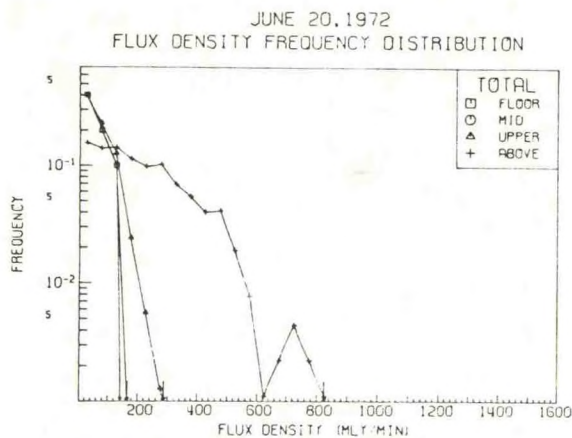


FIG. 20. Smoothed frequency distributions of total radiant flux densities observed within and above the summer fully leafed forest on an overcast day. Milliangleys  $\times 41.84 = \text{J/m}^2$ . ORNL Dwg. 76-15799.

#### Phenoseasonal variation in forest radiation regimes

Figure 21 shows the daily radiative component totals for a clear day in each of the seven phenoseasons defined in Fig. 2 as well as for the two overcast days presented above. As shown, the phenoseasonal course of incident total radiation on the clear days departs considerably from the sinusoidal seasonal variation of potential incident radiation. As would be expected, the minimum total radiation incident on the forest occurs on the winter day, but because of increasing atmospheric turbidity through spring and into summer, the annual observed maximum occurs during the summer leafing forest phenoseason rather than during the summer fully leafed forest phenoseason nearer the summer solstice.

Incident diffuse radiation is minimal during the winter season and slowly increases through the spring. In summer, the incident diffuse radiation increases substantially as a result of increased atmospheric turbidity, then declines again in autumn. Minimum direct beam radiation reaches the forest in winter, while maximum daily totals of incident direct beam are observed in the spring leafing forest phenoseason. After this phenoseason, the direct beam totals are reduced somewhat, despite the high daily totals of radiation incident on the forest because of the increases in incident diffuse radiation.

The daily totals of incident radiation on heavily overcast days are much reduced from those of the clear days and approach the daily totals of clear day diffuse (denoted by stars on Fig. 21). Although the total for the summer overcast day exceeds that of the winter day as would be expected, we have no measures of the relative densities of the cloud cover on these days and hence, this is merely fortuitous.

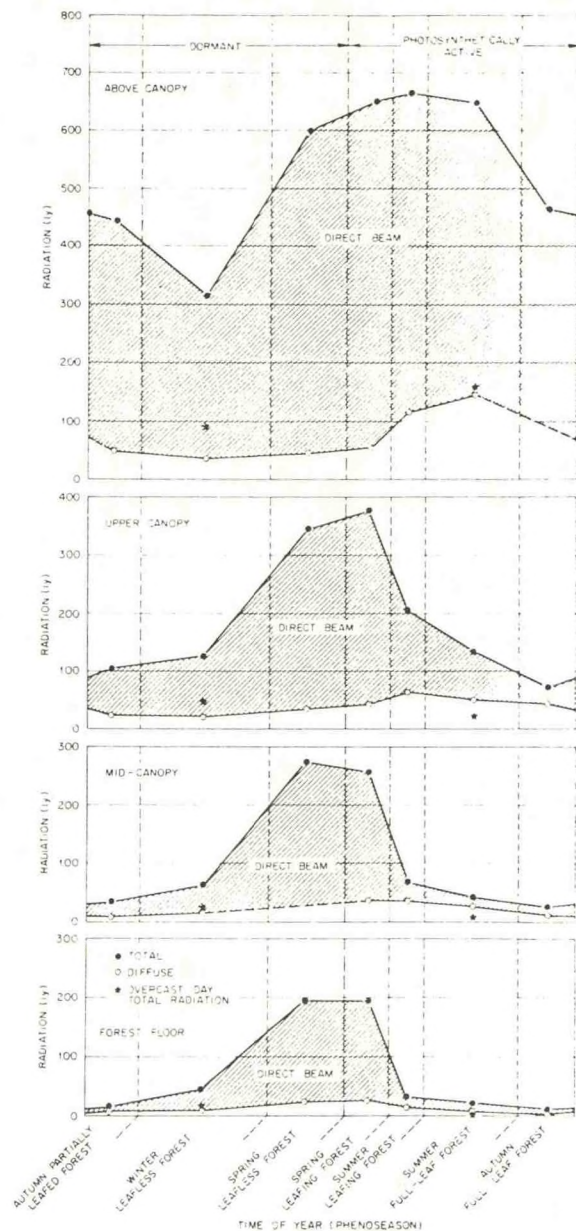


FIG. 21. Annual clear day radiation regimes in and above the *Liriodendron* forest. Starred values are overcast day totals for each of these levels. To convert langleys (ly) to joules per square metre ( $\text{J/m}^2$ ), multiply by  $4.184 \times 10^4$ . ORNL Dwg. 75-1134.

Within the canopy, the seasonal course of total radiation received closely follows that of the radiation incident upon the forest during the winter and early spring. With leaf expansion however, the radiation regimes within the forest change abruptly. Daily total radiation received at the lower two forest levels begins to decrease in the spring leafing phenoseason, while in the upper canopy a continued increase is



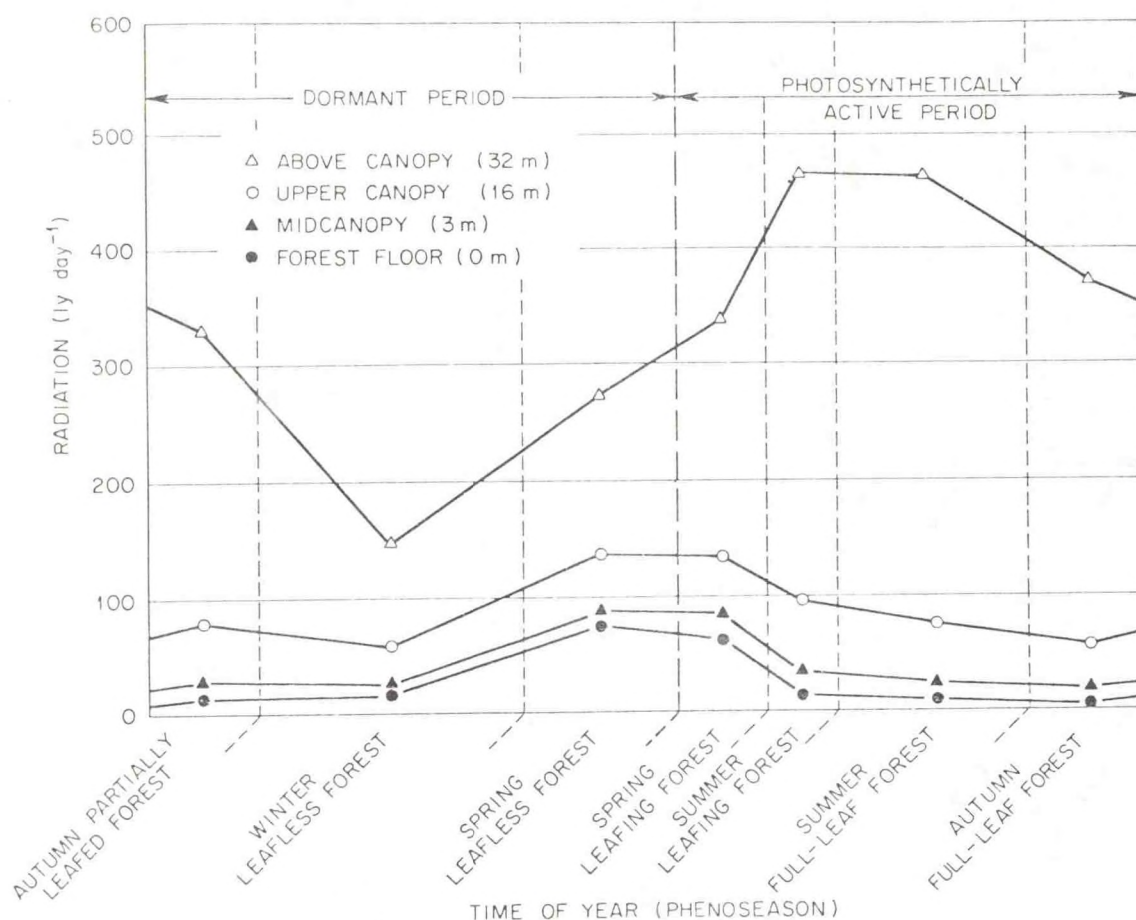


FIG. 22. Approximation of the annual regimes of daily total radiation in and above the *Liriodendron* forest. Langleys  $\times 4.184 \times 10^4 = \text{J/m}^2$ . ORNL Dwg. 75-1133R.

evident. With continued leaf expansion, daily totals drop sharply at all levels in the forest during the summer leafing forest phenoseason despite increasing totals of radiation incident upon the forest. Throughout the summer and early autumn, daily total radiation received within the forest continues to decrease as a result of decreasing incident radiation and lower solar elevations throughout the day. Then with abscission in late autumn, radiation in the forest again increases despite the continued decrease in above-canopy isolation.

Daily totals of diffuse radiation received within the forest on clear days show much less seasonal variation than daily totals of either total or direct beam radiation. Maximum daily totals of diffuse radiation occur in the early summer in the upper canopy and in spring at the lower levels. Minimum diffuse radiation values occur in the autumn fully leafed forest phenoseason at the forest floor, in the autumn partially leafed forest phenoseason at midcanopy, and in winter in the upper canopy. Direct beam radiation

in the forest is maximal through the early spring and minimal in summer and early autumn.

Overcast day totals are reduced in the winter forest and are strongly reduced in the summer fully leafed forest. Because of the leaf cover, overcast summer day totals of radiation in the forest are less than those in the winter leafless forest despite the greater daily total radiation incident upon the forest on the summer overcast day.

While the clear day radiation totals indicate the interactions of changing earth-sun geometry and forest phenology throughout a year, they cannot serve as an approximation of the annual radiation regime in or above the forest because most days are not clear. Using the techniques outlined in the methods section above, we have approximated an annual radiation regime (Fig. 22) in and above this forest using the discontinuous observations of radiation in this forest and the continuous record of solar radiation collected in Oak Ridge, approximately 10 km to the north. The daily totals shown on this figure follow



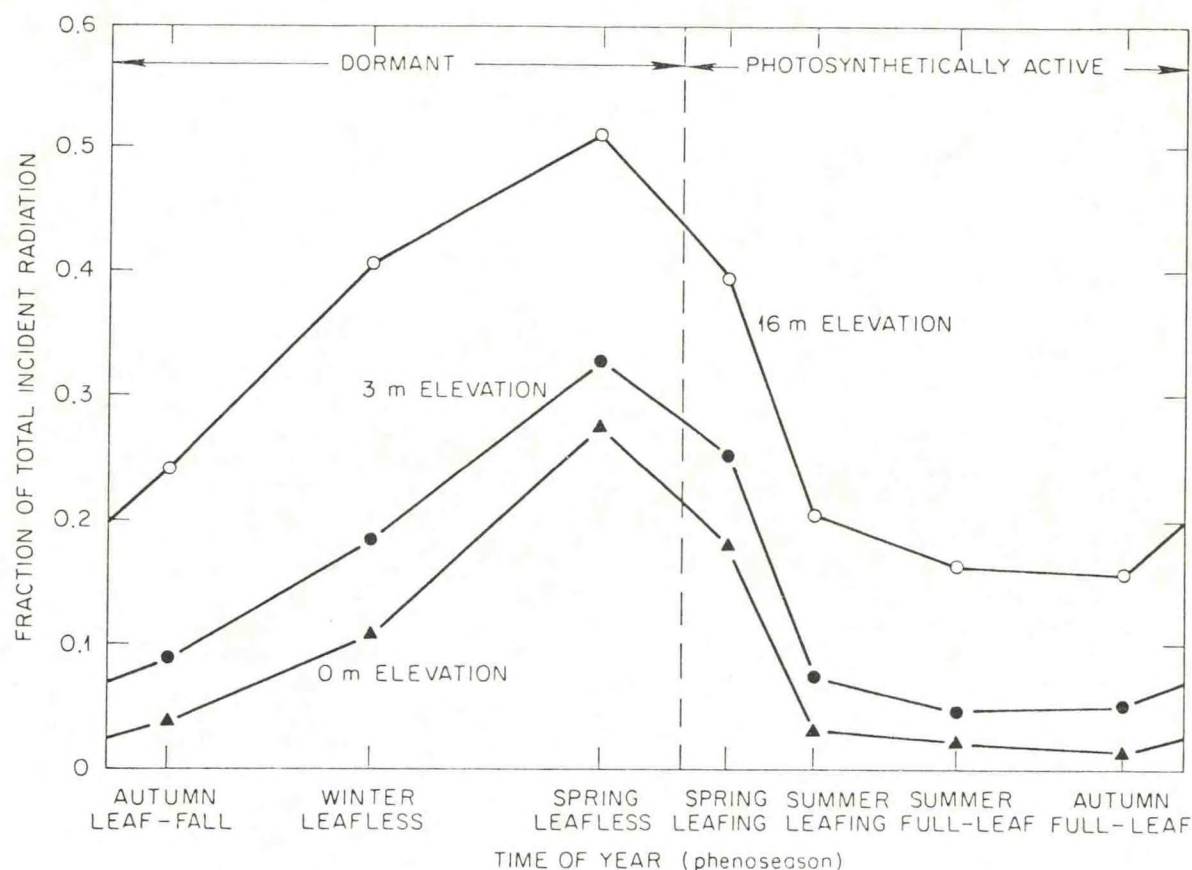


FIG. 23. Derived annual course of average daily fractional penetration in the *Liriodendron* forest. ORNL Dwg. 74-11563.

closely the trends of the clear day data of Fig. 21, but the absolute values are much reduced at all levels in and above the forest. Unlike the clear day totals, maximum average daily totals occur at all levels in the forest during the spring leafless forest phenoseason. The minimum daily totals at all levels occur during the autumn fully leafed forest phenoseason.

Normalizing these daily totals within the forest by that incident upon the forest yields Fig. 23, the annual course of average daily penetration of total radiation in the forest. The interaction between forest phenology and earth-sun geometry is clearly shown on this figure. With increasing solar elevations in the spring, penetration rates increase at all levels in the forest. With the advent of leaf expansion in early April, the penetration rates begin to decline. Then with the stabilization of leaf area, the penetration rates continue to decline, but at very low rates as a result of decreasing solar elevations after the summer solstice. Finally, with leaf abscission in the autumn, these penetration rates again begin to rise as a result of decreased canopy density despite the continued decrease in solar elevations.

From these same data, we approximate the annual incoming radiation budget for this forest in Table 2. Although insolation on the forest during the photosynthetically active portion of the year is over one and one-half times as great as that during the inactive period, less radiation is received within the forest at all levels than in the leafless period because of the presence of leaves. The greatest fraction of the total radiation received within the forest at all levels is received during the spring leafless forest phenoseason. Furthermore, the fraction of the yearly total radiation received during this phenoseason increases with depth to about 45% at the forest floor. Following this phenoseason, these fractions decrease to much lower values in the fully leafed forest phenoseasons. Because of this, the development of the forest floor vegetation peaks during the spring and mostly ceases by summer. Most of the herbaceous plants in this forest complete their annual cycle of growth and reproduction in the spring leafless and leafing forest phenoseasons.

Assuming an exponential attenuation of radiation with depth in the forest and utilizing our knowledge



TABLE 2. Approximation of radiation received within the *Liriodendron* forest throughout the year. To convert langley (ly) to joules per square metre ( $\text{J/m}^2$ ), multiply by  $4.184 \times 10^4$ 

Phenoseason	Duration (days)	Total radiation received (langleys [percent of yearly total])			
		Above (32 m) %	Upper canopy (16 m) %	Midcanopy (3 m) %	Forest floor (0 m) %
Winter leafless	91	13,300 (11.5%)	5,400 (17.5%)	2,400 (16.9%)	1,500 (16.5%)
Spring leafless	55	15,000 (13.0%)	7,600 (24.6%)	4,900 (34.5%)	4,100 (45.0%)
Spring leafing	30	10,200 ( 8.8%)	4,000 (12.9%)	2,500 (17.6%)	1,800 (19.8%)
Summer leafing	26	11,700 (10.1%)	2,400 ( 7.8%)	800 ( 5.6%)	300 ( 3.3%)
Summer full-leaf	67	31,500 (27.2%)	5,100 (16.5%)	1,500 (10.6%)	700 ( 7.7%)
Autumn full-leaf	57	21,100 (18.2%)	3,300 (10.7%)	1,000 ( 7.0%)	200 ( 2.2%)
Autumn partial-leaf	39	12,900 (11.2%)	3,100 (10.0%)	1,100 ( 7.8%)	500 ( 5.5%)
Photosynthetically active period total		74,500 (64.4%)	14,800 (47.9%)	5,800 (40.8%)	3,000 (33.0%)
Dormant period total		41,200 (35.6%)	16,100 (52.1%)	8,400 (59.2%)	6,100 (67.0%)
Yearly total		115,700	30,900	14,200	9,100

of the seasonal and phenological changes occurring, we synthesize these data on the seasonal variation in forest radiation climates in Fig. 24. This figure represents our estimates then, of the annual cycle of radiation regimes in this forest. The penetration of greater amounts of radiation into the leafless forest as solar elevations increase from winter to spring is shown by the height depression of radiation isopleths in spring. With the onset of leaf expansion, this increase is reversed and the isopleths move higher in the forest. After the summer solstice forest structure remains relatively static, and solar elevations slowly decline. With this decline the radiation within the forest declines to the autumn minimum. With leaf abscission in the autumn, radiation isopleths again move slightly deeper into the forest indicating slight increases in radiation received there. With the continued decline in solar elevation after leaf fall is complete, this trend quickly reverses and radiation within the leafless forest declines slightly.

#### SUMMARY AND CONCLUSIONS

The average amount of radiation received at any time within the forest varies directly as the amount of radiation incident at that time. This holds for total radiation and for its direct beam and diffuse components at all times of the year. Only the proportionalities change in time with varying cloudiness, with changing solar elevations, and with phenological changes in forest structure.

Of the two radiative components, direct beam radiation suffers the greatest attenuation by the forest biomass. The penetration of this component is strongly controlled by the interaction of solar elevation and canopy density variation with angular elevation. The greatest attenuation of direct beam radiation occurs in the overstory canopy in all phenoseasons with decreasing attenuation in lower forest strata.

The diffuse component, on the other hand, is less attenuated by the forest biomass and its attenuation is more uniform in the three-canopy strata of the leafless forest than that of the direct beam component. In the fully leafed forest, the greatest amount of attenuation of diffuse radiation occurs in the overstory canopy as well. Because of the differences in the origin of these two radiative components and the structure of the forest, the diffuse component is attenuated less than direct beam radiation in all seasons and phenological phases of the forest.

With the expansion of leaves in spring, attenuation of both direct beam and diffuse radiation increases. Early in the leafing phase, increasing amounts of these components incident on the forest and rising solar elevations offset the increased attenuation by new leaves in the canopy, and absolute quantities of radiation in the forest continue to increase. With continuing leaf expansion, however, attenuation increases and radiation in the forest decreases. After the forest attains full leaf, both diffuse and direct beam radiation continue to decrease within the forest, despite unchanging forest structure. In the overstory canopy, the decrease in direct beam radiation is much greater than the decrease in diffuse as a result of the increasing optical path lengths of direct beam radiation in the forest with the decreasing solar elevations of late summer and early autumn. The decrease in diffuse radiation in the forest results from the decreasing amounts of incident diffuse radiation with time after the summer solstice.

The variability of radiation in horizontal space in the forest is largely the result of the penetration of direct beam radiation. Hence, the degree of spatial variability varies directly as the amounts of direct beam radiation penetrating the forest canopy throughout the year. Because of the apparent movement of the sun across the sky each day, the sunflecks resulting from the penetration of direct beam radiation



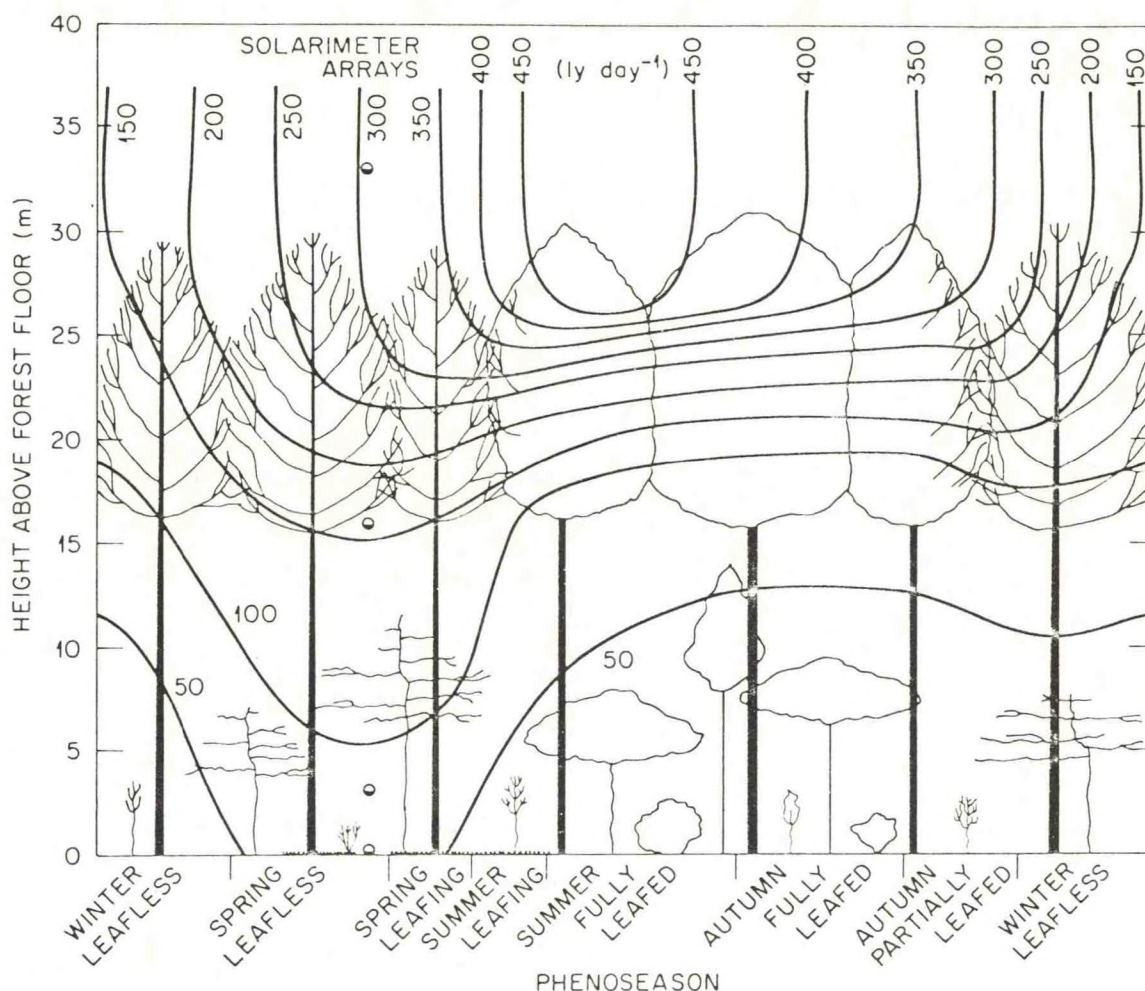


FIG. 24. Synthesized annual course of average daily total solar radiation received within and above a tulip poplar forest. Langleys  $\times 4.184 \times 10^4 = \text{J/m}^2$ . ORNL Dwg. 76-7581.

move across surfaces in the forest, introducing temporal variation as well. Thus, a direct relationship exists between direct beam radiation penetration and temporal variation in daily forest radiation regimes.

Variation in both space and time decreases with depth in the forest. Space variation in the upper canopy greatly exceeds the  $\pm 10\text{-mly/min}$  [ $\approx 418 \text{ J} \cdot \text{m}^{-2} \cdot \text{min}^{-1}$ ] accuracy desirable for energy budget considerations. This implies that more than 12 replications of measurements would be needed in all phenoseasons in the upper canopy to attain this level of precision. Even at the forest floor in the summer fully leafed forest where variation of radiation in horizontal space is generally quite low, our 12 replicated measurements yield variabilities in excess of this level around solar noon. Thus, numbers of replications of measurements needed to attain specific levels of precision vary in vertical space and through time.

In winter, the proportion of radiation penetrating the forest is increased with cloud cover, although absolute values decrease because of lower amounts of incident radiation. Despite the increased penetration of radiation from overcast skies, clear winter day diffuse penetration exceeds that of overcast winter days, indicating that the enrichment of diffuse radiation by reflected direct beam radiation is significant in the winter forest, or that differences in sky brightness distributions between clear and cloudy days effect significant differences in amounts of diffuse radiation penetrating the forest. In summer, the proportion of incident radiation penetrating the forest decreases with increasing cloudiness in contrast to results from other studies reported in the literature. We attribute this difference to a rather different forest structure than has been studied in the past. Our mesic, lower latitude, temperate, deciduous forest, when fully leafed, has greatest amounts of opening at



mid-elevation angles rather than at the zenith. As far as we are able to determine, the previously studied forests had minimal density at the zenith which interacts with overcast sky brightness distributions to allow greater penetration of radiation on overcast days.

As in winter, the summer overcast day penetration rates of total radiation are substantially less than those of the summer clear day diffuse radiation, indicating again the importance of direct beam enrichment of diffuse radiation in the forest on clear to partly cloudy days.

The amount of direct beam radiation that penetrates the forest strongly controls the distribution of radiant flux densities in space and in time within the forest. Maximum amounts of direct beam radiation penetrate this forest in the early spring and, as a result, a substantial portion of the radiation received in the forest arrives at high flux densities. As the leaves expand later in the spring and in early summer, the penetration of direct beam radiation is severely reduced within the forest. This in turn causes a major reduction in the amount of higher flux density radiation within the forest. After the forest attains full leaf, very little radiation is present at any level in the forest at flux densities exceeding 200 mly/min, despite incident flux densities as high as 1,500 mly/min [ $= 62.76 \text{ kJ} \cdot \text{m}^{-2} \cdot \text{min}^{-1}$ ]. With decreasing solar elevations after the summer solstice, further reductions in the penetration of high flux density radiation occur. Then with leaf abscission, slight increases in direct beam penetration effect the penetration of radiation at higher flux densities once again. With the decreasing solar elevations of autumn and early winter, these increases are soon eliminated and the amount of high flux density radiation within the forest decreases from autumn to winter.

Greatest amounts of radiation are received within the forest in the spring before leaf expansion begins. The least radiation is received with the lower solar elevations and shorter day lengths of early autumn while the forest is still fully leafed. With leaf fall later in the autumn, radiation in the forest increases slightly but then decreases again with the winter decline of insolation.

#### ACKNOWLEDGMENTS

The collection and analyses of these data were greatly aided by the assistance of Mike Breed, Mark Hanon, and Vada Maxey, Oak Ridge Associated Universities Summer Trainees; Karen Jamroz and Barbara Rooney, Work-Study Program, University of Tennessee; and Eugene Culver and Jerry Sharp, ATDL. Computer programming for data display by R. T. McMillen, ATDL is hereby acknowledged. Reviews by W. T. Hinds, Battelle Northwest Laboratories, Hanford Reactor Site, Richland, Washington; C. E. Murphy, Jr., Environmental Transport Division, Savannah River Laboratory, Aiken, South Carolina; and S. B. McLaughlin and R. S. Strand, En-

vironmental Sciences Division, ORNL, resulted in significant improvements in this paper. Comments and criticisms of the anonymous Ecological Society referees were of great benefit to the authors and resulted in increased clarity and readability of this report.

This research supported in part by the Eastern Deciduous Forest Biome, US-IBP, funded by the National Science Foundation under Interagency Agreement AG-199, BMS 76-00761 with the U.S. Energy Research and Development Agency, Oak Ridge National Laboratory and in part by the Division of Biomedical and Environmental Research, ERDA, Contribution No. 290, Eastern Deciduous Forest Biome, US-IBP, ATDL Contribution No. 75-18.

#### LITERATURE CITED

- Anderson, M. C. 1964a. Studies of the woodland light climate. 1. The photographic computation of light conditions. *J. Ecology* 52:27-41.
- . 1964b. Studies of the woodland light climate II. Seasonal variation in light climate. *J. Ecology* 52: 643-663.
- . 1964c. Light relations of terrestrial plant communities and their measurements. *Biol. Rev.* 39:425-486.
- Anderson, M. C., and O. T. Denmead. 1969. Short wave radiation on inclined surfaces in model plant communities. *Agron. J.* 61:867-872.
- Brecheen, K. G. 1951. Transmission of shortwave radiation through forest canopy. *Coop. Snow Invest., Corps of Eng., U.S. Army Res. Note SPDGC 627-51*, 18 p.
- Dinger, B. E. 1971. Net photosynthesis and production of *Liriodendron tulipifera* as estimated from carbon dioxide exchange. US-IBP Eastern Deciduous Forest Biome Memo Rpt. No. 71-75, 8 p.
- Dinger, B. E., C. J. Richardson, and R. K. McConathy. 1972. Dynamics of canopy leaf area development and chlorophyll phenology in yellow poplar. US-IBP Eastern Deciduous Forest Biome Memo Rpt. No. 72-164, 15 p.
- Dorno, C. 1919. *Physik der Sonnen-und Himmelstrahlung*. Vieweg, Braunschweig, Germany.
- Drummond, A. J. 1956. On the measurement of sky radiation. *Arch. Meteorol. Geophys. Bioklimatol. Ser. B*, 7:413-436.
- Fritz, S. 1958. Transmission of solar energy through the earth's clear and cloudy atmosphere, p. 17-36. *In* E. F. Carpenter [ed.] *Trans. of the conf. on the use of solar energy: The scientific basis*. Univ. Ariz. Press, Tucson, Vol. 1.
- Gay, L. W., K. R. Knoerr, and M. O. Braaten. 1971. Solar radiation variability in the floor of a pine plantation. *Agric. Meteorol.* 3:39-50.
- Horn, H. W. 1971. *The adaptive geometry of trees*. Princeton Univ. Press, Princeton, N.J., 144 p.
- Horowitz, J. L. 1969. An easily constructed shadow-band for separating direct and diffuse radiation. *Sol. Energy* 12:543-545.
- Hutchison, B. A. 1971. Spatial and temporal variation in the distribution and partitioning of solar energy in a deciduous forest ecosystem. US-IBP Eastern Deciduous Forest Biome Memo Rpt. No. 71-82, 40 p.
- Hutchison, B. A., and D. R. Matt. 1973. Distribution of solar radiation within a deciduous forest. *Eastern Decid. Forest Biome Memo Rpt. No. 72-170*, 26 p.
- Hutchison, B. A., and D. R. Matt. 1976. Beam en-

- richment of diffuse radiation in a deciduous forest. *Agric. Meteorol.* **17**:93-110.
- Kimball, H. H., and I. F. Hand. 1921. Sky brightness and daylight illumination measurements. *Am. Illum. Eng. Soc. Trans.* **16**:235-275.
- Matt, D. R., and B. A. Hutchison. 1974. Response of Lintronic Dome Solarimeters to varying solar radiation flux densities. US-IBP Eastern Deciduous Forest Biome Memo Rpt. No. 74-1, 8 p.
- Miller, E. E., and J. M. Norman. 1971. A sunfleck theory for plant canopies. II. Penumbra effect: Intensity distributions along sunfleck segments. *Agron. J.* **63**:739-743.
- Monteith, J. L. 1959. Solarimeter for field use. *J. Sci. Inst.* **36**:341-346.
- Moon, P., and D. E. Spencer. 1942. Illumination from a non-uniform sky. *Illum. Eng.* **37**:707-726.
- Niilisk, H., T. Nilson, and J. Ross. 1970. Radiation in plant canopies and its measurement, p. 165-177. *In* Prediction and measurement of photosynthetic productivity. Proc. of the IBP/PP Technical Meeting, Trebon, Czech. Center for Agricultural Publishing and Documentation, Wageningen, Netherlands.
- Norman, J. M., E. E. Miller, and C. B. Tanner. 1971. Light intensity and sunfleck-size distributions in plant canopies. *Agron. J.* **63**:743-748.
- Ovington, J. D., and H. A. I. Madgwick. 1955. Comparison of light in different woodlands. *Forestry* **28**: 141-146.
- Pokrowski, G. I. 1929. Über die Helligkeitsverteilung am Himmel. *Phys. Z.* **30**:697-700.
- Ramann, E. 1911. Lichtmessungen in Fichtenbestände. *Allg. Forst. Jagdztg.* **87**:401-406.
- Reifsnnyder, W. E., G. M. Furnival, and J. L. Horowitz. 1971. Spatial and temporal distribution of solar radiation beneath forest canopies. *Agric. Meteorol.* **9**: 21-37.
- Salisbury, E. J. 1916. The oak-hornbeam woods of Hertfordshire, Parts I & II. *J. Ecology* **4**:83-117.
- Schomaker, C. E. 1968. Solar radiation measurements under a spruce and a birch canopy during May and June. *For. Sci.* **14**:31-38.
- Taylor, F. G. 1974. Phenodynamics of production in a mesic deciduous forest, p. 237-254. *In* H. Lieth [ed.] Phenology and seasonality modeling. Springer-Verlag, New York.
- Tsel'Niker, Y. L. 1968. Distribution of photosynthetically active radiation in the open and in the forest under various weather conditions, p. 33-337. *In* V. K. Pyldmaa [ed.] Actinometry and atmospheric optics. Translated from Russian by Israel Program for Scientific Translations, TT 70-505159, Vol. 8.
- Verhagen, A. M. W., J. H. Wilson, and E. J. Britten. 1963. Plant production in relation to foliage illumination. *Ann. Bot. (New Series)* **27**:627-640.





Effects of Atmospheric Parameters on the  
Concentration of Photochemical Air Pollutants

F. A. Gifford  
Steven R. Hanna

Atmospheric Turbulence and Diffusion Laboratory  
National Oceanic and Atmospheric Administration  
Oak Ridge, Tennessee

October, 1976

(Discussion of the paper by Liu, Whitney, and Roth; JAM, 15, August  
1976, 829-35)

ATDL Contribution File No. 76/17

In the paper, "Effects of atmospheric parameters on the concentration of photochemical air pollutants," M. K. Liu, D. C. Whitney, and P. M. Roth (JAM, 15, Aug. 1976, 829-35) describe the results of a sensitivity analysis of a detailed numerical urban air pollution model, applied to the Los Angeles basin on September 29, 1969, a typical smoggy day. The authors emphasize that this numerical model's output can simulate concentration distributions in the real atmosphere, and offer the computational approach as a possible alternative to laboratory and field air pollution studies on account of its lower cost and convenience. They go on to describe many aspects of the "effects of atmospheric parameters on the distribution of photochemical air pollution," based on these numerical modeling results.

What isn't obvious from a casual reading of the paper is that none of the numerical results of the sensitivity analysis has been compared with observed atmospheric data. From the title to the conclusions the authors consistently refer to the model behavior as if it were that of the atmosphere. For example, they state that "the present study sought to assess the response of atmospheric pollutant concentrations to variations in environmental parameters." They further state that "The following paragraphs discuss the response of atmospheric pollutant concentrations to variations in wind speed, vertical diffusivity, mixing depth, radiation intensity and emission rate." Commenting on the model response to assumed percentage step changes

in the average wind over the L. A. basin they state the following.

"The resultant hourly averaged surface concentrations were then compared with those of the base case and average deviations for CO, NO, O<sub>3</sub> and NO<sub>2</sub> were plotted . . . The changes reach their peaks generally about early afternoon. Since the atmosphere serves as an efficient reservoir of pollutants, the response of the model to changes in wind speed cannot be immediate because of the large amount of pollutants initially present in the airshed." They also compare the model response with that of a simple box model and conclude that "the simple box model tends to overpredict." It isn't evident from the text that these and many similar statements all refer to the behavior of the numerical model, not to that of the real atmosphere.

It seems unlikely on simple, intuitive grounds that certain of the model changes computed by the authors can possibly represent real atmospheric changes. Consider their estimate that, as CO emissions vary by 15%, CO concentrations vary by 5%. It is physically obvious that L. A. basin-averaged concentration of a nearly inert pollutant such as CO must be proportional to emissions, once a steady state is reached, in the absence of advection from upwind (background). This property, i.e. mass continuity, is fundamental to air pollution modeling. This being the case it is of interest to compare the observed values of many of the meteorological variables and pollutant concentrations that are available for the L. A. basin for this date with the modeling results.



In Table I we have assembled hourly observed values, averaged over the Los Angeles basin, for the period 0530 to 1630 PST, September 29, 1969, of: windspeed, CO concentration, and the percentage departure of these from their average values over the time period. These observed data are of course not strictly comparable with the output of the modeling exercise. In the sensitivity analysis parameters are varied singly, to determine their separate influence on model output. In the real atmosphere, on the other hand, parameters always vary jointly. A change in wind speed is usually accompanied by one in mixing depth, and so on. Strictly speaking, the changes determined by the sensitivity analysis can never be realized in the atmosphere. However these actual observations are of great interest in view of Liu, Whitney, and Roth's stated goal, which was "to assess the response of atmospheric pollutant concentrations to variations in environmental parameters."

Table I shows that the L. A. basin-averaged wind speed did in this case increase abruptly, by about 100% near the middle of the day. According to one of the main conclusions by Liu, Whitney, and Roth, this wind change should have resulted in a slow decrease in basin-wide average CO concentration, reaching a considerably smaller maximum percentage change. This should have occurred at a time perhaps several hours after the last given observation, no sooner, judging by the curves presented by these authors.

On the contrary, for this particular day, which is the day that provided the meteorological and source-term driving inputs to the authors' model for the sensitivity analysis, the observed L. A. basin-wide average CO concentration did not respond slowly to an abrupt, marked change in the L. A. basin-averaged observed wind speed. It responded rather quickly. Furthermore the observed percentage concentration change in CO was large, not small. Wind speed varied by a factor of 3 during the test period and so, inversely, did CO concentration. Consequently the prediction of a simple urban pollution model such as a box model is, in this case, essentially correct.

To test whether September 29, 1969 was in some way unusual or anomalous, and hence the possibility that the changes shown in Table I are not generally representative, averaged L. A. basin hourly winds and CO concentrations were also examined for 5 additional days. All these days have been studied intensively in Los Angeles air pollution research and the data are readily available. Table II lists values for each hour of CO and wind speed, averaged over all the Los Angeles basin CO monitoring stations and over 9 wind speed stations. Afternoon CO minima and the relevant wind speed maxima are indicated by parentheses, and these form the basis for Table III, which summarizes the times of average and extreme values of L. A. basin-averaged wind speeds and CO concentrations, and the maximum percentage changes of

each relative to their mean values for the day.

These results fully support the conclusions from Table I. The times of maximum wind speed and minimum CO concentration on each day are virtually the same, and the times the average values were reached are fairly close. Consequently the response of the observed CO concentration to wind speed changes over the L. A. basin is prompt, not gradual. The observed percentage CO concentration changes are large in terms of the percentage wind changes.

Of course, for the reason given above, real atmospheric behavior never can be replicated in a model by varying only one parameter in isolation. This should not have been expected nor, for that matter, implied. It is interesting to see if the authors' model can correctly account for L. A. basin-wide CO changes on the same test date if time changes in the other driving parameters, i.e. source strength, solar radiation, mixing depth, etc., are included together with the wind speed changes. Calculated CO concentration values on September 29, 1969, for L. A. basin pollution monitoring stations were included in the comprehensive report by Reynolds, Liu, Hecht, Roth, and Seinfeld (1973). If these are averaged by hour over L. A. basin stations, and the resulting averages correlated with the observed values of Table I, the correlation coefficient is,  $r = 0.65$ . If the observed C-values are correlated with observed basin-wide average values of  $1/u$  for the same period, the result is,  $r = 0.64$ . Thus a simple reciprocal wind speed accounts, in this case, for essentially the same amount of the observed CO-variation as does the authors' model. If a simple diurnal stability



factor is also included, this correlation increases to  $r = 0.74$ , as reported by Gifford (1974).

This research was performed under an agreement between the National Oceanic and Atmospheric Administration and the Energy Research and Development Administration.

#### References

- Reynolds, S. D., M. K. Liu, T. A. Hecht, P. M. Roth, and J. H. Seinfeld, 1973: Urban air shed photochemical simulation model study. U. S. Env. Prot. Agency Report EPA-R4-73-030a.
- Gifford, F. A., 1974: Further comparison of urban air pollution models. In Proc. 5th Meeting of the Expert Panel on Air Pollution Modeling, NATO/CCMS Report No. 35.

Table I

Observed Wind Speed, U, and CO Concentration, C, for  
29 September 1969, Averaged Over the Los Angeles Basin  
for the Time Period 0530-1630 PST

Time (hour)	U(mph)	C(ppm)	$(\Delta U/U) \times 100^*$	$(\Delta C/C) \times 100^*$
5	3.1	6.8	-22 %	-12 %
6	3.3	7.8	-18	6
7	2.9	10.1	-29	31
8	2.2	14.2	-46	85
9	2.1	13.1	-49	71
10	2.0	9.2	-50	19
11	1.9	6.3	-55	-18
12	4.4	6.0	9	-22
13	5.9	5.2	46	-32
14	6.2	4.6	53	-40
15	6.8	4.2	66	-45
16	7.9	4.8	97	-38
Average	4.0	7.7		

\*Percentage departure from average value over the entire period.

Table II

Observed Wind Speeds and CO Concentrations for 5 additional days,  
Averaged over the Los Angeles Basin\*

Hour	9-11-69		9-30-69		10-29-69		10-30-69		11-4-69	
	CO ppm	U mph	CO ppm	U mph	CO ppm	U mph	CO ppm	U mph	CO ppm	U mph
1	5.3	2.3	8.9	1.3	12.6	1.3	12.7	2.6	12.4	1.4
2	5.1	2.0	8.3	1.6	9.4	1.8	11.3	2.2	11.7	1.6
3	5.4	1.5	7.8	1.5	7.8	1.3	9.9	2.2	10.4	1.4
4	5.6	1.4	7.7	1.7	6.9	1.6	7.9	2.7	10.4	1.4
5	6.2	1.8	7.8	1.6	6.8	1.7	7.1	2.7	8.6	2.1
6	7.0	1.4	10.1	1.3	7.3	1.9	7.9	3.0	8.4	1.8
7	8.2	1.4	15.7	1.3	8.6	1.9	11.3	2.6	11.0	1.7
8	9.6	2.0	16.6	1.4	11.9	2.0	14.7	2.7	13.9	1.6
9	9.6	2.1	13.3	1.6	11.9	<u>2.9</u>	13.0	2.7	14.7	1.6
10	8.9	2.4	8.6	<u>3.0</u>	<u>9.9</u>	3.4	<u>8.9</u>	2.5	10.7	<u>3.0</u>
11	8.3	<u>2.3</u>	7.9	3.4	8.1	4.2	5.4	2.6	<u>7.8</u>	3.2
12	<u>7.5</u>	4.4	<u>8.0</u>	4.7	7.8	4.8	4.4	<u>3.1</u>	6.4	3.2
13	7.6	5.2	5.7	5.6	6.4	5.0	4.3	4.2	7.7	4.7
14	7.6	4.7	5.3	6.8	6.0	5.2	(4.0)	5.1	6.2	4.7
15	5.4	5.1	(4.6)	(9.2)	(5.5)	5.3	4.2	(6.6)	5.9	4.7
16	6.5	5.3	5.4	6.9	5.7	(5.5)	5.3	5.8	(5.2)	5.3
17	6.3	5.3	5.7	5.1	8.2	4.7	7.6	5.3	6.3	(5.8)
18	(5.4)	(5.6)	5.1	4.1	11.1	3.6	11.3	4.6	7.3	4.6
19	5.9	4.7	5.4	2.9	13.4	3.1	13.2	2.7	6.6	3.9
20	6.3	3.4	6.6	2.0	18.2	2.1	16.1	2.7	7.0	3.0
21	6.9	2.9	8.0	1.9	17.3	2.2	17.0	2.5	7.2	2.0
22	6.9	2.2	8.4	1.9	16.4	2.7	18.3	1.9	6.2	2.0
23	7.7	2.0	8.3	1.9	16.3	2.8	19.7	2.3	4.6	1.7
24	7.8	1.6	8.3	2.0	15.3	2.7	17.3	2.6	4.1	2.3
	<u>7.0</u>	<u>3.0</u>	<u>8.2</u>	<u>3.1</u>	<u>10.4</u>	<u>3.1</u>	<u>10.5</u>	<u>3.2</u>	<u>8.4</u>	<u>2.9</u>

(\*Afternoon wind-speed maximum and CO minimum values are indicated by parentheses.  
The approximate times at which the average values of these quantities were  
attained previous to these extremes are indicated by horizontal bars.)



Table III

Times of Maximum U, Minimum C, Average U, and Average C, from Table II; observed maximum percentage changes of U and C relative to their averages.

Date	Time, PST				U equals its average	C equals its average	$\left(\frac{\Delta U_{\max}}{\bar{U}}\right) \times 100$	$\left(\frac{\Delta C_{\min}}{\bar{C}}\right) \times 100$
	Of max. U	Of min. C	U equals its average	C equals its average				
9-11	18	18	11	12			+ 86%	-23%
9-29	16	15	12	11			+100%	-46%
9-30	15	15	10	12			+195%	-43%
10-29	16	15	9	10			+ 80%	-45%
10-30	15	14	12	10			+100%	-62%
11-04	17	16	10	11			+100%	-38%
Avg.	16.2	15.5	10.7	11.0			+110%	-43%

Daily Observations of Visible Plume Length at TVA's  
Paradise Cooling Towers

by

Steven R. Hanna and Martin Pike\*

Air Resources Atmospheric Turbulence and Diffusion Laboratory  
Oak Ridge, Tennessee

Abstract

Observations of visible plume length taken each morning at TVA's Paradise Steam Plant cooling towers show only a slight correlation with ambient saturation deficit and wind speed, and very little dependence on season or weather type. Average visible plume height and length are 270 m and 360 m, respectively, with standard deviations of 120 m and 380 m.

\*Oak Ridge Associated Universities Summer Trainee, Union College,  
Schenectady, New York.

ATDL Contribution File No. 76/18.

## 1. Introduction

A predicted climatology of visible cooling tower plume lengths was recently prepared by applying a plume and cloud growth model developed by Hanna (1976) to radiosonde observations during one year at Nashville. The predictions are summarized by Gifford, Hanna, and Hosker (1976). In an attempt to find data to verify the model predictions, we contacted TVA, knowing of their published summaries of cooling tower studies at the Paradise Steam Plant (e.g., Slawson et.al., 1974). The Paradise plant is only about 100 miles from Nashville. It was hoped to use the TVA observations to develop a climatology of visible plume lengths, with weather types broken into five classes: clear, fog, precipitation, clouds>20,000 ft (no precip.), 20,000 ft>clouds>10,000 ft (no precip.), and clouds<10,000 ft (no precip.).

## 2. The Data

J. Coleman of TVA's Air Quality Branch sent us about four linear feet of notebooks containing raw data from the Paradise Cooling Tower Observation Program. Because of personnel shortages, they had been unable to analyze these data, which consist of notes taken by observers each morning of the year for three years. In some cases temperature soundings were taken and pilot balloon wind observations were made. But in most cases only surface temperatures and winds are available. Photographs sometimes supplement the subjective estimates of visible plume lengths. One serious omission is that the observers neglected to note whether precipitation was falling.



There are three natural draft cooling towers at the fossil-powered Paradise Steam Plant. Two service generators of about 700 MWe each and the third services a generator of about 1100 MW. The towers are spaced in a line about 200 m apart.

From each daily observation sheet, the following information was extracted:

Date and observation time

Units operating and their power outputs

Whether or not a photograph, pilot balloon data, and temperature profiles were available

Visible plume direction, length, and angle from vertical

Height of top and base of visible plume

Dry and wet bulb temperature at the surface

Cloud cover: Percent, type, and base height.

There were a few missing days during each year, but we could determine no pattern to them. Rather than analyze all three years, we chose 1974 for detailed analysis. That year seemed to have the most complete set of observations and photographs. There were 193 days used in the analysis. The observed data were used to calculate ambient saturation deficits and categorize the day into one of the five basic weather classes.

### 3. Results

Graphs were constructed in which the visible plume height, length, and resultant length were plotted against saturation deficit, wind speed, the ratio of saturation deficit to wind speed,

and the product of saturation deficit and wind speed. The resultant length is the hypotenuse of the triangle whose sides are the height and the length. There is much scatter in these graphs. Correlations are summarized in Table 1. It is seen that the average saturation deficit and wind speed are 4.9 g/kg and 1.4 m/s. The average visible plume height, length, and resultant length are 270 m, 360 m, and 470 m, respectively. Correlations in all cases have a magnitude less than .28, implying that less than 10% of the variance in, say, visible plume length is accounted for by any of the ambient variables. It is expected that the time at which the observations were taken did not help the correlations, for ambient conditions at plume height are likely to differ quite a bit from ambient conditions at the surface at 8 or 9 a.m. For example, natural fog may occur at the surface, while the relative humidity may be 50% at plume height. The correlations would improve if observations were taken in the afternoon, when the ambient atmosphere is well mixed.

In Figures 1 through 4, some of the data used in Table 1 are plotted. Rather than plot all 193 points, the average of groups of 5 to 10 points are plotted. For the cases indicated by circles, all the data are included, and for the cases indicated by diamonds, the upper and lower extremes have been removed. Of the four graphs, Figures 3 and 4 are the only ones that show a definite relationship between the visible plume parameter and the ambient meteorological parameter.

Table 1

Correlations between Visible Plume Length and Ambient Variables -  
Paradise 1974 Data

x	y	$\bar{x}$	$\sigma_x$	$\bar{y}$	$\sigma_y$	$R_{xy}$
Visible Height(m)	Sat. Def.(g/m <sup>3</sup> )	267	124	4.94	3.47	-.14
	Wind Speed(m/s)			1.44	1.19	-.27
	W.S.*S.D.			7.09	9.03	-.27
	W.S./S.D.			0.95	2.77	-.06
Visible Length(m)	Sat. Def.(g/m <sup>3</sup> )	355	383	4.94	3.47	-.28
	Wind Speed(m/s)			1.44	1.19	-.09
	W.S.*S.D.			7.09	9.03	-.23
	W.S./S.D.			0.95	2.77	+.04
Resultant Length(m)	Sat. Def.(g/m <sup>3</sup> )	466	378	4.94	3.47	-.28
	Wind Speed(m/s)			1.44	1.19	-.13
	W.S.*S.D.			7.09	9.03	-.26
	W.S./S.D.			0.95	2.77	+.02



The variation of visible plume length and height by season is given in Table 2. The visible plume length is more than twice as great in the winter and fall than it is during the spring and summer. The saturation deficit is lower during the cold months, resulting in longer plumes.

Table 2

Seasonal Variation of Visible Plume

Season	Average Visible Plume Height	Average Visible Plume Length
Winter	340m	580m
Spring	250m	200m
Summer	260m	330m
Fall	310m	550m

The data were also broken up according to the five weather classes, but no significant variation could be seen in the visible plume parameters. Similarly, the visible plume parameters were not dependent on the number of cooling towers operating. (Of course assuming that at least one was operating.) Due to the lack of dependence of the observed plume on the observed meteorological conditions, no detailed studies were made.

#### 4. Recommendations for Further Studies

The results of this study indicate the drawbacks of limited experiments which do not have careful supervision. A major problem with the data is that there is no indication of whether precipitation

is falling. This simple observation should be included in future experiments. Another major problem is that the meteorological observations were not made at plume level. This would be less of a problem if the observations were taken during the afternoon, when the atmosphere is well-mixed. However, these data were all taken during the morning, when strong vertical gradients of temperature, wind speed, and relative humidity occur. Consequently the atmosphere could be saturated at instrument level but dry at plume level. The resulting correlations between visible plume length and saturation deficit or wind speed is not good.

The following recommendations can be made:

- i. Observe precipitation.
- ii. If using ground level meteorological observations, limit the experimental periods to the afternoon.
- iii. If morning observations are necessary, obtain vertical profiles of temperature, dew point, and wind speed to heights above the plume height.

## 5. Acknowledgements

The cooperation of Jesse Coleman and his staff of the Air Quality Branch of the Tennessee Valley Authority is greatly appreciated.

## REFERENCES

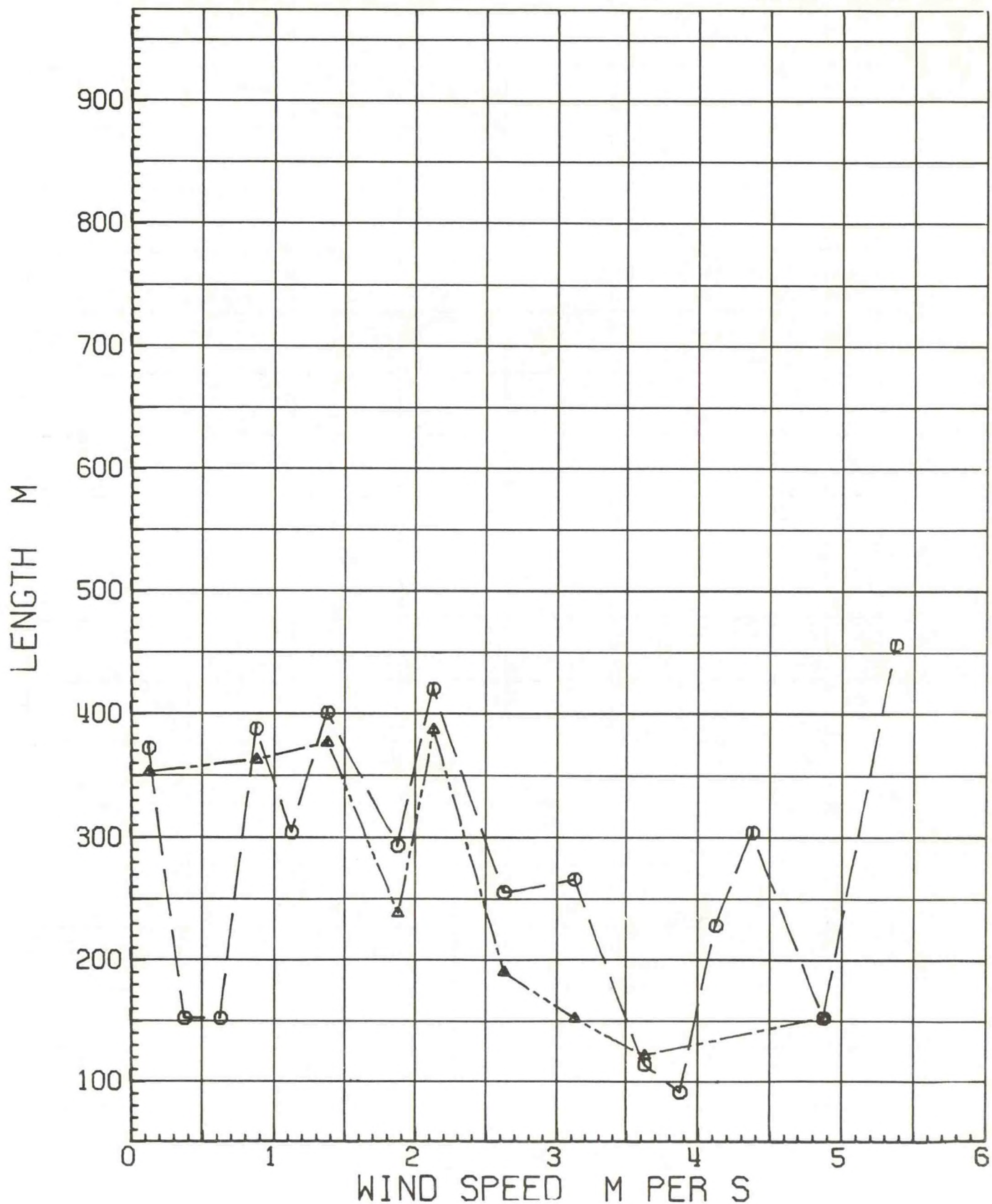
- Gifford, F. A.; S. R. Hanna; and R. P. Hosker; 1976: First Annual Report on Weather Modification Effects of Cooling Towers. ATDL Report 76/11, ATDL, P.O. Box E, Oak Ridge, Tn. 37830, 61 pp.
- Hanna, S. R., 1976: Predicted and observed cooling tower plume rise and visible plume length at the John E. Amos power plant. To be published in Atmos. Environ.
- Slawson, P. R.; J. H. Coleman; and J. W. Frey; 1974: Some observations on cooling tower plume behavior at the Paradise Steam Plant. Cooling Tower Environment-1974, ERDA Symposium Series, CONF 740302, Nat. Tech. Info. Service, U.S. Dept. Com., Springfield, Va. 22161, 147-160.



$r = -.09$

Figure 1.      Circles: All data, groups of 5 to 10.  
                 Triangles: Extremes removed from each group.

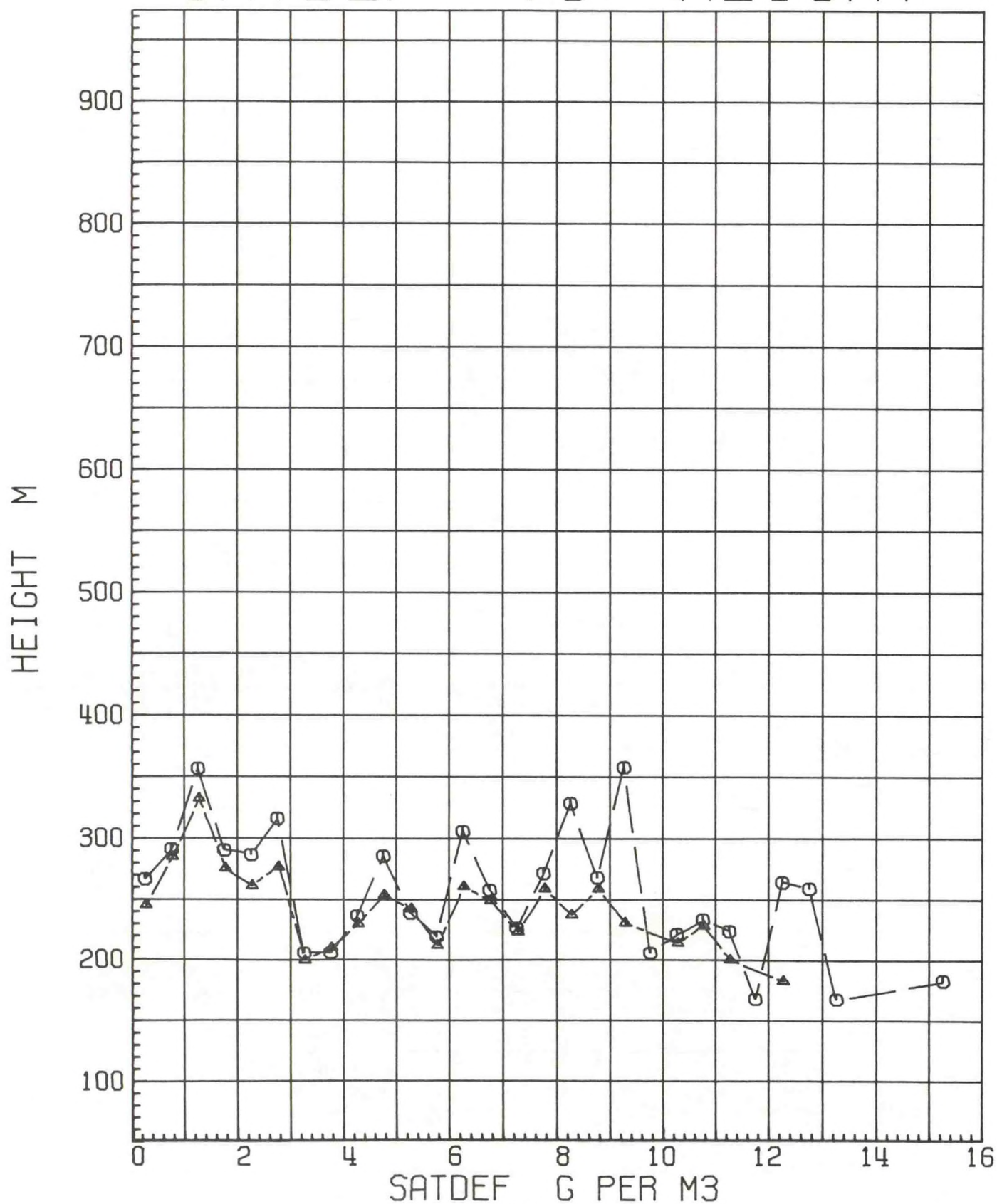
# WIND SPEED VS LENGTH



$r = -.14$

Figure 2. Circles: All data, groups of 5 to 10.  
Triangles: Extremes removed from each group.

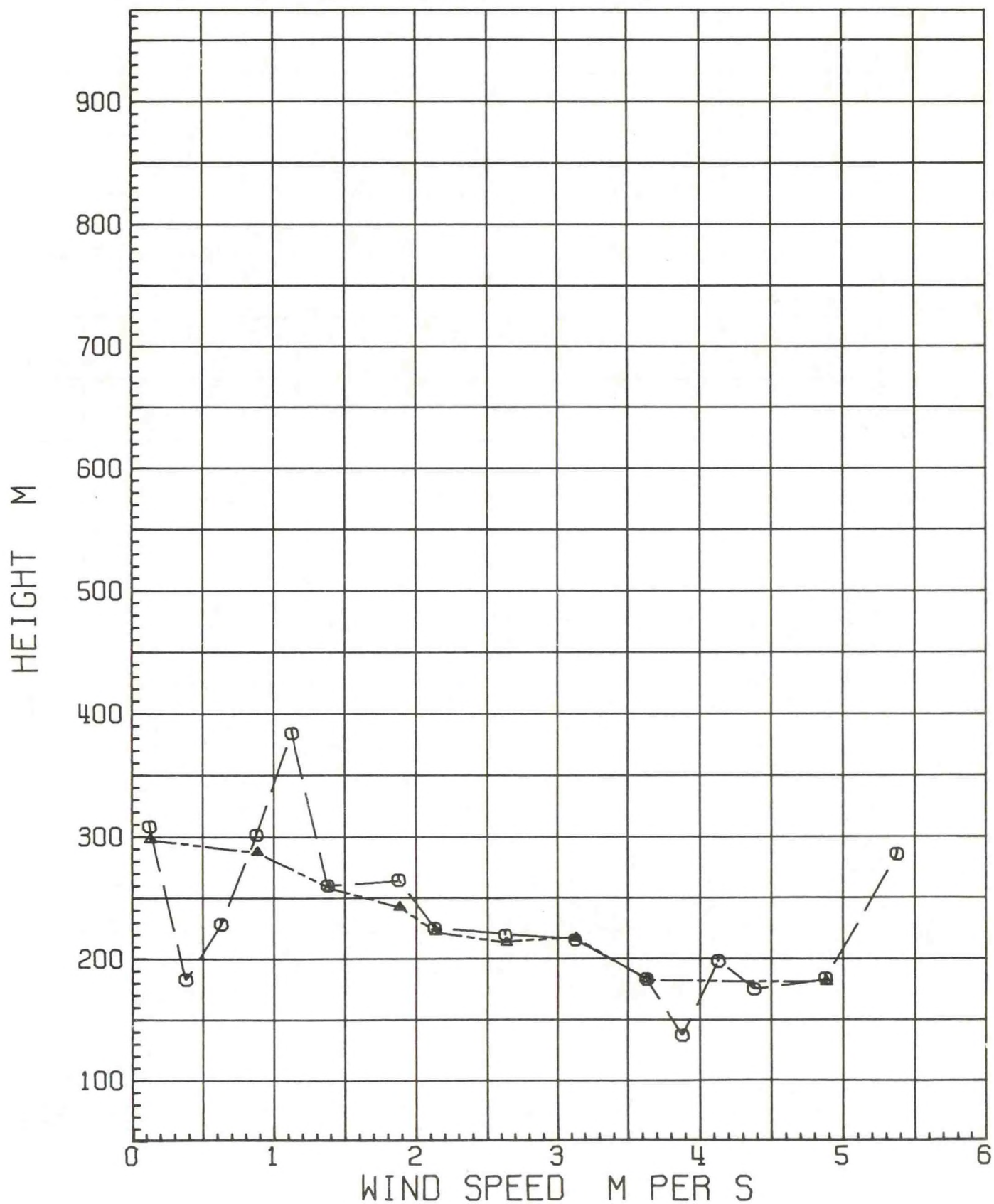
# SATDEF VS HEIGHT



$r = -.27$

Figure 3. Circles: All data, groups of 5 to 10.  
Triangles: Extremes removed from each group.

# WIND SPEED VS HEIGHT

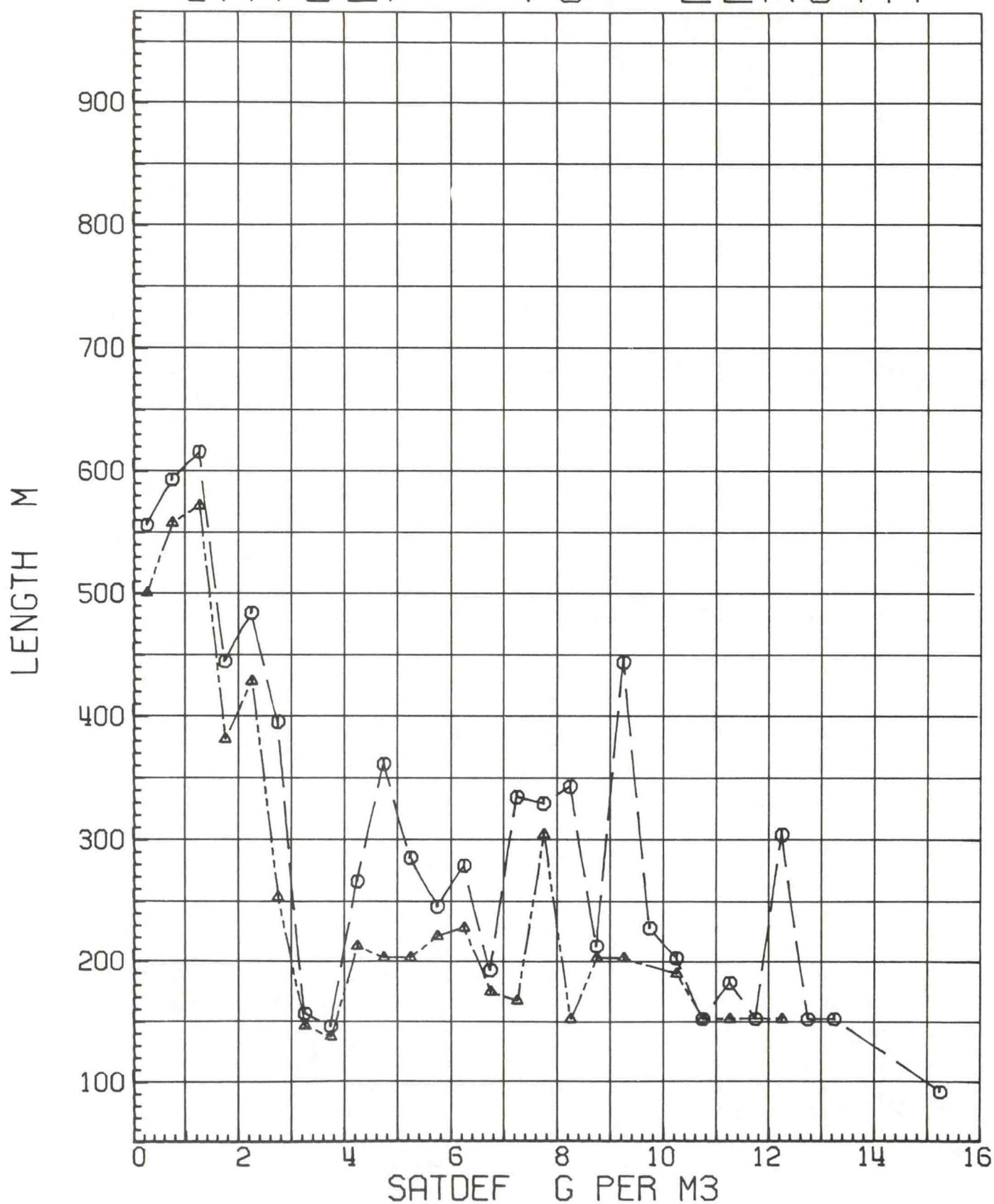




$r = -.28$

Figure 3. Circles: All data, groups of 5 to 10.  
Triangles: Extremes removed from each group.

# SATDEF VS LENGTH



# Secondary Motions in a Cooling Tower Plume

by

Steven R. Hanna and Martin Pike\*

Air Resources Atmospheric Turbulence and Diffusion Laboratory  
Oak Ridge, Tennessee

## Abstract

Time-lapse photography was used to estimate the speed of the vortex in the condensed plume at the edge of a bank of mechanical draft cooling towers. At a distance of about 30 m from the towers, the median tangential speed is about 2 m/s in the downward direction.

\*Oak Ridge Associated Universities summer trainee from Union College, Schenectady, New York.

ATDL Contribution File No. 76/19

## 1. Introduction

Drift deposition is a major environmental effect of cooling towers. Current models of the transport of drift droplets in plumes do not account for the influence of turbulence or secondary motions in the plume (see Cooling Tower Environment - 1974).

It is possible that the centrifugal forces exerted on the drops by secondary motions, as in a strongly bifurcated or downwashed plume, may be sufficient to eject the drops from the plume. Since there are no reported measurements of the magnitude of these secondary motions, it was decided to begin a small experimental program.

## 2. The Experiment

Three banks of mechanical draft cooling towers dissipate about 1000 to 2000 MW of waste heat at the Oak Ridge Gaseous Diffusion Plant. Hanna (1974) reports a series of drift deposition and fog experiments that were performed at these towers. Because of their blocky shape and their orientation perpendicular to the dominant wind direction, these towers are plagued by downwash about a third of the time. When this occurs, a strong secondary vortex forms in the plume on the edge of the tower, as diagrammed in Figure 1. However, this vortex is usually difficult to photograph because it is strongest during windy, humid, overcast conditions. On three days during the winter 1975-1976 it was possible to obtain good photographs of the visible plume, when puffs of condensed plume could be followed through the trajectories



associated with the secondary motions. A 16 mm movie camera with a one second time lapse was set up perpendicular to the plume at a distance of about 400 m. The movie chosen for detailed analysis was taken on 30 January 1976 with west winds of about 7 m/s and a temperature of 5°C.

### 3. Analysis

Several segments were clipped from the film because they contained a visible puff of condensed plume that could be followed for a few seconds. The individual frames were put in slide holders and projected onto a gridded screen so that the cartesian coordinates of the puff position could be plotted. An example of a trajectory is given in Figure 2. At each position, the elevation of the puff center and the plume centerline, and the plume radius and angle were noted. Measurements were limited to distances between 5 m and 50 m downwind of the towers. All speeds are referred to the plume centerline, which rose with a median vertical speed of .2 m/s. The small magnitude of the plume rise is due to downwash.

The first analyses were performed by converting to polar coordinates and accounting for changes in the angle of the cross-sectional plane perpendicular to the plume's axis. However, it was found that the change in angle due to the bending over of the plume did not significantly change the estimated speeds.

The calculations reported here are based on the assumption that the plume's axis is a straight line. Thirty five trajectories were analyzed, with between two and eight points represented in each trajectory. Ninety two individual estimates of tangential speed were made.

#### 4. Results

The calculated vertical speed of the plume's axis ranges from .0 to 2. m/s, with a median of .20 m/s. The tangential speed of the secondary motions, relative to the plume's axis, ranges from -15 m/s to + 4 m/s, with a median of -2 m/s. The minus sign indicates downward motion. Figure 3 contains the frequency distribution of the tangential speeds, showing that two thirds of the observations are within about 1.8 m/s of the median. It is expected that this distribution would approach a Gaussian form if the number and accuracy of the observations were to increase.

#### 5. Future Work

We hope to repeat this experiment at a natural draft cooling tower this winter. Direct in-plume measurements of speeds would be desirable to verify the calculations of speeds using the photography technique.

## References

Cooling Tower Environment - 1974, ERDA Symposium Series CONF-740302,  
Nat. Tech. Inf. Service, U. S. Dept. of Commerce, Springfield,  
Va. 22161.

Hanna, S. R., 1974: Meteorological Effects of the Mechanical-Draft  
Cooling Towers of the Oak Ridge Gaseous Diffusion Plant, loc.cit.,  
291-306.



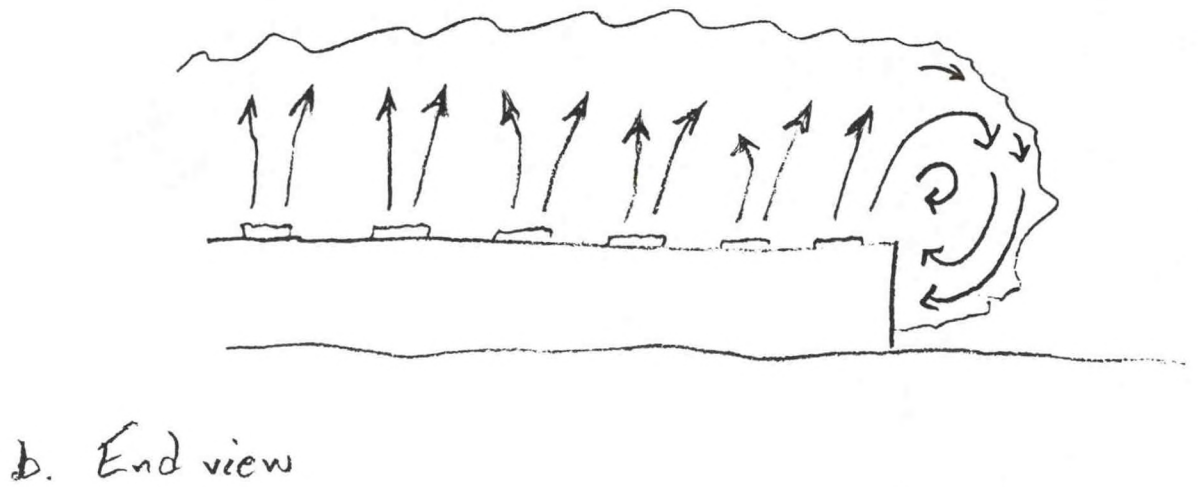
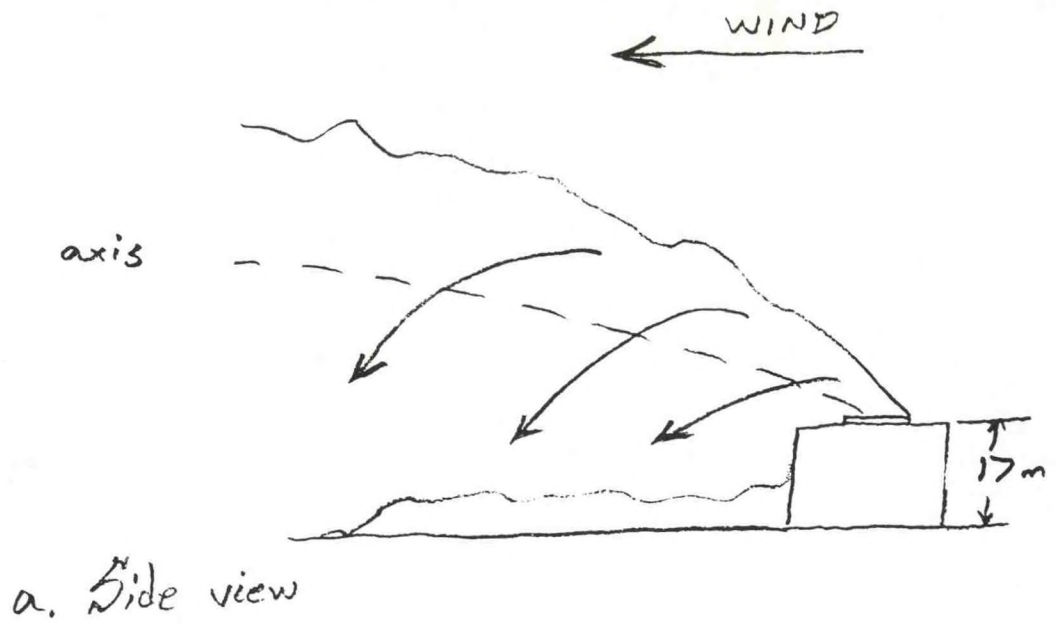


Figure 1 Secondary motions in ORGD cooling tower plume.

Figure 2: The trajectory of puff 2, with positions plotted each second.

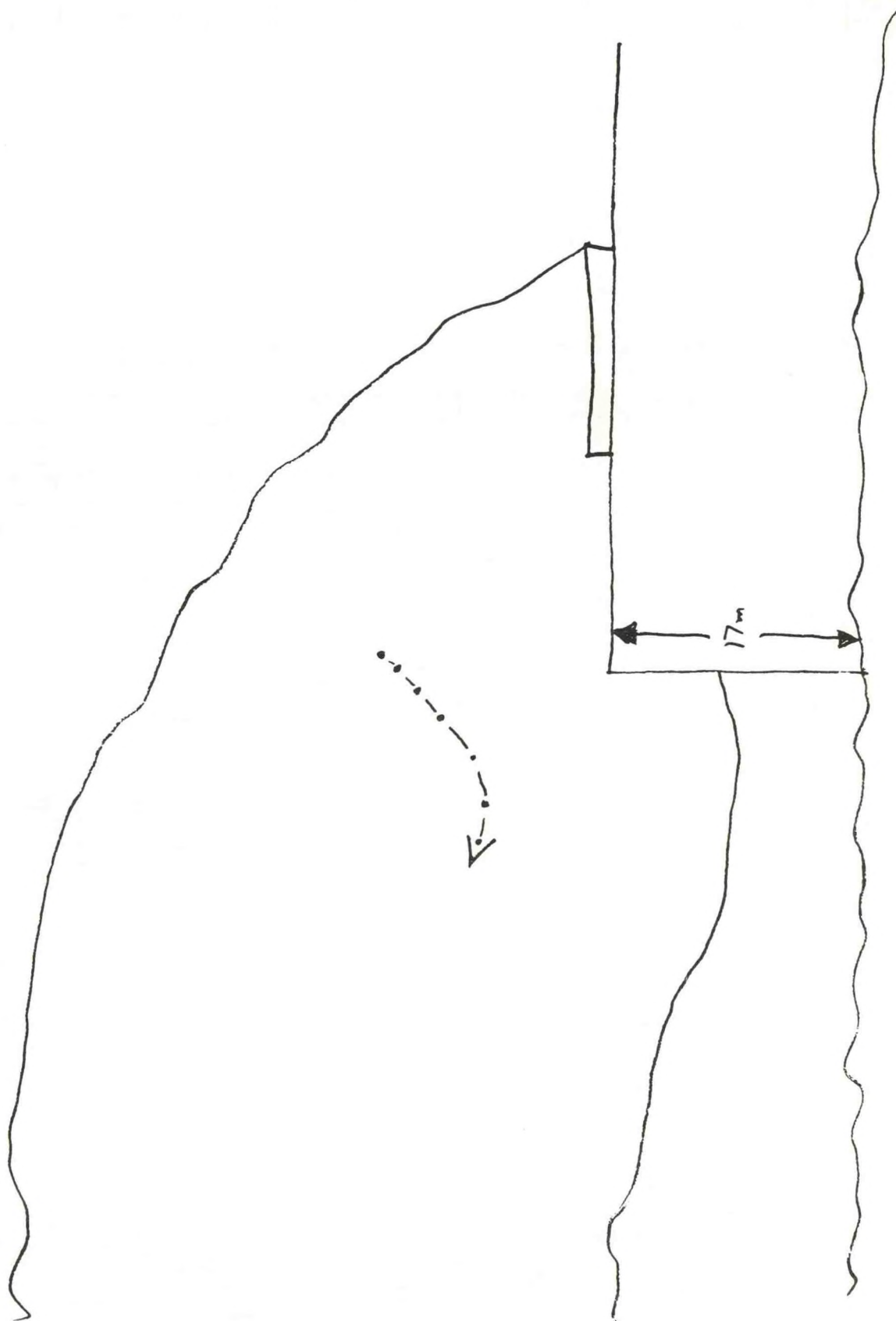
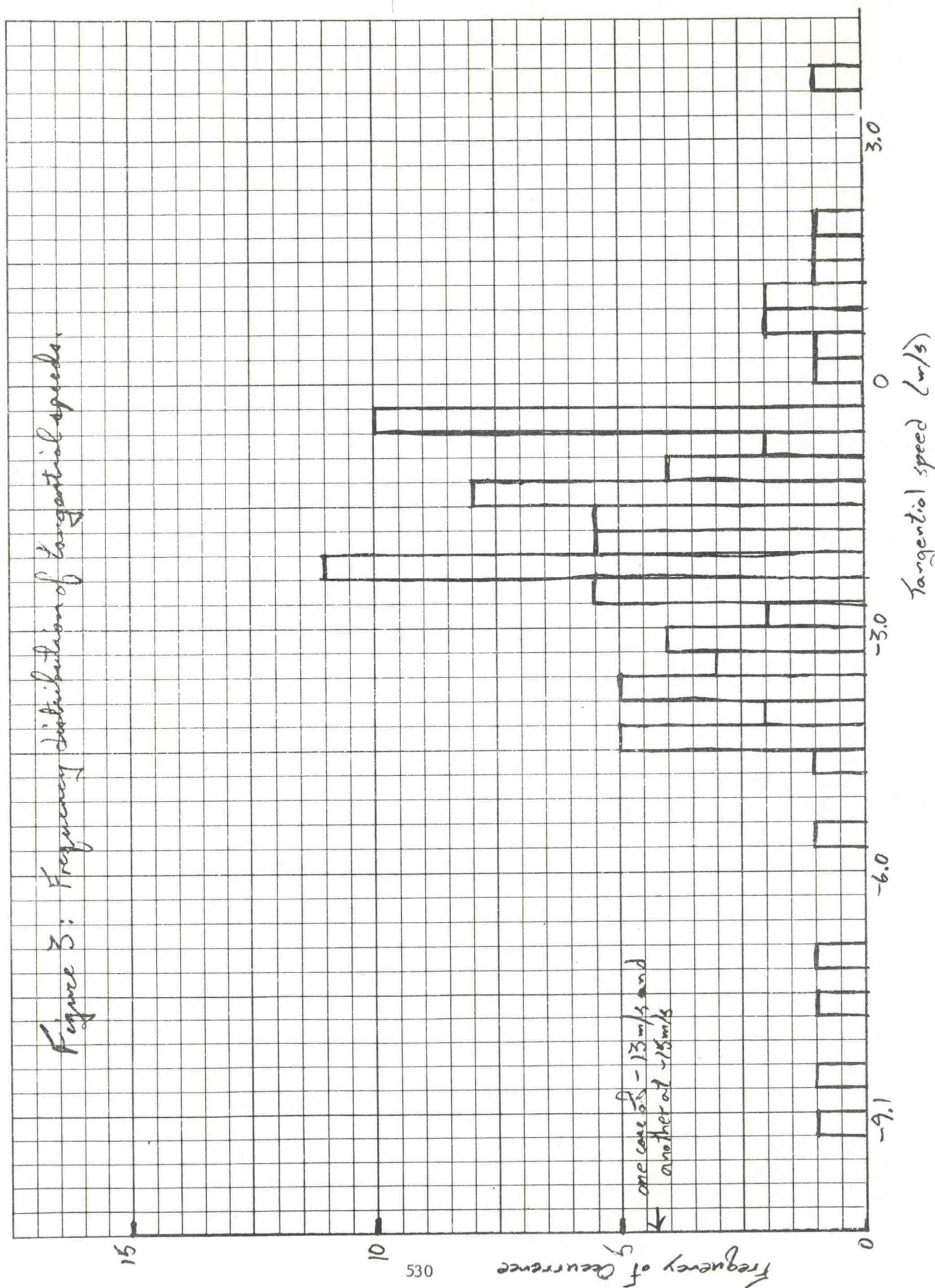


Figure 3: Frequency distribution of tangential speeds.





# Predicted Climatology of Cooling Tower Plumes from Energy Centers\*

by  
Steven R. Hanna

Air Resources Atmospheric Turbulence and Diffusion Laboratory  
National Oceanic and Atmospheric Administration  
Oak Ridge, Tennessee 37830

A one dimensional plume and cloud growth model is applied to four months of radiosonde observations from Nashville, using as initial conditions the plume from single large cooling towers with waste heat outputs of  $10^3$ ,  $10^4$ ,  $10^5$  MW, and a complex of cooling towers with a total waste heat output of  $10^5$  MW. Estimates of average annual plume rise from the four energy sources are 580, 1180, 2460, and 780 m, respectively.

The predicted plume rise, visible plume length, and cloud formation are given as functions of time of day, year, and weather type. For example, a cloud forms at the top of the plume from the  $10^3$  MW tower in 65% of the morning soundings during which ground level fog was observed. A cloud is predicted to occur 95% of the time at the top of the plume from the single  $10^5$  MW tower. It is found that if the towers in an energy center are separated by a distance greater than the average plume rise from one tower, then plume merging is minimized. Observations from TVA's Paradise Steam Plant are used to test the predictions of visible plume length from a single  $10^3$  MW tower.

\*(Scheduled for publication in the JAM, September 1977.)

ATDL Contribution File No. 76/20.

## 1. Introduction

The potential environmental effects of cooling towers include increases in cloudiness and precipitation and shading of the sun by long visible plumes. These problems are intensified as the size of power plants and energy centers increases (see Hanna and Gifford, 1975). Currently operating power plants, such as Paradise, Keystone, or Amos, are approaching energy productions of about 3000 MWe. Minor environmental effects, such as light snowfall (Kramer et al, 1976), have occasionally been observed at these power plants, but there do not appear to be any major effects. It is clear that as the energy releases from power plants increase, at some level there will be serious and unacceptable atmospheric effects. It is desirable to determine this critical point while energy centers are still on the drawing boards. For example, drawings exist for a proposed energy center in Louisiana in which dozens of 1000 MW cooling towers are squeezed into an area of a few square kilometers. The atmospheric scientist can provide specific input to this project by suggesting a minimum spacing between cooling towers, based on calculations of the conditions under which plumes merge.

There have been no comprehensive studies of the climatology of plume types at existing large cooling towers. Even the well-funded Chalk Point Cooling Tower Program (Pell, 1974) does not have climatology as one of its subprojects, although evidently the necessary daily observations are being made. A series of daily

observations of visible plume geometry at TVA's Paradise plant will be described below, but it will develop that there are many serious limitations to these observations. Therefore a good climatological data set for comparison with model predictions is very desirable. Such a data set, which should include at least one year's observations, would include:

1. Accurate morning and evening rawinsonde soundings.
2. Plant operating characteristics at the time of the rawinsondes (total power output, towers operating, temperature and vertical speed at tower opening).
3. Visible plume geometry (from photographs).
4. Reports of cloud formation by plume, and of precipitation falling from plume.
5. Current weather (cloud cover and height, fog, precipitation).
6. Also useful would be aircraft measurements of temperature and mixing ratio in the plume to downwind distances of about 10 km.

All these measurements are necessary to exercise and test a cooling tower plume and cloud growth model.

## 2. A modeling approach to plume climatology

Since such comprehensive climatological data sets for cooling towers do not exist, reliance must be placed at present on modeling studies to simulate the plume properties. The plume model that is used in this paper is based on Briggs' (1975) plume rise theory and Weinstein's (1970) one dimensional cloud growth model, and has been fully described by Hanna (1976a). It is a steady state model in



which the cloud variables (vertical speed, radius, temperature, water vapor content, cloud water content, and hydrometeor water content) are functions only of height. The model has been validated using observations of cooling tower plumes at the John E. Amos Plant (Kramer et al, 1975), the Chalk Point Plant (Meyer, 1976 and Environmental Systems Corporation, 1976), and the Rancho Seco Plant (Gifford, et al., 1976). It also successfully simulated the cloud that formed over an oil refinery near St. Louis (Auer, 1976; Hanna, 1976b).

This model was applied using data from 241 radiosonde observations made at Nashville, Tennessee, during the months of January, April, July, and October, 1974, in order to determine the effects of seasonal changes on plumes. This location was chosen because it is close to the TVA Hartsville power plant (under construction), the TVA Paradise power plant (where studies of cooling towers are underway), and the hypothetical Land-between-the-Lakes energy center site (Gray et al, 1976).

Source characteristics: Four types of sources were assumed, covering the energy range from typical current power plants to large future energy centers. Their characteristics are the following.

- A.  $10^3$  MW single tower: This tower, with radius 30 m, is typical of natural draft cooling towers currently in operation. Initial vertical speed is 4.4 m/s and initial plume temperature is calculated from the environmental temperature and relative humidity using a table published by Kramer et al (1975). The plume is initially saturated and initial cloud water and hydrometeor water contents are both equal to 1 g/kg.

- B.  $10^4$  MW single tower: The waste heat output is slightly larger than that from the largest existing power plants. The extra energy is obtained by keeping all parameters except initial plume radius the same as in the first case. Initial plume radius is increased to 91 m.
- C.  $10^5$  MW single tower: The waste heat output is equal to that proposed for a large energy center. The additional energy is obtained by keeping all parameters except initial plume radius the same as in the first case, but increasing the initial plume radius to 300 m. Since the energy flux is so concentrated, the results of this analysis represent the "worst case".
- D.  $10^5$  MW energy park: There are 100 cooling towers each with the characteristics of case A, divided into 25 groups of 4. The groups are assumed to be spaced on a square grid, 1 km apart. The four towers in each group are in a square array, 200 m apart. Merging of plumes is assumed to occur when the radius of a plume equals one half of the distance between the sources. At that point, the energies of the plumes add linearly, which is accomplished by increasing the plume radius to equal  $\sqrt{N} R$ , where N is the number of plumes merging and R is the radius of a plume before merger.

Model properties: The model follows the plumes until the vertical speed, w, drops to zero, at which point the maximum final plume rise has been achieved. The major characteristics of the calculated plumes that are used in the following analysis are visible plume height and length (determined by the end of the condensed portion of the plume), final plume rise, and liquid water concentrations

at the tops of plumes which are condensed at the final plume rise height. The occurrence or non-occurrence of clouds at the top of the simulated plume are compared for the following six major observed weather types:

1. Clear
2. Precipitation
3. Cloud height  $\geq 20,000$  ft (no prec.)
4.  $10,000 \leq$  cloud height  $\leq 20,000$  ft (no prec.)
5. Cloud height  $\leq 10,000$  ft (no prec.)
6. Fog (no prec.).

In this manner a climatology of visible plume lengths, plume rise, and cloud formation is developed.

### 3. Results

Plume Rise: If condensation occurs in the plume, the resulting release of latent heat can increase the plume rise. For about one-third of the model runs for the single  $10^3$  MW tower, a cloud is predicted to exist at the height of final plume rise. This fraction increases to 95% for the case of the single  $10^5$  MW tower. Examples of the differences in the calculated plumes from the four different sources, based on the particular radiosonde profile shown in Table 1 (11 p.m., 2 July 1974), are given in Figures 1 through 3. For this sounding, the profiles of vertical speed of rise, temperature difference between the plume and the ambient air, and cloud water turn out to be the same at heights below 150 m for the  $10^3$  MW tower and  $10^5$  MW power park. Above 150 m, the groups of four plumes in the power park merge and the combined plume rises about 200 m higher than for the  $10^3$  MW plume. The  $10^4$  and  $10^5$  MW single-tower plumes rise quite high and always contain liquid water, whereas the plumes from the  $10^3$  MW single tower and the  $10^5$  MW power park evaporate at a height of 130 m.



Table 1

Nashville Atmospheric Sounding for 2315 Z, 2 July 1974.  
Initial Plume Temperature is 313.4 K.

Z(M)	Dry Bulb (K)	Dew Point (K)	U(M/S)
0.	302.9	296.6	2.5
127.	301.7	296.0	3.0
1393.	291.2	289.3	3.0
1827.	289.4	284.4	3.5
2214.	286.0	283.0	3.5
2446.	285.3	279.6	3.5
2974.	282.3	278.0	5.0
3033.	282.1	276.1	5.0
3285.	279.8	275.2	5.5
4041.	275.9	264.4	5.0
4441.	273.1	266.0	6.0
4931.	271.4	241.4	4.0
5193.	271.0	241.0	4.0
5509.	268.4	238.4	4.0
5742.	269.0	239.0	4.0
6113.	267.7	237.7	3.5
7465.	256.1	226.1	4.5
8307.	248.8	218.8	6.0
8704.	246.8	216.8	7.5
9098.	244.1	233.4	5.5
9143.	244.2	242.2	13.5
9233.	244.1	244.0	16.5
9371.	243.5	241.9	17.0
9559.	242.5	236.3	18.5
10070.	238.6	232.5	20.5
10377.	236.6	226.2	16.5
10640.	234.0	227.1	15.0
10829.	232.2	202.2	15.5

Table 2

## Average Plume Rise Estimated Using Nashville Radiosonde Observations.

The Range in Plume Rise of the Numbers used in Calculating Each Average is Given in Parentheses.

Month (all 1974)	Morning Rise (m)					Evening Rise (m)					Average Rise (m)				
	10 <sup>3</sup> MW	10 <sup>4</sup> MW	10 <sup>5</sup> MW	10 <sup>5</sup> MW	power parks	10 <sup>3</sup> MW	10 <sup>4</sup> MW	10 <sup>5</sup> MW	10 <sup>5</sup> MW	power parks	10 <sup>3</sup> MW	10 <sup>4</sup> MW	10 <sup>5</sup> MW	10 <sup>5</sup> MW	power parks
Jan.	500 (160- 1340)	880 (320- 1450)	1470 (650- 3600)	610 (160- 1390)		660 (240- 1360)	970 (400- 1690)	1590 (750- 4010)	740 (240- 1530)		580 (160- 1360)	920 (320- 1690)	1530 (650- 4010)	670 (160- 1530)	
Apr.	490 (170- 1430)	1030 (300- 1920)	2340 (780- 4500)	610 (170- 1740)		890 (120- 1600)	1410 (190- 2160)	2550 (420- 4300)	1090 (120- 1880)		690 (120- 1600)	1220 (190- 2160)	2440 (420- 4500)	850 (120- 1880)	
July	470 (200- 1590)	1530 (340- 3110)	3130 (1260- 4950)	890 (210- 3620)		730 (240- 1800)	1590 (520- 2710)	3570 (1690- 5460)	1130 (240- 2980)		600 (200- 1800)	1500 (340- 3110)	3250 (1260- 5460)	1010 (210- 3620)	
Oct.	360 (190- 990)	850 (320- 3160)	2410 (850- 4790)	420 (230- 1200)		550 (260- 1140)	1140 (500- 2160)	2610 (1500- 4600)	770 (210- 2300)		450 (190- 1140)	1000 (320- 3160)	2510 (850- 4790)	600 (210- 2300)	
Avg. annual	450 (160- 1590)	1030 (300- 3160)	2340 (650- 4950)	630 (160- 3620)		710 (120- 1800)	1280 (190- 2710)	2580 (420- 5460)	930 (120- 2980)		580 (120- 1800)	1180 (190- 3160)	2460 (420- 5460)	780 (120- 3620)	

The average plume rises for all 241 soundings, by months and for the four different sources, are listed in Table 2. The calculated increase in plume rise with increase in source strength for the first three types of sources is in approximate agreement with Briggs' (1975) theory for plume rise, which predicts that the plume rise for bent-over plumes is proportional to source strength raised to the one third power. The figures in Table 2 for average annual plume rise show that the ratio of the  $10^4$  MW plume rise to the  $10^3$  MW plume rise is 2.04 and the ratio of the  $10^5$  MW plume rise to the  $10^3$  MW plume rise is 4.25. Briggs' theory predicts that these ratios will be  $10^{1/3}$ , or 2.15, and  $100^{1/3}$ , or 4.65, respectively.

The  $10^5$  MW power park yields an average plume rise that lies generally between those calculated for the single  $10^3$  MW tower and the single  $10^4$  MW tower. Occasionally, all 100 plumes will combine and yield a plume rise close to that calculated for the single  $10^5$  MW tower. In about 90% of the runs, plumes in the group of four towers merge, and in about 15% of the runs, the 25 groups of four all merge. But since merging generally occurs near the top of the plume, it doesn't result in much additional rise. Based on this, a general rule for avoiding plume merging can be stated. The cooling towers should be spaced a distance apart greater than the average plume rise from a single tower. In this way, the edges of the plumes from adjacent towers do not touch, since the radius (proportional to  $.4z$ ) of each plume at its height of final rise is less than half the distance between the towers.

Enhancement of plume rise due to the merging of multiple plumes was studied by Briggs (1974). In his study the ratio of



the enhanced plume rise from N sources to the plume rise from one source, which is denoted by  $E_N$ , is a function of the number of sources, N, the plume rise from one source, H, and the distance between the sources, s.

$$E_N = ((N + S)/(1 + S))^{1/3} \quad (1)$$

where  $S = 6((N-1)s/N^{1/3}H)^{3/2}$

The model results in Table 2 show that the average annual plume rise from a single  $10^5$  MW tower is 580 m. For the small groups in our hypothetical power park ( $N = 4$  and  $s = 200$  m),  $E_N$  equals 1.20. For the entire power park ( $N = 100$  and  $s = 1000$  m),  $E_N$  equals 1.02. In this case the enhancement factors for the groups of four and the entire power park should probably be multiplied together. On this basis the plume rise enhancement factor  $E_N$ , from eq. (1) would be about 1.22 for our hypothetical power park. The plume and cloud growth model yields the result that the average annual ratio of plume rise for the  $10^5$  MW spaced power park to the plume rise for the single  $10^3$  MW cooling tower is 780 m/580 m, or 1.35, in fair agreement with eq. (1).

The seasonal variation of plume rise shown by Table 2 is about what would be expected intuitively. The lowest plume rise usually occurs during winter when the lower atmosphere is more stable. Similarly, afternoon plume rises are 10 to 80% greater than morning plume rises. The diurnal variation is less for large sources, since the morning inversion is usually limited to a layer about 100 to 200 m deep near the ground. However, the annual variation is greatest for the large sources, presumably due to the influence of the deep isothermal or inversion layers which exist during the winter. Also, it should

be stressed that this "climatology" is based on plume rise calculations made from meteorological observations during a period of only four months. Ideally, observations during at least ten years should be used to establish stable climatological estimates.

Cloud at Top of Plume: In many of the model calculations, liquid water is predicted to be present in the plume at the height of final rise. Either a cloud persists from the tower opening through the entire depth of the plume, or else it forms just above the lifting condensation level. The frequencies of cloud occurrence predicted by the model for the six weather classes are given in Table 3, in the case for which the source is the single 1000 MW, 30 m radius tower. On the average, a cloud is predicted to occur at the top of the plume 39% of the time. During precipitation, fog, or cases when the natural cloud height is less than 10,000 ft., a cloud at the top of the plume is predicted about 60% of the time. The reason why the percentage is not 100% during precipitation conditions is that sometimes precipitation falls into relatively dry air near the surface; this occurs, for instance, when warm frontal rain is just beginning or snow flurries are occurring. Clouds at the top of the plume are very unlikely during afternoons that are clear or have high natural clouds. Such high occurrences of clouds are not usually reported from operating cooling towers, since on foggy days, or days with precipitation, it is difficult to see the plume. It should be remembered that the model calculates plumes on all days, instead of just sunny days when the plume is easily visible.

Table 3

Predicted Frequency of Cooling Tower Cloud Occurrence (Liquid  
Water Content Greater than 0 at Height of Final Rise) for 1000 MW  
Tower at Nashville

Weather Class	Observed class freq.		Frequency of cooling tower cloud occurrence within class	
	am	pm	am	pm
1. Clear	.09	.15	.32	0
2. Precipitation	.18		.60	
3. Cloud height $\geq$ 20,000 ft. (no Prec.)	.05	.07	.23	0
4. 10,000 $\leq$ cloud height < 20,000 ft. (no prec.)	.09		.14	
5. Cloud height < 10,000 ft (no prec.)	.24		.53	
6. Fog (no prec.)	.13		.65	
All	1.00		.39	

The frequency of cloud occurrence is predicted to increase as  
source size increases, as shown in Table 4.

Table 4

Frequency of Cooling Tower Cloud Occurrence Estimated  
Using Nashville Radiosonde Observations

Month (all 1974)	10 <sup>3</sup> MW	10 <sup>4</sup> MW	10 <sup>5</sup> MW	10 <sup>5</sup> MW power park
Jan.	.41	.70	.97	.59
Apr.	.34	.59	.96	.43
July	.51	.76	.97	.59
Oct.	.31	.54	.89	.39
All runs	.39	.64	.95	.50



For the  $10^5$  MW power park the frequency of cloud occurrence is roughly halfway between those for single  $10^3$  MW and  $10^4$  MW cooling towers, just as (see Table 2) is true for the plume rise for the power park. A cloud forms nearly all the time (frequency .95) over the single  $10^5$  MW cooling tower. This is a good argument against clustering the waste heat sources as close together as possible. This model predicts that a cloud averaging 2500 m deep would exist nearly continuously over an area with radius 300 m dissipating  $10^5$  MW of heat.

Liquid water content of cloud formed by cooling tower: The liquid water content of a cloud determines the visibility in the cloud and the rainfall rate from the cloud. The removal of large raindrops from the plume has been calculated using a scheme developed by Simpson and Wiggert (1969). It is uncertain whether the estimated rainfall rate at the ground is realistic, because a cooling tower cloud is unlike a natural cloud, in that its base is stationary rather than drifting with the wind.

The average liquid water contents predicted by the model are listed in Table 5. These refer only to those cases when a cloud formed at the top of the plume. The average liquid water contents range between .29 and .63 g/kg, in agreement with typical values reported by Fletcher (1962) of the liquid water content in natural clouds. The largest liquid water

value is 1.49 g/kg. The average liquid water content for the larger sources is significantly greater than that for the  $10^3$  MW source, but there is no significant seasonal variation. In most cases the liquid water content at the top of the plume is less than that in the middle sections of the cloud.

Table 5

Predicted Average and Peak Concentration of Cloud Water at the Top of Plumes Which are Condensed at the Height of Final Rise, Estimated Using Nashville Radiosonde Observations

Month (all 1974)	Average Concentration (g/kg)				Peak Concentration (g/kg)			
	$10^3$ MW	$10^4$ MW	$10^5$ MW	$10^5$ MW power park	$10^3$ MW	$10^4$ MW	$10^5$ MW	$10^5$ MW power park
Jan.	.40	.54	.62	.47	.72	.96	1.49	.98
Apr.	.44	.60	.61	.54	.82	1.15	1.19	1.00
July	.29	.63	.44	.49	.91	1.03	.77	1.25
Oct.	.33	.39	.44	.36	.62	1.02	1.09	.90
All runs	.36	.54	.53	.47	.91	1.15	1.49	.125

Relation of plume rise to inversion height: Based on observations of cooling tower plume rise on cold winter mornings at the John E. Amos power plant, Brennan, et al. (1975) state that the capping inversion height, or mixing-layer depth, determines the final plume rise. Hanna (1976a) has pointed out that this conclusion is not likely to be valid during the summer, when the

capping inversion is much higher than it is in the winter. Consequently the 241 Nashville soundings were analyzed to determine the relation between predicted plume rise from the 1000 MW cooling tower and observed inversion height.

A well-defined capping inversion occurs in 89 of the Nashville soundings; the average plume rise and inversion height for these runs equal 690 m and 1250 m, respectively. Capping inversion heights and plume rise for these soundings are summarized in Table 6. The correlation between plume rise and inversion height is very high for the group of runs for which the estimated plume rise is greater than or equal to the inversion height. If the plume has enough buoyancy to bring it to the capping inversion, the plume will in all likelihood stop there. But in general, a knowledge of the height of the capping inversion permits only an upper limit to be estimated for plume rise.

Table 6

Predicted Plume Rise and Observed Capping Inversion Height for the 1974 Nashville Soundings. The Number of Runs in Each Category is Given in Parenthesis.

Month	Avg. Capping inversion height	Avg. Model plume rise	Correlation Coefficient between Capping Inversion Height and Plume Rise	
			All runs with inversion	Runs with plume rise $\geq$ inversion height
Jan.	920 m	640 m	.31(39)	.99(14)
Apr.	1640	760	.20(25)	.99(5)
July	1700	1250	.78(5)	(0)
Oct.	1280	570	.15(20)	(2)
All runs	1250	690	.33(89)	.99(21)



Visible plume length: The analysis of visible moisture plumes can be conducted with confidence only in the case of plumes that evaporate before they reach the height of final rise. Downwind of this point passive diffusion governs the distribution of excess water, and very little is known about cooling tower plumes in this region. Keeping in mind this limitation, in the case of the single  $10^3$  MW source the average annual visible plume height predicted by the model is 150 m and the average annual visible plume length is 190 m.

Seasonal variations of predicted visible plume length and height for the  $10^3$  MW source are given in Table 7. It can be seen that the average resultant visible plume length is about 40% to 75% greater in January than in July, and that the morning length is about twice the afternoon length. Furthermore, the angle of the plume with the horizontal, which is easily calculated from these values, is about  $30^\circ$  less in the winter than in the summer, presumably due to the greater wind speeds in the winter (8.0 m/s in January compared to 3.4 m/s in July). The shortest plumes are predicted to occur on hot dry days in July, when the visible plume length is only about 50 m, or about one tower diameter.

Table 7

Visible Plume Length and Height Predicted Using Nashville Radiosonde Observations, for Plumes which are not Visible at their Final Height of Rise. The Resultant Plume Length is the Hypotenuse formed by the Visible Plume Length and Height. The  $10^3$  MW Source is used.

Month	Height(m)		Length(m)		Resultant(m)	
	am	pm	am	pm	am	pm
Jan.	230	130	430	170	490	210
Apr.	180	90	330	130	380	160
July	240	120	140	90	280	150
Oct.	240	80	210	110	310	140
All runs	220	100	280	130	360	160

The model predictions of Table 7 can be compared with observations of visible plume geometry at TVA's Paradise Steam Plant (Hanna and Pike, 1976) where there are three large natural draft cooling towers. Morning observations of surface weather conditions and plume geometry, and plume photographs were analyzed for the year 1974, with the results given in Table 8.

Table 8

Observed Morning Visible Plume Geometry at TVA's Paradise Steam Plant, 1974, Compared with Model Predictions from Table 7

Season	Average Visible Plume Height		Average Visible Plume Length	
	Observed	Predicted	Observed	Predicted
Winter	340 m	230 m	580 m	430 m
Spring	250	180	200	330
Summer	260	240	330	140
Fall	310	240	550	210
<hr/>				
Average	290 m	220 m	410 m	280 m

It is seen that the agreement between model predictions and observations is fair. The model underpredicts visible plume height by about 24% and visible plume length by about 32%. This comparison may be biased by the fact that the predicted plume lengths are restricted to cases when the plume is not visible at its height of final rise. Furthermore, the total energy output of the three cooling towers at Paradise is about twice as great as the output assumed in the model.

## 7. Limitations of the Model

Because the plume and cloud growth model is one-dimensional, i.e. variables are functions of height only, it cannot account for horizontal variability in the source, the plume, or the environment. Plume size is parameterized by making the radius a function of height, and mixing with the environment is parameterized by assuming a value for the entrainment coefficient. The distributions of temperature, moisture, etc., in the plume are assumed to be uniform within a cross section perpendicular to the axis of the plume. These limitations are not serious for the study of single plumes, as shown by the success of Briggs' (1975) plume rise theory. However, at many existing power plants, such as Paradise, Amos, Rancho Seco, or Keystone, there are more than one cooling tower on the site, and the plumes from these towers are often observed to merge. Interactions of these plumes cannot in all respects be accurately simulated by a one dimensional model. As discussed above, it has been necessary to resort to gross parameterizations, such as assuming that the plumes completely combine at the point that their edges first touch. Planned energy centers will contain many individual cooling units, and a detailed understanding of their atmospheric effects will require two or three-dimensional models, similar to the multi-cloud model proposed by Hill (1974).



The calculations in this paper for  $10^4$  and  $10^5$  MW energy sources represent the extreme case for which all the energy comes from a single source. The  $10^5$  MW power park assumes a distribution of cooling towers, but plume merging is treated in a highly parameterized way. In a model in which interactions between the plume and the environment can occur, it is expected that the high density of cooling towers would cause the environmental air to be gradually warmed and moistened as it passes over the energy center and through or between the plumes. At the height of final plume rise, it is expected that a broad cloud consisting of the upper portions of all the plumes would drift off downwind.

Another major modeling difficulty is the lack of adequate parameterization for the precipitation rate from relatively narrow, bent over plumes. According to Simpson and Wiggert (1969), precipitation should fall from a cloud whose liquid water content is 1 g/kg. Several of the plumes in this study have liquid water content greater than 1 g/kg, but the effect of precipitation cannot yet be adequately modeled. A research program is needed in which plume microphysics parameters are measured in detail.

The climatology predictions of this model have been compared with a limited set of observations from the Paradise Steam Plant. Further observations should be made of plume climatology, especially the variation of visible plume length and cloudiness with the six weather classes. If models can be satisfactorily validated with measurements from existing power plants, we can be more confident of their extrapolation to large energy centers.

5. Acknowledgements

Some of the calculations in this report were done by Susan Yeh and Martin Pike. Mr. Pike is an Oak Ridge Associated Universities Summer Trainee from Union College, Schenectady, New York. I am grateful to Jesse Coleman of the Tennessee Valley Authority for sending me the Paradise cooling tower observations.

This research was performed as part of ERDA's Meteorological Effects of Thermal Energy Releases program, under an agreement between the National Oceanic and Atmospheric Administration and the Energy Research and Development Administration.

## REFERENCES

- Auer, A. H., Jr., 1976: Observations of an industrial cumulus. J. Appl. Meteorol., 15, 406-413.
- Brennan, P. T., D. E. Seymour, M. J. Butler, M. L. Kramer, M. E. Smith, and T. T. Frankenburg, 1976: The observed rise of visible plumes from hyperbolic natural draft cooling towers. Atmos. Environ., 10, no. 6, 425-431.
- Briggs, G. A., 1974: Plume rise from multiple sources, in Cooling Tower Environment-1974, National Technical Information Service, U. S. Department of Commerce, Springfield, Va., 22161, 161-179.
- Briggs, G. A., 1975: Plume rise predictions. Lectures on Air Pollution and Environmental Impact Analyses. American Meteorol. Soc., 45 Beacon St., Boston, Mass., 59-111.
- Environmental Systems Corporation, 1976: Chalk Point Cooling Tower Project Seasonal Test Data for the Period December 15-19, 1975, Report no. PPSP-CPCTP-8, Prepared by ESC, Knoxville, Tn. for the Md. Power Plant Siting Program, Chalk Point Cooling Tower Project, 157 pp.
- Fletcher, N. H., 1962: The Physics of Rainclouds. Cambridge Univ. Press, London, 386 pp.
- Gray, D. O., F. C. Fitzpatrick, et al., 1976: A Comparison between Dispersed Nuclear Power Plants and a Nuclear Energy Center on Kentucky Lake, Tenn. VIII, Environmental Considerations. ORNL/TM/5312.
- Gifford, F. A., S. R. Hanna and R. P. Hosker, 1976: First Annual Report on Weather Modification Effects of Cooling Towers, ATDL Report 76/11, ATDL, P.O. Box E, Oak Ridge, Tn., 37830, 61 pp.
- Hanna, S. R., 1976a: Predicted and observed cooling tower plume rise and visible plume length at the John E. Amos power plant. To be published in Atmos. Environ.
- Hanna, S. R., 1976b: Comments on "Observations of an industrial cumulus." To be published in Nov. 1976 issue of J. Appl. Meteorol.
- Hanna, S. R. and F. A. Gifford, 1975: Meteorological Effects of Energy Dissipation at Large Power Parks. Bull. Am. Meteorol. Soc., 56, 1069-1076.



- Hanna, S. R. and M. Pike, 1976: Daily observations of visible plume length at TVA's Paradise cooling towers. ATDL Contribution No. 76/18, ATDL, P.O. Box E, Oak Ridge, Tn., 37830, 11 pp.
- Hill, G. E., 1974: Factors controlling the size and spacing of cumulus clouds as revealed by numerical experiments. J. Atmos. Sci., 31, 646-673.
- Kramer, M. L., D. E. Seymour, M. E. Smith, R. W. Reeves and T. T. Frankenberg, 1976: Snowfall observations from natural draft cooling tower plumes. Science, 193, 1239-1241.
- Kramer, M. L., M. E. Smith, M. J. Butler, D. E. Seymour, and T. T. Frankenberg, 1975: Cooling towers and the environment. paper 75-17.3 presented at the 68th Annual Meeting of the Air Poll. Control Assoc., Boston, Mass., June 15-20.
- Meyer, J. H., 1976: Chalk Point Surface Weather and Ambient Atmospheric Profile Data, Report no. PPSP-CPCTP-4, prepared by the Johns Hopkins University for the Maryland Power Plant Siting Program, Chalk Point Cooling Tower Project, 173 pp.
- Meyer, J. H., T. W. Eagles, L. C. Kohlenstein, J. A. Kagan and W. D. Stambro, 1974: Mechanical-Draft Cooling Tower Visible Plume Behavior: Measurements, Models and Predictions. Cooling Tower Environment-1974, CONF-740302, ERDA Symp. Series NTIS, 307-352.
- Pell, J., 1974: The Chalk Point Cooling Tower Project. Cooling Tower Environment-1974, CONF-740302, ERDA Symposium Series, NTIS, 88-127.
- Simpson, J. and V. Wiggert, 1970: Models of precipitating cumulus towers. Mon. Wea. Rev., 97, 471-489.
- Weinstein, A. I., 1970: A numerical model of cumulus dynamics and microphysics. J. Atmos. Sci., 27, 246-255.

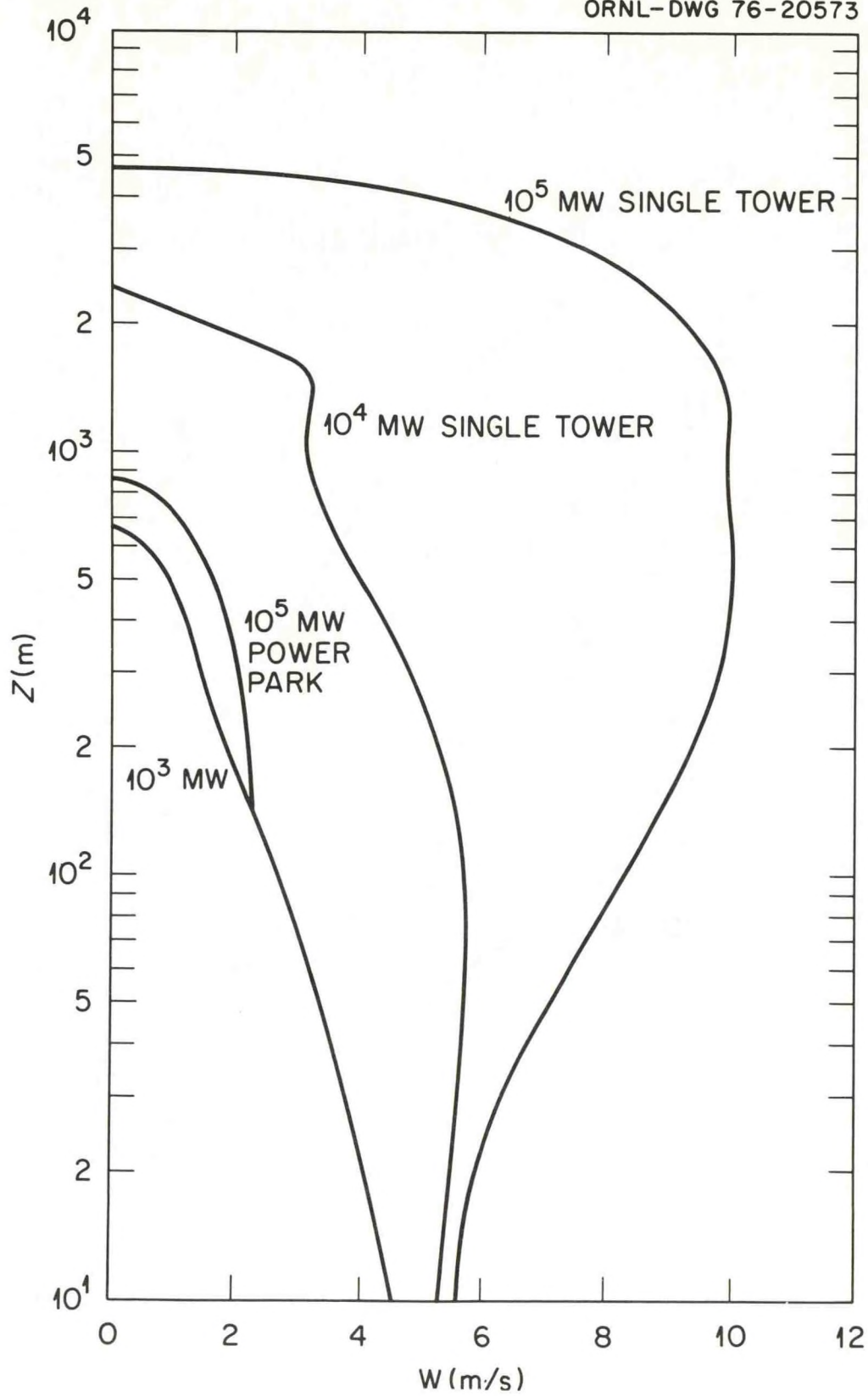


Figure 1: Plume vertical velocity,  $w$ , predicted by the model using the sounding in Table 1.

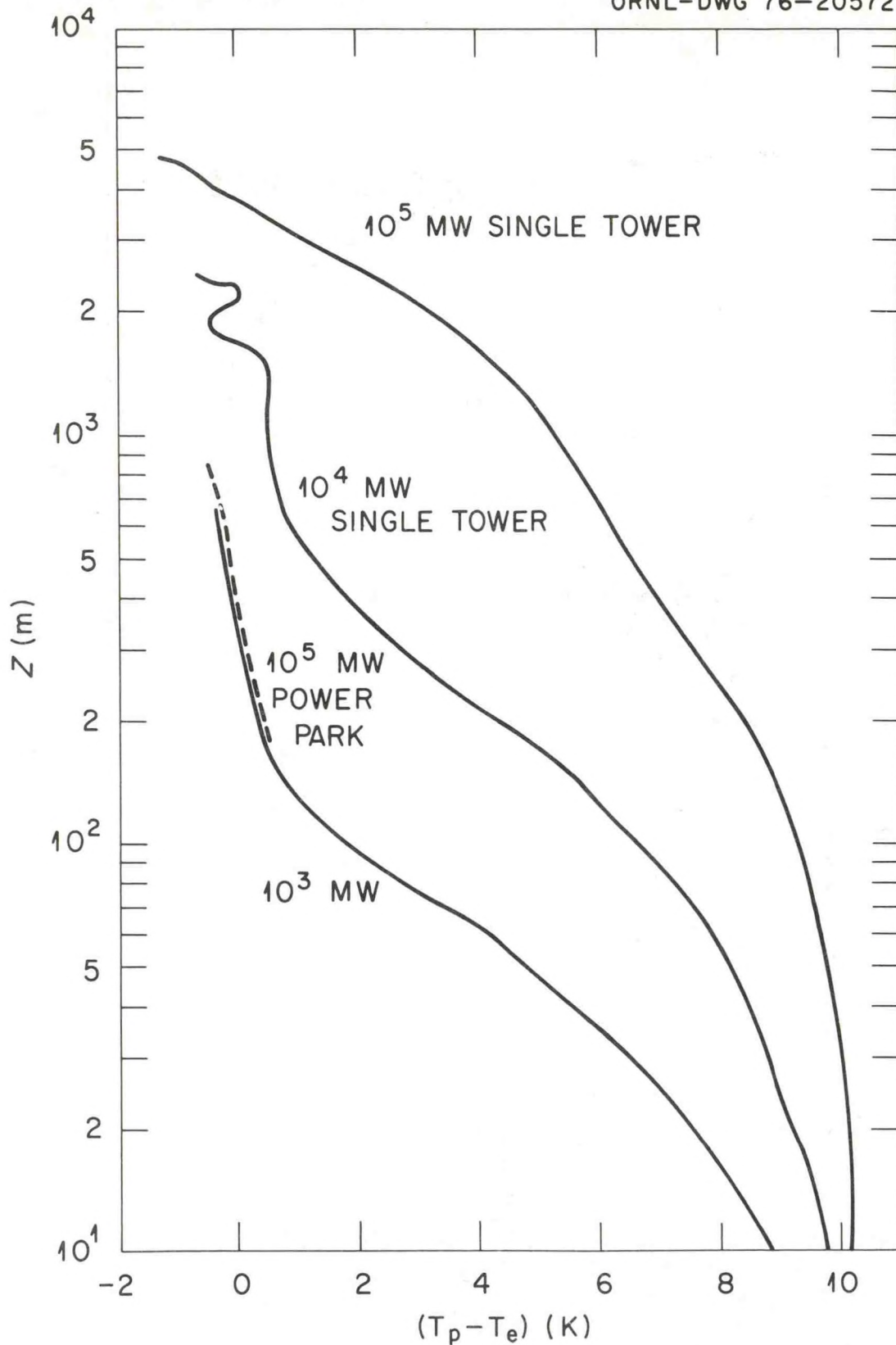


Figure 2: Temperature difference between plume,  $T_p$ , and environment,  $T_e$ , predicted by the model using the sounding in Table 1.



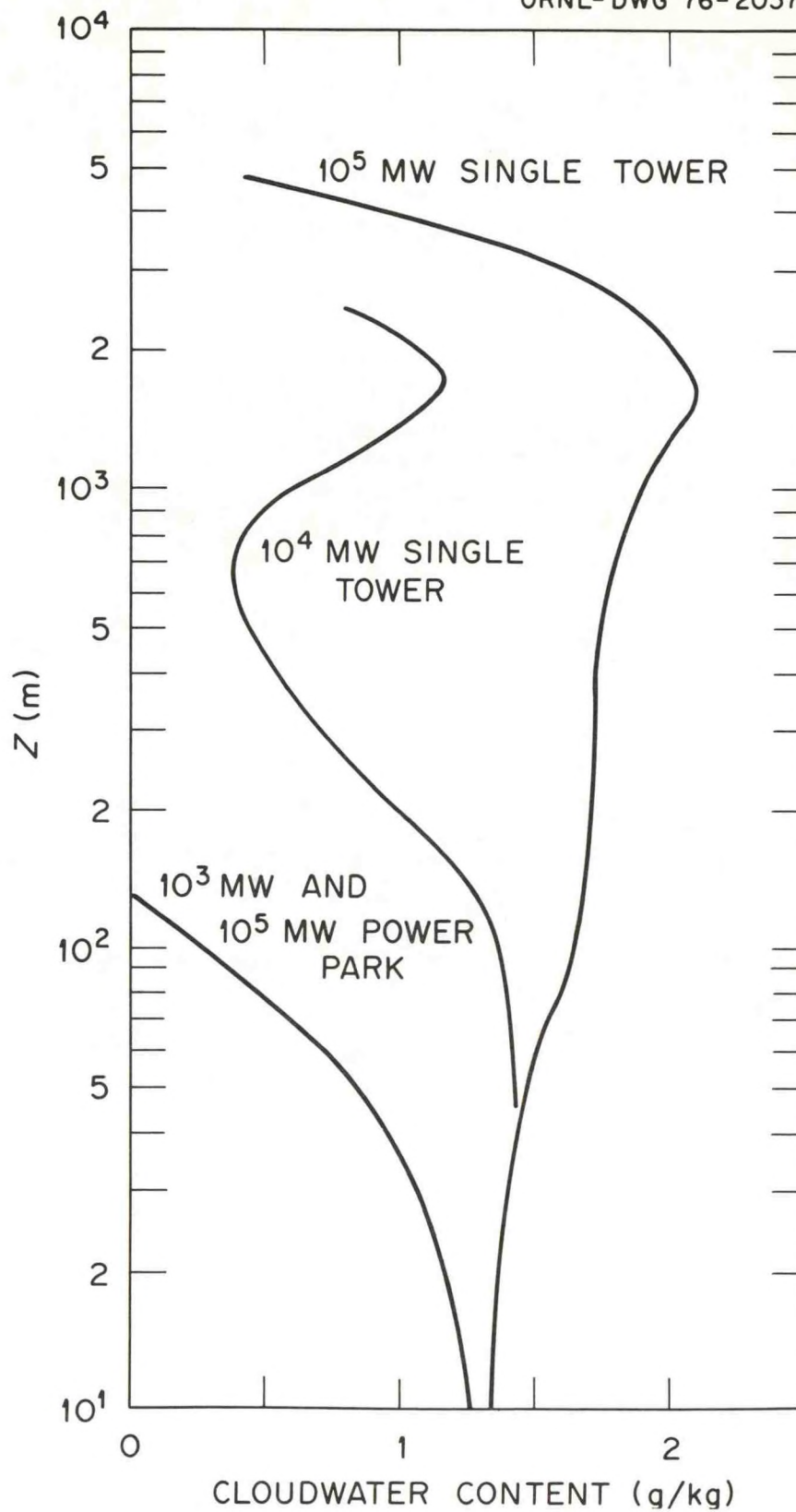


Figure 3: Cloud water content predicted by the model using the sounding in Table 1.



Third Symposium on Atmospheric Turbulence, Diffusion, and Air Quality, AMS, 19–22 October 1976, Raleigh, N.C.

## Summary

Steven R. Hanna<sup>1</sup>

*Chairman, AMS Committee on Atmospheric Turbulence and Diffusion*

### 1. Introduction

There were over 350 registrants for the Third Symposium on Atmospheric Turbulence, Diffusion, and Air Quality, which was held 19–22 October in Raleigh, N.C. This attendance figure ranks this symposium as one of the largest sponsored by the AMS and points out the importance of the specialty areas of turbulence, diffusion, and air pollution meteorology in the atmospheric sciences. The symposium was sponsored by the AMS Committee on Atmospheric Turbulence and Diffusion, the AMS Committee on Meteorological Aspects of Air Pollution, and the Air Pollution Control Association. Todd Crawford was the Program Chairman who deftly fit 102 papers, two panel discussions, a trip to the Environmental Protection Agency (EPA) wind tunnel, a luncheon, a banquet, and two icebreakers into a four day period.<sup>2</sup> On the first three days of the symposium, there were 10–11 hours of scheduled activities each day.

A highlight of the symposium was the banquet on Thursday evening, when AMS member and retired NBC newscaster Frank Blair spoke.<sup>3</sup> He stated how his experiences as a pilot during World War II helped develop his lifelong interest in meteorology. He felt that the weather portion of the "Today" program was often the most important news of the day and deplored some current weatherpersons who use the weather news only as a means for presenting their act.

Preceding Frank Blair's speech, former AMS President Al Blackadar presented the 1976 Charles Franklin Brooks Award to Dean Earl G. Droessler of North Carolina State University.<sup>4</sup> Earl is currently the Chairman of the Scientific and Technological Activities Commission and has served the Society well for many years. I have had contacts with Earl only during the past year, during my term as Chairman of the Atmospheric Turbulence and

Diffusion Committee. However, in these brief contacts, his leadership characteristics and dedication to the AMS were always apparent.

The speaker at the luncheon on Wednesday was Dr. Wilson Talley,<sup>5</sup> Assistant Administrator for Research and Development at EPA. He highlighted the areas in which the subject of the symposium meshed with the missions of EPA. In the question period following his speech, he nimbly handled several loaded political environmental questions that were prompted by the closeness of the elections.

### 2. What's new?

This question was often asked during the symposium. Has anything significant happened since September 1974, when the last symposium in this series convened in Santa Barbara, or are we just rehashing what we knew then? The answer is that there are many new problems but only a few new solutions.

#### *a. Daytime planetary boundary layer*

There is a much better understanding of this problem than there was two years ago, thanks to an excellent field experiment in Minnesota (described by J. Kaimal and S. Caughey), some careful laboratory experiments by G. Willis and J. Deardorff, and clever analyses by several theoreticians. For example, the height of the mixing layer is found to be a very important scaling parameter in determining the variation of winds and temperatures in the boundary layer.

#### *b. Second-order closure*

This theory is now understood and successfully applied by several dozen people. Two years ago it was an enigma understood by only a select few theoreticians. To further its understanding, a panel discussion was held Tuesday evening, with the participants being H. Tennekes, J. Lumley, J. Wyngaard, J. Businger, W. Lewellen, and J. Deardorff. They pointed out that second-order closure can be used to model free convection and counter gra-

<sup>1</sup> Atmospheric Turbulence and Diffusion Laboratory, NOAA, Oak Ridge, Tenn. 37830.

<sup>2</sup> The program, including abstracts, was published in the MAY BULLETIN (57, 621–656).

<sup>3</sup> See page 248.

<sup>4</sup> See page 247.

<sup>5</sup> See page 245.



dient fluxes, where first-order closure ( $K$  theory) fails. J. Lumley stated that 15 flows must be analyzed to fully determine the undetermined constants in second-order closure theory. There are only 6 of the 15 flows left to study, but he feels that it will take up to five or six years to complete the work. His opinion that field data cannot be used to determine the constants was challenged by J. Deardorff. It was felt by J. Wyngaard that the second-order modeling of cloud physics processes is being approached blindly by several persons and that second-order closure fails often in atmospheric applications, such as in the upper part of the convection layer and in the stable layer. All panelists concluded that it may be necessary to go to third-order closure for these more difficult problems.

#### *c. Long-range transport of pollutants*

This problem has grown rapidly during the past two years, due mainly to increased attention to ozone and  $\text{SO}_2\text{-SO}_4$  pollution. There were many case studies published during the past year, and also presented at this symposium, illustrating that high concentrations of pollutants can be detected up to several hundred kilometers from the source region. Models of mesoscale and long-range transport and diffusion have proliferated, but they have often been based on very shaky physical assumptions. For example, there is no basis for extending the Pasquill-Gifford  $\sigma$  curves beyond downwind distances of 10 km, but several models make this extension anyway (e.g., the paper by L. Wendell, D. Powell, and R. Drake). There is no theoretical justification for using instantaneous puffs to simulate diffusion from continuous sources, yet a few papers at this symposium use this assumption, such as those by G. Nordlund and by C. Sheih. How should we account for the spatial separation of wind stations and the relation between the averaging time for the mean wind and the travel time of the pollution plume? And possibly the most important unanswered question is the problem of chemical reactions in the plume over large space and time scales.

Some of these problems were covered in the panel discussion on long-range transport on Thursday evening. The panelists were E. Reiter, P. Altshuller, J. Angell, J. Heffter, W. Johnson, B. Egan, and L. Wendell. All agreed that a set of long-range transport and diffusion experiments was needed to provide the basis for models. Heffter suggested using inert, relatively stable substances such as krypton 85 as tracers, while Angell proposed using constant density balloons. Several panelists emphasized that observations of the detailed wind field were very important and that modelers should carefully account for the difference between mean and turbulent transport and diffusion. Most of the discussion focussed on data needs rather than on models.

#### *d. Transport and diffusion in rugged terrain*

This is another new problem area that has grown rapidly recently owing to the tendency of industries and utilities to select sites in steep-sided valleys or mountainous areas in the Appalachian or Rocky mountains. But here again, the development of adequate models is lagging far be-

hind the acquisition of data. Numerous papers were presented in Session 7 that show that the measured  $\sigma$  in rugged terrain is a factor of  $x$  greater than that suggested by the Pasquill curves. A few persons, such as B. Egan, are looking at the use of potential flow theory to estimate the trajectory of a plume over an obstacle. We hope that by the time of the next symposium in this series, adequate models of transport and diffusion over rough terrain will have been developed.

#### *e. Satellite photos of pollution*

Every two years, we see more and more use of satellite photos of pollution. So far, these are used mainly in a qualitative way, i.e., as a nice picture to liven up a talk. R. Husar, N. Gillani, J. Husar, C. Paley, and P. Turcu used a satellite photo of pollution in the Midwest to help make their point that "blobs" of pollution can be traced for long distances. But we foresee that satellite photos of plumes will be used much more in the future to estimate dispersion parameters and to verify transport models.

#### *f. Rapid response turbulence measurements*

D. Thomson, J. Norman, and R. Miller reported the first rapid response turbulence measurements yet taken in a full-size industrial plume. The detailed graphs of the vertical velocity and temperature distributions across a plume were fascinating and will be of great use to plume modelers.

#### *g. Finite difference schemes*

Use of these schemes for estimating advection of pollutants is coming under careful scrutiny. P. Gresho, R. Lee, and R. Sani, and P. Long and D. Pepper, showed how several commonly used schemes led to unacceptable numerical diffusion after relatively short times, and they recommended the two or three schemes that best preserved the shape and mass of the cloud being advected.

### **3. Quality of papers**

In a letter to the editor in the December 1974 BULLETIN (55, 1482-1483), Frank Hansen criticized the last symposium in this series on several accounts, ranging from entirely too much repetition to poor visual aids. His criticisms are probably valid for nearly all scientific meetings but really should have had some effect on the quality of the Raleigh symposium. I could not see any significant difference between the quality of the Santa Barbara and the Raleigh symposiums, probably because there was nearly the same cast of characters. The visual aids could all be seen from the front row, but less than half of them could be read from the back row. Of course the people in the back should not complain too loudly, because there were always empty chairs near the front. To help solve this problem, the Program Committee for the next symposium is considering screening all visual aids prior to presentation and rejecting those that cannot be seen from the rear of the room.

Another common complaint was that there was not enough time allotted for each paper—the average time was about 12 min. This is the perennial problem of the



Program Committee: should a few excellent papers be presented in detail, or should the gates be opened to one and all? Short papers are fine if the author is well prepared and has a talent for expressing himself without the crutch of pages of differential equations. Unfortunately, more than half of the papers at this symposium gave the impression of being a half hour talk squeezed into 10 min, or else the author barely got through his introduction before the hook came out. Of course the solution to this problem is better preparation. Other ways of handling the large numbers of papers could be poster sessions (which have been tried successfully at other AMS meetings) or summary papers by experts in each subdiscipline.

Also typical of every meeting is the handful of really excellent papers and the handful of downright horrible papers. With our present custom of writing vague and uninformative abstracts, it is difficult for the Program Committee to separate the wheat from the chaff. The Program Committee estimated that only about 5% of the submitted abstracts were sufficiently informative that it could confidently assess the worth of the abstract. We should all read and note well the short article on writing abstracts by Helmut Landsberg in the March 1967 *BULLETIN* (48, 134-135). Perhaps we should allow time in the abstract submission process for the Program Committee to return nondefinitive abstracts to the author for revision.

All registrants were fortunate to obtain the 596 page preprint volume, containing 98 of the 102 papers. Of the four missing papers, three were presented orally at the symposium. The AMS (E. Mazur in particular) is to be commended on its excellent job in organizing the timely production of this volume. However, those of us who opened and closed the volume more than a few times discovered that the pages soon came loose from

the binding. Because their papers were readily available for those who were interested, several speakers chose to use their 12 min in describing new work, discussing only specific aspects of their paper, or philosophizing in general. Hank Tennekes set what must surely be a new record for the shortest oral presentation (not counting those speakers who did not show up) by simply pointing out that observations of inversion rise are not sufficiently accurate to test the several detailed models of this phenomenon that are in existence. Although the preprint volume serves a definitely useful purpose, not enough people respect the admonition at the bottom of the title page: "their appearance in this collection does not constitute formal publication." The papers in the 1971 Raleigh and 1974 Santa Barbara preprint volumes often appear in lists of references. For this reason, all authors should be strongly encouraged to have their papers competently reviewed, and others should be reminded that these papers are basically unrefereed statements of current programs.

#### 4. Further comment

The atmospheric science profession is characterized by a strong mix of theoretical and applied workers, and one of the areas of greatest mixture is the specialty of atmospheric turbulence, diffusion, and air quality. Possibly the greatest benefit of this series of symposiums is the exposure of the theoreticians to the practical problems, and vice versa. This mix should be maintained in future symposiums, rather than splitting the meeting up into two separate sections, as some have suggested. AMS symposiums, as Hansen has pointed out in his letter to the *BULLETIN*, are not perfect, but they serve the very useful function of letting us meet our co-workers, find out what the major problems are, and reorient our own research based on the increased knowledge that we have gained.

Candid photos from the Third Symposium on Atmospheric Turbulence, Diffusion, and Air Quality held in Raleigh, N.C. (Photos courtesy of Ida Kay Jordan of *The North Carolina Leader*.)



Paul Humphrey, Central North Carolina Chapter President, Katherine Perlman, and Arthur Stern, immediate Past President of the Air Pollution Control Association.



Harry Moses, member of the AMS Committee on Meteorological Aspects of Air Pollution, and Elmar Reiter, Colorado State University.





PREDICTIONS OF NOCTURNAL MIXING LAYER PARAMETERS

Gary A. Briggs<sup>\*</sup>  
Air Resources  
Atmospheric Turbulence and Diffusion Laboratory  
National Oceanic and Atmospheric Administration  
Post Office Box E  
Oak Ridge, Tennessee 37830

\*Temporarily assigned to the Atmospheric Modeling and Assessment Branch,  
Meteorology and Assessment Division, Environmental Protection Agency,  
Research Triangle Park, N.C. 27711.

ATDL Contribution File No. 76/22

(WITHDRAWN)



# Hydrometeorological Aspects of Electric Power Production\*

by  
Steven R. Hanna

Air Resources Atmospheric Turbulence and Diffusion Laboratory  
National Oceanic and Atmospheric Administration  
Oak Ridge, Tennessee 37830

## Abstract

Observed atmospheric effects due to waste heat release from cooling towers and ponds are reviewed, including sun shading, ground fog, drift deposition, interference with aircraft, interactions with chemical plumes, high winds, and changes in cloudiness, temperature, and precipitation. It is seen that effects are generally minor from current power production facilities, but that more serious effects can be expected if large energy centers (10,000 MW and up) are built.

The status of physical and mathematical modeling is summarized, and it is concluded that two or three dimensional second or third order closure models must be developed in order to assess the probability of vorticity concentration at large energy centers and adequately explain plume merging.

\*To be published in the proceedings of the conference "Water for Energy Development," held 6-10 December 1976, Pacific Grove, California, sponsored by the Engineering Foundation and the U.S. Water Resources Council.



## 1. Introduction

Fundamental principles of thermodynamics tell us that no method of electric power production is 100% efficient. In fact, the biggest and best electric production facilities are only 20 to 40% efficient. The 60 to 80% of the power that is lost is generally in the form of internal or thermal energy, and is usually carried away by water. Water is used because it is plentiful, easy to transport, and has an excellent thermal capacity. But, in the dispersal of this hot water into the environment, serious hydrometeorological effects can occur. This paper is going to emphasize effects, rather than models or mathematical theories. A fact gap has built up in this research area during the few years that it has been in existence, as model development far outstripped data collection. For example, we now have between 10 and 20 models for predicting drift deposition from cooling towers, but no good set of data to test the models.

There are several reviews that the reader can refer to in order to better grasp the research problems. The ERDA document "Cooling Tower Environment-1974" contains 30 papers which cover topics ranging from visible plume length to social problems to biological effects. McVehil and Heikes (1975) conducted a critical review of cooling tower plume modeling and drift measurement for the American Society of Mechanical Engineers. This document is especially useful in that it compares the predictions of many different visible plume models against some observations, and recommends the so-called "best" model. Meteorological effects of energy dissipation at large power parks are reviewed by Hanna and Gifford (1975), who

suggest that the environmental effects are not severe at present power plants (up to 3000 MW), but that serious effects are possible if power parks (~50,000 MW) are built. A good critical review of the performance of spray ponds and cooling ponds was completed by Drake (1975), who concludes that adequate observations of ponds are nonexistent, and that most existing models do not properly account for variability in atmospheric parameters such as wind speed. Model "olympics," in which all available cooling tower plume models are compared using a common set of input data, are being conducted by Chen and Hanna (1977) and Policastro (1976). Both studies show that model predictions often differ by as much as two orders of magnitude. If anyone were to read through all of the above reviews, he would surely conclude that we are not ready at this time to write a definitive workbook of cooling tower and cooling pond models.

Meteorologists' concern with cooling facilities begins the moment the effluent leaves the source and enters the atmosphere. We traditionally leave problems such as blowdown, in-pond circulations, and drift eliminator designs to the engineers. The major environmental effects discussed in this paper include sun shading, ground fog, drift deposition, interference with aircraft, interactions with chemical plumes, whirlwind generation, and regional changes in temperature, cloudiness, and precipitation. Sections reviewing the state of the art and recommending future research are given for each major effect.

## 2. Sun Shading

When the sun is shaded by the condensation downwind of a cooling pond or in a cooling tower plume, the energy balance at the underlying surface is altered. A reduction in the solar energy received by plants, animals, and all other substances can cause significant changes, such as the mildewing of a painted surface or an increase in fungus on a crop. Over several years or decades, changes in radiation or cloudiness can cause changes in the natural vegetation types occupying an area. Based on the number of reports in the literature this effect is of greatest concern to Europeans at this time, as shown by the work on shading reported by Junod et al, (1974) and Bogh (1974). In Switzerland the government regulations state that "a mean maximum duration of shadow of 15 min/day is tolerable in built up areas around cooling towers" (Junod et al.,1974, p 240).

The condensed water causing the shading is due to the emissions of heat and water from the cooling system. Up to 50% of the heat released from a cooling pond and up to 90% of the heat carried from a cooling tower is in the form of latent heat, or vaporized water. A wet cooling tower releases about  $10^6$  g water vapor per 1000 MW electrical capacity. But even a dry cooling tower can cause clouds to form as moist environmental air is entrained and lifted to its condensation level by the plume. By the time the plume reaches an elevation of 500 m, there is much more environmental air than cooling tower air in the plume. At current power plants (energy outputs up to 2500 MWe) the average visible plume length is about



250 m to 500 m during the summer, and 500 m to 1000 m during the winter (Junod et al., 1974). During very humid environmental conditions, which occur 10% to 30% of the time depending on location, cumulus or stratus clouds are observed up to 50 km downwind of the power plant. However, no comprehensive observations of sun shading at an operating power plant have yet been conducted. Bogh's (1974) model results for the Biblis power station, where light and heat absorption by the plume in three wave-length ranges are accounted for, show that the expected shadowing at nearby villages is 2-5 min/day.

The first step in predicting shadowing is predicting the extent of the condensed plume. There are models available for estimating visible plume length for single sources, and these models have been verified with data from the Paradise (Slawson et al., 1974), Benning Road (Meyer et al., 1974), and Oak Ridge (Hanna, 1974) cooling towers. The simplest model which still emphasizes the physical principles involved was suggested by Hanna (1974), and shown by Briggs (1975) to predict the Benning Road visible plume lengths just as well as several other models. This simple model assumes that the plume temperature equals the ambient temperature at the end of the visible plume, and that the visible plume end occurs when the initial flux of excess water from the cooling tower is just equal to the flux of saturation deficit in the plume:

$$V_o m_o = V(m_s - m_e) \quad (1)$$

In this equation  $V$  is the volume flux ( $m^3/s$ ) in the plume and  $m$  is the water vapor mixing ratio. The subscripts  $o$ ,  $s$ , and  $e$  refer to initial, saturated, and ambient variables, respectively. The following equations for the height and length of the visible plume are obtained:

Windy conditions:

$$\text{height } h = 2R_o (w_o/U)^{1/2} [(m_o/(m_s - m_e))^{1/2} - 1] \quad (2)$$

$$\text{length } l = 1.4((R_o^{3/2} U^{3/4} w_o^{3/4})/F^{1/2}) [(m_o/(m_s - m_e))^{1/2} - 1]^{3/2} \quad (3)$$

Calm:

$$\text{height } h = 5.0R_o [(m_o/(m_s - m_e))^{1/2} - 1], \quad (4)$$

where  $R_o$  and  $w_o$  are initial plume radius and vertical speed,  $U$  is wind speed, and  $F$  is the initial buoyancy parameter, as defined by Briggs (1969):

$$F = (g/T_{po}) w_o R_o^2 (T_{po} - T_{eo}) \quad (5)$$

Here  $T_{po}$  and  $T_{eo}$  are initial plume and ambient temperatures and  $g$  is the acceleration of gravity. Equations (2) and (4) resulted in a correlation coefficient of about .9 between predicted and observed visible plume height at Oak Ridge, Tennessee. The observations are plotted in Figure 1. To proceed from the predictions of equations (2) through (4) to estimates of plume shadowing it is necessary to measure the joint distribution functions of wind direction, wind speed, and saturation deficit at a given site.

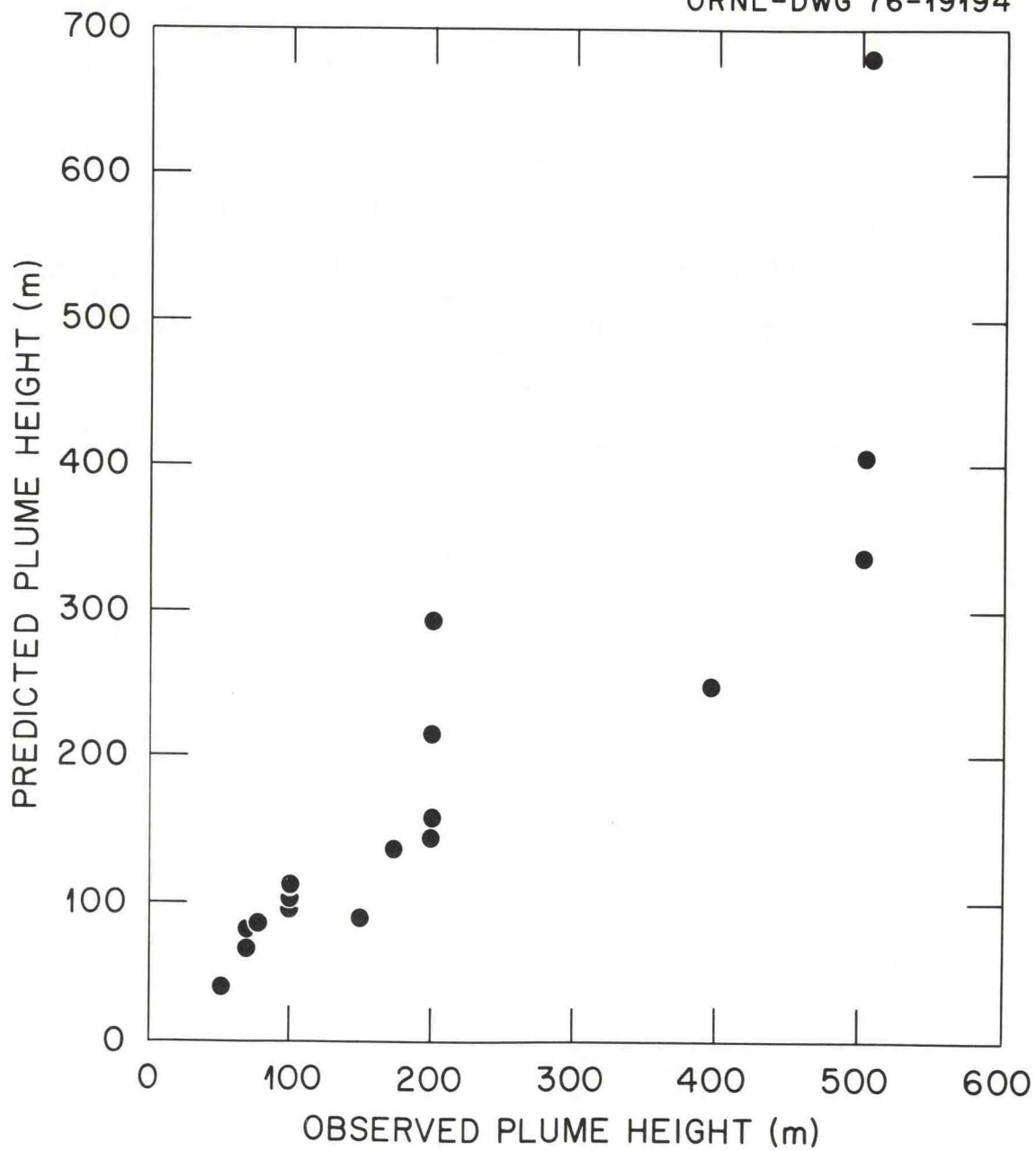


Figure 1: Observed and predicted visible plume height at the Oak Ridge Gaseous Diffusion Plant mechanical draft cooling towers (Hanna, 1974a).



Another major problem is the prediction of the effect on the visible plume length of plume merging from multiple sources. Briggs (1974) provides an empirical formula to estimate the enhancement in plume rise due to plume merging, but it has not yet been adequately tested with field data. The interactions of neighboring plumes with each other and with the environment can be most effectively studied using two and three dimensional atmospheric turbulence models, such as the one reported by Lewellen et al. (1976).

Of course shading can also be caused by stratus and cumulus clouds which are initiated by the waste heat and moisture from a power production facility. There are several cloud models available (see Cotton, 1975, for a good review) but only simple one-dimensional cloud models have been applied to the problem of cloud formation in a cooling tower plume (e.g. Hanna, 1976; Lee, 1976). Hanna's study is concerned with power parks, where up to 50,000 MWe is produced on one site. It is estimated that if all the waste heat is released from a disc 300 m in radius, then a cloud extending to 2500 m height will persist 95% of the time. Consequently sun shading will occur at least 10% of the time at all points within about 10 km of the source.

Sun shading at operating electric production facilities can be measured by setting out an array of solarimeters, or by using radar imagery and satellite photos. Our laboratory is currently studying Landsat photos of the Keystone and Paradise steam plants, in an attempt to detect cloud cover that might have been initiated by the waste heat from these steam plants.

### 3. Ground Fog

When the visible plume reaches the surface, ground fog results, posing the greatest hazard to nearby automobile traffic. Furthermore, vegetation and structures can also be affected by an increase in the incidence of ground fog. Fog is often observed within a few hundred meters downwind of spray ponds and cooling ponds (Drake, 1975), but mainly occurs during atmospheric conditions that favor the formation of natural fog (e.g. cold, calm mornings). Ground fog within a few hundred meters of mechanical draft cooling towers is also common, due to the tendency of the plume to be brought to the ground by downwash behind the towers when the wind speed exceeds three to five meters per second. Downwash is reported about 40% of the time at the cooling towers at the Oak Ridge Gaseous Diffusion Plant (Hanna, 1974a). But because of the strong buoyant forces in the downwashed plumes, they are observed to "lift-off" the ground at a distance of about 500 m from the towers, after they escape from the aerodynamic cavity region downwind of the towers. The "lift-off" phenomenon is being studied at our laboratory using small scale field experiments, and at the EPA wind tunnel in Raleigh by G. Briggs.

Up until about two years ago, many persons would have said that ground fog due to downwash is nonexistent for natural draft cooling towers. But Bogh (1974) reported that the visible plume sometimes touched the ground at German electric production facilities with natural draft cooling towers that are over 100 m

tall. Also, D. Thomson of Penn. State University has noted the Keystone plume touching the ground on a few occasions. It must be emphasized that these occasions are very rare.

A major component of environmental impact statements has been the prediction of ground fog due to diffusion in the plume after it has reached its final rise. Standard stack plume diffusion formulas (e.g., Gifford, 1968) are used, yielding estimates of the distribution of extra hours per year of ground fog in the area within 50 km of the towers. Visibility in the fog is calculated using basic formulas such as Trabert's (1901). These model estimates are often questioned, for there are no observations of ground fog caused by cooling towers anywhere except in the area within a few hundred meters of the towers. The reason why the moisture does not reach the ground has been pinpointed by Austin of the Massachusetts Institute of Technology in an unpublished note. He argues that there is usually a vertical gradient of water vapor in the atmosphere, with the highest value at the ground as shown in Figure 2. The flux of moisture is naturally from high to low values of water vapor. To reach the ground, the water in the cooling tower plume must go against this gradient. The background gradient is not so much of a problem for  $\text{SO}_2$  plumes, because the concentration of  $\text{SO}_2$  in a plume is much greater than the ambient concentration. To model plume water diffusion at distances downwind where the maximum excess water in the plume is less than the difference



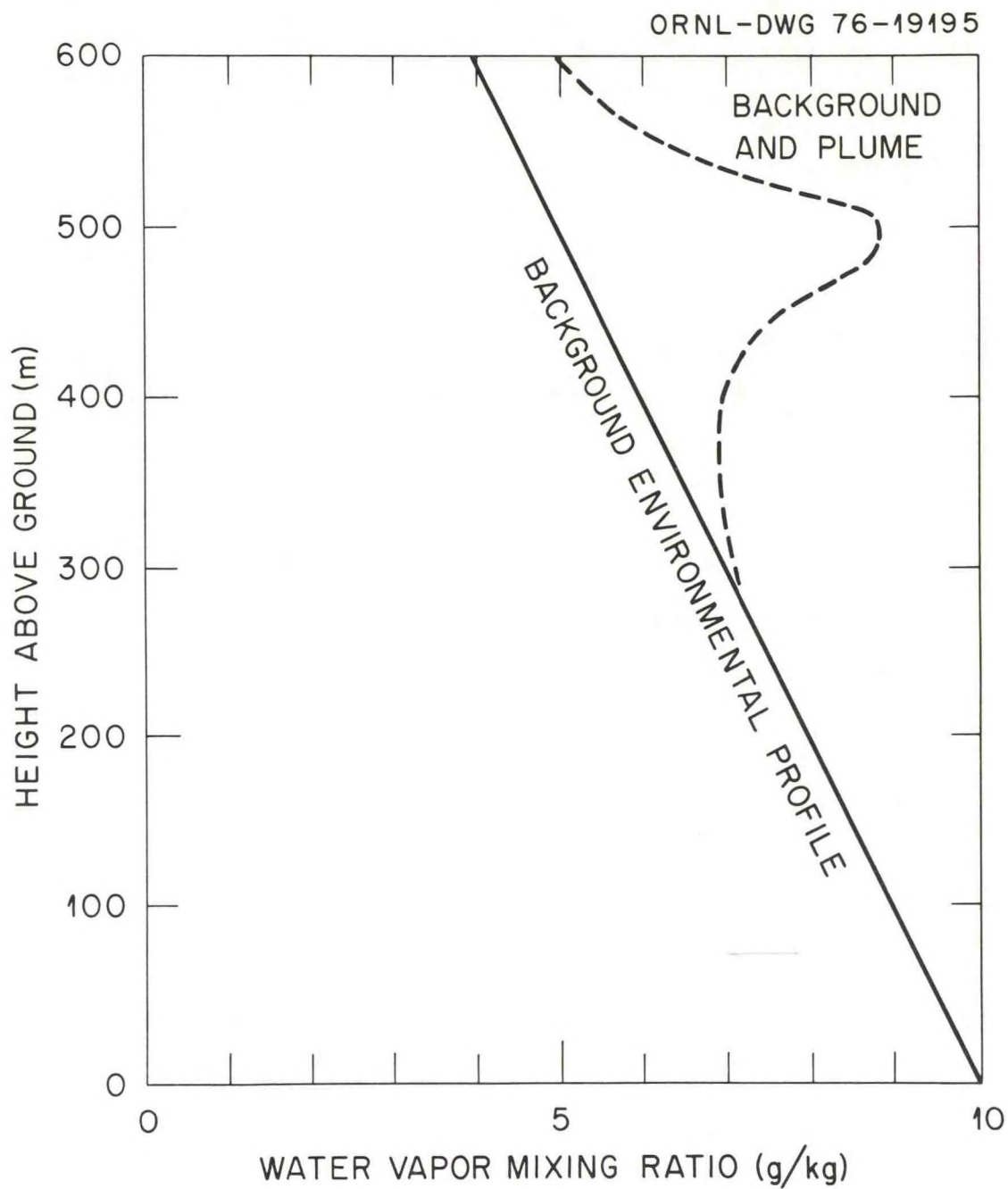


Figure 2: Typical vertical profile of water vapor mixing ratio, with the contribution from a cooling tower plume superimposed. From the usual flux-gradient hypothesis, the flux of water vapor is upward in the layer from the surface to about 350 m.

between the natural water content at the surface and the plume elevation, "K" diffusion theory or second order closure is required.

Measurement programs should be initiated around existing electric production facilities with cooling ponds or towers in order to quantify observations of ground fog. There are several instruments available for sensing fog, most of which operate on the principle of attenuation of a light beam. It is necessary to install several dozens of these instruments and operate them for several years in order to insure that a statistically significant climatology is determined. This type of experiment is now under way in France at a location where a cooling tower that is under construction is expected to produce a plume that impringes on a high plateau adjacent to the tower.

#### 4. Drift Deposition

Ground fog and drift deposition have received the greatest attention in environmental impact reports on cooling towers. Impurities such as herbicides or salts in the circulating cooling water can be carried out the top of the tower by water drops formed as the water splashes over the heat exchange surfaces. After leaving the tower mouth, the drift drops (average diameter about 200  $\mu\text{m}$ ) are carried upward in the buoyant plume but settle relative to the plume updraft due to their large size. They can settle out of the plume and then be carried to the ground, possibly losing mass by evaporation

into the drier environmental air. The efficiency of drift eliminators has progressed so that only about .001% of the circulating water is lost as drift. This amounts to about 2.6 gal/min (156 gm/sec) at a tower such as Chalk Point (Holmberg, 1974). Since the concentration of chlorides in the make up water at Chalk Point is about 4600 ppm, about  $6 \times 10^4$  g of chlorides are sprayed from the tower each day. Much of this drift evaporates to a small dry particle which is carried away by the air. But if all the drift were to fall uniformly over an area with radius 10 km around the tower, the chloride deposition rate would be about  $2 \times 10^{-4}$  g/m<sup>2</sup> day. This is about three orders of magnitude less than the natural salt deposition measured by Moser (1974) at a point about 600 m inland from the New Jersey surf zone. From these figures it can be seen that the effects of drift deposition are slight if the efficiency of the drift eliminators is optimized.

There have been a few preliminary observations taken of the drift deposition around operating cooling towers. For example, Overcamp et al. (1976) report measurements taken during the summer of 1975 of NaCl deposition downwind of the Chalk Point tower, where 22 samplers were located from .18 to 3.23 km downwind of the tower. However, the data are reported as drops/m<sup>2</sup> hr rather than g/m<sup>2</sup> hr and the observations and model predictions differ by an order of magnitude. The Chalk Point program also measured drift deposition



in December, 1975, but the results are uncertain because of the splashing of the drift drops as they hit the sensitive paper (Environmental Systems Corporation, 1976). The results of a second test in June, 1976, have not yet been published.

Wolf et al. (1974) measured chromate deposition downwind of the mechanical draft cooling towers at the Oak Ridge Gaseous Diffusion Plant. Taylor et al. (1974) measured chromium in grass, tobacco, and soil downwind of these towers and found that concentrations significantly above background occurred within about 500 m of the towers. The measurements are difficult to interpret because of the complexity of the source, which consists of three separate banks of towers.

In spite of the lack of observations, there has been a proliferation of drift deposition models. In "Cooling Tower Environment-1974," models by Schrecker et al., Slinn, Pena and Hosker, Hanna, Roffman and Grimble, Laskowski, and Israel and Overcamp are described. McVehil and Heikes (1975) critically reviewed these and other drift deposition models. Chen and Hanna (1977) and Policastro (1976) compared drift deposition models using common input conditions, and found that the magnitudes and downwind locations of the drift deposition maximum predicted by the models differ by two orders of magnitude and several hundred meters, respectively. The models that predict the highest deposition rates are those that assume that the drops begin their downward trajectory at the tower mouth, rather than being carried upward in the rising plume.

In a critical review of methods for calculating drift deposition, Hanna (1974b) recommended that if the final drift drop diameter is less than 200  $\mu\text{m}$ , the drops should be allowed to diffuse according to the Gaussian plume model (Gifford, 1968). The drop plume descends relative to the gaseous plume at a speed equal to the gravitational settling speeds of the drops. Deposition rate then equals the concentration of drift in the air at the surface times the drop settling speed. For drops with diameters greater than 200  $\mu\text{m}$ , the ballistic trajectory technique is recommended. While the drop is in the plume, its vertical speed equals the difference between the vertical speed of the plume and the settling speed. When the drop travels downward a distance equal to the plume radius, it is assumed to break free from the plume. The drop then will evaporate at a rate dependent on its diameter  $D(\text{cm})$ , the mass of solute in it  $M_s(\text{g})$ , the drop settling speed  $V_g(\text{cm/sec})$ , and the saturated  $p_s$  and actual  $p_e$  environmental vapor pressures ( $\text{dynes/cm}^2$ ):

$$dD/dt = ((-7 \times 10^{-10})/D) [1 + 0.59/(DV_g)^{1/2}] [p_s (e^{2.0 \times 10^{-7}/D/(1 + 1.3M_s/D)}) - p_e] \quad (6)$$

If the drop evaporates so that its diameter is less than 200  $\mu\text{m}$ , the Gaussian diffusion formula should be used. As mentioned in section 2, however, if there is a strong vertical gradient of ambient water vapor, the Gaussian assumption is no longer valid and K theory should be used.

Input observations of droplet size distributions at the tower mouth are necessary for the operation of any model. From the few measurements that are available (Holmberg, 1974; Schrecker, 1974; Thomson et al., 1976), it seems that the initial drift characteristics are quite variable, suggesting that observations at the tower mouth should be taken at the same time as ground level drift deposition is being measured.

#### 5. Interference with Aircraft

Because cooling towers and ponds are often located within 100 km of airports, the question has come up whether ponds and plume can affect aircraft. A workshop on aircraft measurements of plumes was held in Oak Ridge in June. Moist plumes are currently being penetrated by the aircraft of several research groups, including Penn. State University (Thomson et al., 1976, Keystone Steam Plant), Meteorology Research, Inc. (Woffinden et al., 1976, Chalk Point Steam Plant), and Battelle Pacific Northwest Lab. (Wolf, 1976, Rancho Seco Nuclear Plant). No one reports icing in the plumes, although this is probably due to the short duration of plume penetration. Turbulence in the plume is reported as moderate to high, but is also of short duration. Some daring pilots fly through the plume at a height of less than one tower diameter above the tower mouth. An abrupt wind shear of about 5 m/s is encountered at either edge of the plume, which requires close attention on the part of the pilot. A record of



plume vertical speed sensed by an aircraft flying near the tower mouth at Keystone is given in Figure 3 (Thomson et al., 1976).

Because of limited visibility, TVA pilots do not fly helicopters in the condensed plume at Paradise (Slawson et al., 1974). It is possible that a serious problem could occur if a commercial or military airplane or helicopter accidentally flew into a plume. In order to determine the possible extent of this problem, existing records of in-plume accelerations and visibilities should be compared with the flight specifications of aircraft which might by chance have to fly through the plume. Also, on a few occasions experimental flights through the plume should be made by various commercial and military aircraft in order to estimate the actual accelerations and visibility losses.

## 6. Interactions with Chemical Plumes

Often cooling towers are built at fossil-fired power plants, where  $\text{SO}_2$  and particles are emitted from a nearby stack. Other types of chemicals may be emitted at refineries or other industries. If the plumes merge, chemical reactions may lead to the production of undesirable substances such as sulfates. It is known that the  $\text{SO}_2$ -sulfate oxidation process occurs more rapidly in a humid environment. In a study at Keystone seven years ago, conducted by the Illinois Institute of Technology Research

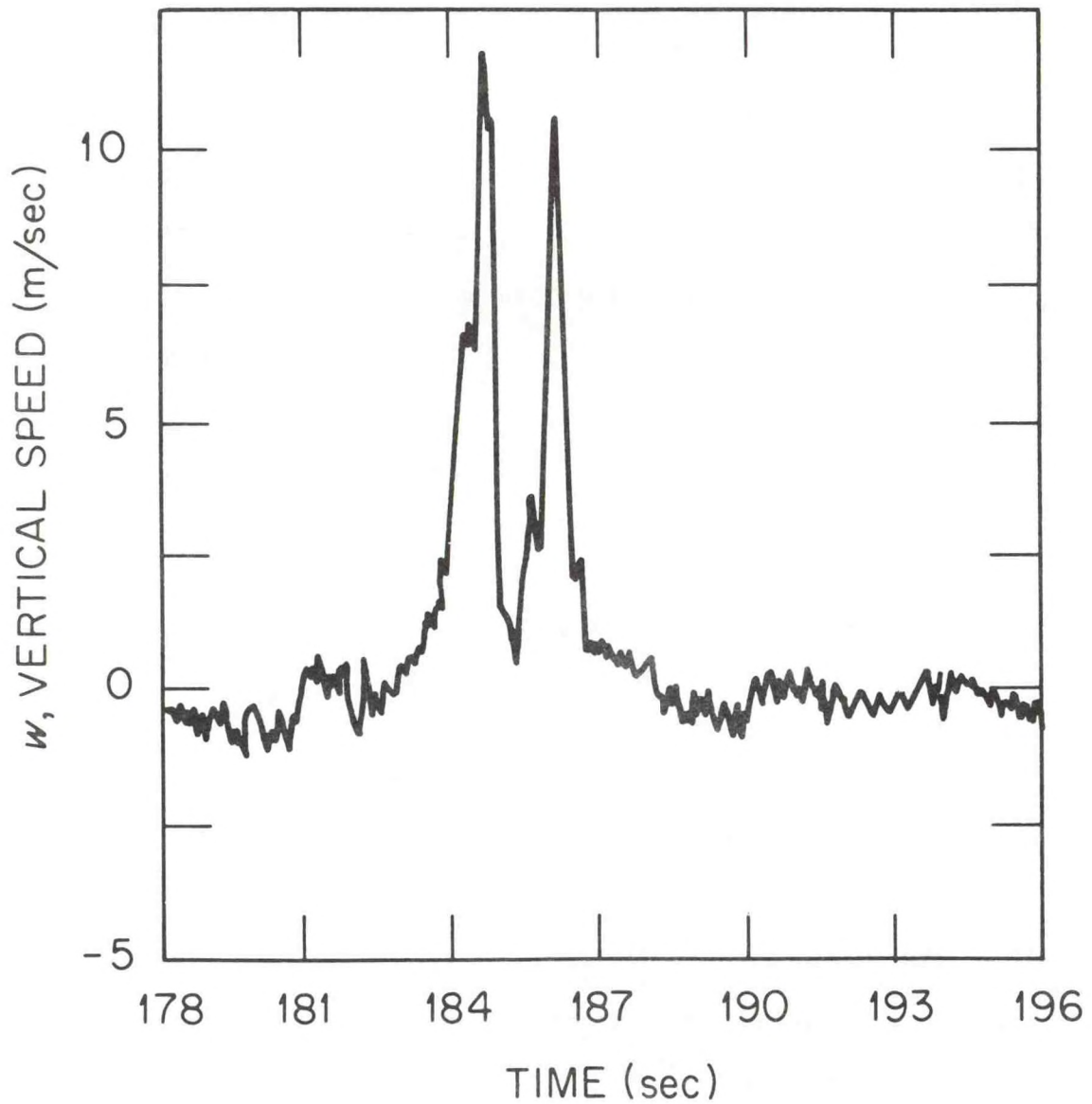


Figure 3: Vertical speed measured through two plumes at Keystone, 93 m above towers 2A and 2B, on 11 March 1975 (Thomson *et al.*, 1976).

Institute (Stockham, 1971) it was determined that acidity in the stack plume increased when the  $\text{SO}_2$  and cooling tower plumes merged. Similar results, also based on the Keystone plant, are reported by Thomson (1976).

Stacks are usually higher than adjacent cooling towers, but the total heat output from the stack is less than that from the cooling tower. Consequently the final plume rise from both sources is nearly the same, about 500 m, and it is not surprising that the stack and cooling tower plumes are often observed to merge. Stockham (1971) used cascade impactors mounted on a helicopter to sample droplets in the merged Keystone plumes. He found that the number ratio of acid drops at pH4-5 to neutral drops at pH6-7 increased from .05 to 3.0 as relative humidity increased from 50% to 95%. The smallest drops had the highest acidity. Thomson (1976) also reported that the smallest drops, those found in the last stage of the impactor, were associated with the highest acid concentrations.

There are two distinct research areas connected with the problem of interactions of cooling tower and chemical plumes. The first is the dynamic problem of the merger of two plumes that have their own distinct circulation systems. When the plumes first touch, only large blobs of air are mixed, and consequently any potential reactants are not well mixed. The other problem is the



question of which chemical reactions take place. There is much work currently underway on sulfur chemistry, due to the recent discovery of high concentrations of sulfate far downwind of urban and industrial sources. Perhaps the ERDA, EPA, and EPRI programs on sulfur chemistry will provide useful input to the cooling tower problem, too.

## 7. High Winds

Very large buoyant plumes can concentrate vorticity existing in the region around the plume, causing the formation of waterspouts and other tornado-like vortices. At currently operating electricity producing facilities, visible vortices are observed only occasionally; e.g. Thomson reports observing a small whirl dangling from the cooling tower plume at Keystone. However, Hanna and Gifford (1975) show that vortices will be much more likely at large energy centers (20,000-50,000 MW), if they are built.

There have been many natural and man made heat sources that have produced vortices, and Briggs (1974) has developed a theory to determine whether a given buoyant source with access to natural vorticity will concentrate this vorticity into a waterspout strong vortex. If the ratio of the tangential velocity of the environmental air,  $V_T$ , to the characteristic vertical speed of the buoyant source,  $V_B$ , is between .15 and .90 it is possible

for vorticity to be concentrated. At values of the ratio  $V_T/V_B$  greater than .90, the buoyancy is not strong enough to concentrate vorticity, and at values of the ratio less than .15, buoyancy is dominant and there is no vortex. The speed  $V_B$  is estimated from  $(F/R)^{1/3}$ , and the maximum speed  $V_T$  on a convective day is assumed by Briggs to equal 1.7 m/s for buoyant sources rising the full depth of the mixed layer,  $z_i$ . On smaller scales  $V_T \approx 6(Hz_i)^{1/3}(R/z_i)$ , where  $H$  is the plume rise.

The result of applying this criterion to various heat sources is summarized in Table 1, illustrating that Briggs' criterion is evidently meaningful for these cases.

TABLE 1. Calculation of the vorticity concentration parameter.

Source	Radius R(m)	Buoyancy flux F(m <sup>4</sup> /s <sup>3</sup> )	$V_B$ (m/s)	$V_\infty$ (m/s)	$V_\infty/V_B$	Observed
Single cooling tower sensible heat	25	3500	5.2	0.32	0.06	Rarely
Cluster of 20 cooling towers	500	70 000	5.2	1.7	0.33	?
sensible heat	5000	70 000	2.4	1.7	0.71	?
Strong natural convection	500	2500	1.7	1.7	1.0	Rarely
Oil burners (Dessens, 1964)	125	6000	3.6	1.6	0.44	Yes
Saturn V (Morris, 1968)	10	1 300 000	51.0	0.13	0.0025	No
Australian bushfires (Taylor et al, 1973)	10 <sup>3</sup>	900 000	13.8	1.7	0.12	Yes

Vortices were observed in Dessens (1964) "Metatron" or oil burner experiment, and in the large Australian (Taylor et al, 1973) bushfires. However they are rarely observed during natural convection, where buoyancy is too weak, or at single cooling towers, where buoyancy overwhelms the tendency to concentrate vorticity. Table 1 shows that vorticity concentration can be expected at large power plants where the crucial combination of energy flux, source radius, and natural vorticity coincide.

Physical modeling and small scale field experiments should be used to further test the validity of the theory of vorticity concentration and study the effects of various source configurations. Snyder (1972) discusses the general scaling rules that apply to wind tunnel models, but we are not yet certain which scaling parameters are most important for this particular problem. It is hoped that it is not necessary to conduct the experiment on the scale used by Dessens (1964), who burned oil at the rate of 800 MW for 20 minutes during each experiment.

Numerical modeling provides another approach to the problem, but is complicated by the need to simulate turbulence in three dimensions and to use enough grid points to cover the vortices that might develop. Two approaches have been considered. The first is based on the work of Deardorff (1974), who calculates the time variability of turbulence quantities at closely spaced grid point. About 20% of the turbulence energy is associated with sub grid scales and is parameterized. However, one 24 hour run



consumes about \$100,000 of computer time, and yields only a single time series of the turbulent variables. To calculate statistically significant averages, several runs must be made. He assumes cyclic boundary conditions, which are not correct for the energy center problem. Because of the problems with boundary conditions and computer time, this option does not seem workable at this time. The other approach is based on second order closure techniques developed by, for example, Lumley and Kajeh-Nouri (1974). Using this method, the average fields of wind speed, temperature, and so on, are calculated at each grid point. However, if the expected vortex is intermittent, it may not be revealed by second order closure modeling. The inclusion of cloud physics terms further complicates the problem and may necessitate going to third order closure.

#### 8. Changes in Cloudiness, Temperature, and Precipitation

Current power plants, with maximum waste energy outputs of 5000 MW, are observed to generate large clouds which occasionally result in light precipitation. Light snowfalls downwind of cooling towers were reported by Culkowski (1961) in Oak Ridge and Kramer et al (1976) in Charleston, West Virginia. The snow in Charleston fell at distances from about 5 km to about 50 km downwind of the John E. Amos plant. Moore (1974) reports no

significant difference in rainfall rates measured around cooling towers in England. There are no reports of thunderstorm generation by cooling tower plumes, although they clearly have the potential to trigger thunderstorms. Furthermore, there are no reports of precipitation caused by spray or cooling ponds. The statistical problems in determining a significant variation in rainfall are so great that it is doubtful that a prediction of a small increase (say, 5%) in rainfall could be verified. Many years of records at a large network of stations are required. A few precipitation networks of this type have begun operation around proposed power plants, such as in Michigan and France, but it will be years before the data can be properly evaluated.

Large urban areas, with waste energy outputs of several hundred thousand MW, are known to affect precipitation patterns (Huff and Changnon, 1973) and cause increased surface temperatures over regions as much as 100 km in diameter (Peterson, 1969). From an energy standpoint it is therefore expected that large power parks (50,000 MW) will increase temperatures and rainfall over a mesoscale region. It is important to set up a network of precipitation, temperature, cloudiness, and fog instruments now, several years before a large facility is built, so that a stable pre-operational climatology can be established.

Preliminary thermodynamic models of cooling tower plumes, including cloud physics processes, have been developed by EG&G (1971), Hanna (1971, 1976), Bhumralkar (1976), and Lee (1976). In addition, Carl Hane (unpublished Battelle Pacific Northwest Laboratory memo) has applied his thunderstorm model using the energy input from a power park. During convectively unstable conditions, a 1000 MW cooling tower can produce a tall cumulus cloud in all of these models. Hanna's (1976) one-dimensional steady-state model, with all variables assumed to be functions only of height, is based on Briggs' (1975) plume rise theory and Weinstein's (1970) cloud model. This model was applied to four month's radiosonde observations from Nashville, using single  $10^3$ ,  $10^4$ , and  $10^5$  MW towers and a  $10^5$  MW energy park as input. It was found that a cloud averaging 2500 m deep existed 95% of the time over a single  $10^5$  MW tower, which is certainly an argument against concentrating the waste heat release from an energy center into as small an area as possible. An example of the profiles of vertical speed temperature, and liquid water content in the model cloud for an unstable summer day is given in Figure 4.

Current models of clouds from power production facilities can be improved greatly by:

- a. Measuring cloud physics parameters in plumes, thus determining whether Kessler's (1969) natural cloud parameterizations are valid for cooling tower plumes.



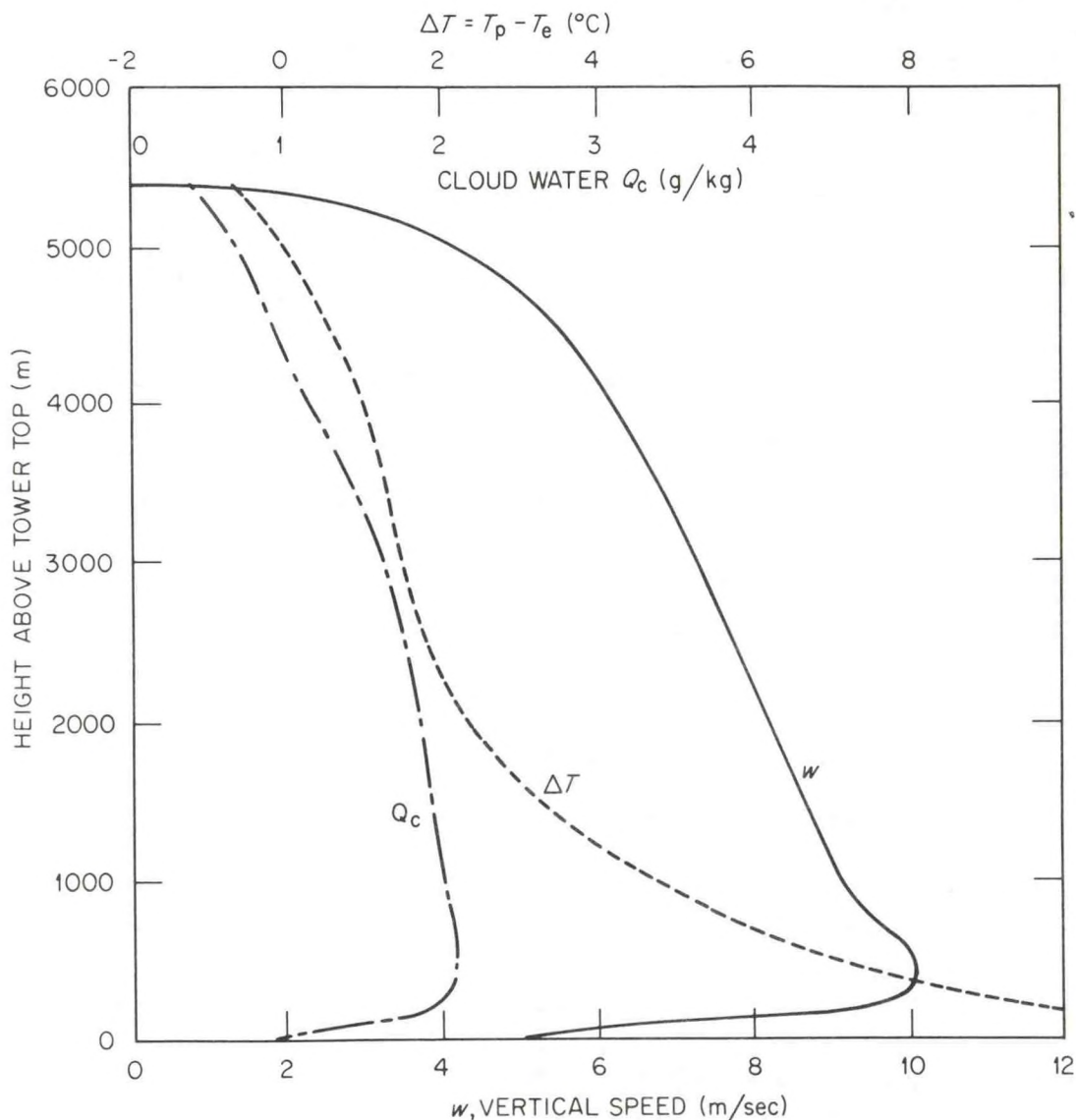


Figure 4: Predicted vertical profiles of vertical speed, temperature difference, and cloud water content in the plume from a cooling tower with 300 m radius releasing  $10^5$  MW. The atmospheric sounding used to generate these results was taken in Nashville at 2315 Z on 14 July 1974. Thunderstorms were observed on this day.

- b. Measuring the initial drop size distribution at the tower mouth.
- c. Determining the correct method for parameterizing rainfall from bent-over plumes.
- d. Developing two and three dimensional models that can account for plume merging and the effects of the plumes on their surrounding environment. Hill's (1974) model of multiple clouds would be a good beginning point.

Satellite photographs are an important tool for analyzing regional weather modification, but have not yet been used in a quantitative way. They are often used at meetings to enhance the visual presentation, but are not used to estimate diffusion or cloudiness increases, for example. Other remote sensors such as radars, lasers, and acoustic sounders would be useful in the study of weather modification around steam plants. It might be reasonable to replace a network of precipitation gauges with a single radar.

#### 9. Further Comments

Many of the research areas identified above are on the frontiers of meteorological research at the present time. It is necessary to work closely with cloud physicists and dynamicists

and computer specialists in order to insure that the most up-to-date concepts are used in the particular application of computer models to problems of atmospheric effects of electric power production.

There are several ongoing programs in the U.S. today which are directly related to the effects discussed above. The largest program, with a budget of about one million dollars per year, is primarily concerned with drift deposition at the Chalk Point steam plant (Pell, 1974). The ERDA program, "Atmospheric Effects of Nuclear Energy Centers," funded at a level of about one-half million dollars per year, is concerned with the potential effects of large (10,000 MW and up) energy centers. In addition, EPRI is sponsoring research in Illinois on the effects of cooling ponds and NRC is sponsoring a review of computer models of visible plumes and drift deposition and the application of Orville's two dimensional cloud model to an energy center. Other work is being conducted by agencies such as TVA and there is a great deal of proprietary work being done for utilities, who are concerned about environmental impact statements for new facilities.

Acknowledgements: This research was performed under an agreement between the National Oceanic and Atmospheric Administration and the Energy Research and Development Administration.



## References

- Alkezweeny, A. J., D. W. Glover, R. N. Lee, J. W. Sloat, and M. A. Wolf, 1974: Measured chromium distributions resulting from cooling tower drift. CTE74, 558-572.
- Bhumralkar, C., 1976: Weather modification caused by waste heat rejected into the atmosphere from cooling towers at large power parks. Proceedings, Third Symp. on Atmospheric Turbulence, Diffusion, and Air Quality, 19-22 Oct. 1976, Raleigh, available from Amer. Meteorol. Soc., 45 Beacon St., Boston, Mass., 02108, 581-585.
- Briggs, G. A., 1969: Plume Rise. AEC Critical Review Series, USAEC-TIC-24635, available from Springfield, Va., National Technical Information Service (NTIS), vi +81 pp.
- Briggs, 1974: Plume rise from multiple sources. In Cooling Tower Environment-1974 (CTE74) 161-179.
- Briggs, 1975: Plume rise predictions, Lectures on Air Pollution and Environmental Impact Analyses, American Meteorological Society, 45 Beacon St., Boston, Mass., 02108, 59-111.
- Bogh, P., 1974: Experience with combined wind tunnel-plume model analysis of cooling tower environmental impact. CTE74, 265-290.
- Chen, N. and S. R. Hanna, 1977: Drift--modeling and monitoring comparisons, presented at annual meeting of Cooling Tower Institute, 27-29 Jan. 1977, Houston.
- Cooling Tower Environment-1974, ERDA Symposium Series, CONF-740302, Nat. Tech. Information Service, U. S. Dept. of Commerce, Springfield, Va., 22161, (\$13.60), 638 pp.
- Cotton, W. R., 1975: Theoretical cumulus dynamics. Reviews of Geophysics and Space Physics, 13, 419-447.
- Culkowski, W. M., 1962: An anomalous snow at Oak Ridge, Tennessee. Mon. Wea. Rev., 90 (5), 194-196.
- Deardorff, J. W., 1974: Three-dimensional numerical study of the height and mean structure of a heated planetary boundary layer. Boundary Layer Meteorol., 7, 81-106.
- Dessens, J., 1964: Man made thunderstorms. Discovery, 25, 40-44.
- Drake, R. L., 1975: A review and evaluation of information on the thermal performance of ultimate heat sinks: spray ponds and cooling ponds. Report BNWL-B-446 by Battelle Pacific Northwest Laboratory, Richland, Wash. 99352, 280 pp.

Edgerton, Germeshausen, and Grier, Inc., 1971: Potential environmental modifications produced by large evaporative cooling towers. Prepared by EG&G, Inc., Boulder, Colo. under Cont. No. 16130 DNH 01/71 from the Water Quality Office, EPA, available from Supt. of Documents, U.S. Govt. Printing Office, Washington, 77 pp.

Environmental Systems Corporation, 1976: Chalk Point Cooling Tower Project Seasonal Test Data for the Period December 15-19, 1975, Report no. PPSP-CPCTP-8, Prepared by ESC, Knoxville, Tn. for the Md. Power Plant Siting Program, Chalk Point Cooling Tower Project, 157 pp.

Gifford, F. A., 1968: An outline of theories of diffusion in the lower layers of the atmosphere. In Meteorology and Atomic Energy--1968. D. H. Slade (Ed.), USAEC Report TID-24190, available from Springfield, Va., NTIS, pp. 65-116.

Hanna, S. R., 1971: Meteorological effects of cooling tower plumes. Presented at Cooling Tower Inst. Meeting, Houston, 25 Jan., 17 pp., available as report no. 48 from ATDL, P.O. Box E, Oak Ridge, Tenn., 37830.

Hanna, S. R., 1974b: Fog and drift deposition from evaporative cooling towers. Nuclear Safety, 15, 190-196.

Hanna, S. R., 1974a: Meteorological effects of the mechanical draft cooling towers of the Oak Ridge Gaseous Diffusion Plant. CTE74, 291-306.

Hanna, S. R., 1976: Predicted and observed cooling tower plume rise and visible plume length at the John E. Amos power plant. To be published in Atmos. Environ.

Hanna, S. R. and F. A. Gifford, 1975: Meteorological effects of energy dissipation at large power parks. Bull. Am. Meteorol. Soc., 56, 1069-1076.

Hill, G. E., 1974: Factors controlling the size and spacing of cumulus clouds as revealed by numerical experiments. J. Atmos. Sci., 31, 646-673.

Holmberg, J. D., 1974: Drift management in the Chalk Point Cooling Tower, CTE74, 128-146.

Huff, F. A. and S. A. Changnon, Jr., 1972: Climatological assessment of urban effects on precipitation at St. Louis. J. Appl. Meteor., 11, 825-843.

Israel, G. W. and T. J. Overcamp, 1974: Drift deposition model for natural draft cooling towers. CTE74, 614-628.



- Junod, A., R. J. Hopkirk, D. Schmeiter, and D. Haschke, 1974: Meteorological influences of atmospheric cooling systems as projected in Switzerland. CTE74, 239-264.
- Kessler, E., 1969: On the distribution and continuity of water substance in Atmospheric Circulations. Meteorol. Monographs, 10, 84 + ixpp, published by the Am. Meteorol. Soc., 45 Beacon Street, Boston.
- Kramer, M. L., D. E. Seymour, M. E. Smith, R. W. Reeves, and T. T. Frankenberg, 1976: Snowfall observations from natural draft cooling tower plumes. Science, 193, 1239-1241.
- Laskowski, S., 1974: Mathematical transport model for salt distribution from a saltwater natural draft cooling tower. CTE74, 598-613.
- Lee, J., 1976: A numerical simulation of atmospheric convection caused by heat dissipation at large power centers. Proceedings, Third Symp. on Atmospheric Turbulence, Diffusion, and Air Quality, 19-22 Oct. 1976, Raleigh, available from Amer. Meteorol. Soc., 45 Beacon St., Boston, Mass., 20108, 563-570.
- Lewellen, N. S., D. A. Oliver, M. E. Teske, and G. G. Williamson, 1976: Status Report on a Low-Level Atmospheric Turbulence Model for Marine Environment. Report no. 289 by Aeronautical Research Associates of Princeton, Inc., 50 Washington Rd., Princeton, N. J. 08540, prepared for U.S. Dept. of the Navy, 77 pp.
- Lumley, J. L. and B. Kajeh-Nouri, 1974: Computational modeling of turbulent transport. Advances in Geophysics, vol. 18A, Academic Press, 169-192.
- McVehil, G., and K. Heikes, 1975: Cooling tower plume modeling and drift measurement. Prepared by Ball Bros. Res. Corp., Boulder, Colo., iv + 125 pp.
- Meyer, J. H., T. W. Eagles, L. C. Kohlenstein, J. A. Kagan and W. D. Stambro, 1974: Mechanical-Draft Cooling Tower Visible Plume Behavior: Measurements, Models and Predictions. CTE74, 307-352.
- Moore, D. J., 1974: Recent Central Electricity Generating Board research on environmental effects of wet cooling towers. CTE74, 205-220.
- Morris, D. G., 1968: Initiation of convective clouds due to static firing of the Saturn V first stage. Bull. Amer. Meteor. Soc., 49, 1054-1058.



- Moser, B. C., 1974: Airborne sea salt: techniques for experimentation and effects on vegetation. CTE74, 353-369.
- Overcamp, T. J., G. W. Israel, and W. J. B. Pringle, 1976: Drift droplet deposition measurements from a brackish-water natural draft cooling tower. Proceedings, Third Symp. on Atmospheric Turbulence, Diffusion, and Air Quality, 19-22 Oct. 1976, Raleigh, available from Amer. Meteorol. Soc., 45 Beacon St., Boston, Mass., 02108.
- Pell, J., 1974: The Chalk Point Cooling Tower Project. CTE74, 88-127.
- Pena, J. A. and C. L. Hosler, 1974: Influence of the choice of the plume diffusion formula on the salt deposition rate calculation. CTE74, 573-584.
- Peterson, J., 1969: The climate of cities: A survey of recent literature. U.S. Dept. of Health, Educ., and Welfare, Pub. Health Ser., Raleigh, N.C.
- Policastro, A. J., W. E. Dunn and R. Carhart, 1976: Generic Report on Environmental Effects of Atmospheric Cooling Systems. Progress Report 1 Nov. 75-31 July 76, prepared by Argonne Nat. Lab., Argonne, Ill. for the Nuclear Regulatory Commission, 59 pp.
- Roffman, A. and R. E. Grimble, 1974: Drift deposition rates from wet cooling systems. CTE74, 585-597.
- Schrecker, G. O., K. R. Wilber, and F. Shafner, 1974: Prediction and measurement of airborne particulate concentrations from cooling-device sources and in the ambient atmosphere. CTE74, 455-482.
- Slawson, P. R., J. H. Coleman, and J. W. Frey, 1974: Some observations on cooling-tower plume behavior at the Paradise Steam Plant, CTE74, 147-160.
- Snyder, W. H., 1972: Similarity criteria for the application of fluid models to the study of air pollution meteorology, Boundary-Layer Meteor., 3, no. 1 (Sept.), 113-134.

- Stockham, J., 1971: Cooling Tower Study, Contract no. CPA 22-69-122, IIT Research Institute, Technology Center, Chicago, Ill. 60616 for EPA Air Poll. Cont. Office, 411 W. Chapel Hill St., Durham, N.C. 27701, 108 pp.
- Taylor, F. G. Jr., L. K. Mann, R. C. Dahlman, and F. L. Miller, 1974: Environmental effects of chromium and zinc in cooling-water drift. CTE74, 408-426.
- Taylor, R. J., S. T. Evans, N. K. King, E. T. Stephens, D. R. Packham, and R. G. Vines, 1973: Convective activity above a large scale brushfire. J. Appl Meteor., 12, 1144-1150.
- Thomson, D. W., 1976: Environmental Impact of Evaporative Cooling Tower Plumes. Dept. of Meteorol., The Penn. State Univ., University Park, Pa., 16802, prepared for ERDA under contract no. E(11-1)2463, 44 pp.
- Thomson, D. W., J. M. Norman, and R. L. Miller, 1976: Airborne measurements of turbulent temperature and velocity fluctuations in cooling tower plumes. Proceedings, Third Symp. on Atmospheric Turbulence, Diffusion, and Air Quality, 576-580.
- Trabert, N., 1901: Die extinction des lichtetes in einem truben medium (Schweite in wolken). Meteorol. Z., 18, 518-520.
- Weinstein, A. I., 1970: A numerical model of cumulus dynamics and microphysics. J. Atmos. Sci., 27, 246-255.
- Woffinden, G. J., J. A. Anderson, and P. R. Harrison, 1976: Aircraft Survey, Chalk Point Cooling Tower Plume, Dec. 1975, Rept. no. 76R-1910 by MRI, Altadena, Calif. 91001 for the Md. Power Plant Siting Program. 32 pp + appendices.
- Wolf, M. A., 1976: Natural draft cooling tower plume characteristics determined with airborne instrumentation. Pac. Northwest Lab. Annual Rep. for 1975 to the USERDA DBER. Part 3 Atmospheric Sciences, BNWL-2000 PT3, 281-288.





Drift — Modeling and Monitoring Comparisons

by

Norbert C. J. Chen  
Engineering Technology Division  
Oak Ridge National Laboratory

and

Steven R. Hanna  
Air Resources Atmospheric Turbulence and Diffusion Laboratory  
National Oceanic and Atmospheric Administration

Presented at  
Cooling Tower Institute  
Houston, Texas  
January 31, 1977 — February 2, 1977

By acceptance of this article, the publisher or recipient acknowledges the U.S. Government's right to retain a non-exclusive, royalty-free license in and to any copyright covering the article.

ATDL Contribution File No. 76/24

## ABSTRACT

Several drift deposition models are compared using a set of standard input conditions. The predicted maximum drift deposition differs by two orders of magnitude, and the downwind locations of the maximum differ by one order of magnitude. The discrepancies are attributed mainly to different assumptions in the models regarding the initial effective height of the droplets.

Current programs in which drift characteristics at the tower mouth and drift deposition downwind of the tower are being measured are summarized. At the present time, drift deposition measurements, sufficiently comprehensive for model verifications, are unavailable. Hopefully, the Chalk Point Program will satisfy this need.

### 1. INTRODUCTION

Congress is looking into the conglomeration of nuclear reactors into energy centers of limited area. The program entitled "Atmospheric Effects of Nuclear Energy Centers," supported by the Energy Research and Development Administration (ERDA), is intended to centralize research on model development and verification in regard to local and regional environmental effects. As a part of this effort, a state-of-the-art review dealing with cooling tower drift was prepared.

Drift from cooling towers can corrode and damage structures in the immediate vicinity of the towers, cause a public nuisance if located near parking lots or high-density traffic areas, and endanger local vegetation. The estimation of salt deposition has relied primarily on predictions from a variety of models, with very few direct measurements. One of the major efforts in our program is to evaluate the assumptions, limitations, and applicabilities of various analytical models for drift deposition prediction. A common set of input parameters — an essential element for model evaluation — is provided for the model comparison.

When a small amount of the circulating water in a cooling tower is entrained and carried aloft by the air stream, the droplets, which vary from a few to several thousand microns in diameter, are referred to as drift. These droplets contain chemicals in roughly the same concentration as in the cooling water. In a modern cooling tower system, with efficient

eliminators, the ratio of drift rate to circulating water rate can be as low as 0.001%.

The drift deposition problem is a complicated one involving several interrelated processes: the dynamics and thermodynamics of drops in a rising plume, the point at which the drops break free from the plume, dispersal by atmospheric turbulence, and possible evaporation in the ambient atmosphere. To make deposition estimates, the source characteristics of the tower, such as tower geometry, amount of water circulated, effluent speed, droplet emission spectra, drift rate, and salt concentration, must be known. Calculations must be made of the plume rise, which in part depends on the initial momentum and buoyancy flux and on the ambient atmospheric conditions. Droplet transport, which depends on meteorological conditions such as the atmospheric relative humidity, turbulence, temperature and its gradient, and wind velocity, must be estimated.

A discussion of the models and a comparison of the predicted ground salt deposition using a common set of input conditions are described in Section 2. Various measurement techniques and comparisons of measured drift emission spectra are described in Section 3.



## 2. MODEL STUDIES AND COMPARISONS USING A COMMON SET OF INPUT CONDITIONS

Ten available models have been reviewed;<sup>(1)</sup> it is found that each model employs some simplifying assumptions to make deposition predictions mathematically tractable. Certain parameters within each require tuning before reliable predictions are possible.

Models are compared (Table 1) by means of some prominent characteristics, with no attempt made to examine all details. Basically, there are two methods for deposition prediction. First, in the ballistic method, the trajectory is determined by the droplet fall velocity and the wind vector. Second, in the tilted Gaussian plume method, the axis of the plume of a given class of droplet sizes falls in proportion to the settling velocity of the mean droplet, with respect to the gas plume. The atmospheric diffusion is simulated by a Gaussian distribution, with the use of Pasquill  $\sigma$  values. Some of the models involve a combined method; that is, the trajectory technique for the large droplets with radii greater than about 100  $\mu\text{m}$  and the Gaussian plume technique for smaller droplets. The majority of models use plume-rise equations derived by Briggs.<sup>(16)</sup> Assumptions concerning breakaway points vary from model to model. Although the treatment of evaporation differs among models, most of them apply the method of Hosler, et al.<sup>(2)</sup>

As stated earlier, before long-term field data become available to verify models, a valuable and effective program is to study the behavior and range of predictions of all current models using a set of identical input parameters. The set of tower and meteorological conditions, listed in Table 2, simulates as closely as possible the conditions at a typical natural-draft cooling tower. Five observed drift-drop-size distributions are plotted in Fig. 4. In addition, the drift-drop size curve arbitrarily chosen for this model comparison is labeled as Curve 6 on the figure.

Given the input data, most of the models estimate that the cooling tower plume will level off at about 500 m above the ground at a downwind distance of about 550 m from the tower. Results of the model calculations are shown in Figs. 1-3 where the individual curves are labeled A, B, C,

Table 1. Summary of model characteristics for ground deposition rate prediction<sup>a</sup>

Investigator	Method	Atmospheric turbulence diffusion	Plume rise formula	Breakaway point	Evaporation
Hosler, et al. <sup>2</sup> May 1972	Ballistic	No	Ns <sup>b</sup>	Drop fall velocity exceeds updraft	Three categories: no evaporation, saturated solution, and dry particles
Roffman & 3-5 Grimble Jan. 1973	K-Theory	Yes, constant K assumed	Briggs	Max. plume rise	Same as Hosler, et al.
Wistrom & Ovard <sup>6</sup> Jan. 1973	Ballistic - large drops; Gaussian - small drops	Yes, PC <sup>c</sup>	Ns <sup>b</sup>	Tower top	Yes
Slinn, <sup>7</sup> Mar. 1974	Ballistic - large drops; Gaussian - small drops	Yes, PC <sup>c</sup>	Briggs	Tower top - large drops; Max. plume rise - small drops	No
Laskowski <sup>8</sup> Mar. 1974	Ballistic-Gaussian	Yes, PC <sup>c</sup>	Briggs or Slawson & Csanady	Drop fall distance exceeds plume radius	Yes
Israel & Overcamp <sup>9</sup> Mar. 1974	Gaussian	Yes, BNL <sup>d</sup> or PC	Briggs or Slawson & Csanady	Drop fall velocity exceeds updraft	Same as Hosler, et al.
Hanna, 10, 11 Mar. 1974	Ballistic - large drops; Gaussian - small drops	Yes, PC <sup>c</sup>	Briggs	Drop fall distance exceeds plume radius	Yes
Wolf, <sup>e</sup> Mar. 1974	Ballistic	No	Briggs	Ns <sup>b</sup>	Yes
Tsai & Johnson <sup>12</sup> April 1974	Ballistic	Ns <sup>b</sup>	Extension of Morton, Taylor, & Turner model <sup>f</sup>	Fall velocity exceeds updraft	Yes
ORFAD <sup>g</sup> 13, 14 Jan. 1975	Ballistic	No	Briggs	Ns <sup>b</sup>	Same as Hosler, et al.
Rao, et al. <sup>15</sup> May 1975	Ballistic-Gaussian	Yes	Extension of Morton, Taylor, & Turner model <sup>f</sup>	Ns <sup>b</sup>	Empirical formula

<sup>a</sup>Effects of downwash and washout are accounted for only by Laskowski.

<sup>b</sup>No specification is given in the model.

<sup>c</sup>Pasquill-and-Gifford stability class.

<sup>d</sup>Brookhaven National Laboratory stability class.

<sup>e</sup>Wolf's model is not reviewed in this report.

<sup>f</sup>B. R. Morton, G. Taylor, and J. S. Turner, "Turbulent gravitational convection from maintained and instantaneous sources," Proc. Roy. Soc. (London) Ser. A234, 1956, 1-23.

<sup>g</sup>Oak Ridge fog and deposition model.

Table 2. Parameters used in the calculations

Saturated plume initially

Plume temperature at exit from tower,  $T_{po} = 305^{\circ}\text{K}$

Ambient temperature near exit from tower,  $T_{eo} = 275^{\circ}\text{K}$

Tower height = 100m

Tower exit diameter = 60m

Efflux velocity = 4.3 m/sec

Amount of circulating water = 31.5 m<sup>3</sup>/sec

Drift rate =  $2 \times 10^{-5}$

Water salinity = 3.45%

Wind speed = 4.3 m/sec

Calculate salt deposition rate for a sector of 22.5°

Frequency of wind direction which blows toward the sector = 1

Ambient relative humidity = 70% (constant with height)

Isothermal ambient atmosphere (slightly stable atmosphere)

Drop size distribution:

Diameter interval ( $\mu\text{m}$ )	Mass mean diameter for interval ( $\mu\text{m}$ )	Mass fraction
0-100	50	0.05
100-200	150	0.3
200-300	250	0.4
300-400	350	0.15
400-500	450	0.075
500-600	550	0.025



etc. Because of an agreement with the persons who developed some of the models, the curves are not identified with their authors. Curves A and B in Fig. 1 are the result of models whose maxima roughly bracket the maxima predicted by the other curves. Curve A is obtained using the trajectory method, assuming that all droplets break away at the tower top and that no evaporation occurs. The resulting deposition pattern has a larger maximum deposition which occurs closer to the source than the pattern of any of the other models. Curve B is obtained by applying the Gaussian diffusion model, assuming that all droplets break away at the height of the maximum plume rise and that they evaporate completely. The resulting deposition pattern has a smaller maximum deposition at nearly all distances on the figure than any of the other models in the range of downwind distance considered. Any model prediction of the maximum deposition falling outside of these two extreme curves would indicate that an error may have occurred.

The curves in Figs. 1-3 group into three general shapes, depending on the assumptions involved in the models: (1) histograms with six steps corresponding to six classes of droplet size, where ground deposition is assumed to be uniform over the particle size range; (2) curves representing the superposition from six isolated Gaussian curves, where turbulent mixing causes overlap in ground deposition between particle-size classes and, hence, smearing of the interface; and (3) curves resulting from a combination of the above two methods — the trajectory technique for large droplets and the Gaussian diffusion model for small droplets. In Curve I, the step function has been smoothed by increasing the number of groups in the droplet-size distribution. At a downwind distance of about 1 km, comparison between the models (with two extreme Cases A and B excluded) shows a disagreement of at least two orders of magnitude in the predicted deposition rates. Furthermore, there is a wide range in the locations of the peak deposition rates. Some of this variance can be identified with differing assumptions concerning the effective height of particle emission and/or the extent of droplet evaporation. It is observed in every individual model in Figs. 1-3 that the maximum deposition rate and the downwind distance where the peak is

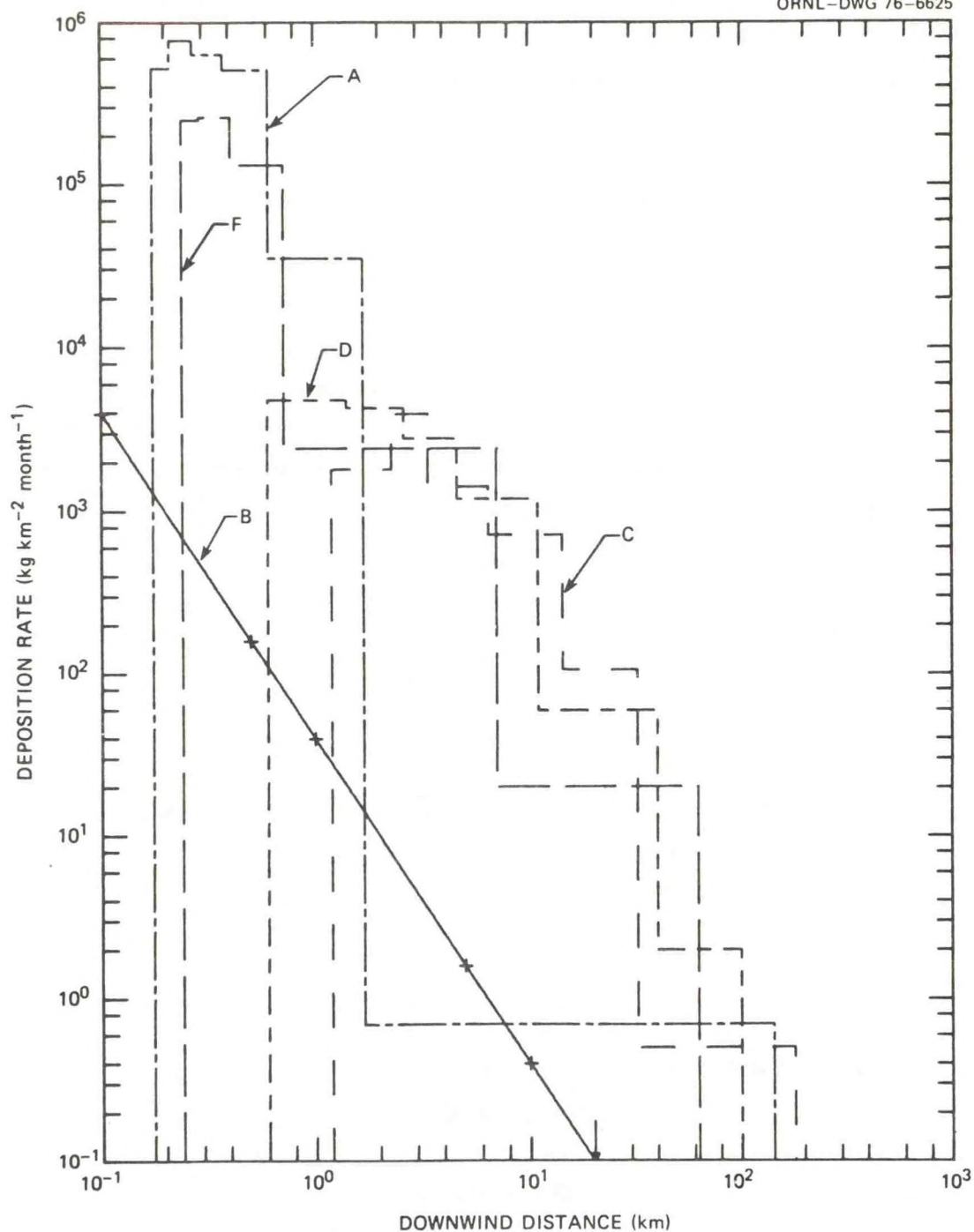


Fig. 1. Model comparison using the input parameters shown in Table 2. The predicted deposition rate is plotted against the downwind distance.

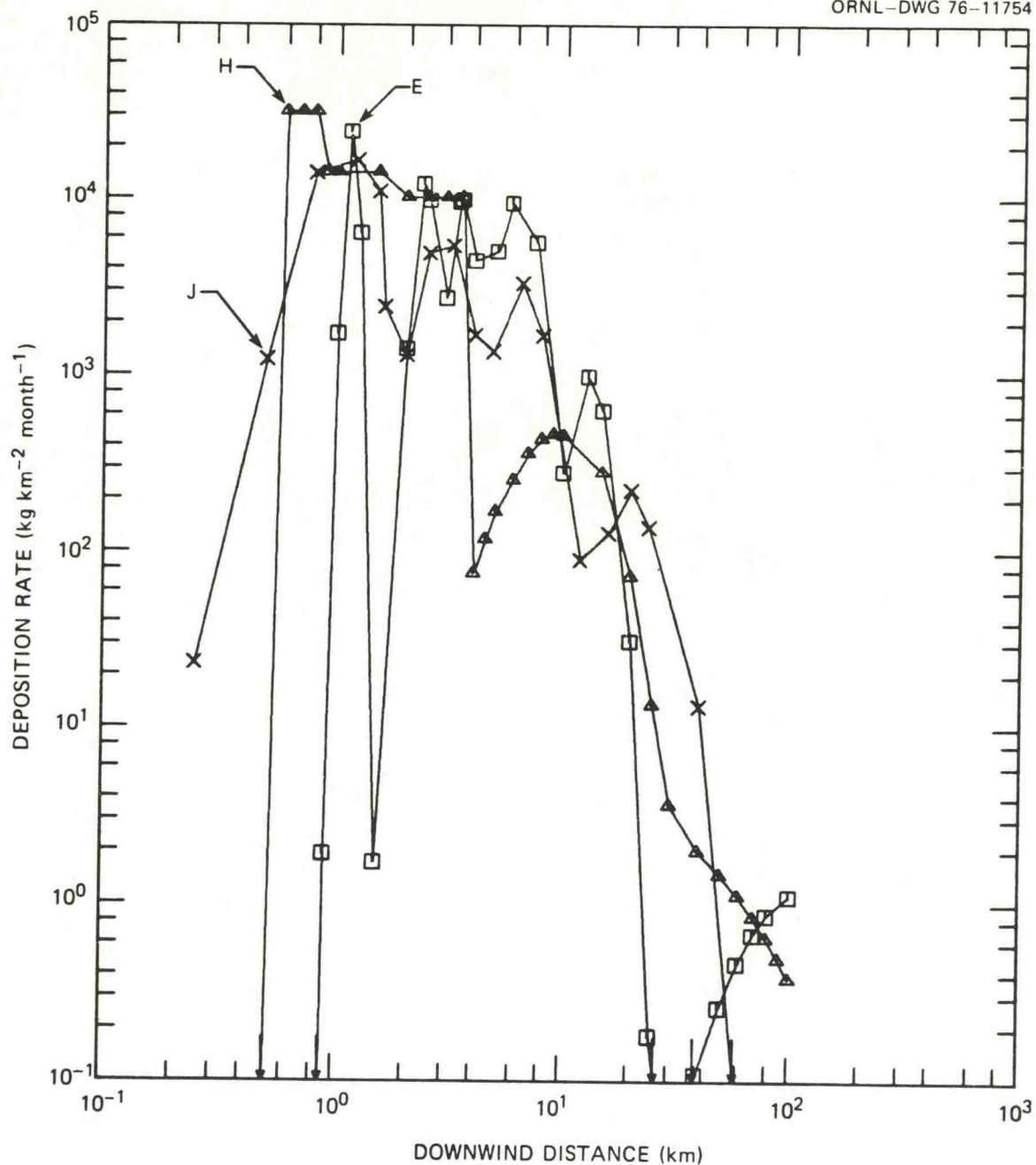


Fig. 2. Model comparison using the input parameters shown in Table 2. The predicted deposition rate is plotted against the downwind distance.



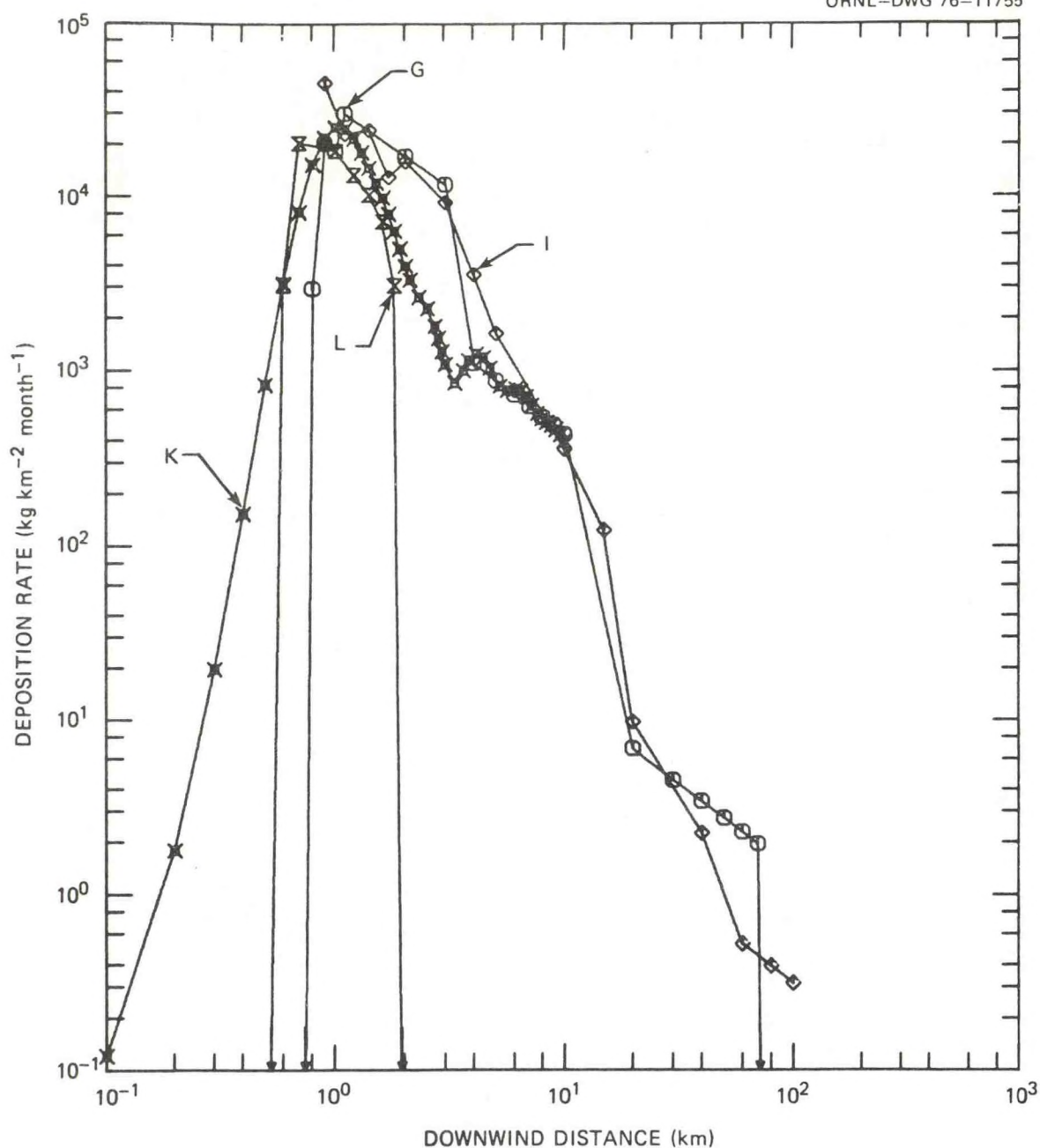


Fig. 3. Model comparison using the input parameters shown in Table 2. The predicted deposition rate is plotted against the downwind distance.

located are mainly determined by the largest droplet size class in the emission spectrum. While the deposition rates fall off rapidly with increasing distance from the tower, the discrepancy between predictions in the far field (for example, at about 100 km) is similar to that at 1 km. Results in the far field obtained by applying Pasquill-Gifford  $\sigma$  curves should be viewed cautiously because the  $\sigma$  values have been extended to distances greater than those from which they were derived.

Whichever method is used, the salt mass should be conserved — one of the essential elements of any model. For the parameters provided, total mass emission of NaCl from the tower is 22 g/sec. By integrating the sector-averaged deposition rate ( $\text{kg}/\text{km}^2/\text{month}$ ), it is found that total salt deposition ( $\text{kg}/\text{month}$ ) predicted by models which use only the trajectory method equals approximately the amount emitted, whereas total salt deposition predicted by the models which use the Gaussian diffusion method is about twice the amount emitted.

The maximum deposition rate, its downwind location, and the ratio of NaCl deposited to that emitted is tabulated for all the models in Table 3. The last column is computed by integrating the averaged deposition ( $\text{kg}/\text{km}^2/\text{month}$ ) over a  $22\text{-}1/2^\circ$  sector from 0.1 to 100 km. The integration interval for model K is from 0.1 to 10 km and for model L from 0.5 to 2 km.

Table 3. Summary of model predicted maximum deposition rate, location, and ratio of NaCl deposited to that emitted

Model	Maximum deposition rate (Kg/Km <sup>2</sup> /month)	Location from source (Km)	NaCl deposited (gm/sec)* NaCl emitted (gm/sec)
C	4,000	From 2.3 to 3.4	1.03
D	4,800	From 0.6 to 1.4	1.02
E	24,000	1.1	1.88
F	260,000	From 0.29 to 0.41	0.95
G	29,400	1.1	0.87
H	31,000	From 0.6 to 0.8	0.91
I	44,000	0.9	0.95
J	16,400	1.2	1.16
K	24,500	1.0	0.41
L	20,000	0.7	0.11

\*The ratio of NaCl deposited to that emitted in all models is computed by integrating the averaged deposition (kg/km<sup>2</sup>/month) over a 22-1/2° sector from 0.1 to 100 km. However, the integration interval for model K is from 0.1 to 10 km and for model L from 0.5 to 2 km.



### 3. TECHNIQUES FOR MEASURING DRIFT

Two basic principles are applied for drift measurement: (1) determination of drift droplet size distribution and (2) determination of total mineral mass flux. In the first type of measurement, the drift rate is calculated from the droplet size distribution in a unit volume and the efflux speed; for the second, the drift is obtained by assuming the chemical composition of the drift droplet to be the same as that of the circulating water in the tower. The measured drift rates are sensitive to the small end of the size spectrum where the mass fraction becomes increasingly greater for towers with efficient drift eliminators (i.e., where the larger droplets have been selectively removed). Moreover, it is difficult to distinguish small drift (in the 10-50  $\mu\text{m}$  size range) from condensed water drops. All the instruments available for drift measurements — at the tower mouth, in the plume, in the background, or on the ground will be reviewed.

Sensitive paper (drop-size distribution)<sup>(10,20-22)</sup> — The impinged droplets produce stains on a chemical sensitive paper. The droplet-size distribution is retrieved from the number and the size of stain. A correction often has to be made because of splattering of the droplet as it hits the paper. In their ground deposition measurements, Israel and Overcamp<sup>(17)</sup> use  $\text{Cl}^-$  as an indicator for  $\text{NaCl}$ . The darkness of the stain produced by the impinged droplet on a specially chemically treated paper varies with the  $\text{NaCl}$  concentration of the drop. The salt deposition is inferred from the measured number flux, provided the salt concentration in the drift water is known accurately.

Coated slides (drop-size distribution)<sup>(6,24)</sup> — The captured droplets on a coated material leave small craters or rings whose size and number are related to droplet size distribution.

Laser scattering (drop-size distribution)<sup>(23,27,29)</sup> — Light scattered by a particle within a sampling volume is received by a photo detector, causing a current pulse proportional to the cross section of the droplet.

ASSP (Small drop-size distribution) — The Axially Scattering Spectrometer Probe is developed by Particle Measuring Systems, Inc., (PMS).<sup>(18,25,26)</sup> A beam of light from a laser on one side of an isokinetic opening illuminates a sampling volume in the center of the opening. A photo detector on the opposite side of the opening senses the forward-scattered light from droplets passing through the sampling volume. The pulse height is proportional to the droplet size.

Isokinetic sampling tube (drift mass flux)<sup>(29)</sup> — A glass tube collector is filled with glass beads. It is designed so that no significant accelerations occur in the air as it enters the tube. The tube is lined with a heating wire which supplies the heat necessary to evaporate all water droplets.

Cyclone separator (drift mass flux)<sup>(6,30)</sup> — Droplets entering the cyclone separator isokinetically are separated from the air by the centrifugal force and collected in a jar.

Chemical balance (drift mass flux)<sup>(31,32)</sup> — Blowdown is stopped, and the evaporation rate from the water basin is assumed to be known. Measurements of the rate of decrease of a tracer concentration in the circulating water provide information on drift rate.

Calorimetry (water mass flux)<sup>(33)</sup> — Droplets passing a throttle in the calorimeter evaporate by a pressure drop, removing heat from the surrounding air. The measured temperature change is proportional to the mass of water evaporated.

High-volume sampler (ambient concentration)<sup>(34)</sup> — The mineral in the drift droplets is collected on a filter mounted in an inlet tube of the air sampler. The collection efficiency is maintained by an infrared heating element.

Airborne particulate sampler (ambient concentration)<sup>(23,27,29)</sup> — This device is operated on the principle of collection by impaction. The collection is independent of wind velocity.

Deposition pan (ground-drift deposition)<sup>(35)</sup> — A pan collects the drift residue that settles out on the ground surface for a predetermined length of time. The residue collected is analyzed by a spectrometer.



The measurement is important for model verification. Measurement of background level should be subtracted from total measurements.

Neutron activation (ground-drift deposition) — A measuring technique proposed by Oak Ridge National Laboratory. Activation by neutrons of certain drift nuclei, such as  $\text{Na}^{23}$  is detected. The quantity is determined by measurable activity detected by a gamma spectrometer. The accuracy depends on, among other things, the cross section of the tracer used and a non-contaminated collector.

Grass interception (ground-drift deposition)<sup>(36)</sup> — Certain chemicals, such as chromium, in the drift are intercepted by the grass. The total drift is inferred from chemical analyses. The measurement is important for the assessment of a long-term ecological impact. The accuracy depends on certain assumptions; among them, the time to reach steady-state concentration in grass and the interception rate by the grass of a tracer.

Tables 4-7 summarize the instruments and measurements listed above. A subjective evaluation of principles of operation, measurement capability, accuracy, etc., on a simple poor-fair-good-very good scale is given. The tables are modeled after Roffman, et al.<sup>(4,5)</sup> and McVehil and Heikes,<sup>(19)</sup> with a few new techniques added.



Table 4. Drift emission measurement at tower mouth

Technique	Principle of operation	Measurement capability			Accuracy
		Droplet size distribution	Size range measured	Mineral mass flux	
Sensitive paper	Collection	Yes	1-50 $\mu\text{m}$ (ESC) <sup>†</sup> 50 $\mu\text{m}$ up (ATDL) <sup>††</sup>	No	Fair
Coated slides	Collection	Yes		No	Fair
Isokinetic sampling tube	Collection	No		Yes	Very good
Cyclone separator	Collection	No		Yes	Good
Laser scattering	Optical	Yes	50-1000 $\mu\text{m}$ (ESC)	No	Good
Chemical balance	Chemical	No		Yes	Poor
Calorimetry	Thermo- and hydrodynamical	NO		No*	Poor

<sup>†</sup>ESC (Environmental Systems Corporation), a company in Knoxville, Tennessee.

<sup>††</sup>ATDL (Atmospheric Turbulence and Diffusion Laboratory), a NOAA laboratory in Oak Ridge, Tennessee.

\*Measures total water content, neither droplet-size distribution nor mineral mass flux.

Table 5. Drift drops plume measurement — aircraft sampling

Technique	Principle of operation	Measurement capability			Accuracy
		Droplet size distribution	Size range measured	Mineral mass flux	
Isokinetic impactor	Collection	No	>50 $\mu\text{m}$	Yes	Good (PSU)*
Chemical film	Collection	Yes	0-1200 $\mu\text{m}$ >30 $\mu\text{m}$	No	Fair (PSU) (MRI)**
ASSP <sup>††</sup>	Optical	Yes	0-30 $\mu\text{m}$	No	Good (BPNL) <sup>†</sup> (MRI)
CPS <sup>‡</sup>	Optical	Yes	30-300 $\mu\text{m}$	No	Good (MRI)
Cascade impactor	Collection	Yes	0.2-30 $\mu\text{m}$	No	Fair (MRI)

\*Used by The Pennsylvania State University for the natural-draft cooling towers at Keystone, Pennsylvania.

\*\*Used by the Meteorology Research, Inc., for the natural-draft cooling towers at Chalk Point, Maryland.

<sup>†</sup>Used by the Battelle Pacific Northwest Laboratory for the natural-draft cooling towers at Rancho Seco, California.

<sup>††</sup>ASSP (Axially Scattering Spectrometer Probe) produced by the Particle Measuring Systems, Inc., Boulder, Colorado.

<sup>‡</sup>Cloud Particle Spectrometer used by MRI.

Table 6. Airborne monitoring — background and tower contribution

Technique	Principle of operation	Measurement capability		Accuracy
		Droplet size distribution	Mineral mass concentration	
High-volume sampler	Collection	No	Yes	Fair
Airborne particulate sampler	Collection	No	Yes	Good



Table 7. Deposition measurement on the ground

Technique	Principle of operation	Measurement capability			Accuracy
		Droplet size distribution	Size range measured	Mineral mass flux	
Sensitive paper	Collection	Yes	1 $\mu$ m up	Yes	Fair (Israel and Overcamp)
Deposition pans	Collection	No	N/A**	Yes	Fair (U. of Maryland)
Neutron activation	Collection	No	N/A	Yes	Unknown (ORNL)*
Grass interception	Collection	No	N/A	Yes	Fair (ORNL)

\*A measuring technique proposed by Oak Ridge National Laboratory.

\*\*Not applicable.

#### 4. RESULTS OF DRIFT MEASUREMENT COMPARISONS

##### 4.1 Droplet Spectra at Natural-Draft Cooling Towers

The spectra of drift droplets above the drift eliminators, at the tower exit and above the tower top have been obtained using sensitive paper, the light-scattering technique, and aircraft measurements, respectively. Figure 4 is modeled after an earlier summary given by Roffman, et al.<sup>(4,5)</sup> with new data from aircraft penetration added. The curves labeled 1, 2, and 3 were obtained by Fish and Duncan,<sup>(20)</sup> Research-Cottrell,<sup>(21)</sup> and GPU,<sup>(22)</sup> respectively, from natural-draft towers. Only the GPU result follows the log-normal distribution curve. The median diameter varies from 80  $\mu\text{m}$  to 195  $\mu\text{m}$ , with a mean value of about 140  $\mu\text{m}$ . However, the median diameter of the new measurements taken by The Pennsylvania State University aircraft is found to be about 600  $\mu\text{m}$ . The size distribution obtained by PSU,<sup>(24)</sup> labeled as Curve 4, is averaged over four sets of data which have a median diameter ranging from 400  $\mu\text{m}$  to 800  $\mu\text{m}$ . The new ESC measurements from Chalk Point, Curve 5, have a median diameter of about 50  $\mu\text{m}$ . Curve 6 is the standard input data used by Chen<sup>(1)</sup> for the model comparison discussed in Section 2.

##### 4.2 Droplet Spectra at Mechanical-Draft Cooling Towers

Figure 5, modeled after Schrecker and Henderson<sup>(27)</sup> but with new data added, shows the cumulative mass distribution (percent of total liquid drift below stated droplet diameter). Curve 1 is the Ecodyne drift mass distribution, which was measured on a mechanical-draft cooling tower equipped with an Ecodyne's Hi-V drift eliminator. More mass fraction in the large end of the droplet spectrum is reported. Curve 2 represents measurements at the Oak Ridge Gaseous Diffusion Plant, over a Marley Tower built in 1950. The drift eliminators were in poor condition at the time of the measurements, and the subsequent drift rate was high. Curve 3 represents results measured at a Turkey Point mechanical-draft cooling tower.<sup>(29)</sup> The drift rate is low because the tower was new and in excellent condition. Curve 4, representing corrected Ecodyne

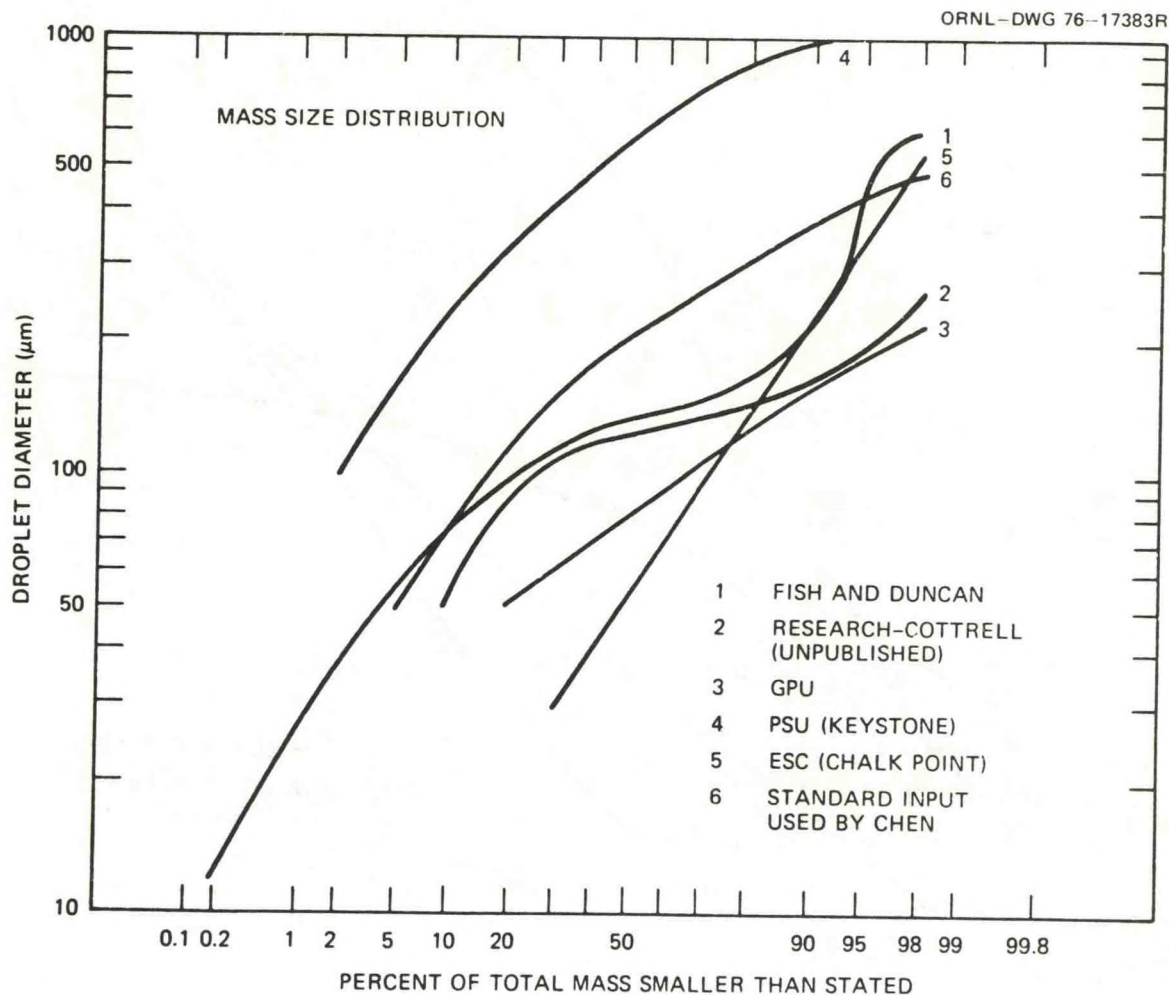


Fig. 4. Cumulative mass distributions of drift droplets for natural-draft cooling towers.



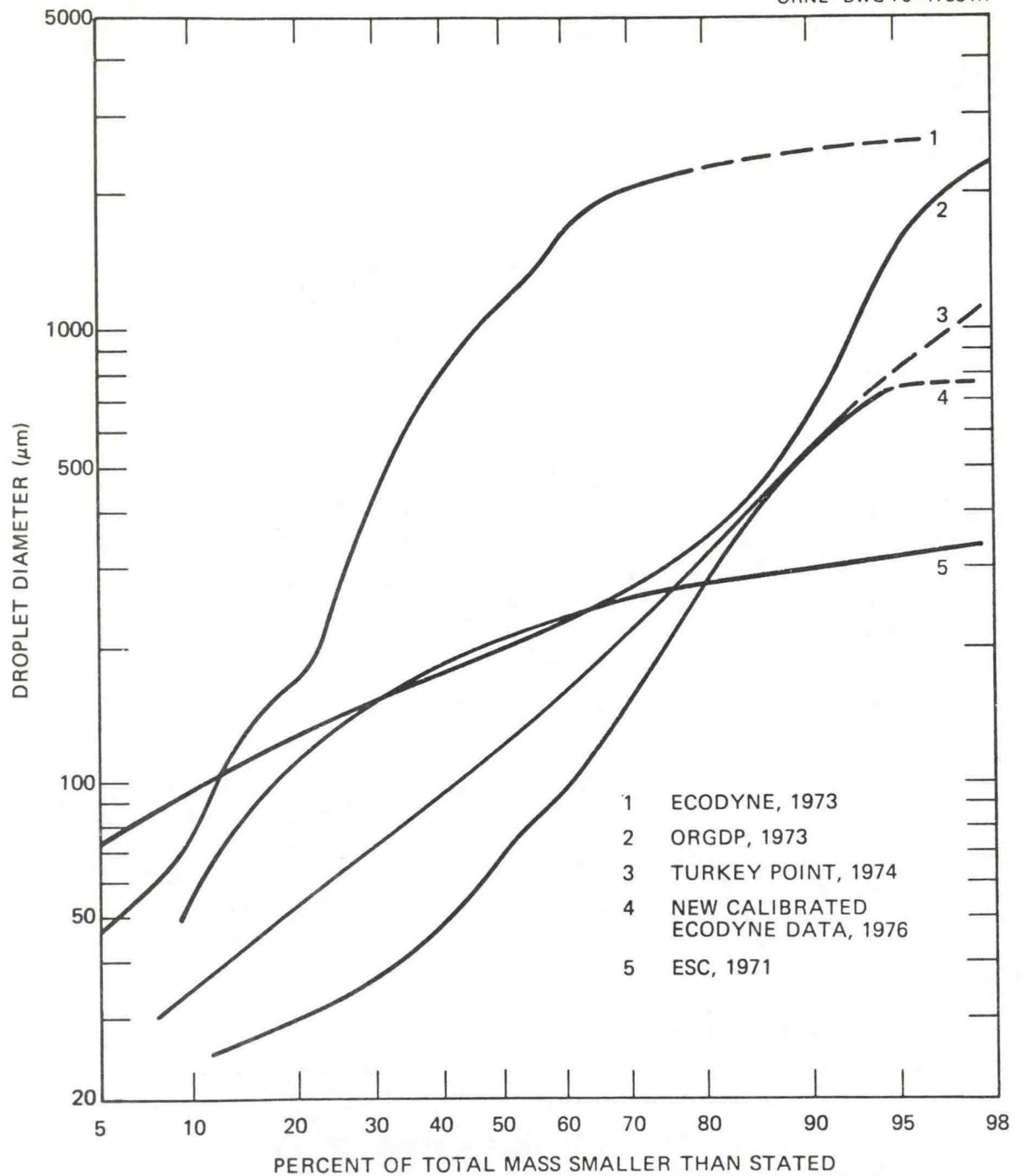


Fig. 5. Cumulative mass distribution of drift droplets for mechanical-draft cooling towers.

data,<sup>(28)</sup> results from a new calibration of stain and droplet size using the same raw data as in Curve 1. This distribution yields the lowest drift rate and shows a considerable shift in mass fraction toward the small end of the droplet spectrum. Curve 5 was obtained by ESC<sup>(23)</sup> from a mechanical-draft tower.

## 5. FURTHER COMMENTS ON MODEL COMPARISONS

Most of the drift deposition models use the stack-plume-rise formulas derived by Briggs.<sup>(16)</sup> Whether these formulas are adequate when applied to cooling tower plumes has not been established and should be tested by measurements.

There are many unproven assumptions in drift deposition models. For example, in some models it is assumed that the droplets escape from the plume at a height where the droplet fall velocity exceeds the updraft. The various updraft assumptions that are used should be verified by aircraft measurements. In some models it is assumed that all droplets break away either from the tower top or at the maximum plume rise. Better justifications should be given for placing the critical droplet diameter at 100  $\mu\text{m}$  in the calculation of drift deposition. In most current models, the trajectory method is used for larger droplets which are supposedly free from turbulent effects near the rising plume. The diffusion method is used for smaller droplets, which are assumed to be influenced by turbulence.

Other areas in which increased understanding is necessary include the calculation of the droplet breakaway points, the dispersal of the droplets by the plume-induced turbulence in the rising plume, and the effects of downwash and terrain. In addition, effects of the centrifugal forces on drift deposition when the plume is bifurcated are not accounted for.<sup>(1)</sup> Of course, whichever method is used, care should be taken that the total amount of salt emitted is conserved.

A main finding in this study is that a difference in the predicted maximum deposition of almost two orders of magnitude exists (from 4,000 to 260,000  $\text{kg}/\text{km}^2/\text{month}$ , with two extreme cases excluded). Furthermore, a difference in the predicted downwind location of peak deposition of an order of magnitude exists (from 0.2 to 3 km). Some of these discrepancies are attributed to different assumptions concerning the height-variation of the plume centerline vertical velocity, the effective height of emission of the droplet, and the extent of its evaporation. The fact that



a given droplet may or may not evaporate to an equilibrium size is affected by many factors, such as where the droplet breaks from the plume updraft, droplet size, salt concentration, and ambient relative humidity. The effective height of emission seems to be the most crucial factor in determining the impact distances and the subsequent deposition.

No model can claim superiority over any other model without field-data verification. Thus, no new models are needed, but field data, especially measurements of ground salt deposition, are needed.

It is found that the maximum deposition and its location are very sensitive to the mass fraction in larger droplets for all present models. Thus, the measurement of droplet-emission spectrum in both size and mass fraction should be as accurate as possible.

There are other sources for deposition besides cooling towers, such as background due to natural sea salt spray and interference from nearby smokestacks. It is necessary to determine these factors before comparisons of predicted deposition against measurements are made.

## 6. A PROPOSED DRIFT DEPOSITION EXPERIMENT

To verify the different deposition models, it is suggested that simultaneous measurements be made of salt concentration in the tower basin, drift-droplet distribution at the tower exit, drift rate, onsite weather conditions, and ground deposition rate distribution. Since the amount of salt to be measured is small, the results will be very sensitive to the instruments and methods used. From the wide scatter of measurements of droplet emission spectra, there appears to be a strong need for good measurements. Simultaneous measurement of droplet emission spectra (namely, the source term) at any specific tower at the tower mouth and along sections normal to the axis of the bent-over plume are desirable.

The ground deposition receptors should be suitably located at 500 m intervals or less from the tower to a point 10 km in the downstream direction of the persistent wind. It is also suggested that more than one collector (sensor) be placed at a given station to provide necessary insurance and calibration.

Deposition depends on, among other things, the joint frequency distribution of wind vector and ambient relative humidity. Thus, onsite hourly averaged wind and relative humidity as a function of height from ground surface to the maximum plume rise are necessary. The sampling period should be longer than the time scale of the plume meandering. An hourly sampling frequency is reasonable for detailed studies of the plume trajectory and its correlation with deposition rate; diurnal variation will smear the maximum and minimum deposition value. For ecological concerns or environmental impact assessments, integrated results from monthly and yearly measurements are adequate.

#### ACKNOWLEDGEMENT

This research was sponsored by the U.S. Energy Research and Development Administration under interagency agreement with Union Carbide Corporation. The calcomplots prepared by Mr. L. Jung of Union Carbide were appreciated.



## REFERENCES

1. N. C. J. Chen, "A Review of Cooling Tower Drift Deposition Models," ORNL/TM-5357, 1976.
2. C. Hosler, J. Pena, and R. Pena, "Determination of Salt Deposition Rates from Drift from Evaporative Cooling Towers," Trans. ASME, Ser. A: J. Eng. Power, 96(3): 283 (1974). (Original document issued by Department of Meteorology, Pennsylvania State University, May 1972).
3. A Roffman and R. E. Grimbale, "Predictions of Drift Deposition from Saltwater Cooling Towers," paper presented at the annual meeting of the Cooling Tower Institute, January 29-31, 1973, Houston, Texas.
4. A Roffman, et al., The State of the Art of Saltwater Cooling Towers for Steam Electric Generating Plants, USAEC Report WASH-1244 (February 1973).
5. A Roffman and Lowell D. Van Vleck, "The State-of-the-Art of Calculating and Predicting Cooling Tower Drift and its Deposition," J. Air Pollu. Control Assoc., 24(9): 855-859 (1974).
6. G. K. Wistrom and J. C. Ovard, "Cooling Tower Drift: Its Measurements, Control, and Environmental Effects," paper presented at the annual meeting of the Cooling Tower Institute, January 29-31, 1973, Houston, Texas.
7. W. G. N. Slinn, "An Analytical Search for the Stochastic-Dominating Process in the Drift Deposition Problem," p. 483 in Cooling Tower Environment - 1974, TIC-ERDA, CONF-470302 (1975).
8. S. M. Laskowski, "A Mathematical Transport Model for Salt Distribution from a Saltwater Natural-Draft Cooling Tower," p. 598 in Cooling Tower Environment - 1974, TIC-ERDA, CONF-740302 (1975).
9. G. W. Israel and T. J. Overcamp, "Drift Deposition Model for Natural-Draft Cooling Towers," p. 614 in Cooling Tower Environment - 1974, TIC-ERDA, CONF-740302 (1975).
10. S. R. Hanna, "Meteorological Effects of the Mechanical-Draft Cooling Towers of the Oak Ridge Gaseous Diffusion Plant," p. 291 in Cooling Tower Environment - 1974, TIC-ERDA, CONF-740302 (1975).
11. S. R. Hanna, "Fog and Drift Deposition from Cooling Towers," Nuclear Safety, 15, 190-196.
12. Y. J. Tsai and D. H. Johnson, "Cooling Tower Drift Model," paper presented at the Fifth Annual Pittsburgh Conference on Modeling and Simulation, April 24-26, 1974.

13. J. V. Wilson, ORFAD, A Computer Program to Estimate Fog and Drift from Wet Cooling Towers, ORNL/TM-4568 (January 1975).
14. M. E. LaVerne, Oak Ridge Fog and Drift Program (ORFAD) User's Manual, ORNL/TM-5021 (in preparation).
15. K. S. Rao, J. S. Lague, and B. A. Egan, "Cooling Tower Drift Model Description," Appendix B of A Study of Environmental Impacts Associated with Cooling Tower Operation at the Proposed Pleasant Prairie, Wisconsin, Power Plant, ERT/P-1235 (1975).
16. G. A. Briggs, "Plume Rise," USAEC Report TID-25075 (November 1969).
17. G. W. Israel and T. J. Overcamp, "A Method to Verify Drift Deposition Predictions from Saline Natural-Draft Cooling Towers," January 1976, submitted for publication to "Atmospheric Environment."
18. The Chalk Point Cooling Tower Program Steering Group, *The Chalk Point Cooling Tower Program, Integrated Experimental Design*, The Johns Hopkins University, Chalk Point, Maryland, August 1975.
19. The American Society of Mechanical Engineers, *Cooling Tower Plume Modeling and Drift Measurement, A Review of the State-of-the-Art*, Research Committee on Atmospheric Emissions and Plume Behavior from Cooling Towers, ASME, New York, 1975. (Original document by G. E. McVehil and K. E. Heikes, issued by Ball Brothers Research Corporation, Boulder, Colorado, March 1975.)
20. B. R. Fish and J. R. Duncan, "Measurement of Liquid Droplet Emission from Cooling Towers and Process Stacks," 65th Annual Meeting of the Air Pollution Control Association, Miami Beach, Florida, Paper No. 72-35, June 18-22, 1972.
21. Unpublished results.
22. "Program to Investigate Feasibility of Natural-Draft Salt Water Cooling Towers," Appendix to Applicant's Environmental Report for Forked River Unit 1, prepared by GPU Service Corporation, Parsippany, New Jersey, 1972.
23. "Development and Demonstration of Low-Level Drift Instrumentation," Office of Research and Monitoring, EPA Corvallis, Oregon, Report No. 16130GNK, prepared by Environmental Systems Corporation, Knoxville, Tennessee, 1971.
24. D. W. Thomson, "Environmental Impact of Evaporative Cooling Tower Plumes," 2nd Technical Progress Report, Department of Meteorology, The Pennsylvania State University, University Park, Pennsylvania 16802, June 1, 1975-May 31, 1976, ERDA Contract E(11-1)2463.



25. G. J. Woffinden, J. A. Anderson, and P. R. Harrison, "Aircraft Survey, Chalk Point Cooling Tower Plume, December 1975," MRI 76R-1410, Submitted to State of Maryland, Department of Natural Resources, Baltimore, Maryland 21201, Contract No. 28-76-04(76), March 15, 1976.
26. M. A. Wolf, "Natural-Draft Cooling Tower Plume Characteristics Determined with Airborne Instrumentation," March 1976, Pacific Northwest Laboratory Annual Report for 1975 to the USERDA Division of Biomedical and Environmental Research, Part 3 Atmospheric Sciences, BNWL-2000 PT3 U2-11.
27. G. O. Schrecker and C. D. Henderson, "Salt Water Condenser Cooling: Measurements of Salt Water Drift from a Mechanical-Draft Wet Cooling Tower and Spray Modules and Operating Experience with Cooling Tower Materials," presented at The American Power Conference, Chicago, Illinois, April 20-22, 1976.
28. G. K. Wistrom, Private Communication, Ecodyne Cooling Products Division, May 1976.
29. Gunter O. Schrecker, Ronald O. Webb, David A. Rutherford, and Frederick M. Shofner, Drift Data Acquired on Mechanical Salt Water Cooling Devices, EPA-650/2-75-060, July 1975.
30. P. A. Jallouk, G. J. Kidd, Jr., and T. Shapiro, Environmental Aspects of Cooling Tower Operation: Survey of the Emission, Transport, and Deposition of Drift from the K-31 and K-33 Cooling Towers at ORGPD, February 1974.
31. J. C. Campbell, A Review of CTI Work on the Measurement of Cooling Tower Drift Loss, TP 68A, Cooling Tower Institute, Houston, Texas, 1969.
32. K. Juris, The Thermal Performance of Natural-Draft Cooling Towers and Influences on Plume Source Strength, Paper 74-9, Annual Meeting Air Pollution Control Association, June 1974.
33. Verein Deutscher Ingenieure, 1974: Lintersuchungen an einem Naturzug-Nass-Kuhlturm (Measurements on an Evaporative Natural-Draft Cooling Tower), Fortschritts-bericht der VDI Zeitschriften, Reihe 15 Nr 5, July 1974.
34. A. Roffman, Drift Losses from Saltwater Cooling Towers - Some Atmospheric Considerations, Amer. Geophysical Union, 54th Annual Meeting, Washington, DC, April 16-20, 1973.
35. C. L. Mulchi and J. A. Armbruster, Effects of Salt Sprays on the Yield and Nutrient Balance of Corn and Soybeans, Cooling Tower Environment-1974, TIC-ERDA, CONF-740302, 1975.



36. F. G. Taylor, Jr., D. D. Gray, and P. D. Parr, "Interception and Retention of Cooling Tower Drift on Vegetation, TP151A, Cooling Tower Institute, Houston, Texas, 1976.

U. S. DEPARTMENT OF COMMERCE  
NATIONAL OCEANIC AND ATMOSPHERIC ADMINISTRATION

ATMOSPHERIC TURBULENCE & DIFFUSION LABORATORY  
P. O. BOX E  
OAK RIDGE, TENNESSEE 37830

POSTAGE AND FEES PAID  
U.S. DEPARTMENT OF COMMERCE  
COM-210



OFFICIAL BUSINESS  
PENALTY FOR PRIVATE USE, \$300

PRINTED  
MATTER

Atmospheric Sciences Library  
Natl. Oceanic & Atmos. Adm.  
8060 13th St., Rm. 806  
Silver Spring, MD 20910

NOAA FORM 61-32A  
(9-73)

NOAA CENTRAL LIBRARY



3 8398 1012 6117 4